






WOODS HOLE
OCEANOGRAPHIC INSTITUTION
REFERENCE ROOM
LIBRARY
COLLECTION

MBL/WHOI

0 0301 0085891 6

WOODS HOLE OCEANOGRAPHIC INSTITUTION
REFERENCE LIBRARY
Exp, ONR. Geophysics Branch
Aug 1961

PHYSICAL OCEANOGRAPHY

Volume II
of
PHYSICAL
OCEANOGRAPHY

by

ALBERT DEFANT

Dr. phil., Dr. rer. nat., h.c.

EMERITUS PROFESSOR OF METEOROLOGY AND GEOPHYSICS

at the

UNIVERSITY OF INNSBRUCK

HONORARY PROFESSOR OF OCEANOGRAPHY

at the

UNIVERSITY OF HAMBURG

and at the

FREE UNIVERSITY, BERLIN

PERGAMON PRESS

NEW YORK · OXFORD · LONDON · PARIS

1961

PERGAMON PRESS INC.
122 East 55th Street, New York 22, N.Y.
P.O. Box 47715, Los Angeles, California

PERGAMON PRESS LTD.
Headington Hill Hall, Oxford
4 & 5 Fitzroy Square, London W.1.

PERGAMON PRESS S.A.R.L.
24 Rue des Écoles, Paris Ve

PERGAMON PRESS G.m.b.H
Kaiserstrasse 75, Frankfurt am Main

COPYRIGHT



1961

PERGAMON PRESS LTD:

LIBRARY OF CONGRESS CARD NUMBER 59-6845

*Printed in Poland to the order of Państwowe Wydawnictwo Naukowe,
by Drukarnia Uniwersytetu Jagiellońskiego, Kraków*

Contents

PART I

SURFACE AND LONG WAVES

I. GENERAL REMARKS ON WAVES	
1. Introduction	1
2. Classification of waves	2
3. Group velocity	12
II. THEORY OF SHORT AND LONG WAVES	
1. Waves with harmonic wave profile. (Stokes' waves)	16
2. Further development of the Stokes wave theory	22
3. Gerstner's rotational waves	26
4. Short-crested waves	29
III. OBSERVATIONS AND MEASUREMENTS OF OCEAN WAVES	
1. Testing of the theory by laboratory experiments	31
2. Observation and measurement of ocean waves	33
3. Comparison between theory and observations	40
4. Stereophotogrammetric survey of the sea surface	46
5. Apparent and real characteristics of waves, the complexity of wind-generated waves	50
6. The energy spectrum and the spectral analysis of recordings of ocean waves	52
7. Statistical relations between the different apparent wave characteristics and their interpretation	57
8. Scales of sea motion and wind	60
9. The mathematical formulation of the actual ocean wave pattern	63
IV. GENERATION, GROWTH AND PROPAGATION OF WAVES	
1. Observations of the generation of waves	66
2. Propagation of a wave disturbance through a region previously undisturbed	68
3. Theories of the generation and the growth of waves	74
4. Theory of the growing of significant waves by wind	87
5. Observations on the growth of waves	93
6. Growing of spectral components of the wind-generated sea	97
7. Swell, observations and theory	99

V. SHALLOW WATER WAVE TRANSFORMATION THROUGH EXTERNAL FACTORS	
1. Shallow water waves; theory and observations	109
2. The solitary wave of Scott Russell	116
3. Changes in form of waves by exterior causes	120
4. Surf on flat and steep coasts	123
5. Calming effect of oil on waves	139
VI. LONG WAVES IN CANALS AND STANDING WAVES IN ENTIRELY OR PARTLY CLOSED BASINS	
1. Long waves in canals	142
2. Standing waves in closed basins	154
3. The character of the oscillation of connected systems	175
4. Observed standing waves in lakes, bays and adjacent seas	182
5. Influence of the earth's rotation on tidal waves and seiches	202
6. Generation and growth of the oscillations of the sea and lake surface	219
7. Dislocation and explosion waves	237
 PART II 	
TIDES AND TIDAL CURRENTS	
VII. PRINCIPAL FEATURES OF TIDAL PHENOMENA	
1. Review of the phenomena	245
2. Tidal observations, gauges	250
VIII. THE TIDE-GENERATING FORCES	
1. Fundamentals for determining tidal forces	254
2. The system of tide-producing forces as a function of the zenith distance	258
3. The harmonic analysis of the tidal potential	263
4. The experimental proof of the tide-generating forces	268
IX. THEORY OF THE TIDES	
1. The equilibrium theory	272
2. The dynamical theory of the tides	279
3. Canal theory of the tides	290
4. Remarks concerning the dynamic theory of tides	296
X. THE HARMONIC ANALYSIS OF TIDAL OBSERVATIONS	
1. The preparation of sea-level recordings and their scientific use	299
2. Characteristics of the tides as shown by their harmonic constants	305
3. Variations in the harmonic tidal constants	308
4. Prediction of the tides. Tide tables, tide predicting machines	311
XI. TIDES AND TIDAL CURRENTS IN THE PROXIMITY OF LAND	
1. Preliminary remarks	320
2. General considerations on the influence of the earth's rotation and of the friction on tides and tidal currents	320
3. Tides in adjacent seas	337

4. The tidal phenomena in narrow embayments	350
5. Relations between tidal current and co-tidal and co-range lines	354
6. Conditions along shores and disturbances on account of bays and islands	357
7. Computation of the tide from tidal current measurements	359
XII. TIDES IN THE MEDITERRANEAN AND ADJACENT SEAS. OBSERVATIONS AND DISCUSSION	
1. The tides of the North Sea	364
2. The tides of the Kattegat and the Baltic Sea	372
3. The tides of the English Channel and the South-western North Sea	377
4. The tides of the Irish Sea	384
5. The tides of the Mediterranean	388
6. The tides of the Strait of Messina	395
7. The tides of the Adriatic	399
8. The tides of the Aegean Sea	403
9. The tides of the Black Sea	404
10. The tides of the Red Sea	407
11. The tides of the Persian Gulf	413
12. The tides of the East Indian Archipelago	417
13. The tides of the Eastern China Sea	423
14. The tides of the Sea of Japan and the Sea of Okhotsk	426
15. The tides of the Bering Sea	433
16. The tides of the Gulf of California	434
17. The tides of the Gulf of Mexico	435
18. The tides of the Gulf of St. Lawrence	439
19. The tides of the Bay of Fundy	443
20. The tides of the White Sea and of the Gorlo	445
21. The tides of the North Polar Basin or Arctic Ocean	446
22. The Tides in Inland Seas	452
XIII. TIDES IN ESTUARIES	
1. Observations	457
2. Theoretical considerations regarding river tides	464
3. Bores	469
XIV. TIDES OF THE OCEANS	
1. First co-tidal chart of the oceans	475
2. Methods used to incorporate the observations presently available in maps of the tides of the oceans	477
3. The charts of the tides in the various oceans	479
4. The M_2 tide as the typical tide wave of the semi-diurnal tides	481
5. The K_1 tide as the typical tide wave of the diurnal tides	491
6. Tidal currents in the Atlantic Ocean	494
7. Theoretical considerations on the semi-diurnal tides in the Oceans especially on those of the Atlantic Oceans	496
XV. THE TIDES IN RELATION TO GEOPHYSICAL AND COSMIC PROBLEMS	
1. The detection of the tides of the solid earth from tidal observations in shallow adjacent seas	504

2. Deformations of the solid earth by tidal load	509
3. Frictional effects of tidal currents and their relation to cosmic problems	512
XVI. INTERNAL WAVES	517
1. Basic facts and theory of the internal waves	537
2. Observations of internal waves in the oceans; testing of the theory	553
3. Internal waves in lakes and in basins	557
4. Causes of internal waves, particularly of those with a tidal character	562
5. The stability of internal tide waves internal breakers	567
6. Stationary internal wave-like displacements	
BIBLIOGRAPHY	571

PART I
SURFACE AND LONG WAVES

Chapter I

General Remarks on Waves

1. Introduction

IN this volume we shall concern ourselves chiefly with such phenomena of the oceans which have as their main characteristic a period, in contrast to the ocean currents, which were discussed in Vol. I. This means that the movement repeats itself after a certain time so that observations for this time interval suffice to determine the process.

The surface of a motionless fluid must satisfy the condition that at every point it is perpendicular to the forces acting on that liquid. When the fluid is at rest, gravity is the only acting force and, therefore, the surface at rest must coincide with a level surface. However, the ocean surface, even when we only consider small parts of it, is never completely at rest. Many factors, especially winds blowing over the ocean, generate waves which are present most of the time; close to the shores we nearly always have a surf. A mirror-like surface is an exception, whereas a sea covered with waves is customary. Besides these short waves, which are easily visible, there are much larger waves which, because of their great dimensions, cannot be detected by visual observation. Over a certain length of time we can observe their effects, and from the combination of such observations we can conclude as to the wave character of these disturbances. These are the waves following earthquakes, volcanic eruptions, etc. (dislocation waves), submarine earth slides and the great phenomena of the tides which affects all the oceans. Each water particle in these wave motions is not subjected to any large local displacement. The water-masses shift relatively little backwards and forwards in a horizontal direction. After a certain time they will generally return to their original position; and in this they differentiate themselves from ocean currents, in which a permanent transport of water takes place in a definite direction. This pendulum movement of the separate water particles and their return to their original position, which applies to nearly all waves, can be considered as oscillations around a steady position.

Before entering upon the nature of the waves proper, we will consider some of their fundamental physical properties and establish some definitions which we will have to use quite often.

In general there are two forces acting on a water surface which is in

a stable equilibrium: gravity and surface tension. If disturbances of this equilibrium occur, both forces tend to restore the equilibrium. If gravity causes the return to the state of equilibrium, we speak of gravity waves, in contrast to capillary waves, for which surface tension is the restoring force. All large waves in the ocean are gravity waves; only when dealing with the smallest waves of a few centimetres length do we have to take the capillary forces into account (see p. 77).

In water waves the disturbing motion of the individual particles is perpendicular to the direction of the wave and, therefore, they belong to a group called "cross waves", in contrast to the "longitudinal waves", where the separate particles oscillate backwards and forwards in the direction of progress. In the longitudinal waves the elasticity of the medium is the force that tries to bring the particles back to their state of rest. This elasticity causes a succession of increases and decreases of the density of the medium. To these longitudinal waves belong the sound waves, which have shown their importance in oceanography by the utilization of echo sounding. They also play an important part in submarine acoustics.

Classification of Waves

We can classify the waves according to the oscillations of the individual particle: (a) in progressive and standing waves, according to the forces which generate and maintain them; (b) in forced and free waves, according to the relation between the velocity of the waves and the depth; (c) in surface or short, or deep water waves and long or shallow water waves. The first class can be subdivided into progressive and standing waves.

(a) *Progressive waves* are characterized by the fact that each water particle in a certain level executes the same closed orbit within a definite time. However, all particles do not participate in this motion with the same phase. The phase lags for the particles in the direction of the wave propagation and is dependent upon the wave velocity. The simplest form of a progressive cross-wave is obtained when we subject the individual particles of the surface to displacements according to the law of harmonic oscillations. If we call this displacement η , we obtain

$$\eta = A \sin a = A \sin \frac{2\pi}{T} t. \quad (I.1)$$

A is the amplitude of the displacement (elongation), $2A$ is its range. a is the angle determining the time of the displacement (phase angle). T , which is known as the period of oscillation, is the time needed by each particle for a complete oscillation. During this time, a passes through all values from 0 to 2π ; consequently, in a unit time the angle $2\pi/T$, so that, for any given time t , a becomes $(2\pi/T)t$ and η takes the second form of (I.1). $t = 0$ determines the time when the movement starts.

Let us now suppose that the individual water particles of the surface execute such harmonic oscillations in a vertical plane and that the energy is transmitted from one particle to another successively in horizontal direction, with each particle starting its motion somewhat later, but this difference in time between each particle remaining the same. Let us designate this time interval as τ . Consider n successive particles; particle 0 will execute the harmonic movement as expressed by (I.1), particle 1 the motion

$$\eta_1 = A \sin \frac{2\pi}{T} (t - \tau),$$

and in general the motion of particle i will be expressed by

$$\eta_i = A \sin \frac{2\pi}{T} (t - i\tau).$$

Particle n should start its harmonic oscillation at the very moment when particle 0 has completed its first harmonic oscillation, then $n\tau = T$. We can replace τ by T/n and the motion of particle i is given by

$$\eta_i = A \sin \frac{2\pi}{T} \left(t - \frac{i}{n} T \right). \quad (\text{I.2})$$

If we designate the horizontal distance between particle 0 and particle n as λ , the distance between particle 0 and particle i as x , then $x : \lambda = i : n$ and we obtain from (I.2) the equation for the motion of each particle in the following form

$$\eta = A \sin \left[\frac{2\pi}{T} t - \frac{2\pi}{\lambda} x \right]. \quad (\text{I.3})$$

This is the general equation for a progressive wave travelling in the direction $+x$ and of an harmonic type. Figure 1 illustrates the development of such a wave for 15 consecutive equidistant particles. Particle 0 has completed its harmonic oscillation at the exact moment of the start of that of particle 12. This moment corresponds to the XII row of Fig. 1. λ is called the wave length; it is the horizontal distance between two particles which are in the same phase of motion; it is, furthermore, the horizontal distance between two corresponding points — like from trough to trough or from crest to crest — for a given time. The form of the wave is an harmonic function and is given by the equation:

$$\eta = A \sin \left(C - \frac{2\pi}{\lambda} x \right).$$

The greatest elevations are called wave crests, the greatest depression wave troughs; their vertical distance is the wave height, whereas the wave amplitude is one-half of the wave height.

Equation (1.3) shows that the waves advance unchanged in the $+x$ direction with a velocity $c = x/t = \lambda/T$. c is called the wave velocity and $1/T = \nu$ is called the frequency of the wave. Often the quantity $2\pi/T = \sigma$ is used which is called the “angular velocity” of the wave. We can similarly

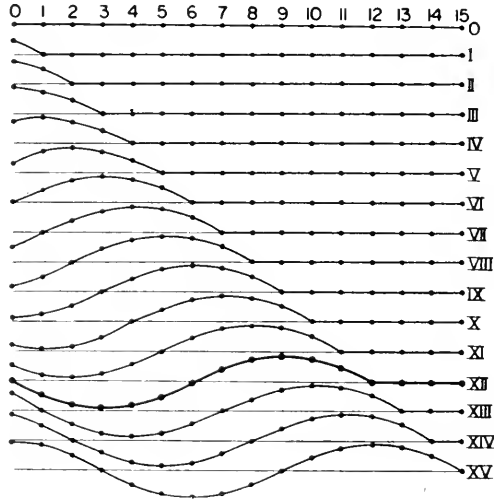


FIG. 1. Development of an harmonic progressive transverse wave.

introduce a quantity $2\pi/\lambda = \kappa$ and call it the “wave number”, because it indicates the number of waves over a distance 2π . We thus obtain the fundamental equations applicable to all waves:

$$\lambda = cT, \quad \sigma = \kappa c, \quad \eta = A \sin(\sigma t - \kappa x). \quad (1.4)$$

In the wave motion discussed so far each particle of the medium executed movements only perpendicular to the direction of propagation of the wave. In water waves we have to add a rhythmic motion in the direction of propagation of the wave, so that each particle, with the passage of a wave, executes an orbit. In this way a system of waves moving with a definite velocity is developed on the surface which is called a wave train.

In case the particles move in circular orbits, we have to replace Fig. 1 by Fig. 2. The water particles numbered from 0 to 15 move in their orbits with the same uniform speed in such a manner that particle 12 starts its movement at the exact moment when particle 0 has completed its circle. Therefore, it is in the same phase as particle 0 and, consequently, the distance 0 to 12 represents the wave length. In this particular case the wave profile is no longer harmonic, because the wave crest and the wave trough have a different form, inasmuch as the wave crest is shorter and steeper, whereas the wave trough is wider and flatter. This curve is a trochoid (p. 28). Within a progressive wave the horizontal flow at the wave crest is in the direction of

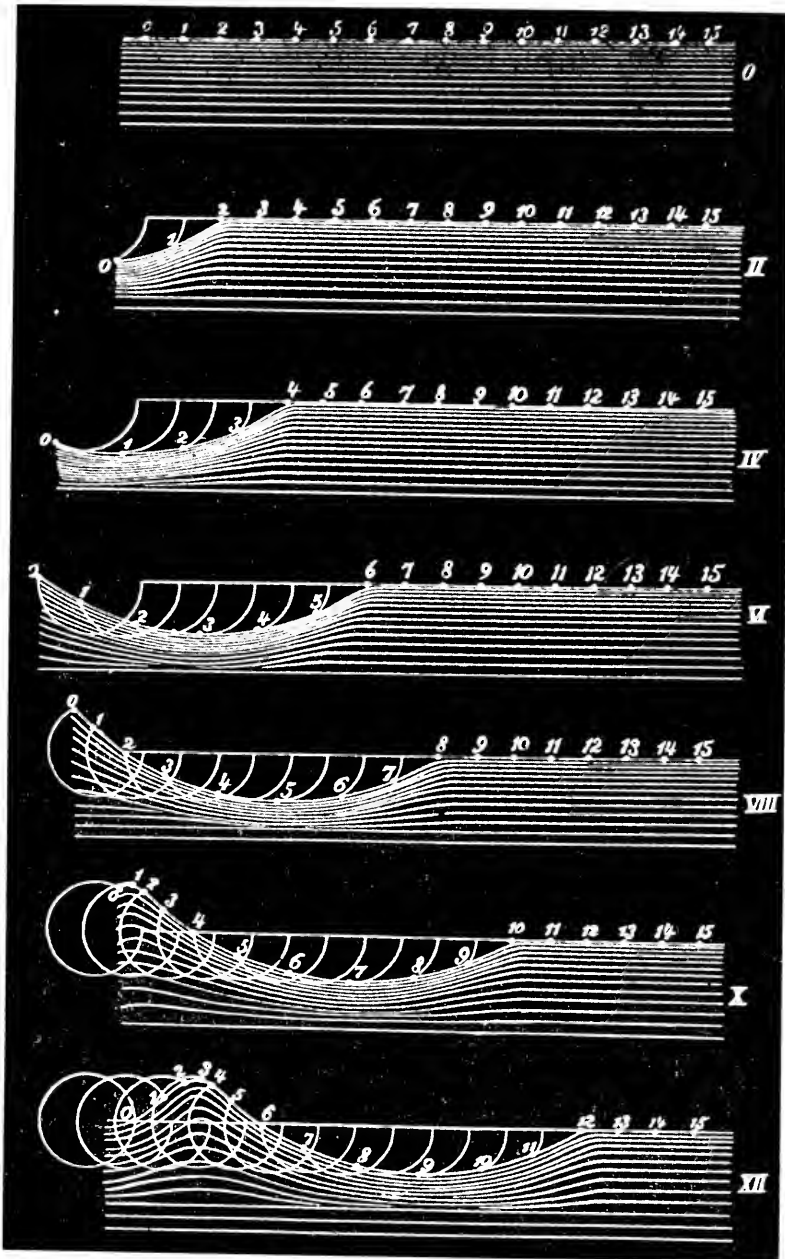


FIG. 2. Wave formation through circular motion of water particles.

progress, and at the wave trough it is opposite to the direction of progress of the wave. The reversal of the current direction takes place at the moment the particle passes through its level of equilibrium; at this point the vertical velocities are greatest, whereas they are reduced to zero at the

highest points of the wave crest and at the lowest points of the wave trough. This distribution of the horizontal and the vertical velocities with the passage of a wave is characteristic for a progressive wave train.

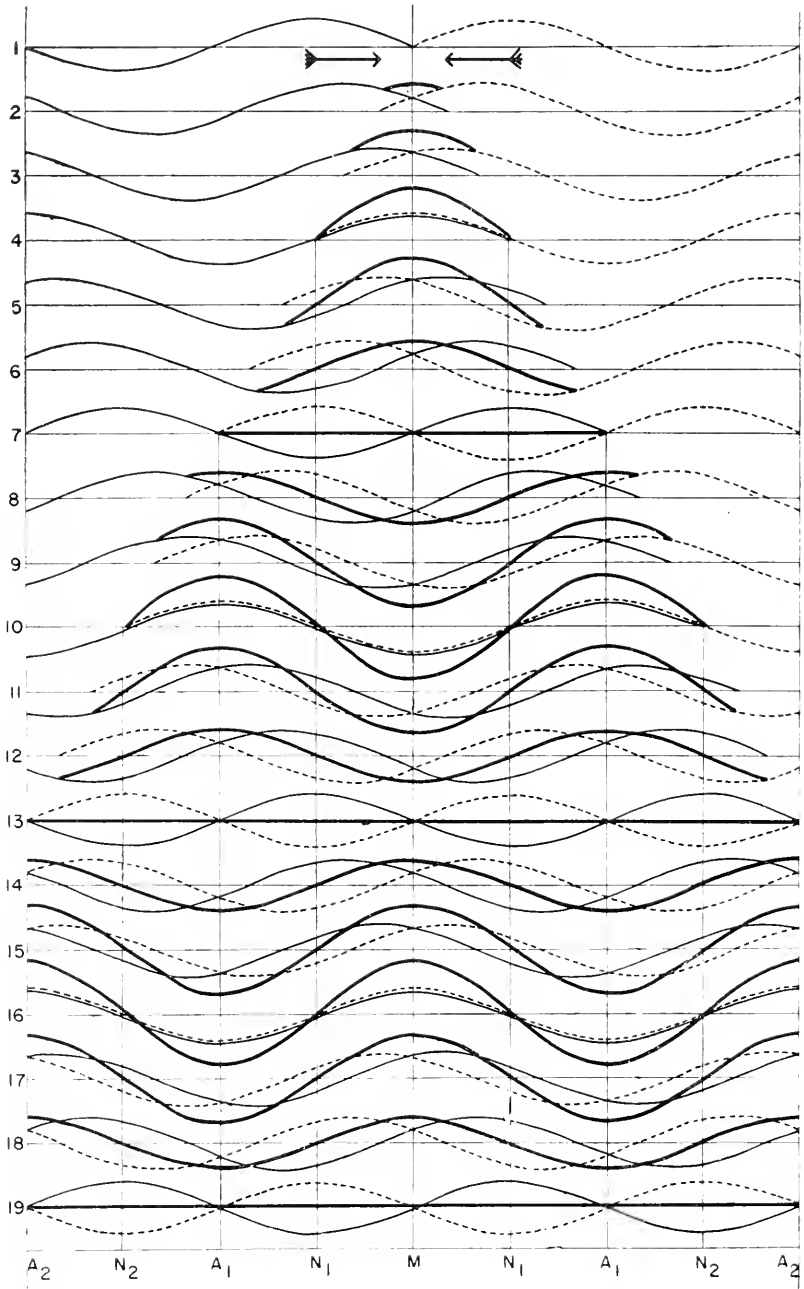


FIG. 3. Standing wave formed by interference of two progressive waves.

Within a standing wave each individual water particle moves in an orbit but, contrary to the progressive waves, the phase is the same for all particles, and the amplitude of the movement is different for each particle. The points where there is no vertical motion are called nodes, and the points where there is no horizontal motion are called antinodes. We can study the properties of standing waves by superposing two progressive waves having the same velocity and the same amplitude but opposite directions. From the superposition results a simple standing wave. Figure 3 represents nineteen different phases of such a case. In 1 both waves meet in the middle M of the figure. In 2 both waves overlap for one-twelfth of the wave length. The heavy line represents the sum of the ordinates of the two waves. In each subsequent phase the original waves have progressed by one-twelfth of the wave length. In 7 each wave has progressed by half its length. The superposition shows that both waves have cancelled each other out, because one wave crest coincides with the wave trough of the other wave. At this particular moment, all particles in the vertical direction go through their state of equilibrium. Then, however, the vertical displacement starts again, in the middle part downwards, in the sides upward. We can see that there are particles which remain always at rest, because they are displaced by the progressive wave going into one direction by exactly the same amount as by the other progressive wave which travels in the opposite direction. Both waves cancel each other and the particle remains at rest. These are the nodes N_1, N_2 etc. There are, furthermore, points called antinodes A_1, A_2 etc. which have the largest vertical displacements, up to the double amplitude of the progressive wave. The antinodes, as well as the nodes, always remain in the same place. The profile of the wave is subjected to continuous changes, but does not move laterally and has no velocity, and therefore such waves have been called standing waves. The wave length of a standing wave is equal to the distance from one node to the next node, or from one antinode to the next antinode. It can be shown that a standing wave results from a complete reflection of a progressive wave on a vertical wall. The superposition of the incoming wave and the reflected wave produces a standing oscillation, with always an antinode at the wall. When η_1 is the vertical displacement on a wave moving to the left, which hits a vertical wall at $x = 0$, and η_2 the vertical displacement of the reflected wave moving in the opposite direction, the superposition of both waves will give a total vertical displacement of $\eta = \eta_1 + \eta_2$. This gives

$$\left. \begin{aligned} \eta_1 &= A \sin(\sigma t - z x), \\ \eta_2 &= A \sin(\sigma t + z x), \\ \eta = \eta_1 + \eta_2 &= 2A \cos z x \sin \sigma t. \end{aligned} \right\} \quad (I.5)$$

This standing wave has its nodes wherever $\cos z x = 0$, viz. at $x = \frac{1}{4}(n+1)\lambda$ ($n = 0, 1, 2, \dots$). It has antinodes wherever $\cos z x = \pm 1$, viz. at

$$x = \frac{1}{2}n\lambda.$$

It is obvious that there exists an antinode at the reflecting wall ($n = 0$). The next node is at a distance from the wall of one-quarter of the wave length.

Standing waves not only have their vertical but also horizontal displacements. However, in this kind of waves, individual water particles do not move in closed orbits, but the particles return through the same points of their trajectories through which they moved forward. Thus the movement of the individual water particles resembles more an oscillation around a point of equilibrium. The distribution of the horizontal and the vertical components of motion within a standing wave is entirely different from that of progressive waves. The particles in a progressive wave move upward at the front side of a wave crest and downward at the rear side, whereas in a standing wave their movement in the entire antinode is everywhere simultaneously upward or downward. There are no vertical displacements in the nodal points, but here occurs the greatest horizontal water displacements, which disappear again in the antinodes. Standing waves thus have the character of a rocking movement of the entire water-mass around fixed nodal lines. This readily explains that in standing waves the current reverses itself everywhere simultaneously, and this happens when the antinodes have the greatest positive respectively negative displacements, viz. at high- and low water. The greatest horizontal velocity is found when the water surface passes through its equilibrium.

A progressive wave $\eta = 2A \cos(\sigma t - \kappa x)$ can be imagined to be composed of the interference of two standing waves. $\eta_1 = A \cos \kappa x \cos \sigma t$ and $\eta_2 = A \sin \kappa x \sin \sigma t$. η_1 and η_2 are two standing waves of equal wave length having a phase difference of a quarter period, and the amplitude of the two systems be equal; consequently, the relation between them is that the antinodes of the one are superposed upon the nodes of the other.

It is to be remembered that, if we disregard a harmonic wave profile, each progressive wave can be represented by a function of $(\sigma t \pm \kappa x)$ (equation I.4); here the negative (positive) sign applies for waves progressing in the positive (negative) x -direction. For standing waves, the function containing the coordinate for the direction x is separated from the time function. As a rule, both appear in the form of a product (I.5). The mathematical treatment of wave processes is facilitated if we consider standing waves as composed of progressive waves. Therefore, it is important that each train of progressive waves can be represented as a superposition of a system of two standing waves with a phase difference of a quarter of the period.

(b) *Free and forced waves.* In every system capable of oscillation we can distinguish free and forced waves. Free waves are generated by a single sudden impulse and for their generation and maintenance they do not require an external force. A system with its equilibrium disturbed by a single impulse would continue oscillating *ad infinitum* in the absence of friction. The amplitude of the oscillations decreases with time according to an e -function (damped

oscillations), due to the ever present internal and external frictional forces, and finally stops entirely. A damped wave can then be represented in a certain locality by

$$\eta = A_0 e^{-\beta t} \cos \sigma t. \quad (\text{I.6})$$

If η_n is the n th point of reversal of the oscillation on the positive side at the time nT , the amplitude at this time will be

$$A_n = A_0 e^{-n\beta T} = A_0 e^{-n\gamma}. \quad (\text{I.7})$$

The quantity $\gamma = \beta T$ is designated as logarithmic decrement of the damped oscillation. It is equal to the natural logarithm of the ratio of two consecutive values of the amplitudes taken in the same direction of displacement, or it is

$$\gamma = \frac{\ln A_n - \ln A_m}{m - n} \quad (\text{I.8})$$

if A_n and A_m represent the n th and m th amplitude of the oscillation in the same direction (KOHLRAUSCH, 1935). The friction of a free oscillating system can be characterized by γ .

The period of the free oscillations depend exclusively on the dimensions of the system, which for a closed basin bay are the length, the depth and the width of the basin. Dissipating forces can increase the period of the free oscillations (see p. 155).

Forced waves are generated in a system capable of oscillation by the continuous action of a periodical external force. The tidal forces of moon and sun subject the water-masses of the oceans to periodical displacements in a horizontal direction, which displacements in turn contribute to the formation of waves. The period of forced waves is always identical to the period of the generating force. However, the amplitude and the phase are not free as is the case with free waves, but they essentially depend on the ratio between forced and the free oscillations of the system. The amplitude and phase of the forced waves depend not only on the generating force, but also on the dimensions of the oscillating system. The amplitude A of the forced waves increases as the period of generating force τ approaches the period of the free oscillations T . Here applies the relation

$$A = \frac{A_k}{\sqrt{\frac{4\tau^2}{T^2} - \frac{4\tau^2}{\tau^2}}} = \frac{A_k}{\sigma^2 - \sigma_k^2} \quad (\text{I.9})$$

in which A_k is the amplitude and σ_k the angular velocity of the generating force. If $\sigma = \sigma_k$ or τ and T are equal, the amplitude of the forced waves increases steadily: the oscillating system then is in *resonance* with the periodical force.

The phase of the forced oscillations is only then the same as the phase

of the generating force, when the period of the generating force of the forced oscillations is greater than the period of the free oscillations, viz. when $\tau > T$. If, on the contrary, the period of the generating force is smaller than that of the free oscillations ($T > \tau$), the phase of the forced waves is opposite to the phase of the generating force. These properties of the forced oscillations pertain to a general dynamic principle of the wave theory and will be frequently referred to in subsequent paragraphs.

(c) *Short and long waves.* We can divide the wave-like motion of water-masses into two different classes, taking as a measure the ratio of the wave-length λ to the depth to the bottom h . If the bottom depth h is smaller than half a wave length, it can be considered as “shallow”; if, on the contrary, the depth exceeds about half a wave length, the water is called “deep”.

In deep water waves, the orbital motion of the water particles decreases fairly rapidly with increasing depth. Close to the surface the individual water particles move in circular orbits. The radii of these orbits decrease with depth and in intermediate depths of approximately half a wave length below the surface, the diameter of the orbits is theoretically one twenty-third of the orbit diameter at the surface. The movement of the wave is restricted to a relatively thin surface layer. Hence the denomination of surface waves. SCOTT RUSSEL (1837, p. 417) named them secondary waves, and in the English literature they are called quite often oscillatory waves. Let us imagine the water-mass is divided into horizontal and vertical filaments of water in a state of rest. The positions of the corresponding filaments during the passage of a wave are shown in Fig. 4. Their distortion is greatest in the

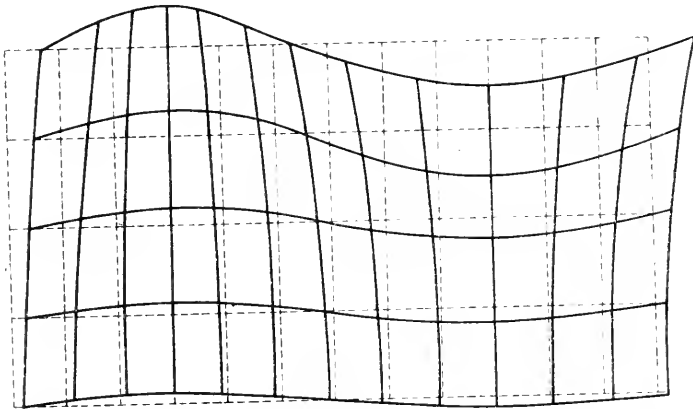


FIG. 4. Behaviour of vertical line of particles during passage of a short wave (great depth).

upper layers and decreases rapidly with depth. In greater depth it becomes imperceptible, and finally it disappears entirely. Thus the comparison made by Leonardo da Vinci between a waving cornfield and such water waves does not apply only to the oscillatory motion of the single particles and to

the progressive form of the surface, but also to the oscillatory motion which decreases rapidly with depth, in as much as the base of the cornsticks remain equally at rest. The only difference is that the length of the stems remains constant, whereas the water columns stretch and shrink as the wave passes by.

In shallow water where h is smaller than half a wave length, the orbital motion reaches to the bottom and is of about the same size in all depths. The motion of the individual water particles then corresponds more to a forward and backward shift of whole water columns whereby they become at times wider and thus shrink in vertical extent or at times narrow and thus stretch depending upon whether they are situated in a wave trough or wave crest. Figure 5 shows rectangles of equal size in a position of rest and during the passing of the wave and the resultant wave at the surface. In these deformations the horizontal components of the velocity and acceleration of the particles play the main role, whereas the vertical acceleration can be neglected. With deep water waves (surface waves) on the contrary, the verti-

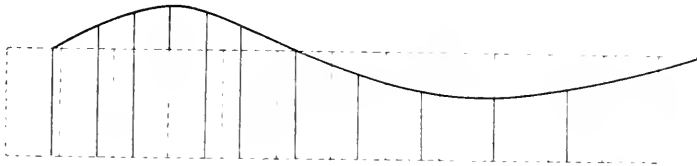


FIG. 5. Behaviour of vertical line of particles during passage of a long wave (shallow depth).

cal component of acceleration must be considered. It is, therefore, quite possible that an ocean is rather shallow relative to the long waves of ocean tides, whereas it must be considered as very deep even for the largest of the ordinary wave trains that can be perceived on its surface. Deep and shallow water, therefore, are only to be considered in relation to the wave length. Waves of tidal periods are the best example of such long waves, which therefore are also called tidal waves; the name long waves is mostly used; Scott Russell called them also primary waves.

An excellent summary of the most outstanding characteristics of ocean surface and long waves has been given by SVERDRUP (1942, p. 521) which we quote here:

	Surface waves	Long waves
Character of wave	Progressive, standing, forced or free	Progressive, standing forced or free
Velocity of progress	Dependent on wave length but independent of depth	Dependent on depth but independent of wave length
Movement of water particles in a vertical plane	In circles, the radii of which decrease rapidly with increasing distance from the	In ellipses which are so flat that practically the water particles are oscillating back

	surface. Motion imperceptible at a depth which equals the wave length. In some types of surface waves the motion is in wide ellipses	and forth in a horizontal plane. Horizontal motion independent of depth
Vertical displacement of water particles	Decreases rapidly with increasing distance from the surface and becomes imperceptible at a depth which equals the wave length	Decreases linearly from the surface to the bottom
Distribution of pressure	Below the depth of perceptible motion of the water particles the pressure is not influenced by the wave	The wave influences the pressure distribution in the same manner at all depths
Influence of the earth's rotation	Negligible	Cannot be neglected if the period of the wave approaches the period of the earth's rotation. The velocity of progress of the wave and the movement of the water particles are modified

Surface waves and long waves are, of course, to be considered as the two extremes of a continuous series of waves. However, the transition zone is relatively small, so that the separation in "short" and "long" waves is appropriate. From this difference in velocities between long and short waves (see p. 18) it results that a group of waves composed of long waves remains undivided, as each wave travels with the same velocity. This is not the case with a group of surface waves, as the long waves travel faster than the shorter ones. The group disintegrates with time. Long waves, consequently, show no dispersion, whereas, in the case of surface waves, dispersion is faster when the difference in the wave lengths becomes greater.

3. Group Velocity

In observing nature, we find that in general an ocean wave does not exist by itself, but that in most cases a train of waves is composed of a system of waves of all possible lengths, each wave progressing with the velocity corresponding to its own particular wave length. The free surface, therefore, is subjected to constant changes, and the wave profile shifts constantly. When observing carefully, e.g. a wave train produced by a stone or a single falling drop of water in a deep water basin, we find that the waves appear in groups. Such an isolated group of waves as a whole shows a velocity smaller than that of the individual waves composing it. Following a single wave in such a group, we see it advances through the group, but, at the same time, it gradually loses its height in approaching the front. The place it formerly

occupied in the group is now occupied in succession by other waves which have moved forward from the rear. It appears as if, on the front end of a group, the waves constantly disappear, whereas new waves appear at the rear. The group is then continuously composed of waves which travel through them. The behaviour of such groups can be best explained, according to Lord Raleigh (LAMB, 1932, p. 382), by the superposition of two systems of waves of equal amplitude, but of a somewhat different wave length and velocity. This overlapping will give the following equation of the free surface:

$$\begin{aligned} \eta &= A \sin(\alpha x - \sigma t) + A \sin(\alpha' x - \sigma' t) \\ &= 2A \cos \left[\frac{\alpha - \alpha'}{2} x - \frac{\sigma - \sigma'}{2} t \right] \cdot \sin \left[\frac{\alpha + \alpha'}{2} x - \frac{\sigma + \sigma'}{2} t \right]. \end{aligned} \tag{1.10}$$

As α and α' differ only very slightly $\alpha = \alpha' + 1\alpha$, the cosine in the first part of this expression changes its value very slowly with x ; so that, at any instance, the wave profile has the form of a sine curve, in which the amplitudes vary between the values 0 and $2A$. The surface thus has the appearance of a succession of groups of waves separated, at equal intervals, by strips of almost smooth water. Figure 6 shows an example of the overlapping of two such waves: $\eta = 1000 \cos 6x \cdot \sin 60x$, for which $\alpha = 66^\circ$ and

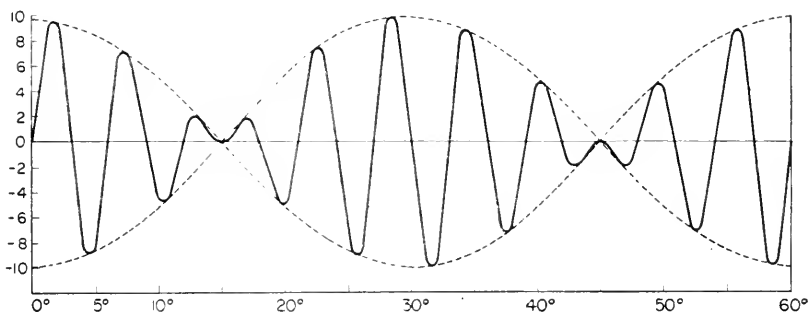


FIG. 6. Superposition of two waves with slightly different wave lengths (ratio 9 : 11). Group maxima 30 units apart.

$\alpha' = 54^\circ$, and which correspond to the wave lengths of approximately $5 \cdot 45^\circ$ and $6 \cdot 66^\circ$. The amplitude becomes = 0 when

$$6x = (2n + 1) \frac{1}{2} \pi \quad (n = 0, 1, 2 \dots), \quad \text{this means,}$$

in intervals of 30° . It looks as if the entire train of waves is composed of wave groups, each of which has a length of 30° . The periodical phenomenon under consideration can be explained by a superposition of two waves having approximately the same wave length. It is easy to follow the path of such wave groups by means of Fig. 7. It shows the superposition of two wave systems whose velocities c_1 and c_2 correspond to a ratio of 17 to 15, and their wave length to the ratio 5 to 4. One can easily see that the wave groups

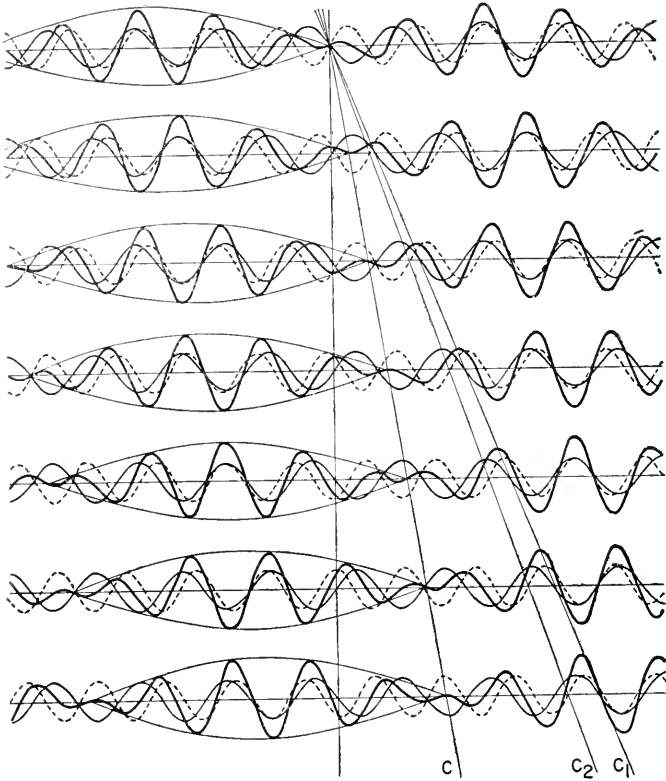


FIG. 7. Behaviour of wave groups resulting from the superposition of two wave systems (ratio of wave lengths 5:4); (ratio of wave velocities 17:15) (From Grimsel-Tomaschek, *Lehrbuch der Physik*, vol. 1, p. 405).

travel much slower than the separate waves. The behaviour of the separate waves within the groups can be seen in this figure. The distance between the centres of two successive groups, according to (I.10) is $2\pi/(\kappa - \kappa') = 2\pi/\Delta\kappa$ and the time needed by the system to cover this distance is $2\pi/(\sigma - \sigma') = 2\pi/\Delta\sigma$. The velocity of group C is consequently $(\sigma - \sigma')/(\kappa - \kappa') = \Delta\sigma/\Delta\kappa$, or in case there is only a slight difference between the respective values of the denominator and the numerator, $C = d\sigma/d\kappa$. With $\lambda = 2\pi/\kappa$, one obtains with (I.4) $C = d\lambda c/d\lambda$ or $C = c - \lambda(dc/d\lambda)$ (I.11) when c is the wave velocity.

Generally the wave velocity increases with the wave length, and therefore the group velocity is smaller than the wave velocity. Progressive waves at the surface of a water layer of a depth h have a wave velocity of $c = [g/\kappa \tanh \kappa h]^{1/2}$ (see p. 18, equation II.10). The group velocity of a train of such waves will be

$$C = \frac{1}{2} c \left[1 + \frac{2\kappa h}{\sinh 2\kappa h} \right]. \quad (\text{I.12})$$

When the water is deep (short waves), the ratio between the group velocity and the wave velocity is $\frac{1}{2}$; this ratio increases with decreasing water depth, and becomes equal to 1, when the depth is small in proportion to the wave length (long waves). In many natural phenomena dealing with superposed wave trains, the group velocity is undoubtedly of more importance than the velocity of separate waves, which can seldom be observed independently of each other. What shows is the group velocity of the wave train, and in many cases discrepancies between observation and theory are attributable to confusion of the two quantities.

Equation (I.11) is commonly derived from the interference of two wave systems of the same amplitude and of a slightly different wave length; this, however, should not be interpreted to the effect that the group velocity only has any significance in case there are such interferences. According to its intrinsic nature, it is much more general. For general deductions see ROSSBY (1945, p. 187) and MUNK (1947).

Chapter II

Theory of Short and Long Waves

I. Waves with Harmonic Wave Profile. (Stokes' Waves)

THE basic prerequisite for a wave theory is that the motion of the water mass obeys the hydrodynamic equations and the equation of continuity. If this is the case, it only means that this motion is possible, and not whether and under which conditions it occurs. This theory can first be considered from the viewpoint that the motion of the individual water particles is stationary and irrotational, i.e. that the motion can be generated from rest by the action of ordinary forces. Then there exists a velocity potential φ which will satisfy the equation of continuity in the form

$$\frac{\partial^2 \varphi}{\partial x^2} + \frac{\partial^2 \varphi}{\partial z^2} = 0. \quad (\text{II.1})$$

Instead of the three equations of motion, we have the equation of Bernoulli

$$\frac{\partial \varphi}{\partial t} + \frac{c^2}{2} + \frac{p}{\rho} + gz = F(t), \quad (\text{II.2})$$

in which we substitute for the gravity potential gz . Let us consider oscillations of a horizontal sheet of water. We will confine the problem first to cases where the motion is in two dimensions, of which one (x) is horizontal and the other (z) vertical, counted positive upwards; water surface at rest $z = 0$, water depth $z = -h$. The waves then present the appearance of a series of parallel straight ridges and furrows perpendicular to the plane xz . The amplitude of the waves shall be small at first and we will neglect frictional influences.

One of the kinematic boundary conditions to be fulfilled by the motion of the water masses is that at the bottom ($z = -h$) the vertical velocity component $w = \partial \varphi / \partial z$ must disappear; the other boundary condition requires that at the free water surface the normal component of the fluid velocity be equal to the normal component of the surface itself. If ξ and η are the horizontal and vertical displacements of the surface, then with sufficient approximation:
for

$$z = 0: \frac{\partial \eta}{\partial t} = w = \frac{\partial \varphi}{\partial z}. \quad (\text{II.3})$$

In addition to these kinematic boundary conditions there is a dynamic boundary condition to be fulfilled at the free surface, namely that pressure and counter pressure be equal. If we neglect the influence which the atmosphere exerts on the water motion (see p. 83), this condition is simply reduced to the requirements that the pressure at the surface be equal to the uniform air pressure p_0 . If the motion is small, we can neglect in (II.2) the square of the velocity c in a first approximation and, provided the function $F(t)$, and the additive constant p_0/ρ , be supposed merged in the value of $\hat{c}q/\hat{c}t$ we obtain for

$$z = 0: \eta = -\frac{1}{g} \frac{\hat{c}q}{\hat{c}t}. \quad (\text{II.4})$$

The equation (II.1) with the boundary conditions give the possible wave motion in the water mass of the depth h (AIRY, 1845; STOKES, 1880. vol. I, p. 197; LAMB, 1932. p. 227).

If q is a simple-harmonic function of x

$$q = P \cos(\alpha x - \sigma t). \quad (\text{II.5})$$

According to (II.1) P must satisfy the differential equation

$$\frac{d^2 P}{dz^2} - \alpha^2 P = 0,$$

of which the general solution is $P = Ae^{-\alpha z} + Be^{+\alpha z}$. The boundary condition at the bottom $\hat{c}q/\hat{c}z = 0$ for $z = -h$ gives

$$Ae^{-\alpha h} = Be^{+\alpha h} = \frac{1}{2} C$$

and from (II.5) results*:

$$q = C \cosh \alpha(z+h) \cos(\alpha x - \sigma t). \quad (\text{II.6})$$

From the equations (II.3) and (II.4) we obtain $\hat{c}\eta/\hat{c}t$ and η . If we differentiate again with respect to t we get $\hat{c}^2\eta/\hat{c}t^2$. By equating both terms we get the wave frequency in the form:

$$\sigma^2 = g\alpha \tanh \alpha h. \quad (\text{II.7})$$

If we write

$$\eta = A \sin(\alpha x - \sigma t), \quad (\text{II.8})$$

then we obtain for the velocity potential

$$\varphi = \frac{gA}{\sigma} \frac{\cosh \alpha(z+h)}{\cosh \alpha h} \cos(\alpha x - \sigma t). \quad (\text{II.9})$$

The relation (II.8) represents an infinite train of progressive waves with a harmonic wave profile, travelling in the $+\alpha x$ -direction with the velocity

* Hyperbolic functions are used more often and therefore we give here their relationship with the exponential functions:

$$\sinh x = \frac{e^x - e^{-x}}{2}, \quad \cosh x = \frac{e^x + e^{-x}}{2}, \quad \tanh x = \frac{e^x - e^{-x}}{e^x + e^{-x}}, \quad \operatorname{sech} x = \frac{1}{\cosh x}.$$

$$c = \frac{\sigma}{\varkappa} = \sqrt{\left(\frac{g\lambda}{2\pi} \tanh \frac{2\pi h}{\lambda}\right)}. \quad (\text{II. 10})$$

When the wave length is smaller than double the depth ($\lambda < 2h$) we can assume that $\tanh(2\pi h/\lambda) = 1$, and therefore

$$c = \sqrt{g\lambda/2\pi} \quad \text{or} \quad c = gT/2\pi. \quad (\text{II. 11})$$

The velocity is independent of the depth but proportional to the square root of the wave length.

If, on the other hand, the wave length is moderately large compared with h , we have $\tanh(2\pi h/\lambda)$ nearly equal to $(2\pi h/\lambda)$, and we obtain the velocity of long waves (LAGRANGE 1781)

$$c = \sqrt{gh}. \quad (\text{II. 12})$$

It is independent of the wave length and proportional to the square root of the depth.

To determine the orbit of the individual water particles, we can compute with the aid of (II.9) from the velocities u and v the component displacements in the horizontal and vertical directions:

$$\left. \begin{aligned} \underline{x} = x_1 - x_2 &= A \frac{\cosh \varkappa(z+h)}{\sinh \varkappa h} \cos(\varkappa x - \sigma t), \\ \underline{z} = z_1 - z_2 &= A \frac{\sinh \varkappa(z+h)}{\sinh \varkappa h} \sin(\varkappa x - \sigma t). \end{aligned} \right\} \quad (\text{II. 13})$$

This gives for each individual particle an elliptic-harmonic orbit. The horizontal and vertical semi-axes are

$$A \frac{\cosh \varkappa(z+h)}{\sinh \varkappa h} \quad \text{and} \quad A \frac{\sinh \varkappa(z+h)}{\sinh \varkappa h}.$$

Both axes decrease from surface to the bottom ($z = -h$). Only a horizontal movement can exist at the bottom, where the vertical semi-axis vanishes. Figure 8 shows such orbits and the position of small perpendicular water filaments at rest in a shallow water wave ($h/\lambda = 0.2$). For

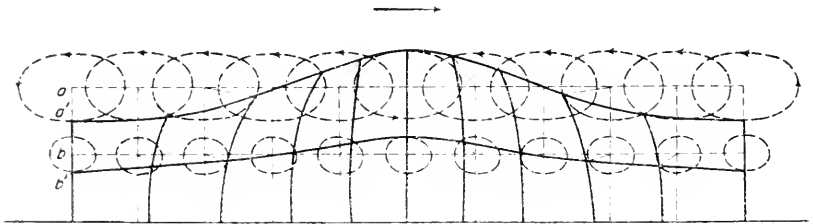


FIG. 8. Orbital motion and positions of water filaments in a progressive wave travelling to the right in shallow water ($h/\lambda = 0.2$).

deep water waves ($h > \lambda$) the quantities η and ξ become $Ae^{\varkappa z}$, and each individual particle describes a circular orbit with a constant angular velocity $\sigma = \sqrt{2\pi g/\lambda}$. The radii of the circle are given by the formula $Ae^{\varkappa z}$ and decrease with depth in a geometrical progression. The velocity of the particles is $2(A\pi/T)e^{\varkappa z}$.

Table 1 and Fig. 9 show, according to Airy, for different values of h/λ listed in the first column, the ratio of the horizontal motion at the bottom to that at the surface listed in the second column and shown in curve one; the third column and curve 2 gives the ratio of the vertical to the horizontal

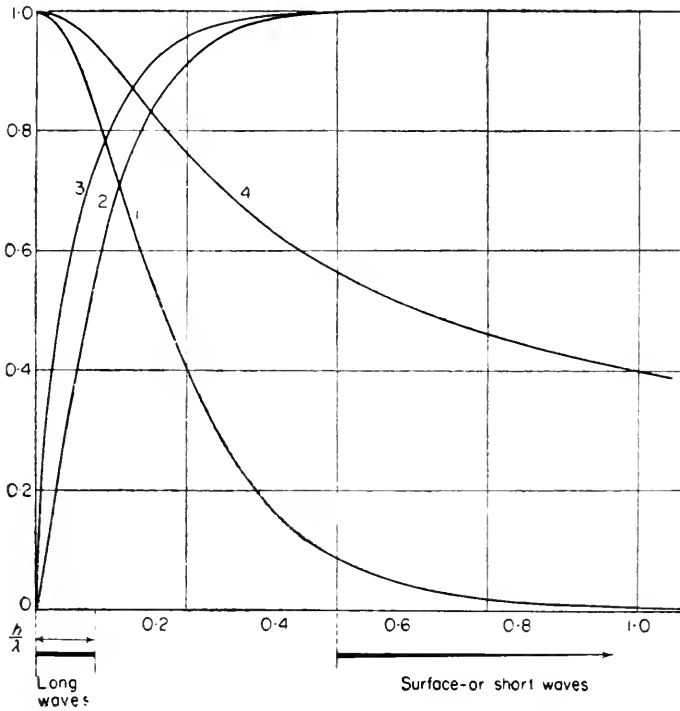


FIG. 9. Relation between orbital motion and velocity of propagation and the ratio h/λ .

- (1) $\text{sech } h$: horizontal motion $\frac{\text{bottom}}{\text{surface}}$, (2) orbit: $\frac{\text{vertical}}{\text{horizontal}}$ diameter at the surface,
 (3) $\frac{\text{velocity of waves}}{\text{velocity of short waves}}$, (4) $\frac{\text{velocity of waves}}{\text{velocity of long waves}}$.

axis of the elliptic orbit of a surface-particle; the fourth and fifth columns (curves 3 and 4) give the ratios of the wave velocity to that of waves of the same length on water of infinite depth, and to that of long waves on water of the actual depth respectively. This presentation shows clearly that deep water waves start with $h = \frac{1}{2}\lambda$, whereas the long waves extend up to a maximum where $h = 0.1\lambda$; the interval between those two belongs to a transition zone with more complicated conditions.

LORD RAYLEIGH (1876) has given another elegant derivation of the wave theory when the disturbance is small compared with the wave length. If waves travel in a certain direction with a velocity c and if we give the water-mass a velocity equal but opposite to the direction of propagation, the motion becomes steady, while the forces acting on the individual particles remain the same. PRANDTL (1942) uses this method in a brief derivation of the velocity of propagation of surface or short waves. A "reference system" travelling with the waves has a horizontal velocity in the wave crest $u_1 = c - 2\pi r/T$, r being the radius of the orbit and T the time of a revolution (period of the waves). Then $2\pi r/T$ is the velocity on the circular orbit. The horizontal velocity in the wave

trough is $u_2 = c + 2\pi r/T$. The wave height is $h = 2r$, so that according to the equation of Bernoulli for steady currents

$$u_2^2 - u_1^2 = 2gh = 4gr,$$

on account of the equality of pressure. With these values for u_1 and u_2 the left side of the equation becomes $8\pi cr/T$, and $c = gT/2\pi$, which corresponds to (II.11).

Table 1. Characteristic values of surface waves

Depth wave length $h : \lambda$	Ratio:	Ratio:	Ratio: water velocity	
	Horizontal motion bottom/horizontal motion surface ($\operatorname{sech}^2 zh$)	Vertical axis/horizontal axis of elliptic orbit of surface particles ($\tanh^2 zh$)	to wave velocity deep water waves of same length $c : \sqrt{(g/\lambda)}$	to wave velocity shallow water waves of same length $c : \sqrt{(gh)}$
0.00	1.000	0.000	0.000	1.000
0.01	0.998	0.063	0.250	0.999
0.02	0.992	0.125	0.354	0.997
0.03	0.983	0.286	0.432	0.994
0.04	0.969	0.246	0.496	0.990
0.05	0.953	0.304	0.552	0.984
0.06	0.933	0.360	0.600	0.977
0.07	0.911	0.413	0.643	0.970
0.08	0.886	0.464	0.681	0.961
0.09	0.859	0.512	0.715	0.951
0.10	0.831	0.557	0.746	0.941
0.20	0.527	0.850	0.922	0.823
0.30	0.297	0.955	0.977	0.712
0.40	0.161	0.987	0.993	0.627
0.50	0.086	0.996	0.998	0.563
0.60	0.046	0.999	0.999	0.515
0.70	0.025	1.000	1.000	0.477
0.80	0.013	1.000	1.000	0.446
0.90	0.007	1.000	1.000	0.421
1.00	0.004	1.000	1.000	0.399
∞	0.000	1.000	1.000	0.000

The streamlines of the wave motion in surface waves, relative to a reference system at rest, are shown in Fig. 10. The broken-line circles represent the orbits for individual particles. It can be seen how rapidly the dimensions of these orbits decrease with increasing depth (see vol. I, pt. 2.). In a depth of one wave length the radius is reduced to $Ae^{-2\pi}$, i. e. approximately the one five-hundredth of its size at the surface.

The energy of a wave system of progressive waves can easily be calculated. A narrow strip of unit width and of unit length dx , parallel to the direction of propagation, with a vertical elevation at the surface η according to (II.8), has a potential energy $\frac{1}{2}g\eta^2 dx$. In the unit area the potential energy amounts to

$$P = \frac{1}{2} g \rho A^2 \sin^2(\kappa x - \sigma t)$$

and for one wave length $P = \frac{1}{4} g \rho A^2 \lambda$.

A water particle has in its orbit an angular velocity $A e^{\kappa z} 2\pi/T$ and the kinetic energy of a volume element $dx dz$ is represented by

$$\frac{\rho}{2} \frac{4\pi^2}{T^2} A^2 e^{2\kappa z} dx dz.$$

In order to obtain the energy for the whole water column, this expression must be integrated for dz from $-\infty$ to 0. Considering (II.11), the kinetic energy per unit area will be $K = \frac{1}{4} g \rho A^2$ that per wave length $\frac{1}{4} g \rho A^2 \lambda$. Consequently, at any time the total energy per unit area in the case of a progressive wave will be

$$E = \frac{1}{2} g \rho A^2. \tag{II.14}$$

The energy at any instant is always half potential, and half kinetic. The energy of a progressive wave system of amplitude A , therefore, is equal to the work required to raise up a waterlayer of thickness A through a height $\frac{1}{2}A$. One has to remember that, in considering a part of the ocean surface, its

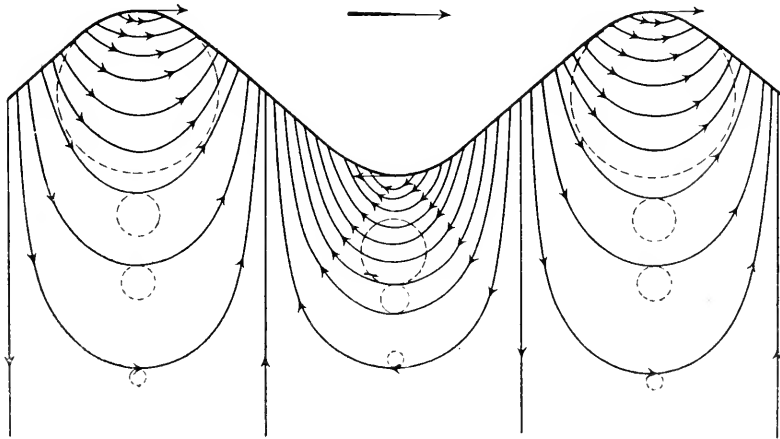


FIG. 10. Streamlines and orbits in a short wave travelling to the right.

wave energy depends not only on the wave height, but also on the wave length. The long waves being mostly at the same time the highest ones, have more energy than short waves.

In each progressive wave there is a transport of energy in the direction of propagation of the wave. If v is the velocity of this energy transport, then vE is the amount of energy propagated across vertical planes which are a unit width apart; for surface waves, according to LAMB (1932, p. 383), this is

$$vE = \frac{1}{2} g \rho A^2 c \sin^2 \kappa(x - ct). \tag{II.14a}$$

The mean value for a wave length is

$$vE = \frac{1}{4} \rho g A c^2 = \frac{1}{2} E c. \quad (\text{II.14b})$$

This equation can therefore be interpreted that either the entire energy is propagated at half the wave velocity or half the energy at full wave velocity. The latter interpretation appears to be the better one, because, according to the above expression for P , $vE = cP$, which means that the potential energy is transmitted with the wave velocity. To satisfy (II.14), $P = \frac{1}{2} E$. It should be observed that the potential energy is a periodical function, which advances in phase with the deformation of the surface, whereas the kinetic energy is evenly distributed along the entire wave and is independent of the position or the velocity (SVERDRUP and MUNK, 1947) with which the surface deformation advances. See Fig. 11.

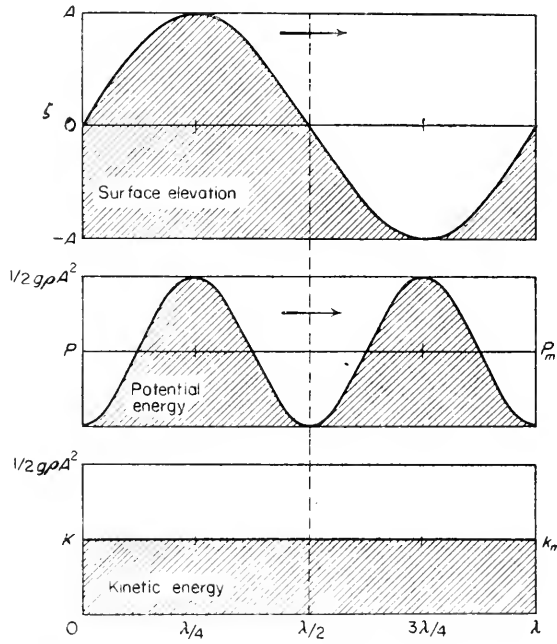


FIG. 11. Variation of the potential and kinetic energy along a wave length of a progressive wave over a great depth.

2. Further Development of the Stokes Wave Theory

The wave theory developed so far has as a condition that the wave height must be small compared to the wave length. The profile of the wave was a simple-harmonic. This condition is fulfilled at the beginning of the development of a wave. But with the increase of the wave amplitude this restriction should be abandoned. The determination of the wave-forms which satisfy the conditions of uniform propagation without change of type, when

this restriction is abandoned, forms the subject of a classical research by STOKES (1847).

Stokes developed his theory by using Rayleigh's method by superposing a wave disturbance upon a steady current.

If in the case of infinite depth, neglecting small quantities of the order A^3/λ^3 , a stationary wave disturbance of the wave length λ is superimposed on a steady motion with the velocity c the velocity potential φ and the stream function ψ will be:

$$\left. \begin{aligned} \frac{\varphi}{c} &= -x + Ae^{\kappa z} \sin \kappa x, \\ \frac{\psi}{c} &= -z + Ae^{\kappa z} \cos \kappa x. \end{aligned} \right\} \quad (\text{II. 15})$$

The equation of the wave profile of the disturbed surface $\psi = 0$ is found by successive approximations from z

$$\begin{aligned} z &= Ae^{\kappa z} \cos \kappa x = A(1 + \kappa z + \frac{1}{2}\kappa^2 z^2 + \dots) \cos \kappa x \\ &= \frac{1}{2}\kappa A^2 + A(1 + \frac{3}{8}\kappa^2 A^2) \cos \kappa x + \frac{1}{2}\kappa A^2 \cos 2\kappa x + \frac{3}{8}\kappa^2 A^3 \cos 3\kappa x + \dots \end{aligned}$$

if

$$A(1 + \frac{3}{8}\kappa^2 A^2) = a$$

we obtain

$$\eta = \frac{1}{2}\kappa a^2 + a \cos \kappa x + \frac{1}{2}\kappa a^2 \cos 2\kappa x + \frac{3}{8}\kappa^2 a^3 \cos 3\kappa x + \dots \quad (\text{II. 16})$$

With increasing amplitude the wave profile differs more and more from the simple-harmonic type. The wave crests become narrower and steeper, wave troughs wider and flatter. The wave profile as expressed in equation (II.16) corresponds to the equation of a trochoid, in which the circumference of the rolling circle is $2\pi/\kappa = \lambda$ and the length of the arm of the tracing point is a . So far his profile corresponds to that of the Gerstner waves (see p. 26). The ratio of $2a/\lambda = \frac{1}{10}$ represents already a high value (see p. 48) and, neglecting the terms of 3rd order in κa we omit in (II.16) a value less than one thirtieth of the wave height.

BURNSIDE (1916) raised the question as to the convergence, both of the series which form the coefficients of the successive cosines when the approximation is continued and of the resulting series of cosines. He even doubted the possibility of waves of rigorously permanent type. LEVI-CIVITA (1925, p. 264; GEPPERT, 1929, p. 424) has proved the convergence and the existence of waves of a permanent type in agreement with hydrodynamic principles. The wave profile of a permanent wave as calculated by Levi-Civita differs very little from the profile computed by Stokes and Gerstner (trochoids), and for small amplitudes there is practically no difference. With increasing amplitude there is a gradual transition of the wave profile from the harmonic type to the trochoidal form, and a further increase of the wave height will change the profile again. If the trochoidal form were exact instead of being

merely approximate, the extreme form would have cusps at the crests, as in the case of Gerstner waves (Fig. 15). This, however, is not the case. STOKES and MITCHELL (1893, p. 430) have shown that the extreme form has angles of 120° , similar to a roofline. The ratio between the height and the length of this steepest wave form was 0.142 or approximately 1:7, and its velocity of propagation was 1.2 times greater than for waves with infinitely small heights.

THORADE (1931, p. 31) explains this striking result as follows. Figure 12 shows a small part of a wave in the vicinity of the crest, where the water surface can be adequately represented by two planes AB and $A'B'$; He adds the negative velocity $-c$ according to the method of Rayleigh, and he obtains a steady current towards the left, which is bounded by the crest acting as a solid wall;

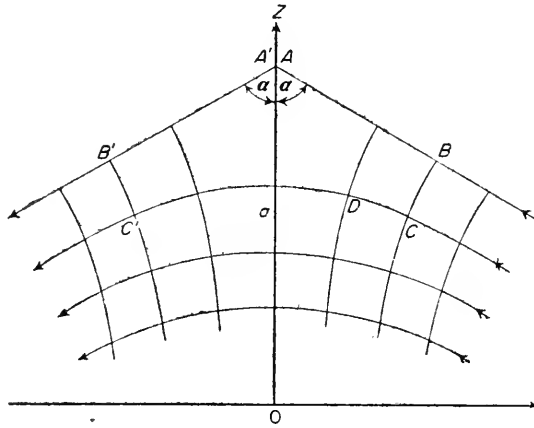


FIG. 12 Streamlines and equipotential lines in the crest of the highest possible Stokes's wave.

The stream lines then follow the deathered lines CC' ; the system of lines CB , $C'B'$ perpendicular to CC' represent equipotential curves, whose successive distance is inversely proportional to the velocity. If one knows the angle 2α formed by two rigid walls, and provided that in greater depth the stream lines are horizontal, then both systems of lines are completely determined, as shown in LAMB (1932, § 63, p. 68). On account of the continuity of the current, the velocity in A must be zero; it decreases in approaching A and increases again afterwards. Below A the horizontal component increases, until it reaches $-c$ when the stream lines are horizontal, but in the crest of each stream line the vertical component is always zero. The condition of continuity and the condition of irrotational motion determine the entire field of streamlines. In this case an additional condition is that the surface BAB' is a free surface, and the fixed walls can therefore be removed without changing the motion. This condition fixes the angle 2α . Calculation gives for the value of $\alpha = 60^\circ$.

The equation of continuity in the present case is $\partial u/\partial x + \partial w/\partial z = 0$, the condition of irrotational motion $\partial w/\partial x - \partial u/\partial z = 0$. We introduce instead of rectangular co-ordinates (x, z) polar co-ordinates (r, ϑ) with their centre in A (Fig. 13). Then $x = r \sin \vartheta$ and $z = a - r \cos \vartheta$, and the transformation of co-ordinates gives for both conditions the equations:

$$\frac{\partial u}{\partial r} \sin \vartheta - \frac{\partial w}{\partial r} \cos \vartheta + \frac{\partial u}{r \partial \vartheta} \cos \vartheta + \frac{\partial w}{r \partial \vartheta} \sin \vartheta = 0,$$

$$\frac{\partial u}{\partial r} \cos \vartheta + \frac{\partial w}{\partial r} \sin \vartheta - \frac{\partial u}{r \partial \vartheta} \sin \vartheta + \frac{\partial w}{r \partial \vartheta} \cos \vartheta = 0.$$

This gives the two equations:

$$\partial u/\partial r + \partial w/r\partial\theta = 0 \quad \text{and} \quad c w\partial r - \partial u/r\partial\theta = 0.$$

The wave profile in the vicinity of A is given by $\eta = a - r\cos\alpha$.
Bernoulli's theorem has the form of

$$\frac{p}{\rho} + \frac{1}{2} q^2 + g(a - r\cos\alpha) = \text{constant},$$

if the total velocity along BA is q .

This requires that, with p constant (free surface)

$$q^2 = 2gr\cos\alpha.$$

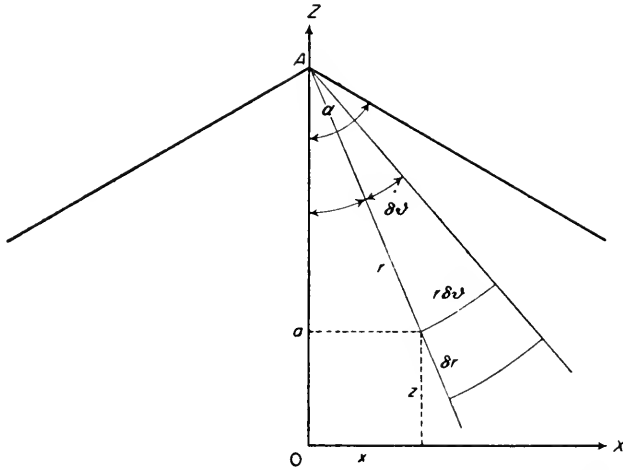


FIG. 13. Transformation from rectangular into polar co-ordinates.

In the vicinity of A, therefore, q must be proportional to \sqrt{r} or $u = C\sqrt{r}f(\theta)$ and $w = C\sqrt{r}g(\theta)$. With the previous equations, we then obtain $\frac{1}{2}f'(\theta) + g'(\theta) = 0$ and $\frac{1}{2}g(\theta) - f'(\theta) = 0$, which leads to the differential equation $4g''(\theta) + g(\theta) = 0$, with the solution $\theta = A\cos\frac{1}{2}\theta + B\sin\frac{1}{2}\theta$. With $\theta = 0$, $w = 0$ and we obtain $u = -C\sqrt{r}\cos\frac{1}{2}\theta$ and $w = +C\sqrt{r}\sin\frac{1}{2}\theta$. In each point (r, θ) the current vector forms with the $-x$ -axis the angle $\frac{1}{2}\theta$. This also applies to the surface, where $\theta = \alpha$, for which $\alpha + \frac{1}{2}\alpha = 90^\circ$, or $\alpha = 60^\circ$.

A simpler derivation of this condition can be obtained starting with the stream function according to LAMB (1932, § 63 (3), p. 69). If the stream function in polar co-ordinates (r, θ) has the form $\psi = Cr^n \cos n\theta$ with the condition that $\psi = 0$ when $\theta = \pm\alpha$, this will lead to $n\alpha = \frac{1}{2}\pi$. From this we obtain $q = nCr^{n-1}$, where q is the resultant fluid-velocity. But since the velocity vanishes at the crest, its value at a neighboring point of the free surface will be given by $q^2 = 2gr \cos \alpha$. Comparing q and q^2 , we see that $n = \frac{3}{2}$ and therefore $\alpha = \frac{1}{3}\pi = 60^\circ$.

The condition of uniform pressure at the free surface along the entire wave profile ($\psi = 0$) here again leads to a relation between wave velocity and wave length. The total velocity is obtained from u and w from (II.15), and the square will be $c^2 + A^2 e^{2xz} - 2A c e^{xz} \cos \alpha x$. Therefore Bernoulli's theorem gives for the free surface

$$\frac{p_0}{\rho} + \frac{c^2}{2} + \frac{1}{2} A^2 e^{2xz} - c A e^{xz} \cos \alpha x + g\eta = \text{const.}$$

If we develop the e -functions in series and substitute (II.16) for η , we obtain

$$c = \sqrt{\left[\frac{g\lambda}{2\pi} \left(1 + 4\pi^2 \frac{a^2}{\lambda^2} \right) \right]}. \quad (\text{II.17})$$

The velocity of progressive waves with a wave profile not changing its type slightly increases with the relative wave height, i.e. with the steepness of the waves; however, the discrepancy with the simple formula is not great, as a/λ appears only in the second order. The somewhat more exact value derived by Levi-Civita also corresponds with the first terms of (II.17).

The Stokes waves of the permanent type show the characteristic that they possess relatively to the undisturbed surface a certain momentum in the direction of wave propagation. The individual particles in these progressive waves of permanent type do not have closed orbits, but they show a slow but constant advance in the direction of the wave propagation. This is explained by the fact that, in the case of rather large wave heights, a particle which moves in the wave crest at the surface to the right has a smaller velocity in the wave trough in the opposite direction and that it does not come back to its initial position below the former wave crest. The particle, in this way, does not cover circles but loops. According to Stokes, the velocity of this current in a depth z is

$$u' = \kappa^2 a^2 c e^{-2\kappa z} = \pi^2 \delta^2 c e^{(-4\pi z)/\lambda}$$

when δ is the ratio of the wave amplitude $2a = H$ to the wave length λ (δ is called the wave steepness). The velocity of the current decreases rapidly with increasing depth. Rayleigh (THORADE, 1931, p. 31) showed that, in an irrotational wave motion there always must be a water transport, which is also valid for other waves; LEVI-CIVITA (1922, p. 85) has given the theoretical proof of this statement. The mean velocity Q is given by the equation $Q = \frac{1}{2}(a/h)^2 gh/c$. If $a = 10$ cm, $h = 500$ cm and $c = 50$ cm/sec, we obtain for $Q = 2$ cm/sec; compared with c , this is a small amount, which should not be neglected generally.

3. Gerstner's Rotational Waves

In 1802, GERSTNER developed a wave theory which gives an exact solution of the hydrodynamical equations for waves over infinite depth. The exact equations, according to Gerstner, express a possible form of wave motion. Contrary to the Stokes waves, the motion in this fluid is rotational. The vorticity is greatest at the surface and diminishes rapidly with depth. The sense of the vorticity is opposite to that of the revolution of the individual particles in their circular orbits and, therefore, unfavourable for the generation of such waves, because it is impossible to originate these waves by the action of ordinary forces on the surface at rest.

The derivation of the equations is facilitated by using the Lagrangian

equations of continuity motion (see vol. I). If the x -axis is horizontal in the free surface at rest and if the positive z -axis is vertical downwards, and $\rho = 1$, we have

$$\left. \begin{aligned} \frac{d^2x}{dt^2} \frac{\partial x}{\partial a} + \left(\frac{d^2z}{dt^2} - g \right) \frac{\partial z}{\partial a} + \frac{\partial p}{\partial a} &= 0, \\ \frac{d^2x}{dt^2} \frac{\partial x}{\partial \gamma} + \left(\frac{d^2z}{dt^2} - g \right) \frac{\partial z}{\partial \gamma} + \frac{\partial p}{\partial \gamma} &= 0, \\ D = \frac{\partial x}{\partial a} \frac{\partial z}{\partial \gamma} - \frac{\partial x}{\partial \gamma} \frac{\partial z}{\partial a}, \quad \frac{dD}{dt} &= 0. \end{aligned} \right\} \quad (II.18)$$

a and γ are the co-ordinates of this particle at rest at true t . Figure 14 shows that in general

$$x = a + r \sin \theta, \quad z = \gamma + r \cos \theta,$$

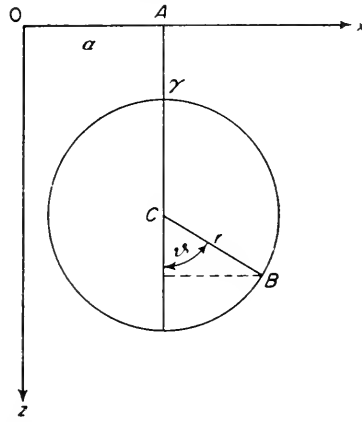


FIG. 14. Orbit of a water particle B (a and γ are the co-ordinates of its centre).

and if $\theta = (\kappa x - \sigma t)$, the path of any particle will be a circle with a radius r , which can be a function of the depth γ . After a time $T = 2\pi/\sigma$ and at a distance $\lambda = 2\pi/\kappa$, this circular motion is repeated. If such a motion is possible, then the equations (II.18) must be satisfied. The expression for D gives

$$D = 1 + \kappa r \frac{\partial r}{\partial \gamma} + \left(\frac{\partial r}{\partial \gamma} + \kappa r \right) \cos \theta.$$

As D should be independent of t ,

$$\frac{\partial r}{\partial \gamma} = -\kappa r, \quad r = A e^{-\kappa \gamma}. \quad (II.19)$$

The radii of the circular orbits decrease with depth with an e -power. As $e^{2\pi/g} = 2.01$, we have the simple rule established by Rankine, according to which, with each increase of depth of one-ninth of the wave length, the amplitude is reduced to half of the previous amount. Accordingly,

$$D = 1 + \kappa r \frac{\partial r}{\partial \gamma} = 1 - \kappa^2 r^2 = 1 - \kappa^2 A^2 e^{-2\kappa \gamma}. \quad (\text{II.20})$$

The two equations (II.18) further give

$$\frac{\partial p}{\partial a} = (\sigma^2 - \kappa g) r \sin \vartheta \quad \text{and} \quad \frac{\partial p}{\partial \gamma} = (\sigma^2 - \kappa g) r \cos \vartheta + g - \sigma^2 \kappa r^2.$$

The boundary condition of uniform pressure at the free surface requires that $\sigma^2 - \kappa g = 0$. This is identical with the equation (II.7) for water of infinite depth, which means that the velocity of propagation of the Gerstner waves is also

$$c = \mathbf{J} (g\lambda/2\pi).$$

The equations for pressure are then reduced to

$$\partial p / \partial a = 0 \quad \text{and} \quad \partial p / \partial \gamma = g(1 - \kappa^2 r^2).$$

Consequently, when $\gamma = 0$, i.e. for the free surface, the pressure p_0 must be equal to the atmospheric pressure:

$$p = p_0 + g \left[\gamma - \frac{\kappa}{2} A^2 (1 - e^{2\kappa \gamma}) \right]. \quad (\text{II.21})$$

The constant A , which is the wave amplitude, can only increase to such an extent that D in (II.20) does not vanish or becomes negative. As γ varies between 0 and ∞ , this requires that

$$A^2 \leq \frac{1}{\kappa^2} = \left(\frac{\lambda}{2\pi} \right)^2. \quad (\text{II.22})$$

As long as $A < \lambda/2\pi$, the equation of the surface is at any time a trochoid; when the amplitude becomes equal to $\lambda/2\pi$, we have the extreme case with acute angles at the crest (cycloid). If $A > \lambda/2\pi$, we have a curve with loops, which is impossible for steady motion. This is in agreement with (II.22). Figure 15 shows in thin, solid circles the orbits of the water particles and

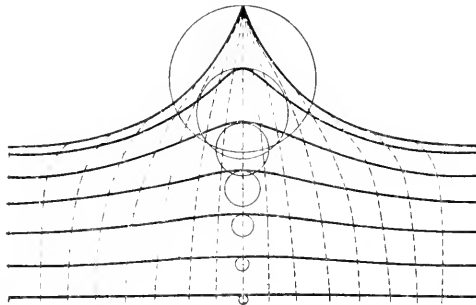


FIG. 15. Profile of a Gerstner wave: trochoid. Thin circles: orbits of the particles; dotted curves: position of line of particles during passage of a wave.

the decrease of the orbits with increasing depth: the dotted lines represent the successive places of filament of particles which are vertical when they pass through a crest or a trough. The solid drawn lines are the possible wave profiles, which are trochoids, and their extreme form is a cycloid.

Stokes has already proven that a system of waves of the Gerstner type in an ideal fluid cannot be originated from rest. It can be supposed that by properly adjusted pressures applied to the surface of the waves the surface takes the shape of Gerstner waves. According to Stokes, we require as a generating condition an initial horizontal motion in the direction opposite to that of the propagation of the waves ultimately set up. A wind blowing over a water surface tends to provoke a steady horizontal current in the direction of the waves. Therefore, this is an unfavourable condition for producing Gerstner waves.

4. Short-Crested Waves

The previous theoretical investigations assume infinitely long wave crests which advance perpendicularly to the direction of progress of the wave. The surface should look like a sheet of corrugated iron. In reality, however, the ocean surface looks like crepe paper. JEFFREYS (1925, 1926) has given the theory for these short-crested waves. We can represent this wave by

$$\eta = A \cos(\sigma t - \kappa x) \cos \kappa' y, \tag{II.23}$$

in which the wave advances in the $+x$ -direction with a wave length $\lambda = 2\pi/\kappa$, the length of the crest being $\lambda' = 2\pi/\kappa'$. Figure 16 shows, according to Thorade,

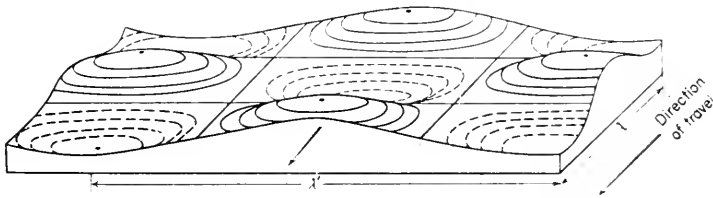


FIG. 16. Three-dimensional wave motion ($\lambda' = 7\lambda$). (By Thorade.)

a topographical map of the surface for $\lambda' = 7\lambda$. This presentation is still too regular compared to the actual mixed-up waves as they occur in nature, but there is already a difference with the waves discussed earlier. If x and y are the axes in the horizontal direction and z is positive upwards, we can express the velocity potential by

$$\phi = -\frac{\sigma}{r} A e^{r z} \sin(\sigma t - \kappa x) \cos \kappa' y, \tag{II.24}$$

in which $r^2 = \kappa^2 - \kappa'^2$. The amplitude has been selected in such a way that the conditions for the continuity and irrotationality are satisfied. We can deduct

from (II.24) the velocity components u , v , w , and the co-ordinates of a particle referred to the centre of its orbit.

This gives:

$$\left. \begin{aligned} \xi &= \frac{\kappa}{r} A e^{r z} \sin(\sigma t - \kappa x) \cos \kappa' y, \\ \xi' &= -\frac{\kappa'}{r} A e^{r z} \cos(\sigma t - \kappa x) \sin \kappa' y, \\ \eta &= A e^{r z} \cos(\sigma t - \kappa x) \cos \kappa' y. \end{aligned} \right\} \quad (\text{II.25})$$

If we use again Rayleigh's method by adding a wave velocity $-c$, we transform the wave motion into a steady motion, and the square of the total velocity of a particle $(u-c)^2 + v^2 + w^2 = c^2 - 2uc$ if we neglect $u^2 + v^2 + w^2$ against c^2 . Bernoulli's theorem then is

$$\frac{p_0}{\rho} + g\eta + \frac{1}{2}(c^2 - 2uc) = \text{const};$$

which is only possible when $g = c\kappa\sigma/r$. If $\sigma/\kappa = c$, we obtain

$$c = \sqrt{\left[\frac{g\lambda}{2\pi} \right] \left(1 + \frac{\lambda^2}{\lambda'^2} \right)} \quad (\text{II.26})$$

The velocity of propagation increases when the crests become shorter. We can deduct from (II.25) that the orbits are no longer circular, but elliptical, and the plane of the ellipse is parallel to the direction of propagation (x -axis), but it forms an angle a with the vertical plane xz . This angle a is given by $\tan a = \kappa'/r \tan \kappa'/y$. These planes, therefore, are only vertical in the troughs and in the crests; elsewhere they are inclined, and the vertical axis is larger than the horizontal. The ellipses are standing up, which might seem strange. It has not been possible to find out if such waves really exist. Another strange fact is that the energy of such three-dimensional waves per unit area is smaller than for a similar two-dimensional wave.

When $t = 0$, we have according to equation (II.23) $\eta = A \cos \kappa x \cos \kappa' y$. The potential energy of a wave crest can be computed by integrating $\frac{1}{2} g \rho \eta^2 dx dy$ from $-\frac{1}{4}\lambda$ to $+\frac{1}{4}\lambda$ and from $-\frac{1}{4}\lambda'$ to $+\frac{1}{4}\lambda'$ and by dividing afterwards by the area $\frac{1}{4}\lambda\lambda'$. We then obtain $E_p = \frac{1}{8} g \rho A^2$. The kinetic energy is calculated by integrating $\frac{1}{2} \rho q^2 dx dy dz$, in which q is the total velocity. The limits of the integration are the same as previously, and the additional limits are $z = 0$ to $z = -\infty$. After dividing by $\frac{1}{4}\lambda\lambda'$, we obtain $E_k = \frac{1}{8} g \rho A^2$.

Per unit area we find again that the energy is half potential and half kinetic and that the total energy is $\frac{1}{4} g \rho A^2$, which is only half that of a two-dimensional wave system of smaller amplitude (equation II.14).

Chapter III

Observations and Measurements of Ocean Waves

1. Testing of the Theory by Laboratory Experiments

THE first attempts to check experimentally the theoretical results of the wave theory date back as far as LEONARDO DA VINCI (1452–1519), who always endeavoured to support his views by experiments. The first systematical experiments in wave tanks were made by the WEBER brothers (1825). However, the wave tanks used by them were not large enough and too narrow to avoid disturbances at the ends. The results were also influenced by friction at the side walls. Later on, SCOTT RUSSELL (1845, p. 311) undertook measurements under more favourable circumstances; he was principally concerned with a kind of waves different from the wind waves of the oceans (waves of translation) (see p. 116). Later on the theories by Stokes, Airy and others have been tested in hydraulic dynamic laboratories which were better equipped. But the depths in wave tanks are generally small in proportion to the generated wave lengths, and the term “surface waves” can only be used with certain reservations. At the bottom of the tank the water particles are still in motion, and the friction at the bottom is liable to retard the propagation of the waves. Recent experiments with long and relatively deep tanks are significant and important, as they permit a survey of the principles on which the whole wave theory is built.

We shall discuss the experimental tests made during 1938 and 1939 by MITCHIM in the hydraulic laboratory of the University of California (1940). The tank had the shape of a canal with a length of slightly over 18 m, a depth of 92 cm and a width of 30 cm. Through glass walls one could observe and photograph waves travelling through the canal. He made 28 series of observations on waves with a constant wave length varying between approximately $\frac{1}{2}$ and $1\frac{1}{2}$ m. Such waves can still be considered as surface waves in proportion to the depth h because h/λ did not become smaller than 0.5; according to Table 1 and Fig. 9, however, this is the lower limit for such waves. We will show in diagrams the main results of the extensive observations. Figure 17 shows for each series the relation between the velocity of propagation and the wave length and the solid line corresponds to the theoretical

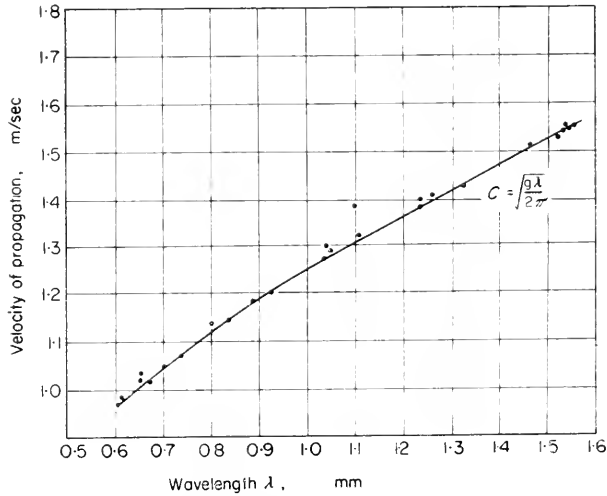


FIG. 17. Relationship between wave velocity and wave length according to experiments in a wave tank.

relation $c = \sqrt{g\lambda/2\pi}$. This equation satisfies very well the observations. Deviations average 0.39%. Figure 18 shows the results of the evaluation of photographs of orbits of floating particles. These orbits were circles every-

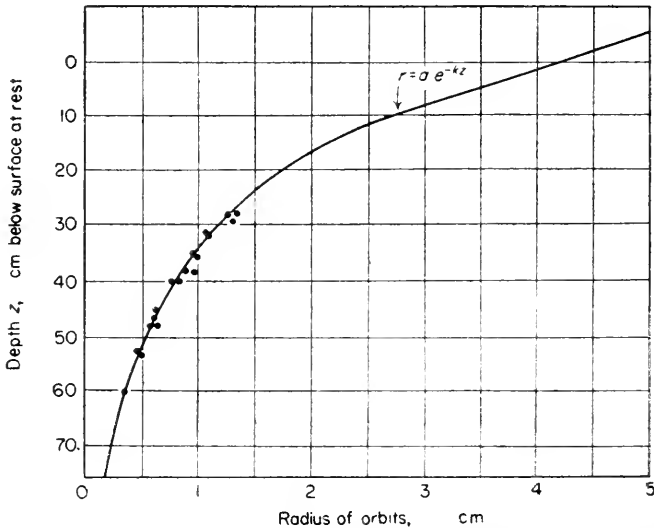


FIG. 18. Relationship between radii of orbits and depth according to experiments in a wave tank.

where, and the decrease of their radii, with increasing depth corresponds exactly to the theory, as shown by the figure. Figure 19 shows the velocity of water transport connected with wave motion in the direction of propagation of the wave, according to the text on page 26.

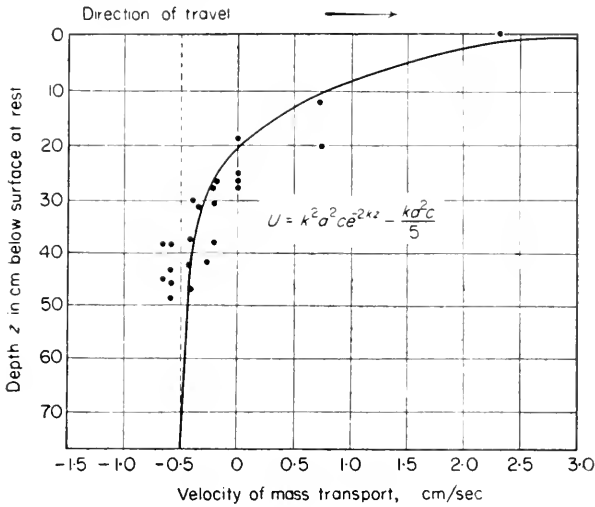


FIG. 19. Relationship between velocity of water transport and depth when depth of water is 75 cm (wave tank experiments).

Considering the difficulty in determining this velocity, we can say that there is a satisfactory agreement between the theory and observations. But this agreement does not necessarily apply to large waves generated by the wind upon the ocean surface in respect to their length, period and velocity. We have to consider, in addition, that the height of the wave and the length of the crest are important factors not to be neglected in ocean waves.

2. Observation and Measurement of Ocean Waves

It is relatively simple to observe ocean waves from aboard a ship. Such observations are almost without any exceptions limited to the determination of the velocity c , the wave length λ and the period T . In most cases, these observations are based on evaluation or on measuring by means of simple instruments and, consequently, they are subject to numerous sources of errors. This is particularly true for the determination of the wave height. Only recently stereophotogrammetric observations of waves, and especially of wave profiles, have given reliable observations. The results of this new method will be discussed in a subsequent chapter, and we will first deal with direct visual observations.

Amongst the numerous scientific observations of ocean waves, which were gathered in a systematic manner during oceanographical expeditions, those made by Cornish deserve special attention. Another comprehensive study of waves was given by LARISCH-MÖNICH (1925) in a monograph titled *Sturmsee und Brandung*. His method of work is wave photography. By means of excellent photographic pictures, giving all kinds of phases in wave development, he has attempted to explain the complex mechanism of wave

motion and the various relations between it and the generating force of the wind. We wish to call special attention to this valuable collection of wave photographs.

Waves, in the open ocean, are generated by winds which change their direction very often and suddenly, especially outside the region of the trade winds. Therefore, simple uniform wave systems over large areas cannot be expected. These wave systems, with their great velocity of propagation, travel great distances from their source. These waves, which were not generated in the area under observation by the wind prevailing at that particular moment, but are coming from great distances, are called swell. They are not subjected any longer to the direct influence of the wind and can, therefore, be considered as free waves. By their roundish, and long-streched profile, which they maintain despite their length and height, they look different from the real wind waves. These wind waves, under the direct influence of the wind, have considerably shorter wave lengths and shorter crests, which break very easily; their profile is unsymmetrical and steeper on the front than at the rear side.

Long and high swells from the region of the trade winds of the two hemispheres travel into the equatorial zones of calm, and occasionally intersect here (cross sea). No less typical are the high and long swells, which are almost permanently present in the calm area of the *Hors* latitudes, in the polar border regions of the trade winds of both hemispheres. North-west storms (in the Northern Hemisphere) which originate in the rear of atmospheric low-pressure regions whip wind waves into mighty seas which gradually move out from their source of origin. Eventually, they travel as far as the north-east trade wind region and sometimes even into the Southern Hemisphere. It is not difficult for an observer aboard a ship, especially if he has some experience, to distinguish between "sea" and "swell". When the sea is rough, one wave system will generally surpass the others by its dimensions and thus strike the eye; frequently they have a different direction of propagation, so that, by observing them carefully, they are easily distinguishable.

In principle, it is not difficult to observe the period, velocity and length of ocean waves. In case of a ship anchored in the direction of propagation of the waves, the period of the waves can be determined by means of a stop-watch, checking the times at which the consecutive wave crests pass the point of observation; or one observes the passage of n waves. If the time required for this was t_1 , the wave period is $T = t_1/n$. The wave velocity is obtained from the time required by the wave crest to cover the distance from the bow to the stern of the ship. If this time is t_2 and the length of the ship l , the velocity c will be l/t_2 . From c and T , the wave length can be calculated from $\lambda = cT$. If the waves are shorter than the ship ($\lambda < l$), their length can be marked out on the ship hull and measured (preferably by two observers).

If the ship is moving, it is necessary to know and to take into account

the course, direction and speed of the ship. The preceding formulae undergo a change if the ship and the waves travel in the same or opposite direction, then the speed of the ship has simply to be subtracted or added respectively algebraically to the wave velocity. If the speed of the ship is V , the wave velocity and the wave length will be, respectively

$$c = (l/t_2) \pm V \quad \text{or} \quad \lambda = t_2(c \pm V).$$

If the course of the ship is not perpendicular to the wave crests, but makes an angle α , the above formula only gives the apparent wave velocity. In order to obtain the real one, it must be multiplied by $\cos \alpha$; the angle here must be smaller than 45° , else the result is not sufficiently accurate.

It is more difficult to determine the wave period when the ship is travelling. An observer located in A (see Fig. 20) observes in t_1 sec the passage of n waves

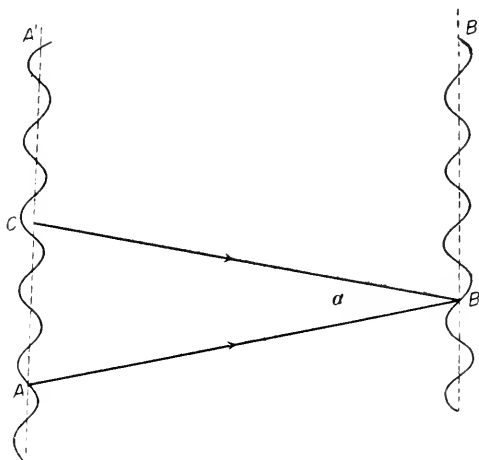


FIG. 20. Determination of wave period and wave velocity.

(apparent period = t_1/n). For this observer AA' would be the last wave front counted by him. For an observer who shifted from A to B , BB' is the last one, as he did not count the waves on the stretch CB . Therefore, we have to add to the n waves, CB/λ waves. As $CB = Vt_1 \cos \alpha$, the period will be

$$T = t_1 : \left(n + \frac{Vt_1 \cos \alpha}{\lambda} \right) = \frac{t_1}{\lambda} : (n\lambda + Vt_1 \cos \alpha).$$

It is easy to establish that the wave length $\lambda = cT$ will then be $\lambda = \left(\frac{l}{t_2} \frac{t_1}{n} \right) \cos \alpha$, i.e. the wave length is found from the apparent wave velocity multiplied by the apparent period and by the cosine of the angle between the course of the ship and the direction of the waves (THORADE, 1931, p. 24).

The wave length can also be measured directly by throwing out a log board or a small buoy and letting the marked rope unwind long enough

for the log and the buoy, respectively, to line up with the stern of the ship simultaneously on a wave crest. On account of the sag of the cord there is a considerable error by obtaining too great wave lengths.

It is much more difficult to measure correctly the wave height. If the waves are of considerable height, so that the horizon is concealed by them from the observer when the ship is in a wave trough, he can climb up high enough in the shrouds in the middle of the ship to see the crest of the approaching wave line up with the horizon and thus determine the wave height. In using this visual method, attention should be paid to the fact that, at the time of the observation, the ship must lie entirely on a flat keel in the wave trough, otherwise the observation would be worthless. In a similar way, WILKES (1845, p. 135) determined the height of the ocean waves, looking from the shrouds of a ship in a wave trough across two successive wave crests. Figure 21

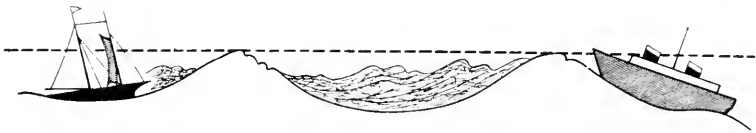


FIG. 21. Wave height measurement. (By Ch. Wilkes.)

illustrates this procedure. It should be considered that, in consequence of its buoyancy, the ship makes dipping motions. This causes considerable errors in the observations. In the wave trough the ship dips less than at the top of the wave crests. Especially in observing the wave height, these corrections should be made by means of very fine aneroid barometers. Neumayer was the first to refer to this method, which was then frequently used later. The conversion factor from pressure variations to differences in height varies slightly with atmospheric pressure: at a pressure of 1039.9 mbar (780 mm Hg), a height difference of 40.5 in. (1.03 m) corresponds to a pressure increase of 0.13 mbar (0.1 mm Hg), whereas at 986.6 mbar (740 mm Hg) the difference for 0.13 mbar (0.1 mm) is 42.5 in. (1.08 m). The error resulting from dipping oscillations can be estimated at ± 40 in. (1 m) at the least. Furthermore, there are errors arising from the elastic after-effect of the aneroid and from short period variations of air pressure which have a different origin. Only very sensitive aneroids and great care in measurements will give useful results. If the wave heights are too small to be determined by the above-mentioned methods, they can be estimated from high ships, provided one can watch the exterior of the marked hull. In the open sea it is easy to carry out such measurements from a small boat.

In former times it was left to the observer to decide which waves he was going to measure, and observation instructions were rather vague. Thus, the results of wave measurements were entirely inhomogeneous and could hardly be compared. A procedure to standardize wave observations was recently agreed upon. The aspect of a travelling wave system, as well as the

record of a wave registering instrument (see below), show that the surface of the ocean is composed of many very irregular wave groups. Due to this fact, it can be expected that the determination of the elements of a wave will give entirely different results depending on which parts of such a wave train are considered and which are not. Figure 22 gives a typical record of a wave

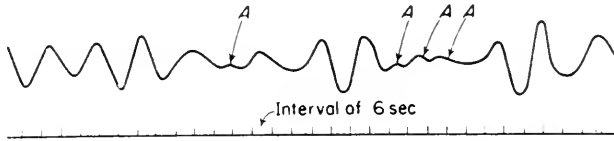


FIG. 22. Registration of a wave train by a wave recorder of the Admiralty.

train made by the Admiralty's wave recorder. It shows the variations of the ocean surface with time at a fixed point and, therefore, represents the up and downward motion of an object floating at the ocean surface as seen by an observer. This record shows at once the difficulties encountered in the case of visual observation of the average period and height of the waves at this point. In order to get representative values and to be able to obtain comparative values with other observers, it seems necessary to consider particularly such waves which do not change during their travel. These are in the first place the waves which occupy the middle of the individual wave groups. Recent instructions require that the observer should note the period and height of these higher waves in each group, neglecting flat and ill-developed waves (*A* in Fig. 22) in the intermediate region between wave groups. The average period and height of fifteen to twenty of the higher waves is to be determined. The individual waves do not belong to one group and, therefore, the observations must not necessarily be on successive waves.

These waves were called "significant" waves (see p. 87) by SVERDRUP and MUNK. It is not until a large number of such exact determinations of wave elements will be available that discordances in the results of individual observers and of individual series of observations will disappear.

Wave-measuring instruments have been built by FROUDE and PÂRIS (1867, p. 731); they were only used occasionally by scientific expeditions. The principle on which both devices work is the fact that the orbit of the water particles is large in the surface layers, whereas the orbit decreases rapidly with increasing depth. A few metres below the surface it is so small that it can almost be neglected. We can construct a long divided staff which is weighted at the lower end and has a floating anchor. This rod will float without participating in the up and downward movement of the wave motion. We can then measure the variations of the water level on the affixed scale. The Froude instrument has its floating anchor made of a horizontal canvas-covered frame tied to the staff by means of cords. This frame, which lies in almost completely stationary water layers, damps nearly every vertical

movement of the staff (see Fig. 23). The construction of the instrument built by Pâris is fundamentally similar, except that it is somewhat more stable. A ring-shaped float around the lath is pushed up and down by each wave. These motions are recorded by an automatic recording device affixed to the top of the staff. PABST (1933) (Hamburg ship-building laboratory) developed

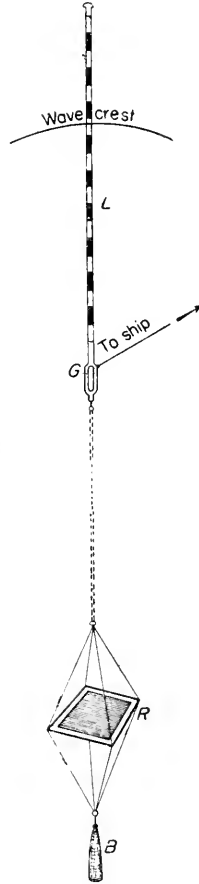


FIG. 23. Wave height meter by Froude.

a buoy which proved to be satisfactory for measuring waves, but it seems to be very difficult to make it work when the sea is rough. No measurements with this device have been published.

Recently wave-recording instruments have been developed or built which either record approaching waves at a point not too far distant from the coast or from aboard a ship. Such instruments have been described by DEACON (1946, p. 13) for the Admiralty Research Laboratory, Teddington, and almost simultaneously by KLEBBA (1945) for the Woods Hole Oceanographic Institution. Although the various instruments which were developed differ

in many important respects, they are all based upon the following principles. Surface waves induce pressure fluctuations in the entire column of water between the surface and the sea bottom. For any given depth of water and wave height the amplitude of these fluctuations depends on the wave period in such a manner that waves of very short period are virtually eliminated. The pressure fluctuations at the bottom are measured by an underwater unit. A slow leak placed in this underwater instrument permits the selection of wave periods, as that the instrument will eliminate very long waves, as, for example tidal waves. The pressure fluctuations are converted into electrical modulations which are transmitted by means of a cable to a shore recorder (see Fig. 24). The natural wave is modified in three stages: (a) waves of short

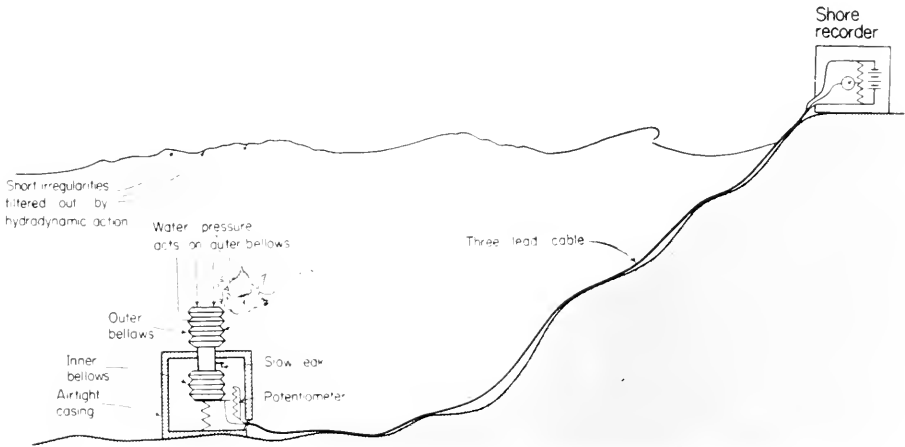


FIG. 24. Wave recorder (schematic).

period are eliminated by hydrodynamic filtering; (b) waves of very long period are removed by the slow leak in the underwater unit device; (c) the remaining waves are recorded and then subjected to a harmonic analysis, for further study.

The effect of the hydrodynamic filtering can be characterized by the ratio $\Delta p/\Delta p_0$, in which Δp and Δp_0 respectively are the amplitudes of the pressure fluctuation at the bottom, immediately beneath the surface where h is the water depth. From the equation (II.9) it is easy to deduce that

$$\frac{\Delta p}{\Delta p_0} = \frac{1}{\cosh \kappa h}$$

when $\kappa = 2\pi/\lambda$. According to the equation (II.7), however

$$\sigma^2 = \left(\frac{2\pi}{T}\right)^2 = \frac{g}{\kappa} + \tanh \kappa h$$

and the hydrodynamic filtering effect can be computed as a function of depth

and of the wave period (MUNK, 1947). It can be shown that wave periods of less than 4, 8 and 15 sec are practically eliminated in depths of 40, 150 and 600 ft.

The underwater unit is different for each of the instruments developed. We quote Munk "As a rule, the exterior pressure variations are transmitted through an outer bellows into a second bellows inside the instrument casing. Thus the pressure of the air inside the two bellows always equals the pressure in the water outside. The air inside the bellows can pass through a slow leak into the instrument casing, so that the average pressure inside the casing equals the average pressure in the water, that is the hydrostatic pressure p_h . The leak is so slow that the pressure inside the instrument does not change appreciably during one wave period.

"The total displacement of the inner bellows depends on the difference in pressure between the inside and the outside of the bellows and therefore measures the deviations of pressure from the hydrostatic mean. These deviations have an amplitude Δp .

"For waves of very long periods the fluctuation of air pressure in the instrument casing cannot be neglected. Indeed waves of tidal period are almost completely eliminated from the record, as the slow leak is able to compensate for the gradual rise and fall of sea level during a tidal cycle. In the general case the amplitude response of the instrument is proportional to $r^2/(1+r^2)$, where $r = T_r/T$. T_r is the 'resonance' period, which depends on the size of the slow leak, the air volume of the instrument, and the water depth. T_r has been assumed to equal about one hour. Owing to the combined effect of hydrodynamic filtering and the slow leak, waves of short and very long period are effectively eliminated. Maximum sensitivity is achieved in the desired range by a proper choice of depth for the underwater unit and of size for the 'slow leak'."

The methods used for measuring waves from aboard a ship are more difficult and require the ship to stop during the measurements. The dimensions of the waves at the ocean surface can be derived from the movements which the ship makes under the influence of the passing waves. A picture of such a recording is given in Fig. 44 (p. 100). Such measurements are, of course, more intricate and can only be performed on commercial ships by trained personnel.

3. Comparison between Theory and Observations

To compare observations with theory, we need the following relations in metres per second:

$$\begin{aligned} c &= 1.25 \lambda, & c &= 1.56 T, & T &= 0.80 \lambda, \\ \lambda &= 0.64 c^2, & T &= 0.64 c, & \lambda &= 1.56 T^2. \end{aligned}$$

The fact should be stressed that a confirmation of these formulas by

observation of ocean waves is not by any means conclusive with regard to the wave profile. As a matter of fact, all these theories give very much the same result as to the relation between the velocity of propagation c and the wave length λ , and the period T respectively, which is given numerically in the above formulae. Table 2 gives a few correlated numerical values according to the preceding formulae, together with the frequently needed values for α and σ .

Table 2. Surface, short or deep water waves

Velocity c (m. sec)	Wave length λ (m)	Period T (sec)	Wave number $\alpha = \frac{2\pi}{\lambda}$ (cm^{-1})	Frequency $\sigma = \frac{2\pi}{T}$ (sec^{-1})
0.32	0.063	0.198	0.0	31.7
0.57	0.209	0.365	0.3	17.22
0.99	0.628	0.634	0.1	9.90
1.81	2.09	1.16	0.03	5.43
3.13	6.28	2.01	0.01	3.13
5.72	20.9	3.65	0.003	1.72
9.90	62.8	6.34	0.001	0.99
18.10	209.0	11.6	0.0003	0.54
31.30	628.8	20.1	0.0001	0.31

The numerous observations collected from various sources were mostly grouped by the different observers into average values, in order to eliminate random errors resulting from individual measurements. A most satisfactory agreement between observation and theory has been obtained. A very meritorious compilation of older observations (previous to 1914) was made by ZIMMERMAN (1920, p. 663). From this are taken Figs. 25 and 26, which

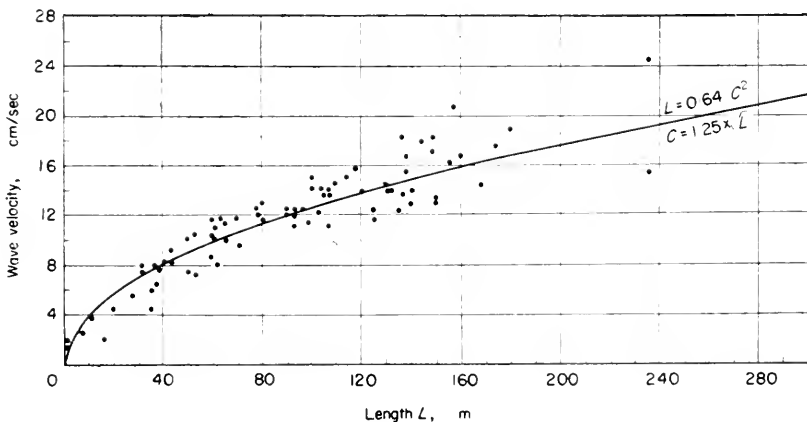


FIG. 25. Wave length and wave velocity of ocean waves (Zimmermann).

show the deviation to be expected from the theoretical values. Figure 25 gives the ratio between the wave length λ and the wave velocity c , Fig. 26 gives the ratio between wave length λ and period T . Each point corresponds to a group of observations made by nine investigators. The solid curve

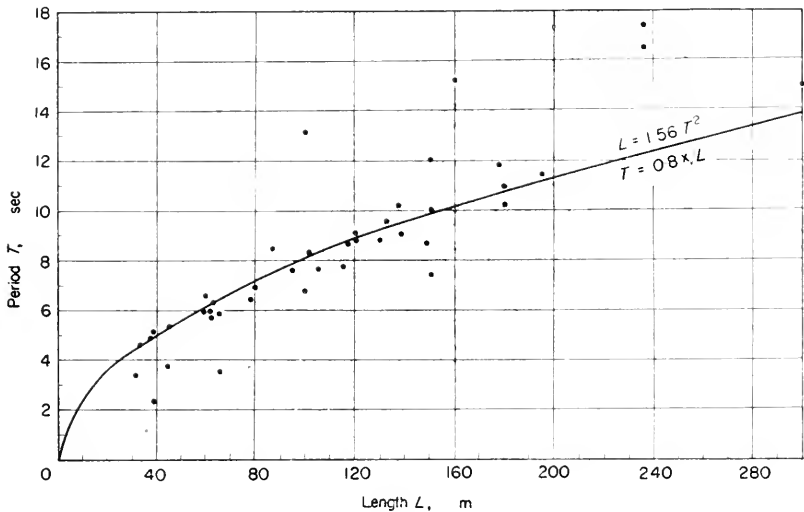


FIG. 26. Wave length and period of ocean waves (Zimmermann).

corresponds in both cases to the theoretical ratio between the two values. In general, observations agree well with the theory. The 143 observations made in 1914, at the suggestion of Zimmermann, by naval officers on German steamers show that only in eight cases values beyond the interval of 1.55 and 1.57 were found for the formula $c = 1.56T$. A very good comparison between observations and theories has been given by Thorade in Table 3, based on observations by PÂRIS (1871, p. 111), ABERCROMBY (1888, p. 263), SCHOTT (1893, p. 82) and GRASSENMAGER (1896, p. 190).

In this table are given for each group the wave velocities c_λ respectively c_T , which were computed from the observed wave length λ and from the observed period T . Furthermore, the ratios $c:c_\lambda$ and $c:c_T$ in per cent in which c represents the observed velocity. The values are very close to 100%, which is much better than can be expected from such heterogeneous observations. Therefore, we can state that the equations previously mentioned have been successfully tested by the observations. There is not much sense in discussing extreme values for velocity, length and period of the waves, because it all depends on the time at which a wave is observed. We might mention the very big waves which have a length of 250–350 m and even up to 450 m; with periods varying from 17 to 20 sec and with velocities of propagation from 25 to 30 m/sec (LARISCH, 1925). It has been established that wave heights from 10 to 12 m are not exceptional, and extremely high waves from

Table 3. Comparison between velocities deducted from observations and computed from wave length and period (according to H. Thorade)

Author	Year	Ocean	c/c_2 (%)	c/c_T (%)	Remarks
Pâris	1871	All Oceans	96 ± 2	96 ± 3	5 groups, totalling about 4000 observations
de Benaze	1874	Atlantic Ocean	96 ± 2	—	25 groups, swell
de Benaze	1874	Atlantic Ocean	109 ± 3	—	14 groups, wind waves
S. M. S. "Gazelle"	1874/76	All Oceans	100 ± 2	101 ± 5	4 groups, storm
Abercromby	1888	Pacific Ocean	106 ± 3	114 ± 7	6 groups, storm
Schott	1893	Atlantic and Indian Ocean	99 ± 2	99 ± 3	7 groups, wind waves
Gassenmayer	1896	Atlantic Ocean	104 ± 1	109 ± 3	8 groups, swell
Gassenmayer	1896	Atlantic Ocean	90 ± 2	83 ± 4	20 groups, wind waves
Gassenmayer	1896	Atlantic Ocean	99 ± 7	96 ± 3	8 groups, swell
Average			100 ± 1	100 ± 2	97 groups

17 to 18 m have been observed and photographed by the stereophotogrammatic method. Gigantic waves of these dimensions seem to occur only in the high Southern latitudes where storms last for a long time without changing their direction. In the North Atlantic the extreme values for waves are about 150 m long and from 12 to 13 m high. In exceptional circumstances we find higher waves through interference. Smaller seas and lakes have far smaller waves, as tabulated by THORADE in Table 4.

Table 4

Name	Area (km ²)	Maximum wave		Observed by
		Height (m)	Length (m)	
Lake of Geneva	570	1.7	34.5	FOREL (1895, p. 43)
Lake Superior	81,000	$6-7\frac{1}{2}$	85-100	GAILLARD (1904, p. 82)
English Channel	75,000	<5-6	—	LARISCH (1925, p. 98)
North Sea	580,000	~6*	<45	LARISCH (1925, p. 99)
Western Mediterranean	820,000	6.7	100	CORNISH (1910, p. 36)
East China Sea	$1\frac{1}{4} \cdot 10^6$	6.5	100	PÂRIS (1871, p. 119)

* In the Southern North Sea 4m.

Beside the relations between length, velocity and period of the waves, we can establish one for the height of the waves. It can only be applied to waves which have grown to their full development. The influence of the wind on the growth of waves will be dealt with later (see p. 87). The numerous

simultaneous observations of wind velocity and wave height have been used to derive a mathematical relation between both values. Difficulty is that the wind velocity is evaluated after the Beaufort-scale, and the reduction of the values to m/sec is different according to the different observers and, therefore, the observations are not always comparable. Another difficulty is that very often the force of the wind is measured at deck height of the ship and is different from the wind acting on the ocean surface. For this reason, it is not surprising that the relations between the wind velocity v (m/sec) and the wave height h (m) have shown variations according to the different observers. Therefore, we will obtain a relation derived by Cornish $h = 0.37v$ which mathematically is not exact, but is rather a rule which tries to represent average conditions.

This equation assumes that for a given wind velocity with a sufficient duration, and if the fetch is long enough, there is a definite maximum wave height.

We will discuss in another chapter the growth of the waves and the experiments which determine the relation between the wave height and the duration of the wind action (see p. 87). Table 5, by Cornish shows the values of the different characteristics of a wave in relation to the wind velocity.

Table 5. Maximum dimensions of waves relative to wind force
(According to V. Cornish)

Wind force Beaufort	Wind velocity v (m/sec)	Wave velocity c (m/sec)	Wave period T (sec)	Wave length λ (m)	Wave height h (m)	Ratio $\lambda : h$	Ratio $(h : v)$
6½	14.0	11.0	7.0	66	6.6	10.0	0.472
7	15.6	12.5	8.0	100	7.5	13.3	0.480
8	18.8	15.0	9.6	144	9.0	16.0	0.479
9	22.0	18.0	11.4	204	10.7	19.2	0.486
10	26.4	21.0	13.5	285	12.6	22.6	0.478
11	30.4	24.3	15.5	376	14.5	25.5	0.510

Table 6. Relation between wind force and wave height
(According to E. Zimmerman)

Number of observations	29	32	44	23	12
Average wind velocity v (m/sec)	6.0	10.0	14.0	18.0	24.0
Average wave height h (m)	1.32	2.21	3.20	6.85	10.4
Maximum wave height	3.5	6.0	10.0	15.0	17.0
Minimum wave height	0.3	0.8	0.8	2.5	3.5
Ratio, $h : v$	0.22	0.22	0.23	0.38	0.43

Table 6, by ZIMMERMANN in 1914, is an analysis of 143 values of the relation between wave height and wind velocity. It gives the average values

of the wind velocity and the corresponding maximum and minimum wave height. From this table it is easy to see that the deviation is quite large for each group. Figure 27 is a graphic presentation of these average values and the values given by Cornish in Table 5. Cornish's values are distributed

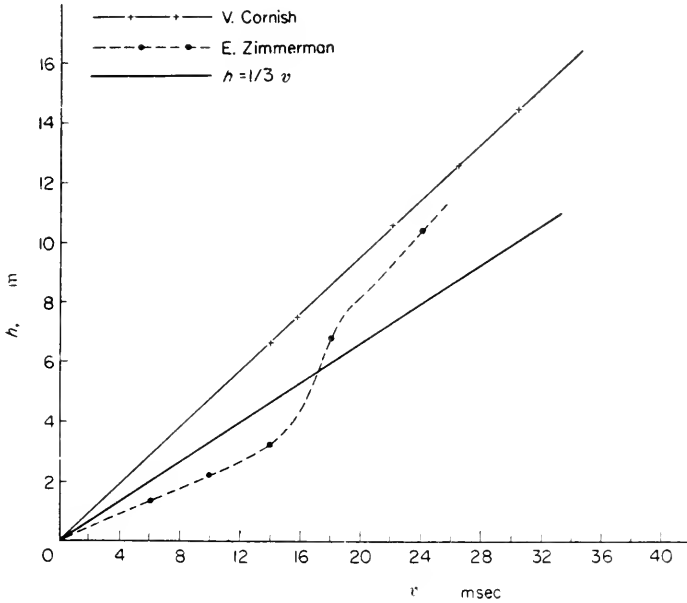


FIG. 27. Relationship between wave height h and wind velocity w for well-developed ocean waves $-+-+$, according to Cornish; $- \cdot - \cdot - \cdot$, according to Zimmermann (averaged from observations); $—$, $h = 1/3 v$.

along a straight line which passes through the origin. The inclination coefficient is about 0.48 and a little larger than the average value given by Cornish previously. The heavy solid line corresponds to the equation $h = \frac{1}{3}v$, which can be used for wind velocities below 6 Beaufort. Similar values were observed in the Baltic (BRUNS, 1936).

A distinct effect of the *thermal stratification* on the waves has been found in wave measurements on ocean weather ships (ROLL, 1952; BROWN, 1953), at lakes (BURLING, 1955) as well as in laboratory experiments (FRANCIS, 1954). Appreciable temperature differences between air and water (e.g. the air 6°C colder than the water) are connected with greater wave heights (approx. 22%) and greater wave lengths (approx. 15%) as compared to equal temperature conditions in both layers, with the same wind velocity. These differences are certainly caused by the unstable stratification of the air above the water, giving rise to strong turbulence and small vertical wind shear. Thus, the wind forces can exercise a greater influence on the surface of the sea.

4. Stereophotogrammetric Survey of the Sea Surface

KOHLSCHUETTER (1909, p. 135) on the "Planet" Expedition was successful in taking photographic pictures. Since then great improvements have been made, both in the photographic material and in the measurement of the stereo pictures. The fundamental conditions for stereophotogrammetry, which are not always easy to fulfil aboard ships, are: the base-line should have an appropriate length and the cameras must be high enough above the sea surface. The great development of (Stereoplanigraph of Zeiss or aerocartograph of Hugerhoff) instruments to measure the plates have eliminated the necessity of both photographic plates being in the same plane. Now it is only necessary that in the measuring instrument the plates have the same orientation as at the time of the exposure, and give again a good stereoscopic picture. The Zeiss cameras used by the "Meteor" Expedition 1925–7 had a device which consisted in that below to the wave cameras there were two other cameras solidly attached at an angle of 90° . These auxiliary cameras photographed each other (Fig. 28). For each picture they obtained four plates and on each

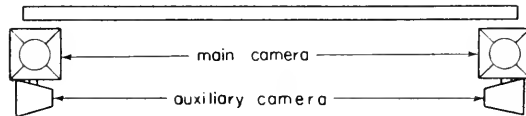


FIG. 28. Position of the main and auxiliary cameras for stereophotogrammetric wave pictures.

plate there was a horizon. There are sufficient points to determine the exact position of the main plates. By evaluating the plates we obtain a topography of the sea surface and we can measure this map in any desired direction (SCHUMACHER, 1939, p. 8; WEINBLUM and BLOCK, 1935). The size of the field depends on, and increases with, the length of the base line and the height of the camera's above the sea surface. We obtain a plot in the shape of a triangle with the point in the direction in which the picture was taken. This field will be characterized by the height of this triangle (the depth of the field) and by the width of the boundary line in the back. Table 7 gives the length of the basis and the height of the cameras above the sea surface which have been used up till now for stereophotogrammetric pictures. It also gives the error in distance and height which can be expected by the evaluation from a stereoplanigraph. The ideal solution, of course, is to have a base line so long and so high that even in rough seas a picture containing several wave trains can be obtained, which can be measured. One can see, for instance, that a base-line of 6 m as used by "Meteor" Expedition was too small and that, in such a case, it is a matter of luck to have in the field of observation a full wave length from trough to trough or from crest to crest when the sea is rough. The conditions on the "Deutschland" were already much better and made it possible to secure several wave lengths on one picture. The

Table 7. Accuracy of the stereophotogrammetric wave pictures

Ship	Year	Base length (m)	Height of camera above sea surface (m)	Field		Distance of camera (m)		Distance of camera (m)			
				Approx. depth (m)	Length of rear boundary line	50	150	50	150	250	250
"Preussen"	1904-5	22.18	9	22.5	150	3	30	82	1	2	3
"Planet"	1906-7	4.10	5	—	—	11	100	—	2	7	—
"Meteor"	1925-7	6.00	13	150-200	150-175	2	15	43	0	1	2
"Deutschland"	1929	14.77	24	550	450	—	5	14	—	0	1
"Westfalen"	1933	14.80	9	450	500	—	—	—	—	—	—
"San Francisco"	1934	7.58	15	200	150	—	—	—	—	—	—

Error in distance (cm)

Error in height for waves 10 m high (cm)

greatest number of stereophotogrammetric pictures were taken during the "Meteor" Expedition in 1925-7. To complete these observations, more pictures were taken by the "Deutschland" on two winter cruises in the North Atlantic, and the excellent pictures were discussed, together with the "Meteor" observations, by SCHUMACHER (1939). The discussion includes 17 maps of the "Meteor" Expedition and 13 of the "Deutschland", which have all been published in the results of the "Meteor" Expedition on a scale of 1:1000. The contours are at an interval of 20 cm and they show extremely clearly the multitude of forms. Furthermore, from each map there have been selected a number of profiles, which have been added to the discussions. Average waves were computed, which have been obtained by grouping several profiles and by eliminating small irregularities. In this process the wave length was standardized on 25, 50, 100 and 200 m. These average waves constitute an excellent material for the study of wave profiles. Furthermore, we have to mention the stereophotogrammetric pictures taken by WEINBLUM (1935) on the "San Francisco" in 1934 in the North Atlantic, and the pictures taken on the "Westfalen" in the summer of 1933 which SCHUMACHER (1936, p. 239) published.

The complete analysis of all maps gives much information on wave lengths and wave heights and on the steepness of waves. All these data have been condensed in Table 8. From this table we can see that with a well-developed sea we often find wave lengths of 150 m and over. It is evident that in earlier days the wave lengths were undervaluated because of the flat wave crests. The concept of wave height has not been clearly established for natural waves, because normally neither two successive troughs nor two successive crests are in the same level. At present we accept as wave height, the average between the wave trough and wave crest at the front and at the rear of the wave. From Table 8 we can derive that as an average the wave height is not too large, most values vary between 3 and 6 m. The largest difference in levels measured by stereophotogrammetry on a picture taken on the "San Francisco" was $18\frac{1}{2}$ m and seems to belong to a wave of 16 m height. We can, therefore, accept Cornish's statement that in many cases waves have exceeded the height of 21 m.

According to the measurements by Schumacher, the ratio between the wave height and the wave length varies from 1:17.6 to 1:92.2. This value is for a swell near decay. Wind waves values vary from 1:19 or 1:20; waves generated by trade winds from 1:28 to 1:33. Maximum values of 1:10 and more occur, according to KRUEMMEL (1911, vol. II, p. 82), only for waves in their initial stages; when the waves are older, this ratio becomes smaller and is, then, dependent on the stage of development of the wave. 101 waves measured by Schumacher had the following distribution in percentages:

$$h/\lambda = 1 : 20 : 25 : 30 : 35 : 40 : 45 : 50 : 55 : 60 : 65 : 70$$

7 4 15 8 23 19 11 7 4 1 1

Table 8. Compilation of stereophotogrammetric wave pictures taken by different expeditions

Expedition	Place	Wind Force in Beaufort	State of the sea	Wave length λ (m)	Wave height (m)	Slope of the wave or steepness			Remarks
						Maximum	Average		
							Leeward	Windward	
"Meteor" 2	S. Atlantic Westwind Zone, 48½ S., 17 W.	5-6	5-6	71	3.4	0.20	0.09	0.09	Swell
"Meteor" 4	S. Atlantic, Drake Strait	5-6	4-5	26	0.7	0.21	0.08	0.12	
"Meteor" 7	S. Atlantic, Westwind Zone	5-6	4-5	92	2.4	0.11	0.05	0.06	Swell
"Meteor" 9 & 10	High Southern latitudes	1	1	117	1.5	0.05	0.03	0.03	Weak Swell
"Meteor" 12	S.E. Tradewind 22½ S., 29 W.	5-6	3-4	24	0.8	0.17	0.05	0.08	Swell
"Meteor" 13	S.E. Tradewind 21½ S., 19 W.	4	3	118	2.3	—	0.04	0.03	Swell
"Deutschland" 1	N. Atlantic N.W. of Azores	6-7	6	89	2.7	0.15	0.05	0.07	Swell
"Deutschland" 2		6-7	6	76	2.9	0.26	0.07	0.09	Swell
"Deutschland" 3		6-7	6	69	1.9	0.11	0.06	0.07	
"Deutschland" 5		6-7	6	189	3.2	0.09	0.03	0.05	Swell
"Deutschland" 6		3		153	5.5	0.20	0.06	0.06	Swell
"Deutschland" 7		3		146	1.9	0.09	0.03	0.04	Swell
"Deutschland" 8		9	7	138	7.2	0.26	0.10	0.08	Wind Sea
"Deutschland" 10		8-7	6-7	129	4.8	0.26	0.09	0.06	Swell
"Deutschland" 11	N. Atlantic S.E. of Newfoundland	6	6-7	138	2.7	0.07	0.04	0.04	Swell
"Deutschland" 12		4	4	148	3.0	0.09	0.04	0.03	Swell
"Deutschland" 13		4	4	128	1.7	0.07	0.04	0.05	Swell
"San Francisco" 24	N. Atlantic 19 N., 67½ W.	6-7	—	~ 70	7.5	0.04	—	—	
"San Francisco" 36	N. Atlantic 45 N., 30½ W.	9	—	~180	13.5	0.33	—	—	
"San Francisco" 7	about 50 N., 13½ W.	9-10	—	80-10	7	0.23	—	—	
"San Francisco" 9				~150	9	0.30	0.1		
"San Francisco" 10				180-200	11	0.30	—		
"San Francisco" 11				Over 200	18.5	0.26	0.14		
"San Francisco" 19				—	11	0.40	—		
"San Francisco" 20				~200	13	0.40	—		
"San Francisco" 20				—	8.5	0.78	—		
"Westfalen"	N. Atlantic N.E. Tradewind	6	4-5	~ 80	3.2	Up to 0.36	about 0.15	—	Tradewind

The division of the frequency maxima in two regions shows perhaps the border between wind waves ($> 1:35$) and swell ($< 1:35$). The average steepness of the wave profile on the leeside and the windside are within a narrow range. They are of the magnitude 0.05, which corresponds to an angle of inclination of about 3° . But on short distances we have sometimes extraordinary large waves inclinations, as is shown by the maximum values in the table. Values of 0.4 (about 22°) have been observed, and 0.2 (about 12°) are frequent. These values are very important in relation to the stability of ships.

It is of interest to discuss the angle formed by the wave crests. The observations available are too few to be grouped e.g. according to swell o.a. Mostly the angle is in excess of 120° . Of 52 values we have 41, which is about four-fifths, lying between 149° and 165° . Schumacher could find only very few angles smaller than 120° , which corresponds to the limits of a Stokes's wave. Weinblum concurs that the waves measured by him did not have any angle formed by the crest smaller than 120° .

The wave profiles derived from the contour lines have not a simple mathematical form. An approximation to a cosine form could not be found, and even a trochoid profile could only be established in a few well-shaped waves. Looking at the profiles as presented by Schumacher, one has the impression of a very irregular appearance of the sea. But by grouping and averaging and by elimination of the very numerous irregularities, he gets for well-shaped wave trains a profile which is very similar to the form of a trochoid. In Fig. 29 several profiles have been compiled and compared

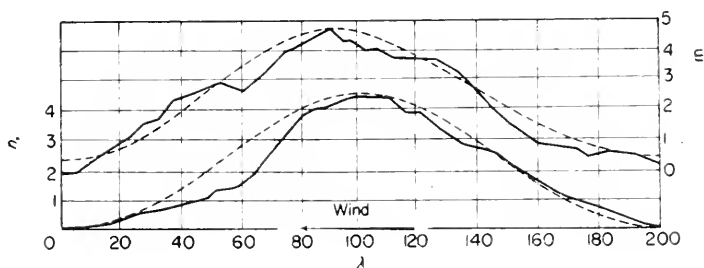


FIG. 29. Comparison between averaged waves and trochoid profile, (mean values of several profiles, wave length reduced to 200 m). Dotted lines: trochoid (height scale exaggerated 10 times).

with the corresponding trochoid of similar height. One can recognize a certain similarity, especially on the windward side. On the leeside, the real wave profile is below the trochoid. Such deviations, which make the crests steeper and the troughs flatter, have already been observed in the pictures of Kohlschuetter taken on the "Planet". The deviation on the leeside, which corresponds to the Stokes theory, seems to be characteristic of the wave profile for well-developed waves (see p. 80).

The stereophotogrammetric wave maps are morphological instantaneous

pictures. These pictures do not give any information as to the motion of the waves. We might consider perhaps the instantaneous pictures of the sea surface between two wave crests or between two wave troughs as a picture giving the change of the surface during a wave period. Kohlschuetter has interpreted the pictures of the sea surface at a definite interval as a wave motion and to derive from this motion the orbits of average waves. A complete wave length was divided in twelve equal parts and around each division he placed an orbit according to the trochoid theory, but instead of taking the corresponding point of the trochoid, he took the point of the real wave profile lying vertically beneath the trochoid point. Although these twelve points are side by side in space they are considered to succeed each other in time. These twelve points were then considered as an orbit of the observed wave profile. This is only permissible if the wave profile remains constant during its travel, which might be acceptable for one wave length if the movement is harmonic. Figure 30 represents one of the six cases on which Kohlschuetter



FIG. 30. — wave profile according to stereophotogrammetric pictures taken on the "Planet"; ----, trochoid of the same height; ·····, real orbit (wave height not exaggerated in height) (Kohlschütter).

worked. The wave profile shows again the characteristic deviation from the form of a trochoid. On the left, the points give the derived orbit. The troughs are flatter and the crests are steeper, and, therefore, the orbit is not circular but oval, with the pointed end on top. These experiences of Kohlschuetter have not been repeated recently, probably because the fundamentals are not considered too accurate.

A good way to broaden our knowledge in the mechanics of ocean waves would be to take a stereophotogrammetric moving picture. This would be essential for the research on orbits.

5. Apparent and Real Characteristics of Waves, the Complexity of Wind-Generated Waves

In former times, the numerical investigation of the wind-generated sea consisted in determining some average value of wave period, wave length or propagation velocity, and wave height. Such average values apply only to ideal wave trains, that is, to an infinite succession of congruent waves of permanent form. Therefore, it was not to be expected to find definite relations between these quantities on the one hand and to the wind force on the other. The wind does not generate a single wave, and especially not a simple harmonic wave. As soon as the first formation of waves appears

on the sea surface, energy supplied by wind to waves is distributed more and more over a certain range or wave length with different heights as the sea grows. A spectrum of ocean waves is being formed, with wave components ranging from ripples to large billowing waves in a storm sea. Therefore, it is not possible to describe the wind-generated wave pattern by the previously used quantities which apply only to some kind of a fictitious single wave train.

The basic values of wave motion as obtained from visual observations or wave recorders shall be ascribed to "apparent waves". The apparent wave height \hat{H} is to designate the height difference between a wave crest and the preceding trough. The apparent wave period \hat{T} gives the time difference and the apparent wave length \hat{L} the distance between succeeding crests at a fixed position. As the motion of the sea is not a periodical phenomenon in the mathematic-physical sense, but rather a superposition of a large number of partial waves whose frequencies are in an irrational proportion, the structure of the oscillation is subject to perpetual changes and the above "apparent basic values" give only a rough approximation of the motion of the sea. The *true* quantities, that is, the amplitude, the period and the height of harmonic wave components, can neither be observed nor directly measured. A spectrum of sea motion can be obtained quantitatively only by means of harmonic analysis. More recent systematic observations of apparent wave quantities in deep water are not very numerous (SEIWELL, 1948; PUTZ, 1952; NEUMANN, 1952*b*, 1953*a, b*; WATTERS, 1953; DARLINGTON, 1954; ROLL, 1953, 1954), but they stress the importance of such investigations. An example of the frequency distributions obtained in this way is given in Fig. 31.

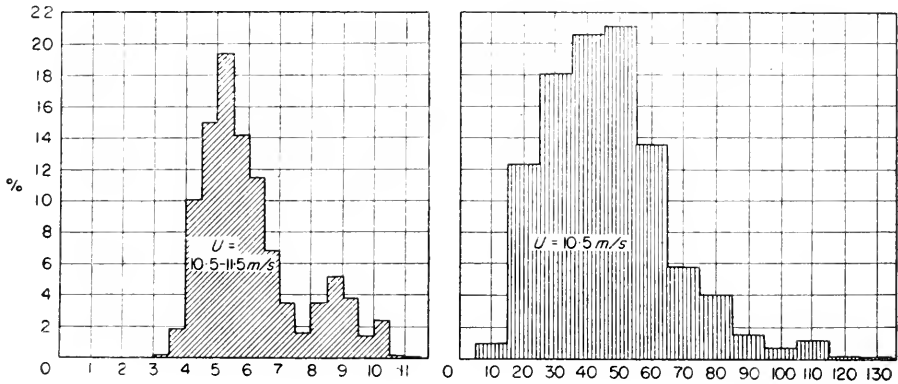


FIG. 31. Distribution of frequency of apparent wave periods and wave lengths in a heavy sea. (After Roll, 1957.)

The results of visual observations on the high seas differ in some respects from those obtained off-shore by pressure recorders at the sea bottom, but they are similar to the frequency distributions from Radar observations.

6. The Energy Spectrum and the Spectral Analysis of Recordings of Ocean Waves

The actual complex wave pattern characterized by the distribution of the apparent periods \tilde{T} and the apparent heights \tilde{H} is closely related to the spectrum of the wind-generated waves. It is not difficult to derive theoretically this spectrum from very simple basic assumptions (NEUMANN, 1953*b*, 1954). It will be pointed out that theoretically all periods T of the frequencies $\sigma = 2\pi/T$ are present in this spectrum. Analogous to the distribution of thermal radiation in the individual frequency intervals of continuous spectra, it is postulated that to a given range ΔT there belongs an energy interval ΔU . Then, the *spectral energy density* of the sea motion can be defined by the ratio

$$W_T = \frac{\delta U_T}{\delta T} \quad [\text{erg cm}^{-2} \text{ sec}^{-1}]. \quad (\text{III.1})$$

The spectral wave energy ΔU_T for the average period T in the interval ΔT is proportional to the square of the spectral wave height H_T in the same interval. Therefore

$$H_T^2 = \frac{\delta h_T^2}{\delta T} \quad [\text{cm}^2 \text{ sec}^{-1}], \quad (\text{III.2})$$

where h_T^2 is the square of the heights of individual waves in the spectrum. With sufficient accuracy for our purpose and with (II.14)

$$\delta U_T = W_T dT = \frac{1}{8} g^2 \frac{\delta h_T^2}{\delta T} dT \quad [\text{erg cm}^{-2}] \quad (\text{III.3})$$

can be defined as the mean energy per unit area of the sea surface of waves whose periods lie between $T - \frac{1}{2}\Delta T$ and $T + \frac{1}{2}\Delta T$. The total energy in the wind generated wave pattern will be given by

$$U = \frac{1}{8} g^2 \int_0^{\infty} \frac{\delta h_T^2}{\delta T} dT. \quad (\text{III.4})$$

The spectral wave height will be not only a function of the wave period (or wave length), but it also will depend on the wind velocity.

Again, analogous to the classical theory of thermal radiation, it must be assumed that the spectral wave energy δU_T or the energy density W_T , represented as a function of the period T , will attain a maximum with a certain wave of a period T_{max} and, with a further increasing period, it will drop until it practically disappears. This form of the spectrum is also suggested by the frequency distribution of the composite sea motion.

In order to arrive at a mathematical form of the energy-distribution curve, one may use the empirical relation derived from the statistics of basic values of the *apparent waves* (NEUMANN, 1953*a*, *b*):

$$(H/L)_T \sim \exp[-(gT/2\pi v^2)] \quad (\text{III.5})$$

where v is the wind speed.

The relation valid for the single wave components

$$L = \frac{gT^2}{2\pi} \quad (\text{III.6})$$

can be substituted for the spectral wave steepness, and from (III.3) with $\sigma = 2\pi/T$ we obtain the spectrum of the wave frequencies:

$$\delta U_T = W_\sigma d\sigma = -C \rho g^3 \tau^3 \sigma^{-6} \exp\left[-\frac{2g^2}{\sigma^2 v^2}\right] d\sigma. \quad (\text{III.6a})$$

The constant C [sec^{-1}] must be determined, similar to a respective constant in Planck's Law of Radiation, from the total wave energy of the fully arisen wind generated waves for a given wind velocity. Figure 32 shows for three

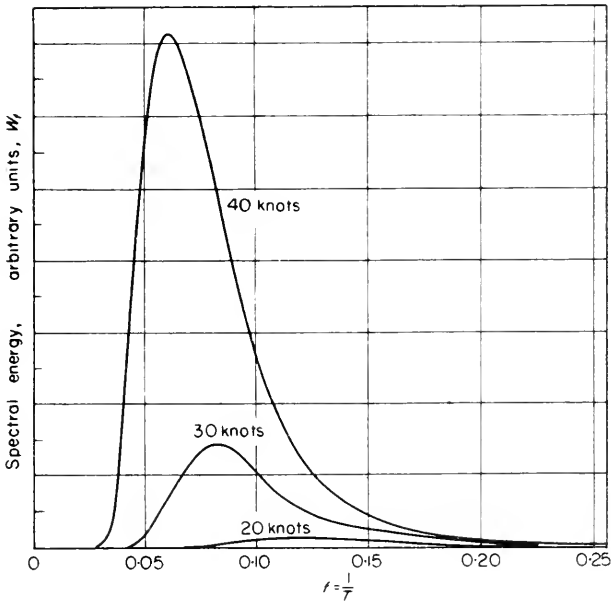


FIG. 32. Wave spectra for fully arisen sea at a wind speed of 20, 30 and 40 knots, respectively.

different wind velocities the energy distribution $W_\sigma = f(\sigma)$ for a fully arisen sea. The scale of the ordinate is proportional to the square of spectral wave heights.

Depending upon the wind velocity, the range of wave components with a significant amount of energy covers a more or less broad band on the f -scale, although all periods between 0 and ∞ are theoretically possible. The examples in Fig. 32 show that the relatively small wave energy, or the relatively small spectral wave heights for a 20 knot wind cover significant

frequencies between $\sigma = 0.083$ and $\sigma = 0.300$, that is, in terms of periods between 12 and 3 sec. The maximum of spectral energy is concentrated in an optimum band around $\sigma_{\max} = 0.124$ or $T_{\max} = 8.1$ sec.

With increasing wind speed the range of significant frequencies extends more and more towards smaller σ values, and with a 30 knot wind the significant range is between about $\sigma = 0.048$ and $\sigma = 0.24$, or between $T = 21$ and $T = 4$ sec. The optimum band is displaced to lower frequencies at $\sigma_{\max} = 0.0826$ or $T_{\max} = 12.1$ sec.

The frequency of the optimum band, σ_{\max} , is found from equation (III.6) by differentiating the energy distribution function with respect to σ . One obtains

$$\sigma_{\max}^3 = \frac{1}{3} g. \quad (\text{III.7})$$

The law that the product of the frequency of the energy maximum and the wind speed is constant ($= \frac{1}{3} g$), corresponds to Wien's law in the theory of thermal radiation. It is one of the theoretical results which can easily be checked by observations, if in the future reliable spectral analyses are available from sea surface wave records of pure fully arisen wind generated sea.

Equation (III.7) can also be written

$$T_{\max} = 0.785v \quad (\text{III.8})$$

where T_{\max} means the period of the energy maximum in the energy curve for the wind speed v . With increasing frequency the spectral energy rises rapidly to the maximum σ_{\max} , whose position is given by (III.8). Beyond this value it drops approximately inversely proportional to the sixth power of σ .

The total wave energy in the spectrum between the period 0 and T , or between the frequency ∞ and σ is obtained by integrating 3.12 between these limits (PIERSON, NEUMANN and JAMES, 1953):

$$U_{\sigma}^{\infty} = C_0 g^3 \pi^3 \left[\frac{3}{8} \sqrt{\frac{\pi}{b^5}} \cdot \Phi(x) - \frac{e^{-x^2}}{b^5} \left\{ \frac{x^3}{2} + \frac{3x}{4} \right\} \right], \quad (\text{III.9})$$

where $b = 2g^2/v^2$ and $x^2 = b^2/\sigma^2$; (III.10); $\Phi(x)$ is the error integral. The function (III.9) is called the *co-cumulative power spectrum* of waves and the curve which represents this function in a graphical form is called the CCS-curve. Examples of such CCS-curves are shown in Fig. 33 for wind velocities between 20 and 30 knots. The ordinate is scaled in E -values which are related to the wave energy U by equation:

$$U = \frac{1}{2} g_0 E. \quad (\text{III.10})$$

E has the dimension of a (length)². This is done in order to facilitate the practical use of the CCS-curves.

The total wave energy in the case of *fully arisen sea* follows from equation (III.6) by integration between the limits $\sigma = \infty$ and $\sigma = 0$ or from equation (III.9) with $x = \infty$:

$$U = C \rho \pi^3 \sqrt{\frac{\pi}{2} \cdot \frac{3}{32} \frac{1}{g^2} v^5}. \tag{III.11}$$

The total energy accumulated in the composite wave motion of a fully arisen sea increases in proportion to the fifth power of the wind speed. The constant C can be determined from observations (NEUMANN, 1953a), and one obtains with $C = 8.27 \times 10^{-4} \text{ sec}^{-1}$, $\rho \sim 1$ and $g = 981 \text{ cm/sec}^2$ and v in cm/sec

$$U = 3.125 \times 10^{-9} v^5 [\text{erg cm}^{-2}]. \tag{III.12}$$

The actual wave spectrum of a sea is obtained by harmonic analysis of recordings of sea motion; this procedure is based on the conception that

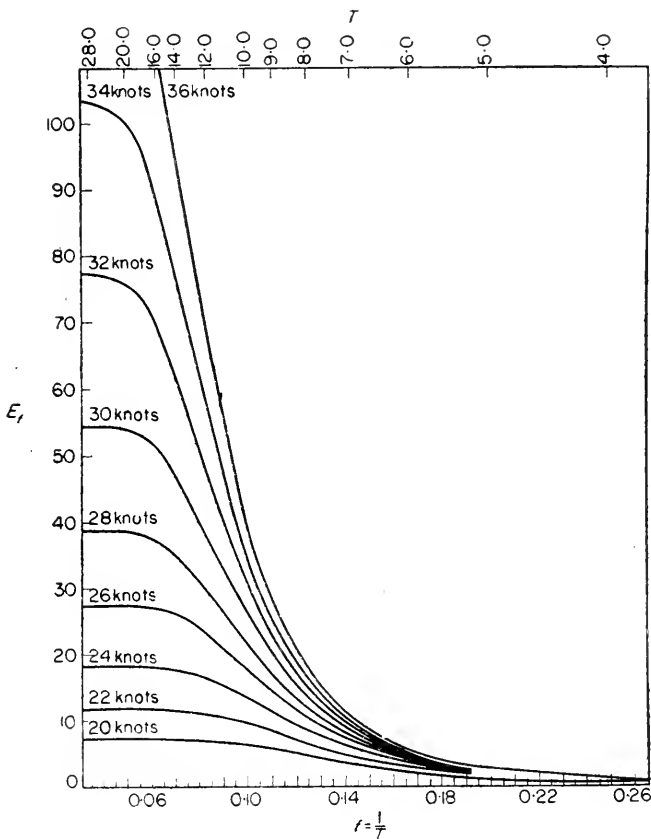
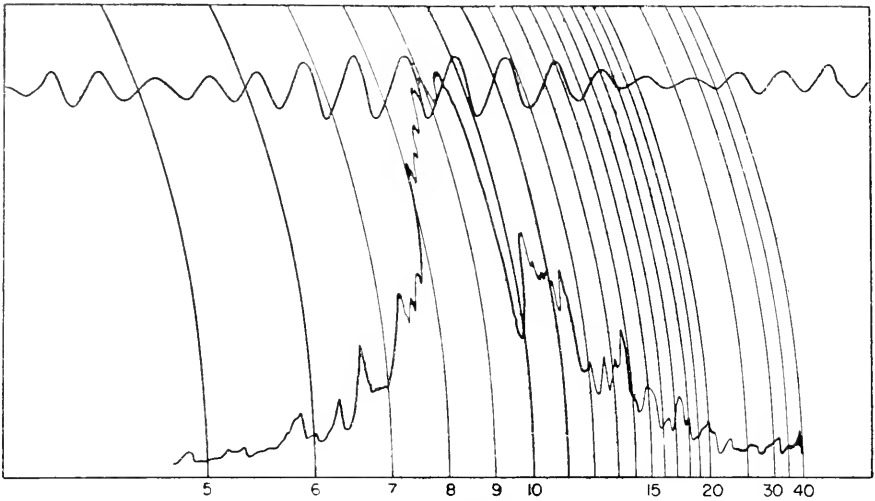


FIG. 33. Co-cumulative power spectra for ocean waves at wind velocities between 20 and 36 knots. The ordinate E_f are proportional to the total wave pattern and determine the height characteristics of the sea.

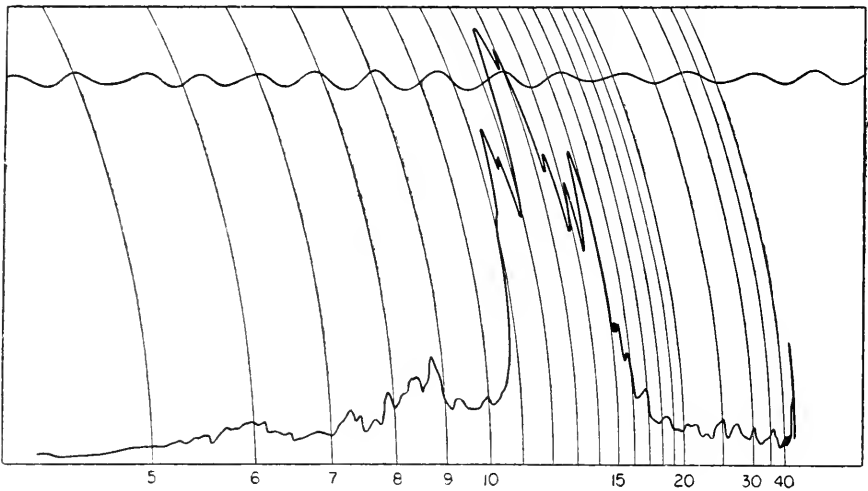
the actual wave motion results from a linear superposition of harmonic waves according to the principle of Fourier. The wave analysis is done by



3.375"/min

Period of waves, sec

11-26-46



3"/min

Period of waves, sec

11-26-46

FIG. 34. Above: Results of mechanical periodogram analysis of Wave Record B 713a, Bermuda, 21 February, 1947, depth 120ft. Below: Results of periodogram analysis of Wave Record 53-X Cuttyhunk. (E coast of USA), 15 September, 1946, depth 75ft.

wave analysators which disintegrate a section of a wave recording into a "wave spectrum". Examples of such wave spectra are to be found in Fig. 34. In the upper diagram there is shown a section of a 20 min wave record, below the continuous spectral distribution is given. The greatest development occurs in the 8 to 10 sec band of the "wave train" and maximum

energy is indicated for 8.8, 9.0 and 9.5 sec. The lower diagram shows in the same form, a wave spectrum of a pressure record. This is a typical swell spectrum with a narrow period range of 11–15 sec.

SEIWELL (1949) and WADSWORTH (1949) have doubted the results of wave analysators, which they considered as physically unfounded. They feel that a period analysis by autocorrelation will lead to more plausible and physically more simple results. Frequently, there was only one single harmonic wave upon which local oscillations are superposed by chance. The former, the “cyclic” component, corresponds to the situation forced by the wind, the latter, the “oscillatory” components, are regarded as depending upon accidental local disturbances. These doubts are only in part justified. In some cases with a narrow frequency range Seiwell and Wadsworth may be right, but in general the wave pattern is much more complicated, and the assumption that this pattern is formed by the superposition of a great number of waves with different periods, amplitudes and heights will be more correct.

7. Statistical Relations Between the Different Apparent Wave Characteristics and their Interpretation

It is possible to compute the average period \bar{T} , that is, the average of time intervals between succeeding wave crests at a fixed position, from the theoretical energy spectrum of wind generated waves. This value is calculated by

$$\bar{T} = 2\pi \left(\frac{\int_0^{\infty} \delta U_{\sigma} d\sigma}{\int_0^{\infty} \delta \sigma^2 U_{\sigma} d\sigma} \right)^{1/2}. \quad (\text{III.13})$$

We obtain for the average period

$$\bar{T}/v = \pi \sqrt{3/g} \quad \text{or} \quad \bar{T} = 0.555 v \quad (\text{III.14})$$

where v is given in m/sec^{-1} . If v is given in knots, then $\bar{T} = 0.258 v$.

With equation (III.8) we obtain the ratio

$$T_{\text{max}}/\bar{T} = \sqrt{2} = 1.414. \quad (\text{III.15})$$

Therefore, the apparent wave with the “average period” \bar{T} is not identical with the energy-richest wave of the spectrum, but its period is considerably smaller than the period T_{max} .

From the energy spectrum of sea motion one can easily estimate in which period range the most important wave components must be found. The energy richest part of the spectrum, which contains 92% of the total wave energy, can be said to give the actual pattern of the sea motion. This main part can be limited such that 3% of the total energy at the short-wave end

(in Fig. 27 in the right portion of the CCS-curves) and 5% at the long-wave end are supposed to be cut off. In this way, we get the limit periods T_u and T_0 , which, together with \tilde{T} and T_{\max} , define the total period characteristics. These limit values are given for different wind speeds in Table 10b. NEUMANN (1954) has shown that the theoretical values agree very well with the observations.

The determination of the "average wave length \tilde{L} " of the composite sea motion is more difficult. It is not allowed to compute \tilde{L} from the classical formula valid for harmonic waves with \tilde{T} . Using the theoretical wave spectrum for a fully arisen sea, PIERSON (1953) has computed the average "apparent wave length" \tilde{L} as a function of the average "apparent period" \tilde{T} and found

$$\tilde{L} = \frac{1}{3} \frac{3}{2\pi} \frac{g}{2\pi} \tilde{T}^2 = 0.577 \frac{g\tilde{T}^2}{2\pi}. \quad (\text{III. 16})$$

This relation is valid only for infinitely long wave crests. Taking into account the length of the wave crests, PIERSON derived an other relation between the average values of the apparent wave length and the apparent period by extending the energy spectrum to two dimensions:

$$\tilde{L} = \frac{2}{3} \frac{g\tilde{T}^2}{2\pi}. \quad (\text{III. 17})$$

Thus, the average apparent wave length of short-crested wind-generated waves is only two-thirds of that value which can be computed from the apparent wave period by means of the classical formula. This relation is not yet verified by observations, but we know that in general the application of the classical formula with the apparent wave period gives too large apparent wave lengths.

The characterizations of wave height data in terms of the average wave height \tilde{H} , the height of the highest third of the waves ($\frac{1}{3}$ highest, or significant waves) $\tilde{H}_{1/3}$, or the highest tenth of the waves (1 to 10 highest waves) $\tilde{H}_{1/10}$, give useful descriptions of the ocean wave pattern for many practical purposes. Observations indicate that, in general, a similar distribution of wave heights prevails in the wave pattern generated by different winds, although the absolute heights and the wind speed vary considerably. According to a summary by MUNK (1952), the ratios of the average wave heights \tilde{H} , and of the average of highest 10% $\tilde{H}_{1/10}$, to significant wave heights ($H_{1/3}$) are

$$\left. \begin{aligned} \tilde{H}/\tilde{H}_{1/3} &= 0.65 \\ \tilde{H}_{1/10}/\tilde{H}_{1/3} &= 1.29 \end{aligned} \right\} \text{(computed from wave records).} \quad (\text{III. 18})$$

As was shown by LONGUET-HIGGINS (1952), the distribution of the apparent wave heights can be computed with the following assumptions:

(1) The wave spectrum is composed of a frequency band which must not be too wide.

(2) The ocean wave pattern is formed by the supersposition of a large number of waves of small amplitude and a random distribution of phases.

It has proved convenient to express all quantities by the energy E defined in equation (III.10). It represents the sum of the squares of the amplitudes of the individual component wave trains, which go to make up the actual wave motion as it is observed; E is with equation (III.10) related to total potential energy of the composite wave motion, and can be calculated for any stage of wave development by equation (III.8). Table 8a contains the statistical height distribution of apparent waves in a wind generated wave train.

Table 8a. Statistical distribution of the heights of apparent waves in a composite ocean wave pattern

(after LONGUET-HIGGINS, 1952)

In long observation series there occur:

10% of all waves higher than $3.04 \sqrt{E}$	60% of all waves higher than $1.42 \sqrt{E}$
20% of all waves higher than $2.54 \sqrt{E}$	70% of all waves higher than $1.20 \sqrt{E}$
30% of all waves higher than $2.20 \sqrt{E}$	80% of all waves higher than $0.94 \sqrt{E}$
40% of all waves higher than $1.92 \sqrt{E}$	90% of all waves higher than $0.64 \sqrt{E}$
50% of all waves higher than $1.66 \sqrt{E}$	100% of all waves higher than $0.00 \sqrt{E}$

The most important characteristics of wave height data can be found from the

most frequent value (mode)	$H_f = 1.414 \sqrt{E}$	(III.19)
average value (mean)	$\bar{H} = 1.772 \sqrt{E}$	
significant value	$\tilde{H}_{1/3} = 2.832 \sqrt{E}$	
average of highest ten percent	$\tilde{H}_{1/10} = 3.600 \sqrt{E}$	

It follows

$$\bar{H}/\tilde{H}_{1/3} = 0.625 \quad \text{and} \quad \tilde{H}_{1/10}/\tilde{H}_{1/3} = 1.27 \quad \text{(III.20)}$$

which is in good agreement with equation (III.18). These results demonstrate that the statistical theory is capable of reflecting the actual conditions in a very satisfactory manner, and it seems that the statistical distribution of apparent wave heights does not so much depend on the width of the frequency band. As an example of the application of the theoretical results we will consider the case of a fully arisen sea at a wind speed of 30 knots ($v = 15.43 \text{ m/sec}^{-1}$). Equation (III.12) gives $U = 27.4 \text{ erg cm}^{-2}$ or $E = 5.48 \text{ m}^2$. The same value can be obtained from Fig. 33. Then the characteristic heights are: $\bar{H} = 4.1 \text{ m}$, $\tilde{H}_{1/3} = 6.6 \text{ m}$ and $\tilde{H}_{1/10} = 8.4 \text{ m}$. According to Table 8a, 10% of the total waves present will be higher than 7.1 m, 20% higher than 6.0 m, 30% higher than 5.15 m, 40% higher than 4.5 m and 50% higher

than 3.9 m. The average period \bar{T} is 8.6 sec; besides, $T_{\max} = 12.1$ sec, $T_0 = 16.7$ sec and $T_u = 4.7$ sec.

8. Scales of Sea Motion and Wind

For practical purposes, the state of the sea (sea motion) has been defined by a number from a scale divided into ten parts. The different steps of this scale have been defined by international meteorological congresses and were gradually improved. Unfortunately, different authors have used difference scales which were not always comparable. The scales which are used most often are the scales adopted in Paris in 1919 (Paris scale), the Douglas scale adopted in Copenhagen in 1929 and the new scale adopted at the International Meteorological Conference held in Berlin in 1939 (see Table 9)

Table 9. State of the sea

Scale	Douglas scale, Copenhagen, 1929	Paris scale, Paris, 1919	International scale, Berlin, 1939
0	Calm sea	Calm — glassy	Calm — glassy
1	Smooth sea	Very smooth — slightly rippled	Calm — rippled
2	Slight sea	Smooth — rippled	Smooth
3	Moderate sea	Slight — rocks buoy	Slight
4	Rough sea	Moderate — furrowed	Moderate
5	Very rough sea	Rather rough — much furrowed	Rough
6	High sea	Rough — deeply furrowed	Very rough
7	Very high sea	High — rollers, steep fronts	High
8	Precipitous sea	Very high — rollers with steep fronts	Very high
9	Confused sea	Phenomenal — precipitous	Phenomenal *

* As might exist at the centre of a hurricane.

They are quite helpful in building up statistics of the wave movements and wave measurements for a certain part of the ocean, provided the observations are extended over a sufficient length of time. We should not forget that, like evaluating the wind force according to the Beaufort scale, the evaluation of the sea surface by a number is not applicable to a certain point, but it embraces the state of the sea over a very large area. Therefore, we work with field values, and not with point values. This, however, is not a disadvantage, because in this way we evaluate the average state of a large sea surface, which is more advantageous for practical purposes.

SCHUMACHER (1939, p. 82) has worked up the enormous number of observations from the logs of the old sailing ships. These observations of the state of the sea which extend over all oceans have been classified according to the Paris scale of 1919. His results have been reproduced in Fig. 35 and they show the frequency of the different state of the seas in particular parts of the oceans. It is surprising to see that very calm and smooth seas are

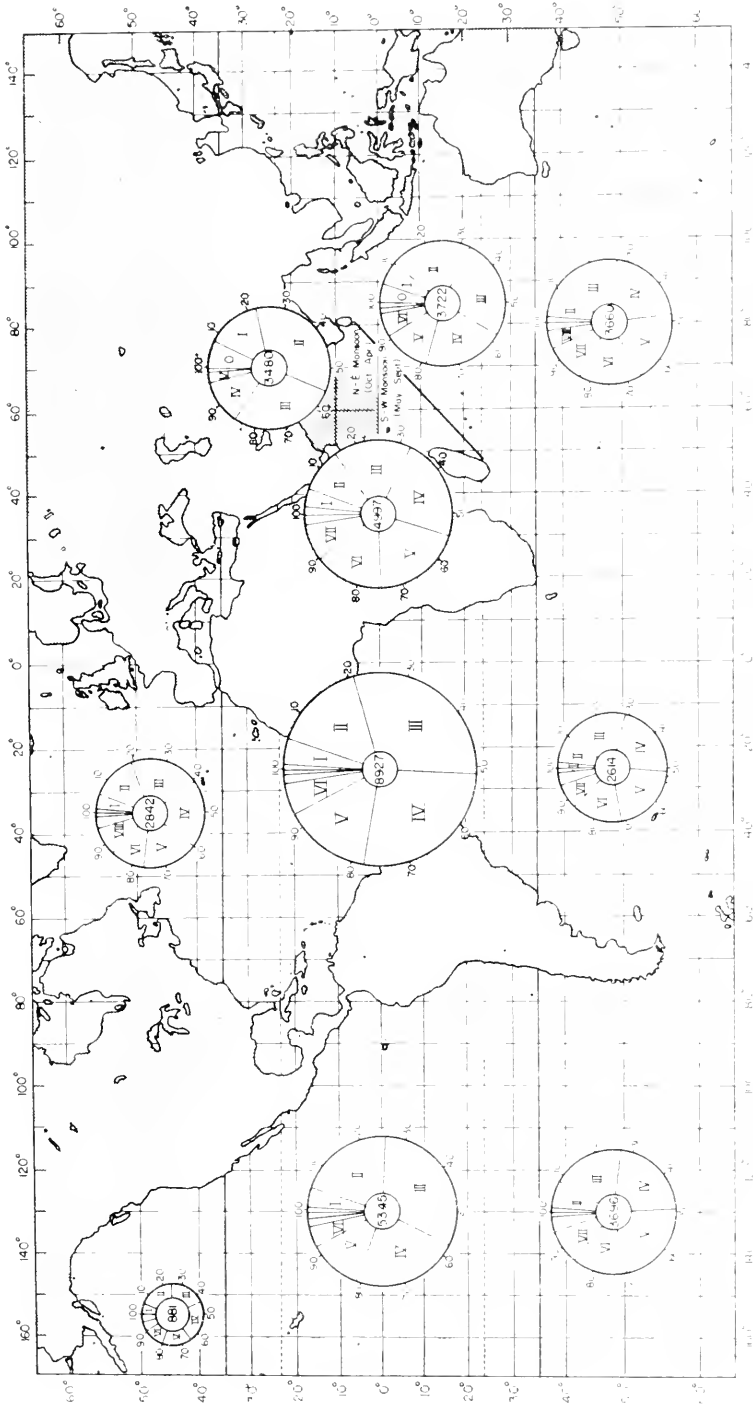


FIG. 35. Frequency in percentage of swell according to observations on German sailing vessels (Schumacher). The roman figures in the sections denote the scale number of swell (0 IX). The area of the sections is proportional to the frequency of the corresponding scale number of swell. The total area of the large circle is proportional to the total number of observations, indicated by the number in the centre.

predominant: in the lower latitudes (zone of the trade winds and doldrums) more than 50% of all observations fall between the scale points 0 and 3. Even in the middle southern latitudes (the west wind zone), about 50% of the observations fall in the categories 0 to 4. In the northern and north-western part of the Indian Ocean it is necessary to make a division for the two main seasons, because of the change of the monsoon (from May to September: the south-west monsoon and from October to April: the north-east monsoon). These tropical seas are in the south-west monsoon period about just as agitated as the annual average of the west wind zones. However, in the season of the north-east monsoon 84% of all observations indicate a slight sea; state of the sea 4 or 5 are exceptional.

The presentation by Schumacher should be considered a first trial. It has, however, been very useful and it seems that a more detailed statistical presentation of many more observations on the state of the sea will give excellent results.

Schumacher has also tried to relate the scale of the state of the sea to absolute values derived from wave measurements. Such comparisons were also attempted in former times, but they were rather inaccurate as they were based only on estimates of wave motion.

The International Maritime Commission organized from 14th to 19th November, 1938, an international week to observe swell in the Atlantic Ocean, in which 210 ships and 70 coastal stations participated. The extensive ob-

Table 10. *State of the sea motion and dimensions of the swell*
(for winds 0-5 Beaufort)

Swell scale figure	0	1	2	3	4	5	6	7	8	9	
Swell	height in m	--	1.3	2.0	2.1	2.6	3.5	4.3	3.6	3.9	(2.4)
	length in m	--	43	69	54	85	88	80	94	130	(4.4)
Wind force Beaufort	Douglas scale 1929	1.0	1.8	2.7	3.8	5.0	6.3	7.0	8.5	8.8	(5.0)
	Paris scale 1919	0.5	1.7	2.7	3.7	4.7	5.7	6.7	8.0	9.5	--

<i>Force of the wind and period of the swell</i>													
Wind force Beaufort	0	1	2	3	4	5	6	7	8	9	10	11	12
Average wave period in sec	8.7	8.8	8.7	8.1	8.4	8.5	9.0	8.5	9.4	10.5	8.6	10.5	--

servations were subjected to a thorough analysis by KEYSER (1946). Table 10 gives a compilation of the statistical comparison of actual sea-scale values

as well as height and length of the swells which were observed. This table contains only observations for winds from 0 to 5 Beaufort, in order to be reasonably sure that only swell and no waves produced by strong winds were observed. The proof that generally this was the right procedure is shown in the bottom lines of the table, where the average period of waves is given for each wind speed, and there is no correlation between the two quantities.

The characteristics of sea motion (state of the sea) with different wind speeds, which are based on the statistical wave values, can be derived from the most important spectral features of wind generated ocean waves. Such characteristics can, of course, only be given for fully arisen seas, because the ocean wave pattern at the time of generation depends not only upon the wind speed v but also upon the wind duration t and the fetch F . To a fully arisen sea belong minimum values F_m and t_m , given in the right of Table 10a. This table contains the most important wave values for fully arisen seas; it is, besides other tables, based upon the energy spectrum for all states of generation for given values of F and t (PIERSON, NEUMANN and JAMES 1953) of utmost practical importance for the prediction of sea-motion characteristics.

9. The Mathematical Formulation of the Actual Ocean Wave Pattern

The state of the sea surface at a fixed point and at a certain time can, without doubt, be described by the interference of a very large number of harmonic waves of relatively small amplitudes, which progress in different directions. They have different frequencies and become superposed with random phases. It has been attempted to give a general representation of the sea motion by means of a step-by-step approximation. The investigations by PIERSON (1952) are of importance in this connection, which he suggested from procedures in theoretical statistics and in part carried out himself. PIERSON presents *the motion of the sea surface* at a fixed point (zero point) by the following integral as a pure function of time

$$\eta_j(t) = \int_0^{\infty} \cos[\sigma t + \delta(\sigma)] \{ [h(\sigma)]^2 d\sigma \}. \quad (\text{III. 21})$$

This unusual integral cannot be solved by common methods; it represents a mathematical abstraction which can be approximated with desirable accuracy by a partial sum. $h^2(\sigma)$ is the energy spectrum according to (III.4), $\delta(\sigma)$ is of the character of a random phase; all values between 0 and 2π are of equal probability and are independent of one another. To each σ there belongs a certain $\delta\sigma$, where

$$W[\sigma < \delta(\sigma) < 2\pi\sigma] = a, \quad (\text{III. 22})$$

that is, a is the probability of $\delta(\sigma)$ falling within the range $0-2\pi\sigma$. In order

Table 10a. Wind and state of the sea

Specification	Sea motion													
	Wind *		Characteristics of heights (m)			Characteristics of period (sec)		Characteristics of wave lengths (m)		Min. fetch (km)	Min. wind duration (h)			
	Beaufort	Knots	Mean wind speed	\tilde{H}	$\tilde{H}_{1.3}$	$\tilde{H}_{1.10}$	$T_u - T_0$	T_{max}	\tilde{T}	\tilde{L}	L_{max}^\dagger	\tilde{L}	F_m	t_m
Calm	0													
Light air	1	1-3	1.2	0.011	0.02	0.023	Up to 1 sec	0.47	0.33	0.33	0.34	0.12	0.1	0.07
Light breeze	2	4-6	2.57	0.06	0.09	0.112	0.4-2.8	2.0	1.4	1.4	6	2	1.2	0.7
Gentle breeze	3	7-10	4.37	0.18	0.30	0.365	0.8-4.9	3.4	2.4	2.4	18	6	11	2.3
Moderate breeze	4	11-16	6.94	0.55	0.88	1.12	1.6-7.6	5.4	3.9	3.9	47	16	45	4.8
Fresh breeze	5	17-21	9.77	1.3	2.1	2.7	2.8-10.6	7.7	5.4	5.4	93	31	120	9.2
Strong breeze	6	22-27	12.58	2.5	4.0	5.2	3.8-13.6	9.9	7.0	7.0	153	51	260	15
Moderate gale	7	28-33	15.69	4.5	7.0	8.8	4.8-17.0	12.4	8.7	8.7	240	80	540	24
Fresh gale	8	34-40	19.03	7.0	11.3	14.2	6.0-20.5	14.9	10.5	10.5	345	115	980	37
Strong gale	9	41-47	22.63	11.0	17.4	22.2	7.0-24.2	17.7	12.5	12.5	490	163	1780	52
Whole gale	10	48-55	26.49	15.8	25.2	32	8.0-28.2	20.8	14.7	14.7	675	225	2900	73
Storm	11	56-63	30.6	22.2	35.0	45	10-32	24	17	17	900	301	4600	101

* The characteristics of sea motion are computed for the wind speeds (m/sec) tabulated under "Mean wind speed". Values for the upper and lower limits of the Beaufort scale can be found by interpolation.

† L_{max} is the wave length of the energy-richest wave component in the spectrum. Wave lengths of this order will be observed mainly in the highest swell outside the wind fetch.

to determine the integral (III.21) it is dissolved into a partial sum of corresponding terms, so that

$$\eta(t) = \lim_{\substack{\sigma_{2n+2} - \sigma_{2n} \rightarrow 0 \\ \sigma_{2n} \rightarrow \infty}} \sum_{n=0}^q \cos[\sigma_{2n+1}t + \delta(\sigma_{2n+1})] \{h^2(\sigma_{2n+1})[\sigma_{2n+2} - \sigma_{2n}]\}. \quad (\text{III.23})$$

For practical purposes it is not necessary to subdivide the interval into too small parts. A satisfactory approximation will also be obtained by a sufficiently large but finite frequency band. This new kind of representation of the sea motion corresponds much better to natural conditions than those used formerly. Towards a practical application only the first steps have been made; PIERSON has also extended this method to short-wave sea motion, but final results are still missing (see ROLL, 1957).

Chapter IV

Generation, Growth and Propagation of Waves

1. Observations of the Generation of Waves

OBSERVATIONS on a large water surface show that, when the equilibrium is disturbed, waves propagate from this point in all directions; the crests of these waves are concentric circles. This is easy to understand, when we think of the nature of wave motion. Pressure disturbances are transmitted from the point of disturbance to the neighboring water particles and thus generate a wave. It is more difficult to understand how a continuous force, like the wind, blowing over the surface previously at rest, can put it into a rhythmic oscillation. The effect of an air current on the water surface is not only the development of a wind current, but also the generation of small horizontal pressure differences which can cause wave formation. These pressure differences are caused by the eddy motion of the wind, or its turbulence which is the principal source of wave generation.

We quote SCOTT RUSSELL (1844, p. 317) and (LAMB, 1932, p. 630) the description of the process of wave generation. "A wind velocity of less than half a mile an hour ($8\frac{1}{2}$ in. or 23 cm/sec) does not sensibly disturb the smoothness of the reflecting surface. A gentle zephyr flitting along the surface may destroy the perfection of the mirror for a moment, but when it disappears, the surface is as smooth as before; if the wind has a velocity of about a mile an hour (45 cm/sec) the surface of the water becomes less capable of distinct reflection, and it is to be noticed that the decrease of this reflecting power is due to the presence of those minute corrugations of the superficial film which form waves of the third order (capillary waves). At this first stage of disturbance the phenomena on the surface cease almost simultaneously with the intermission of the disturbing cause, so that a spot which is sheltered from the direct action of the wind remains smooth. The waves of the third order are incapable of travelling spontaneously to any considerable distance, except when under the continued action of the original disturbing cause. While it remains it gives that deep blackness to the water which the sailor is accustomed to regard as the index of the presence of wind, and often as the forerunner of more."

“The second state of the development of wave motion is to be observed when the velocity of the wind acting on the smooth water has increased to two miles an hour (90 cm/sec). Small waves then begin to rise uniformly over the whole surface of the water, these are waves of the second order. Capillary waves disappear from the ridges of these waves, but are to be found sheltered in the wave troughs between them and on the anterior slopes of these waves. The regularity of the distribution of these secondary waves over the surface is remarkable; they begin with about an inch of amplitude and a couple of inches long; they enlarge as the velocity or duration of the wave increases; by and by the coterminal waves unite; the ridges increase, and if the wind increases the waves become cusped, and are regular waves of the second order (gravity waves). They continue enlarging their dimensions, and the depth to which they produce the agitation increases simultaneously with their magnitude, the surface becomes extensively covered with waves of nearly uniform magnitude.” Scott Russell’s wave of the first order is the “solitary wave.”

Similar observations were made by Apstein (see KRUEMMEL, 1911, p. 57) aboard the “Valdivia” and on the research steamer “Poseidon” in the open ocean, partly by means of photographs of the ocean surface taken from a very short distance. Mostly several kinds of waves were present simultaneously. The capillary waves cover all areas hit by the wind; their length is about 2–3 cm, their crests are, without exception, slightly curved; the shape of these wave crests, which have a length of about 9–15 cm, make the water surface look to be covered with irregular “rhombic corrugations”. Beside these “elementary” waves appear, as next larger size, waves of 6–12 cm length and, following these, waves of 18–25 cm, also 30 cm length. At a wind speed of 100 cm/sec, waves several metres long appear, and the length of the crest is at an average 3–5 times the wave length. Until longer wave crests and regular wave trains are formed, the water surface has the appearance of a piece of crepe paper rather than of a sheet of corrugated iron.

All these observations deal rather with the qualitative aspect of the process of wave formation, whereas the quantitative indications are mostly based on estimates and not on instrumental measurements. Jeffreys made a few more exact observations of this kind on ponds near Cambridge, in order to test the theoretical results. He observed, with wind speeds of less than 104 cm/sec, small disturbances which did not have the characteristics of waves. Only beyond this limit did the first distinct waves appear and at wind speeds of 104, 110 and 116 cm/sec the wave length was 8·0, 8·8 and 9·8 cm. Stanton, on the contrary, found in wave tanks, with wind velocity of 250 cm/sec, wave lengths of only 6 cm. More thorough systematical investigations, taking into account all factors which might influence wave formation, would be most desirable, the more so as the theory of the process

of wave formation is far ahead of observations and needs to be checked by experiments.

2. Propagation of a Wave Disturbance Through a Region Previously Undisturbed

Before going more thoroughly into the theory of the generation and growth of water waves, it is advisable to know something about the propagation of the waves which, after being generated at a certain point, advance from this source in a given direction. The theoretically very difficult memoirs by POISSON (1816, p. 71) and CAUCHY (1827) give the nature of such a propagation. A disturbance is produced on the surface of an infinitely large water mass of great depth. The problem now is to find out how the disturbance changes the form of the surface and how does the disturbance propagate. We can imagine that this disturbance is composed of an infinite number of sine and cosine waves of all possible wave lengths, according to Fourier's Theorem, and we can discuss the further development of this package of waves.

The formulation of the problem can be accomplished in two ways: (1) we start with an initial elevation of the free surface without initial velocity; (2) we start with an undisturbed surface (and therefore horizontal) and an initial distribution of surface pressure impulse.

Every kind of disturbance can be brought back to a combination of these two basic kinds. The results from the theory are essentially identical for both kinds of initial disturbances, so that it will be sufficient to deal only with one of them. In doing so, it will be well to distinguish between the cases in which, the propagation of the disturbance takes place only in one direction (canal waves) or occurs in all directions (circular waves). The results are not essentially different, so far as the form and the velocity of the propagation are concerned. Therefore, we will only concern ourselves with canal waves. The theoretical developments of these cases can be found in LAMB'S *Hydrodynamics* (1932, p. 384). The disturbance at a point $x = 0$ in the canal is confined to the immediate neighborhood of the origin. If b is the width of the canal and F the area between the disturbed and the undisturbed water surface, then Fb will be the volume of water originally lifted up above the surface and causing the disturbance by falling back to the level of the undisturbed surface. It will then cause a change in the level at a far distant point which has the form

$$\eta = \frac{F}{x} \sqrt{\frac{2w}{\tau}} \cdot [C(w) \cos w + S(w) \sin w], \quad (\text{IV. 1})$$

with

$$w = \sqrt{\frac{gt^2}{4x}}.$$

$C(w)$ and $S(w)$ are the integrals of Fresnel, which are of great importance in the theory of the diffraction of light. Tables of these integrals can be found in JAHNKE and EMDE (1933). When the quantity w is larger, i.e. after

a relatively long period of time, the values of the functions $C(w)$ and $S(w)$ are simplified to the extent that we obtain approximately

$$\eta = \frac{F}{x} \int \frac{w}{\pi} \cdot \cos(w-45^\circ) = \frac{Ft}{2} \int \frac{g}{\pi x^3} \cdot \cos(w-45^\circ) \quad (IV.2)$$

LAMB (1932, p. 385) writes: "It is evident that any particular phase of the surface disturbance, e. g. a zero or a maximum or a minimum of η is associated with a definite value of w and therefore that the phase in question travels over the surface with a *constant acceleration*. Consequently, an endless series of waves travels from the disturbed region, and the amplitude of these waves would rapidly decrease with increasing distance from the origin, if only the distance was taken into consideration. However, inasmuch as the amplitude is at the same time proportional to the time t , it constantly increases. This result, at first sight, seems contradictory, but finds its explanation in the assumption of the initial accumulation, of a finite volume of elevated water on an infinitely narrow base which implies an unlimited store of energy." It is mathematically possible to consider an initial elevation distributed over a band of finite breadth: then all peculiarities of a concentrated linesource of disturbance disappear, but the formulae become much more complicated without altering essentially the results. Thorade has given in Fig. 36 a graphical

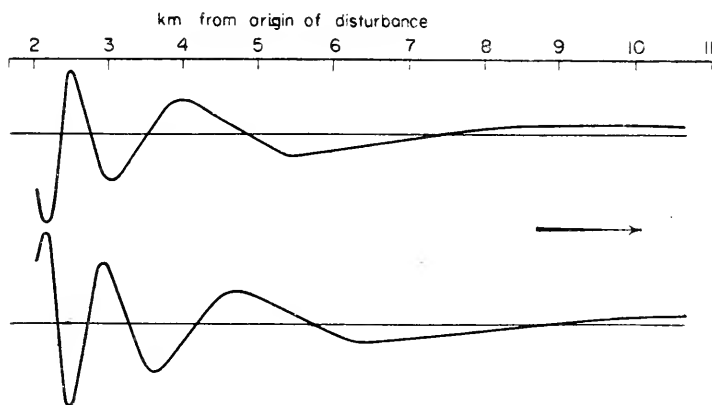


FIG. 36. Progress of a single disturbance according to Poisson and Cauchy's theory (computed by Thorade). (130 and 140 sec after the disturbance. One has to assume that the right part of the curves are extended so far that they cross the x -axis, go through a minimum and then tend asymptotically towards the x -axis.)

presentation, according to (IV.2), of the front waves computed for a distance of 10 km from the origin after 130 sec and after 140 sec and also the surface wave. We can no longer speak of a simple-harmonic wave profile. The wave crests and wave troughs have different lengths; the wave crests flatten out and at the same time lengthen as the disturbance moves on, as observed in

nature. The same follows from (IV.2). Nodes appear when $w = (2n-1)\frac{1}{2}\pi + \pi/4$ ($n = 1, 2, 3, \dots$). The first one at the time t_1 is near x_1 , the next one near x_2 ; the wave length then is $x_2 - x_1$ and

$$\frac{gt_2^2}{4x_1} - \frac{gt_1^2}{4x_2} = \pi.$$

If the difference between both quantities w remains equal, then at a later time t_2 , the quantities gt_2 , x_1 and x_2 and also the distance $x_2 - x_1$ have increased correspondingly. Each wave, therefore, lengthens while propagating, and this explains the accelerating pace of the wave disturbance. For sufficiently great values of t , the changes in length and the height from wave to wave are very gradual, so that in first approximation a considerable number of consecutive waves may be represented by a curve of sines. In a progressive wave for this short distance $\sigma t - \kappa x = (gt^2)/(4x)$. When we vary in this expression only the time t , we obtain the wave period

$$T = \frac{4\pi x}{gt}. \quad (\text{IV.3})$$

Whilst if we vary x alone we obtain the wave length

$$\lambda = \frac{8\pi x^2}{gt^2}. \quad (\text{IV.4})$$

The wave velocity then is

$$c = \frac{\lambda}{T} = \frac{2x}{t} = \sqrt{\frac{g\lambda}{2\pi}}. \quad (\text{IV.5})$$

This, however, is the velocity of propagation of an infinitely long train simple-harmonic surface waves according to Stokes equation (II.11). Each individual wave, therefore, behaves in first approximation like other simple water waves. But when we consider a group of waves having approximately a wave length λ_0 , then at a time t_0 and at a locality x_0 , $\lambda_0 = 8\pi x_0^2/gt_0^2$ and the velocity of the group

$$\frac{x_0}{t_0} = \frac{1}{2} \sqrt{\frac{g\lambda_0}{2\pi}}, \quad (\text{IV.6})$$

which is half that of the component wave. The group does not maintain a constant amplitude as it advances. This is in agreement with the relation on p. 12.

These theoretical results are confirmed by many observations, in wave tanks and in nature. Only a portion of the energy of a wave advancing in calm water travels along with the wave form, whereas the remaining portion of this energy remains available for the next wave. In this manner, each single wave in a wave train in deep water acquires energy from the preceding wave and leaves a portion of its energy for the wave following it. Due to this

process, it appears to an observer at a given distance from the wave source that the first waves of a long wave train are of a very small height. This height can be so small, that these waves often escape the observer's attention. Then the wave height increases with time and, when the wave train is only composed of a finite number of waves, i. e. when the wave source only sends out a finite number of waves, the maximum wave height is found in the centre of the group, whereafter it decreases again. The rate of travel of the place in the group where there is maximum wave height always equals the group velocity, although each wave travels with its own wave velocity (see p. 12). On the contrary, when there is a continuous generation of waves of constant height at the source, one will find that after a transient stage of wave growth, a steady state condition involving constant wave height will be approached.

SVERDRUP and MUNK (1947) based their study of the propagation of a disturbance into an area of calm, on considerations of energy.

It has been previously shown, equation (II.14*b*) that the energy of a wave, and also of a wave group, is propagated with half the wave velocity $vE = (\frac{1}{2}E)c$; inasmuch as half of the wave velocity is equal to the velocity C of the wave group, we can also say that all the energy advances with the group velocity C , $vE = EC$ so that $v = C$. Here is again the question (1) does all the energy travel with the group velocity C ; or (2) does half of the energy travel with the wave velocity c ? In order to decide between these two possibilities, we consider the flow of energy through a parallelepiped of unit width, length dx , which extends from the surface to a depth where wave motion is negligible. The time rate of change of energy within this parallelepiped must equal $-\partial vE/\partial x$, the net inflow in the direction of the x -axis, and therefore

$$\frac{\partial E}{\partial t} + \frac{\partial vE}{\partial x} = 0. \tag{IV.7}$$

The first of the two interpretations gives

$$\frac{\partial E}{\partial t} + C \frac{\partial E}{\partial x} = 0,$$

with the solution

$$E = f(x - Ct).$$

It does not explain in which manner E varies with x .

The second interpretation of equation (IV.7) gives the differential equation

$$\frac{\partial E}{\partial t} + c \frac{\partial \frac{1}{2}E}{\partial x} = 0. \tag{IV.8}$$

As the energy of a wave is proportional to the square of the wave height, equation (IV.8), taking into consideration the necessary physical boundary

conditions, will explain the transient state in wave height when the wave advances into calm areas.

The process of the transmission of energy, according to observations on wave propagation in deep water was qualitatively expressed in the following form by GAILLARD (1935, p. 194) and quoted here from SVERDRUP and MUNK (1942):

“Suppose that in a very long trough containing water originally at rest, a plunger at one end is suddenly set into harmonic motion and starts generating waves by periodically imparting an energy $\frac{1}{2}E$ to the water. After a time interval of n periods, there are n waves present and equals the time in periods since the first wave entered the area of calm.

“If the position of a particular wave within this group is indicated by m and equals the distance from the plunger expressed in wave lengths, $m = 1$ represents the wave just generated by the plunger, $m = \frac{1}{2}(n+1)$ will be the centre wave and $m = n$ the wave which has travelled farthest. Let the waves travel with constant velocity c and neglect friction.”

The first wave generated by the plunger's first stroke will have the energy $\frac{1}{2}E$. One period later this wave will have advanced one wave length, leaving behind one-half of its energy or $\frac{1}{4}E$; it now occupies the space of a wave length of the previously undisturbed area, into which it brings the energy $\frac{1}{4}E$. A second wave has been generated by the plunger occupying the position next to the plunger, where $\frac{1}{4}E$ was left behind by the first wave. The energy of the second wave equals $\frac{1}{4}E + \frac{1}{2}E = \frac{3}{4}E$. This is repeated, and when three waves are present on the water surface, the one which has just advanced into the undisturbed area has an energy of $\frac{1}{8}E$, the second one of this series $\frac{1}{8}E + \frac{1}{2}$ of $\frac{5}{8}E = \frac{5}{8}E$, the third one $\frac{1}{2}$ of $\frac{3}{4}E + \frac{1}{2}E = \frac{7}{8}E$, and so forth. Table 11 shows the distribution of energy in such a short wave train.

In any series, n , the deviation of the energy from the value $\frac{1}{2}E$ is symmetrical about the centre wave. Relative to the centre wave all waves nearer the plunger show an excess of energy and all waves beyond the centre wave show a deficit.

For any two waves at equal distances from the centre wave the excess equals the deficiency.

In every series, n , the energy first decreases slowly with increasing distance from the plunger, but in the vicinity of the centre wave it decreases rapidly. Thus, there develops an “energy front” which advances with the speed of the central part of the wave system, that is, with half the wave velocity.

According to the last line in Table 11 a definite pattern develops after a few strokes: the wave closest to the plunger has an energy $E(2^n - 1)/2^n$ which approaches the full amount E with increasing n , the centre wave has an energy $\frac{1}{2}E$, and the wave which has travelled the greatest distance has very little energy ($E/2^n$).

An exact distribution of energy and therefore also of the wave height

Table 11. Distribution of energy in a short wave train

Series number n	Wave number, m							Total energy of group
	1	2	3	4	5	6	7	
1	$1/2 E$	—	—	—	—	—	—	$1/2 E$
2	$3/4$	$1/4 E$	—	—	—	—	—	$2/2$
3	$7/8$	$4/8$	$1/8 E$	—	—	—	—	$3/2$
4	$15/16$	$11/16$	$5/16$	$1/16 E$	—	—	—	$4/2$
5	$31/32$	$26/32$	$16/32$	$6/32$	$1/32 E$	—	—	$5/2$
6	$63/64$	$57/64$	$42/64$	$22/64$	$7/64$	$1/46 E$	—	$6/2$

in a wave train starting at a source and propagating in undisturbed water is obtained through the elegant solution of the differential equation (IV.8), as given by SVERDRUP and MUNK (1947). It is superfluous to go into these mathematical developments here; an example computed for $n = 900$ will show the most important results, and is present in Fig. 37. It gives the change

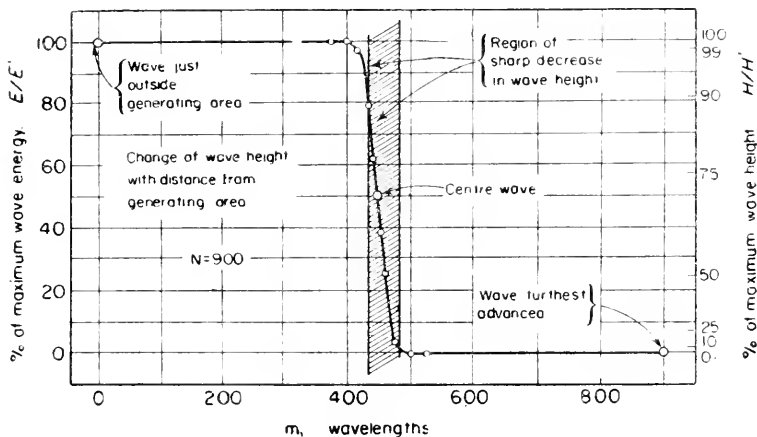


FIG. 37. Change of wave height with increasing distance from source region in a wave train advancing through water originally at rest. Deep water waves (Sverdrup and Munk).

of wave height with increasing distance from the source (indicated by m in wave lengths) when it is assumed that the deep water waves produced are uniform and are advancing through water originally at rest. The ratio of the energy E' of a certain wave to the wave with maximum energy E drops from 90 to 10% of the maximum value over a small wave range (in Fig. 37 from $m = 485$ to $m = 435$; centre wave $m = 450.5$) in the vicinity of the centre wave. This region of sharpest decrease in energy is at the same time the region of sharpest decrease in wave height, as the latter is proportional to the square root of energy. The region of sharpest decrease in wave height travels with the group velocity C . The height of the waves in front of this

region is so small that they will pass unnoticed, so that, due to the continuous transmission of energy into the undisturbed water in front of the wave train, the speed of propagation of a disturbance will appear to be one half of the wave velocity, even though each wave travels with the full wave velocity. This will be especially important in predicting the spreading of a wave disturbance into undisturbed water.

These results by Sverdrup and Munk are in good agreement with those found by Poisson and Cauchy; they have the advantage of being much clearer than these latter.

3. Theories of the Generation and the Growth of Waves

(a) General Remarks

The generation of waves by the action of an air current on a water surface will be more easily understood when we return to the dynamic fundamentals of wave processes based on Bernoulli's Theorem. Let W , in Fig. 38, be

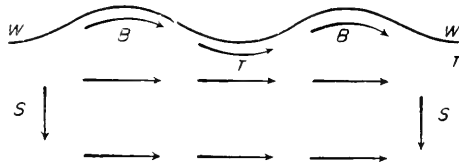


FIG. 38. Stationary waves and Bernoulli's theorem.

a wave-shaped wall extending in a horizontal direction, which has as its lower boundary a current moving to the right. The motion of the water-masses exercises pressures upon this wall. At a point B , where the section across the current is greater, the velocity must be smaller, whereas at a point T , where the section is smaller, the velocity must be greater. In other words, in steady motion the pressure is greatest where the velocity is least and vice versa. When the motion is steady the velocity is constant in magnitude and direction at every point. Consequently, the water motion, according to Bernoulli's Theorem, will generate an excess pressure at the point B , and a deficit in pressure at the points T . The consequence of this is that the water motion will try to exaggerate the deformation of the wall. Between B and T , consequently, there is a "dynamic" pressure gradient in the direction opposite to that of the current (to the left). The force of gravity acting on the water mass in the direction S generates pressure forces which increase with depth. Should gravity act alone, the pressure at all points below B would be greater than at the points below T , and between B and T there would be a "hydrostatic" pressure gradient to the right (in the direction of the current). Current and gravity, therefore, produce between B and T , pressure gradients acting in opposite directions. The velocity of the current can now be selected in such a way that the two equalize each other and that the differences in

pressure between B and T vanishes. Then there is equilibrium in all forces present and the wall can be removed without changing the situation. We have a water current with a stationary wave surface. For an observer who is moving with the inner velocity of current to the right, we have surface waves travelling to the left with a constant velocity, whereas the deeper water is motionless. The process of stationary wave motion can be based in principle on the fact that the statical and dynamical pressure differences within the water masses are in equilibrium. See EINSTEIN (1916, p. 509) and CORNISH (1934, p. 139, Notes of H. JEFFREYS).

We can see that, in this case, the air above the wavy water surface must have the same velocity as the velocity of propagation of the waves (to the left), in order that there be equilibrium. If this is not the case, the wave motion is no longer in equilibrium. If the wind velocity is greater than the wave velocity, then the negative pressure generated in O in Fig. 39 by the air

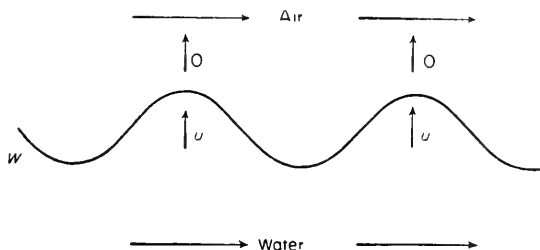


FIG. 39.

movement in a wave crest is greater than the excess pressure caused in U by the water motion. Then there exists an excess pressure in the wave crests on the side of the water, which tries to lift the water surface. The wave must increase in height. If, on the contrary, the wind velocity is smaller than the wave velocity, the wave must lose some of its amplitude, so that it approaches again a stationary, stable condition.

These fundamental considerations show that, each time there is the slightest disturbance of the water surface by air in motion, the smooth sea surface represents an unstable situation and the wavy water surface a stable situation and that to each wind velocity at the sea surface corresponds a fixed, stationary wave system. HELMHOLTZ (1889, p. 761, 1890, p. 853) was the first to conclude, from general viewpoints that the generation of waves is related to an unstable condition of the smooth sea surface. It can be proven that a wavy surface is in a stable, stationary condition, when in a system of two superposed layers of water and air in motion the difference of the potential and kinetic energy of the system is at a minimum. The determination of the wave form belonging to this system is very difficult. WIEN (1894, p. 509) has elaborated the thoughts expressed by Helmholtz and has derived a number of theoretical wave profiles which satisfy these conditions. The results obtained by him, however, are

not very satisfactory, because they do not agree with the observations. More research work on this theory has been done by BURGERS (1927, p. 333) and ROSENHEAD (1931).

LORD KELVIN (1871) showed earlier that surface waves can be formed in the absence of friction as a consequence of the dynamic pressure variations previously discussed and, that this was the principal cause for the generation of waves by the wind. Later on, Rayleigh has shown in a simple way how a system of progressive waves may be maintained against dissipative forces by a properly adjusted distribution of pressure over their slopes. This is especially true when the pressure is largest on the wind side and smallest on the lee side of the wave (LAMB, 1932).

This shows that through an excess of pressure on the rear slopes of the waves, combined with a tangential stress on the exposed wave crest when the wind velocity is greater than the wave velocity, the wave crests will become larger and that the energy lost by friction has been equalized by the work accomplished by these forces on the surface. The following investigations, made by different authors at the same time, have accentuated this concept of wave formation. In order to gain a good insight into all the factors which have to be considered we will discuss each one, its relation and its influence on the formation of waves. Many equations will be derived later in the section dealing with internal waves on boundary surfaces of the density (chap. XVI).

(b) *Stability of Internal Waves in Moving Water Masses*

If we have two superposed homogeneous fluids with a density ρ_1 and ρ_2 then there is a possibility of internal waves on their boundary surface having the character of short or deep water waves. Their wave velocity is given by the equation

$$c_0 = \sqrt{\left(\frac{g\lambda}{2\pi} \frac{\rho_1 - \rho_2}{\rho_1 + \rho_2} \right)}. \quad (\text{IV.9})$$

The wave velocity as expressed in equation (II.11) is reduced in equation (IV.9) with the square root of the difference in density of both water layers. The equation (IV.9) is in reality only valid when both layers have an infinite depth, but if the water depth is several times a multiple of the wave length (short waves), then the discrepancy with the exact formula (see equation (XVI.17)) is extremely small.

If both water masses have a motion parallel to their common boundary layer and have the velocities U_1 and U_2 , the wave velocity of the internal waves is

$$c' = \frac{\rho_1 U_1 + \rho_2 U_2}{\rho_1 + \rho_2} \pm \left[\frac{g}{z} \frac{\rho_1 - \rho_2}{\rho_1 + \rho_2} - \frac{\rho_1 \rho_2}{(\rho_1 + \rho_2)^2} (U_1 - U_2)^2 \right]^{1/2}, \quad (\text{IV.10})$$

in which $z = 2\pi/\lambda$. The first member of this equation can be considered the average velocity of both currents and, in relation to this velocity, the internal

waves have a velocity of propagation $\pm c$, which is given by the equation

$$c^2 = c_0^2 - \frac{\rho_1 \rho_2}{(\rho_1 + \rho_2)^2} (U_1 - U_2)^2. \quad (IV.11)$$

One can easily recognize that the values from c in (IV.11) becomes imaginary, in other words that the wave motion becomes unstable, when

$$(U_1 - U_2)^2 > \frac{g}{z} \frac{\rho_1 - \rho_2}{\rho_1 \rho_2}.$$

As the right member of the equation decreases unlimitedly with λ , this would mean that, in the absence of all other factors, the smallest wind will be capable of generating waves of extremely small wave lengths.

(c) *Influence of the Surface Tension*

The wave lengths of the waves which are generated first (capillary waves) are extremely small. Therefore it is to be expected that the surface tension has to be considered if the condition of pressure on the boundary surface is to be fulfilled. If both media are at rest, the velocity of propagation of the waves on the boundary surface is now given by (IV.13) if we designate the capillary coefficient, or surface tension by T

$$c'_0 = \sqrt{\left(\frac{g}{z} \frac{\rho_1 - \rho_2}{\rho_1 + \rho_2} + \frac{Tz}{\rho_1 + \rho_2} \right)}. \quad (IV.13)$$

If the values of λ are sufficiently large, the first term of this equation becomes large relative to the second term, in other words the decisive factor in a wave motion is the gravity. However, if λ is very small, then the second term is more important, and the wave motion is conditioned mainly by the surface tension.

Although the wave length decreased continuously from ∞ to zero, the wave velocity tends towards a minimum and then increases again. If we put $T/\rho_1 - \rho_2 = T'$, this minimum value c'_{\min} is given by

$$c'_{\min} = \left[\frac{\rho_1 - \rho_2}{\rho_1 + \rho_2} \cdot 2(gT')^{1/2} \right]^{1/2}$$

and the corresponding wave length is

$$\lambda_{\min} = 2\pi \sqrt{\frac{T'}{g}}.$$

We can compute that for $\lambda > 3\lambda_{\min}$ the influence of the surface tension on the wave velocity will not exceed 5%, and the influence of the gravity decreases to a like degree if $\lambda < \frac{1}{3}\lambda_{\min}$. For water-air at 20°C, T is approximately 74 (cm/sec⁻²), while $g = 981$ (cm/sec⁻²) $\lambda_{\min} = 172$ cm and $c'_{\min} = 23.15$ cm/sec.

Waves with a wave length smaller than λ_{\min} are called capillary waves or, after Kelvin, ripples. These theoretical results are in good agreement with observations of MATTHIESON (1889) and KAPLAN (1950).

If in the case of two superposed currents, we take the capillarity into consideration, then we have to add to the equation (IV.10) to the right side the term $T\kappa/(\varrho_1 + \varrho_2)$ and we obtain for the wave velocity of such waves again the equation (IV.11), with the change that instead of c_0 we now have c' of the equation (IV.13). For quantities fulfilling the inequality

$$(U_1 - U_2) \geq \frac{g}{\kappa} \frac{\varrho_1^2 - \varrho_2^2}{\varrho_1 \varrho_2} + T\kappa \frac{\varrho_1 + \varrho_2}{\varrho_1 \varrho_2}, \quad (\text{IV.14})$$

the velocity of propagation of the wave becomes imaginary, in other words the slightest disturbances cause the formation of small waves, and the amplitudes of these waves will increase gradually. The equation on the right-hand side has a minimum for

$$\kappa = \kappa_0 = \left[\frac{g}{T} (\varrho_1 - \varrho_2) \right]^{1/2} \quad (\text{IV.15})$$

or for a wave length $\lambda_0 = \lambda_{\min}$. The smallest difference in velocities where there exists the possibility of wave formation is

$$(U_{0,1} - U_{0,2})^2 \geq 2 \frac{\varrho_1 + \varrho_2}{\varrho_1 \varrho_2} g T (\varrho_1 - \varrho_2)^{1/2}, \quad (\text{IV.16})$$

also:

$$U_{0,1} - U_{0,2} \geq \frac{\varrho_1 + \varrho_2}{\varrho_1 \varrho_2} c_{\min}.$$

In case the media are water of 15°C and 35‰ salinity and air where $\varrho_1 = 1.026$ and $\varrho_2 = 0.00122$

$$U_{0,1} - U_{0,2} \geq 671 \text{ cm/sec}, \quad (\text{IV.17})$$

whereas $\lambda_0 = 1.7$ cm and $c_{\min} = 23$ cm/sec. The wind will only start generating waves when its velocity is about 6.7 m/sec, which corresponds to a force on the Beaufort scale of 4. The first waves are of the order of the capillary waves. This result is not in accordance with the observations and we can, therefore, see at once that the capillarity is not as important an element in the formation of waves as it was believed formerly.

(d) Frictional Influences

The amplitude of waves in a wave train due to the internal friction would decrease gradually and the wave would finally disappear completely, were it not for the fact that energy is fed continuously into the wave train. We have mentioned previously that the first capillary waves which come on to a motion-

less water surface disappear instantaneously the moment the force acting on the water surface subsides. The damping force is the internal friction or viscosity.

According to p. 17, we have for free oscillatory waves on deep water, and neglecting viscosity a certain velocity potential

$$q = -Acc^{\kappa z} \cos \kappa(x - ct)$$

belonging to a wave train

$$\eta = A \sin \kappa(x - ct) . \tag{IV.18}$$

From this it follows that the total velocity is

$$q^2 = w^2 + w'^2 = \kappa^2 c^2 A^2 e^{2\kappa z} .$$

The energy used up by the viscosity per unit time is, according to LAMB (1932, p. 677),

$$R_\mu = \frac{\mu}{2} \int \int \frac{\partial q^2}{\partial z} dS$$

in which μ is the coefficient of viscosity of water and dS is a unit area of the volume under consideration. We select a volume of water which extends vertically from the surface with a width b and with the length λ , to the bottom. Then with the above-mentioned value for q , we have

$$R_\mu = 2\mu\kappa^3 c^2 A^2 \cdot \lambda b . \tag{IV.19}$$

The loss of energy through viscosity per unit area is then

$$R_\mu = -2\mu\kappa^3 c^2 A^2 . \tag{IV.19a}$$

The total energy of the wave for the same volume is according to equation (II.12)

$$E = \frac{1}{2} \rho \kappa c^2 A^2 \cdot \lambda b . \tag{IV.20}$$

If we equalize the velocity of the decrease of energy with the loss of energy through friction, we have

$$\frac{d}{dt} \left(\frac{1}{2} \rho \kappa c^2 A^2 \right) = -2\mu\kappa^3 c^2 A^2 , \tag{IV.21}$$

or

$$\frac{dA}{dt} = -2\nu\kappa^2 A$$

and from this follows:

$$A = A_0 e^{-2\nu\kappa^2 t} , \tag{IV.22}$$

in which A_0 is the amplitude at the time $t = 0$ and $\nu = \mu/\rho$ is the kinematic coefficient of viscosity. The damping factor τ or modulus of decay which

represents the time in which the wave amplitude has been reduced to the fraction e of its original value ($e = 2.718$), becomes $\tau = 1/2v\lambda^2$ or in terms of the wave length (IV.23)

$$\tau = \frac{\lambda^2 \rho}{8\pi^2 \mu} . \quad (\text{IV.23})$$

In the case of water

$$\tau = 0.712\lambda^2 \text{sec} .$$

if the wave length be expressed in cm. We can see that these capillary waves are destroyed very rapidly by viscosity, whereas for a wave length of 1 m the necessary time τ would be about 2 h. This modulus of decay increases very rapidly. A wave with a period of 8 sec would travel more than 2 years before friction would reduce its height to 63% of its original value, as a consequence of friction; in that time it could circle the equator 10 times. The internal molecular viscosity is therefore always negligible. However, we observe a very rapid decrease of wave height of ocean waves and, therefore, it becomes obvious that where we have turbulent flow, we have to substitute the eddy viscosity for the molecular viscosity; according to the theory of wind currents, this eddy viscosity is about a million times greater than the molecular viscosity. It is not known whether the motion of the water on their orbits is turbulent. However, we have to put the coefficient for eddy viscosity for a wave motion many times smaller than for wind currents, because the decrease of the angular velocity of the particles with increasing depth would become too large, contrary to the observations. It is probable that the decrease of wave height is mainly caused by the air resistance encountered by the travelling wave.

(e) Investigations of the Wind Fields above the Waves

So far such systematical investigations, which are important in the study of wave formation, have not been conducted. Whatever is known about it is based on direct visual observations and occasional experiments. The lower layer of air flowing over the water is slowed down by the water surface which causes a vertical velocity gradient. The upper layer of air moving more rapidly creates a sucking action upon the lower layer of air and also on the water surface. The pressure exercised by the air on the water will be distributed irregularly, depending on the turbulence of the current at the surface. The consequence of this is an upward and downward motion of the water. Wind gusts and internal turbulence in the air create variations in pressure in points lying near each other in space, and these pressure differences cause the initial formation of waves. As shown some time ago by SCHMIDT (1934, p. 57) there are variations in the vertical component of the air motion, hurling small air bubbles like missiles, up and down. The water surface immediately follows these variations of pressure and wave formation sets in.

Apart from these first effects of the wind, one can observe a continuous action of the wind in well-developed wave trains. When an air current blows over the wave crests, phenomena appear which are similar to those when wind flows over a fixed obstacle. Only when the flow of air is small compared to the wave velocity, the streamlines of the air motion join the wave profile. The pressure exerted on the windward side of the wave will be greater than that on the lee side. Air pockets will develop in the wave troughs and on the lee side. When the wind becomes much stronger, lee eddies are formed, which, with large wave heights, become characteristic for the wind distribution above the water. Weickmann has experimented in 1930, during the "Meteor" Expedition in the waters of Iceland-Greenland, with small balloons floating just above the water, and the results showed clearly the streamlines of the air above the wave profile, as described by DEFANT (1929, p. 165). Despite the difficulties of this experiment, the air movements on a small scale were similar to those occurring on a large scale above dunes and which are used by gliders. Apparently there must be an excess pressure on the windward slopes of the waves and a pressure deficit at the leeside, which try to increase the wave height for such a time until the loss of energy by friction is compensated by the work done by the pressure forces.

MOTZFELD (1937, p. 193) and STANTON (1932) have measured in a wind tunnel the pressure distribution on models of water waves in order to test the distribution of pressure caused by wind on a wavy surface. These models consisted of (1) a train of three sine waves with a wave length $\lambda = 300$ mm and a height $2A = 15$ and 30 mm respectively; (2) a train of six waves with a trochoid profile with $\lambda = 150$ mm and $2A = 14.5$ mm, and finally (3) a train of six waves with sharp crests (crest angle 120°) with $\lambda = 150$ mm and $2A = 20$ mm.

Figures 40 and 41 show for the second and the third case the streamlines of the air motion over the wave-shaped surface and the total pressure on the streamlines. Where the crests are rounded, the streamlines hug to the wave profile, being more crowded over the crests than over the wave troughs. The wave profile with sharp crests shows the strong air current upward at the windward slope of the wave, whereas on the leeside an eddy reaches from the crest to the bottom of the trough. The wave shape of the streamlines has shifted a distance of approximately one-fourth of the wave length in the direction of the wind with reference to the profile of the wave. Considering the total pressure on the streamlines, it shows that behind the wave crests at the lower streamlines there is a loss of energy which then reaches the inside of the current more downstream. With decreasing static pressure the energy on the lower streamlines increases again. This energy increase has its origin inside the current, because there is here a continuous decrease of the total pressure on the streamlines. During these tests, the air resistance (pressure resistance) of the waves W_d was measured and it was found according to

$$c_d = \frac{W_d}{\rho(z^2, 2)\lambda}, \tag{IV.24}$$

it was for the four models 0-00085, 0-0024, 0-0028 and 0-0195 respectively.

The experiences made by Motzfeld prove that the distribution of pressure on the water surface becomes unsymmetrical through the influence of friction.

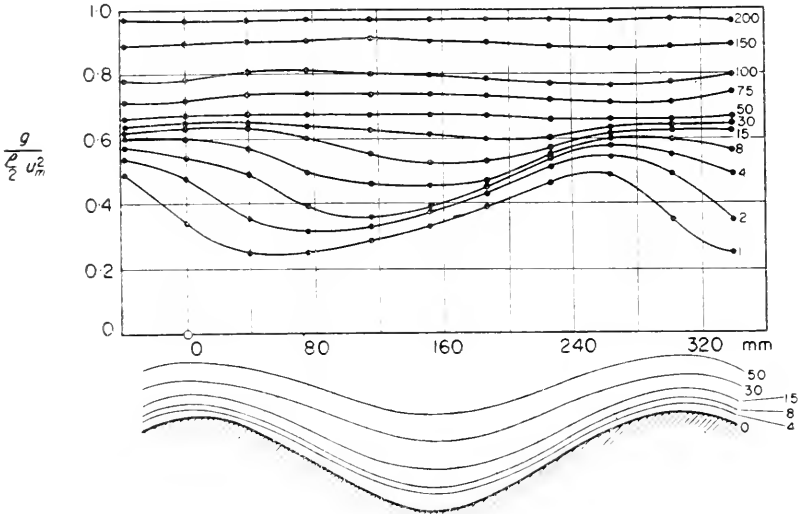


FIG. 40. Streamlines of the air motion over the wave-shaped surface and the total pressure on the streamlines. Wave with a trochoid profile with $\lambda = 150$ mm and $2A = 145$ mm.

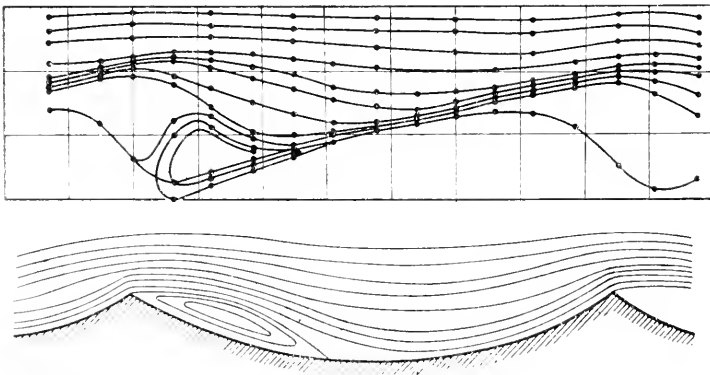


FIG. 41. The same as in Fig. 40. Wave with sharp crest (crest angle 120°) with $\lambda = 150$ mm and $2A = 20$ mm (according to Motzfeld, 1937).

Consequently, in case the wind velocity exceeds the wave velocity, the wind must add work to each wave crest and the wave constantly receives energy from the wind. Concerning the wind field above ocean waves, see especially ROLL (1948).

(f) *The Action of Normal Pressure Forces and of the Tangential Stress of the Wind on the Waves*

All waves, once generated, suffer a loss in intensity coupled with decreased wave height through viscosity and through air resistance. To generate and maintain waves on the surface, it is necessary to supply energy from the outside, mainly by wind blowing over the water surface. The question as to how waves are generated and grow can be brought back to what the action of the wind is on the waves. JEFFREYS (1925, p. 189; 1926, p. 241) has made the first test of a theory of wave generation which goes beyond the general description given by Lord Kelvin of the influence of an unsymmetrical distribution of pressure on the wave formation. According to JEFFREYS (1925) the principal supplier of energy R_N is the wind pressure Δp , which he assumes to be proportional to the product of the square of the relative wind velocity $(U-c)^2$, the density of the air ρ_2 , and the slope of the surface in the direction of the wind $\partial\eta/\partial x$. We thus have

$$\Delta p = s\rho_2(U-c)^2 \frac{\partial\eta}{\partial x},$$

wherein s is an unknown proportionality constant called by Jeffreys "sheltering coefficient". As $\partial\eta/\partial t$ is the elevation of the surface in unit time, the pressure Δp performs in unit time over the area $dx dy$ the work

$$s\rho_2(U-c)^2 \frac{\partial\eta}{\partial x} \frac{\partial\eta}{\partial t} dx dy.$$

For an area of the width b and of the length λ we then obtain with the help of (IV.18) an equation for energy transferred to a wave by normal pressure.

$$R_N = \frac{1}{2}(s\rho_2)(U-c)^2 \kappa^2 A^2 c \cdot b\lambda. \tag{IV.25}$$

(for $c < U$).

This equation (IV.25) is for waves with a velocity smaller than the wind velocity. If the latter exceeds the wave velocity and if the relative wind blows in the direction opposite to the wave motion, a negative sign must be inserted into the equation for Δp , which means that Δp is 180° out of phase with the slope, and we obtain

$$R_N = -\frac{1}{2}(s\rho_2)(U-c)^2 \kappa^2 A^2 c \cdot b\lambda \quad (\text{for } c > U). \tag{IV.25b}$$

The loss of energy through viscosity is given by the equation (IV.19). Jeffreys assumes that a wave can only grow when the energy it receives R_N is greater than the energy dissipated by viscosity R_μ . Jeffreys' criterion for the growth of deep water or surface waves is then

$$\frac{(U-c)^2}{c} \rho_2 \geq \frac{4r_1 \rho_1}{s\rho_2} \kappa. \tag{IV.26}$$

If we neglect the influence of the surface tension, then equation (IV.9) is applicable to c and the equation (IV.26) becomes

$$(U-c)^2 c \geq 4 \frac{r_1 g}{s} \frac{\rho_1}{\rho_2} \cdot \frac{\rho_1 - \rho_2}{\rho_1 + \rho_2}. \quad (\text{IV.27})$$

The smallest wind velocity U which is capable of generating and maintaining waves is the one which gives a maximum in the left hand term of equation (IV.27). It occurs when $c = \frac{1}{3}U$ and, in this case,

$$U_{\min}^3 = 27 \frac{r_1 g}{s} \frac{\rho_1}{\rho_2} \cdot \frac{\rho_1 - \rho_2}{\rho_1 + \rho_2}, \quad (\text{IV.28})$$

and with (IV.9) the corresponding wave length follows from

$$\lambda_{\min}^3 = s^2 \frac{g}{v_1^2} \frac{\rho_1^2}{\rho_2^2} \cdot \frac{\rho_1 - \rho_2}{\rho_1 + \rho_2}.$$

It is not possible to test Jeffreys' suppositions by experiments, because the value of the sheltering coefficient s is unknown. Jeffreys can only deduct from his observations of the first waves generated by the wind ($\lambda = 8-10$ cm at a minimum wind velocity of 104-110 cm/sec, see p. 67) that s has plausible values between 0.318 and 0.229, which he considers to confirm his theory. For $U_{\min} = 110$ cm/sec and $\mu = 0.018$, $g = 980$ and $\rho_2 = 1.25 \times 10^{-3}$ one obtains $s = 0.27$. The corresponding wave velocity $\frac{1}{3}U_{\min}$ is approximately 35 cm/sec and the wave period $T_{\min} = 0.22$ sec, which would be in agreement with observations.

Motzfeld, in his laboratory experiments in a wind tunnel, has submitted Jeffreys' theory to a test and was able to prove that the air resistance of the waves in Jeffreys' hypothesis in respect to the pressure distribution leads to values c_d of a pressure resistance coefficient which do not agree as to the order of magnitude with those derived from the laboratory tests. Therefore, he does not find a satisfactory solution of the problem in the hypothesis of Jeffreys. In Jeffreys' postulate the pressure coefficient has a value $c_d = sA^2k^2$, which is proportional to the square of the ratio $A/\lambda = \delta$, the average slope of the wave. Motzfeld, elaborating on Jeffreys' postulate, puts $c_d = sA^n k^n$, in which s and n are at first unknown, but which can be derived empirically from laboratory experiments. He thus finds for the value of the coefficients in the two first model tests $n = 1.5$ and $s = 0.014$. The value of s , consequently, is about 20 times smaller than the value claimed by Jeffreys. STANTON (1937, p. 283) has obtained a similar result with his tests on small wooden models of waves placed in the wind tunnel. The pressure distribution was measured along the wave profile and allowed the numerical determination of the sheltering coefficient s . It is of the order of magnitude of 0.05, i.e. about 5 to 10 times smaller than found by Jeffreys. It follows that the normal

pressures exercised by the wind on the wave surface cannot by themselves account for the generation and the growth of waves, especially as a transmission of energy from the air to the water can only take place when the wind velocity exceeds the wave velocity.

Another hypothesis for the transfer of energy consists in that a tangential stress is exercised on the water surface through the boundary friction between water and air. A computation of Jeffreys showed that, when we take the tangential stresses proportional to the square of the relative velocity between water and air, a minimum wind velocity of 480 cm/sec would be required to generate waves on a water surface, and these first waves should have a length of 140 cm. This value, however, is contradictory to observations, for which reason Jeffreys was of the opinion that the tangential stresses of the wind can hardly be accepted as the initial cause of wave formation. The average rate at which energy is transmitted to a wave by tangential stress equals

$$R_T = \frac{1}{\lambda} \int_0^\lambda \tau u_0 dx, \quad (\text{IV. 29})$$

if u_0 is the horizontal component of particle velocity in its orbit at the sea surface and where τ is the stress which the wind exerts on the sea surface. According to ROSSBY (1936), the stress of the wind with wind velocities of above 500 cm/sec is

$$\tau = k^2 \rho_2 U^2, \quad (\text{IV. 30})$$

ρ_2 being the density of the air, U the wind velocity at a height of 8–10 m and $k^2 = 0.0026$ the resistance coefficient (see, *Physical Oceanography* vol. 1). This value k^2 is valid provided that the difference between the wave velocity and the wind velocity is not too great. If this condition is not fulfilled, k^2 should probably be increased. Introducing equation (IV.30) in equation (IV.29) assuming τ to be independent of x :

$$R_T = k^2 \rho_2 U^2 \int_0^\lambda u_0 dx. \quad (\text{IV. 30a})$$

For waves of small amplitude (see II. 9)

$$u_0 = \left(-\frac{\partial \varphi}{\partial x} \right)_{z=0} = g \frac{A}{\sigma} \sin(kx - ct) = \pi \delta c \sin k(x - ct).$$

$\delta = H/\lambda = 2A/\lambda$ is the average slope or steepness of the wave, and the integral in equation (IV.30a) vanishes. These seem to be the main reason why Jeffreys assumed that the tangential stress of the wind is of no importance for the generation of waves. SVERDRUP and MUNK (1947), however, draw the attention to the fact that for Stokes's waves of finite amplitude (see p. 26) accompanied by mass transport $u' = \pi^2 \delta^2 c e^{-2\pi z}$ the value for

for the surface is $u'_0 = \pi^2 \delta^2 c$. One obtains for the transfer of energy by tangential stress

$$R_T = k^2 \pi^2 \rho_2 \delta^2 c U^2 \quad (U > 500 \text{ cm/sec}). \quad (\text{IV.31})$$

If we take this transfer of energy also into account, the energy of waves can increase only if $R_N + R_T$, the rate at which energy is added by both normal and tangential stresses of the wind, exceeds R_μ , the rate at which energy is dissipated by viscosity, or when

$$\pm s \rho_2 (U - c)^2 c + 2k^2 g_2 U^2 c > 4\mu g, \quad (\text{IV.32})$$

in which $+$ refers to $c < U$. This equation replaces the Jeffreys criterion (IV.27) for the growth of waves. This cancels the conclusion drawn from the Jeffreys criterion that the waves cannot attain a velocity exceeding the wind velocity. According to (IV.32), waves can go on growing even after their velocity exceeds that of the wind, which is in agreement with observations. This is then an action of the tangential stress which accelerates the motion of the particles in the wave crest and slows it down in the wave trough, which equals an increase of energy, just when the wave moves faster than the wind. Since it must be assumed that the wave velocity increases the longer the wave travels, the ratio $\beta = c/U$ will indicate the state of development of the wave and can appropriately be considered a parameter which describes the age of the wave.

Equation (IV.32) is valid only for $U > 500$ cm/sec and, therefore, cannot be applied to the problem of the first formation of waves which takes place, when U is approximately 100 cm/sec. At wind velocities less than 500 cm/sec the sea surface is hydrodynamically smooth according to ROSSBY (1936), and the relation between the stress and the wind velocity differs from that expressed in (IV.30).

The effect of molecular viscosity is always small compared to the wind effect; thus, Sverdrup and Munk show that:

for $U = 500$ cm/sec $\beta = 0.1$, and $c = 50$ cm/sec respectively,

for $U = 1000$ cm/sec $\beta = 0.1$, and $c = 100$ cm/sec respectively,

$R_\mu/(R_T + R_N)$ becomes -0.296 and -0.036 respectively. Consequently, for all very small values of β and for moderate and large values of U , R_μ is small compared to $R_T + R_N$ and can be neglected when dealing with the growth of waves.

(g) *New Considerations and Measurements*

The arrangements given in the preceding sections on influences of wind pressure upon the water and on the boundary friction between air and water have recently been improved. W. WÜST (1949) has applied these arrangements

to the initial generation of waves and obtained for the minimum velocity a value of about 70 cm/sec. A similar result was arrived at by NEUMANN (1949). At first he tried to get a quantitative value of the frictional coefficients c_d for actual waves. By means of corresponding comparison values he determined these coefficients as a function of wind speed and found a simple proportionality between c_d and δ (the slope of the wave), contrary to JEFFREYS and MOTZFELD (see p. 84). The balance equation, which states that the energy supplied by the wind must at least be equal to the energy dissipated by friction if the wave is to be generated or maintained, leads in the case of deep water to a lower limit of wind speed for the generation of initial waves

$$U_{\min} = 69.6 \text{ cm/sec.} \quad (\text{IV. 33})$$

This value agrees very well with the value given by Wüst. Neumann finds for the length of the initial waves

$$L_{\min} = \frac{\pi}{9g} U_{\min}^2 \pm \sqrt{\left[\left(\frac{\pi}{9g} U_{\min}^2 \right)^2 - \frac{4\pi^2 T}{g} \right]}. \quad (\text{IV. 34})$$

The root becomes zero for $U_m = 69.5$ cm/sec and $T = 73$ cm³/sec⁻², that is, the first wave has a length of 1.72 cm and a minimum velocity of $c_{\min} = 23.15$ cm/sec. However, these are the values for the smallest capillary waves. This result is due to the fact that the energy transmitted to the waves by the wind attains a maximum when U is three times the wave velocity. For the generation of the slowest waves with $c_{\min} = 23.15$ cm/sec the influence of a wind $U_{\min} = 3c_{\min} = 69.5$ cm/sec is most favourable. New determinations of the minimum wind speed and of the length of the initial waves in wind-wave channel experiments gave mostly $U_{\min} = 200\text{--}300$ cm/sec (WEINBLUM, 1938; W. WÜST, 1939; SCHOOLEY, 1955), that means much too high values. Observations and measurements by ROLL (1951) at undisturbed water surfaces show that in closed water basins the first distinctly noticeable waves will not appear in the immediate vicinity of the *windward edge* but only at a certain leeward distance from it. This distance increases rapidly with decreasing wind speed, and for $U = 100$ cm/sec it amounts to about 40 m. Thus, there are considerable differences between the wave generation in nature and in experiments. It is quite obvious that in the relatively short-wave channels, as used in laboratories, much higher wind speeds are required than in nature to generate the first waves.

4. Theory of the Growing of Significant Waves by Wind

The former theories of wave generation supposed that initially there must be small disturbances on the sea surface which may then grow by the wind. ECKART (1953) has studied the cause of such primary disturbances. First, he considered the effect of a *single gust* on the water surface. The disturbed

pressure system (low pressure in front and high pressure in back) moves over the water surface with the mean wind speed, the wind pressure being perpendicular to the disturbed surface. He was able to show that such a pressure disturbance generates a V-shaped "wake" similar to that generated by ships. After the gust has passed, the waves progress as a group of free gravity waves. The question as to the occurrence of the observed wave heights remained unsolved, as the pressure differences associated with the passage of the gust are not sufficient to form so high waves.

The first theory of wave growth by wind was given by MOTZFELD (1937), based on his model experiments in wind channels. The main relation starts out from the principle that, according to the conservation of energy, the time variation of the total wave energy (equation IV.20) must be equal to the difference between the energy supplied and the energy dissipated by internal friction (equation IV.19). For the energy supply Motzfeld takes only the work of normal pressure according to equation (IV.25), where he substitutes A^2k^2 by $A^n k^n$ according to his experiments (see p. 82). The influence of the wind stress on the sea surface is ignored. It is found that to each wind speed and to each amplitude there belongs a corresponding *stationary* wave length, and to each wind speed a maximum wave length, which occurs with a wind speed of $U = 3c$. In this theory it is not possible to make the computed wave values agree with the observed values, even if the surface tension is considered in addition.

A more comprehensive theory of the growing of waves was developed by SVERDRUP and MUNK (1946, 1951). It is based on the formerly shown complexity of the actual wind sea and on the dependence of the wind sea upon the *effective fetch* on the one hand, and upon the *wind duration* on the other. If the wind duration were unlimited, the wind sea would depend solely upon the wind speed and the effective fetch. With a sufficiently long fetch a stationary final state, corresponding to the given wind speed, would be reached ("fully arisen sea"), and everywhere the energy supplied by the wind would equal the energy dissipation. In this case all wave values would be *independent of the time* at all places, even though simultaneous local differences may exist. This ideal case may occur in small sea areas if the wind duration is long enough. If, however, the sea region affected by a homogeneous wind field is unlimited, the structure of the wind sea is determined by the wind speed and wind duration. Also in this instance the stationary state of a "fully arisen sea" is reached after a certain wind duration. There are no *local differences* in this ideal case, but uniform time variations at all places. This case will occur on the ocean most easily with a short wind duration (ROLL 1957). The theory of Sverdrup and Munk takes full account of the differences in time and space of the wind sea, in other words, here the ocean waves are not "conservative" and do not maintain their identity during propagation.

It has been pointed out (p. 36 ff.) that the new instructions for wave observations aim at obtaining the *characteristics of wave trains*. Experience shows that a careful observer will always note wave values fitting the defined values of significant waves. The significant waves behave differently than do the classical waves composing a single wave train. The individual waves of such a train are conservative and as its wave length remains unchanged, in the neighborhood of a geometrical point which travels with a group velocity C (see p. 14) we obtain

$$\frac{d\lambda}{dt} = \frac{\partial\lambda}{\partial t} + C \frac{\partial\lambda}{\partial x} = 0 \quad \text{or} \quad \frac{\partial c}{\partial t} + \frac{c}{2} \frac{\partial c}{\partial x} = 0. \quad (\text{IV.35})$$

We can see from this relation that a steady state ($\partial c/\partial t = 0$) cannot exist simultaneously with an increase of the wave velocity (or period) with distance in fetch. Nor can there exist a transient state during which the wave velocity (or period) increases with time, while it remains uniform over the area under consideration ($\partial c/\partial x = 0$).

These conclusions are in contrast with experience as to the behaviour of the significant waves. When a wind of constant velocity blows for a long time over a limited stretch of water (a lake), a steady state will soon be established. At any fixed locality the characteristics of significant waves do not change with time, but on the downward side of the lake the waves are higher and longer than on the upwind side. If, on the other hand, a uniform wind blows over a wide ocean, the waves grow just as fast in one region as in any other region and the significant waves change with time, but they show no alteration in a horizontal direction.

The discrepancy between the behaviour of significant waves and individual waves lies in the fact that the crests of significant waves do not maintain their identity, i. e. significant waves are not conservative in the storm area. This follows from the wave picture resulting from the superposition of several simple conservative wave trains, as shown in Fig. 7. In all events, in order to agree with the observations, the relations between waves and wind, fetch, duration, must be based upon a study of significant waves. Such a study represents a radical departure from the study of the conservative waves of the classical theory.

To deduct the fundamental relations between waves and wind, SVERDRUP and MUNK (1947) determine the energy budget of conservative and significant waves, giving particular consideration to the manner in which the energy progresses with the wave. We will first discuss the transient or unsteady state.

The total energy per unit crest width of a wave equals $E\lambda$, where E is the mean energy per unit surface area. The energy added each second by the normal pressures of the wind is $\pm R_N\lambda$ (IV.25) and that which is added by tangential stress equals $R_T\lambda$ (IV.31). Only half the energy, the potential

energy, travels with the wave (see p. 22); the kinetic energy, on the contrary, is constantly gathered at the forward edge of the wave and left behind at the rear edge. This can be illustrated by considering a parallelepiped of unit width, extending to a depth below which wave motion is negligible and whose forward and rear edges travel beneath two adjacent wave crests (see Fig. 42).

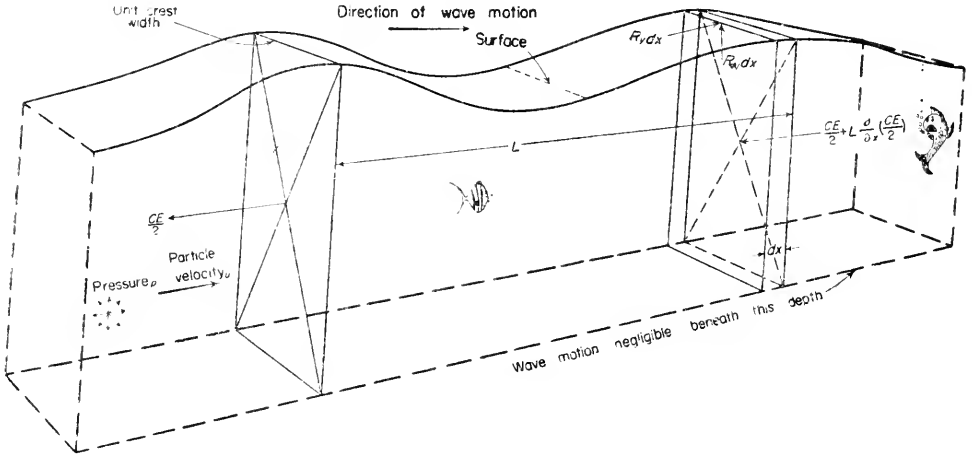


FIG. 42. Energy changes of an individual wave of length L (λ in text) travelling from left to right with a velocity c .

At the forward edge of the moving parallelepiped energy is gained at the rate of

$$c \frac{E}{2} + \lambda \frac{\partial}{\partial x} \left(c \frac{E}{2} \right)$$

and at the rear edge energy is lost at the rate $c \frac{1}{2} E$. The total energy budget is therefore

$$\frac{d(E\lambda)}{dt} = \left[R_T \pm R_N + \frac{\partial}{\partial x} \left(c \frac{E}{2} \right) \right] \lambda. \tag{IV.36}$$

The rate at which the wave length increases and therefore at which the parallelepiped “stretches”, is determined by the difference in speed between the two adjacent wave crests:

$$\frac{d\lambda}{dt} = \frac{\partial c}{\partial x} \lambda \quad \text{or} \quad \frac{\partial c}{\partial x} = \frac{1}{\lambda} \frac{d\lambda}{dt} \quad \text{or again as} \quad c^2 = \frac{g\lambda}{2\pi}$$

this equation can be written

$$\frac{\partial c}{\partial x} = \frac{2}{c} \frac{dc}{dt}.$$

We thus obtain from the equation (IV.36):

$$\frac{dE}{dt} + \frac{E}{c} \frac{dc}{dt} - \frac{c}{2} \frac{\partial E}{\partial x} = R_T \pm R_N. \quad (\text{IV.37})$$

This relation applies to a train of conservative waves, but not to significant waves, because experience shows that under the stated conditions the energy of the significant waves is independent of x ; therefore, $\partial E/\partial x = 0$, with this condition the equation (IV.37) takes the form

$$\frac{dE}{dt} + \frac{E}{c} \frac{dc}{dt} = R_T \pm R_N. \quad (\text{IV.38})$$

The integration of (IV.38) gives the change with time of the significant waves at any locality in the storm area. Initially the significant waves will have originated in the immediate neighbourhood of the locality under consideration. As the time increases, the waves reaching this locality will have travelled a longer time and originated at larger distances. In practice, the distance from which waves can come is limited by the dimensions of the storm area or by a shore line. This distance is called the fetch. The time necessary for the waves to travel from the beginning of the fetch to the locality under consideration is called the minimum duration t_{\min} . If the duration of the wind exceeds t_{\min} , the character of the significant waves which are present in the fetch remains constant in time and a steady state is established.

To examine the steady state, consider a parallelepiped fixed in space of unit width and of the length δx , but otherwise similar to the one shown in Fig. 42. Since the parallelepiped is fixed in space, potential energy flows into the volume at the rear edge at the rate $c \frac{E}{2}$ and leaves at the forward edge at the rate

$$c \frac{E}{2} + \frac{\partial}{\partial x} \left(c \frac{E}{2} \right) \delta x.$$

The local change in energy must equal the sum of the amounts which enter or leave the parallelepiped and one obtains

$$\frac{\partial E}{\partial t} + \frac{c}{2} \frac{\partial E}{\partial x} + \frac{E}{2} \frac{\partial c}{\partial x} = R_T \pm R_N. \quad (\text{IV.39})$$

This equation applies only to conservative waves. In order to apply it to significant waves which are present over a limited fetch after a steady state has been reached, we must write $\partial E/\partial t = 0$ and we obtain:

$$\frac{c}{2} \frac{dE}{dx} + \frac{E}{2} \frac{dc}{dx} = R_T \pm R_N. \quad (\text{IV.40})$$

In the equations (IV.38) and (IV.40) the $+$ and $-$ sign applies respectively,

when we have $c < U$ and $c > U$ respectively. The solution of the equation (IV.40) gives the height and velocity as function of fetch after a steady state has been reached, i.e. for $t \geq t_{\min}$. It will be shown that t_{\min} depends upon fetch and wind velocity. The value of t_{\min} determines whether the equation (IV.38) (the duration equation) or the equation (IV.40) (the fetch equation) is to be used for determining the characteristics of the significant waves.

Each of these relations contains two unknowns, the energy and the wave velocity. As the energy depends only on the wave height, we can consider this latter and the wave velocity as the unknowns. A third relation is necessary for the solution of these equations. Sverdrup and Munk form this relation from empirical data derived from observations, and therefore their theory is based only partly on purely theoretical deductions.

In the past many fruitless attempts have been made to relate wave steepness to wind velocity or other variables, but it has not been attempted to relate steepness, $\delta = H/\lambda$ to wave age $\beta = c/U$. Such a relationship is suggested by dimensional considerations and, if existing, has the advantage of being

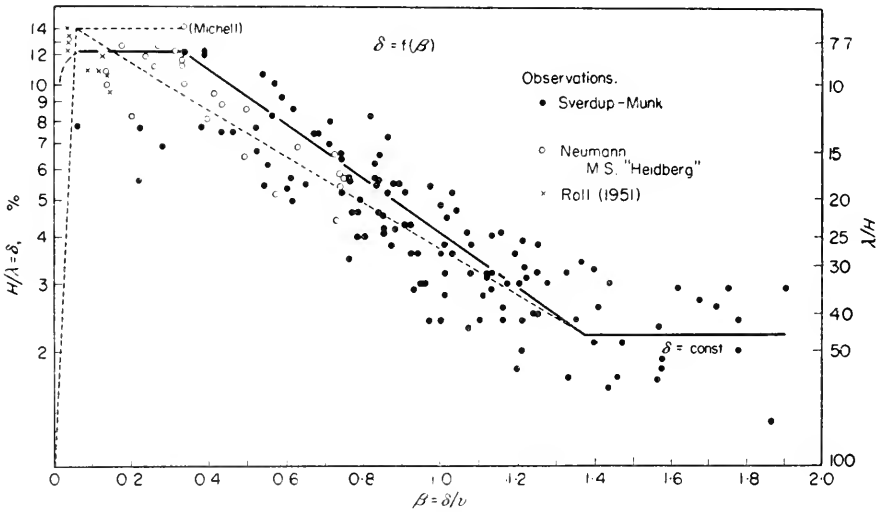


FIG. 42a. Wave height δ as a function of $\beta = c/U$.

independent of fetch and duration. The question can be examined by sets of more recently collected observations. The corresponding values of the two non-dimensional parameters δ and β are plotted in Fig. 42a, which clearly demonstrates that the two variables are related (SVERDRUP and MUNK, 1947; NEUMANN, 1952). The data were collected from observations at many different localities and, although these values are scattered, there is nevertheless a marked relation between the values. The heavy drawn curve has been fitted

to the average values and to the observations. More recent observations suggest that a rapid increase of the wave steepness in the first stages of development up to the maximum value $\delta = \frac{1}{2}$. This value seems to remain constant to about $\beta = \frac{1}{3}$. Since this first stage is passed very fast, it will probably have only little influence on the following development of the wave pattern.

With these relations, the equations (IV.38) and (IV.40) can be solved. These solutions can be given as relations between non-dimensional parameters and can be compared with observations. It is not possible to give here the rather long derivations of these solutions and we must refer to the original paper.

The results are presented in the form of diagrams giving the most important wave quantities and their dependence on fetch and duration. BRETSCHNEIDER (1952) has summarized the results into one diagram (Fig. 43), which presents all the basic information on the generation of waves. It contains, first of all, the dependence of c/U and gH/U^2 on the quantity gF/U^2 that is, on F the fetch and U the wave velocity, *for an unlimited wind duration*. The variation of these quantities is so large that, to represent it graphically, one needs a 4×5 cycle logarithmic paper. The curves represent the theory, the points the observations. The latter were greatly increased by Bretschneider, who included data which have been obtained from wave-channel experiments, from measurements on small lakes, and from observations and wave-recorder measurements of ocean waves. Thus, the entire curve is covered by observations points.

The duration curve tU/F and the curve H/L versus gF/U^2 also have been presented in Fig. 43. These curves give in a similar manner the wave velocity and the wave height as a function of wind duration t for unlimited fetch. Also here there is a close agreement with the observations. The curve tU/F was determined assuming that for a given fetch length, waves generated by a particular wind velocity reach their limiting values in a particular time. This time increases as the fetch length increases, resulting in increased limiting values of wave height and period. For any particular fetch length and wind velocity, there is a duration of wind, after which no future increase in height and period occurs. This limited time is the time required for the energy front associated with the significant waves to advance at the variable group velocity from the beginning of the fetch to the end of the fetch.

5. Observations on the Growth of Waves

We have seen previously that there is a fair agreement between the theory and observations on wave velocity, wave length and the wave period. It was always more difficult to reconcile observations and theory on the wave height, especially now that it is recognized that one has to consider the fetch and the duration of the wind. The theory developed by Sverdrup and Munk has

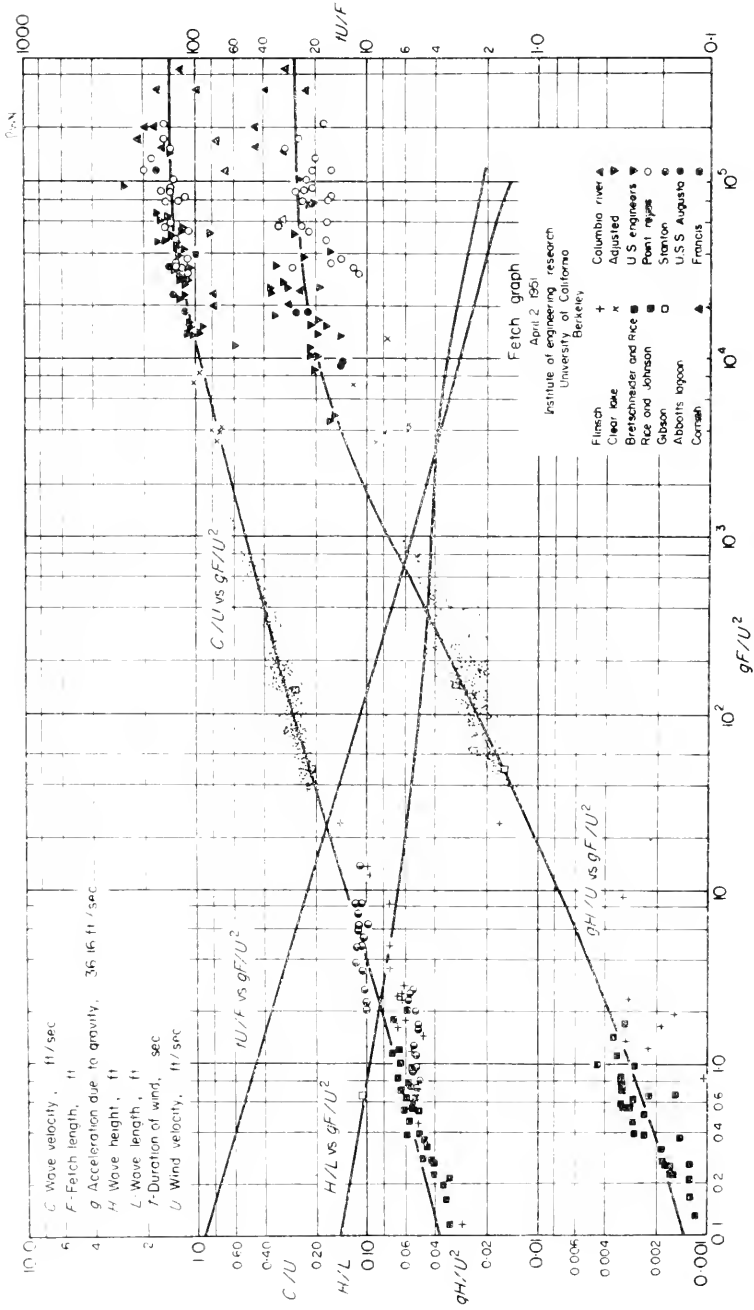


FIG. 43. Wave height and velocity as functions of fetch. Theoretical relationship shown by curves, observations by symbols.

shown in which way these two variables have to be considered in the growth of waves. In order to test the theory we need complete observations, consisting of at least the following five variables:

- (a) Significant wave height H .
- (b) Significant wave period T , or velocity c or length λ .
- (c) Wind velocity U .
- (d) Wind fetch x .
- (e) Wind duration t .

It must, furthermore, be borne in mind that the waves in any one region are the result, not only of local winds but also of winds in other areas, and that the relation between wind and waves during the periods of growth or of decay (sea or swell) should be considered separately.

The observations which have been entered as points in Fig. 43 have been collected from different series of older and newer observations, where it was possible to determine the non-dimensional parameter through special observations. However, generally it is not possible to have such complete series of observations available.

From earlier days we have empirical relations between the wave height, the distance and the duration of the fetch, and also between the wave height, the wave velocity and the force of the wind. However, these relations are only approximate, e.g. STEVENSON (1851, p. 189, 1852, p. 358) has established an empirical formula giving the "greatest" wave height H as function of the fetch (both in cm), according to which $H = 0.105 \sqrt{x}$. The formula was established by means of data from lakes, where the value of x ranged from a few kilometres up to 250 km. For the Mediterranean Cornish has verified the relation for fetches up to 830 km, and it is generally assumed that the relationship holds for values of x up to 1000 km. The formula is incomplete, since it does not take the wind velocity into account, but it is intended to apply at the highest wind velocity which can be expected to occur. Figure 43 gives the dimensionless relationship between H , x and U , and Stevenson's formula fits this relation only when there is a definite connection between the wind force and the fetch.

BOERGEN (1890, p. 1) has given an empirical formula for the relation between wave height and duration of the wind; it is a linear formula, in which $H = H_m/(1 + a/t)$. H is the wave height to be determined and H_m the maximum wave height for any given wind velocity and t the duration of the wind action; for $t = 0$, $H = 0$, and for $t = \infty$, $H = H_m$. The coefficient a must be determined from observations. Although a comparison of this formula with theory is not possible, its chief features seem to be in agreement. Boergen has attempted to combine the three factors: wind, velocity, duration of the wind action and active length of the fetch, and devised the formula

$$A = \frac{A_{\max} U}{\left(1 + \frac{aU}{D}\right) \left(1 + \frac{\beta}{t}\right)}. \quad (\text{IV.41})$$

a and β are constants to be determined empirically. A_{\max} is the wave amplitude of matured waves, that is after a great fetch and lengthy wind action. Thorade reasons rightly that this equation in the form

$$A = A_{\max} U (1 - e^{-\beta t}) (1 - e^{-\delta(D/u)}) \quad (\text{IV.42})$$

would be more justified. Boergen has tried to test his formula to observations made by Paris; KRÜMMEL (1911, Vol. II, p. 66), however, is of the opinion that the observations are not suited for this purpose.

The relationship between wave height and wind velocity as given by Sverdrup and Munk is $H = (2\pi/g) U^2 \delta \beta^2$, i. e. it depends not only on the wind velocity, but also on the fetch and the duration of the wind, since δ and β are functions of these variables. The maximum wave height is found by setting in this relation $\beta = \beta_M$, and for $\delta = \delta_m$, and therefore depends upon the wind velocity only. $H_m = (0.26/g) U^2$, a relation which is in good agreement with a formula suggested by ROSSBY and MONTGOMERY (1935, p. 1011) from quite different considerations.

Linear relations between wind velocity and general wave height (not maximal) have been derived and were already discussed previously. It was pointed out that both the length of the fetch and the duration of the wind action exert an influence on the wave height and that the simple linear relations of Cornish and Zimmermann are only rough approximations of the reality.

Table 12. Average wave characteristics in tradewind regions

Locality	Observations made by	U (cm/sec)	c (cm/sec)	β (c/U)	δ (H/λ)
Tradewind, N. Atlantic Ocean	"Meteor"	935	858	0.93	0.029
Tradewind, N. Atlantic Ocean	"Meteor"	670	780	1.16	0.024
Tradewind, N. Atlantic Ocean	"Pâris"	590	1120	1.90	0.029
Tradewind, Indian Ocean	"Pâris"	720	1260	1.75	0.029
Western Pacific Ocean	"Pâris"	860	1240	1.44	0.030
Westerlies, South Atlantic Ocean	"Pâris"	1240	1400	1.13	0.032
Westerlies, Indian Ocean	"Pâris"	1490	1500	1.01	0.045
China Sea	"Pâris"	1300	1140	0.88	0.042

The same applies for the relation of wave velocity and wind velocity. Here also partly linear and partly more complicated formulae were selected. According to Zimmermann, $c = 2.35U^{2/3}$ and hence c exceeds U for minor velocities above 1331 cm/sec but, according to Cornish, $c = 0.8U$, and ac-

According to Schott, $c = 0.76U$, that is, the wave velocity is less than the wind velocity. According to the newer theory, it is perfectly possible that $c > U$. Observations from the trade wind region, where the wind blows over large areas with great uniformity and moderate velocity, show clearly that wave velocities may exceed wind velocities in the generating area. Table 12 by Sverdrup and Munk is a compilation of wave characteristics in tradewind regions and is highly instructive.

6. Growing of Spectral Components of the Wind-Generated Sea

The introduction of the wave spectrum in studying the characteristics of the wind-generated sea led to the problem of the growth of the *individual* components of sea motion. NEUMANN (1952, 1953, 1954) and, in another way also DARBYSHIRE (1952), have tried to solve this problem. Since the ocean waves will only grow as long as the energy supplied by the wind exceeds the loss in energy, the complete energy equations permit to compute this growing theoretically. The computations by Neumann are physically more founded than those by Sverdrup and Munk, as Neumann took into account the internal friction and turbulence in the water as well as the periodical changes of wind stress along the profile. Again, the results are represented in diagrams with dimensionless wave quantities and become especially clear when the co-cumulative energy spectra (CCS-curves) are used. An example is given in Fig. 43a for wind speeds of 10 to 36 knots. The energy spectrum in this figure is the same as in Fig. 33, but Fig. 43a contains also duration or fetch lines.

The intersection points of the CCS-curves with the duration or fetch lines, respectively, show the limit of the development of the composite wave motion at the given duration or fetch. Physically, it means that the state of development is limited by a certain maximum amount of total energy which the wave motion can absorb from the wind with the given conditions. The E value of the ordinate of each intersection point is a practical measure of the total energy accumulated in the wave motion of the non-fully arisen state, limited either by the fetch or duration. From the $E = \frac{1}{2}(g\rho)E^*$ value, the wave height characteristics can be computed, as in the case of a fully arisen sea.

The upper limit of significant periods in not fully arisen sea is approximately determined by the "frequency of intersection", f_i , that is, the frequency of the intersection point between the CCS-curve of a given wind speed and the given fetch or duration line, respectively. By this, theoretically, the wave spectrum is cut off abruptly at a given maximum period, T_i (or minimum frequency, f_i) without considering possible wave components with periods a little longer than $T_i = 1/f_i$, which are just in the beginning stage of development. These wave components probably have a small amplitude, and contribute so small amounts of energy to the total wave energy that they may be neglected in most practical cases of wave forecasting.

JAMES (1954) checked Neumann's theory by comparing it with ocean wave records and obtained very satisfactory results; the results found by

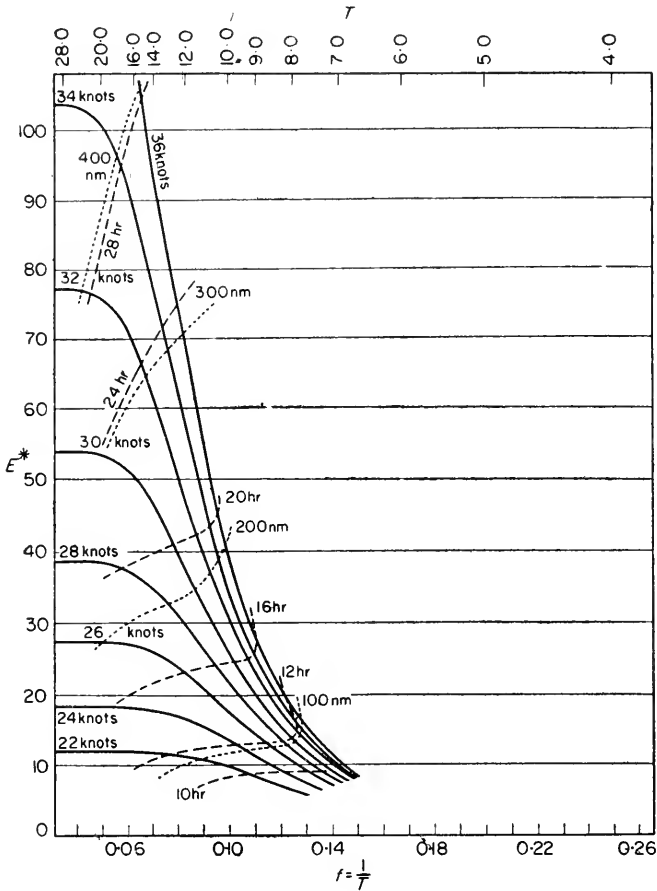


FIG. 43a. Duration and fetch graph for wind speeds from 22–36 knots as a function of duration and fetch respectively. -----, isolines for duration in hours; ······, isolines for fetch in nautical miles.

RATTRAY and BURT (1956), however, who studied the wave heights in a storm weather situation, are not so good, so that it is not possible to form a final judgement.

The investigations by DARBYSHIRE (1952) are based on direct measurements of the development of wind sea spectra off the British west coasts and in lakes. He found empirical relations between wind and waves for fully arisen sea as well as for the times of generation with different duration and fetch. The basic assumption of the physical relations is the following: there is no energy exchange between the different wave components of the spectrum, so that they progress independent of one another, with the corresponding

group velocity $c_g = \frac{1}{2}c$ and grow by wind. One of the main results of Darbyshire's is that the wave spectrum is fully arisen already after a fetch of 200–300 nm, with the longest wave period of the spectrum being, in sec, $\frac{1}{3}v_g$, where v_g means the maximum gradient wind speed. The period of the highest waves is $T_{\max} = \frac{1}{4}v_g$ and the steepness of the higher waves $d_{\max} \sim 1/11 v_g$. All results are summarized in an amplitude spectrum containing the stages of generation and the fully arisen waves

$$[h(\sigma)]^2 = \frac{8\pi^2 C'}{\sigma^4} \exp \left\{ -2.0 \left[\frac{2\pi g}{\sigma v_g} - 4.6(1 + 1.25 \times 10^{-4}F)(1 - e^{-0.231F}) \right]^2 \right\}. \quad (\text{IV.43})$$

In this equation v_g is the gradient wind speed and F the fetch in nm. For great values of F the equation gives the simple energy spectrum of the fully arisen sea, the wind speed v at the sea surface is $0.667 v_g$. The constant C' was found to be $22 \text{ cm}^2 \text{ sec}^{-2}$. In general, the theory of Darbyshire seems to be verified by the observations. In some cases there will be differences in the results gained from Neumann's and Darbyshire's theories. The reason for these differences will probably be the fact that each theory assumes an entirely different mechanism of wave generation by wind. As mentioned above, in Darbyshire's theory each component of the wave spectrum grows independently of the other components present; whereas Neumann assumes that after the beginning of wind action short-period steep waves develop from the initial waves which soon break up, that is, become unstable. They are run under by the longer waves and in part give their kinetic and potential energy to the longer waves. After this stage and with sufficiently long duration and fetch long waves develop, which progress with the wind speed. After Neumann, the longer waves will appear and grow only after the shorter ones are fully arisen. These discrepancies between the two conceptions will be settled only by further research.

7. Swell, Observations and Theory

(a) Observations on the Propagation of Swell

A strong wave motion, generated by a storm of long duration, travels from the generating area with a great velocity. Alteration of the wave profile transforms the wind-sea into a swell. As soon as the wind decreases in force, the waves change their shape quite characteristically. The irregularities in form in the wave profile smooth out, the shorter wave disturbances vanish first and only the waves of greater height and length remain. This is the swell, where the waves are not any longer subjected to action of the wind ($U < c$). In a system of waves of different lengths, the waves of greater wave length move with a greater velocity than the shorter ones. One can observe how these smaller waves apparently climb backwards to the crests of the large waves. Finally, only the large waves remain and the wave trains acquire shapes

with long crests and almost straight fronts. This is a well-developed swell, propagating in its original direction independently of the wind.

In the area of generation the ratio between wave height H and wave length λ is about 1:20, and occasionally 1:10; according to COUNT VON LARISCH (1925), this ratio is for swell 1:30 to 1:100; great wave lengths and small heights are predominant and round trochoidal profiles are their characteristic shape (see Table 8). The stereophotogrammetric picture one sees is a mixture of waves of the most varied wave lengths, which last only a short time, on account of the different velocities of its components. The long waves, with their greater velocity, rapidly leave the wind area and the long waves with small height dominate entirely in the swell. Owing to the smaller energy per unit area the short-crested waves will be destroyed more rapidly by friction and by turbulence. Photogrammetrical pictures have confirmed that waves with great wave length are also present in the generation area. In the storm area they become inconspicuous because of the usually steeper and chopped waves.

A wave group can be represented by the superposition of two normal wave trains of nearly equal wave length. The phenomena of the reappearance of particularly high wave crests (see p. 13) can also be explained in this manner. Such a superposition is graphically illustrated in Fig. 6. It shows the wave composed of "wave groups" alternating with smooth surfaces, where the amplitude of the wave decreases to zero. Figure 44 reproduces the

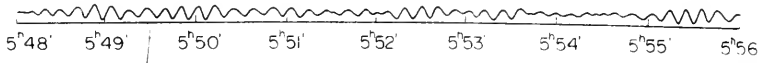


FIG. 44. Registration of waves on a "Petravic" pendulum. "Meteor", 30 March 1925.

records of a "Petravic" pendulum which registered the approaching waves aboard the "Meteor" while the engines were stopped. The wave groups present can easily be represented by the interference of two wave systems of nearly the same wavelength (see also Fig. 22).

The simple theory of interferences cannot explain all phenomena relative to wave groups, for instance, the question how it is possible that a field of waves continues to travel after the generating force has ceased to exist.

Swell is particularly characteristic in the trade wind regions, where in the winter months of the respective hemispheres it grows to considerable proportions. It always comes from the poles and originates in the storm areas which cross from west to east the higher mid-latitudes. When a large storm area remains for some time over a region at sea or travels slowly eastward, enormous wind-seas develop mostly on the backward side of the depressions. These waves are very long; consequently, they travel with great velocity towards lower latitudes, and will reach eventually the polar boundary

of the tradewind region, which they penetrate sometimes. Strong swells have been observed to cross the whole region of the tradewinds and penetrate into the equatorial calm zone, and even into the tradewind area of the other hemisphere. This occurs in the North Atlantic Ocean, where the swell generated by the north-westerly storms of the moderate latitudes travels across the zone of the north-east tradewind and the equatorial regions of calm air into the region of south-east tradewind. For instance on Ascension Island (8°S. lat.) and even on St. Helena (16°S. lat.), there is sometimes a strong surf (the famous “rollers”) from a swell generated about 4000 nautical miles distance. If the storm waves have an original wave length of 150 m and keep up their original velocity of 15 m/sec, they can travel the distance of 4000 miles within 137 h = 5 days and 17 h. This time, however, will be shorter, as the wave velocity increases with the increase of the wave length.

In the same way, the imposing swell causing the constant surf at the coast of Guinea (the Kalema) originates from a region near Tristan de Cunha in the moderate latitudes of the southern hemisphere. It consists of very long waves, whose average period in a series of 60 waves was 15.1 sec with extreme values of 6 and 24 sec. The waves, therefore, had the enormous length of 350 m and travelled with a velocity of 23½ m/sec; they only need 1 day for 1100 miles and only 2-3 days to reach the coast of French Guinea.

The swell in the trade-wind region of the North Atlantic Ocean and the surf on St. Helena are correlated to the north-westerly storms of the North Atlantic Ocean, as shown by the comparison of their monthly variations.

Table 13. Yearly number of breakers at St. Helena and number of storms in North Atlantic Ocean

Month	July	Aug.	Sept.	Oct.	Nov.	Dec.	Jan.	Feb.	March	Apr.	May	June
Breakers (1856-75)	3	2	1	7	25	43	62	100	40	9	1	5
N.W. storms	2	5	15	23	45	90	100	68	65	35	8	2
All storms	2.1	2.1	4.3	8.0	13.2	16.2	19.3	19.3	17.9	11.8	4.1	2.0

Table 13 gives the official computation of the rollers on St. Helena during 20 years from 1856 to 1875 and the frequencies of the north-westerly storms in the North Atlantic Ocean north of 25° N. lat. registered by Toynbee (KRUEMEL 1911, vol II, p. 116); the same table includes the yearly course of storms in the region 30°-50°N., 70°-30°W. in the North Atlantic. The maximum frequency of the rollers respectively of the north-westerly storms has here been given the value 100; the general distribution

of storms according to the maps of the Atlantic Ocean of the German Seewarte is given in per cent of all observations. In the equatorial area of calms there is generally a strong north-westerly swell in the northern winter and spring, which is a consequence of the winter gales in the northern hemisphere, whereas in summer the swell is more from the south and the south-west, which are caused by wintery storms in the high latitudes of the southern hemisphere.

The behaviour of swells on the European coast has been observed by CORNISH (1910); he found that wave lengths of a very long period (12–20 sec) are not exceptional; once he found an average period of 22.5 sec, which would correspond to a wave length of more than 1200 m in the open ocean. Thorade once observed, from gauge recordings in Heligoland, waves with a period of about 15 sec.

There is as yet no absolute certainty as to whether the large waves of the swell are already present in the storm area, and concealed there by the amplitudes of the stronger wind-sea; according to Poisson and Cauchy's theory, it is not right to deduct the wavelength of the wave in the generating area from the length and period of the waves in the swell; it was found that the wave length increases considerably as the waves travel (p. 68, Fig. 36).

The relation between a swell and the storm-waves which generated it, has been investigated more or less successfully in some special cases. Krümmel reports a few interesting cases in the southern part of the Indian Ocean (Pâris) and in the southern Atlantic Ocean (Gassenmayer) in which it is quite probable that there really was a connection between these two phenomena. He investigated more thoroughly in a synoptical way several cases in the North Atlantic Ocean by drawing charts of the state of the waves based on the diary of the German Seewarte. Observations were made during the international wave week held from 14th to 19th November, 1938, in the northern Atlantic Ocean. A synoptical presentation of the observations for each day at 12 G.M.T. was given by Keyser. Figure 45 gives a simplified example of these charts; it shows the distribution of the swells for the entire northern Atlantic Ocean for the 15th of November. This chart shows also the distribution of pressure at the ocean surface; however, the winds have been omitted, in order not to clutter up the picture. They can be derived with sufficient accuracy from the pressure distribution. The direction and the force of the swell according to the Douglas scale is given for each separate position of the ships. An attempt was made to draw from these values the wave fronts of the existing swell. One wave-train spreads from the western North Atlantic to the north-east, thereby increasing in force. A second wave-train covers the eastern part of the ocean and spreads to the south-east almost perpendicularly to the first one. The first wave-train is probably the result of an extensive low-pressure region, which on November 14th travelled rapidly eastward from northern North America and which was on 15th November with its centre above the Davis Strait. The second

wave-train is the remainder of a strong swell which developed on the southern side of a cyclone which moved towards the British Isles, thereby decreasing in force. Simultaneously the force of the swell decreased.

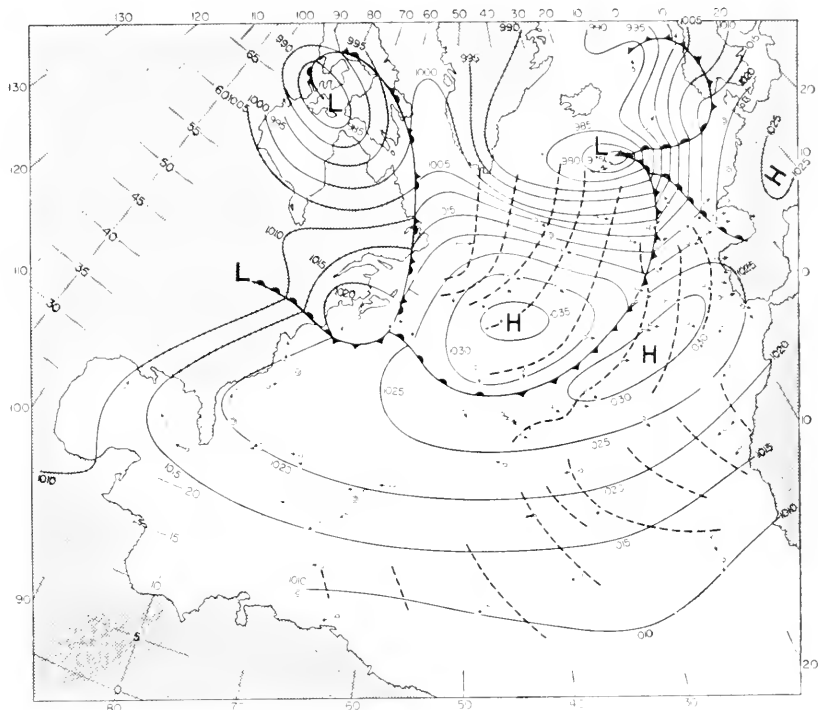


FIG. 45. Swell in North Atlantic 15 November 1938, 12h G.M.T. (Keyser).

Particularly interesting is the study of the propagation of a strong swell which started at the end of February 1886 from a storm area south of Newfoundland (40°N. , 55°W.) and which could be followed, according to the ships logs, right across the subtropical and tropical Atlantic Ocean to the coast of Ascension Island (March 1886). This study allows some insight into the behaviour of swells during such a long travel over large oceanic areas. The main results have been summarized in Table 14. Seven reliable time measurements, recorded in the ships logs, permitted to follow a particularly high wave-train in its progress through the trade-wind region. The distances have been measured from the assumed centre of the hurricane (on 25th February) in 40°N. , 55°W. along the great circle. Even though the time of the start for determining the "age of the swell" is uncertain, the time differences between the observations of the individual ships are probably dependable. The velocity computed from these observations is approximately 30 n.m. per hour at the start, increasing then to $41\frac{1}{2}$, and off Ascension it was

48½ n.m. per hour. The wind-sea might have had periods of 8, maximum 9 sec i.e. velocities of 24 to 27 n.m. per hour in the storm region, and the velocity of propagation of the swell can be assumed to have been accelerated with increasing age. Thorade wanting a more precise answer to this question has submitted the values of Table 14 to an analysis by the method of the least squares and found that the observations are in somewhat better

Table 14. Tracking a heavy North Atlantic swell from 25th February to 1st March 1886

Ship	Longitude N.	Latitude W.	Distance miles nautical	Time of observation		Age of the swell (h)	Velocity computed from age of the swell (m/sec)
				Day	Hour		
Start	40°	55°	0	25 Feb.	—	—	
“Terpsichore”	16° 22′	38° 1′	1670	27 Feb.	16h	49	18.6
“Ida”	8° 57′	35° 40′	2130	28 Feb.	12h	69	21.1
“Sakkarah”	14° 7′	26° 0′	2170	28 Feb.	12h	70	21.2
“Johanna”	8° 12′	31° 3′	2300	28 Feb.	10h	68	20.9
“Pernambuco”	10° 8′	27° 43′	2310	28 Feb.	12h	70	21.2
“Moltke”	6° 45′	31° 14′	2370	28 Feb.	14h	72	21.4
“Strassburg”	7° 37′	26° 35′	2470	28 Feb.	16h	78	22.2
“Buccaneer”	7° 50′ S	14° 27′	3640	1 Mar.	22h	102	25.0

agreement with the hypothesis of accelerated progression of the Poisson-Cauchy theory than the hypothesis of uniform velocity. Unfortunately, *no other similar cases* are available for a check on the theory, although the observations for this could probably be found in the ship journals. The questions, how swell propagates in the ocean, how their wavelength and period increase in progressing belonged until recently to the unsolved problems of ocean waves. Thanks to the new theory of SVERDRUP and MUNK (1947), we now know more about the development of the swell, even though the observations along this line still leave very much to be desired.

(b) *Theory for the Decay of Waves and Application of Same to the Swell*

In order to survey the values characteristic of the swell, it will be suitable to realize the conditions as given by Fig. 46*a*. At the point *P* a swell is observed whose characteristic wave values are H_D and T_D , while t_D is the time of occurrence. This swell component comes from the point *A* on the windward side of the area of wave generation with a fetch *F* and a width *B*. The lateral spreading is given by the angle θ , and at the time $t = 0$ the wave values in *A* are H_F and T_F . The problem of the swell consists in computing the transformation of the waves outside their area of generation.

After the waves have left the generating area, they travel through a region of calm, where the wind velocity is small compared to the wave velocity. The waves receive no energy by normal pressures but, on the contrary, air resistance causes a loss of energy. According to the equation (IV.25*b*), this loss of energy per unit area equals

$$R_N = -\frac{\rho_0 g}{2} \kappa^2 A^2 c^3 = -\frac{\rho_0 g}{8} g^2 H^2 c^{-1}, \quad (\text{IV.43})$$

the transfer of energy due to tangential stress of the wind can be neglected ($R_T = 0$).

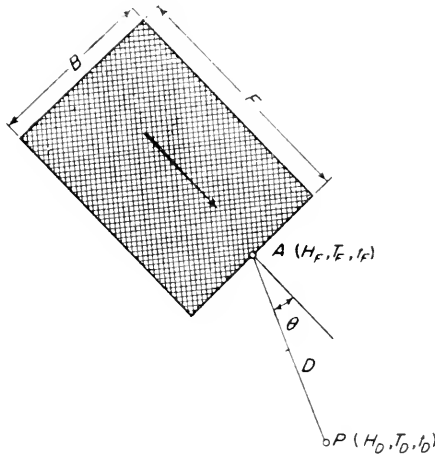


FIG. 46a. Registration of swell.

The swell composed of different wave systems can now be explained by means of the significant waves. The theory of Sverdrup and Munk for the decay of waves is closely related to the theory of the growth of waves and thus explains for the first time, on a general physical basis, this important phenomenon of ocean waves. The differential equation for the change of wave velocity with propagation of the wave is simplified and can be solved without introducing other hypotheses and constants. The most important results is that the period of the waves increases with increasing distance from the end of the fetch, whereas the wave height decreases simultaneously. The distance is called the distance of decay D . The theory shows that the ratio between the period at the end of the decay distance and the period at the end of the fetch $T_D:T_F$, and the ratio between the corresponding wave heights $H_D:H_F$, as well as the ratio between the travel time and the period at the end of the fetch $t_D:T_F$ can be represented as functions of the same non-dimensional parameter D/gT_F^2 . The observations then available to Sver-

drup and Munk were but sparse and unreliable, but in the main they confirm the theoretical results. The theory clearly shows that, while the swell waves travel from the storm area, the period, wave length and velocity of propagation increase and the wave height decreases. Later on, SVERDRUP (1947*a*) completed his theory. Assuming that swell generally has the same characteristics as the waves in the generating area, it is shown that the air resistance which the swell encounters leads to a selective dissipation. The energy associated with the shorter period waves is dissipated more rapidly than that of longer period waves, and consequently the energy maximum shifts toward longer periods, that is, the period of the significant waves increases. The effect is modified by following or opposing winds. Numerical examples are in satisfactory agreement with results from the formerly semi-empirical graphs.

This result was fully confirmed by DARBYSHIRE (1952). Using his wave spectrum and introducing a coefficient of friction proportional to the wave steepness (see p. 87), he explained the transformation of swell waves by the different extinction of the spectral components progressing independently of one another. This extinction is due to the air resistance. GROEN and DORRESTEIN (1950), and later BOWDEN (1950), give a completely different explanation for the energy loss of swell waves. The former regard the turbulence friction as the main cause of the loss of energy, and take the *turbulence coefficients* to be proportional to the $4/3$ power of the wave length (after VON WEIZSÄCKER, vol. I no. 1), while Bowden takes them to be proportional to the velocity and amplitude of the waves. Both assumptions are capable of explaining completely the transformation of swell waves. It was not possible to decide whether this transformation is due more to air resistance or to turbulence friction. This fact will not be changed by the application of a refined method by GROEN (1954). It was also possible to prove that the tidal currents exercise an influence on the swell waves (DEACON, 1949; DARBYSHIRE, 1952).

Hitherto, only the influence of air resistance and of turbulent friction has been discussed. We shall now deal with the influence of *dispersion* on the transformation of swell waves. Since long waves progress faster than shorter waves, the wave spectrum of a wave pack will gradually change. The apparent wave period of the swell must increase with time with increasing fetch whereas at a fixed point the period decreases. At the same time the dispersion requires a decrease in wave energy. This leads to a reduction of the heights of significant waves. The first study of the transformation of swell waves on the basis of the effect of dispersion was made by BREIT-SCHNEIDER (1952), who started out from the wave values of significant waves. He wants to determine, on the one hand, the dependence of the wave heights of a swell H_D upon the fetch F , upon the height of the wind-sea at the end of the wind-field and upon the decay distance, and, on the other hand, the dependence of the period T_D upon the fetch, upon the period of the wind-

sea T_F and upon the decay distance. The results were given in the form of dimensionless parameters which can be checked against the observations. The conclusions drawn confirm what had been expected from qualitative considerations: For a given wave period T_F and a decay distance D the increase of the period and the decrease of the height of a swell are the greater the shorter is the fetch. These conclusions are more comprehensive than those of SVERDRUP and MUNK, who investigated only the influence of T_F and D . Besides, the graphs show that the theoretical results fit the observations only in part, which is not surprising if one regards the simultaneous influence of so many factors.

PIERSON, NEUMANN and JAMES (1952, 1953) have treated this problem in an entirely different way. Based on the energy spectrum of short-crested wind generated waves, they try to solve the influence of dispersion and of lateral angular spreading. For the case of a *line-shaped* source of wave generation, having a width B , Fig. 46b gives the quantities used. T_1 designates

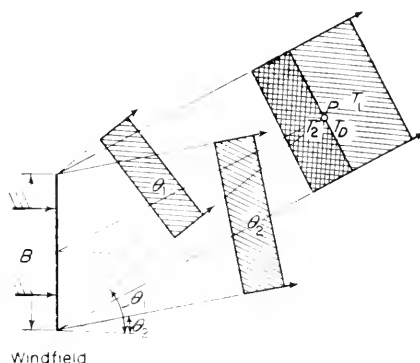


FIG. 46b. Registration of a swell filter in a linear area of wave origin. P point of observation of swell.

the period of those waves which have just passed the point of observation P at the time t_D , T_2 the period of the waves which just reach P at the time t_D . θ_1 and θ_2 are the angles of propagation of those waves which just pass “above” and “below” P . Using the group velocity for each period, T_1 can be computed from the duration of the emission of such waves from the source, θ_1 and θ_2 from the width B . The wave periods and directions existing in P at the time t_D are between T_1 and T_2 and θ_1 and θ_2 , respectively. The formerly broad energy spectrum is contracted into a narrow spectral band of the swell in P at the time t_D . The entire process is similar to the effect of a *filter*. The period range of the swell can be determined by applying this method to the energy

spectrum of the wind generated sea; then it is possible to compute the structure of the swell at any place. With increasing distance between P and the wave source the frequency band and the scope of the direction of the swell will become narrower, the crests longer and the periods more uniform. Therefore, the principal features of "old swells" can be easily understood. This theory by Pierson, Neumann and James seems to give a correct interpretation of the development of swells and, together with the above considerations, will give an insight into this kind of ocean waves.

Chapter V

Shallow Water Waves and Their Transformation through External Factors; Surf

SURFACE or short waves generated by wind on deep water travel eventually on to shallow water, where their profile changes when the depth becomes equal to the wave length.

In order to understand the phenomena accompanying this transformation, it is necessary to deal first with the theory of the shallow water waves, that is with waves whose vertical motions, in shallow water, can no longer be regarded as small in relation to their horizontal motions.

1. Shallow Water Waves; Theory and Observations

As shown in the second chapter (see p. 16) there is a gap between surface waves and tidal waves which is filled by waves where the water depth varies between $\frac{1}{10}$ to $\frac{1}{2}$ of the wave length. The orbits of the single water particles in such waves are flat ellipses, whose vertical axes become gradually smaller until they vanish at the bottom, where the ellipses degenerate into straight lines. Figure 8 shows the wave profile and the position of the line of particles which is vertical at rest. The velocity of propagation of such waves is given by equation (II.10), and the middle section of Fig. 9 shows its relation to the ratio $h:\lambda$. The extreme values in either direction are the well-known equation for the velocity of surface or deep water waves $c = \sqrt{g/\lambda}$ and for the long waves of small amplitudes $c = \sqrt{g/h}$. In a first approximation the wave profile, for small amplitudes in shallow water, is very similar to a harmonic form, but with large amplitudes the profile changes differently for small and great depths. A short time ago, STRUIK (1926, p. 595) was able to prove, by using a similar analysis as used by LEVI-CIVITA (1925) for deep water waves, that waves of a permanent type are possible in shallow water. However, it is not yet known how the waves are generated and maintained. KORTEWEG and DE VRIES (1895, p. 422) developed a theory of a system of oscillatory waves of finite height in a canal of limited depth. It gives wave profiles with steep crests and wide troughs as they are regularly encountered in rather high shallow water waves. Regarding the theory of these waves, we refer to LAMB'S *Hydrodynamics* (1932, para. 253, p. 426).

The wave profile of these cnoidal waves has the form

$$\eta = 2A \operatorname{cn}^2 \left(2K \frac{x}{\lambda} \right), \tag{V.1}$$

in which cn represents the Jacobi elliptical function and K the complete elliptic integral of the first kind. The module k is computed from the relation

$$\frac{\lambda}{h} \sqrt{\frac{2A}{h}} = \frac{4Kk}{1-3}, \tag{V.2}$$

where h is the depth (from wave trough to bottom) and $2A$ the wave height measured from trough to crest. We can replace the module k by $\sin \alpha$. For $\alpha = 0$, $k = 0$ and for small values of λ we obtain in a first approximation sine waves, which means a harmonic wave profile in the sense of the Stokes theory. If, on the other hand, $\alpha = 90^\circ$, then $k = 1$ and, with $K = \infty$, $\lambda = \infty$. The wave profile nears a sech-function and thus corresponds to that of the solitary wave (p. 116). The theory of Korteweg and de Vries is important because it bridges the gap between “long” and “short” waves.

To test the theory on observed waves, THORADE (1931, p. 183) proceeded as follows: From the observed wave length λ and the values h and A the value at the left side of (V.2) is computed. From Table 15 or from a graphical presentation the auxiliary angle α is obtained. With this value we find in the Table on p. 134 of functions by JANNKE and EMDE (1933) the numerical

Table 15. For determining cnoidal wave profiles

$\frac{\lambda}{h} \sqrt{\frac{2A}{h}}$	α°	$\frac{\lambda}{h} \sqrt{\frac{2A}{h}}$	α°	$\frac{\lambda}{h} \sqrt{\frac{2A}{h}}$	α°	$\frac{\lambda}{h} \sqrt{\frac{2A}{h}}$	α°
0.32	5°	2.29	35°	4.83	65°	7.71	82°
0.63	10	2.66	40	5.44	70	8.39	84
0.95	15	3.03	45	5.78	72½	9.35	86
1.28	20	3.42	50	6.18	75	10.1	87
1.61	25	3.85	55	6.62	77½	10.9	88
1.95	30	4.31	60	7.17	80	12.5	89

values of the elliptic integral $F(k, \varphi)$ for $\varphi = 1^\circ, 2^\circ, \dots, 90^\circ$, where $F(k, \frac{1}{2}\pi) = K$. We then obtain the values of x corresponding to each φ from $x = (\lambda/2K) \cdot F(k, \varphi)$ and then $\eta = 2A \cos^2 \varphi$.

Figure 47 gives for standard waves $\lambda = 1$ and $2A = 1$ the corresponding wave profiles for several values of α between 10° and 89° . With a constant wave length and a constant wave height, α approaches rapidly the limit of 90° with decreasing depth, and the wave crests become narrower and steeper, the wave troughs wider and flatter. If $\alpha = 89^\circ$, the wave train

consists almost exclusively of narrow, steep wave crests, separated by a stretch of almost smooth surface. Such degenerated waves have sometimes really been observed in shallow water (for $\lambda = 50$ m, a wave height of 4 m, and

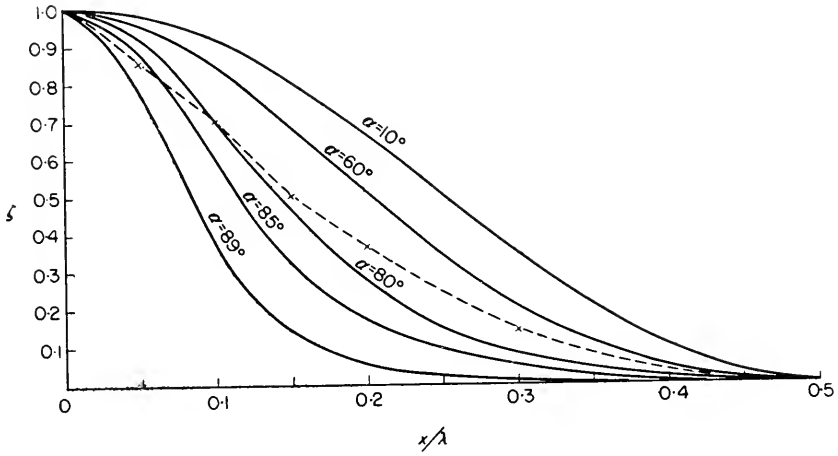


FIG. 47. Cnoidal wave profiles for several water depths, wave lengths and wave heights (+ values for the normalized four half wave lengths of 24 February and 6 September 1911 near Heligoland).

a depth below the wave trough of 4 m, α becomes indeed 89°). Thorade has computed wave profiles for different kinds of shallow water waves, which are reproduced in Fig. 48. It shows that like cnoidal waves, there is a steepen-

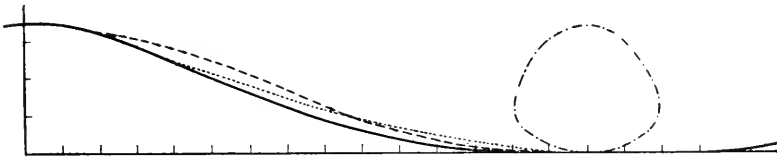


FIG. 48. Theoretical profiles of different kind of long waves (Thorade) (Height scale doubled). ----, sinus wave after Laplace-Airy (Stokes's wave); ·····, waves according to Stokes-Struik; —, cnoidal waves by Korteweg de Vries; - - - - , orbit of *cn* waves (normal height scale).

ing of the wave crests and a widening of the wave troughs. The orbit of the *cn* waves is pointed at the top; it remains in this form of the orbits derived by Kohlschuetter from the wave pictures taken on the "Planet" Expedition (see p. 49), Figs. 29 and 30. The Struik wave shows a pointed crest about the same as the *cn* wave, but a flatter trough. The velocity of propagation of the *cn* waves is given by

$$c = \sqrt{gh} \left[1 + \frac{A}{2k^2h} \left(1 - \frac{E}{K} \right) \right], \tag{V.3}$$

in which K and E are the complete elliptic integrals of 1st and 2nd kind; the deviation from the Lagrangian value $\int (gh)$ is very small for great wave lengths.

The extensive and detailed experiments of the WEBER brothers (1825) in their inadequate wave tank have been partly used by Thorade to attempt a test of the theory. It has, however, been found that they do not suffice to answer all problems. Most of the experimental series deal with shallow water waves. Their velocity of propagation should correspond to the equation of Laplace (p. 18) $c = \int (8/\pi) \tanh^2 zh$. In the case of long waves, they would have to conform to the equation by Lagrange $c = \int (gh)$. KRÜMMEL (1911, vol. II, p. 22) has given the comparison with the values of Lagrange, whereas Thorade (1931, p. 189) has given the comparison with the Lagrangian values.

Table 16 gives a comparison between these observed values in the tanks and velocities computed according to the equations by Laplace and Lagrange. We can see that for increasing depth the Laplace formula is in better agreement with observations.

Table 16. *Shallow water wave in Weber's wave tank*

Depth (h) cm		2.7	5.4	8.1	10.8	16.2
Wave length (cm)		27	68	81	95	119
Wave Velocity (cm sec)	Observed	55	76	85	90	94
		Computed to				
	Lagrange	52	73	89	103	126
	Laplace	48	70	84	95	113

A more recent long series of observations has been made from the Scripps Institute of Oceanography at La Jolla (California), and Fig. 49 is a com-

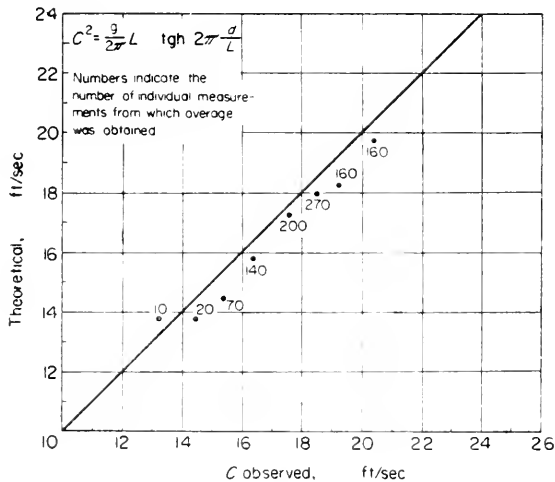


FIG. 49. Observed and computed wave velocities in shallow water from observations at the pier of the Scripps Institute of Oceanography, La Jolla, California.

parison between observed values and the wave velocity calculated according to the Laplace formula. The observations were grouped to eliminate random observational errors. The agreement is good, notwithstanding a slight tendency of the observed wave velocities to exceed the theoretical ones. However, deviations are small.

A few good stereophotogrammetric wave pictures made by ECKHARDT (1931) for the construction of the harbour of Heligoland, can be used for testing the theoretical results. Those taken on 24 February and 6 November, 1911 are particularly remarkable. Figure 50 shows in the first series of pictures a partial section of the wave plane south-west of the western breakwater, where the wave-train is not yet disturbed by the harbour construction. More to the north, there was a rather strong shock surf against the breakwater. From both series of pictures an average wave-train was derived, for an appropriate zone (in the first case over a width of 200 m, in the latter case over a width of 450 m) by drawing longitudinal profiles, if possible perpendicular to the wave crests and by averaging same. This could be done, in view of the very uniform waves in the area. Small irregularities were thus eliminated and a good wave profile obtained. Figures 51 and 52 give these

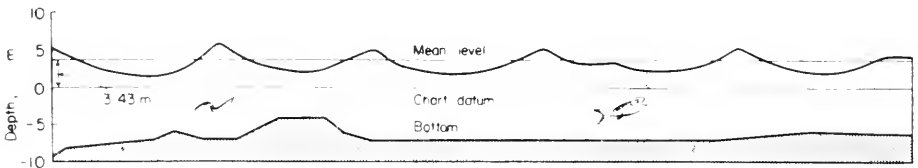


FIG. 51. Average from five wave profiles taken from a stereo photogrammetric picture 24 February, 1911 South-west of East Heligoland breakwater. Wind: W.N.W., 17–20 m/sec. When picture was taken mean water level was +3.43 over zero level. Average wave length: $114 \text{ m} \pm 8 \text{ m}$; average wave height: 3.32 m; wave velocity: 10–12.5 m/sec (height scale 1:5.1).

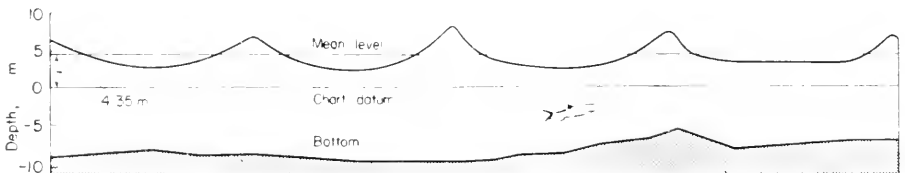


FIG. 52. Average from ten wave profiles on 6 November, 1911, same location as Fig. 51. Wind: W. 18–20 m/sec; Mean water level was +4.35 m over zero level. Average wave length: $143 \pm 10 \text{ m}$; Average wave height: 4.5 m; Wave velocity: 10–15 m/sec (height scale 1:5.1).

typical average waves for both cases, and also all the data necessary for their use. The average wave length and the average wave height were in the first case 114 and 3.32 m, in the latter one 143 and 4.5 m. The graphs show the typical profile of the shallow-water waves with the sharp crests and the wide flat wave troughs; also that in travelling the wave length increases somewhat: in the first case from about 110 to 133 m (except the last wave,

which appears to be disturbed in its length), in the latter case from 136 to 153 m. In both cases the depth decreases in the direction of propagation from about 8 to 6 m, and 9 to 7 m respectively, except for a small elevation of the ocean bottom up to a depth of 4 m underneath the second wave trough in the first case, and a larger elevation up to a depth of 6 m beneath the fourth crest in the second case. The profile keeps its form, but during its travel the crest becomes sharper on both sides. The trough is very flat and in many localities the wave trough is practically level over a large surface. This flattening shows particularly well in the median waves in the second case; the last wave has an absolutely flat trough.

To test the theory, the first four half waves were averaged. These average wave profiles are shown in Fig. 53. To compute the cnoidal wave profiles,

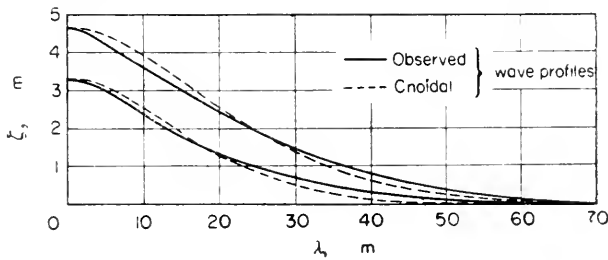


FIG. 53. Comparison between observed and cnoidal wave profiles. Upper figure: 6 November, 1911; lower figure: 24 February, 1911; Average values of four half wave lengths. -----, cnoidal wave profile; ———, observed wave profile.

we have the following value: $\frac{1}{2}\lambda = 57.0$, and 71.5 m respectively, and for $2A = 3.32$ and 4.67 m respectively; then we take $h = 9.5$ and 12.5 m respectively (from below the wave trough), so that in both cases α becomes $77\frac{1}{2}^\circ$. The computed cnoidal wave profiles have been entered in the figure as dotted lines. They correspond fairly well with the observed wave profile, but in both cases we find the same systematical deviation: in the upper part of the wave slope the computed profile is above, while in the lower part it is below the observed curve. The deviations are not very large, but characteristic. If we vary α , we still have the same deviations. As Fig. 47 shows, the values of α in the crest are larger than 80° , whereas in the wave trough they are about 65° and 60° . The last wave in Fig. 52 fits pretty well $\alpha = 88^\circ$, but would require for a wave length of 153 m and a wave height of 3.4 m a water depth underneath the wave trough of 8.75 m. The observed water depth varies between 7.7 and 9.7 m, with an average of 8.7 m, which corresponds to the theoretical value.

According to equation (V.3), the velocity of propagation is in the first case $c = 10.56$ m/sec, in the second case $c = 12.18$ m/sec. The observed values are not accurate and are not comparable to the theoretical values; the values do fit the Laplace equations better than the equations of Lagrange.

GAILLARD (1924) derived from 533 waves of very different amplitudes that Stokes's equation (II.10) is valid. He also pointed out that, with decreasing depth the wave length decreases, which causes a decrease in the wave velocity. If the bottom slopes up very slightly, he found that the empirical formula

$$\frac{c_1}{c_2} = 0.9 \sqrt{\frac{h_1}{h_2}}$$

is applicable, in which c_1 and c_2 represent the velocity of the same wave corresponding to a depth h_1 and to the shallower depth h_2 . We can see that in shallow water waves the cnoidal waves represent quite well the actual waves.

2. The Solitary Wave of Scott Russell

SCOTT RUSSELL (1845, p. 311) during his experiments in wave tanks (6.10 m long, 30.5 cm wide, rectangular basin), found a particular type of wave, which he called the solitary wave. The wave was generated on one end of the tank, ran through it and was reflected on the other end. He repeated this reflection 60 times, and he could, in this way, observe the wave over a length of 360 m. This wave consists of a single elevation, of a height not necessarily small as compared with the depth and which, if properly started, may travel for a considerable distance along a uniform canal with little or no change of type. The velocity of propagation of this wave is constant and is given by

$$c = \sqrt{g(h+a)} \quad (\text{V.4})$$

in which a is the height of the wave crest (the maximum elevation above the undisturbed level). Scott Russell considers the wave profile a trochoid.

It has been tried to generate waves which consisted only of a wave trough, having the same amplitude as the solitary crest. However, the experiments were unsuccessful and the wave thus generated always broke up in shorter waves after a relatively short time.

BAZIN (1865) confirmed the results obtained by Scott Russell by experimenting in two long canals of rectangular shape, one 450 m long, 1.99 m wide, 1.95 m deep, and also in another canal 500 m long, 6.5 m wide and 2.4 m deep. He also found that the form of the wave profile was quite permanent and that the wave velocity was expressed correctly by equation (V.4). Even if the water is in motion, equation (V.4) is valid, if we take the wave velocity relative to the velocity of the water. If we have waves travelling in a direction opposite to the current, we get a change in the wave profile, and finally the wave breaks up. According to Scott Russell, this would happen when $h = a$, but Bazin found that it happens a little earlier.

BOUSSINESQ (1871, 1877) and RAYLEIGH (1876, p. 257) have developed independent theories on the solitary wave in which they considered the vertical

velocity component. Scott Russell's solitary wave may be regarded as an extreme case of Stokes's oscillatory wave of permanent type, the wave length being great compared with the depth of the canal. The theory showed that the wave profile is not a trochoid as assumed by Scott Russell, but given by the formula

$$\eta = a \operatorname{sech}^2 \frac{x}{2b}, \tag{V.41}$$

in which b is a quantity depending on the wave height A and the depth h . Figure 54 shows the wave profile of the solitary wave and the theoretical wave

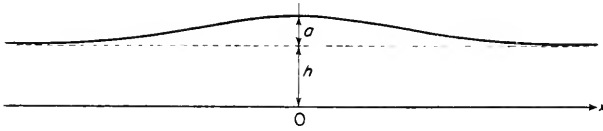


FIG. 54. Profile of the solitary wave.

line according to equation (V.4). With increasing wave amplitudes the agreement is not so good now. MC COWAN (1891) found sharper pointed crests. The waves are no longer permanent, and the limiting value of the waves a/h was found to be $0.68 h$, in which case the velocity is given by $c^2 = 1.56 gh$ (see also MICHELL, 1893; and GYWGHTER, 1900).

The theory of the solitary wave starts as usual with the equations of motion

$$\frac{du}{dt} = -\frac{1}{\rho} \frac{\partial p}{\partial x}, \quad \frac{dw}{dt} = -\frac{1}{\rho} \frac{\partial p}{\partial z} - g \tag{V.5}$$

and the equation of continuity

$$\frac{\partial u}{\partial x} + \frac{\partial w}{\partial z} = 0. \tag{V.6}$$

The origin of the co-ordinates is at the bottom of the ocean and η is the elevation of the water above the undisturbed level h . If U is the average horizontal velocity component in the whole water column of a height $h + \eta$, then we can give the equation of continuity the form

$$\frac{\partial \eta}{\partial t} + (h + \eta) \frac{\partial U}{\partial x} = 0, \tag{V.7}$$

in which

$$(h + \eta)U = \int_0^{h+\eta} u dz.$$

We can now integrate the second equation of motion from any level where there is a pressure p to the surface $z = h + \eta$, where the pressure $p = 0$. From the equation (V.6) we can obtain by integration from $z = 0$, where $w = 0$, to z

$$w = -\frac{\partial U}{\partial x} dz = \frac{z}{h + \eta} \frac{\partial \eta}{\partial t},$$

and from the integration of the second equation of motion we have

$$\frac{p}{\rho} = g(h + \eta - z) + \frac{(h + \eta)^2 - z^2}{2(h + \eta)} \frac{\partial^2 \eta}{\partial t^2}. \tag{V.8}$$

If we substitute this value for p in the first equation of motion (V.5) and if we integrate this relation over the whole water column from 0 until $h + \eta$, and neglecting small quantities, we obtain,

$$\frac{\partial U}{\partial t} + U \frac{\partial U}{\partial x} + g \frac{\partial \eta}{\partial x} + \frac{h}{3} \frac{\partial^3 \eta}{\partial x \partial t^2} = 0. \tag{V.9}$$

We can substitute for the time t the velocity of propagation c of the wave disturbance and if we give the disturbance the general form of $\eta = f(x - ct)$ and $U = F(x - ct)$, eliminating the first and second differential, we obtain

$$\frac{\partial U}{\partial t} = -c \frac{\partial U}{\partial x} \quad \text{and} \quad \frac{\partial^2 \eta}{\partial t^2} = c^2 \frac{\partial^2 \eta}{\partial x^2},$$

and equation (V.9) gives us

$$\frac{\partial}{\partial x} \left(cU - \frac{U^2}{2} - g\eta - \frac{c^2 h}{3} \frac{\partial^2 \eta}{\partial x^2} \right) = 0. \tag{V.10}$$

Since there were $\eta = 0$, also $U = 0$ the value between parentheses is always equal to 0, so that in general we have

$$cU - \frac{U^2}{2} - g\eta - \frac{c^2 h}{3} \frac{\partial^2 \eta}{\partial x^2} = 0. \tag{V.11}$$

We can eliminate U through the equation of continuity (V.7) and equation (V.10) and then have $U = [c/(h + \eta)]\eta$ and from equation (V.11) we obtain in first approximation

$$c^2 = gh \left[1 + \frac{3}{2} \frac{\eta}{h} + \frac{h^2}{3\eta} \frac{\partial^2 \eta}{\partial x^2} \right]. \tag{V.12}$$

This is the formula for the velocity of propagation of a wave disturbance η according to Bousinesq; this velocity is dependent on the wave form η and also on the curvature of the water surface. It is possible to get a wave profile η of the permanent type, and in which the influences of η and $\partial^2 \eta / \partial x^2$ cancel each other; the terms can then be replaced by a constant a . The velocity of propagation of the disturbance would then be $c = \sqrt{[gh(1 + a)]}$.

This condition would give a differential equation

$$\frac{\partial^2 \eta}{\partial x^2} + \frac{9\eta^2}{2h^3} - \frac{3a\eta}{h^2} = 0.$$

Multiplying this by $\partial \eta / \partial x$ and integrating, and assuming that the bottom of the wave is a horizontal straight line (for $\eta = 0$, $\partial \eta / \partial x = 0$) we obtain

$$\frac{\partial \eta}{\partial x} = \frac{\eta}{h} \sqrt{3 \left(a - \frac{\eta}{h} \right)}. \tag{V.13}$$

$\eta = a$ for the crest of the wave and here also $\partial \eta / \partial x$ must be equal to 0. This condition is satisfied if according to equation (V.13) $\eta = ah$. For the velocity of propagation of the wave we obtain

$$c = \sqrt{[g(h + a)]}. \tag{V.14}$$

This is the equation Scott Russell derived from his experiments. Except for $\eta = 0$ and for the value

derived from equation (V.13), the wave profile has no horizontal tangent, the wave disturbance consists of a single crest. The wave profile relative to the middle of the crest has the form

$$\eta = a \operatorname{sech}^2 \left(\frac{ct - x}{2} \cdot \sqrt{\frac{3a}{h^3}} \right). \tag{V.15}$$

For this wave profile (see Fig. 54) we have no definite “wave length”, but we can establish, an approximate wave extent by assuming the limit there where the elevation η is one-tenth of its maximum value. This will occur for $x_\lambda \sqrt{3a/h^3} = 3.636$; if $a = 2$ m and $h = 12$ m, the length of the wave disturbance will be 130 m. Boussinesq has shown that if the ratio a/h is small, the path of each particle is an arc of a parabola having its axis vertical and its apex upwards, when the solitary wave passes by. The wave disturbance is not periodic but there is a permanent displacement of the water particles, which is associated with mass transport. LAMB (1932), describes Lord Rayleigh’s derivation of the solitary wave. The result is slightly different, as we have to substitute in equation (V.15) the root $\sqrt{[h^2(h+a)]}$ for h^3 . The Rayleigh equation gives, therefore, for larger values of the ratio a/h flatter slopes, but the difference is not very considerable.

According to Lamb, the cnoidal waves of Korteweg and de Vries can be derived from the above-mentioned formulas. The equation (V.13) has the form

$$\left(\frac{\partial \eta}{\partial x} \right)^2 = \frac{3\eta^2}{h^2} \left(a - \frac{\eta}{h} \right) + C, \tag{V.16}$$

and the solitary wave requires that the constant C is equal to zero. However, in a general way C is different from 0, and the right side of this equation (V.16) must vanish, both for the wave crest and for the wave trough. This will give us a cubic equation of the form $\eta^3 - ah\eta^2 - \frac{1}{3}h^2C = 0$ which must have three real roots. As $a > 0$, this requires, as the discriminant shows, that $c < -4a^3/9$. As C is negative, the two roots $\eta_1 = a$ and $\eta_2 = b$ must be positive and the third one $\eta_3 = -ab/(a+b)$ negative. We then obtain easily

$$ah = \frac{a^2 + ab + b^2}{a + b} \quad \text{and} \quad C = -\frac{3a^2b^3}{h^3(a + b)}$$

and the equation (V.16) takes the form

$$\left(\frac{\partial \eta}{\partial x} \right)^2 = \frac{3}{h^3} (a - \eta)(\eta - b) \left(\eta + \frac{ab}{a - b} \right). \tag{V.17}$$

If we put $\eta = a \cos^2 \chi + b \sin^2 \chi$, we obtain from the integration the equation

$$\eta = b + (a - b)cn^2 \frac{2Kx}{\lambda}, \tag{V.18}$$

$$\operatorname{mod} k = \sqrt{\frac{a^2 - b^2}{a^2 + 2ab}}$$

At the same time we have

$$\lambda = 4K \sqrt{\frac{h^3(a + b)}{3(a^2 + 2ab)}} \quad \text{and} \quad c = \sqrt{[gh(1 + \epsilon)]}.$$

If we know the values of three out of the four quantities, h, a, b , and λ then we have determined mathematically the value of the fourth one. Equation (V.18) represents the cnoidal waves (equation V.1).

3. Changes in Form of Waves by Exterior Causes

When the wind increases in force, the wave crests become higher and sharper and the waves will show a tendency to break. We observe the formation of foam on the wave crests and this will occur with a wind force of about 4 Beaufort. This is so constant that the appearance of foam on the ocean is a characteristic for this wind force. If the wave height increases to the limit of the cycloid and above, the motion of the water particles in the wave crest becomes discontinuous, which will lead to the breaking of the wave crest and to the making of foam. But after the explanations of the preceding chapters, this usual explanation is not any longer valid. If wind velocity and wave height are not any longer in equilibrium (unsteady state) then with too great a wind we have the deficiency in pressure in the faster moving air become greater and greater, and the excess pressure on the side of the water in the wave crests is increasing. The displacement upwards of the water particles becomes stormy and unsteady (p. 75). The water is mixed with air and, consequently, we have foam on the wave crests. The first formation of foam on relatively small waves for a wind force of 4 can be attributed to a not yet attained steady state between wind and waves. We have to compare this to the foam which appears, when the larger waves increase their unsymmetric wave profile and the wave crest topples over. This happens either because the wind becomes too strong and forces the wave profile to become asymmetric, or because the water depth decreases and produces the surf.

With very strong winds, we observe these enormous breakers, which can become highly destructive. We observe very high waves and mighty breakers where a swell runs against a strong current, i.e. in estuaries and in areas with strong ocean currents and tidal currents. In the vicinity of the wave crest, the orbit of the wave motion becomes compressed through the opposing currents, the crests become higher and steeper until they break in the direction of the current. Waves change considerably when approaching the shores, especially when the water depth becomes smaller than half the wave length. The character of the wave changes from a short wave in a deep ocean to a long wave in the vicinity of the shore. The wave velocity decreases from the moment that the wave enters shallow water until it breaks, but the wave period remains unchanged. When a wave continues in shallow water, its wave length becomes smaller and, in general, the wave height becomes larger because the wave fronts are compressed.

GREEN (1837) has investigated the influence of the reduction of the cross-section of the wave motion and its influence on the wave height. He found that the wave height is inversely proportional to the fourth root of the water depth; the influence of the variation of the cross-section becomes more important if a wave enters a funnel-shaped estuary, and the wave height changes here inversely proportional to the square root of the width of the

water basin. LORD RAYLEIGH (1876, p. 260) has shown that this follows from the law of conservation of energy.

SVERDRUP and MUNK (1946) have presented this problem in a simple way. In deep water, half of the total energy E_0 travels at a velocity c_0 (see p. 22). In shallow water, only a fraction n of the energy E travels at a velocity c . The fraction n is sometimes used to express the relationship between the wave and group velocities. The ratio of the energies equals

$$\frac{E}{E_0} = \frac{1}{2n} \frac{c_0}{c}, \tag{V.19}$$

and the ratio of wave heights is proportional to the square root of the energy

$$\frac{H}{H_0} = \sqrt[4]{\frac{E}{E_0}} = \sqrt[4]{\left(\frac{1}{2n} \frac{c_0}{c}\right)}. \tag{V.20}$$

As the wave period remains constant, and $\lambda = cT$, the height H will be approximately proportional to the fourth root of the depth. The ratio c/c_0 and n have both been expressed theoretically by Stokes as functions of a ratio h/λ_0 , where h is the depth and λ_0 the wave length in deep water. This ratio has been called "relative depth"; the exact derivation was given by MUNK and TRAYLOR (1947). Figure 55 shows the theoretical relationship

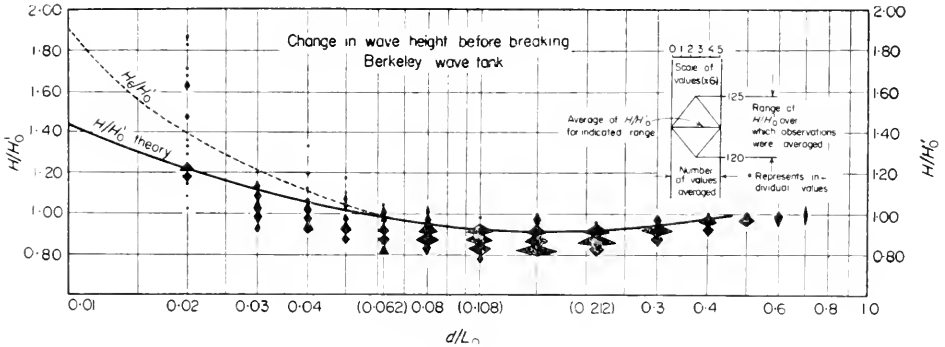


FIG. 55. Ratio wave height over deep-water wave height as function of relative depth. Line gives theoretical relationship, filled-in figures show distribution of observed values. Theory and observations both show initial decrease followed by increase (Sverdrup and Munk).

between H/H_0 and h/λ_0 , according to Sverdrup and Munk, from whom we quote the following paragraphs.

“As the wave comes into shallow water, the theory shows first a decrease of 8% in wave height and then an increase. The changes are small and difficult to detect from individual observations. A statistical study of a large number of observations made at the University of California in a wave tank gives evidence of the dip and the subsequent increase. Field observations have confirmed the computed increase, but have been too inaccurate to

confirm or deny the small initial decrease in wave height. The observations shown in Fig. 55 refer only to waves before they break during a short interval immediately preceding the breaking, an increase in wave height takes place, which is more rapid than the one given by the Stokes theory. The reason for this discrepancy can be found in the rapid change in the wave profile where the wave height is not any longer proportional to the square root of the energy" (see p. 130).

One of the most characteristic features of the onrushing swell on a sloping beach in the form of breakers is the very regular formation of long-crested waves. JEFFREYS (1924) explains that, when a wave system composed of different wave lengths advances into shallow water, the dissipation of energy destroys the short-crested waves before the low crested waves of the swell.

AIRY (see LAMB, 1932, para. 188, p. 281) has shown that when the elevation η is not small compared with the mean depth h waves are no longer propagated without change of type. The waves become steeper and steeper because on the front slope of the wave the water particles are moving faster, whereas on the rear slope of the wave the water particles move slower, and we get to a point where the vertical accelerations can no longer be neglected in comparison to the horizontal ones. The observation shows that the wave topples over and breaks. Applying the method of successive approximations, we can derive the gradual development of an asymmetric wave profile. The second approximation adds a second term to the simple wave train which increases the duration of the fall and decreases the rising time of the water surface. The wave profile has then the following form:

$$\eta = a \cos \kappa(x - ct) + \frac{3}{4} \frac{g \kappa a^2}{c^2} x \sin 2\kappa(x - ct). \quad (\text{V. 21})$$

The second term in the equation contains the factor x in the amplitude. This means that this first approximation is valid only for a small distance x . At a certain distance x the unsymmetry of the wave profile becomes so large that the approximation (V.21) can hardly be maintained. This limit is attained when the amplitude of the second term becomes equal to that of the first one. This happens when

$$\frac{3}{4} \frac{g \kappa a}{c^2} x = 1.$$

The distance the wave can travel without overturning will be

$$\frac{4}{3} \frac{c^2}{g \kappa a}.$$

FJELSTAD (1941) solved mathematically the differential equations for this change of profile. He neglected only the vertical accelerations so that he was justified to substitute for the pressure its hydrostatic value. He considered com-

pletely that the differential equations were not linear. The solution is valid irrespectively if one starts either with Euler's equations or the Lagrangian equations of motion.

The approximation by Airy (V.21) applies to a simple two-dimensional wave train. Jeffrey analysed in the same manner a three-dimensional wave system with shorter crested waves, as already discussed on p. 29. If we take as an undisturbed wave form

$$\eta = b \cos \kappa'(x - c't) \cos \mu y,$$

we find here too that if b attains the order of magnitude of depth, the wave profile becomes asymmetric. In a first approximation

$$\eta = b \cos \kappa'(x - c't) \cos \mu y + \frac{3}{8} \frac{g \kappa' b^2 c'^2}{c^4} x \sin 2\kappa'(x - c't) \cos 2\mu y. \quad (\text{V.22})$$

As found before, the waves will overturn at a distance of about

$$x = \frac{8}{3} \frac{c^4}{g \kappa' b c'^2}.$$

In order to determine which of the two wave systems can keep itself longest before breaking we establish the ratio of the two distances where the waves break. This ratio is $\kappa' c'^2 b / 2 \kappa a c^2$. Inasmuch as c' is larger than c , the value of c' will be $> \kappa' b / 2 \kappa a$, as long as μ is not large in comparison to κ' .

From observations made far out from the coast it was found that the amplitudes of the long-crested waves are so small that they are barely noticeable in a cross-sea. Consequently, b is many times larger than a . Furthermore, the short-crested waves of a cross-sea have a short length as compared with the long waves of the swell; we therefore have $\kappa' > \kappa$. For these two reasons, the value of the above-mentioned ratio is very large. This means that when a cross-sea enters into shallow water close to the beach, the short-crested waves are destroyed rather soon by collapsing and overturning. They vanish from the oncoming waves, whereas the long-crested swell is maintained. Numerical examples show that, generally, a stretch of water 500—1000 m long consists only of long-crested swell, and this is also confirmed by observations.

4. Surf on Flat and Steep Coasts

The further development of shallow water waves advancing towards the coast depends upon whether they can expand on a gradually sloping beach or whether they progress against a steep coast where the water remains relatively deep.

(a) Coastal Surf

If the coast is gently sloping, the surf is regular and constant provided the height of the waves is not too large and can be followed up qualitatively, although not by mathematical analysis. In a wave system travelling from deep water towards a soft sloping shore, the orbits which are in deep water perpendicular to the wave front and to the water surface at rest, become inclined from this vertical plane. Finally, these orbits will be parallel to the plane of the beach. The projection of the orbit on the horizontal plane is, therefore, a straight line in front of the coast; on approaching the shore, it becomes an ellipse which gradually changes its main direction. When the

angle formed by the orbit and the vertical plane exceeds 45° , the transversal horizontal component of motion in the ellipse will exceed the vertical one. In addition to this change of plane of the orbits, there is a decrease in the velocity of propagation of the wave, as a consequence of decreasing depth. The wave crests turn parallel with the shore line (see p. 127). BJERKNES (1921) has illustrated by two examples the geometrical viewpoint when the waves run on to the shore (Fig. 56). In connection with these presentations, we

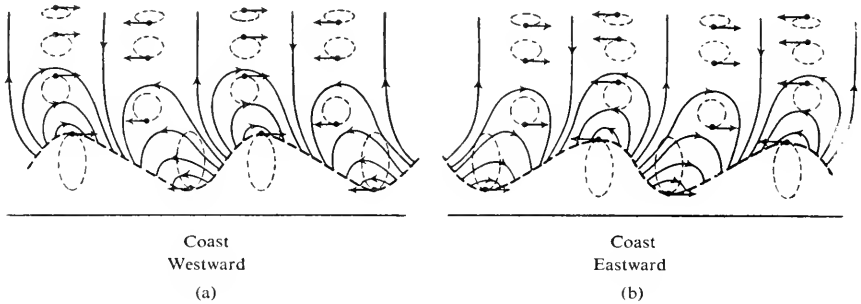


FIG. 56. Wave advancing on a straight even beach. Horizontal projection of streamlines (full lines) and orbits (dotted). a: westward; b: eastward travelling wave; shore sloping slightly to the north.

should always remember that for the dynamics of the wave process, the vertical displacements always remain decisive; for the exterior form of the process, the horizontal components of motion are decisive. Case a deals with a wave travelling westward in ocean towards a beach sloping up northward; case b deals with a wave which travels eastward, the topography of the bottom remaining the same as in case a. The orbits and the horizontal component of the streamlines have been drawn in their projection on the horizontal plane in the figure. In case a, the orbital motion at the shore is anticyclonic and the waves run up the beach area from east to west; in case b, on the contrary, it is cyclonic and the waves run up from west to east. The rolling of the ocean waves up the well delineated and gently rising beach area is a regular process.

The wave length of the waves rolling on to the shore becomes shorter and, consequently, the wave height increases. With waves of great amplitude, this increase causes them to topple over, and the wave process degenerates into an eddy with a horizontal axis. Several authors have measured the critical depth over which waves will start breaking (see SCOTT RUSSELL, 1844, p. 352; BAZIN, 1865, p. 509; STEVENSON, 1864, p. 72; GAILLARD, 1935; and FORCHHEIMER, 1924, p. 379). It is assumed that the waves start to break as soon as the wave height equals the water depth. From observations in nature it appears, however, that with head-wind or in calm weather the wave starts breaking when the depth beneath the undisturbed level is 0.72 of the wave height $2A$. With a wind in the direction of propagation of the

waves and a stronger sloping beach, this ratio $h:2A$ can increase to 2.71. The crest of the breaking wave is then at $0.65-0.85 \times 2A$ above the surface at rest. The approaching wave gives the impression of having a larger water volume than the retreating wave. This may partly be due to an optical illusion because, in accordance with the nature of the eddy, the water starts already flowing back in the rear part of the wave, while in the front and upper part the water is still advancing. According to WHEELER (1903, p. 37), a substantial amount of water oozes through the gravel beach.

KRÜMMEL (1911, vol. II, p. 110) emphasizes that the breaking of the waves is not only dependent on the ratio between depth and wave height, but also on the dimensions of the orbits in the deeper layers and at the bottom. The breaking of the waves is, therefore, also influenced by a disturbance of the horizontal water motion in greater depth. Gaillard found that if the beach is shaped in terraces and its slopes vary between 1:30 and 1:90 the critical depth increases to 1.84 of the wave height. Coastal banks which are located far into relatively deep water, or shoals in the open ocean are generally visible by an increase in the swell. Often-times it produces a heavy surf and thus the position of the shoals is indicated. According to a compilation made by Krümmel, surf phenomena occur for ocean depths ranging from 15–20 to 200 m and over, probably as a consequence of a terrace-like topography of the ocean bottom (CIALDI, 1860). These strong currents extending into great depths without a particularly high visible swell at the surface are called groundswell by seamen.

More accurate observations and analyses have provided a theory about the cause of a wave to break when approaching the shore. SVERDRUP and MUNK (1946, p. 828) have elaborated on an interesting observation that at the approximate moment of breaking, a wave behaves like the solitary wave of Scott Russell. This seems to follow from the theory of shallow water waves and of the solitary wave. According to the theory of KORTEWEG and de VRIES (1895) the profiles of the cnoidal waves correspond very closely to those of waves in shallow water, just before they break. It was shown on pp. 110 and 119 that the solitary wave is theoretically a special case of these cnoidal waves. Therefore, it can be expected that the shallow water waves behave in breaking like the solitary waves.

When the water becomes so shallow that the ratio of depth h to wave height H reaches the value of 1.28 (see p. 117), then the water at the crest moves faster than the crest itself, and the wave breaks (Sverdrup and Munk). From the theory of the solitary wave and from the assumption of conservation of wave energy one can derive a relationship in which the ratio of wave height H at the moment of breaking to wave height over deep water H_0 is a function of the initial steepness (ratio: wave height to wave length in deep water) H_0/λ_0 . The solid line in Fig. 57 shows graphically this ratio. The dots are observed values on the Atlantic and Pacific beaches. Although

individual observations deviate considerably from the theory, on the average the theoretical relationship seems to apply for all but the steepest storm waves. One may conclude that friction cannot play a decisive role in the trans-

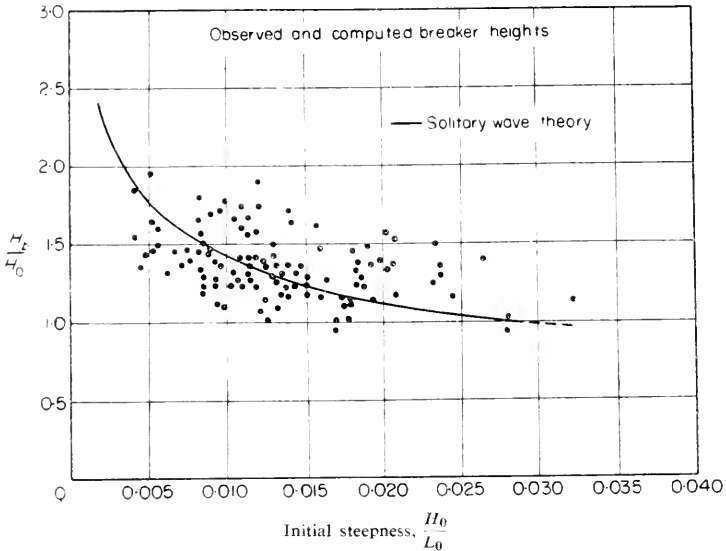


FIG. 57. Theoretical and observed ratio breaker height to deep water wave height as function of initial steepness (Sverdrup and Munk).

formation of waves travelling from deep into shallow water. Sverdrup and Munk state that a careful analysis of all available data covering slopes of beaches from 1/20 to 1/100 shows that the loss of energy due to friction does not exceed 10% of the original wave energy and is even much smaller on the average.

It is confirmed by a large number of observations in the laboratory and in the field that surf waves start breaking at a ratio of depth and wave height of 1.28. However, there are three exceptions not covered by the theory:

(1) Abrupt changes in the beach slope may lead the waves to break already at considerable depths.

(2) Very steep storm waves break in water deeper than the depth indicated.

(3) Very flat waves break in water of smaller depth than indicated.

After eliminating all cases of abrupt changes in beach slope from 555 individual observations in different localities, the average observed ratio of depth over breaker height equals 1.27 as compared to the theoretical value of 1.28. Individual observations lie roughly between 1.1 and 1.5, and this deviation cannot be altogether ascribed to accidental circumstances one differing strongly from the next. The deviations will also result from the fact that the profiles of individual breakers differ: some are steeper, others less steep than the solitary wave. But on the average the breakers seem to resemble the profile given by the solitary wave theory and follow the theoretical rules.

A special topography of the beach can produce a repeated surf. The water-mass which broke during the first surf process moves on over the beach as a rather low wave, which can break again when the depth decreases more. This action can even repeat itself. Figure 58 gives, according to Krümmel,

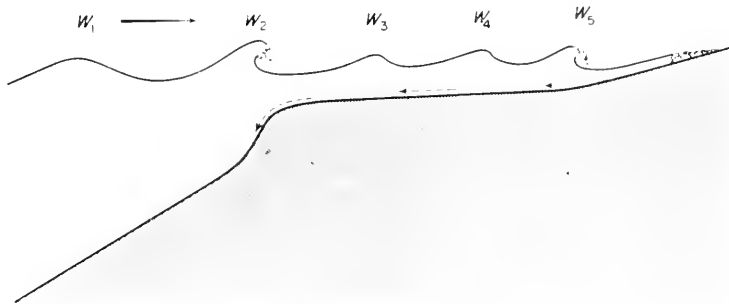


FIG. 58. Multiple surf (W_2 to W_5). Rip current at bottom (Krümmel).

a picture of such a repeated surf. Associated with such a surf is a “rip current”, which is a current particularly strong at the bottom, and which carries from the beach towards the sea any objects that are not fixed to the bottom.

(b) *Refraction of Ocean Waves*

The preceding explanations refer to waves which travel towards the shore and whose crests are parallel to the depth contours of the beach, and their direction of propagation remains constant. This is no longer the case when they approach the coast at an angle. The wave crests then tend to turn parallel to the shore. The reason is that the wave velocity decreases with decreasing depth, so that the part of the wave crest nearest to the shore moves slower than the crest in deeper water which races ahead. Figure 59 makes this clear. This endeavour of the crest line to become parallel with the coast is similar to the one causing the bending of light rays in optical systems. It is called wave refraction.

GAILLARD (1904, p. 66) and STEVENSON (1864, p. 165) observed the changes which waves undergo on account of different contours of the coast. Gaillard found that a wavy coastline may cause a decrease in swell, in view of the tendency of the waves to establish the wave front parallel to the coast and consequently to stretch their crests. The swell is becoming less pronounced when it moves into a harbour through a narrow opening. If b is the width of the opening, an arc-shaped diffraction wave is formed, which at the distance m from the entrance has a radius m . If this arc has the length B , the ratio between the later and the earlier wave height, according to Stevenson, is

$$\sqrt{\frac{b}{B} - 0.0269 \left(1 + \sqrt{\frac{b}{B}}\right)^4} m$$

(everything in m). If waves are deflected by a breakwater and the angle of

deflection is α , the wave height will decrease by

$$h_2 : h_1 = 1 - 0.06 | \alpha$$

provided the deflected waves can expand freely. However, if the waves, after having been deflected, move by the breakwater without hitting it, we have

$$h_2 : h_1 = 1 - 1.04 | \alpha$$

(see FORCHHEIMER, 1924, p. 378).

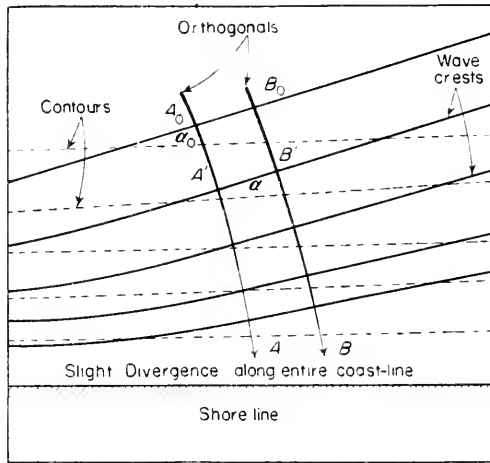


FIG. 59. Refraction of waves along beach with straight parallel depth contours. The wave crest along the orthogonal B is always in deeper water than along A and therefore moves with greater velocity. As a result, the waves tend to turn parallel to the shore.

BLATON (1937) was the first who attempted to give a theoretical explanation by transposing similar problems from geometrical optics to gravitational waves, in applying the principle of Fermat. MUNK and TRAYLOR (1947) have investigated this problem thoroughly and were able to devise a theory for forecasting purposes.

The process of refraction for a beach with depth contours running parallel to the shore is governed by Snellius's Law

$$\frac{\sin \alpha}{\sin \alpha_0} = \frac{c}{c_0}, \tag{V.23}$$

in which α is the angle between the wave crest and the contours at any depth and c the wave velocity at the same depth under consideration; the parameters with subscript refer only to deep water, where the direction and the velocity of the waves are constant.

If the topography of the bottom is more complicated for which the depth contours are neither straight nor parallel, the changes in the direction of

propagation and in the height of the waves can be found graphically by constructing a "refraction diagram", a term first used by O'BRIEN and MASON (1940).

A refraction diagram is one on which the position of wave crests at the sea surface is shown by a series of lines. These are evenly spaced in deep water — that is, in water of depth greater than half the wave length. Beyond this depth the effect of bottom contours on any of the wave characteristics is negligible. At shallower depths the relation between wave velocity and water depth is known (see later reference), and a refraction diagram can be constructed by advancing various points on a crest through distances determined from any chosen time interval and the average depth. The direction of advance is drawn normal to the crest. In Fig. 59 for example, the chosen time interval is one wave period, and the distance A_0-A' . The distance B_0-B' represents the advance of point B during the same time interval, but for the average depth between B_0 and B' . The lines A_0-A' and B_0-B' are normal to the wave crests. By locating a set of points, A', B', C', \dots , the new crest can be found with sufficient accuracy by drawing a smooth line through these points. Advancing one wave length at a time, the crests may be carried into any depth of water desired, and the completed diagram shows the continuous change in the direction of a wave advancing from deep into shallow water.

Description of a practical procedure for constructing refraction diagrams, together with the necessary graphs and tables, can be found in the forecasting manual (Written by Sverdrup and Munk and published by the Hydrographic Office, 1944). The completed diagram can be interpreted in one of two ways:

(1) As a series of lines representing the positions of a single wave crest at various times as the crest advances towards shore. Crest interval is then defined as the interval between these times. In Fig. 59 the crest interval equals one wave period.

(2) As a series of lines representing the position of certain wave crests at a single instant; a crest interval of one wave length means that every crest is represented (Fig. 59), because the advance of any point on a crest during one wave period equals one wave length by definition. A crest interval of two wave lengths means that only every second wave crest is shown; a crest interval of one-half wave length, that the position of every crest and trough is shown.

Wave height is defined as the vertical distance between crest and trough. In order to evaluate the effect of refraction on wave height, a set of orthogonals, that is, a family of lines which are everywhere perpendicular to the wave crests, must be constructed. The lines A_0-A and B_0-B in Fig. 59 are orthogonals; they may be visualized as the wakes behind two surfboards which are continuously oriented normal to the crest, that is, in the direction of wave motion. Assuming that the wave energy is transmitted in the direction

of wave motion, the total flow of energy between two orthogonals must remain constant. Thus, if orthogonals converge, the crests are compressed, and the energy per unit crest length is relatively large; if orthogonals diverge, the crests are stretched, and the energy per unit crest length is relatively small.

It has been derived previously that the change in wave height, when the waves enter into shallow water follows the relation

$$\frac{H}{H_0} = \sqrt[3]{\left(\frac{1}{2n} \frac{c_0}{c}\right)}. \quad (\text{V.24})$$

The breaking waves, with their sharp crests isolated by long flat troughs, have the appearance of "solitary" waves (see pp. 116 and 121), for which the height is proportional to the cube root of the energy. We then have, instead of the relation (V.24), the relation

$$\frac{H_b}{H_0} = \frac{1}{3 \cdot 3 \sqrt[3]{(H_0/\lambda_0)}}, \quad (\text{V.25})$$

in which H_0/λ_0 is the slope of the wave or wave steepness in deep water. These relations are only valid when the orthogonals are parallel, which is to say with rectilinear propagation of waves. Munk and Traylor show that, when the orthogonals are convergent or divergent, equation (V.25) must be corrected with a factor which takes into account the variation in distance s between two adjacent orthogonals. Let H designate the wave height and s the distance between adjacent orthogonals on the refraction diagram. Parameters with subscript 0 again apply in deep water, those with subscripts b at the breaker point, and parameters without subscript at any depth intermediary between deep water and the breaking point.

$$\frac{H}{H_0} = \gamma K, \quad \frac{H_b}{H_0} = \gamma_b K_b, \quad (\text{V.26})$$

where γ and γ_b are the right-hand terms of equations (V.24) and (V.25) and have constant values along a fixed depth contour

$$K = \sqrt[2]{\frac{s_0}{s}} \quad \text{and} \quad K_b = \sqrt[3]{\frac{s_0}{s}} \quad (\text{V.27})$$

vary along a depth contour and will be referred to as the "refraction factors".

Equations (V.26) are derived from the postulates that the energy flows along orthogonals and that energy is conserved. This, in turn, implies two assumptions:

(1) The effect of diffraction (which would bring about the flow of energy across orthogonals from regions of high waves to regions of low waves) can be neglected.

(2) The effect of bottom friction is negligible. The validity of these assumptions is borne out by the good agreement between computed changes in

breaker height according to equation (V.26), and observations along the beach north of La Jolla, California. There has been a tendency in the literature to emphasize the effect of bottom friction on wave motion and other wave characteristics. Studies dealing with generation of waves by wind and with absolute changes of wave height in shallow water and the dynamics of breaking waves indicate that the wave motion in general is not appreciably affected by frictional processes.

Refraction type examples: beach with straight and parallel depth contours. For this simple case the change in wave direction can be expressed analytically by equation (V.23). Figure 59 is a schematic drawing of wave refraction along a straight coastline with parallel depth contours. Figure 60 is an aerial photo-

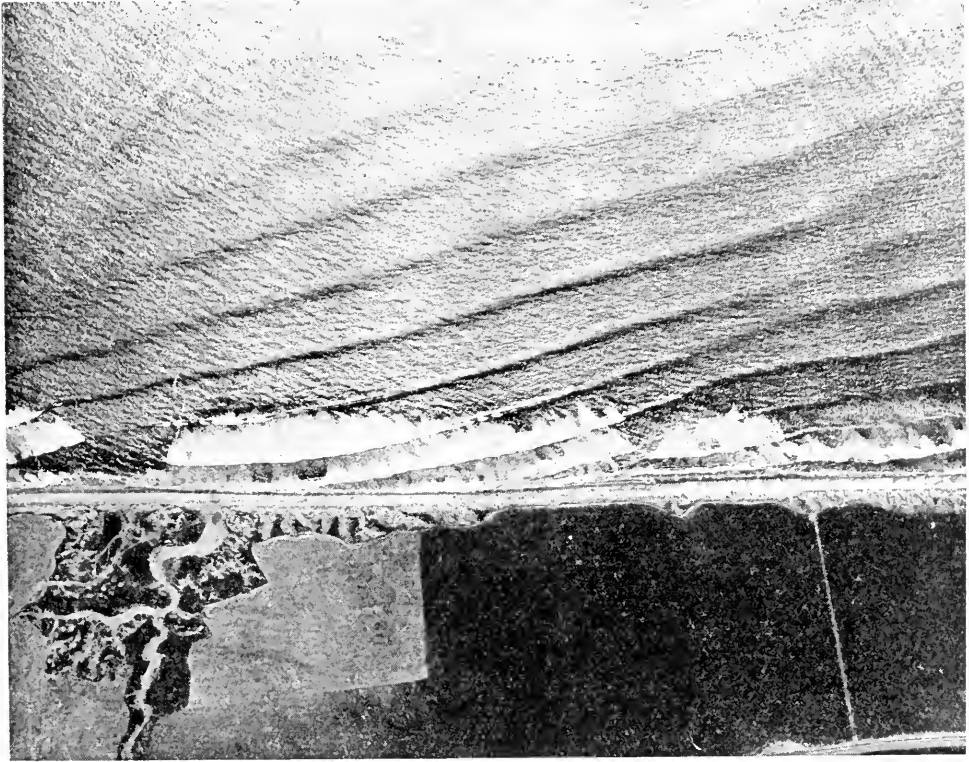


FIG. 60. Aerial photograph showing swell turning parallel to shore north of Oceanside, California.

graph showing long waves from the south-south-west coming into the beach north of Oceanside, California. There is a divergence of the orthogonals indicated by the values of s computed from the equation

$$\frac{s}{s_0} = \frac{\cos \alpha}{\cos \alpha_0} \tag{V.28}$$

Combining equations (V.23), (V.27), and (V.28) leads to equation

$$K = \left[\frac{\cos^2 \alpha_0}{(1 - [c/c_0] \sin \alpha_0)^2} \right]^{1/4}, \tag{V.29}$$

$$K_b = \left[\frac{\cos^2 \alpha_0}{(1 - [c_b/c_0] \sin \alpha_0)^2} \right]^{1/6} \text{ in which } \frac{c}{c_0} = \frac{\lambda}{\lambda_0} = \tanh \frac{2\pi h}{\lambda}.$$

Figure 61 presents a comparison between the positions of the wave crests according to Fig. 60 and the positions computed from these formulas.

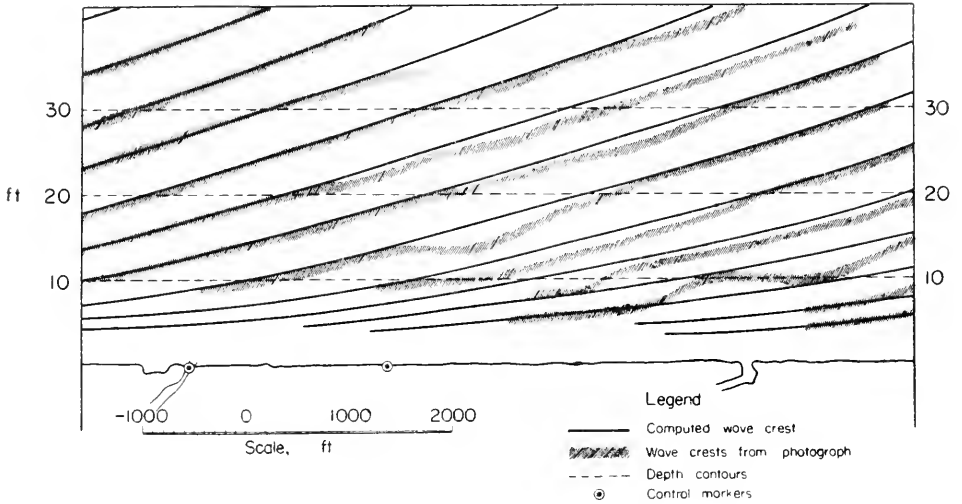


FIG. 61. Comparison between observed position of wave crests shown in Fig. 60 and positions computed according to Snellius's law (Sverdrup and Munk).

Waves coming from an angle into a beach with straight and parallel depth contours are reduced in height according to equation (V.26), but the reduction is uniform along the entire beach, and no variation in wave height along the beach will result. As an example of variation in wave height, consider a coastline which forms a sharp bend at point *B* (Fig. 62). On both sides of point *B* the coastline and the depth contours are straight and parallel. Assume that waves of 14-second periods come from the north-north-west. The angle α is drawn between the orthogonals and the bottom gradient, which is consistent with our earlier definition. Table 17 gives the computed direction and relative height at the 10-foot contour, which is assumed to lie outside the breaker zone. Along the beach section *A-B*, which is relatively exposed to the incoming swell, waves are about 50% higher than along section *B-C*. This can also be seen from the fact that the divergence of orthogonals along *A-B* is less than the divergence along *B-C* (Fig. 62).

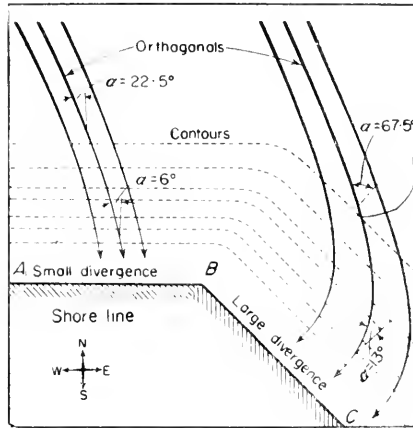


FIG. 62. Refraction of waves along two sections of straight beaches with different exposures. The divergence along section *A-B* is less than along *B-C*, and the wave height along *A-B* exceeds therefore the wave height along *B-C* (Munk and Traylor).

Table 17

Section of coastline (Fig. 62)	<i>A-B</i>	<i>B-C</i>
Wave angle in deep water (α')	22.5°	67.5°
Wave angle at 10 ft. depth (eq. V. 23)	6.0°	13.0°
Refraction factor (eq. V. 29)	0.97	0.63

Submarine canyons. Portions of wave crests over the centre of a canyon are in deeper water and move ahead faster than the portions on either side (Fig. 63). Consequently, the waves fan out, resulting in divergence (low

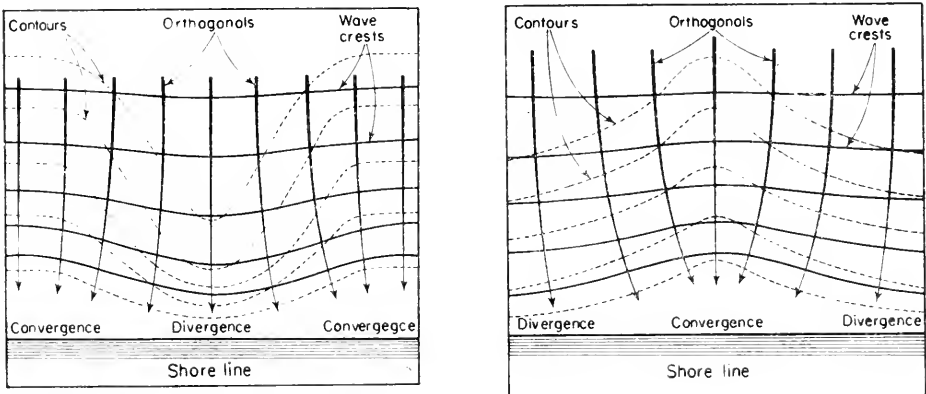


FIG. 63. Left: refraction of waves by a submarine canyon. Divergence (low waves) over the mouth of the canyon and convergence (high waves) on either side. Right: refraction of waves by a submarine ridge. Convergence over the ridge.

waves) over the head of the canyon and convergence (high waves) on either side.

Submarine ridges. Underwater ridges near shore have an effect opposite to that of canyons. Waves passing over the ridge are in shallower water and are therefore retarded, and on either side waves move ahead, creating a convergence over the ridge. This is borne out by frequent observations of unusually violent breakers over the shoal portion of underwater ridges.

Other interesting cases are the influence of promontories, of bays and islands on the surf, for which MUNK and TAYLOR and ARTHUR (1946, p. 168) have given good examples and which fully confirm the theory. It seems quite possible to forecast the direction and force of the expected surf with the aid of previously computed refraction diagrams for wave systems of definite periods. The investigations are also of importance in connection with the action of the surf on the topography of beaches.

(c) Surf Breaking against Cliffs

If a wave train moves towards a vertical surface or against a shore sloping down steeply into great depths at a sharp angle, it will be totally or partly reflected. The reflected wave superimposes itself on the approaching one and the result is a complete or incomplete standing wave. The water motion in front of the wall then remains more or less at rest and, in an extreme case, the wave attains twice the height of the approaching wave. With such a simple reflection, there will be no shock from the approaching wave against the vertical wall, because there are only vertical displacements of the water particles (antinode). When there is such a motion, a vessel can venture to come up close to the wall (breakwater, etc.) without risk of damage. In general, however, the result of the reflection is not such a regular process, and the incoming and reflected waves mix up confusedly.

If the waves are high and move fast, they generally bounce against the steep shore in breaking or shortly before; huge water-masses from the wave crests are thrown jet-like against the wall. This is the shock or cliff surf.

The shock waves are, of course, closely related to the place where the wave crests overturn, and this place is dependent on the wave velocity and on the slope of the beach, as well as on the latter's nature. The waves, when hitting a barrier, exert a dynamic pressure, which is added to the generally far smaller static pressure. When a liquid hits perpendicularly a large wall, the particles change their motions gradually by a right angle, until the total energy of motion in the direction of the pressure is counterbalanced by the counterpressure of the wall. If the cross-section of the approaching water-mass is F , then the mass of the shock in the unit of time with a velocity U is ρFU and its momentum ρFU^2 , so that the shock pressure at the wall becomes $P = \rho FU^2$. STEVENSON (1864, p. 285) was the first to determine this shock pressure of surf waves and built a spring dynamometer which, based on the principle of railway buffers, determined numerically the shock pressure of the waves. Experiments made with such an instrument in 1843 and 1844 at the cliffs of Skerryvore (in the west of Scotland) gave an average

0.298 kg/cm² (611 lb./sq ft) for five summer months and 1.018 kg/cm² (2090 lb./sq ft) for six winter months, with a maximum of 2.97 (6090 lb./sq ft). At Dunbar on the north coast of Scotland, the maximum found was 3.83 (7840 lb./sq ft) and near Buckie, over several years of reading, 3.28 kg/cm² (6720 lb.). As a result of experiments on how the pressure varies with height, it was found that the shock pressure of the waves is strongest at high-water level and decreases rapidly with increasing water depth. Off the German coast of the North Sea, FRANZIUS and SCHILLING (1901, p. 22) found as largest shock pressure 1.5 kg/cm², at the Baltic coast 1.0 kg/cm², so that it can be assumed that at points exposed to the beating of the waves the largest shock pressure varies between 1.5 and 2.5 kg/cm². More recently, experiments have been made with manometer and oscillograph pressure gauges respectively, which have given values of the same order of magnitude; the highest pressure hitherto recorded of 6.9 kg/cm² was observed on the east mole of the harbour of Dieppe on 23rd February 1933, by means of a recording device which was located 35 cm above the base of the vertical wall, and which was hit by a wave 5 m high (horizontal velocity 8.50 m/sec, initial vertical velocity 23 m/sec). The breaker had a height of 3.6 m, a length of 40 m and a wave velocity of 6 m/sec (DE ROUVILLE, 1938). Other measurements, made simultaneously with several recording dynamometers, were reported from the east coast of North America (Portland, Maine). However, the pressure values remained far below the maximum value observed at Dieppe. A comprehensive survey has been compiled by D'ARRIGO (1940).

GAILLARD (1904), at North Beach (Florida), studied the relationship between the dimensions of the waves and the shock pressure. The shore line at that point is straight, the beach is flat, and the pressure gauges were mounted on upright poles, 8×8 in., in such a manner that they received the full shock of the waves. When we take $p = k\rho(\frac{1}{2}u^2)$ as dynamical pressure, the pressure coefficient $k = 2p/\rho u^2$ and, theoretically, it can attain a maximum value 2. Gaillard assumes u is the sum of the wave velocity c and the velocity v of the water particles in their orbit, so that

$$u = c + v = \sqrt{\left(\frac{g\lambda}{2\pi} \frac{b}{a}\right)^2} + \sqrt{\left(\frac{2\pi g}{\lambda}\right)^2} ab,$$

in which a and b are the semi-axis of the orbit at the surface. He thus obtains Table 18, from which we can see that the shock pressure, even with relatively large waves, hardly attains the average value of 0.5 kg/cm²; the pressure coefficient here is 1.2, which is considerably below the theoretical maximum value. The destructive force by a breaker is estimated by D'AURIA (1890–1891) as follows: a breaker with a frontal height h , a length λ , with a velocity u (approximately equal to c) has per unit width the kinetic energy $(\rho h \lambda) u^2$. The onrush occurs during the time $\lambda:u$. If during this time the total kinetic energy has been used up, then, according to the impulse theorem,

$$\frac{P}{2} \frac{\lambda}{u} = \text{mass} \cdot \text{velocity} = \frac{\rho h \lambda u}{2} \quad \text{or} \quad \frac{P}{2} = \frac{\rho h}{2} u^2,$$

where the average resistance $= \frac{1}{2}P$. The greatest resistance may be approximately twice as much. If spread at the vertical wall over an area of the height h , the maximum shock pressure per unit surface of a breaker will be $p = u^2$, which is in agreement with the result obtained by Gaillard.

This force is able to displace horizontally and lift considerable water masses simultaneously. With a velocity u , a water mass can climb a height $u^2/2g$. for instance with 10 and 14 m/sec respectively the height can be 5 to 10 m. Therefore, it is not surprising that breakers can cause enormous destructions. KRÜMMEL (1911, vol. II, p. 118) has given a compilation of such surf breakers with a powerful visible effect.

Table 18. *Pressures of wave impacts for different sizes of waves*
(According to Gaillard)

Maximum wave dimension		Wave velocity (c in m/sec)	v Computed (m/sec)	Maximum pressure observed (P in kg/cm ²)	Pressure coefficient observed (k)
Height $2A$ in m	Length (λ in m)				
0.61	14.0	2.56	0.88	0.072	1.16
0.76	18.3	1.87	0.98	0.112	1.45
0.91	22.9	3.57	1.13	0.157	1.36
1.22	25.0	3.72	1.24	0.198	1.53
1.52	36.6	4.63	1.62	0.228	1.11
1.83	45.7	5.55	1.89	0.325	1.12

BAGNOLD (1939), of the College of Science and Technology in London, threw a new light on this process of surf breaking. These experiments were made in a wave tank approximately 11 m long, $1\frac{1}{2}$ m high and $\frac{1}{2}$ m wide. The waves were generated at one end and caused to overturn at the other end (often after several reflections) by travelling on to an adequately sloping surface and then to break by hitting a vertical wall. Different devices on this wall were fixed to determine the pressure produced by the surf breakers, either by visual observations or by recording continuously. The purpose of the experiments was mainly to find a numerical relation between the maximum shock-pressures and the dimensions of the observed waves. In Fig. 64 are shown three different possibilities when surf hits a vertical wall whose base is always submerged. In the first case, the wave overturns at such a distance from the wall that no breaker will hit it. In the second case (*2a*) the wave overturns just in time for the tip of the breaker A to reach the wall before the breaker founders (*2b*). In this process, a large air cushion B is enclosed between the wall and the lower part of the surf front. As this front advances, the air in this space is being compressed (*2c*) and then explodes vertically with a scarcely audible noise with a formation of many squirts (*2d*). In this case the position of the lower point E in the surf eddy, is always below the normal surface at rest. In the third case, the wave overturns still later and, according to Bagnold, this is the only case in which shock-pressures can occur. The enclosed air cushion is much smaller in the horizontal direction than before, and the point E is already in ascending motion, before it contacts with the wall at A . Also, in the vertical direction, the dimension of the air cushion

is smaller than it was previously. Only in this case, the noise of the surf is sharp.

It was expected that, by experimenting in the wave tank, the process could be controlled in such a manner that each experiment could be repeated in

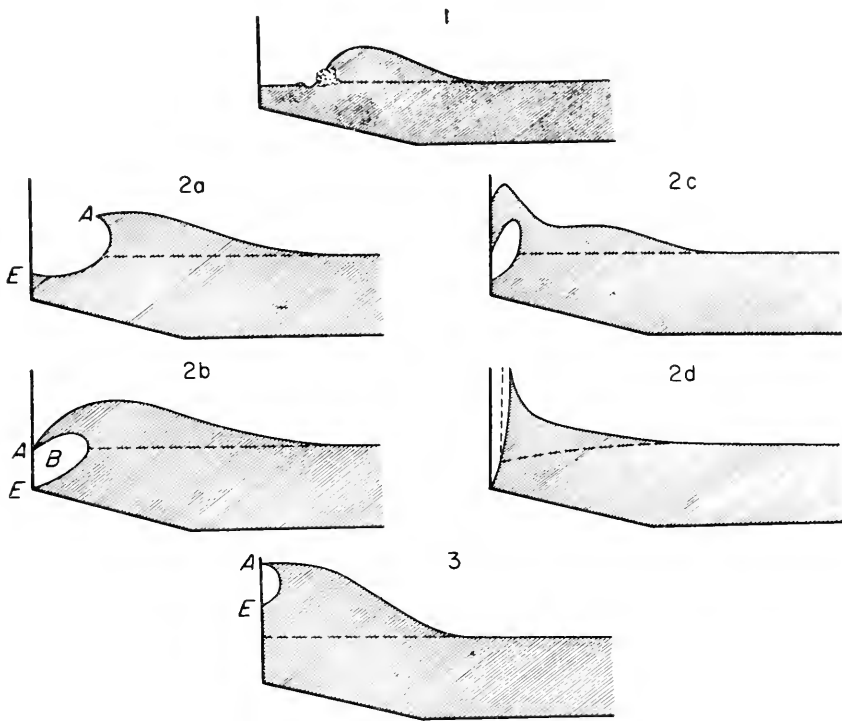


FIG. 64. Several possibilities in the behaviour of the breakers on a vertical barrier (Bagnold).

the same way at any time, thus permitting an exact analysis of the phenomenon, especially of the maximum pressure. Although the greatest precautions were taken, this could not be attained. With external circumstances unchanged, and one wave being quite similar to the other, the maximum shock-pressure turned out to be different in each case, and it seems that the smallest, hardly noticeable changes in the wave itself and in the outside factors cause variations in the shock. The development of small air cushions has also a considerable influence and much depends upon whether one single air cushion is formed or whether, as shown in Fig. 65, it is split up into several small cushions. The greatest shock-pressure that could be observed for a normal wave of 25.4 cm high, and a velocity of 1.80–2.40 m/sec was, according to visual observations, 5.6 kg/cm². The tests showed that the shock-pressure became very small when the thickness of the enclosed air cushion exceeded half its height and that its intensity increased when this thickness decreased.

Despite the great diversity in maximum pressures, the area enclosed by the time-pressure curve remained constant. The higher the maximum pressure, the smaller its duration will be. Figure 66 gives a graphic presentation of a time-

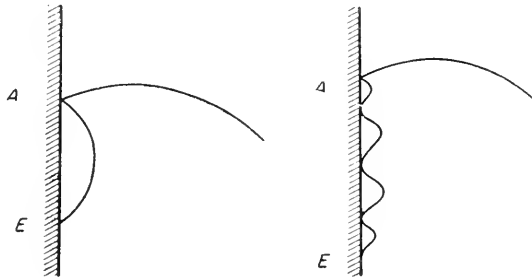


FIG. 65. Normal shape of an imbedded air pocket and its disintegration into several parts

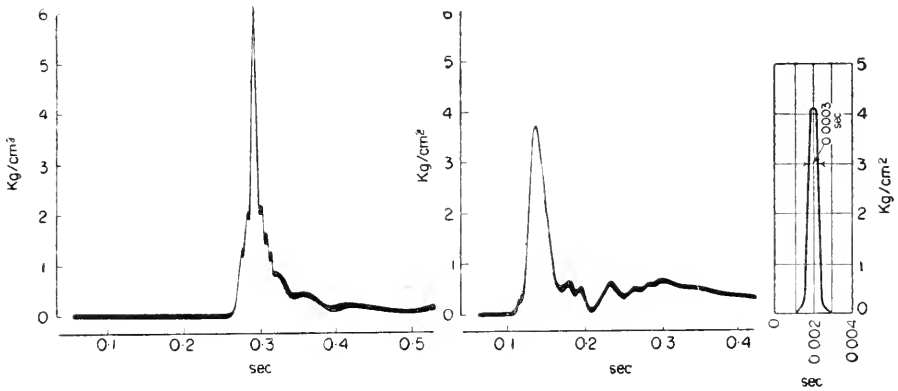


FIG. 66. Left: normal curve of shock pressure in Bagnold's experiments. Right: recordings of pressure at the vertical breakwater at Dieppe.

pressure curve, showing how rapidly the pressure increases and decreases in shock-surf; besides, there are two recordings of shock-pressures of a surf wave against the breakwater of Dieppe. We can see that the order of magnitude of the shock-pressures of the waves is the same in the tank as in nature. The maximum pressure obtained in the test was 5.6 kg/cm², as mentioned above. The linear dimensions in nature are increased in the proportion 12:1, and one could expect here maximum pressures of 70 kg/cm². However, the maximum pressure found in Dieppe was only 6.9 kg/cm² and the values, in all other respects, remain of the same order of magnitude as the laboratory tests. Bagnold is of the opinion that this striking fact must be ascribed to the considerable difference existing between sea water and fresh water used in laboratory tests. The formation of foam which occurs

so easily with sea water, the circumstance that in nature the entire water-mass of surf waves is interspersed with innumerable bubbles, and perhaps also the fact that sea water is rich in plankton, apparently contribute to this considerably different behaviour in the two cases.

5. Calming Effect of Oil on Waves

Substances which are either mixed freely with the water, such as mud, ice, seaweed, eelgrass, etc., or cover the sea surface, like some oils, and even fresh water, can prevent the regular development of waves and cause existing waves to decay rapidly. The wave-stilling action of mud and ice is a well-known phenomenon. The ice crystals formed by the freezing sea water dampens the swell very rapidly. The wave energy is dissipated more quickly by increased friction. The same applies to drift ice in polar seas which dampens considerably the wave action and reduces the swell. Sea weeds and eel grass in sufficient quantity can also prevent development of a strong swell. It has often been observed that rainfalls have a wave calming effect. It should be remembered that fresh water has a considerably lower density than the saline sea water and that so long as it does not mix with the lower layers, it can spread out over the surface in a thin layer. In this manner it has the same effect as a thin layer of oil spreading over the surface. The wave dampening action of the rain vanishes very soon because the difference in density rapidly decreases through mixing. An old and successful way to calm large waves in the stormy seas is to pour oil on the surface. Canvas bags filled with tow or twist, can absorb a large quantity of oil, which is released drop by drop through tiny holes punched into the canvas; this oil spreads with great rapidity over the surface as an extremely thin film suppressing all capillary waves and leaving only the long waves of the swell. It removes the breakers, if the swell is not too high; the oil-covered surface becomes very smooth. This smoothing action is completed within a few minutes (GROSSMANN, 1892). Experience has taught that not all oils have such action and that viscous heavy animal oils, like fish oil, cod liver oil, also rape seed or colza oil are more effective than mineral oils; petroleum and soap solutions proved to be useless. Even a small quantity like one or two litres of oil per hour is sufficient to smooth a surface of 20–100 m around the vessel. There is no doubt whatsoever as to the calming effect of oils on windsea and swell.

The damping effect of oil has been associated for a long time with the surface tension of the water and of the damping liquid (KÖPPEN, 1893). Each wave motion tends to alternate the contraction and expansion of the surface as can be rapidly deduced from Fig. 4. An expansion of the surface counteracts the surface tension. A smaller surface tension must, therefore, facilitate the wave formation. The surface tension of sea water is approximately 78, that of olive oil 37, or rape seed oil and cod liver oil 32 to 33, of petroleum 31 to 32 dynes, which is only about half that of pure water. The addition of

damping liquid reduces consequently the surface tension of the upper layer and capillary wave action of the oily surface is started more easily than with sea water alone and, therefore, a damping action cannot set. The calming effect of the waves by oil cannot be attributed to the difference in surface tension of water and oil alone.

Because the surface tension of sea water is greater than the tensions at the surfaces of separation of oil-water and oil-air, a drop of oil on the water will spread rapidly into a very thin film. If this layer becomes sufficiently thin, that is of the order of magnitude of one-hundred thousandth or one-millionth of a millimetre, it is found that the surface tension is no longer constant but increases when thickness of the layer is reduced and vice versa. Each expansion of the surface results in a reduction of the thickness of the oil film and, consequently, an increase in surface tension and vice versa. Therefore a surface opposes any motion connected with an expansion of the surface. The contaminated water surface therefore behaves as an elastic skin. The expanding and contracting movements of the surface accompanying the wave motion generate alternating tangential drag on the water, with a consequent increase in the rate of dissipation of energy and reducing the possibility of wave formation. The expansions are greater where the waves are shorter and steeper. Moreover, the expansions are greater in the place where the waves are cusped than in the flat troughs and consequently the calming effect of the oils will be more apparent with shorter waves, and will be more visible at the wave crests than in the wave troughs. This is exactly what has been observed.

The calming effect of a thin layer of oil can also be considered as a result of the greater viscosity of the oils, even though this explanation, physically speaking, is not as correct as the one mentioned before. The damping time for waves, according to equation (IV.23) is

$$\tau = \frac{\lambda^2}{8\pi\nu},$$

in which $\nu = \mu/\rho$ is the kinematic viscosity of the liquid. For water ν is of the order of magnitude 0.01, for petroleum and liquid oils only little more (0.011-0.06), for olive oil ν is already 80 times ($\nu = 0.808$), for rape seed oil 70 to 100 times ($\nu = 1.2$) greater than for pure water. The damping time for such liquids is, therefore, many times smaller than for water. A capillary wave of $\lambda = 5$ cm vanishes on water in 32 sec, on rape seed oil in 0.26 sec; a wave of $\lambda = 20$ cm needs for this 507 sec, on rape seed oil only 0.4 sec; a wave 1 m long on water takes $3\frac{1}{2}$ h, on rape seed oil only 1.75 min. One also observes that petroleum, due to its small viscosity, similar to that of water, cannot have a great wave calming effect. The great viscosity of the new surface should therefore, be decisive. In this explanation little consideration is given to the effect of the abnormal behaviour of the water surface contaminated by oils in regard to the surface tension, also the fact that the oil spreads on the water in an extremely thin layer, which makes the effect of the alternating variations in the surface tension possible.

An exact theory by REYNOLDS (1880) and AITKEN (1883, p. 56) starts with these variations considering the oil layer as a quasi-elastic skin, the effect of which is the greater, the shorter the wave length is. If this wave length becomes sufficiently small, the surface is practically inexpandible and the horizontal velocity at the surface will vanish. In deriving the relations on the influence of

internal friction on water waves, the condition for the normal tension remains the same as in the case of pure water; however, the condition that the tangential stress must vanish is now replaced by the one indicated above. We then obtain for disturbances of the surface with a wave number κ and with a frequency σ a modulus of decay of $\tau_1 = (2 \sqrt{2}) / (v^{1/2} \kappa \sigma^{1/2})$ instead of the value $1 / (2v\kappa^2)$.

The ratio of this to the modulus obtained on the hypothesis of constant surface tension will be

$$\frac{\tau_1}{\tau} = 4 \sqrt{2} \left(\frac{v\kappa^2}{\sigma} \right)^{1/2} = \text{prop. } \frac{1}{\lambda^{3/2}},$$

which is by hypothesis small. That is the damping time is the greater, the smaller the wave length and many times smaller than with water that has not been contaminated.

Chapter VI

Long Waves in Canals and Standing Waves in Entirely or Partly Closed Basins

1. Long Waves in Canals

(a) Canal of Uniform, Rectangular Cross-section

IN the general wave theory it has already been shown that, when the water depth becomes small in proportion to the wave length, the nature of the wave motion is changed completely, and that the propagation of the waves at the surface of such a water-mass obeys another law as surface waves or short waves, do. The equations applying to "long waves" can easily be derived from the equations of motion, if the characteristic features of these waves are considered at the time the basic equations are formulated. These characteristics are chiefly the following: on account of the small water depth relative to the wave length, the vertical motions become less important than horizontal motion, and the vertical acceleration of the water particles can be neglected. This means that at any point the pressure is in each case equal to the statical pressure exercised by a column of water extending from the free surface to the depth of the point under consideration. From the neglect of the vertical acceleration follows that the horizontal motion is always the same for all water particles in a vertical plane perpendicular to the direction of propagation of the wave; in other words, the horizontal velocity u is a function of the direction x and of the time t only.

In a straight canal with a horizontal bed and parallel vertical sides and with a constant, regular cross-section we place the x -axis parallel to the length of the canal, the z -axis vertical and upwards.

Let the ordinate of the free surface corresponding to the abscissa x , at time t , be denoted by $h + \eta$, where h is the ordinate in the undisturbed state. Then the pressure at any chosen point will be

$$p = p_0 + g\varrho(h + \eta - z), \quad (\text{VI.1})$$

where p_0 is the (uniform) external pressure. Hence

$$\frac{\partial p}{\partial x} = g\varrho \frac{\partial \eta}{\partial x}. \quad (\text{VI.2})$$

The equation of horizontal motion, viz.:

$$\frac{\partial u}{\partial t} + u \frac{\partial u}{\partial x} = -\frac{1}{\rho} \frac{\partial p}{\partial x}$$

is further simplified in the case of infinitely small motions by the omission of the term $u(\partial u/\partial x)$ which is of the second order so that

$$\frac{\partial u}{\partial t} = -g \frac{\partial \eta}{\partial x}. \tag{VI.3}$$

Now let

$$\xi = \int_0^t u dt, \tag{VI.4}$$

i.e. we introduce the horizontal displacement ξ instead of the horizontal motion u for the water particles in the x -direction until the time t . Equation (VI.3) may now be written

$$\frac{\partial^2 \xi}{\partial t^2} = -g \frac{\partial \eta}{\partial x}, \tag{VI.5}$$

which is the equation of motion for long waves. The ordinary form of the equation of continuity

$$\frac{\partial u}{\partial x} + \frac{\partial v}{\partial z} = 0.$$

Thus

$$v = -\int_0^z \frac{\partial u}{\partial x} dz = -z \frac{\partial u}{\partial x}, \tag{VI.6}$$

if the origin be for the moment taken in the bottom of the canal. This formula shows as a consequence of our assumption that the vertical velocity of any particle is simply proportional to its height above the bottom. At the free surface we have $Z = h + \eta$ and the equation of continuity in a canal with a rectangular cross-section is found by

$$\eta = -h \frac{\partial \xi}{\partial x}. \tag{VI.7}$$

If we eliminate from equations (VI.5) and (VI.7) either η or ξ we obtain

$$\frac{\partial^2 \xi}{\partial t^2} = gh \frac{\partial^2 \xi}{\partial x^2} \quad \text{and} \quad \frac{\partial^2 \eta}{\partial t^2} = gh \frac{\partial^2 \eta}{\partial x^2}. \tag{VI.8}$$

It is easy to prove that its complete solution has the form

$$\xi \text{ or } \eta = F(x-ct) + f(x+ct) \tag{VI.9}$$

in which $c = \sqrt{gh}$, and where F and f are arbitrary functions. In other words, the first term is a progressive wave travelling with velocity c in the

direction of x -positive. In the same way the second term of equation (VI.9) represents a progressive wave travelling with velocity c in the direction of x -negative and it appears, since equation (VI.9) is the *complete* solution of equation (VI.8), that any motion whatever of the fluid, which is subject to these conditions, may be regarded as made up of waves of these two kinds.

If in any case of waves travelling in one direction only, without change of form, we impress on the entire water mass a velocity $-c$, equal in force and in opposite direction to the velocity of propagation, the motion becomes steady, whilst the forces acting on any particle remain the same as before. Bernoulli's theorem for the free surface gives then

$$\frac{p}{\rho_0} + g\eta + \frac{1}{2}(u-c)^2 = \text{constant} . \quad (\text{VI.10})$$

If b is the width of the canal, a water-mass $b(h+\eta)(u-c)$ flows through the cross-section $b(h+\eta)$ to the left, whereas for a cross-section not yet reached by the wave the mass flown through is $-bhc$. If the slope of the wave-profile be everywhere gradual, and the depth h small compared with the wave-length, the horizontal velocity may be taken to be uniform throughout the depth and approximately equal to the velocity. The equation of continuity then gives

$$u = \frac{c}{h+\eta} \eta \quad (\text{VI.11})$$

or, if η is small compared to h , $u = c/h\eta$. If we substitute in (VI.10), we obtain

$$\frac{p}{\rho} + g\eta + \frac{c^2}{2} \left(1 - \frac{\eta}{h}\right)^2 = \text{constant} . \quad (\text{VI.12})$$

With the condition for a free surface $p = \text{const.}$ and by developing into series, we obtain the relation

$$g\eta + \frac{3}{2}c^2 \frac{\eta^2}{h^2} + \dots = c^2 \frac{\eta}{h} .$$

If η^2 is small compared to h^2 , we get for c the Lagrangian formula $c = \mathbf{J}(gh)$; a closer approximation gives

$$c = \mathbf{J}(gh) \cdot \left[1 + \frac{3}{2}(\eta/h)\right] . \quad (\text{VI.13})$$

This equation by ST. VENANT (1870) states that the wave velocity in this second approximation is also independent of the wave length, but it varies with the height, and consequently, such a wave cannot be propagated without change of profile. AIRY (1842) has shown, in applying the method of successive approximations, what variations occur; a complete solution for this has been given by FJELSTAD (1941). In an advancing wave system, the front slopes become steeper, the rear slopes flatter, until finally a point is reached

where it is no longer possible to neglect the vertical acceleration. The wave crests overturn and break.

Table 18a gives the Lagrangian velocity of propagation c for various depths. The appendix contains an extensive table. The bottom line of the

Table 18a. Wave velocity according to Lagrange for several depths

h in m	100	200	500	1000	1500	2000	3500	5000
c in m/sec	31	44	70	99	121	140	185	221
c in n.m./h	61	86	136	192	236	272	360	430
Travel time of a wave over a distance equal to the earth's circumference, h	354	251	159	112	92	79	60	50

table gives the time needed by a wave to travel over a distance equal to the circumference of the earth $2\pi R$. In order that a long wave complete this distance within one day (24 h), the water depth should be 22 km. This result is important in relation to the theory of the tides.

(b) Canal with uniform arbitrary cross-section

KELLAND (1839, p. 497) has extended the results obtained for a canal of constant rectangular cross-section to a uniform canal of any form of section. The equation of horizontal motion (VI.5) remains unchanged, but the form of the cross-section of the canal is introduced into the equation of continuity. If the area of the section is S when the surface is undisturbed, its width at the free surface b , we obtain, in case there are no cross-currents or pressure gradients perpendicular to the canal, the equation of continuity

$$\frac{\partial(\xi S)}{\partial x} + \eta b = 0. \tag{VI.14}$$

If S and b are constant and $\bar{h} = S/b$ denotes the mean depth of the canal, we can also use in this case the Lagrangian equation

$$\eta = -h \frac{\partial \xi}{\partial x},$$

if the mean depth \bar{h} is substituted for h . If, however, the width b is not constant, when the wave passes by, which is the case for a canal with sides inclined, conditions are changed and the Lagrangian equation cannot be applied. MACCOWAN (1892) has dealt with a canal with sides inclined and he studied the question if the change of the wave profile caused by the propagation of the wave with a velocity (VI.13) could be cancelled through an appropriate form of the slope, so that the wave form would be again permanent. This can be done, whereby the cross-section below the water

Table 18b. Velocity of long waves according to Lagrange's Equation in n.m. for 45° latitude

Depth (m)	0	1	2	3	4	5	6	7	8	9
0	0.0	6.1	8.6	10.5	12.2	13.6	14.9	16.1	17.2	18.3
10	19.3	20.2	21.1	22.0	22.8	23.6	24.3	25.1	25.8	26.5
20	27.2	27.9	28.6	29.2	29.8	30.4	31.0	31.6	32.2	32.8
30	33.3	33.9	34.4	35.0	35.5	36.0	36.5	37.0	37.5	38.0
40	38.5	39.0	39.5	39.9	40.4	40.8	41.3	41.7	42.2	42.6
50	43.0	43.5	43.9	44.3	44.7	45.5	45.6	46.0	46.4	46.8
60	47.2	47.5	47.9	48.3	48.7	49.1	49.5	49.8	50.2	50.6
70	50.9	51.3	51.7	52.0	52.4	52.7	53.1	53.4	53.8	54.1
80	54.4	54.8	55.1	55.5	55.8	56.1	56.5	56.8	57.1	57.4
90	57.8	58.1	58.4	58.7	59.2	59.3	59.7	60.0	60.3	60.6

Depth (m)	0	10	20	30	40	50	60	70	80	90
100	60.9	63.8	66.7	69.4	72.0	74.6	77.0	79.4	81.7	84.0
200	86.1	88.2	90.3	92.3	94.3	96.3	98.2	100.0	101.9	103.7
300	105.4	107.2	108.9	110.6	112.2	113.9	115.5	117.1	118.6	120.2
400	121.7	123.2	124.8	126.2	127.7	129.1	130.6	132.0	133.4	134.8
500	136.1	137.5	138.8	140.1	141.5	142.8	144.0	145.3	146.6	147.8
600	149.1	150.3	151.5	152.7	154.0	155.2	156.4	157.5	158.7	159.9
700	161.6	162.2	163.3	164.5	165.6	166.7	167.8	168.9	170.0	171.1
800	172.2	173.3	174.3	175.4	176.4	177.4	178.4	179.5	180.6	181.6
900	182.6	183.6	184.6	185.6	186.6	187.6	188.6	189.6	190.6	191.5

Depth (m)	0	100	200	300	400	500	600	700	800	900
1000	192.5	201.9	210.9	219.5	227.8	235.8	243.5	251.0	258.3	265.3
2000	272.2	279.0	285.5	291.9	298.2	304.4	310.5	316.3	322.1	327.8
3000	333.4	338.9	344.3	349.7	354.9	360.1	365.2	370.3	375.4	380.4
4000	385.0	389.8	394.5	399.2	403.8	408.3	412.9	417.3	421.7	426.1
5000	430.4	434.7	438.9	443.2	447.3	450.4	456.6	459.6	463.6	467.6
6000	471.5	475.4	479.3	483.2	487.0	490.8	494.5	498.3	502.0	505.6
7000	509.3	512.9	516.5	520.1	523.7	527.2	530.7	534.2	537.6	541.0
8000	544.5	547.9	551.2	554.6	558.0	561.1	564.5	567.8	571.1	574.2
9000	577.5	580.6	583.8	587.0	591.6	593.3	596.5	599.5	602.6	605.6

level remains entirely free; on the contrary, the width b_z of the canal above this level must satisfy the equation

$$b_z = b_0 \left(1 - \frac{2z}{\bar{h}} \right)^{-3/2}.$$

The origin of the co-ordinates lies in this level, the x -axis in the direction of the canal, the z -axis upwards, the y -axis in a direction perpendicular to the x -axis and \bar{h} is the mean depth of the lower part of the canal (Fig. 67).

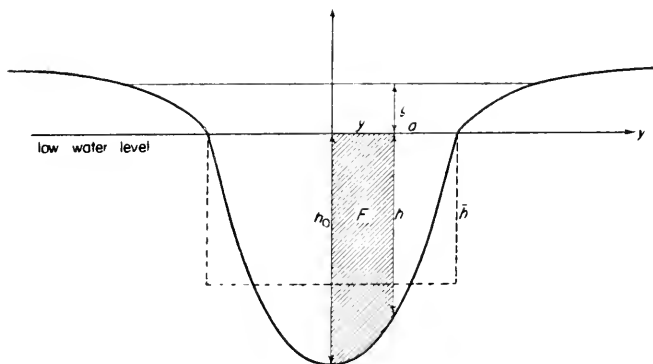


FIG. 67. Section of canal to compute the transverse current with longitudinal waves in a canal (MacCowan).

It is not necessary that, like in the figure, the cross-section of the lower part of the canal be symmetrical to the centre line, only the upper part must satisfy this condition. The sharp bend of the slope appearing in the low water line reminds, as Thorade remarks, of the channels of the Watten, but it is doubtful whether, cross currents can be completely disregarded in such cross-sections. THORADE (1931, p. 76) has estimated the cross-currents which are possible in such cases, provided there is no transversal slope of the water surface.

In the shaded part of the cross-section F in Fig. 67 reaching from $y = 0$ to y , the flow section is $F + y\eta$ and the the volume of the flow per second $M = u(F + y\eta)$. Through a second cross-section at a distance δx flows a volume $M + (\partial M / \partial x) \delta x$. The amount of water staying per second in the considered volume element is $-(\partial M / \partial x) \delta x$. Let v be the velocity of the cross-current, which will be equal to zero in the middle of the canal if the cross-section is symmetrical; in the lateral distance y the velocity will be v and through the profile $(h + \eta) \delta x$ flows the volume $v(h + \eta) \delta x$. In this volume element there remains per second the water volume $-v(h + \eta) \delta x$. The increase in volume must result in a rise of the water surface $\partial \eta / \partial t$ per second above a surface $y \delta x$. This gives following equation:

$$(F + y\eta) \frac{\partial u}{\partial x} + yu \frac{\partial \eta}{\partial x} + v(h + \eta) + \frac{\partial \eta}{\partial t} y = 0.$$

If we add the equation of continuity (VI.7) in which ξ is replaced by u (\bar{h} is the mean depth) and neglect the members of second order, this equation is simplified to

$$vh = (\overline{hy} - F) \frac{\partial u}{\partial x} \quad \text{or} \quad vh = \frac{F - \overline{hy}}{h} \frac{\partial \eta}{\partial t}.$$

If we put

$$\eta = Z \cos(\sigma t - \kappa x); \quad u = U \cos(\sigma t - \kappa x) \quad \text{and} \quad v = V \sin(\sigma t - \kappa x) \tag{VI.15}$$

we obtain

$$\frac{V}{U} = \frac{2\pi}{\lambda} \cdot \frac{\overline{yh} - F}{h}.$$

This means that the ratio of the maximum values of the cross-current and longitudinal current is proportional to the area by which the hatched part F exceeds the rectangle yh ; besides, \overline{u} is proportional to λ and \overline{h} . For a canal with a rectangular cross-section we have always $F = \overline{yh}$, so that everywhere $v = 0$; for a concave canal (as in Fig. 67) we always have $F > \overline{yh}$ until at $y = \frac{1}{2}b = a$ (half the width of the canal) $F = \frac{1}{2}Q = \overline{ah}$, and there v also becomes zero. Therefore, v has always the same sign as $\partial\eta/\partial t$. If the water rises in the canal, the cross-current flows from the middle to the bank; if it drops, it flows from the bank to the middle. These conclusions, of course, apply only if there is no transversal slope of the water surface in the canal.

AIRY (1842, par. 358–63) has expressed the opinion that, in a wide canal, in which cross-currents are probable, the wave crests are bent because the wave will travel faster in the middle of the canal than at the shallower sides. But rather soon it was recognised that this idea did not seem to be conclusive. Much later PROUDMAN (1925, p. 466) has proven that for a canal with a parabolic cross-section, Airy's assumption in regard to the bending of the wave crests is not correct. The crest line is always a straight line perpendicular to the canal, and the effect of different velocities of each part of the wave are equalized. To the contrary, the wave height perpendicular to the canal does not remain constant and increases towards the bank. At high water, the current flows in the direction of the canal and the cross-current is zero; with falling tide the current flowing towards the middle of the canal becomes stronger and attains its maximum, when the surface goes through its position of equilibrium, then it decreases again and becomes again zero at low water, when the current flows again in the direction of the canal, but now in the opposite direction. With rising water, the cross-current flows from the middle to the banks. The current, therefore, can be represented by an ellipse with a different direction of rotation at both banks; in the middle of the canal there is only an alternating current.

The equations of motion and the equation of continuity, in this case have the form

$$\left. \begin{aligned} \frac{\partial u}{\partial t} = -g \frac{\partial \eta}{\partial x}; \quad \frac{\partial v}{\partial t} = -g \frac{\partial \eta}{\partial y}, \\ \frac{\partial}{\partial x}(h \cdot u) + \frac{\partial}{\partial y}(h \cdot v) + \frac{\partial \eta}{\partial t} = 0. \end{aligned} \right\} \tag{VI.16}$$

Moreover, the solution must satisfy the condition that (VI.18)

$$hv = 0 \quad \text{for} \quad y = \pm a, \tag{VI.17}$$

when a is the half width of the canal (origin of co-ordinates in the middle of the canal). We assume a solution of the equation (VI.15), in which Z, U, V must only be functions of y . If we introduce these values into (VI.16), these functions must fulfill the following equations ($c = \sigma/\varkappa$)

$$U = \frac{g}{c} Z, \quad V = -\frac{g}{c} \frac{dZ}{dy}, \quad \frac{d}{dy} \left(h \frac{dZ}{dy} \right) + \left(\frac{\sigma^2}{g} - \varkappa^2 h \right) Z = 0. \quad (\text{VI.18})$$

The boundary condition (VI.17) becomes

$$h \frac{dZ}{dy} = 0 \quad \text{for } y = \pm a. \quad (\text{VI.19})$$

If we consider a canal of parabolical cross-section, then

$$h = h_0 \left(1 - \frac{y^2}{a^2} \right), \quad (\text{VI.20})$$

in which h_0 is the maximum depth in the middle of the canal. The mean depth of the water is $\bar{h} = \frac{2}{3} h_0$. The equations (VI.18) and (VI.19) now become

$$\frac{d}{dy} \left[\left(1 - \frac{y^2}{a^2} \right) \frac{dZ}{dy} \right] + \left[\frac{\sigma^2}{gh_0} - \varkappa^2 \left(1 - \frac{y^2}{a^2} \right) \right] Z = 0, \quad (\text{VI.21})$$

and

$$\left(1 - \frac{y^2}{a^2} \right) \frac{dZ}{dy} = 0 \quad (\text{for } y = \pm a).$$

A symmetrical solution can be represented in the form of an infinite series

$$Z = A_0 + A_2 \frac{y^2}{a^2} + \dots + A_n \frac{y^n}{a^n} \quad (\text{VI.22})$$

(n even whole numbers). The substitution gives for the coefficients

$$2A_2 + \left(\frac{\sigma^2 a^2}{gh_0} - \varkappa^2 a^2 \right) A_0 = 0. \quad (\text{VI.23})$$

and

$$(n+2)(n+1)A_{n+2} - (n-1)A_n + \left(\frac{\sigma^2 a^2}{gh_0} - \varkappa^2 a^2 \right) A_n + \varkappa^2 a^2 A_{n-2} = 0.$$

The determination of the coefficients A results in continued fractions similar to those developed by Laplace in his theory of tides, and to a relation between σ and \varkappa , which determines the wave velocity c . We then obtain

$$\varkappa^2 = \frac{3}{2} \frac{\sigma^2}{gh_0} \left(1 + \frac{1}{30} \frac{\sigma^2 a^2}{gh_0} \right). \quad (\text{VI.24})$$

The average depth of the canal being $\bar{h} = \frac{2}{3} h_0$ we find

$$c = \sqrt{(g\bar{h})} \cdot \left[1 - \frac{4\pi^2 a^2}{90} \right] \left(\text{if we put } a = \frac{a}{\lambda} \right). \quad (\text{VI.25})$$

Consequently, in first approximation, the wave velocity $\sqrt{(g\bar{h})}$ which checks with the rule of Kelland according to which the Lagrangian equation applies, when we take the mean depth of the canal as the water depth. If A_0 is the wave amplitude in the middle of the canal, we have

$$\left. \begin{aligned} Z &= A_0 \left[1 + \frac{4\pi^2 a^2}{6} \frac{y^2}{a^2} + \frac{16\pi^4 z^4}{216} \frac{y^4}{a^4} + \dots \right], \\ U &= \frac{g}{c} Z \quad \text{and} \quad V = -\frac{g}{c} A_0 \frac{2\pi a}{3} \frac{y}{a} \left[1 + \frac{4\pi^2 a^2}{18} \frac{y^2}{a^2} + \dots \right]. \end{aligned} \right\} \quad \text{(VI.26)}$$

Thus if a canal has the following dimensions 200 km wide ($a = 100$ km) $h_0 = 100$ m and $A_0 = 100$ in the middle of the canal, with a wave period $T = 12$ h 25 min (tidal wave period), the distribution of wave heights and of the ratio $V:U$ across the canal (Table 18c) the wave velocity becomes

Table 18c

y/a	0.0	0.1	0.2	0.3	0.4	0.5
Wave height	100	100	101	102	103	105
$V:U$	0.00	0.037	0.073	0.109	0.144	0.178

$c = 0.9966 \sqrt{gh}$ and one recognizes the good approximation with (VI.25) when the expression between brackets is ignored. In a parabolical canal a wave travels with rectilinear crests and constant velocity when the wave height is almost constant. There is no doubt that, when the cross-sections of the canal are more complicated, the influence of the bottom configuration in the transversal direction on the formation of the waves is equally small as in the case under consideration as far as the wave crests and the wave velocity are concerned.

(c) Wave Motion in a Canal of Variable Section in the Direction of Propagation

If we introduce in the equation of continuity (VI.14) which is also valid in this case, the surface of the cross-section $S = b\bar{h}$, in which \bar{h} is the mean depth over the width b , we get

$$\eta = -\frac{1}{b} \frac{\partial}{\partial x} (\bar{h} b \xi), \quad \text{(VI.27)}$$

where \bar{h} and b are functions of x . The dynamical equation has the same form (VI.5) as before. By eliminating ξ we obtain

$$\frac{\partial^2 \eta}{\partial t^2} = \frac{g}{b} \frac{\partial}{\partial x} \left(\bar{h} b \frac{\partial \eta}{\partial x} \right). \quad \text{(VI.28)}$$

The laws of propagation of waves in a canal of gradually varying rectangular section were first investigated by GREEN (1837). RAYLEIGH (1876) showed (see p. 121) that, considering the principle of energy, it follows from the variation in the cross-sections that the amplitude of the wave in such a canal is inversely proportional to the square root of the width and the fourth root of the depth.

If we take a solution of the equation (VI.28) similar to that with a constant h , we can assume

$$\eta = \eta_0 \cos \sigma(t - \varphi), \quad \text{(VI.29)}$$

whereby we substitute the unknown function $\varphi(x)$ for x/c . If we introduce this expression into (VI.28)

and separate the terms with $\cos\sigma(t-\varphi)$ and $\sin\sigma(t-\varphi)$, which by themselves must be zero, we obtain the relations

$$\frac{d}{dx} \left(bh \frac{d\eta_0}{dx} \right) + \left(\frac{b}{g} - hb\varphi'^2 \right) \sigma^2 \eta_0 = 0$$

and

$$(hb)' \eta_0 \varphi' + 2hb\eta_0' \varphi' + hb\eta_0 \varphi'' = 0.$$

From the last equation follows $hb\eta_0^2 \varphi' = \text{constant} = C$; so that

$$\frac{d}{dx} \left(hb \frac{d\eta_0}{dx} \right) + \left(\frac{b}{g} - \frac{C^2}{hb\eta_0^4} \right) \sigma^2 \eta_0 = 0. \tag{VI.30}$$

If the variable velocity, according to Kelland, were $\mathbf{v}'(gh)$, then $\varphi = \int \frac{dx}{\mathbf{v}'(gh)}$; then the second term at the left of the equation (VI.30) will vanish provided that

$$\eta_0 = \text{prop } b^{-1/2} h^{-1/4}. \tag{VI.31}$$

The equation (VI.30) is therefore satisfied assuming that the first term can be neglected. But (VI.31) is the law of amplitude by Green which has as a condition that

$$\frac{d}{dx} \left(hb \frac{d\eta_0}{dx} \right) \ll \frac{b\sigma^2}{g} \eta_0. \tag{VI.31a}$$

It can be shown that $\frac{1}{2}(b''/b)$, $\frac{1}{4}(b'/b)^2$, and $\frac{1}{4}(h''/h)$, $\frac{1}{16}(h'/h)^2$ and $\frac{1}{2} \frac{b'}{b} \frac{h'}{h} \ll \left(\frac{2\pi}{\lambda} \right)^2$ respectively. In order that, for instance

$$\frac{\lambda^2}{h^2} h'^2 \ll 64\pi^2,$$

dh/dx must be small compared to h/λ . The same applies for the other terms $\frac{1}{2}(b'/b)$, $\frac{1}{4}(b'/b)^2$, $\frac{1}{4}(h'/h)$, $\frac{1}{16}(h'/h)^2$ and $\frac{1}{2}(b'h'/bh) \ll (2\pi/\lambda)^2$ respectively. (VI.31a) is equivalent to the condition that $\lambda(db/dx)$, and $\lambda(dh/dx)$ are small compared with b and h respectively. In other words, it is assumed that the transverse dimensions of the canal vary only by small fractions of themselves within the limits of a wave length. Therefore, it is not to be expected that the law of Green applies to long waves, such as tidal waves and sea-quake waves, (see p. 237), whereas it can be used, for instance, for shorter shallow water waves.

It was customary to substitute the mean or average depth h for the exact depth h in the equation $c = \mathbf{v}(g/h)$ (when the depth changes in the direction of the propagation of the wave). Sometimes the average depth of a sea was computed from the duration of travel of a long wave. The bad results (see p. 239) obtained have shown that the use of the simple formula $c = \mathbf{v}(gh)$ is not permissible. DU BOYS (see FOREL, 1895) has tried to avoid these difficulties in assuming for the travel time of a long wave

$$t = \int \frac{dx}{\mathbf{v}[gh(x)]}. \tag{VI.32}$$

Green's investigations have shown that this formula can only be used under certain conditions, which are not satisfied for all long waves in nature.

THORADE (1926a, b, p. 217), investigated the behaviour of a long wave,

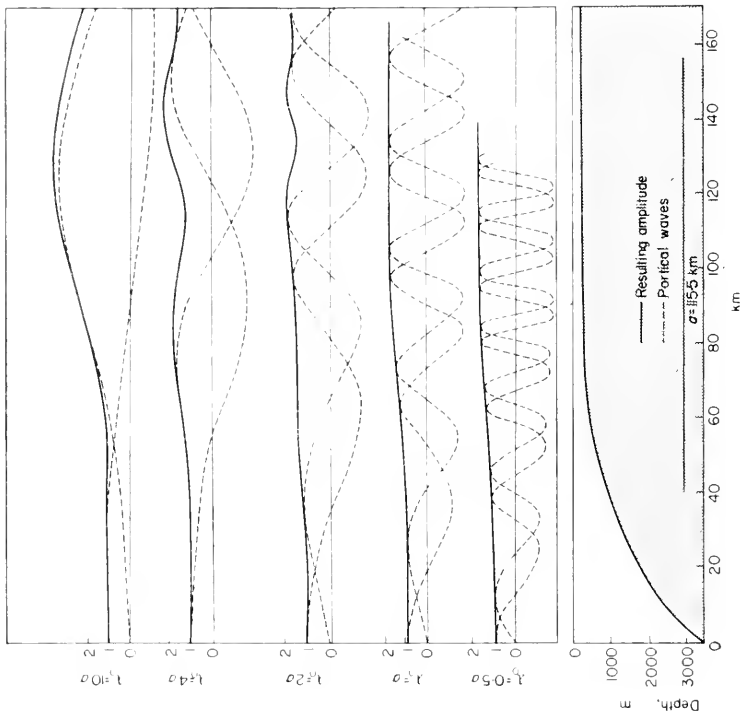


FIG. 68.

Variation in profiles of long waves traveling over a concave slope. The dotted partial waves indicate the wave profile in two moments, $\frac{1}{4}$ periods apart. The profiles after $\frac{1}{4}$ respectively $\frac{3}{4}$ period are obtained by a mirror image of the curves with respect to the x -axis. The scale indicating the depths and wave height are exaggerated for the latter ones more than for the first ones.

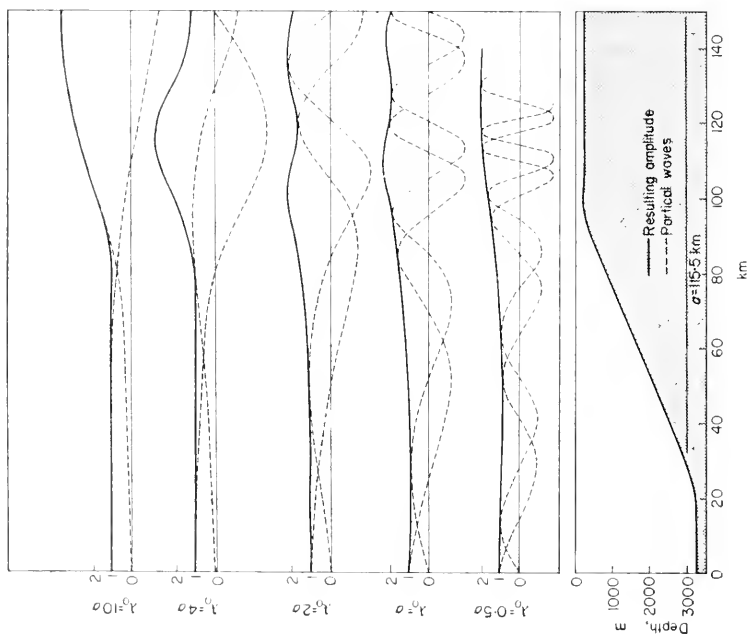


FIG. 69.

Variation of profiles of long waves travelling over a convex slope (See Fig. 68).

when the depth changed rapidly. He determined the shape of a long wave, travelling from deep ocean (depth h_0) over a concave, convex or flat slope into a shallow sea (depth h_1). The dimensions of the bottom profile corresponded approximately to those of the continental shelf, which slopes down from the shelf to the deep sea. His method consisted in the splitting up of a progressive wave

$$\eta = \eta_0 \cos(\sigma t - \kappa x)$$

into two standing waves

$$\eta = \eta_1 \cos \sigma t + \eta_2 \sin \sigma t,$$

whose behaviour was examined separately. Their superposition then represents the progressive wave. Figs. 68 and 69 are examples, namely for $h_0 = 3200$ m and $h_1 = 200$ m, for a slope 100 km long, which is defined by the bottom $h = h_0(1 \pm x^2/a^2)$ and $a = 115.5$ km. The wave length over the deep water is λ_0 . The dotted wave trains represent the partial waves η_1 and η_2 and are at the same time wave profiles for $\sigma t = 0^\circ$ and 90° . For $\sigma t = 180^\circ$ and 270° the wave profiles are obtained by inverting η_1 and η_2 and it can be seen that when the wave passes over the slope its wave length decreases with its amplitude increasing. For $\lambda_0 = a$ and smaller values Green's formula still applies with fairly close approximation, but for greater wave lengths the two partial waves do not fit any longer and are displaced in such a way that there are important deviations from this equation. The variation in amplitude (full line) does not agree any longer with this law

$$\sqrt[4]{h_0} : \sqrt[4]{h_1} = 2,$$

but follows the simpler one

$$\sqrt[3]{h_0} : \sqrt[3]{h_1} = 4.$$

Therefore, the ratio shows a considerably higher value than Green's equations.

Table 19. Travel time of high water in minutes over a slope 100 km long and rising from 3200 m to 200 m depth ($a = 200: \sqrt[3]{3} = 115.5$ km)

Wave length over 3200 m depth	0.5a	a	2a	4a	6a	10a	Very large	According to Green	computed from 100 km/ $\sqrt[3]{gh}$	
Rising {	Slope									
	Concave	14.3	14.4	14.5	16.2	18.5	22.1	26.0	14.3	12.0
	Convex	22.7	22.7	22.1	20.3	21.7	28.6	65.0	22.7	17.2
Flat	15.1	15.1	15.5	16.3	18.6	22.2	27.8	15.1	12.9	
Falling {	Concave	14.3	14.1	13.9	11.1	7.9	7.0	6.5	14.3	12.0
	Convex	22.7	22.6	22.1	20.5	18.3	17.0	16.1	22.7	17.2
	Flat	15.1	15.1	14.5	12.4	8.9	7.5	7.0	15.1	12.9

Also the travel time, where a distinction should be made between that of the wave crest and that of the high tide, are different from those obtained from Green's hypothesis, as can be seen from Table 19 for the travel times of high tide. The difference as against those computed from the Green-Du Boys equation is considerable, especially for the ones computed from the mean depth \bar{h} .

Thorade's papers are important for tidal waves coming from the deep ocean on to the continental shelf. Unfortunately, there are hardly any observations available to test the theoretical results. Tidal waves passing over irregularities of the ocean bottom, as for instance a wavy bottom, shallow places and the like, will show variations in their wave length and amplitude. It would certainly be well worth while to make systematical observations on such variations.

2. Standing Waves in Closed Basins

(a) *Constant Rectangular Section*

The equations of motion as formulated in (VI.8) also has a solution in the form of a standing wave, for the reason that the superposition of two progressive waves with corresponding phase difference always causes a standing wave.

This standing wave can also result from the superposition of an incoming wave and its reflection from a vertical wall. If the reflection occurs at $x = 0$ at the vertical wall, and if η_1 is the incoming, η_2 the reflected wave then

$$\begin{aligned}\eta_1 &= \frac{1}{2} a \cos(\sigma t - \kappa x), & \eta_2 &= \frac{1}{2} a \cos(\sigma t + \kappa x), \\ \eta &= \eta_1 + \eta_2 = a \cos \kappa x \cos \sigma t.\end{aligned}\tag{VI.33}$$

Equation (VI.8) required that $c = \sigma/\kappa = \frac{1}{n} (gh)$, or that the period of the oscillation $T = \lambda/\frac{1}{n} gh$ or

$$T = \frac{2l}{n \frac{1}{n} (gh)},\tag{VI.34}$$

when n is a positive integer greater than zero and l the length of the rectangular basin (Merian's formula). It is readily seen that n is the number of nodes of the standing wave.

For ($n = 1$) we obtain the longest period of the free oscillating water-mass $T = 2l/\frac{1}{n} (gh)$; in the centre of the basin ($x = \frac{1}{2}l$) there is one nodal point ($\eta = 0$) with maximum values of ξ , which also follows directly from solving for

$$\xi = -\frac{a}{h\kappa} \sin \kappa x \cos \sigma t \quad \text{and} \quad u = \frac{ca}{h} \sin \kappa x \sin \sigma t.\tag{VI.35}$$

For $n = 2, 3$, etc., we have two, three, etc., node oscillations. For the n th nodal oscillation, the node is situated at

$$x_k = \frac{l}{2n} (2k + 1),$$

in which k will be $0, 1, \dots$ to $(n-1)$. The antinodes, on the contrary, are situated at $x_B = (l/n)k$ and $k = 0, 1, \dots$ to n .

The streamlines of a two-nodal standing wave are represented in Fig. 70. It shows that, at the antinodes the horizontal motion of the particles disappears completely, and the vertical motion is at a maximum, whereas at the nodal points the movements are reversed.

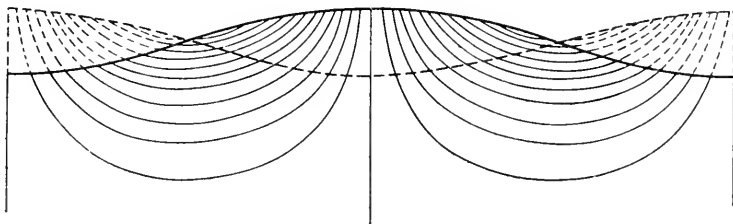


FIG. 70. Streamlines of a binodal standing oscillation.

When the depth is not negligible compared with the wavelength λ , we obtain with equation $T = 2l/c$ as a more exact equation for the period of the free oscillation with one node (see VON DER MUEHL, 1886, p. 575).

$$T = 2 \sqrt{\left(\frac{\pi l}{g} \coth \frac{\pi h}{l} \right)}.$$

If $\pi h/l$ is small, we obtain as a second approximation instead of (VI.34)

$$T = \frac{2l}{n \sqrt{gh}} \left[1 + \left(\frac{\pi h}{2l} \right)^2 \right].$$

We also wish to point out that in the equation for the period of oscillation (VI.34) the density of the oscillating medium does not appear. Forel has proven this by means of laboratory tests in a trough with water, mercury and alcohol.

(b) Effect of Friction on Oscillations in a Rectangular Basin

The motions related to the oscillations of a water-mass in a basin are subject to frictional influences which are due, on one hand to molecular friction and, on the other hand to frictional stresses at boundary surfaces, namely at the bottom and the walls of the basin. The free oscillations of a water-mass in a basin of a given cross-section would last indefinitely, once they are generated, were it not that the energy is gradually dissipated through friction. When there are no other disturbing influences, the amplitude of the oscillations decreases gradually, whereas the period of the oscillations increases slightly through friction. The influence of the friction can be illustrated by adding to the right side of the equation of motion for the horizontal displacement of the water-mass (VI.8) another term of the form

$-\beta(\partial\xi/\partial t)$. The frictional force is thus assumed to be proportional to the horizontal velocity u , an assumption which can indicate only roughly the real frictional influences but which permits to make numerical computations. This gives some idea of the effects of friction. The quantity β has the dimension $[\text{sec}^{-1}]$ and characterizes the boundary friction at the bottom and on the walls of the basin.

The equation of motion

$$\frac{\partial^2 \xi}{\partial t^2} = -\beta \frac{\partial \xi}{\partial t} + c^2 \frac{\partial^2 \xi}{\partial x^2} \quad (\text{VI.36})$$

has a solution in the form $\xi = ae^{\gamma t + i\kappa x}$, and by substituting we find that

$$\gamma^2 + \beta\gamma + c^2\kappa^2 = 0 \quad \text{or} \quad \gamma = \frac{1}{2}\beta \pm i\sqrt{(c^2\kappa^2 - \frac{1}{4}\beta^2)}.$$

If with $\kappa = n\pi/l$, $\xi = 0$ for $x = 0$ and $x = l$ and when, moreover, we put for the free constants

$$a_1 = \frac{1}{2}Ae^{+i\epsilon} \quad \text{and} \quad a_2 = -\frac{1}{2}Ae^{+i\epsilon}$$

we obtain as the final equation of oscillation for ξ

$$\xi = Ae^{-\frac{1}{2}\beta t} \cos \left| (c^2 - \kappa^2 - \frac{1}{4}\beta^2)(t - \epsilon) \right| \sin \kappa x. \quad (\text{VI.37})$$

The damping factor is represented by $e^{-(\frac{1}{2}\beta)t}$ and the logarithmic decrement λ can be computed from the decay of the amplitude (see p. 9). The coefficient of friction β can be computed from the logarithmic decrement; when A_1 is the amplitude at the start and T the period, the amplitude after n half waves is

$$A_n = A_1 e^{-(\frac{1}{2}\beta)n(\frac{1}{2}T)},$$

and from the equation (VI.37) results

$$\lambda = \frac{1}{4}\beta T. \quad (\text{VI.38})$$

If we designate by $T_n = 2l/n_1(gh)$ the period without any effect of friction, the period of the damped oscillation T_r will be from (VI.37)

$$T_r = \frac{2l}{n \sqrt{gh - \frac{\beta^2 l^2}{4\pi^2}}} = T_n \left(1 + \frac{\beta^2 T^2}{32\pi^2} + \dots \right). \quad (\text{VI.39})$$

For water depths of 50–100 m β is of the order of magnitude of 10^{-5} sec^{-1} and the factor of T^2 in the brackets is of the order of magnitude of 3×10^{-13} . This leads to belief that the influence of the friction on the period of the oscillations of water-masses in closed basins is small under normal circumstances.

The influence of the molecular friction on standing waves can be determined more correctly by starting from the complete equations of motion with the usual frictional terms. Its solution leads to simple results, assuming that

the kinematic coefficient of viscosity ν is small, which is the case for water. For a standing wave in a rectangular basin of the length l HIDAHA (1932) finds in this manner that in a first approximation the period of the free oscillation is not different from Merian's formula, but that the amplitude of the n th nodal oscillation decreases with the damping factor $\tau = l^2/(2n^2\pi^2\nu)$. This is the same damping factor found previously for the decrease in amplitude of waves of the wave length $2l/n$ through friction (see p. 79).

Using greater values of ν , far more correct solutions of the equations of motion are obtained where the frictional terms and the corresponding boundary conditions are taken into consideration. Solutions of this kind have been given by DEFANT (1932); they are to be found also in a paper of PROUDMAN and DOODSON (1924, p. 140), to which we will refer later. However, they do not show the frictional influences as clearly as the simple assumption stated previously.

The stresses in different fluids under similar circumstances of motion will be proportional to the corresponding values of μ ; but if we wish to compare their effects in modifying the existing motion we have to take account of the ratio of these stresses to the inertia of the fluid. From this point of view the determining quantity is the ratio $\mu/\rho = \nu$, the kinematic coefficient of viscosity.

The equations of motion and of continuity now takes the form

$$\frac{\partial u}{\partial t} = -g \frac{\partial u}{\partial x} + \nu \frac{\partial u^2}{\partial z^2} \quad \text{and} \quad \frac{\partial}{\partial x} \int_{-h}^0 u dz + \frac{\partial \eta}{\partial t} = 0, \tag{VI.40}$$

when ν is the kinematic coefficient of viscosity ($\text{cm}^2 \text{sec}^{-1}$) and when the origin of the co-ordinates lies in the undisturbed water surface and the depth is $-h$.

We have to add, the boundary conditions that $u = 0$ for $x = 0$ and $x = l$, as well as for $z = -h$; also no wind on the water surface and $\partial u/\partial z = 0$ for $z = 0$. Part of the condition is fulfilled at once, if we start with u proportional to $\sin \kappa x$, where $\kappa l/\pi = n$ ($n = 1, 2, 3, \dots$).

For the general solution one can select the form

$$\left. \begin{aligned} \kappa \eta &= \cos \kappa x \cdot e^{-(\epsilon\nu/h^2)t}, \\ \frac{\nu}{gh^2} u &= \sin \kappa x \cdot v(z) e^{-(\epsilon\nu/h^2)t}. \end{aligned} \right\} \tag{VI.41}$$

ϵ is a numerical parameter and $v(z)$ a certain function of z . If we put

$$a = \frac{\nu^2}{g\kappa^2 h^5}, \tag{VI.42}$$

the equation of continuity gives

$$\frac{1}{h} \int_{-h}^0 v(z) dz = a\epsilon,$$

and the equation of motion

$$h^2 \frac{d^2 v}{dz^2} + \epsilon v + 1 = 0.$$

A solution of the latter equation, when the boundary conditions are fulfilled, is

$$v(z) = \frac{1}{\epsilon} \left\{ \frac{\cos \epsilon^{1/2}(z/h)}{\cos \epsilon^{1/2}} - 1 \right\},$$

whereas the former gives an equation for ϵ in the form

$$\tan \epsilon^{1/2} = \epsilon^{1/2} + a\epsilon^{5/2}. \tag{VI.43}$$

To each root of this equation ϵ_s corresponds a $v_s(z)$, and the general solution of the two equations (VI.40), when A_s are constant coefficients, is

$$\begin{aligned} \kappa \eta &= \cos \kappa x \sum_s A_s e^{-(\epsilon_s v/h^2)t}, \\ \frac{v}{gh^2} u &= \sin \kappa x \sum_s A_s v_s(z) e^{-(\epsilon_s v/h^2)t}. \end{aligned} \tag{VI.44}$$

Most important is the determination of the roots ϵ_s of equation (VI.43), if a is given, which Proudman had done in an elegant manner. First, it can be shown that, if a is considered as a function of ϵ , this equation has a minimum for the values

$$\epsilon^{1/2} = 1.1122 \text{ and } a = 0.5370. \text{ For values } a < 0.5370$$

there are no real values smaller than $\frac{1}{2}\pi$, but there are two conjugated complex roots. The real values can be computed approximately from $\frac{1}{2}\pi r$ ($r = 3, 5, 7, \dots$), except if a is very small, from $\epsilon^{1/2} = \frac{1}{2}\pi r - \theta$ in which

$$1/\theta = \frac{1}{2}r\pi + a(r\frac{1}{2}\pi)^5$$

($r = 3, 5, 7, \dots$).

For the complex roots when $a < 0.5370$ we put $\epsilon^{1/2} = \xi + i\eta$ and $a = a + ib$, where ξ, η, a and b are real and we then derive

$$a = \frac{(t - \xi - \eta t T) + i(T - \eta + \xi t T)}{(1 - i\eta T)(\xi + i\eta)^5},$$

in which

$$t = \tan \xi \quad \text{and} \quad T = \tanh \eta.$$

We now must find these correlated values for ξ and η , for which $b = 0$. The numerical determination occurs in such a way that, with an arbitrary value of η , ξ is being varied until the relation for a gives $b = 0$. Table 20 gives such correlated values up to $\xi = \pi$, according to Proudman and Doodson; an extension to $\xi = 100$ was made by LETTAU (1934, p. 13). As $\epsilon_s = (\xi^2 - \eta^2) + 2\xi\eta i$ and if

$$A_s = p + iq$$

$$R = -2 \sqrt{p^2 + q^2}$$

$$\tan \gamma = q/p$$

we obtain as a contribution to κy :

$$R \cos \kappa x \cdot \exp \left[-(\xi^2 - \eta^2) \frac{v t}{h^2} \right] \cdot \cos \left(2\xi \eta \frac{v t}{h^2} - \gamma \right). \tag{VI.45}$$

This is a standing wave with a damping coefficient

$$\gamma = (\xi^2 - \eta^2) \frac{\nu}{h^2}$$

and the period

$$T_r = \frac{\pi h^2}{\xi \eta \nu} = \frac{T}{2 \xi \eta \alpha}, \tag{VI.46}$$

when T is the period according to Merian's equation.

The value of α is determined with (VI.42) for a given basin by its dimensions and the magnitude of the frictional constants; Table 20 gives the corresponding value of $2 \xi \eta$ which can also be taken from a graph.

Table 20. Computation of the period of the free oscillation in a rectangular trough, taking into account the effect of friction

η	ξ	α	$\xi^2 - \eta^2$	$\frac{1}{2 \xi \eta \alpha}$
0.00	1.1122	0.5370	1.237	∞
0.20	1.1307	0.4732	1.239	3.21
0.40	1.1837	0.3376	1.241	1.82
0.60	1.2670	0.2132	1.245	1.41
0.80	1.3757	0.1284	1.253	1.27
1.09	1.5708	0.0615	1.272	1.17
1.50	1.8916	0.02440	1.328	1.13
2.00	2.3362	0.00936	1.458	1.11
2.84	3.1416	0.00268	1.822	1.08
3.75	4	9.77×10^{-4}	1.937	1.068
4.75	5	4.00	2.437	1.052
5.75	6	1.931	2.937	1.044
6.75	7	1.041	3.437	1.037
7.75	8	0.610	3.937	1.032
9.75	10	0.250	4.937	1.025
14.75	15	4.94×10^{-6}	7.437	1.017
19.75	20	1.562	9.937	1.013
29.75	30	0.309	14.937	1.008
49.75	50	4.00×10^{-8}	24.937	1.005
69.75	70	1.041	34.937	1.003
99.75	100	0.251	49.937	1.0005

Equation (VI.46) for the period of the free oscillating system has lost the simple form of Merian's equation and it is only from numerical examples that we can derive how much the friction increases the period. According to (VI.42) α becomes rapidly very small with increasing depth, and $2 \xi \eta \nu \alpha$ tends to unity, so that T_r will differ only little from T , i.e. the deeper the

basin, the less the period will be affected by friction; the same applies for the logarithmic decrement, which is inversely proportional to the depth of the water-mass.

An example will illustrate the computation. Let us assume a closed basin of $l = 100$ km and $h = 20$ m. Let the frictional coefficient be $\nu = 100$ cm²/sec; then T will correspond to 3.96 h. From (VI.42) it follows that $a = 0.00322$ and from a graph of $\xi - \eta$ and $2\xi\eta\sqrt{a}$ over \sqrt{a} we get the values $\xi = 2.994$ and $\eta = 2.692$. We thus obtain $T_f = 4.35$ h or an increase through friction of 9.9% of the period of the free oscillation. The damping coefficient is $\gamma = 4.29 \times 10^{-5}$ sec⁻¹ = 2.57×10^{-3} min⁻¹ with a logarithmic decrement $\lambda = 0.336$. We can compare these values with the Vättern lake in Sweden with a length $l = 124$ km, greatest depth 120 m, mean depth approx. 54 m. Since for this lake $T = 2.99$ h one obtains the values $\gamma = 0.7 \times 10^{-5}$ min⁻¹ and $\lambda = 0.06$ (see p. 184).

(c) *Variable Cross-section. Theories of Seiches*

Oblong lakes can be considered as basins of variable width and depth. It is to be expected that periodic fluctuations of the water-level will be observed when the water-masses in the lake basin, once the equilibrium is disturbed, oscillate back into equilibrium position. Already in the eighteenth century such oscillations were reported to have been observed in the Lake of Geneva. According to an old chronicle by Schulthaiss, oscillations of this kind were noted at the Lake of Constance as early as in 1549. FOREL (1895) was first in making systematical and methodical observations of the oscillations of the Lake of Geneva in 1869. Since then, these oscillations have been observed in other lakes; they are known as "Seiches". These seiches are free oscillations of a period that depends upon the horizontal dimensions, the depth of the lake and upon the number of nodes in the standing wave. Forel compared the observed periods of the free oscillations of the lake of Geneva with the period derived from Merian's equation: $T = 2l/\sqrt{gh}$ which only applies to a rectangular basin of constant depth. He substituted for the depth h the mean depth of the lake, but the result was not very satisfactory; later on, Du Boys proposed that, if the travel time of the wave is $T = 2l/c$ for a distance $2l$, when the depth h is a constant, the period of a lake with varying depth should be

$$T = 2 \int_0^l \frac{dx}{\sqrt{gh}}$$

in which h represents the depths along a line connecting the lowest points of the bottom of the lake called "Talweg" (valley-way). Although a little better, this relation still left many discrepancies unexplained, especially for the harmonics (multinodal seiches). Forel rightly wondered why the depths of the "Talweg" are taken for h , instead of the mean depths of the single cross-sections, as it is these cross-sections which determine the oscillating process in the whole lake.

The problems connected with free oscillations (seiches) in closed basins of an oblong form, but of variable width and depth, have been the subject

of very complete theoretical investigations. The literature on the seiches theories is very extensive and, therefore, we can only refer here to the most important works. The theoretical considerations only apply for oblong basins, i.e. such basins where there are no components of the horizontal motion in a direction perpendicular to the “Talweg” so that the motion of the water is always parallel to the x -axis, i.e. along the “Talweg” of the lake (see STENIJ, 1932).

The equation of motion has the same form as it had previously [see equation (VI.5)], whereas the equation of continuity [see equation (VI.27)] becomes

$$\eta = -\frac{1}{b(x)} \frac{\partial}{\partial x} (S(x)\xi), \tag{VI.47}$$

if $b(x)$ and $S(x)$ are respectively the variable width at the surface and the variable cross-section of the lake at the point x of the “Talweg”. The boundary conditions, neglecting the friction, are

$$\xi = 0 \quad \text{for } x = 0 \quad \text{and } x = l.$$

(i) *The theory of Chrystal* (1904, p. 328; 1905a, p. 599; 1905b, p. 637). If we introduce into the equations (VI.28) and (VI.47) two new variables

$$u = S(x)\xi \quad \text{and} \quad v = \int_0^x b(x)dx \tag{VI.48}$$

and if we put

$$S(x)b(x) = \sigma(v), \tag{VI.49}$$

we obtain

$$\frac{\partial^2 u}{\partial t^2} = g\sigma(v) \frac{\partial^2 u}{\partial v^2} \quad \text{and} \quad \eta = -\frac{\partial u}{\partial v}. \tag{VI.50}$$

For a lake of a constant width b , but of a variable depth $h(x)$ we obtain, if we put $u = h(x)\xi$,

$$\frac{\partial^2 u}{\partial t^2} = gh(x) \frac{\partial^2 u}{\partial x^2} \quad \text{and} \quad \eta = -\frac{\partial u}{\partial x}. \tag{VI.51}$$

The equations (VI.50) and (VI.51) are identical if we replace x with the variable v . CHRYSTAL proceeds as follows: a great number of cross-sections close to each other are drawn. The width of these cross-sections at the surface is $b_1 \dots b_2 \dots b_n$. The area of each section is called $S_1 \dots S_2 \dots S_n$. The surface of the lake from section o to section i is designated v_i . Chrystal draws a curve which has as abscissa v_i and as ordinate the product $\sigma_i = b_i S_i$. This curve is called by Chrystal, the “Normal curve”. A comparison of (VI.50) and (VI.51) shows that the oscillations of an arbitrarily shaped lake [$b(x)$, $S(x)$] are the same as those of a rectangular basin with variable cross-section in the x -axis, provided the “normal curve” is the “Talweg” of the lake. The form of

the oscillations is geometrically similar in both cases, so that it is sufficient to deal with the simpler case. This “normal curve” alone is decisive for the forms of oscillations of the lake under consideration.

If we select, according to the oscillation

$$u = A(x)\cos(\omega t + \epsilon) \quad \text{when} \quad \omega = 2\pi/T,$$

then the first of the equations (VI.50) gives

$$\frac{d^2A}{dx^2} + \frac{\omega^2}{gh(x)}A = 0, \tag{VI.52}$$

which is to be solved. The problem, therefore, lies in the determination of the form of the oscillations of a basin of constant width but of variable rectangular cross-sections. A requirement by the theory is to have the “normal curve” of a lake substituted by one or several mathematical curves. The “normal curve” can be approximated with sufficient accuracy by a curve or parts of several simple analytical curves.

Chrystal has given the solution for various longitudinal profiles $h(x)$, in which

h	horizontal	$h = h_0$
h	two sloping straight lines	$h = h_0 \left(1 \pm \frac{x}{a}\right)$
h	convex parabolic	$h = h_0 \left(1 + \frac{x^2}{a^2}\right)$
h	concave parabolic	$h = h_0 \left(1 - \frac{x^2}{a^2}\right)$
h	convex “quartic”	$h = h_0 \left(1 + \frac{x^2}{a^2}\right)^2$
h	concave “quartic”	$h = h_0 \left(1 - \frac{x^2}{a^2}\right)^2$.

Table 21. Period of free oscillation of basins with various longitudinal profiles

Period of free oscillation	Main period T_1	Harmonics		
		T_2/T_1	T_3/T_1	T_4/T_1
Longitudinal profile Two sloping straight lines	$1.305 T_0$	0.628	0.434	0.343
Concave parabolic	$1.110 T_0$	0.577	0.408	0.317
Rectangular	$1.000 T_0$	0.500	0.333	0.250
Convex parabolic	$0.950 T_0$	0.472	0.312	0.234

If $T_0 = 2l/\sqrt{gh_0}$, lakes with such longitudinal profiles will have the following periods for the uninodal and multi-nodal (harmonic) oscillations (Table 21). This compilation shows that convex forms shorten the time of all oscillations compared with the simple, horizontal profile, whereas concave forms increase it. Furthermore, it is shown that the nodes of the harmonics tend to move towards the shallow ends of the lake. The shallower the extreme ends of the lake, the stronger this movement is. This is clearly shown in Fig. 71, which indicates the position of the nodes for the uninodal and multi-

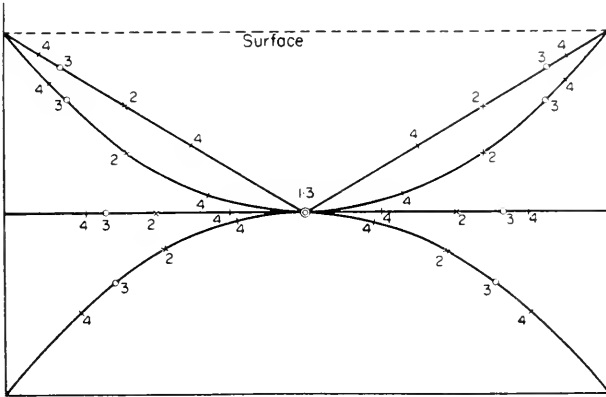


FIG. 71. Positions of nodal lines of oscillations having 1-4 nodes in basins of different shapes. The numbers at the different curves (bottom shape) give the positions of the nodes for the 1-4 nodal oscillations.

nodal oscillation of the different longitudinal profiles. A number of theoretical investigations of free oscillations in water basins of different "Talweg", is also given by HIDAKA in "Problems of water oscillations in various types of basins and canals", Parts I to X, mostly in *Mem. Imp. Mar. Obs. Kobe*, 1931-1936.

The application of Chrystal's method to certain basins requires that the "normal curve" be replaced by carefully selected sections of the above mentioned longitudinal profiles. Where these sections join, the horizontal and vertical displacements ξ and η must tend to the same values, from both sides, and at the end of the lake ξ must vanish. The general solutions for the simple longitudinal profiles contain sufficient number of constants to satisfy these requirements. As a final result of the elimination of these free constants, there remains a transcendental equation for the determination of the period of the free oscillation after a computation which grows more intricate with the number of sections. The computation to find the position of the nodes is very long, and therefore Chrystal's method has not been applied often in practice; but wherever it has been used it has given very satisfactory results. (In the following paragraph an example of this is being given p. 182).

(ii) *The Japanese Method.* Investigating the oscillations in several bays along the Japanese coast, HONDA, TERADA, IOSHIDA and ISITANI (1908, p. 1, see also DEFANT, 1911, p. 119) have developed a method to determine the period of the free oscillation of the water-masses of an irregularly shaped basin, which method is based essentially on Rayleigh's theory of air oscillations in a tube of variable cross-section. Here is a brief outline of the method: if the kinetic and potential energy of the oscillating system can be expressed by quadratic functions of a co-ordinate q , in such a way that

$$T = \frac{1}{2} a \left(\frac{\partial q}{\partial t} \right)^2 \quad \text{and} \quad V = \frac{1}{2} c q^2,$$

then the Lagrangian equations of motion give the equation of oscillation for the system LAMB (1932, p. 251).

$$a(\partial^2 q / \partial t^2) + c q = 0$$

and the period of free oscillation of the system simply results from

$$\omega^2 = \left(\frac{2\pi}{T} \right)^2 = \frac{c}{a},$$

when $q = A \cos(\omega t - \varepsilon)$. Therefore if both T and V can be expressed by quadratic functions the period of oscillation of the system can be determined without directly deriving the equations of motion.

Considering an oblong basin, we put $S(x)\xi = X$, and as, according to (VI.47), $b(x)\xi = -\frac{\partial X}{\partial x}$

then

$$T = \frac{1}{2} \rho \int_0^l \frac{1}{S} \left(\frac{\partial X}{\partial t} \right)^2 dx \quad \text{and} \quad V = \frac{g\rho}{2} \int_0^l \frac{1}{b} \left(\frac{\partial X}{\partial x} \right)^2 dx.$$

Now if we assume for X an expression of the same form as is obtained if S were a constant, then

$$X = \sum A_n \sin \frac{n\pi}{l} x \cos \omega_n t.$$

If we select as a new co-ordinate $q_n = a_n \cos \omega_n t$, then we get after a long computation

$$T = \sum_n \{A_n + \Delta A_n\} \left(\frac{\partial q_n}{\partial t} \right)^2 + \sum_n \sum_m \Delta A_{n,m} \frac{\partial q_n}{\partial t} \cdot \frac{\partial q_m}{\partial t}$$

and

$$V = \sum_n \{C_n + \Delta C_n\} q_n^2 + \sum_n \sum_m \Delta C_{n,m} m q_n \cdot q_m$$

in which

$$A_n + \Delta A_n = \frac{\rho}{2} \int_0^l \frac{1}{S} \sin^2 \frac{n\pi}{l} x dx \quad \text{and} \quad C_n + \Delta C_n = \frac{1}{2} \frac{n^2 \pi^2 g \rho}{l^2} \int_0^l \frac{1}{b} \cos^2 \frac{n\pi}{l} x dx.$$

The summation has to be done over all $n \neq m$. When the lake approaches a rectangular basis of constant cross-section ΔA_n and ΔC_n become small. If both $S(x)$ and $b(x)$ do not vary too rapidly

and to greatly, the double in these equations are small compared with the first term and can be neglected. The period of oscillation of the lake can then be computed in first approximation from

$$\omega_n^2 = \left(\frac{2\pi}{T_n}\right)^2 = \frac{C_n + \Delta C_n}{A_n + \Delta A_n}.$$

After a few transformations, we finally obtain

$$T_n = \frac{2l}{n\sqrt{gh_0}} \left[1 + \frac{1}{2} \int_0^l \left(\frac{\Delta S}{V} + \frac{\Delta b}{O} \right) \cos \frac{2n\pi}{l} x dx \right], \quad (\text{VI.53})$$

in which V is the volume and O the surface area of the whole lake and ΔS and Δb are the deviations from the mean values S_0 and b_0 and $S_0/b_0 = h_0$, where S_0 is the mean area and b_0 the mean width of the mean cross-sections. The term in parentheses is the correction to be applied to Merian's formula for the period of free oscillation of an irregularly shaped lake. The first part of this correction represents the effect of the variations in cross-section, the second one that of the variations in width. It is easy to see that there will be an increase of the period when the lake narrows in the centre whereas the period will decrease when the lake narrows at the end.

To apply equation (VI.53), one makes a numerical integration by dividing the lake in a sufficient number of cross sections perpendicular to the "Talweg", which are carefully measured. This method, which is limited to lakes with a fairly regular shape, gives only the period, and does not give any information, either on the position of the nodal lines, nor on the relative magnitude of the horizontal and vertical water displacements, caused by the oscillations. In this respect this method is inferior to the other ones.

(iii) *Defant's method* (1918). It finds its origin in the equations of motion and of continuity transformed by STERNECK (1915). Their solution can be adapted accurately to the most complicated shape of basins by stepwise integration, using finite difference-method. Besides the period, Defant's method gives at the same time the relative magnitude of the vertical and horizontal displacements and, consequently, also the position of the nodal lines along the entire basin. In this it is superior to other methods, even though it generally requires considerable work (see DEFANT, 1918, p. 78).

As a solution of the equation of motion (VI.5) and of the equation of continuity (VI.47), one assumes, periodic functions of t in the form

$$\xi = \xi_0(x) \cos\left(\frac{2\pi}{T} t - \varepsilon\right) \quad \text{and} \quad \eta = \eta_0(x) \cos\left(\frac{2\pi}{T} t - \varepsilon\right)$$

in which ξ_0 and η_0 represents the horizontal and vertical displacements and are functions of x only. If we substitute these expressions into the equations (VI.5) and (VI.47), we obtain for the small variations $\Delta\xi$ and $\Delta\eta$ which occur along a small distance Δx of the "Talweg", the relations

$$\Delta\eta = \frac{4\pi^2}{gT^2} \xi \Delta x \quad \text{and} \quad \xi = -\frac{1}{S} \int_0^x \eta b dx. \quad (\text{VI.54})$$

Furthermore, we have to add the boundary conditions, which for both ends of the lake $x = 0$ and $x = l$ require $\xi = 0$. The first approximation for the period of the free oscillation with one node T_1 gives Merian's formula (VI.34), if we substitute for h the mean depth of the lake. Then $a = (4\pi^2/gT^2)\Delta x$ is known approximately. If the cross-sections drawn along the "Talweg" are closely spaced, it can be assumed in a first approximation that the changes of the displacement between two successive cross-sections are linear. For the practical computation, the equations (VI.54) then take the easier form:

$$\left. \begin{aligned} \eta_2 &= \eta_1 + a \frac{\xi_1 + \xi_2}{2}, \\ \xi_2 &= -\frac{1}{S_2 \left(1 + \frac{av_2}{4S_2}\right)} \left[q_1 + \left(\eta_1 + a \frac{\xi_1}{4} \right) v_2 \right], \\ q_2 &= q_1 + \frac{\eta_1 + \eta_2}{2} v_2. \end{aligned} \right\} \quad (\text{VI.55})$$

The quantities with the subscripts 1, 2 represent respectively the value for two successive cross-sections, whereas v_i is the surface area of the sea between section $(i-1)$ and the i . The quantity q_0 is equal to zero. First, an approximate value of T is found by means of Merian's formula (VI.34), using the average depth of the basin. The result is an approximate value of a . The computation is then started at one end of the basin $x = 0$, $\xi_1 = 0$, and where $\eta_1 = 100$ cm (an arbitrary value). The second equation (VI.55) then gives ξ_2 and introducing this value in the first equation of (VI.55) we get the vertical displacement η_2 at the second cross-section. The third equation then gives q_2 . Now all quantities are given at the second cross-section, and from there to the next cross-section the computation can then be continued, repeating the previous computation with the new values of ξ and η . If the approximate period which was derived from Merian's formula (VI.34) is correct for the simplest seiche, the computation must arrive at a value q and $\xi = 0$ at the other end of the lake, in order to fulfil the boundary condition. The computed value will usually differ from zero and, hence, it will be necessary to select another value of the period, i.e. another value of a and to repeat the entire computation. If this second value of the period does not lead to a correct result, one has to select a third one, which can then usually be determined by suitable interpolation. The final result will give relative values of the displacements and its related currents, and the exact locations of the nodal line, and finally also the currents related with the oscillations within the lake. According to (VI.4), $u = d\xi/dt$, the horizontal component of the current

$$u = -\frac{2\pi}{T} \xi_0(x) \sin\left(\frac{2\pi}{T} t - \varepsilon\right) = \frac{2\pi}{T} \xi_0 \cos\left[\frac{2\pi}{T} \left(t + \frac{T}{4}\right) - \varepsilon\right]. \quad (\text{VI.56})$$

The largest current intensity corresponding to the seiches therefore is $(2\pi/T)\xi$ and its phase differs by one quarter period from that of high tide.

This method is not limited by the exterior form of the oscillating water-mass; however, it naturally gives the unequivocal results, especially when the main direction of the oscillation is determined by the direction of the longitudinal extent of the lake. For a correct application, it requires a good knowledge of the orographic nature of the lake. An example of the application of the method will be given on p. 198.

(iv) *Proudman's Method.* This method starts with the equation of motion (VI.50) of Chrystal, which if

$$u = S\xi = A \cos(\omega t + \varepsilon)$$

is transformed into

$$\frac{d^2A}{dv^2} + \frac{\lambda}{\sigma(v)} A = 0, \quad (\text{VI.57})$$

which is similar to equation (VI.52) and in which $\lambda = \omega^2/g$ the function $\sigma(v) = b(x)$. $S(x)$ is given by the "normal curve" of the lake. (VI.57) is to be solved with the boundary conditions that $A = 0$ for $v = 0$ and $v = a$, that is to say the entire surface of the lake. Proudman (1914) has given an exact theoretical analysis of this differential equation, and also the procedure of computing the free oscillations of a basin of any shape. DOODSON, CAREY and BALDWIN (1920) have applied this method to the lake of Geneva with excellent results. This method is better than the one by Chrystal, in so far as it is not necessary to adapt the "normal curve" to fragments of analytical curves, which is always very difficult with an irregular "normal curve". We will only discuss here the characteristic features of this method.

As a solution of (VI.57) we can establish an infinite series of the form:

$$A = \sum_{n=0}^{\infty} (-\lambda)^n J_n(v) = J_0 - J_1\lambda + J_2\lambda^2 - J_3\lambda^3 + \dots$$

The determination of the functions $J_n(v)$ considering the boundary condition $v = 0$ gives

$$J_0(v) = v, \quad \frac{\partial J_1}{\partial v} = J_1 = \int_0^v \frac{v}{\sigma(v)} dv$$

and

$$J_1 = \int_0^v J_1' dv$$

and generally

$$J_n'(v) = \int_0^v \frac{J_{n-1}}{\sigma(v)} dv \quad \text{and} \quad J_n(v) = \int_0^v J_n' dv.$$

As the normal curve $\sigma(v)$ is known, the integrals can be easily computed by simple summations, but not for the ends when $v = 0$ and $v = a$, as for these $\sigma(v) = 0$ and the expressions under the integrals are indefinite. At the first place, however, where $v = 0$, all $J_n = 0$, so that only the $J_n(a)$ are to be computed. In order to overcome this difficulty, Doodson divides the lake into two equal parts at $v = \frac{1}{2}a$ and determines the J_n by two integrations first, starting from one end (east end) J_n^e , and then the J_n^w from the other end (west end) up to the middle of the lake. As, due to the unsymmetry of the lake, the two parts are not identical, the J_n values obtained for the middle of the lake will not agree. As the equations of (VI.57) are linear, it is possible to adjust the two values to each other by a multiplication factor. For the other end of the basin the theory then gives the conditional equation

$$\sum_{r=0}^n (J_{n-r}^e J_r^{w_1} + J_{n-r}^{e_1} J_r^w) = J_n(a),$$

in which the argument $\frac{1}{2}a$ has to be taken for the functions J and J in the left-hand term of the expression in parentheses. As these values are known for the middle of the lake, the J_n can also be determined for the other end.

Doodson and his collaborators determine these J_n for 10 values of v of the western and the eastern half. When $v = 0$, the $J_n(0) = 0$ and, therefore there are in all, till $v = a$, 18 values of J_n . At both ends of the lake, A must be equal to 0. This condition is automatically fulfilled for the end $v = 0$, as here all $J_n = 0$; for the other end, however, $v = a$ must be

$$\sum_n (-\lambda)^n J_n(a) = J_0(a) - \lambda J_1(a) + \lambda^2 J_2(a) - \dots + \lambda^{18} J_{18}(a) = 0.$$

This is the equation for the determination of the values of λ , which according to (VI.57) define the periods of the free oscillations of the lake. This equation is solved by Doodson according to the method of Horner.

Figure 72 shows the normal curve of the lake of Geneva and Fig. 73 the distribution of the vertical displacement along the lake for the uni- and two-nodal Seiches. According to the method of Proudman, the periods are

T_1	T_2	T
74.45 min	35.1 min	28 min,

whereas Forel has observed the following values:

$$74.0 \text{ min} \quad 35.5 \text{ min} \quad \dots$$

The position of the nodal lines are also agreeable with those derived from the limnographic recordings. Fig. 73, moreover, shows very clearly how much the profile of the seiches can deviate from a cos-line in irregularly shaped lakes. The method of Proudman has not yet been tested for other lakes.

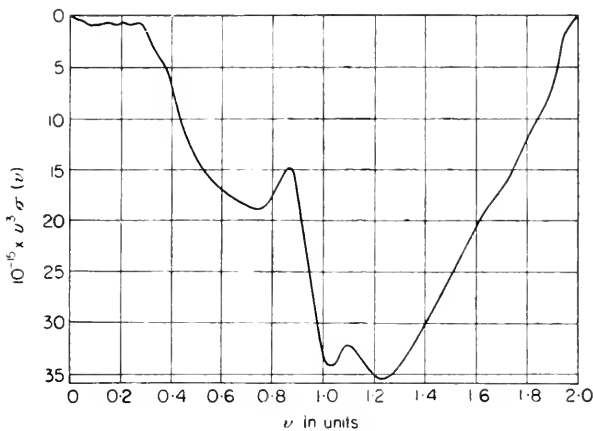


FIG. 72. Normal curve of the Lake of Geneva (each unit represents 17.052 km).

(v) *The method of Hidaka.* HIDAKA (1932, 1936) has also devised a method for computing the period of oscillation and the distribution of vertical displacement for enclosed water-masses, taking fully into account the variable cross-sections and depths of the basins. It is based on the application of the

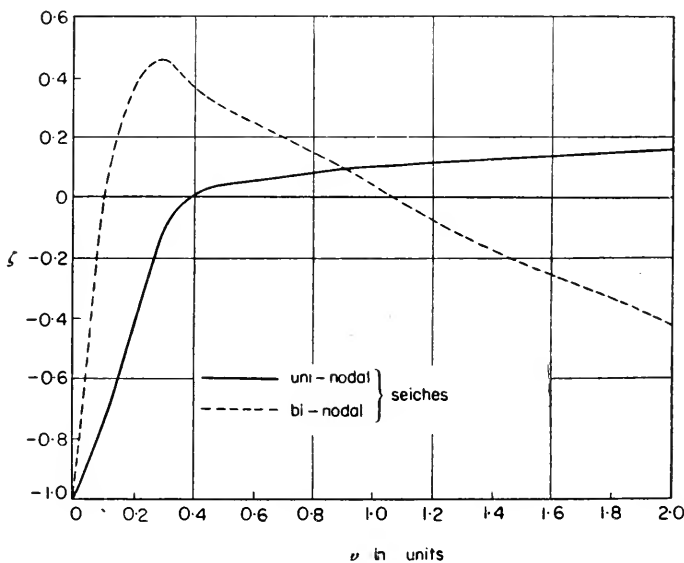


FIG. 73. Range of the uni- and bi-nodal seiches in the Lake of Geneva. Same scale as Fig. 72. —, uni-nodal; ----, bi-nodal.

Ritz theorem of the calculus of variations to the integration of the Chrystal differential equation (VI.57). If we introduce $v/a = z$ as a new variable and if $\sigma(z)$ is the normal curve of the lake as a function of z , we obtain

$$\frac{d^2A}{dz^2} + \frac{\lambda}{\sigma(z)} A = 0 \tag{VI.58}$$

with

$$\lambda = \frac{4\pi^2 a^2}{gT^2}.$$

Equation (VI.58) is to be solved with the boundary conditions $A(0)$ and $A(1) = 0$. This differential equation, according to the said theorem of the calculus of variation, is equivalent to the relation

$$\int_0^1 \left\{ \left(\frac{dA}{dz} \right)^2 - \frac{\lambda}{\sigma(z)} A^2 \right\} dz = J(A) = \text{Minimum}. \tag{VI.59}$$

We now assume a solution A in the form of a finite series

$$A = A_0\psi_0 + A_1\psi_1 + A_2\psi_2 + \dots + A_m\psi_m, \tag{VI.60}$$

in which the $m+1$ functions ψ_i must satisfy the same boundary conditions as A itself: $\psi_i(0) = \psi_i(1) = 0$ for $i = 0, 1, 2, \dots, m$. If we choose $\psi_i(z) = z(1-z)z^i$ then these boundary conditions are fulfilled and A becomes

$$A = \sum_{i=0}^m z(1-z)z^i A_i. \tag{VI.61}$$

The determination of the unknown A_i results from the fact that after substituting (VI.61) into (VI.59) $J(A)$ must be a minimum. This requires that

$$\frac{\partial J}{\partial A_0} = 0, \quad \frac{\partial J}{\partial A_1} = 0 \text{ etc., } \dots, \quad \frac{\partial J}{\partial A_m} = 0.$$

After a few calculations, we finally obtain for determining A_i the equation

$$\sum_{i=0}^m \left\{ \left(\frac{ij}{i+j+1} - \frac{2(i+1)(j+1)}{i+j+2} + \frac{(i+2)(j+2)}{i+j+3} \right) - \lambda \int_0^1 \frac{z^2(1-z)^2 z^{i+j}}{\sigma(z)} dz \right\} A_i = 0. \tag{VI.62}$$

The integral can only be evaluated, if $\sigma(z)$ can be represented as an analytical function of z . In order to avoid singularities at the end of the lake, Hidaka puts

$$\sigma(z) = hz(1-z)\varphi(z),$$

in which h is a constant with the dimensions (L^3) and $\varphi(z)$ represents a function of z which is always positive in the interval $0 \leq z \leq 1$. $\varphi(z)$ must now be approximated as well as possible from the normal curve by a suitable analytical function. Hidaka has done this for the Lake of Yamanaka and then evaluated the integral. If the normal curve is irregular, such a function cannot easily be found; in that case it is better, as Neumann has done in the case of the Baltic, to compute the integral directly by numerical integration, in which, of course, the limiting values at $z = 0$ and $z = 1$ in (VI.62) require special attention.

Equation (VI.62) then gives $m + 1$ simultaneous, homogeneous equations.

$$\begin{aligned} \left(\frac{1}{3} - J_0\lambda\right) A_0 + \left(\frac{1}{6} - J_1\lambda\right) A_1 + \left(\frac{1}{10} - J_2\lambda\right) A_2 + \dots &= 0 \\ \left(\frac{1}{6} - J_1\lambda\right) A_0 + \left(\frac{2}{15} - J_2\lambda\right) A_1 + \left(\frac{1}{10} - J_3\lambda\right) A_2 + \dots &= 0 \\ \left(\frac{1}{10} - J_2\lambda\right) A_0 + \left(\frac{1}{10} - J_3\lambda\right) A_1 + \left(\frac{3}{35} - J_4\lambda\right) A_2 + \dots &= 0 \\ \dots \quad \dots \quad \dots \quad \dots \quad \dots \quad \dots & \end{aligned}$$

They can only exist when their determinant vanishes:

$$\begin{vmatrix} \frac{1}{3} - J_0\lambda & \frac{1}{6} - J_1\lambda & \frac{1}{10} - J_2\lambda & \dots & \dots \\ \frac{1}{6} - J_1\lambda & \frac{2}{15} - J_2\lambda & \frac{1}{10} - J_3\lambda & \dots & \dots \\ \frac{1}{10} - J_2\lambda & \frac{1}{10} - J_3\lambda & \frac{3}{35} - J_4\lambda & \dots & \dots \\ \dots & \dots & \dots & \dots & \dots \\ \dots & \dots & \dots & \dots & \dots \end{vmatrix} = 0 \tag{VI.63}$$

in which

$$J_n = \int_0^1 \frac{z^2(1-z^2)z^n}{\sigma(z)} dz .$$

In case that in (VI.61) A only consists of three terms ($m = 2$), we get $A = z(1-z)(A_0 + A_1z + A_2z^2)$ and the determinant is restricted to the terms shown in (VI.63). From this we obtain as a determining equation for λ the cubic equation:

$$\begin{aligned} &(J_0J_2J_4 - J_0J_3^2 - J_1^2J_4 - 2J_1J_2J_3 - J_2^2) \lambda^3 - \\ &- \left[\frac{3}{35}(J_0J_2 - J_1^2) + \frac{1}{5}(-J_0J_3 + J_1J_2 + J_1J_3 - J_2^2) + \frac{2}{15}(J_0J_4 - J_2^2) + \frac{1}{3}(-J_1J_4 + J_2J_3 - J_2J_4 - J_3^2) \right] \lambda^2 + \\ &+ \left[\frac{1}{700}J_0 - \frac{3}{350}J_1 + \frac{53}{2100}J_2 - \frac{1}{30}J_3 + \frac{1}{60}J_4 \right] \lambda - \frac{1}{10500} = 0 \end{aligned}$$

The roots of this equation must all be positive and can be determined by applying the “regula falsi” or the method of Newton. If they are λ_1 , λ_2 and λ_3 , the second of the equations (VI.58) gives as period of the uni-nodal, two-nodal and three-nodal seiches the values

$$T_i = \frac{2\pi a}{\sqrt{\lambda_i g}} . \tag{VI.64}$$

Hidaka has applied his method to Lake Yamanaka, which has a beautiful, regular shape and has obtained results which agree exceptionally well with the observed periods of this lake. Neumann has applied this theory to the large, almost completely closed water-masses of the Baltic Sea. We will refer later to this important paper (p. 194).

(vi) *The method of Ertel.* ERTEL (1933) has developed a new and an elegant method which follows the wave mechanical perturbation theory. The only restriction to its application is that the lake should extend preponderantly in the x -direction, so that transversal oscillations can be disregarded. It starts out from the Chrystal equation, to which we can give the form

$$\frac{\partial^2 A}{\partial z^2} + \frac{\omega^2}{q(z)} A = 0. \tag{VI.65}$$

It is identical with equation (VI.58) if we put

$$\frac{\omega^2}{q(z)} = \frac{\lambda}{\sigma(z)},$$

in which

$$q(z) = (g/a^2)\sigma(z) \quad \text{and} \quad \sigma(z)$$

is the normal curve of the lake, referred to the abscissa $z = \frac{v}{a}$

$$(0 \leq z \leq a, \quad \text{if} \quad 0 \leq x \leq l).$$

If we assume a rectangular cross-section of constant depth of the width b_0 and an area $S_0 = b_0 h_0$, then $b_0 l = a$ and $q_0 = gh_0/l^2$. Considering here only the longest free oscillation, we have for this rectangular basin

$$\frac{\partial^2 A_0}{\partial z^2} + \frac{\omega_0^2}{q_0} A_0 = 0, \tag{VI.66}$$

with $A_0(0)$ and $A_0(1) = 0$. Its solution is

$$A_0 = \frac{1}{2} \sin(\pi z), \tag{VI.67}$$

and its proper frequency is

$$\omega_0 = \pi \sqrt{q_0}, \tag{VI.68}$$

or as period of the free oscillation Merian's formula $T_0 = 2l/\sqrt{gh_0}$. This amplitude in (VI.67) has been selected so that

$$\int_0^1 A_0^2 dz = 1 \quad (\text{normalized eigenfunction}). \tag{VI.69}$$

In order to obtain a general solution of (VI.65) we make the usual assumption in the perturbation theory

$$A = A_0 + \Delta A \quad \text{and} \quad \frac{\omega^2}{q(z)} = \frac{\omega_0^2}{q_0} + \Delta \left(\frac{\omega^2}{q(z)} \right), \tag{VI.70}$$

and substituting in (VI.65), we obtain

$$\frac{\partial^2 \Delta A}{\partial z^2} + \frac{\omega_0^2}{q_0} \Delta A = -\Delta \left(\frac{\omega^2}{q(z)} \right) A_0. \tag{VI.71}$$

Ertel transforms the perturbation term $-l \left(\frac{\omega^2}{q} \right) A_0$ into $\frac{\Delta\omega^2}{q_0} - \omega_0^2 \frac{\Delta q}{\Delta q_0^2}$, neglecting quantities of second order, which can be done only if $\frac{\Delta q}{\Delta q_0} \ll 1$, as was shown by FR. DEFANT (1953). This will not always be so; therefore, one must use equation (VI.71).

For the frequency of uni-nodal seiches, we then obtain with (VI.67)

$$\omega^2 = \frac{\omega_0^2}{2} \cdot \frac{1}{\int_0^1 \frac{1}{\sin^2 \pi z} [1 + (\Delta q/q_0)] dz} \tag{VI.72}$$

For $\Delta q = 0$ (rectangular basin $q = q_0$) the integral becomes 1/2 and $\omega = \omega_0$. With the two-nodal or multi-nodal seiches, πz in (VI.72) must be substituted by $2\pi z$ or $n\pi z$. This method was first applied by Fr. Defant in the determination of the free oscillations of Lake Michigan. The periods obtained deviate by less than 1% from those computed by means of other methods. It can be shown that the ‘‘Japanese method’’ (see p. 164) is a special case of the method given by Ertel. It does not give especially good results as compared to other procedures, because Ertel did not consider terms of higher order in $\Delta S/S_0$ and $\Delta b/b_0$.

As the homogeneous equation (VI.66) has the solution (VI.67), the inhomogeneous equation (VI.70) can only be solved according to the theory of differential equations, if the condition (VI.73) is satisfied:

$$\int_0^1 \Delta \left(\frac{\omega^2}{q(z)} \right) A_0^2 dz = 0. \tag{VI.73}$$

(d) Standing Waves in Partially Open Basins

A water-mass in a basin not enclosed on all sides, but communicating in one or several points with a considerably larger body of water, can also have standing waves. We have then to deal with the free oscillations of bays and canals. In such oscillations the water-masses will be drawn in a horizontal direction from the great body of water of the ocean; there must always be a nodal line across the opening of such bays and canals. The longest free oscillation of a bay must, therefore, be identical with that of a basin consisting of two identical sections which are mirror images in respect to the opening which joins the two parts. If the length of the bay is l its cross-section rectangular and its depth constant (canal closed on one side of rectangular cross-section and of a depth h) then

$$T = \frac{4l}{\sqrt{gh}} \tag{VI.74}$$

It will be necessary to introduce a correction for a canal or bay with a wide opening to the free ocean, in whose width b at the opening is an appreciable fraction of the length of the canal l . This correction increases the period, similar to the behaviour of vibrations of air in pipes which are open at one end. As a matter of fact, in the oscillatory processes at the opening, the water not only flows forth and back in the longitudinal direction of the canal, but it is also drawn from the side and thrown back sideways. The investigations made by RAYLEIGH (1897) show, as is to be expected, that the correction is the greater, the wider the opening of the bay is in proportion to its length. The corrected period of the free oscillation then is $T(1 + \epsilon)$, if T is the period computed according to Merian's formula (VI.74). For ϵ we find, if b is the width and l the length of the canal closed on one side,

$$\epsilon = \frac{b}{\pi l} \left\{ 3 - \ln \frac{\pi b}{4l} - \gamma \right\}, \tag{VI.75}$$

in which γ is Euler's constant 0.577215. Different ratios $b:l$ gives the values for $1 + \epsilon$ (Table 22).

Table 22

$\frac{\text{Width}}{\text{Length}}$	1	1/2	1/3	1/4	1/5	1/10	1/20
Correction factor	1.371	1.297	1.240	1.203	1.176	1.110	1.066

It can be seen from these values that when the width of the bay equals the length, the increase in the period is 37% but is reduced to about 11% if the width is one-tenth of the length. PROUDMAN (1925, p. 247) has pointed out that this mouth correction only applies if the shore from which the canal

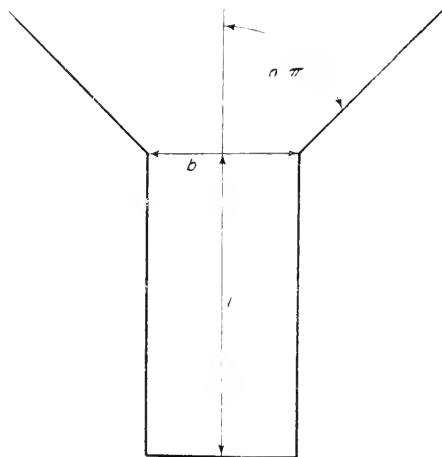


FIG. 74. Computation of the correction for the opening.

branches out is straight and if there is a uniform distribution of a current transverse to the open end of the canal. If the coastline is funnel-shaped and

makes an angle $n\pi$ with the centre axis of the canal (see Fig. 74) equations (VI.75) is replaced by

$$\varepsilon = \frac{1}{2n} \frac{b}{\pi l} \left(\beta_n - \ln \frac{1}{2n} \frac{6}{4l} - \gamma \right), \tag{VI.76}$$

in which

$$\beta_n = n \int_0^1 \frac{1 - (1-t)^n}{t} dt. \tag{VI.77}$$

The influence of the shape of the opening proves to be very great. Thus we find for

According to Rayleigh's equation

$n = 1/4$	$1/2$	$3/4$	$1/2$
$n\pi = 45^\circ$	90°	135°	90°
Correction factor $(1 + \varepsilon) = 1.285$	1.259	1.233	1.265

For a canal of the length l open on both ends we obtain again as period of the longest oscillation $T = 2l/\sqrt{gh}$; nodal lines are present at both ends and, except these, this oscillation has no further nodal lines.

The longest possible period of a standing oscillation is therefore the same as the period of a lake of similar shape, but in a lake antinodes are located at the ends of a lake, whereas in a canal open on both ends, nodes are found at the ends.

The computation of the period of the free oscillation of ocean bays and canals (straits) of irregular shape can be made after the methods explained previously; particularly well suited for this is the method of a step by step approximation, because it can also be applied in the case of very complicated bottom configuration. For ocean bays the computation is started at the inner end with an arbitrary value of η and $\xi = 0$ and, if the period is selected correctly, we must obtain $\eta = 0$ at the opening. However, we can also start at the opening with ξ arbitrary and $\eta = 0$, and we then obtain, if T is correctly selected, $\xi = 0$ at the inner end.

3. The Character of the Oscillation of Connected Systems

(a) *Free Oscillations of Connected Systems*

The determination of the period of the free oscillation of the lakes and ocean bays with a complicated configuration becomes difficult with the methods previously mentioned, especially if the cross-sections become so narrow that the whole area of oscillation can no longer be adequately represented by one and the same oscillatory function of time and place. In such cases, the total oscillatory system is split up into separate parts, which are considered as separate areas for theoretical oscillatory problems. Together they form the total oscillatory system. The following example will illustrate

this. An oblong lake communicates at one end with a second basin through a narrow canal. If the opening to the second basin is sufficiently narrow, there will be in the oblong lake seiches, with, in first approximation, an anti-node at the end partially closed, so that the oscillation of the lake will reach approximately the narrow connecting passage. In this connecting canal there will be variations in the water level and consequently periodical horizontal currents. Oscillations can start also in the second basin. In this way, the water-masses in the connecting canal oscillate back and forth with the period of the free oscillation of the lake, but the physical process in the canal is quite different from the seiches in a lake. However, it reacts back on the oscillations in the oblong lake, and the resulting period of the whole oscillatory system is somewhat different from the period of the free oscillation of the oblong lake when it is completely closed and also completely different from the case where the oscillation in the connecting canal is unhampered. Such connecting oscillatory systems have been described in the well-known work on the oscillations of Japanese bays by HONDA (1908) and his collaborators. An interesting case has been computed by STERNECK (1916) (see also DEFANT, 1917, p. 329) in his solution of the Euripus problem. ENDROES (1927, p. 74) has pointed out the remarkable long period of oscillation of lakes composed of separate basins and explained them to be compensating oscillations of connected systems. ZEILON (1913), too, has dealt with similar problems in investigating the oscillations of the Gullmar-Fjord. NEUMANN (1943, p. 409) has given an extensive analysis according to a new method. We will first explain, with the help of hydrodynamics, the case of free oscillations in two lakes communicating by means of a narrow canal.

Let us assume that a short and narrow rectangular canal II connects an oblong rectangular basin I with a smaller basin III. Let their length be l , their width b and their depth h and the suffixes 1, 2, 3 refer to each quantity

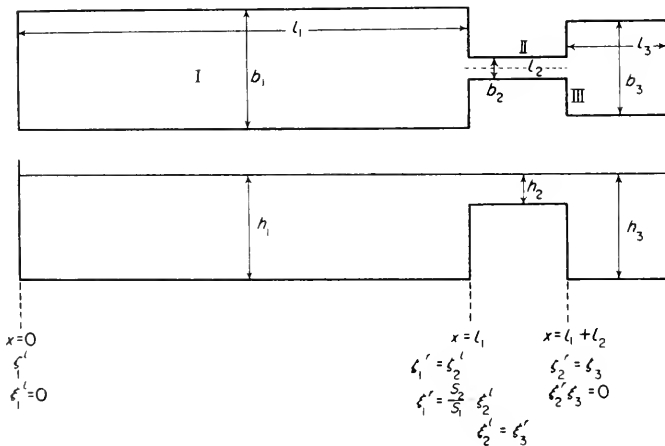


FIG. 75. Computation of the free periods of linked systems.

in its respective basin. Let their surface be $O = bl$, their cross-section $S = bh$, their longitudinal section $F = lh$, and their volume $Q = llhb$. Let the horizontal and vertical displacements of the water particles be ξ and η (see Fig. 75; everywhere in this figure ξ stands in place of η).

Suppose basin I oscillates regularly (seiches); then there will be in the connecting canal II periodical pressure variations and a corresponding periodically alternating current, whereas in basin III the oscillations are caused through the filling and emptying of the basin in the same rhythm as the free period of the complete system. The resulting period of the connected system ω depends, of course, first of all on the dimensions of the system, which will be expressed in the boundary conditions. These boundary conditions have been added to Fig. 75 underneath the three points $x = 0, l_1$ and $l_1 + l_2$ and do not need any further explanation. L and R as upper indices mean left and right of the section in question.

The oscillations in III are simple variations in level caused by water flowing in or out at $x = l_1 + l_2$ and the condition for continuity gives

$$S_2 \xi_2 = O_3 \eta_3. \tag{VI.78}$$

In II the equation of motion (VI.5) applies

$$\frac{\partial^2 \xi_2}{\partial t^2} = -g \frac{\partial \eta_2}{\partial x} = -\frac{g}{l_2} (\eta_2^R - \eta_2^L), \tag{VI.79}$$

because this is a simple pressure current.

All ξ and η in the oscillatory system are proportional to a periodical function of the time, and therefore $\xi, \eta \sim e^{i\omega t}$. Considering (VI.78) and the boundary condition at $x = l_1$, it follows from (VI.79)

$$\left(1 - \frac{\omega_3^2}{\omega^2}\right) \omega^2 \frac{S_1}{S_2} \xi_1^R + \frac{g}{l_2} \eta_1^R = 0, \tag{VI.80}$$

in which

$$\frac{gh_3 S_2}{O_3 h_3 l_2} = c_3^2 \frac{a_2}{O_1} = \omega_3^2 \tag{VI.81}$$

$$c_3 = \sqrt{gh_3} \quad \text{and} \quad a_2 = \frac{S_2}{l_2}.$$

In analogy to the theory of the resonators of Helmholtz, a can be designated as the “conductivity” of the canal and

$$\omega_3 = \frac{2\pi}{T_3} = c_3 \sqrt{\frac{a_2}{Q_3}}$$

is then in agreement with Rayleigh’s equation for the natural frequency of such a resonator.

The equation (VI.80) represents a relation between ξ_1^R and η_1^R of basin I. A second equation can be derived from the equation for the oscillations

of this basin itself. From the equations (VI.8) and (VI.6) we obtain, when considering the boundary condition $x = 0$ and neglecting the time factor $e^{i\omega t}$,

$$\xi_1 = \frac{\xi_1^R}{\sin \kappa l_1} \sin \kappa x \quad \text{and} \quad \eta_1 = -h_1 \kappa \frac{\xi_1^R}{\sin \kappa l_1} \cos \kappa x \quad (\text{VI.82})$$

with $\kappa c_1 = \omega$.

The second equation gives for the right side $x = l_1$ the second relation between ξ_1^R and η_1^R , in the form

$$\kappa h_1 \cot \kappa l_1 \xi_1^R + \eta_1^R = 0. \quad (\text{VI.83})$$

The two equations (VI.80) and (VI.83) can only exist when their determinant vanishes, which gives the equation for the frequency ω of the connected system. After a few transformations, we obtain

$$\cot \kappa l_1 = \frac{S_1 \kappa}{a_2} \left(1 - \frac{\omega_3^2}{\omega^2} \right). \quad (\text{VI.84})$$

The period T of the system is given if we put $\omega_3 = 2\pi/T_3$ and $T_1 = 2l_1/\mathbf{1} (gh_1)$ (period of I when completely closed at the right):

$$\cot \pi \frac{T_1}{T} = \frac{2\pi S_1}{c_1 a_2} \cdot \frac{1}{T} \left(1 - \frac{T^2}{T_3^2} \right). \quad (\text{VI.85})$$

This formula applies only on the condition that in the connecting canal there will be compensating currents and no oscillations. This is identical with the condition that the cross-section of the canal be small, compared with S_2 , which is the cross-section of the lake. Equation (VI.85) can also be applied for irregularly shaped lakes provided that first T_1 be determined considering the width and depth according to one of the preceding methods, and then T be corrected by equation (VI.85).

If κl_1 is small (l_1 small compared to the wave length of the total oscillation), we can substitute in the equation (VI.84) $1/(\kappa l_1)$ for $\cot \kappa l_1$ and after a few transformations we obtain

$$T = 2\pi \sqrt{\left(\frac{l_2}{b_2 h_2 g} \frac{F_1 F_3}{F_1 + F_3} \right)}. \quad (\text{VI.86})$$

This is the equation derived by Honda and his collaborators. Equation (VI.86) corresponds with the relations which have been derived in hydraulics for the oscillations in U -shaped tubes and for oscillations in a "Wasserschloss", see FORCHHEIMER (1924, p. 344) who also considers the damping through friction. This method can also be applied to Seiches.

One can derive in the same way the period of a bay connected with a small basin through a narrow canal. If the opening of the bay into the open ocean lies at $x = 0$, the equation for its period will be

$$\tan \pi \cdot \frac{T_1}{2T} = -\frac{2\pi S_1}{c_1 a_2} \frac{1}{T} \left(1 - \frac{T^2}{T_3^2} \right), \quad (\text{VI.87})$$

in which $T_1 = 4l_1/\sqrt{gh_1}$ represents the period of the free oscillation of the bay closed at one end, and corrected for the opening.

Neumann has tested his theory by interesting experiments in a wave tank, which, in spite of inherent difficulties have shown a very satisfactory agreement between the theory and the observation. Applications of these formulas are given in the following paragraph.

(b) *The Impedance Theory of Neumann*

It is very difficult to deal with the theory of combinations of basins such as they occur very often in nature. It, therefore, was an excellent idea of NEUMANN (1944, p. 65, 193) to apply the impedance of oscillating systems, which was proved to be so valuable in the theory of electrical and acoustic oscillations, also to the oscillations of water-masses. In this manner, it is possible to derive in an elegant way the equations for the period of the various combinations of lakes and bays. It is true that the formulas thus derived apply only for rectangular basins of constant width and depth, but they can also be applied, with small changes, to lakes and bays of irregular shape. We will give here only the fundamentals of the theory; the applications and the proof of its manifold uses will be presented later (p. 186), along with a number of examples based on observations.

The general periodical motion of water-masses in lakes and bays follows the equation (VI.36) if the frictional influences are also considered. If we introduce $\xi \sim e^{i\omega x}$ and if we assume that the oscillations are produced by a force X acting in the horizontal direction we obtain as the fundamental equation of the forced oscillations of a system (see DEFANT, 1916, p. 29)

$$\frac{\partial^2 \xi}{\partial t^2} + \beta \frac{\partial \xi}{\partial t} + \sigma^2 \xi = X, \tag{VI.88}$$

in which $\omega = \sigma$ is the natural frequency of the system.

We will now put $X = Ae^{i\omega t}$, in which ω is the frequency of the exciting force, and if we assume

$$u = \frac{\partial \xi}{\partial t} = Ue^{i\omega t}, \quad \xi = \frac{1}{i\omega} Ue^{i\omega t}$$

then from (VI.88) follows

$$U \left(i\omega + \beta + \frac{\sigma^2}{i\omega} \right) = A. \tag{VI.89}$$

In analogy with Ohm's law for alternating currents and in accordance with the definition in the theory of acoustical filters, the quantity

$$Z = \frac{A}{U} = \beta + i\omega + \frac{\sigma^2}{i\omega} \tag{VI.90}$$

is called the impedance of the hydrodynamical oscillatory system. It can be

shown that for this quantity the following equation can be used as its definition:

$$Z = \frac{p_0}{S(\partial\xi/\partial t)_{\max}} = \frac{\text{amplitude of pressure}}{\text{area} \times \text{amplitude of velocity}}. \quad (\text{VI.91})$$

If this quantity is known, the natural frequencies ω of the system can be computed from $Z = 0$, if frictional influences are disregarded (otherwise from $Z = \text{minimum}$).

The correctness of this argument can be proved from (VI.90). Without friction $\beta = 0$, $Z = 0$ only when $\omega = \sigma$, which means the system oscillates with its natural frequency.

In a canal closed on one end (head of the canal $x = 0$, opening $x = -l$, depth h , width b) there follows from (VI.8)

$$\xi = \xi_0 \sin \frac{\sigma x}{c} e^{i\sigma t} \quad \text{and} \quad \left(\frac{\partial \xi}{\partial t} \right)_{\max} = -i\sigma \xi_0 \sin \frac{\sigma l}{c} \quad (\text{for } x = -l).$$

From (VI.91) follows

$$Z = \frac{g\varrho h_{\max}}{S(\partial\xi/\partial t)_{\max}}$$

and as, according to (VI.7),

$$\eta = -h \frac{\sigma}{c} \xi_0 \cos \frac{\sigma x}{c} e^{i\sigma t}$$

with $S = bh$

$$Z = -\frac{i\varrho c}{S} \cotg \frac{\sigma l}{c}. \quad (\text{VI.92})$$

$Z = 0$ gives as the period of the free oscillation the well-known formula $T = \frac{4l}{\sqrt{gh}}$.

Neumann has computed for the various parts of an oscillatory system their impedance Z . The most important cases are (using the customary designations, $q = bh$ cross-sectional surface of a connecting canal, $S = bh$ that of a lake, ϱ density of water and λ wavelength:

(1) Basin closed on one end

$$Z = -\frac{i\varrho c}{S} \cot \frac{\sigma l}{c} \quad (\text{VI.93})$$

with $l = \frac{1}{4}\lambda$. For a canal closed at both ends the formula remains the same, but we have $l = \frac{1}{2}\lambda$.

(2) Basin open at both ends

$$Z = \frac{i\varrho c}{S} \tan \frac{\sigma l}{c} \quad (\text{VI.94})$$

with $l = \frac{1}{2}\lambda$.

(3) Narrow flow-off opening or narrow canal (Cross-section q , length l' *)

$$Z = \frac{i\varrho \sigma l'}{q}. \quad (\text{VI.95})$$

* An effective length $l' = l + a$ can be introduced in lieu of the geometrical length l to take into consideration the co-oscillation of water-masses of the open ocean near the entrance.

(4) For a basin connected with the open ocean by a narrow opening we obtain, provided the dimensions of the basin are of equal magnitude in all directions,

$$Z = \frac{i\rho\sigma l}{q} - \frac{i\rho c^2}{Q\sigma}. \tag{VI.96}$$

In this case, the water level in the whole basin rises and falls simultaneously and higher forms of oscillation are not easily produced. The impedance is composed by two parts: one given by (VI.95), which is that of the flow-off opening, and secondly that of the closed water volume $Z = -\frac{i\rho c^2}{Q\sigma}$ (VI.97); which results from (VI.93), if $\sigma l/c$ is small, so that $\cot\sigma l/c$ can be replaced by $c/\sigma l$.

(c) Free Oscillations of Combination of Basins

In dealing with these oscillatory systems it is to be noticed that the impedance of each part is added in the same manner as the resistances of electrical circuits. A distinction should here be made as to whether the basins are connected "in parallel" or in "series". The following example will illustrate this. Figure 76 shows the oscillatory system of a ramified closed canal: Canal I

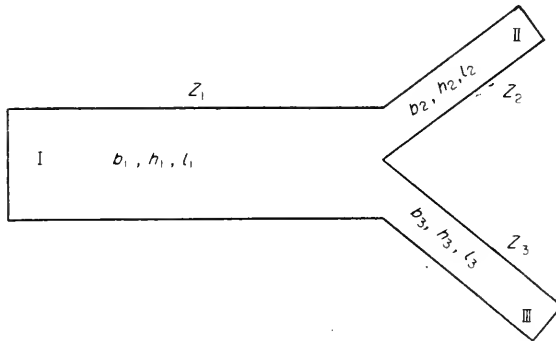


FIG. 76. Closed canal which branches out.

forks into the canals II and III. Here the canals II and III with their impedances Z_2 and Z_3 are placed "parallel" behind I with the impedance Z_1 . If P is the total impedance of II and III, then we have:

$$\frac{1}{P} = \frac{1}{Z_2} + \frac{1}{Z_3} \quad \text{or} \quad P = \frac{Z_2 Z_3}{Z_2 + Z_3}. \tag{VI.97a}$$

On the contrary, if I and (II and III) are connected in series, the total impedance of the entire system is

$$Z = Z_1 + P = Z_1 + \frac{Z_2 Z_3}{Z_2 + Z_3}. \tag{VI.97b}$$

The natural frequency then results from

$$\frac{1}{Z_1} + \frac{1}{Z_2} + \frac{1}{Z_3} = 0.$$

If we introduce the values for Z_1 from (VI.93), we obtain as the equation for the period of the system

$$b_1 c_1 \tan \frac{\sigma l_1}{c_1} + b_2 c_2 \tan \frac{\sigma l_2}{c_2} + b_3 c_3 \tan \frac{\sigma l_3}{c_3} = 0. \quad (\text{VI.98})$$

Similarly, we obtain:

If canal I is open towards the ocean, II and III being closed

$$-b_1 c_1 \cot \frac{\sigma l_1}{c_1} + b_2 c_2 \tan \frac{\sigma l_2}{c_2} + b_3 c_3 \tan \frac{\sigma l_3}{c_3} = 0.$$

If canals I and II are open, III being closed

$$-b_1 c_1 \cot \frac{\sigma l_1}{c_1} - b_2 c_2 \cot \frac{\sigma l_2}{c_2} + b_3 c_3 \tan \frac{\sigma l_3}{c_3} = 0.$$

If all three canals are open:

$$b_1 c_1 \cot \frac{\sigma l_1}{c_1} + b_2 c_2 \cot \frac{\sigma l_2}{c_2} + b_3 c_3 \cot \frac{\sigma l_3}{c_3} = 0.$$

These frequencies are identical with those derived by ZEILON (1913) in the usual hydrodynamical way. Neumann has also derived the equations for the periods for other basins with different configurations.

(4) Observed Standing Waves in Lakes, Bays and Adjacent Seas

(a) *Seiches in Lakes*

It is not our intention to give here an extensive review of oscillations observed in lakes, as this would fit better into a text-book of hydrology. A compilation of older literature can be found in Forel, in Chrystal, as well as in the text-book of limnology by HALBFASS (1923). Good reviews have also been given by ENDROS (1908, p. 39; 1927, p. 74). We will only mention here a few essential points of these phenomena which are particularly characteristic and which are connected with the theoretical explanations given previously.

At present, there are only a limited number of oblong lakes, for which a complete analysis of the seiches and a comparison between observations and theory has been given. Table 23 contains a compilation of observed and computed periods for some lakes, as well as enumerations of the methods used for the computation. We can see that the agreement between observation and theory is always very good, and even better than could be expected when influences of a secondary nature (friction, Coriolis-force, etc.) are

Table 23. Observed and computed values of the period of several lakes (in minutes)

Period	Loch Earn		Loch Treig		Lake Garda		Lake of Geneva			
	Observed	Computed	Observed	Computed	Observed	Computed	Observed	Computed		
	(1)	(2)	(3)	(2)	(4)	(5)	(6)	(7)		
T ₁	14.52	14.50	14.76	9.18	9.14	9.15	42.92	42.83	74.0	74.45
T ₂	8.09	8.14	8.36	5.15	5.10	5.18	28.58	28.00	35.5	35.1
T ₃	6.01	5.74	—	—	—	—	21.79	20.10	—	28.0
T ₄	3.99	4.28	—	—	—	—	14.95	14.83	—	—
T ₅	3.54	3.62	—	—	—	—	12.07	11.9	—	—
T ₆	2.88	2.93	—	—	—	—	9.87	10.1	—	—

Period	Lake Yamanaka		Lake Vättern		Lake Michigan			Lake Tanganika		
	Observed	Computed	Observed	Computed	Computed			Observed	Computed	
	(6)	(7)	(8)	(9)	(10)	(11)	(12)	(13)		
T ₁	15.61	15.47	178.99	177.94	9.08	9.04	9.02	4.5	4.37	4.30
T ₂	10.57	—	97.52	95.95	4.92	4.87	4.69	2.3	2.33	2.0
T ₃	5.46	—	80.74	79.17	—	—	—	1.7	1.85	1.60
T ₄	—	—	57.89	59.83	—	—	—	—	—	—
T ₅	—	—	48.10	49.77	—	—	—	—	—	—
T ₆	—	—	42.59	42.46	—	—	—	—	—	—

- (1) According to Chrystal's method (Chrystal, 1908).
 - (2) According to Hidaka (1931).
 - (3) According to Chrystal and McLagan — Wedderburn (1905).
 - (4) According to Defant (1908), also Vercelli (1909).
 - (5) According to Proudman's method.
 - (6) According to Hidaka (1932).
 - (7) According to Chrystal's method (Bergsten 1926).
 - (8) According to Defant's method.
 - (9) According to Chrystal's method.
 - (10) According to Ertel's method.
 - (11) According to F. Servais (1957).
 - (12) According to Defant's method.
 - (13) According to Hidaka's method.
- } Fr. Defant (1953).
 } F. Servais (1957).

neglected. This proves that these secondary influences are really unimportant in comparison to the importance of the configuration of the basin. The most careful and thorough analysis of the seiches in a great lake has been given by BERGSTEN (1926) in his work on the seiches of Lake Vättern (Sweden). On account of its narrow, uniform shape and its great length of 124 km, this lake was particularly well-suited for the investigation of the variations

of its level. As an example of such oscillations, Fig. 77 shows simultaneous registrations at both ends of the lake. It shows the uninodal seiche, and it can be noticed how the displacements of the water level at one end are the mirror image of the displacements at the other end.

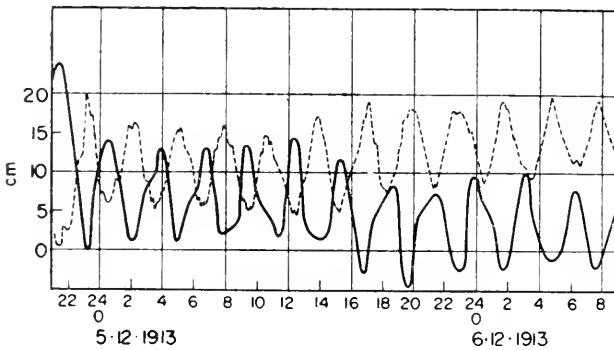


FIG. 77. Simultaneous recordings of the uni-nodal seiche in Lake Vättern at Bastedalen and Jönköping.

Bergsten divided the lake (Fig. 78) in four parts, and could very well approximate the normal curve, by means of parabolical and quartic curves and then apply Chrystal's method for the determinations. The result can be

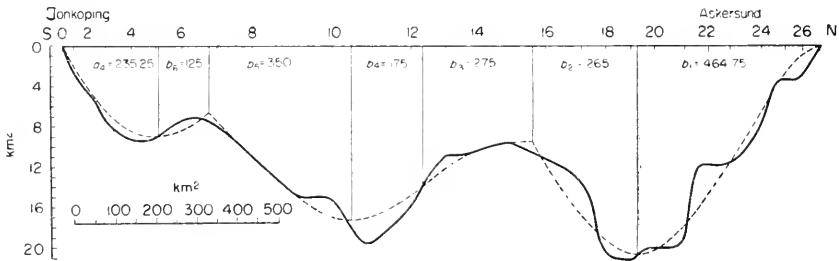


FIG. 78. Normal curve of Lake Vättern and its approximation by parabolic and quartic curves (broken) (Bergsten).

found in Table 23. The mean period of the uni-nodal seiche is 178.99 min, the extreme values of the single series are 180.8 and 174.6 min. The differences are caused partly by the different height of the water level at the time of the observation, and partly by the difficulty in determining correctly the phase of the first and the last wave of the series. There is a discrepancy of only 0.6% between the observed mean value and the theoretical value, which is reduced to 0.2%, if friction is taken into account by determination of the damping coefficients. For the multinodal seiches the agreement becomes worse, but even for the five-nodal seiches the discrepancy does not exceed 4%. These discrepancies may be caused by the difficulties in establishing the period of oscillation of these shorter waves.

In recent times, also, other lakes were investigated according to the methods described above. FR. DEFANT computed the seiches of Lake Michigan, applying methods by Defant, Christal and Ertel. The results obtained were in good agreement, so that all these methods seem to be equivalent.

A comprehensive study by SERVAIS (1957) on the seiches of Lake Tanganyika was published recently. Besides an exact computation of the seiches of this lake after methods by Defant and Hidaka as well as newer formulae by Fredholm and Goldberg, it gives a detailed review of all seiche theories, to which special attention is drawn. For the results see Table 23. Furthermore, Servais gives a special theory for transversal seiches and obtains good results, applying it to the Lakes of Geneva and Tanganyika.

The seiches in their simplest form only appear, of course, in oblong lakes, and the previous theories pertain to this special case. If the bottom configuration of the lake is more complicated, the seiches become more involved. Seiches of different periods are produced, depending on which parts of the lake are oscillating and of the direction of the forces causing the oscillations. A typical example of this are the seiches of the Chiemsee (Bavaria), which have been thoroughly examined by ENDRÖS (1903). The complicated orographical configuration of this lake favours several oscillation axes, and parts of the lake oscillate separately, so that there can be simultaneously eight oscillations in the lake. It is obvious that the seiches of such a lake can only be studied by detailed pictures taken simultaneously at different points on shore. Generally, all observed periods could be assigned to specific areas and the periods did agree with the ones computed from the dimensions of the oscillating water-masses.

Only in few lakes did the theory fail to be successfully applied. These exceptions occurred always when the configuration of the basins was very exceptional. Endrös has drawn attention to several cases where, besides the regular seiches, there are also oscillations of an exceptionally great period. He has been able to prove that this is due to the rising and falling of the entire level of the lake, and that this process should be considered as a periodic compensation with a second basin through a narrow canal. Such cases have been fully explained by the impedance theory of Neumann.

If the oscillating system consists of two different basins 1 and 2, connected by a canal (b, h, l) which has a cross-section q , then the impedance of the entire system equals the sum of the impedances of each individual part. With equations (VI.93) and (VI.95) we obtain

$$Z_1 + Zq + Z_2 = -\frac{c_1}{S_1} \cot \frac{\sigma l_1}{c_1} + \frac{\sigma l}{q} - \frac{c_2}{S_2} \cot \frac{\sigma l_2}{c_2} = 0$$

or

$$\frac{2\pi}{T} \frac{l}{q} = \frac{c_1}{S_1} \cot \pi \frac{T_1}{T} + \frac{c_2}{S_2} \cot \pi \frac{T_2}{T}$$

in which T_1 and T_2 are the periods of partial oscillation, when each basin is assumed to be completely closed at the connecting canal q . These periods can be determined accurately by using one of the methods previously explained, and then it is not difficult to determine the period of the oscillation of the connected system.

Examples are the Hallstättersee (Salzkammergut, Austria), the Königssee and the Waginger-Tachinger See (Bavaria) and others which consist of two parts connected by a more or less narrow canal. The computations made by Neumann of the period of the connected system have shown that there is a very satisfactory agreement between the observations and the theory (see Table 24).

Table 24. Lakes composed of two inter-connected parts

(l and b in km, h in m, S in 1000 m²)

		Period of oscillation				
		Computed	Observed ENDRÖS 1905, 1906, 1927			
Hallstättersee						
Southern Basin:	$l_1 = 5.47$	$b_1 = 1.08$	$h_1 = 81.0$	$S_1 = 87.5$	16.25	16.4 min
Northern Basin:	$l_2 = 2.79$	$b_2 = 0.72$	$h_2 = 23.0$	$S_2 = 16.5_5$		
Connecting Canal:	$l = 0.20$	$b = 0.40$	$h = 13.6$	—		
Königssee						
Northern Basin:	$l_1 = 5.28$	$b_1 = 0.69_5$	$h_1 = 114.5$	$S_1 = 79.54$	11.0	10.6 min
Southern Basin:	$l_2 = 2.22$	$b_2 = 0.64_4$	$h_2 = 59.8$	$S_2 = 38.5$		
Connecting Canal:	$l = 0.38$	$b = 0.27$	$q = 8.1$	—		
Waginger-Tachingersee						
Wagingersee:	$l_1 = 6.9$	$b_1 = 1.123$	$h_1 = 14.1$	$S_1 = 16.82$	64	about 62 min
Tachingersee:	$l_2 = 3.9$	$b_2 = 0.683$	$h_2 = 8.8$	$S_2 = 6.03$		
Connecting Canal:	$l = 0.14$	—	$q = 0.09$	—		

The damping of the seiches in lakes permits one to estimate the influence of friction on the oscillation. ENDRÖS (1934, p. 130) has given a compilation of the logarithmic decrements of the seiches of many lakes, part of which is reproduced in Table 25. It shows that there is a great variation in logarithmic decrements, ranging from the smallest value of 0.015 in the Lake of Geneva to its twenty-fold, viz. 0.310 in the Waginger-Tachinger See. Therefore, the successive amplitudes decrease for the Lake of Geneva by 0.3%, for the Waginger-Tachinger See by 48%. The values of the damping factor $\frac{1}{2}\beta = \frac{2\lambda}{T}$ show still greater variations. Leaving the large value of a fish-pond near Freising out of consideration, the Lake of Geneva has again the smallest value, viz. $0.4 \times 10^{-3} \text{ min}^{-1}$, the Königssee the fifty-fold of this, viz. $19.6 \times 10^{-3} \text{ min}^{-1}$. It can be concluded from the compilation by Endrös that the strongest

Table 25. Logarithmic decrements of seiches in lakes

(According to Endrös)

Lake	$\lambda \times 10^3$	Period in minutes	$\gamma = \frac{\beta}{2} \times 10^3$ in min^{-1}	Lake	$\lambda < 10^3$	Period in minutes	$\gamma = \frac{\beta}{2} \times 10^3$ in min^{-1}
Lake of Geneva	15	73.5	0.41	Frisches Haff	170	465	0.73
Lake Garda	23	42	1.09	Lake Erie	194	858	0.43
Lake Yamanaka	52	15.6	6.6	Lake Balaton	194	576	0.68
Lake Vättern	60	179	0.7	Kurisches Haff	250	550	0.7
Chiemsee	65	41	3.2	Wäger- Tachingensee	310	62	10
Fish-pond near Freising	89	1.02	175				
Königssee	114	11.6	19.6				

damping occurs in lakes composed of basins which are connected with each other by a narrow canal. This is the case with the Wäger-Taching See, the Königssee, and others. Another group which has a great damping factor is the shallow lakes, like the Lake Balaton, the Kurisches Haff, etc. It seems, on the whole, that every great disturbance in the morphology of the basin is accompanied by an increased damping of the seiches; this increase can take such proportions that the variation of the water level comes very close to being aperiodical.

(b) Oscillations in Bays

It has been clearly proven from the tide-gauge registrations that all ocean from the smallest to the largest, execute oscillations with a nodal line at the opening of the bay. These “disturbances” in the tidal curves are so frequent that smooth tidal curves are very rare. HONDA, TERADA, YOSHIDA and ISITANI (1908) have reproduced in scale models the oscillations as they occur in nature in the bays along the Japanese coast. Figure 79 gives as an

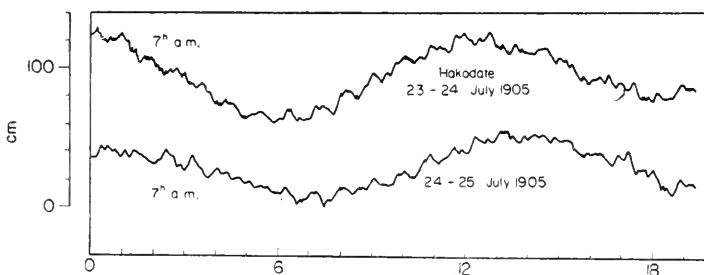


FIG. 79. Tide curves in the Bay of Hakodate and oscillations of short period in the bay.

example tidal curves of the Bay of Hakodate on which the short-period oscillations of sea level in the bay are superimposed. The principal seiches

(with the nodal line at the opening) had a period of 45.5–57.5 min; there is also a transverse oscillation with a period of 21.9–24.5 min. The computed periods were 45.3 and 23.6 min; the scale model gave 47.0 and 23.6 min. Figure 80 shows the streamlines of the most frequent oscillations, which were also the easiest to reproduce in the model.

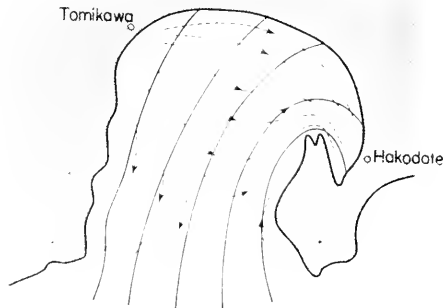


FIG. 80. Oscillations in the Bay of Hakodate.

These standing waves have also been observed in the bays and channels of the European coasts, and a mere look at the coastal configurations on charts will suffice to locate the points where they can be expected. Thus, WESTPHAL (1899, p. 53) has been able to find in the tide-gauge registrations seiches-like variations of the ocean surface for a number of German coast localities and PAULSEN (1906, p. 13) has done the same for Danish localities around the Baltic and Belts.

Numerous seiches have been observed in the Mediterranean. PLATANIA (1904–7), ODDONE (1908) and FOREL (1895, p. 229) have given a compilation for a number of localities on the Italian shore. At the west coast of Sicily, from Trapani to Sciacca, there is a phenomenon, referred to as the “Marubio”, which has the character of seiches with large oscillations of the sea level. Airy identified seiches in the harbour of Malta, which he assumed to be standing waves on the coastal shoal extending towards Sicily and in the Tunisian straits. Krümmel made the remark that they might be the oscillations of the harbour of La Valetta, with an average period of oscillation of 23.4 min; the dimensions of the bay agree very well with the observed period.

Seiches-like oscillations exist in the bays and channels of the Adriatic. STAHLBERGER (1874) has been the first to give a paper on the sea-level registrations in the Gulf of Fiume; later on, MAZELLE (1907) has tried to derive quantitatively from these registrations the oscillations between the islands and in the numerous bays, which are accompanied by strong currents (called stigazzi). An extensive paper by STERNECK (1914) on the seiches in the Adriatic is available. He has found, from the dimensions of the bays and

canals under consideration, a plausible explanation based on Merian's formula for most observed periods. In general, the oscillations in these bays and harbours have a period smaller than half an hour. Only on Trieste there is sometimes a seiche with an average duration of 3.2 h which is always accompanied by great variations in water level (the average of fifteen cases was approximately 75 cm, with a maximum of 156 cm). These are oscillations of the whole Gulf of Trieste, which can be imagined to be closed off from the open sea by a line drawn from Capo Salvatore to a point located somewhat to the west of Grado. This line is, in fact, the nodal line of the oscillation. Merian's formula with a correction for the opening of 1.2943 gives a period of 3.1 h, in good agreement with the average observed period (see CALOI, 1938). It seems, however, that part of the Adriatic west of this nodal line participates in the oscillation, because the tide gauge at Falconera (about 30 km to the west of Grado) clearly shows an antinode with a phase opposite to that of Trieste. Smaller oscillations (0.78 h and less) registered in Trieste are oscillations of the Bay of Muggia and of the harbour. For the causes of the great seiche of 3.2 h we refer to p. 224.

In the eastern part of the Mediterranean there occur also seiches at any point where the configuration of the coast is appropriate for free oscillations of the water-masses. If the amplitude of the tide is small and the seiches rather large, then it happens that the tides are concealed by the seiches.

The most famous example of standing waves in the Mediterranean is considered to be the currents in the narrows between the Greek mainland (Phokin and Voiotia) and the island Euboea. FOREL (1879, p. 859) was the first to relate the rapidly changing currents (4 m/sec) in the narrows of Khalkis with the seiches in the northern and southern channels. KRUEMMEL (1888, p. 331), submitted the observations of Miaulis to a thorough discussion, which confirmed to him the correctness of Forel's assumption. Endrös (1914) and Sterneck (1916) (see also DEFANT, 1917, p. 329) have solved the Euripus problem, on the basis of hydrodynamical considerations. The narrows at Khalkis are composed of two parts each of 18 m length and approximately 6 m respectively 1 m depth (total cross-section 126 m²), and separated by a small island. The currents in these narrows are very irregular, which is to be attributed to differences in the level of the sea surface north and south of the narrows. Endrös considers these differences in the water level to be caused by (1) difference in the tides north and south of the narrows; (2) the occurrence of seiches in the northern and southern channels; (3) piling up of water in the channels by the winds.

The tides of the Aegean Sea reach the narrows of Khalkis from the north through the Trikeri and Oreos channel and from the south-east through the Gulf of Petali. Both Endrös and Sterneck were able to compute from the observations of Miaulis the tidal constants of the semi-diurnal tides for the northern and southern harbour of Khalkis. They found that the large dif-

ference of the amplitudes of the tides was the main cause of the Euripus currents. The maximum differences of 1 m in the northern harbour and of 20 cm in the southern harbour changes its sign every 6 h and, consequently, causes these strong currents. The "reversal of the high waters" in Khalkis was previously considered a peculiarity; it describes the fact that the times of the high and low water on the 9th lunar day are just interchanged from those of the 6th lunar day. The same is true for the 23rd in comparison with the 21st lunar day. It is a phenomenon which necessarily results from the tidal constants and which is somewhat strengthened by the fact that the ratio of $S_2 : M_2$ for Khalkis is 0.64, which is considerably higher than the normal value of 0.46.

The narrows of Khalkis can be considered as a wall which almost completely closes the Evoikos and Evripon Euripus, because, as a consequence of its small cross-section, there can hardly be any exchange of the water-masses through it. Therefore, the tides of both the northern and the southern canal will be a co-oscillation with the tides of the Aegean Sea at the respective openings of the canal. Sterneck has computed these co-oscillating tides for the two canals, taking fully into account their bottom configuration, and he obtained the range of the tide along the longitudinal axis of these canals up to the narrows of Khalkis, as represented in Fig. 81. Despite the nearly

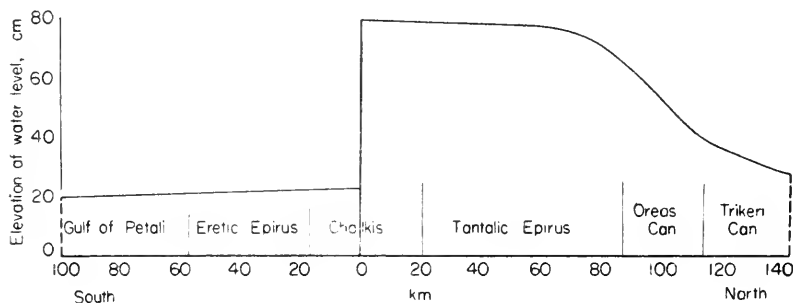


FIG. 81. Range of the semi-diurnal tide in the Euripus Channel co-oscillating with the Aegean Sea in the north and in the south.

equal amplitude of the semi-diurnal tide at both the north and south opening of the channel in the Aegean Sea, the amplitude of the tide in the northern canal rises first rapidly and then slower to 79 cm in the northern harbor of Khalkis. In the southern harbour, on the contrary, the rise is very small and the amplitude only attains 23 cm. These theoretical values show a very good agreement with the observations of Miaulis. They also explain fully the anomalous value of the ratio $S_2 : M_2$ for the penetrating tides and the small value of the diurnal tides. They also explain the reversal of the high water hours, which is linked with the reversal of the regular current before and

after the quadratures. The regular part of the Euripus currents, therefore, is a consequence of the variety of the tides in the northern and southern harbours of Khalkis.

In both of these harbours there are always seiches. Contrary to the tides, these seiches are of small amplitude in the northern harbour; Miaulis observed during one month, despite stormy weather, only once amplitudes of 15 cm during two oscillations; otherwise they were smaller than 5 cm. The seiches in the southern harbour are a daily occurrence and have greater amplitudes. The period of the seiches for Khalkis north is 1.44 h, for Khalkis south 1.84 h. The Japanese method (p. 164) was used to explain the period of these seiches. It gave for the Evripon Euripus (node at the opening near the Isle of Kavalianis) 1.87 h, in accordance with the observations. The regularly shaped bay, the narrowing near the opening and the funnel-shape of the adjoining Gulf of Petali call for greater amplitudes, as it was observed. The period of the free oscillations of the entire northern canal with a correction for the opening is 6.49 h for the uni-nodal wave and 1.04 h for the two-nodal wave. It is doubtful, considering the complicated form of the northern canal, whether such oscillations occur. They have not been observed. It is possible that the 1.44 h seiche is the one of the Talantic Euripus combined with the seiche of the Mali Gulf, with an opening in the Oreos channel. If we consider this as a closed system, the period of the free oscillation will be 0.96 h, hence smaller than the observed period of 1.44 h. With this disagreement it can be expected that the amplitudes of the seiches in the northern harbour, if there are any at all, will be small. Since in the southern harbour the amplitude of the tide is small, the seiches become especially important for the Euripus currents. According to their period, they can, under certain circumstances, cause the current to alternate fourteen times in the course of 24 h in the narrows of Khalkis. If we consider these irregular currents as the actual Euripus problem, then Forel, in referring to the seiches, was the first to give a correct explanation.

A close scrutiny of the differences in the level in the northern and southern harbours of Khalkis permits to get a better insight into the phenomena of the reversal of the currents. Endrös concluded from the observations of Miaulis that these currents are not horizontal displacements, like in the vicinity of the nodes in standing waves, but a compensating gradient current. The reversal in the direction of the current occurs simultaneously with the change of sign of the difference in level, and not at the time of extreme levels in the north and the south of the narrows, as would happen in the case of the water-masses oscillating through the narrows. The number of changes in the direction of the current during one day depends also, however, on the general daily level in the entire area of the Euripus. These variations in level are superimposed on the tidal and seiches currents and they fix the sequence of the changes in the current. The variations of the daily mean level originates

partly from the unperiodical variations of the ocean surface of the entire Aegean Sea and partly from the piling up of the water by the wind.

The basis of explanation of the entire phenomenon is the fact that there can be no uniform oscillation in the area of the narrows of Khalkis. Both canals leading up to Khalkis from the north and the south oscillate individually, and the ensuing differences in level north and south of the narrows are compensated by currents between them. It is easy to understand that the great frictional influences in the shallow and narrow straits prevent free oscillations, and that there can only be an aperiodical adjustment of the differences in level.

(c) *Oscillations of the "Haffe"*

Most interesting are the standing waves in "Haffe" which are mostly outstretched water-masses of small depth, which are connected with the open sea by one or several openings. In the Baltic the most typical examples are the Frisches Haff and the Kurisches Haff, which are connected with the open Baltic by the Pillauer Channel and the Memeler Channel respectively.

In the Frisches Haff (length 90 km, mean depth less than 3 m) there are, according to the gauge registrations at Pillau and other localities, seiches with a duration of 8.0 h, and — although less often — seiches of 5.0 h. The first is probably the oscillations of the entire, more or less enclosed water-mass of the Haff with a nodal line lying approximately at the Passage Mouth, whereas the latter period might be the two-nodal seiches, (See LETTAU, 1932, p. 229, and MOELLER, 1937, p. 262). The oscillations are strongly damped and show a logarithmic decrement of 0.229.

The gauge placed in the Kurisches Haff in the channel from Memel to the Baltic shows, as an average of a large number of cases, a period of oscillation of 9.2 h, which might correspond to that of the uni-nodal seiche, and besides, a period of oscillation of 4.12 h, which will be that of the two-nodal seiche (see LETTAU, 1932). Here also the damping is great, considering the shallowness of the Haff (length 85 km, mean depth 4.0 m) (according to Endrös, $\lambda = 0.25$).

The impedance method can be used to good advantage for a theoretical investigation on the period of the free oscillations of incompletely enclosed lakes. A lake with one side or one end open will lose or receive periodically at each oscillation a certain amount of water, and this process must influence the period of the free oscillations of the lake. One is inclined to assume that such process generally causes an increase of the period of a lake supposedly completely enclosed. However, NEUMANN (1944, p. 200) was able to prove that this is not the case. The impedance theory clearly shows that there is a decrease of the period, according to the position of the opening with respect to the nodes and antinodes. LETTAU (1932) has tried to solve this problem by starting from the principle of conservation of energy. The result was an increase in the period of the lake, which does not seem right.

Possibly an error was made in applying the energy principle, inasmuch as the energy equation used is not satisfied at all times. We can distinguish three parts in a Haff as shown in Fig. 82: sections 1 and 2, situated on either side

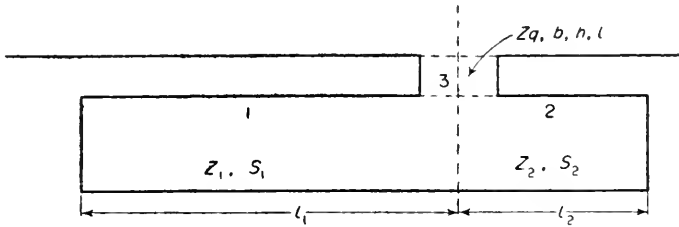


FIG. 82. Computation of the free period of a sea partially closed.

of the opening are considered as separate areas of oscillation with the impedances Z_1 and Z_2 , the outlet opening has the impedance Z_q . During the oscillations, water from 1 will flow both into 2 and through the lateral outlet. 2 and 3, therefore, must be regarded as connected “in parallel” to each other and these two connected “in series” to 1. Consequently, the condition of the natural frequency is

$$\frac{1}{Z_1} + \frac{1}{Z_2} + \frac{1}{Z_q} = 0.$$

With the corresponding expressions for Z , we obtain, assuming Z_1 and Z_2 are basins closed on one side:

$$\frac{S_1}{c_1} \tan \frac{\sigma l_1}{c_1} + \frac{S_2}{c_1} \tan \frac{\sigma l_2}{c_2} = \frac{a}{\sigma},$$

if $a = bh/l$ (dimensions of the outlet). In case the outlet opening is moved towards the far end of the lake, we get $l_2 = 0$ and the equation for the period

$$\frac{S_1}{c_1} \tan \frac{\sigma l_1}{c_1} = \frac{a}{\sigma}.$$

This relations shows that the period is shortened compared to the period of the fully closed basin.

In applying this to the Frisches Haff, the section 1 is the narrow southwestern part from the mouth of the Nogat to the deep of Pillau, section 2 the remaining part of the Haff to the mouth of the Pregel including the Fischhauser Wick, and section 3 the Pillauer Seetief. The application of Defant’s method gave for 1 and 2 the partial periods 6.63 and 3.11 h and with the numerical values:

	Average cross-section (S)	Mean depth (h)	Length	Width (b)	Depth (h)
Sect. 1:	$22.5 \times 10^3 \text{m}^2$	2.58 m	Sect. 3: 2.04 km	4.45 m	8.8 m
Sect. 2:	$23.0 \times 10^3 \text{m}^2$	2.92 m			

The above-mentioned equation gives as the period of the free oscillation of the entire Haff basin 8.05 h, which is in agreement with the observed

period of the fundamental oscillation. If the Haff is completely enclosed, we find 9.7 h. The influence of the opening on the side consists in a decrease of the period by about 1.7 h.

In the case of the Kurisches Haff, conditions are more complicated. Merian's formula, assuming this Haff to be closed near Memel, gives for the period of the fundamental oscillation 7.6 h, Defant's method according to Lettau only 7.0 h, which decrease is understandable, because the narrowing of the lake at one end causes it. The observed period, however, is 9.2 h. The opening of the Haff near Memel cannot be the cause of this considerable increase. Only the exact records of oscillatory conditions of the Kurisches Haff can eliminate this disagreement.

(d) Standing Oscillations in Adjacent Seas

Because of the large horizontal dimensions of the basins, the period of these free oscillations will be very great, sometimes one day and more. The superposition of smaller partial oscillations and forced oscillations (e.g. tides) will often cover up the free oscillations. These are the main reasons why the free oscillations of the adjacent seas have thus far been so little investigated, even though such work is indispensable for clearing up all oscillatory phenomena in these seas, including the tides.

NEUMANN (1941, p. 180) investigated the Baltic seiches-like oscillations which have already been described for some sections in the Baltic. The variations of its sea level designated by MEISSNER (1922, p. 121) as "seiches of the Baltic" cannot be the free oscillations of the entire Baltic, on account of the shortness of their periods, but they are merely oscillations of smaller sections of bays and shores. The free oscillations of the Baltic became very important from a practical point of view when they were associated with the sometimes disastrous floods in the inner Gulf of Finland (Leningrad). STENIJ (1936) has shown that the free oscillations of the water-masses of the Baltic are one of the causal factors for these floods. It was attempted by DUBNOW (1936) to consider the oscillations of the Baltic by means of a basin model, but there is no good agreement between the results of his experiments and the actual observations. Neumann was the first to investigate the free oscillations by analysing accurately the tide gauge observations distributed over the entire coast, in order to study simultaneously oscillatory processes. The existence of free oscillations all over the Baltic was in this way satisfactorily proven. A statistical examination of the variations of the sea surface in Ystad (southern point of Sweden) and Koivisto (at the head of the Gulf of Finland) for the years 1935 and 1936 gave the most frequent period, which was for both localities 26.75–28.25 h, on the average 27.5 h, which is the uni-nodal seiche in the system Baltic–Gulf of Finland.*

* A shorter period between 25 and 26 h in Koivisto, which is lacking in Ystad, might be the oscillation of the Gulf of Finland itself.

The examination of the individual records showed that it is not uncommon for the oscillations to occur in a row of three or four and more successive waves and attain in the Gulf of Finland a range of over 1 m. We will give as an example the record from 10 to 15 December 1932 illustrated in Fig. 83,

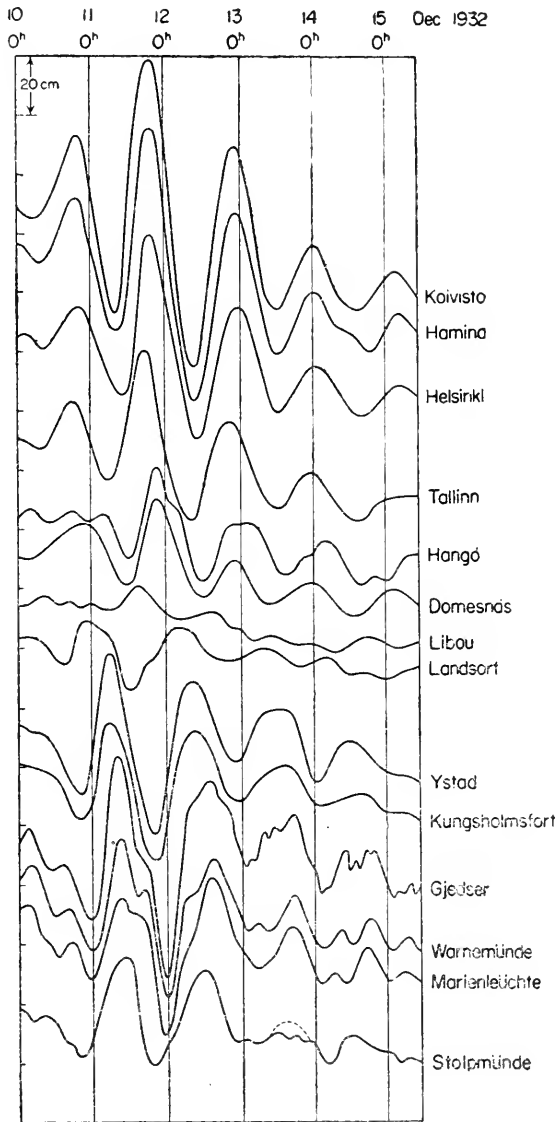


FIG. 83. Level of the Baltic measured by various gauges from 10 December 00^h (G.M.T.) to 15 December 1932, 10^h (G. Neumann).

which can be considered as particularly typical of the uni-nodal oscillation of the system Baltic—Gulf of Finland. In Koivisto the range of the first wave

exceeds 1 m; towards the entrance of the Gulf of Finland the amplitudes decrease rapidly, and at Landsort and Libau the oscillations have nearly vanished. The south-west part of the Baltic, on the contrary, oscillates in the opposite phase and the amplitudes increase up to Gjedser. From here on, the amplitudes in the south-western part of the Baltic no longer increase; they rather decrease. In the Belts, in Korsoer and Frederica, it is impossible to find a correlation with the oscillatory process of the Baltic except at two extremes. Here as in Copenhagen, the regular tidal oscillations are preponderant. Figures 84 and 85 give, for the first oscillation of this case, the two

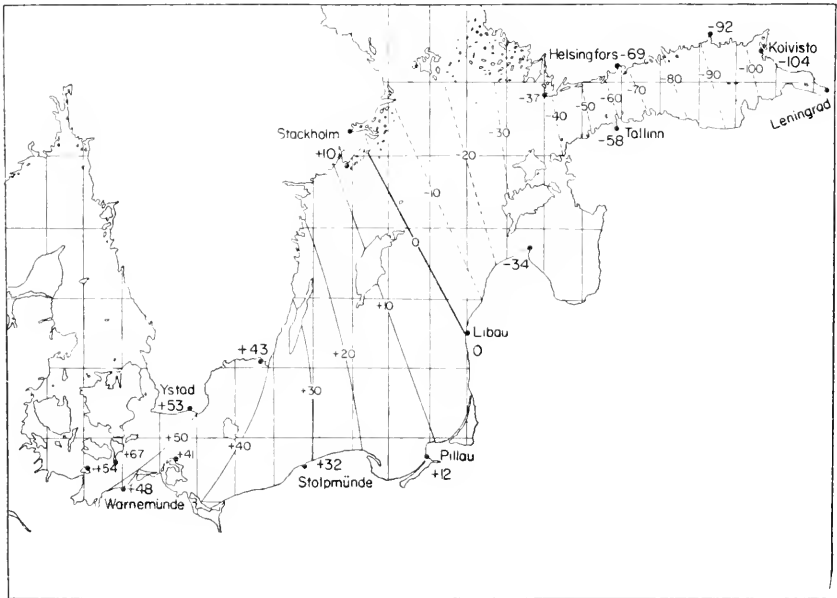


FIG. 84. Co-range lines of the oscillation of 11–12 December, 1932 in the Baltic. The dotted lines indicate the amount in cm of depression, the full drawn lines the amount of elevation for the first half period.

extreme positions of the water surface in the entire area of the Baltic. We can see how well the amplitudes fall along the line of the oscillation, and there is no doubt that we have here the uni-nodal free oscillation of the system Baltic—Gulf of Finland. The observed period is 27·3 h.

The two-nodal wave appears quite often; however, it has always a smaller amplitude and, in the few cases in which it occurs without the fundamental oscillation, it does not persist after one or two oscillations. It is less persistent than the uni-nodal seiche; the Baltic seems to be less suited for its development.

There are also free oscillations in the system Baltic—Gulf of Bothnia with a period of about 40 h; however, in this case the oscillating basin is divided into two unsymmetrical sections by the nodal line, and this is why the oscillations of this basin seldom occur.

The closing of the Baltic basin towards the Belts is established morphologically. The first narrowing of the cross-sections is near the Darser sill (saddle depth only 18 m), the second one in the western part of the Fehmarn-

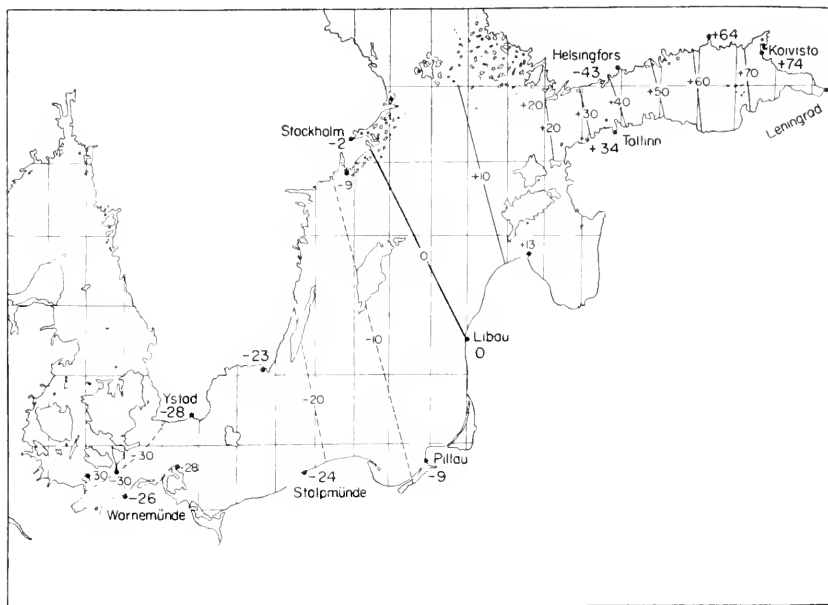


FIG. 85. Co-range lines for the watermass oscillating back to its original position (see Fig. 84).

belt near the sandbank Öjet. In both cases the cross-section is only about 1/30 to 1/40 of the mean cross-section of the Baltic. If we take the western border line first at the Fehmarnbelt, the second time in the small Belt near the line Aarö-Assens, Neumann obtains for both oscillating systems according to the methods of Defant and Hidaka, the fundamental period of the Baltic, as listed in Table 26.

The agreement of the periods computed by fundamentally different methods is very good. Figure 86 shows the theoretical distribution of the vertical ($2\eta_0$) and of the horizontal ($2\xi_0$) water displacements of the uni-nodal oscillation. The position of the nodal line of this oscillation is not symmetrical, but is somewhat displaced towards the north in the vicinity of the northern point of Gotland. This is in excellent agreement with the observed position (see Figs. 84 and 85). From the entrance in the Gulf of Finland (approximately at cross-section 38) the range increases very rapidly and attains at the eastern end (Leningrad) values which are nearly twice as large as those at the western end (Luebecker Bucht). This is also confirmed by observations. It is remarkable that, for the two-nodal wave, the opposite is true. Due to the large widening and deepening of the Baltic in the middle sections, the greatest horizontal water displacements and, hence, also the greatest current

Table 26. *Theoretical free periods of the Baltic*

Oscillating system	Western boundaries	Oscillation				
		Uni-nodal		Two nodes		Three nodes
		Method of Computation				
		Defant	Hidaka	Defant	Hidaka	Hidaka
Baltic —	Fehmarn	27.5	27.5	19.3	18.1	11.3
Gulf of Finland	Aarö-Assens	29.5	29.3	24.3	22.0	13.4
Baltic —	Fehmarn	39.1	—	—	—	—
Gulf of Bothnia —						
Gulf of Finland	Aarö-Assens	39.7	—	—	—	—

velocities caused by the oscillation, do not occur in the centre of the basin near the nodal line, but at the points where the cross-section narrows, at the Darser sill and at the entrance of the Gulf of Finland.

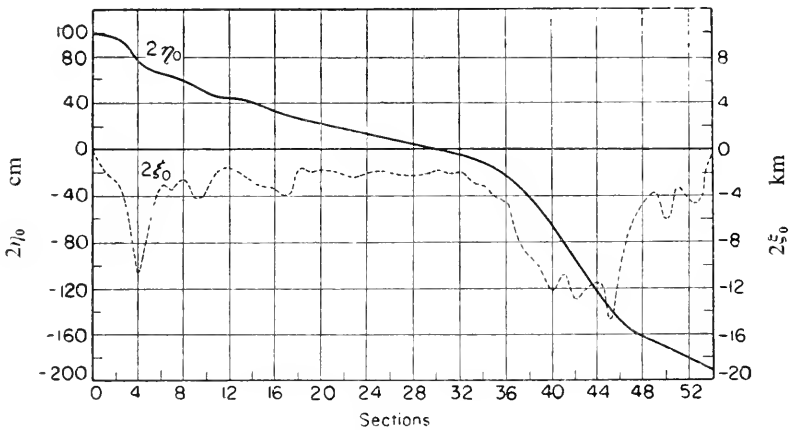


FIG. 86. Theoretical distribution of the vertical ($2\eta_0$) and horizontal ($2\xi_0$) displacement of the uni-nodal oscillation of the Baltic—Gulf of Finland ($T = 27.5$ h).

The important question is, to what extent the Beltsea participates in the oscillatory process of the Baltic. Neumann has been able to prove that, according to observations, this oscillation process does not continue into the Bay of Kiel. The bays west of the Darser sill participate only in the process in so far as, in the first half of the oscillation, they simply fill up, whereas in the second half they are again emptied. We have here a practical application of the case which was dealt with theoretically on p. 177. If we designate the Baltic as basin 1, the Darser sill as the connecting canal 2 and the basins east of the same as basin 3 (see Neumann, 1941) we obtain from the equation (VI.85) as the fundamental period of the system Gulf of Finland — Baltic —

Darser Sill — Mecklenburg Bay and Kiel Bay, $T = 27.70$ h by inserting in (VI.85) the numerical values provided by the survey of the Baltic. However, one can also compute from the observations the water-masses transported back and forth across the Darser sill during one period of oscillation and, with these values as the western boundary condition, determine the period after Defant's method. One then obtains as the period of the uni-nodal oscillation 27.6 ± 0.7 h, and for the two-nodal oscillation 17.5 ± 0.6 h. These values are in good agreement with the observed free periods of the Baltic.

The Adriatic Sea, due to its regular shape, is particularly suited for free oscillations. As a matter of fact there are indications of such seiches in the tidal gauge registrations, which often attain a very large amplitude. Because the range of the tide in this sea is not negligible, these variations in level should be studied in the following way. The partial tides computed from the observations are used to construct a tidal curve. The difference between this theoretical and observed tidal curve is plotted and analysed. In this manner, VON KESSLITZ (1910) has found for Pola and VERCELLI (1941, p. 32) for Zara oscillations of the following periods:

(1) About 22 h; it occurs especially at the northern end of the Adria with regular wave trains of a large amplitude (30 cm and above), particularly with sirocco and bora weather.

(2) About 11 h; it is less frequent than the former and it seems to occur only with special weather conditions (bora in the northern section, stormy sirocco in the southern section of the Adria) with rather irregular amplitudes.

(3) About $8\frac{1}{2}$ h.

(4) Finally $3-2\frac{1}{2}$ h which appear more frequently than the two previous ones, and they are more discernible in the registrations because of their shorter duration. Figure 87 gives a good example of the 22 h oscillation.

This long oscillation seems to be the uni-nodal seiche of the entire Adria with a nodal line at the opening Otranto-Valona. For $l = 802$ km and an

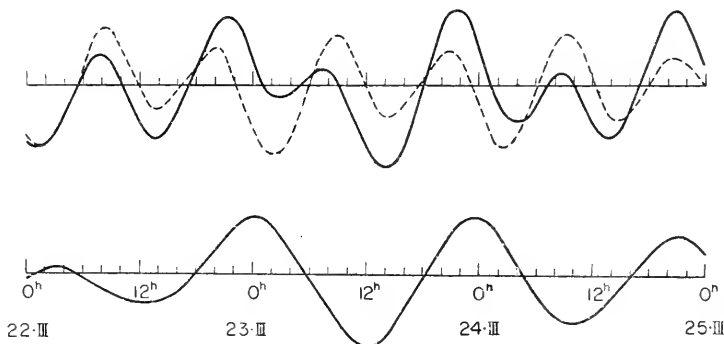


FIG. 87. Record of the tide at Pola from 22 to 24 March 1906. The dotted line is the theoretical tide curve. The full drawn line is the observed curve. Below; the difference between both curves. 3 waves with an average period of 22.2 h.

average depth of 235.7 m. Merian's formula gives a period of 18.39 h and, with a correction for the mouth of 1.167, a period of 21.4 h. It fits quite well the observed value of 22 h. The Japanese method, however, gives a negative correction for both the width and the cross-section, so that the theoretical value is reduced to 15.62 h. It is questionable whether, in view of the rather large correction due to the form of this sea, the Japanese method can still be used. The narrowing of a bay at the opening must lengthen the period and not shorten it (see DEFANT, 1911, p. 126). If this oscillation is not the uni-nodal period of the free oscillation of the Adria, it could not be explained by its dimensions. STERNECK (1915, p. 44) finds, by integrating step by step the equations of motion, for the Adria a period of 21.12 h, which is increased to 23.34 hours by a correction factor for the opening 1.105.

The 11 h wave can only be the uni-nodal seiche of the Adria, if the strait of Otranto is assumed to be closed. Oscillations of this kind are perhaps not entirely excluded, on account of the great narrowing of the bay at the opening; the unusual wind conditions which accompany this oscillation might also be the cause. The $8\frac{1}{2}$ oscillation then is the first harmonic oscillation of the Adria with a node at the opening and a second one inside, whereas the short, 3 h waves which often occur might be transverse oscillations. The average cross-sections of the Adria give as period of such transverse oscillations approximately $2\frac{1}{2}$ h, which is in agreement with the observed values.

The Black Sea can be considered as a completely closed basin with regard to its seiches. Both STERNECK (1922) and KURTSCHATOFF (1925) have only been able to find short-period oscillations from tide registrations, which are to be considered as local bay and shore oscillations. A careful analysis of the tidal curves made by ENDRÖS (1932, p. 442) has shown that a small seiche of a definite duration can be read from the curves after elimination of the small tides. However, on account of the little development of these seiches, the Black Sea, despite its large dimension, must be regarded as a badly tuned oscillating basin. Endrös found periods of 7.4, 6.4 and 5.5 h. The first period seems to be essentially an oscillation of the north-western shallow section of the sea (Bay of Odessa). Endrös believes that the two other oscillations are of the entire water-mass of the Black Sea along the main deep basin towards the southwest (Burgas, 5.5 h), and towards the middle of the western shore (Constanza, 6.4 h). These two periods are very similar, and when they occur simultaneously, it is very difficult to separate them by analysis. The 5.5 h wave must be attributed to the uni-nodal longitudinal oscillation of the main basin in the direction Poti-Burgas. Sterneck found for the theoretical period of this longitudinal oscillation, using the Japanese method, 4.98 h, DEFANT (1918, p. 78) using the residual method, 5.12 h. In both computations the Bay of Odessa was omitted. If the water-masses oscillate more from the middle of the lake towards the south-

west, the period increases to 6.4 h, because the sea becomes shallower and because the “Talweg” becomes longer. Endrös reaches a remarkable conclusion, that there are in the Black Sea three different main directions of oscillation, each having a different period, which coincide at the eastern end, whereas they split up in the western part.

Opposing this interpretation, DEFANT (1933, p. 56) remarked that, in view of the enormous extension of the area of the Black Sea, it is perhaps no longer permitted to neglect the deflecting force of the earth’s rotation (see p. 217), and that the periods of 6.4 h and 5.5 h might be oscillations influenced by the rotation of the earth. He supports his objection by comparing the Black Sea with a circular basin having the same main oscillation. The longest oscillation of such a circular basin (a nodal line at a diameter), neglecting the earth’s rotation, is found from the equation $\sigma_0 a / \sqrt{gh} = 1.84$, in which $\sigma_0 = 2\pi/T_0$ and a the radius of the circular boundary and h the depth of the basin. If the basin is rotating with an angular velocity ω , a simple oscillating motion is no longer possible (LAMB, 1932), (GOLDSTEIN, 1929, p. 213). Instead, two rotating waves develop having their centre in the middle of the basin. One of these waves moves in the same direction as the rotation (positive wave), the other one in the opposite direction (negative wave). Their angular velocity and their period depend on a quantity

$$\beta = \frac{4\omega^2 a^2}{gh}.$$

When $\beta = 0$ (no rotation), the angular velocities and periods of both waves are equal. Their superposition gives the simple standing wave. With rotation, however, their periods and angular velocity become different. If the value of β becomes sufficiently great, the wave period nears the period of the rotation.

In small lakes β is so small, that the influence of the Coriolis force is almost imperceptible. However, if the lake has dimensions as large as those of the Black Sea, the influence can make itself felt. If we put $T_0 = 6$ h, then $\beta = 0.391$, quite different from zero, and we find for the periods of the positive and of the negative waves respectively 5.47 and 6.49 h. The influence of the earth’s rotation is very important and, in view of the striking similarity of these periods with those by Endrös, it cannot be denied that perhaps there is actually some influence of the earth’s rotation on the oscillatory system.

The Sea of Azov is one of the shallowest basins with large dimensions (length 390 km, mean depth about 10 m). It is a region where very strong winds pile water up to 5 m in the shallow north-eastern Bay of Taganrog. This causes oscillations of large amplitude. Kurtschatoff found 24.5 h for the uni-nodal seiche reaching from the south coast to the Bay of Taganrog. The enormous variation of 2.5 m at the end of the north-eastern bay near Taganrog can be computed from the largest amplitude of 80 cm observed in Temrjuk (at the south-eastern angle). The dimensions of the sea fit this longest oscillation. Furthermore, a great number of other seiches have been observed, among which those with a period of 14.8 and 12.8 h stand out. Endrös regards the former as the binodal seiche of the entire Sea of Azov, and it is very noticeable at Jeisk. It cannot have, however, the same direction as the principal oscillation, otherwise Jeisk and Temrjuk could not have the same phase. Endrös considers the 1.28 h wave as an oscillation in a curved direction west–north–south-east. Oscillations in this sea are very complicated

and not yet fully solved; neither is there any certainty yet as to the extent of the influence exercised by the Strait of Kertsch.

We want to mention the variations of the level of the great North American lakes, which were investigated by HENRY (1902). These investigations were followed by the extensive work of HAYFORD (1922) towards determining the correct mean level of the lakes. ENDRÖS (1908) determined the principal period of Lake Erie from the curves added to the paper by Henry. He found a main period of 14.3 h, and the harmonic oscillation of 8.8 h to be a two-nodal, those of 5.7 and 4.1 h three- and four-nodal seiches respectively. All periods and phases agree with the theory. Another wave of long duration which averages 12.65 h is — as shown by ENDRÖS (1930) — the semi-diurnal tide. These results seem to be in contradiction with the findings of Hayford, who found periods of 12.8, 13.0 and 13.8 h for the principal oscillation in Buffalo, and periods of 12.5, 12.9 and 13.9 h in Cleveland, whereas the harmonic oscillations agree with the values given by Endrös. This deviation from the value of 14.3 h indicated previously can be explained from the fact that Hayford has not eliminated the tidal waves from the curves, so that the values found by him represent the superposition of the free oscillations with the ever present tidal wave. This superposition, however, gives oscillations with a period varying between 12.5 and 13.9 h. Endrös found for Lake Erie a large logarithmic decrement of $\lambda = 0.237$ h, which is caused by the islands located in the western part.

Hayford did not find in Lake Michigan and Lake Huron well-developed oscillations, because of special conditions in the basins. Endrös proved in both lakes a distinct oscillation with a period of approximately 45 h, which he explains as a compensating motion between these two great lakes through the connecting Straits of Mackinac.

A theoretical investigation of the seiches in Lake Michigan was made by Fr. DEFANT (1953). He computed the free periods of the uni-nodal and two-nodal seiches after different methods. In the mean, 9.05 h were found for uni-nodal seiches and 4.84 h for two-nodal seiches. The simple, swinging motion of the seiches is changed into weak amphidromies contra solem when the Coriolis force is taken into account. Then the amplitude of the transverse oscillations amounts to about one fifth of that of the longitudinal oscillations. It seems that there are as yet no actual observations.

5. Influence of the Earth's Rotation on Tidal Waves and Seiches

(a) *Horizontal Motions in Progressive and Standing Waves*

It is customary to observe principally the vertical displacements of the water-masses η , whereas little attention is paid to the horizontal displacements ξ . In the simplest case of progressive and standing waves in a uniform canal of constant depth h , we have the following relations for these displacements:

Progressive wave	Standing wave	} (VI.99)
$\xi = a \cos(\sigma t - \kappa x)$	$\xi = a \cos \kappa x \cos \sigma t$	
$\eta = ah \kappa \sin(\sigma t - \kappa x)$	$\eta = ah \kappa \sin \kappa x \cos \sigma t$	
$u = -a \sigma \sin(\sigma t - \kappa x)$	$u = -a \sigma \cos \kappa x \sin \sigma t$	

The horizontal velocity in the wave results from the equation $u = d\xi/dt$. Equations (VI.99) show that with progressive waves the greatest velocities coincide with the greatest rise and fall of the free surface. The free surface rises and falls because of the convergence and divergence of the horizontal motion of the water particles. Within a progressive wave the horizontal flow at the wave crest is in the direction of progress of the wave, and at the trough it is opposite to the direction of progress. Within a standing wave, on the contrary, the horizontal velocity is zero at every point, at the time when the wave reaches its greatest height, and is strongest at the nodes; at the antinodes (crest and trough) it is constantly zero (p. 6). The vertical velocity is always zero at the nodes halfway between the trough and the crest.

Because it is possible, for standing waves in seas and bays, to compute the horizontal and vertical displacements ξ and η for each cross-section, it is easy to compute the horizontal velocities and to compare them with the results of current measurements. There are only very few of these measurements, even though they constitute an important indicative feature as to the oscillatory form of completely or partly closed basins. NEUMANN (1942, p. 1) has analysed the currents connected with the seiches in the Baltic. From ξ computed according to the residual method he derived the distribution of the horizontal current velocities in the direction of the "Talweg", assuming an amplitude of 50 cm at the head of the Gulf of Finland. These values are shown in Fig. 88 by the broken line; the dotted curve indicates

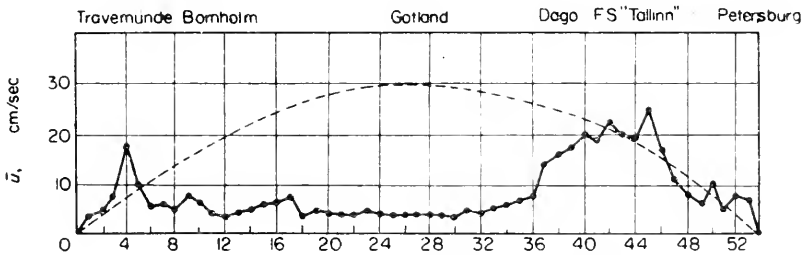


FIG. 88. Current velocities computed by the stepwise integration along the "Talweg" of the Baltic assuming an amplitude of the seiches of 50 cm at the closed end of the Gulf of Finland (the dotted line is for a rectangular basin of constant depth).

the distribution of the current computed by equations (VI.99) for a rectangular basin ($l = 1473$ km, $h = 55$ m). The distribution of the current velocities is changed by the complicated basin configuration compared to a rectangular basin. At the Darser Sill and at the opening into the Gulf of

Finland one has to count with velocities of the seiches of 15–20 cm/sec, whereas in the centre of the Baltic the values are being reduced to the order of magnitude of 5 cm/sec.

Neumann has used the current observations made on lightships in the Gulf of Finland, in order to prove the variations in the current which accompany the uni-nodal free oscillation. The current observations made by the lightship "Tallinn" show the same period as the free oscillation (27.5 h) and a difference in phase with the free oscillation of approximately 7 h, which corresponds to the theoretical value $\frac{1}{4}T$. These periodically varying currents, which in one instance reached an amplitude of 45 cm/sec, do cause a periodically varying transversal slope of the sea surface in a line Helsingfors–Reval.

When studying drift and wind currents, attention should be paid to possible periodic currents resulting from the free oscillations of the water-masses.

(b) Progressive Waves in a Rectangular Canal Considering the Rotation of the Earth

Like any moving object on the earth, horizontal water displacements are subjected to the Coriolis force. Fully developed, this force is capable of modifying the currents considerably. In most cases it should not be neglected, as it is of the same order of magnitude as the pressure forces. If the amplitude of the periodical horizontal velocity of the wave is U the Coriolis force will be $2\omega \sin \varphi U$, and its direction is perpendicular to the direction of propagation of the wave. Since U changes its sign the Coriolis force during one half of the wave period is directed to the left, during the other half to the right. Gravity acts in the vertical direction on the moving water particle. Together they give a resultant, which is inclined by a small angle γ towards the vertical. Its tangent is given by

$$\tan \gamma = \frac{2\omega U \sin \varphi}{g}.$$

If the surface is always perpendicular to the resulting force, it should also make an angle γ with the horizontal plane. The order of magnitude of this angle is very small. At $\varphi = 45^\circ$ we have $\tan \gamma = 1.027 \times 10^{-7} U$ and with $U = 20$ cm/sec $\gamma = 0.4''$. The slope of the sea surface is, therefore, extraordinarily small. However, considering that the slope of the sea surface is equally small when long waves pass by, we cannot neglect the transverse slope caused by the earth's rotation. In a tidal wave of 200 km length and an amplitude of 25 cm the slope of the waves is on the average 5×10^{-6} , the transverse slope caused by Coriolis force is approximately 1×10^{-6} , thus of the same order of magnitude. In a canal of a width b the rise and fall of the surface caused by the action of the Coriolis force is $\frac{1}{2} b \tan \gamma$, which can become important, provided that b is sufficiently large.

The horizontal velocity u varies at one point with the period of the wave T and, therefore, the Coriolis force will cause corresponding variations in the

level of the surface in the transverse direction (transverse oscillations). If at one point $\xi = A \cos(\sigma t + \varepsilon)$, then

$$u = -\sigma A \sin(\sigma t + \varepsilon) = \sigma A \cos(\sigma t + \varepsilon + \frac{1}{2}\pi) = \sigma A \cos[\sigma(t + \frac{1}{4}T) + \varepsilon].$$

This means that the phase of the transverse oscillations has shifted against the phase of the longitudinal oscillations by one quarter period. It is here assumed that the surface adjusts itself immediately to the resultant between gravity and Coriolis force, i.e. that there be always equilibrium between all acting forces. It remains to be seen whether this applies for all cases.

Let us now examine more closely the effect of the earth's rotation on a wave progressing in a canal of constant, rectangular cross-section. The equations of motion are the same which we used in the theory of stationary ocean currents.

$$\left. \begin{aligned} \frac{\partial u}{\partial t} - fv &= -g \frac{\partial \eta}{\partial x} \\ \frac{\partial v}{\partial t} + fu &= -g \frac{\partial \eta}{\partial y} \\ \frac{\partial \eta}{\partial t} &= -\left(\frac{\partial hu}{\partial x} + \frac{\partial hv}{\partial y}\right) \end{aligned} \right\} (f = 2\omega \sin\varphi). \tag{VI.100}$$

Likewise, the equation of continuity. Only the Coriolis force has to be added to the equations (VI.16).

If we assume that the periodical disturbance η has the form $e^{i\sigma t}$, then u and v become also proportional to $e^{i\sigma t}$ and, eliminating this time factor, $e^{i\sigma t}$, (VI.100) becomes

$$\left. \begin{aligned} i\sigma u - fv &= -g \frac{\partial \eta}{\partial x} \\ i\sigma v + fu &= -g \frac{\partial \eta}{\partial y} \end{aligned} \right\} \text{and } i\sigma \eta = -\left(\frac{\partial hu}{\partial x} + \frac{\partial hv}{\partial y}\right). \tag{VI.101}$$

In the case of uniform depth where h is constant, the elimination of u and v leads to the oscillatory equation in a rotating system in the form:

$$\frac{\partial^2 \eta}{\partial x^2} + \frac{\partial^2 \eta}{\partial y^2} + \frac{\sigma^2 - f^2}{gh} \eta = 0 \quad \text{or} \quad (\nabla^2 + k^2)\eta = 0 \tag{VI.102}$$

when

$$k^2 = \frac{\sigma^2 - f^2}{gh}$$

and ∇^2 is the Laplacian operator. The velocities u and v must obey the same differential equations.

We can write the equation for wave motion in a rotating canal the (longitudinal axis of the canal is chosen to be the x -direction) of constant width a

which has as its boundary condition that all transverse motion v disappears at its walls, with motion in the x -direction only. One obtains for the Northern Hemisphere:

$$u = (g/c)\eta, \quad v = 0 \quad \text{and} \quad \eta = Ae^{-(f/c)y} \cos(\sigma t - \kappa x), \quad (\text{VI.103})$$

in which $c = \sqrt{gh}$.

The wave velocity is not influenced by the earth's rotation, but the wave height is not the same everywhere in a cross-section of the canal. The wave-height increases from the side of the canal preceding the rotation to the other side in an exponential function. If on one side it is η_0 , then on the other side it is

$$\eta_0 e^{-(f/c)a}.$$

Table 27 shows this influence for two cases. The velocity of the water in the x -direction of the canal — there are no transverse movements — has

Table 27. Amplitude across a canal for Kelvin waves

(In percent of the amplitude at that side of the canal succeeding rotation)

	Width of canal in km							
	10	25	50	75	100	250	500	1000
At $\varphi = 45^\circ$, $h = 90 \text{ m}$, $c = 30 \text{ m/sec}$	96.6	91.8	84.2	77.3	70.9	42.4	16.2	3.2
At $\varphi = 90^\circ$ (Pol), $h = 50 \text{ m}$, $c = 22.1 \text{ m/sec}$	93.6	84.9	72.0	61.1	51.9	19.4	3.8	0.15

always the same phase as the vertical displacement, to which the amplitude is proportional. The wave preferably limits itself, in case of wide canals, to one side of the canal, namely the one which follows the rotation. These KELVIN (1879) waves named after their discoverer, are characterized by great amplitudes on the right-hand side and by small amplitudes on the left-hand side, looking in the direction of travel of the wave. At high water, when the current flows in the direction of progress, the wave crest slopes down from right to left, and the component of gravity acting down that slope is exactly balanced by the deflecting force of the earth's rotation acting in the opposite direction. At low water, the directions of the slope and of the current are reversed.

The peculiarity that transverse oscillations do not occur with Kelvin waves is only valid in rectangular canals, in which the Coriolis force is balanced at any time by the transverse slope of the surface. If the cross-section of the canal is of a different shape, there will be periodical transverse motions which — as proven by PROUDMAN (1925, p. 465) — are not symmetrical to

the middle of the canal. For the equations (VI.100) one can select a solution in the form of the equation (VI.15). Then (VI.18) is replaced by

$$\left. \begin{aligned} \sigma U - fV &= \kappa g Z, \\ \sigma V + fU &= -g \frac{dZ}{dy}, \end{aligned} \right\} \quad \text{(VI.104)}$$

and

$$\frac{d}{dy} \left(h \frac{dZ}{dy} \right) + \left(\frac{\sigma^2 - f^2}{g} - \kappa^2 h + \frac{f\kappa}{\sigma} \frac{dh}{dy} \right) Z = 0,$$

whereas for the boundary conditions at the walls of the canal

$$h \left(\frac{dZ}{dy} + \frac{f\kappa}{\sigma} Z \right) = 0$$

replaces (VI.19) for $y = \pm a$, if the canal has the width of $-a$ to $+a$.

With the boundary condition for $y = -a$, we can derive from these equations

$$hV = \frac{\kappa^2}{\sigma} e^{-(f\kappa/\sigma)y} \int_{-a}^{+y} \left(\frac{\sigma^2}{\kappa^2} - gh \right) Z e^{-(f\kappa/\sigma)y} dy \quad \text{(VI.105)}$$

and the boundary condition for $y = +a$ takes the form

$$\int_{-a}^{+a} \left(\frac{\sigma^2}{\kappa^2} - gh \right) Z e^{-(f\kappa/\sigma)y} dy = 0. \quad \text{(VI.106)}$$

As Z is always positive, this equation is equivalent to the condition

$$\frac{\sigma^2}{\kappa^2} = gh_1, \quad \text{(VI.107)}$$

in which h_1 is a kind of an average value between the largest and the smallest value of h .

When the profile of the canal slopes up on both sides, there must at least be two values of y , for which h becomes $= h_1$; let these be y_1 and y_2 . Then we see that $hV e^{-(f\kappa/\sigma)y}$ increases from zero at $-a$ to a maximum at $y = y_1$, then decreases to a minimum at $y = y_2$, and finally becomes again zero on the other bank for $y = +a$. Therefore, V must change its sign between y_1 and y_2 , so that V is positive for $-a < y < y_1$ and negative for $y_1 < y < +a$, i.e. on both sides of the canal the transverse motions are in an opposite direction.

Although with the above-mentioned equations the problem is solved, we cannot gain an insight into the entire oscillatory process until we calculate special cases. If $\sigma = +f$, which would be applicable to a semi-diurnal wave at the Pole, or to a diurnal wave at 30° latitude, one obtains from (VI.104)

$$\frac{\sigma}{g} (U + V) = \kappa Z = -\frac{dZ}{dy},$$

so that, besides a constant factor,

$$\kappa Z = e^{-\kappa y} \tag{VI.108}$$

(VI.106) becomes

$$\int_{-a}^{+a} \left(\frac{\sigma^2}{\kappa^2} - gh \right) e^{-2\kappa y} dy = 0. \tag{VI.109}$$

There is only one real value of κ , which fulfils this equation.

Proudman deals especially with a canal with a parabolic cross-section (see equation (VI.20) which was explained on p. 148) for a non-rotating earth. From (VI.109) we obtain the conditional equation for κ in the form

$$\frac{\tanh 2\kappa a}{2\kappa a} = \frac{1}{1 + 2\sigma^2 a^2 / gh_0}. \tag{VI.110}$$

For $a = 100$ km, $h_0 = 100$ m and $\sigma = 1.4 \times 10^{-4}$ sec⁻¹ (semi-diurnal tide) $\sigma^2 a^2 / gh_0 = 0.2$, and one obtains, according to (VI.110), for the ratio of κ^2 and the value $\frac{3}{2} \sigma^2 / gh_0$, which applies in the case of a narrow canal or when the earth's rotation is neglected (see equations (VI.24) and (VI.25)), the following values:

$\sigma^2 a^2 / gh_0$:	0.1	0.2	0.3	0.4	0.5	0.6	0.7	0.8	0.9	1.0
$\frac{\kappa^2}{\frac{3}{2}(\sigma^2 / gh_0)} = \frac{\bar{c}^2}{c^2}$:	1.04	1.09	1.13	1.18	1.22	1.27	1.32	1.38	1.43	1.49

\bar{c} and c are the velocities of propagation respectively of a canal at rest and rotating. It is obvious that if the canal is rotating the velocity of progress decreases when the width of the canal increases.

Moreover, we can derive values for U and V in a simple manner from (VI.108) with the aid of (VI.106). If we select $\sigma^2 a^2 / gh_0 = 0.1, 0.5$ and 1.0 , we obtain the distribution of the velocities in the longitudinal and transverse direction of the canal as represented in Fig. 89. We see that the transverse current is distributed very unsymmetrically in respect to the centre of the canal. This transverse current vanishes the closer to the left side of the canal, in the direction of the wave propagation, the greater $\sigma^2 a^2 / gh_0$ is. In the narrow strip to the left, the transverse velocities also are smaller, the greater this value is. Only on the right side of the canal the transverse velocity is noteworthy in proportion to the strength of the current in the longitudinal direction of the canal.

Poincaré Waves. Besides the Kelvin waves, there can be in a canal other waves which are called Poincaré waves (1910, p. 126) after the name of their discoverer. If we assume again a solution of the equations of motion in the form (VI.15) and the depth of the rectangular canal to be constant, U , V and Z must fulfil the equation (VI.104), of which the last one takes the form

$$\frac{d^2 Z}{dy^2} + \left(\frac{\sigma^2 - f^2}{c^2} - \kappa^2 \right) Z = 0.$$

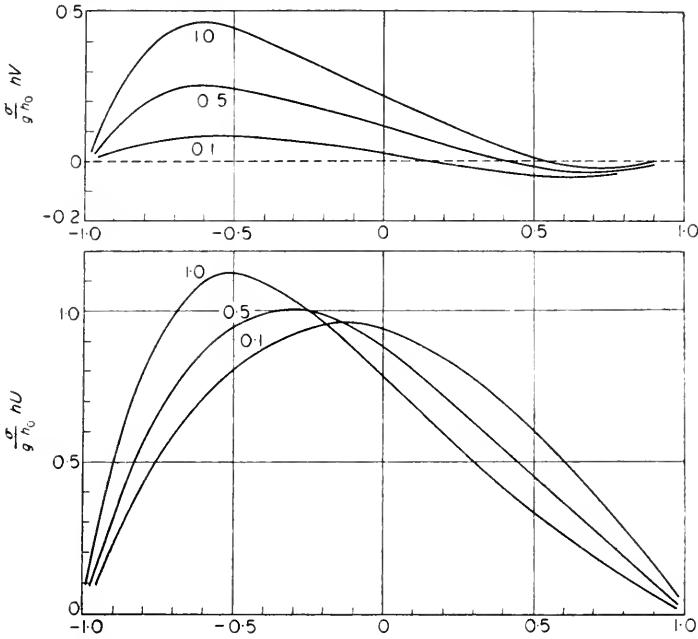


FIG. 89. Distribution of the transverse velocity (upper) and longitudinal velocity (below) in the opposite sens of progress of the wave. The numbers along the curves correspond to the values $(\sigma^2 a^2)/(g h_0)$. (The velocities have been multiplied by the factor $(\sigma h)/(g h_0)$ which becomes zero at the border.)

The boundary conditions at the walls of the canal $y = \pm a$ are again $v = 0$. If n is an odd integer ($n = 1, 3, 5, \dots$) and if we put

$$\frac{\sigma^2 - f^2}{c^2} - \kappa^2 = \left(\frac{n\pi}{2a}\right)^2 \tag{VI.111a}$$

we obtain a complete solution in the form

$$\left. \begin{aligned} u &= A \left(\frac{\sigma}{\kappa h} \cos \frac{n\pi}{2a} y + \frac{\pi g}{2af} \sin \frac{n\pi}{2a} y \right) \cos(\sigma t - \kappa x), \\ v &= -A \frac{f}{\kappa h} \left(1 + \frac{\pi c^2}{4a^2 f^2} \right) \cos \frac{n\pi}{2a} y \sin(\sigma t - \kappa x), \\ \eta &= A \left(\cos \frac{n\pi}{2a} y + \frac{\pi \sigma}{2af\kappa} \sin \frac{n\pi}{2a} y \right) \cos(\sigma t - \kappa x). \end{aligned} \right\} \tag{VI.111b}$$

The period of the n -nodal free transverse oscillation of the canal is $T_q = 4a/n\kappa$, the period of the inertia oscillation $T_i = 2\pi/f = \frac{12 \text{ sidereal hours}}{\sin \varphi}$ and the period of the longitudinal wave in the canal $T = 2\pi/\sigma$. Equation (VI.111a) then becomes

$$1 - \left(\frac{T}{T_i}\right)^2 - \left(\frac{T}{T_q}\right)^2 = \frac{c^2 \kappa^2}{\sigma^2}. \tag{VI.111c}$$

This means that these Poincaré waves are only possible when $T < T_i$ and also $T < T_q$, i.e. the period of the wave must be shorter than half a pendulum day and, at the same time, shorter than the natural period of the transverse oscillations of the canal. This condition greatly reduces the possibility of the occurrence of such waves. Thus, in narrow canals only Kelvin waves with tidal periods are possible. However, it is possible that Poincaré waves will play an important part in the development of the tides in ocean sections comparable to wide canals. If the depth of the canal is not constant in its cross-sections, the problem becomes much more difficult mathematically. PROUDMAN (1946, p. 211) gave a thorough discussion of this question. He assumed a frictionless motion of the water-masses for the middle section of the canal, but assumed a dissipation of energy on the two sides where the depth is smaller. This corresponds more to real conditions and permits a more accurate application.

Another kind of oscillations is still possible in a canal. A solution of the equation (VI.102), which is also valid for v , is

$$v = \exp\left[-s_n x + i \frac{n\pi}{2a} y\right], \quad \text{if } s_n^2 = \left(\frac{n\pi}{2a}\right)^2 - k^2 \quad \text{(VI.112)}$$

in which $n\pi/2a > k$. As v should vanish for $\pm a$, v can only take the forms:

$$\left. \begin{aligned} v &= A_n e^{-s_n x} \sin \frac{n\pi}{2a} y \cdot e^{i\omega t} && \text{for even integers } n (= 2, 4, \dots), \\ v &= A_n e^{-s_n x} \cos \frac{n\pi}{2a} y \cdot e^{i\omega t} && \text{for odd integers } n (= 1, 3, \dots). \end{aligned} \right\} \quad \text{(VI.113)}$$

With the aid of these relations and equation (VI.101), we can compute easily the corresponding values of η and u . These oscillations have the form of standing transverse waves in the canal, with amplitudes decreasing with a power of e along the canal from a point $x = 0$. They are practically limited to a small section of the canal. This kind of oscillations was introduced by TAYLOR (1920), in order to fulfil the condition of total reflection of a Kelvin wave in a canal closed at one end. If we wish to compute the oscillations of a rectangular canal closed at both ends (total reflection at both ends of the canal), Poincaré waves should be added to the Kelvin waves, so as to fulfil the boundary conditions (p. 216).

(c) Reflection of a Kelvin Wave. Free Oscillations in a Rotating, Rectangular Basin of Uniform Depth

The superposition of two Kelvin waves progressing in a rectangular canal in an opposite direction does not result at all times at any cross-section of the canal in a horizontal water-motion zero, where a transverse barrier could be erected which would close the canal without changing the water-motion.

Let us add to the wave (VI.103) travelling in the $+x$ -direction a wave progressing in the negative direction in the form

$$\eta = Ae^{+(f/c)y} \cos(\sigma t + \kappa x). \tag{VI.114}$$

We then obtain if $A = \frac{1}{2}$, $\kappa = 1$ and $\alpha = f/c = 0.7$, the distribution of amplitudes and phases of the superposed waves as shown in Fig. 90. The

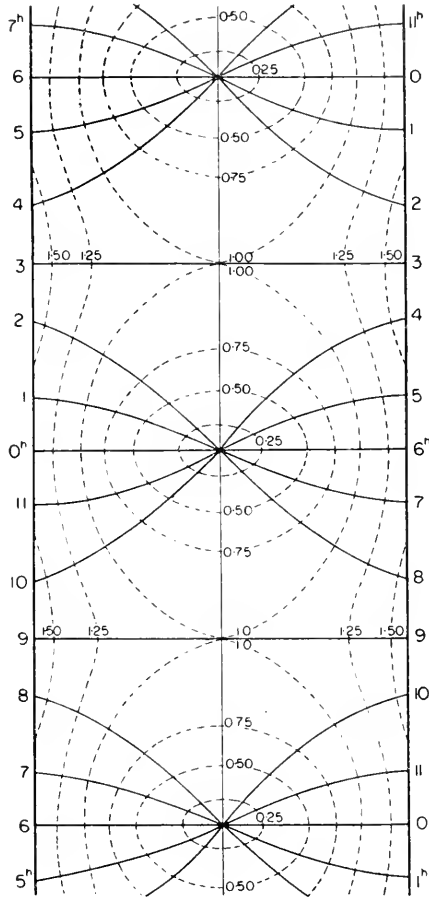


FIG. 90. Superposition of two Kelvin waves travelling in opposite directions in a canal with a uniform rectangular section. Period: 12 h. Amplitude of each wave: $A = \frac{1}{2}$, $\alpha = 0.7$ (corresponding to a canal width of 400 km, depth of 40 m and $\varphi = 44.5^\circ$).

assumed values correspond approximately to a canal width of 400 km and a depth of 40 m at $44\frac{1}{2}^\circ$ latitude. The period of the wave is assumed to be 12 h. The wave picture has completely lost the nature of a standing wave, as it would be in a system at rest. Instead, the wave is split up in cells which

succeed each other. In each cell the wave is rotating and in the centre of each cell the amplitude is reduced to zero. Such star-shaped distributions of the lines of equal phase are called amphidromies. The succession of these amphidromies in a canal gives the impression that on the left-hand side of the canal a wave is progressing with varying amplitude in the $+x$ -direction and on the right-hand side a similar wave in the $-x$ -direction. The amplitudes are always greatest along the wall of the canal. According to (VI.103), the horizontal velocity u in the direction of the canal is proportional to η , and the phases of the horizontal water motion are given by the same lines of equal phase as for η . Perpendicularly to the canal the velocity is everywhere zero. When the water moves in one direction in the left section of the canal, it moves in the opposite direction in the right section.

The distribution of the amplitudes shows that nowhere on a line transverse to the canal, the amplitude is constantly zero, and this cannot be achieved by selecting another difference of phase for the two waves travelling in opposite directions. In order to reduce to zero the motion caused by the superposition of two Kelvin waves, it is necessary to add a definite disturbance in the canal towards its closed end. This disturbance will depend essentially upon the period of the wave and the dimensions of the canal, especially upon its width.

The problem of the reflection of a Kelvin wave on a transverse wall was solved by TAYLOR (1920). First of all, he takes the superposition of two Kelvin waves progressing in opposite direction as a particular solution, as illustrated in Fig. 90. The transverse motion v is equal to zero everywhere, and at a specific cross-section $x = x_1$ there is in the canal a current in the longitudinal direction of the canal $u = u_1$. Taylor has succeeded in finding a second particular solution for the transverse motion v in the canal which, according to the boundary conditions, vanishes at the longitudinal walls of the canal, but which at the same time agrees to a current in the direction of the canal giving for the cross-section $x = x_1$ exactly the same value u_1 as the first solution.

The difference between the two solutions is then the complete solution, because it fulfils the boundary conditions, according to which the transverse velocity is zero everywhere at the longitudinal walls of the canal and at the closed end of the canal ($x = x_1$) the longitudinal velocity always vanishes. The mathematical difficulties of the problem lie in establishing certain values fixing the cross-section at which the longitudinal currents of both solutions must become equal. Taylor's solution says that in a given canal rotating with a certain angular velocity, a total reflection of a penetrating Kelvin wave at its closed end occurs only then, when its frequency is smaller than a value depending on the dimensions of the canal. At some distance from the closed end, the reflection is practically identical with the superposition of two Kelvin waves moving in opposite directions (Fig. 90); in the inner section of the

canal, however, a disturbance has to be added, through which the boundary condition is fulfilled. Taylor's condition for the total reflection is

$$\sigma_2 - f^2 < gh \frac{\pi^2}{b^2} \tag{VI.115}$$

in which b represents the width of the canal.

As $\sigma = \frac{2\pi}{T}$, $f = \frac{2\pi \sin \phi}{12 \text{ hours}}$ and as $\frac{2b}{\sqrt{gh}} = T_q$ the natural period of the canal in the transverse direction, this relation can also be given the form

$$\left(\frac{T_q}{T}\right)^2 < 1 + \left(\frac{T_q \sin \phi}{12 \text{ hours}}\right)^2 \tag{VI.116}$$

in which the periods are to be taken in hours.

If we take for the wave the semi-diurnal tidal period (12 hours) we obtain from (VI.116)

$$\frac{T_q}{T} < \frac{1}{\cos \phi}, \tag{VI.117}$$

for 45° of latitude = 1.42, i.e. if total reflection is to occur at the closed end of the canal (bay), the natural period of the transverse oscillations in tide waves must not, for average conditions, exceed $1\frac{1}{2}$ times the tidal period.

Although Taylor's results apply strictly only for canals with a rectangular cross-section, they nevertheless can be used to fairly correctly evaluating the possibility of a reflection of Kelvin waves in the case of a more complicated configuration of the basin.

The solution by Taylor is mathematically very elegant, but difficult. A simpler one, in connection with Taylor's solution, has been given by DEFANT (1925, p. 25). Let the origin of the co-ordinate system be situated in the center of the canal, its width be π and extend along the y -axis from $-\frac{1}{2}\pi$ to $+\frac{1}{2}\pi$. The superposition of two Kelvin waves progressing in opposite directions gives for the horizontal velocities in the x - and y -direction at the point $x = x_1$ of the canal,

$$\left. \begin{aligned} u_0 &= S \left(\cosh ay \sin \frac{\sigma x_1}{c} \cos \sigma t + \sinh ay \cos \frac{\sigma x_1}{c} \sin \sigma t \right) \\ v_0 &= 0, \end{aligned} \right\} \tag{VI.118}$$

where $a = f/c$ and $c = \sqrt{gh}$. A second solution of the equations of motion (VI.102) is being sought, which will give also always $v = 0$ for $y = \pm \frac{1}{2}\pi$, but for $x = x_1$ the value u_0 of the solution (VI.118). The difference between the two solutions then always is that at the longitudinal walls the transverse current is zero, but at the cross-section $x = x_1$ the longitudinal current is zero, so that a barrier-like partition can be erected here, without disturbing the wave motion in the canal. Taylor derives the second solution from the differential equation in v , (VI.102), by putting

$$v = v_1 \cos \sigma t + v_2 \sin \sigma t, \tag{VI.119}$$

v_1 and v_2 must then fulfil this equation. A solution satisfying the boundary condition for $y = \pm \frac{1}{2}\pi$, $v = 0$ and extending practically over a small area in the x -direction, has the form:

$$v_1 = \sum_{\text{even } n} C_n e^{-S_n x} \sin ny \quad \text{and} \quad v_2 = \sum_{\text{odd } n} C'_n e^{-S_n x} \cos ny. \tag{VI.120}$$

For v_1 the sum only refers to the even integer numbers n , for v_2 only to the odd numbers. Furthermore, $s_n^2 = n^2 - k^2$ (see p. 210). In order that the e -power remains real and the disturbance makes itself felt only on a finite portion of the canal, $n^2 > k^2$ and, as the smallest number of n is 1, $k^2 < 1$. This leads to the conditional equations (VI.115) and (VI.116). To the transverse currents belong longitudinal currents in the form

$$u_1 = \sum_{n=1}^{\infty} A_n e^{-s_n x} \cos ny \quad \text{and} \quad u_2 = \sum_{n=1}^{\infty} A'_n e^{-s_n x} \sin ny. \tag{VI.121}$$

The constants A_n and A'_n can be expressed by the constants C_n and C'_n by means of the differential equations (VI.122), which follow from the equations (VI.101) by the elimination of η :

$$\frac{\partial u_1}{\partial y} - \frac{\partial v_1}{\partial x} + \frac{f}{\sigma} \left(\frac{\partial u_2}{\partial x} + \frac{\partial v_2}{\partial y} \right) = 0, \quad \text{and} \quad \frac{\partial u_2}{\partial y} - \frac{\partial v_2}{\partial x} - \frac{f}{\sigma} \left(\frac{\partial u_1}{\partial x} + \frac{\partial v_1}{\partial y} \right) = 0. \tag{VI.122}$$

If we introduce the equations (VI.120) and (VI.121) into these equations and if we consider that the coefficients of $\sin ny$ and $\cos ny$ must vanish, we obtain for the ratios $A_n : A'_n$ the following values

$$\left. \begin{aligned} &\text{for } n \text{ even } \left. \begin{aligned} \frac{A_n}{A'_n} &= \frac{n}{\psi_n}, \\ \frac{A_n}{A'_n} &= \frac{\psi_n}{n}, \end{aligned} \right\} \\ &\text{and for } n \text{ odd } \left. \begin{aligned} \frac{A_n}{A'_n} &= \frac{\psi_n}{n}, \\ \frac{A_n}{A'_n} &= \frac{n}{\psi_n}, \end{aligned} \right\} \\ &\text{in which } \psi_n = \frac{f\sigma}{s_n c^2}. \end{aligned} \right\} \tag{VI.123}$$

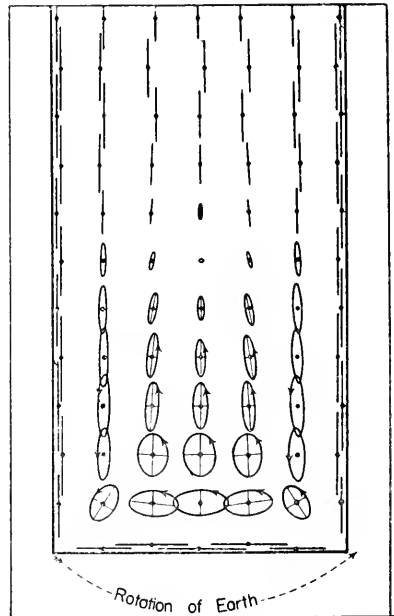
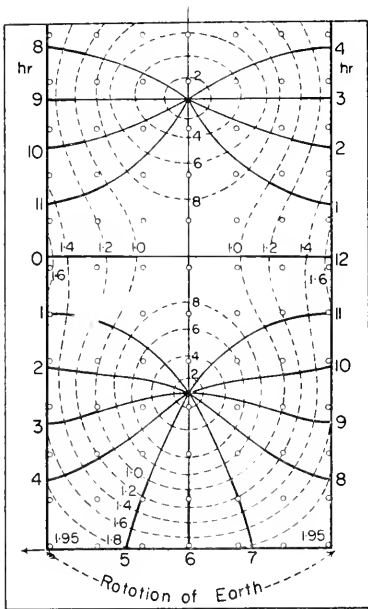


FIG. 91. Total reflection of a Kelvin wave at the closed end of a rectangular bay on a rotating earth. Co-tidal lines and amplitudes (Taylor).

FIG. 92. Current diagrams corresponding to Fig. 91.

In order that, for a definite, but still unknown value $x = x_1$ the difference between the longitudinal currents of both solutions be always zero, we must have for all values $-\frac{1}{2}\pi \leq y \leq +\frac{1}{2}\pi$,

$$\left. \begin{aligned} \sin \frac{\sigma x_1}{c} \cosh \alpha y &= \sum_{n=1}^{\infty} A_n \cos ny, \\ \cos \frac{\sigma x_1}{c} \sinh \alpha y &= \sum_{n=1}^{\infty} A'_n \sin ny. \end{aligned} \right\} \quad \text{(VI.124a)}$$

With equations (VI.123) and (VI.124a) we can determine the constants A_n, A'_n and x_1 . Since the rapidly converging series contain an infinite number of coefficients, we may accomplish every desired accuracy during the fulfilment of these conditions. For instance if we choose the five points $y = 0, = \pm \pi/4$ and $= \pm \pi/2$, at which (VI.124a) should be satisfied, we obtain from (VI.124a) by use of (VI.123) a number of equations sufficient to determine the unknowns A_1, A_2, A_3, A_4 as well as A'_1, A'_2, A'_3 and x_1 :

$$\left. \begin{aligned} A_1 + A_2 + A_3 + A_4 &= \sin \frac{\sigma x_1}{c}, & (1) \\ -A_2 + A_4 &= \sin \frac{\sigma x_1}{c} \cosh \alpha \frac{\pi}{2}, & (2) \\ A_1 - A_3 - 1.415 A_4 &= 1.415 \sin \frac{\sigma x_1}{c} \cosh \alpha \frac{\pi}{4}, & (3) \\ A'_1 - A'_3 &= \cos \frac{\sigma x_1}{c} \sinh \alpha \frac{\pi}{2}, & (4) \\ A'_1 + 1.415 A'_2 + A'_3 &= 1.415 \cos \frac{\sigma x_1}{c} \sinh \alpha \frac{\pi}{4}, & (5) \\ A_1 - \psi_1 A'_1 &= 0, & (6) \\ A_2 - \frac{2}{\psi_2} A'_2 &= 0, & (7) \\ A_3 - \frac{3}{\psi_3} A'_3 &= 0. & (8) \end{aligned} \right\} \quad \text{(VI.124b)}$$

If we combine these equations in the following way, (1-2)+(2+3), then (4+5)+(6, 7) and (4+(6 and 8)+(1-2), they will only have as unknowns A_1-A_2 and x_1 . The elimination of A_1 and A_2 gives an equation for $\tan(\sigma x_1/c)$. This procedure will fix all constants and the place in the canal where the incoming wave is reflected. If $k = 0.5$ and $\alpha = 0.7$ which, with a period of 12 h (semi-diurnal tidal period), corresponds to a bay with a rectangular cross-section having a width of 465 km and a uniform depth of 74 m at approximately 53° of latitude, we get, according to the above method, $\tan(\sigma x_1/c) = 0.383$ against 0.385, as found by Taylor (1920) by another, more accurate way.

If one wishes to know more about oscillations in such a canal, closed at one end, he must compute numerically some special cases. Taylor has done this for a bay having the same dimensions as mentioned in the previous paragraph and which corresponds to the North Sea and computed the distribution of the amplitudes and the phases, as well as the currents inside the

canal which are shown in Figs. 91 and 92. Comparing with Fig. 90, we can see the changes caused by the closing of the canal. The inside amphidromy in front of this barrier is developed regularly on all sides and it looks as if the wave penetrates into the canal at the left side and leaves the amphidromy at the right side of the canal, turning around its centre. The outside amphidromy is identical with the one shown in Fig. 90. The amplitudes are always largest at the bay shores and attain a maximum in the two corners of the bay.

In the outward sections of the canal, the currents (Fig. 92) run always parallel to the sides of the canal, and their distribution here is identical with the currents produced by the superposition of two Kelvin waves. In the inside section of the canal, the currents are parallel to the wall — as is required — but in the middle they are not any longer alternating currents, but have become currents which rotate in the direction of the wave. The current figures are ellipses, and their eccentricity decreases towards the middle. Just in front of the closed end of the canal the major axis of the ellipse is parallel to the transverse barrier, whereas it is parallel to the longitudinal walls towards the opening. At the same time, the transverse velocity decreases and vanishes completely in the outer section of the canal. The current distribution for four phases ($t = 0, 1\frac{1}{2}, 3$ and $4\frac{1}{2} h$) can be found in DEFANT (1923*a*, p. 57).

The free oscillations of a rotating basin could be easily computed, in case the basin has a circular or an elliptical shape (see GOLDSTEIN, 1929, p. 213). RAYLEIGH (1903, 1909) has given a solution for a rectangular basin of uniform depth, for the case where the rotating velocity is relatively small which does not apply to the rotating earth. Taylor arrived at a general solution following the same method which he used for the reflection of a Kelvin wave in a canal closed at one side. An appropriate second solution of the equations of motion is added to the superposition of two Kelvin waves, in such a manner that the longitudinal current is always zero at the transverse barriers closing the canal at both ends. This will give the condition for the natural period of the rotating rectangular basin.

We now assume that the superposition of two Kelvin waves moving in opposite directions has the form:

$$\left. \begin{aligned} u_0 &= S \left(\cosh \alpha y \cos \frac{\sigma x}{c} \cos \sigma t - \sinh \alpha y \sin \frac{\sigma x}{c} \sin \sigma t \right), \\ v_0 &= 0. \end{aligned} \right\} \quad (\text{VI. 125})$$

The origin of the co-ordinate system is laid in the middle of the basin; let its width be π , extending from $-\frac{1}{2}\pi \leq y \leq +\frac{1}{2}\pi$, its length $2l$ and $-l \leq x \leq +l$. The second solution is supposed to have the form (VI. 119). As it is now required that in two points x the longitudinal current equals (VI. 125), and when $n^2 > k^2$, we have to put v_1 and v_2 :

$$v_1 = \sum_{\text{even } n} C_n \sinh S_n x \sin n y \quad \text{and} \quad v_2 = \sum_{\text{odd } n} C'_n \cosh S_n x \cos n y. \quad (\text{VI. 126})$$

To this transversal current belong longitudinal currents of the form

$$u_1 = \sum_{n=1}^{\infty} A_n \cosh S_n x \cos ny \quad \text{and} \quad u_2 = \sum_{n=1}^{\infty} A'_n \sinh S_n x \sin ny. \tag{VI.127}$$

We obtain for the ratios $A_n : A'_n$ exactly the same expressions as in (VI.123). The condition that for $x = \pm l$ the difference between the two longitudinal currents (VI.125) and (VI.127) always vanishes, requires for all y :

$$\left. \begin{aligned} \cos \frac{\sigma l}{c} \cosh ay &= \sum_{n=1}^{\infty} A_n \cosh S_n l \cos ny, \\ \sin \frac{\sigma l}{c} \sinh ay &= \sum_{n=1}^{\infty} A'_n \sinh S_n l \sin ny. \end{aligned} \right\} \tag{IV.128}$$

If we restrict ourselves to a certain number of y -points, we obtain a sufficient number of equations (with VI.123) to compute σ/c , which will give the natural period of the basin.

The assumption that the differences between the longitudinal currents vanish for $y = 0$ and $y = \pm \frac{1}{2}\pi$, gives already a good first approximation. We obtain the simple relation

$$\frac{\sigma l}{c} \tan \frac{\sigma l}{c} = \frac{ls_1}{u} \tan s_1 l \frac{1 + \cosh \frac{1}{2} \alpha \pi}{\sinh \frac{1}{2} \alpha \pi}. \tag{VI.129}$$

Taylor has found in another way that for a basin which is twice as long as it is wide ($l = \pi$) and whose rotation period is equal to the longest free oscillation of the non-rotating system (which means $f/c = \alpha = 1$), σ/c must be $= 0.429$. From (VI.129) we obtain by repeated tries (as σ/c is also hidden in s_1) $\sigma/c = 0.433$, which comes very close to Taylor's value.

We find that for long, narrow basins (l a multiple of π) the term on the right-hand side in (VI.128) increases rapidly and, therefore, σ/c nears $\frac{1}{2}\pi$. This means that for this kind of basin the period of oscillation differs slightly from the period of a similar basin at rest (see later the case of the Baltic, p. 219).

In the example given above $\sigma/c = 0.5$ for the basin without rotation, and we find that the period in case of rotation is being increased at the ratio: $0.50 : 0.429 = 1.14$, i.e. by 14%.

The wider the canal in proportion to its length, the greater the increase of the period. The standing wave of the free oscillation is changed into an amphidromy (rotatory wave) with its centre in the middle of the basin.

A special investigation of free tidal oscillations in a rotating square sea was made by CORKAN and DOODSON (1952).

(d) *Influence of the Earth's Rotation on the Seiches in Closed Basins*

The reason for not considering the influence of the earth's rotation on the seiches of the lakes is that, in view of the small expansion of the oscillating water-masses this influence is hardly noticeable. In dealing with the free oscillations of large lakes and oceans, this can no longer be neglected. The disturbance caused by the earth's rotation can be summarized by computing the transverse oscillations caused by the variations in velocity of the

longitudinal current. The amplitude of these transverse oscillations, according to the explanations given on p. 204, is given by

$$A' = \frac{b}{2} \tan \gamma = \frac{b f}{2 g} U,$$

if U is the amplitude of the periodic variations of the current in the longitudinal direction of the lake; its phase is shifted by one quarter period against that of the longitudinal oscillation.

Thus, at any point of the lake the vertical displacement of the transverse oscillation $\eta' = A' \sin \sigma t$ is added to the vertical displacement of the longitudinal oscillation $\eta = A \cos \sigma t$, so that the superposition takes the form

$$Z = A \cos \sigma t + A' \sin \sigma t = M \cos \sigma(t - \tau)$$

in which $M = \sqrt{A^2 + A'^2}$ and $\tan \sigma \tau = A'/A$. From the latter relation we can compute the time of the maximum and minimum height.

There are not many cases in which the influence of the earth's rotation has thus been determined. Neumann has calculated, according to the above method, from the computed current velocities of the longitudinal oscillations (period 27.5 h), the amplitudes of the transverse oscillations A' for several localities of the Baltic and found the following values for the Gulf of Finland:

	Helsinki	Hangö	Tallinn
Amplitude of the longitudinal oscillations (cm)	35	21	30
Amplitude of the transverse oscillations (cm)	9	9	8
Time of high water (hours)	1.1 h	1.8 h	26.4 h

The time ($t = 0$) is counted here from the moment of high water in Koivisto (innermost part of the Gulf of Finland). Consequently, there is a delay in Helsinki and in Hangö, on the northern side of the gulf, of 1.1 and 1.8 h respectively, whereas on the southern side, in Tallinn, high water occurs 1.1 h earlier than in Koivisto. Between Helsinki and Tallinn the difference in time of the high water is 2.2 h, and the extremes occur earlier in Tallinn than in Helsinki.

All cases closely investigated by Neumann on the basis of gauge registrations show the phase displacement required by the theory, which averages 2–3 h. Figure 93 shows two of these cases, illustrating clearly the earlier occurrence of the maximums in Tallinn against Helsinki. The longitudinal

oscillation thus assumes the nature of a rotatory wave; however, the deviations from a simple standing wave are small.

The increase of the period caused by the earth's rotation will be unimportant. An evaluation can be made from the relation (VI.129). We simplify the Baltic as a rectangular basin of the length $2l = 1500$ km, a width,

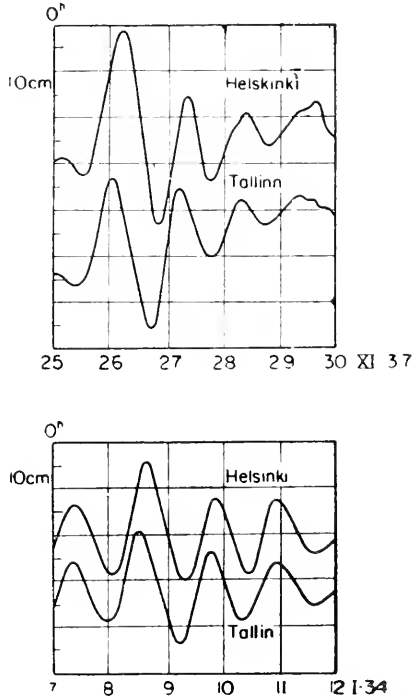


FIG. 93. Uni-nodal oscillation of the system Baltic—Gulf of Finland at Helsinki and Tallinn (Neumann).

$B = 150$ km and a depth $h = 77$ m. The period of the uni-nodal longitudinal oscillation is then 29.7 against 27.5 h of the real Baltic. As $f = 1.24 \times 10^{-4}$ and $c = (\pi/B) \sqrt{gh}$ and in first approximation $a = f/c = 0.2$ and $l = 5\pi$ the relation (VI.129) gives $\sigma/c = 1.56$ so that $\sigma/c = 0.0993$ and $T/(T \text{ at rest}) = 1.007$.

The increase of the period caused by the earth's rotation, therefore, is only about 0.7%, which is very little. Nevertheless, this influence makes itself felt very definitely in the time of high water on both sides of the Baltic.

6. Generation and Growth of the Oscillations of the Sea and Lake Surface

(a) Causes of the Seiches

Forel showed that sudden changes in the atmospheric pressure cause frequently seiches of great amplitude, whereas the influence of the wind

apparently is of secondary importance. CHRYSTAL (1908, p. 464) arrived at the same conclusion in his thorough investigations of the seiches of Loch Earn. The following disturbing forces can generally be regarded as the causes of oscillatory motions in lakes and bays:

(1) The sudden return to its equilibrium of a surface previously disturbed by the passage of an atmospheric disturbance over a section of the lake.

(2) The sudden oscillation back to a state of equilibrium of a watermass previously piled up by wind.

(3) Sudden or rapid receding of an accumulation of water produced by an extremely rapid influx across a section of the lake (violent rainfalls).

(4) Shocks of rain drops falling on the water surface.

(5) Sudden changes in air pressure, as expressed in microbarograms (registrations of variographs).

(6) Shock pressures of wind gusts on the lake surface.

(7) Subsiding of the electrical attraction on the surface by thunder clouds.

One should always remember that, in general, these disturbing forces have little intensity. On the other hand, it should also be borne in mind that, as shown by EMDEN (1905), small quantities of energy are capable of developing seiches. Chrystal emphasizes that for Loch Earn which, as the Lake of Geneva, must be counted among the deep lakes, the disturbing forces 1, 5 and 6 cause seiches. He also corroborates Russel's opinion already expressed in 1890, that slight pressure disturbances across the lake surface develop standing waves, especially when there is a certain synchronism with the natural modes of oscillations of the lake. For the influence of seismic waves, see ODDONE (1910, p. 115). BERGSTEN (1926) has been able to prove that the seiches in the Lake Vättern are attributable mainly to piling up effect by wind. This contrast to the theory of Forel and Chrystal is explained by the fact that the Lake Vättern with its large water surface is a shallow lake, and the effect of piling up by wind is, therefore, much more apparent than in deep lakes, where the current in deeper layers can compensate more rapidly this effect. Figure 94 (above) illustrates the start of a seiche by the influence of the wind. On 17 January 1920, at 2 p.m., there blew a south-westerly wind of a force of 8 Beaufort, which at 9 p.m. turned to W 9. The limnogram shows how with the change of the wind at 9 p.m. the water level receded rapidly and the potential energy of the wind drift caused a uninodal seiche of 5–6 cm. In many cases it can be proved that sudden changes in pressure can also cause seiches. Figure 94 (below) illustrates the case on 31 May 1925 in Bastedalen. The microbarographic disturbance at about 10 a.m. shows approximately the same period as the uni-nodal seiche of the lake and thus contributes to the further development of the oscillation already present.

The action of the separate forces causing seiches was investigated by Okada, Fujiwhara and Maeda (1913, p. 210) in a special case, in which a thunderstorm on Lake Biwa in Central Japan caused a seiche of 17 cm amplitude.

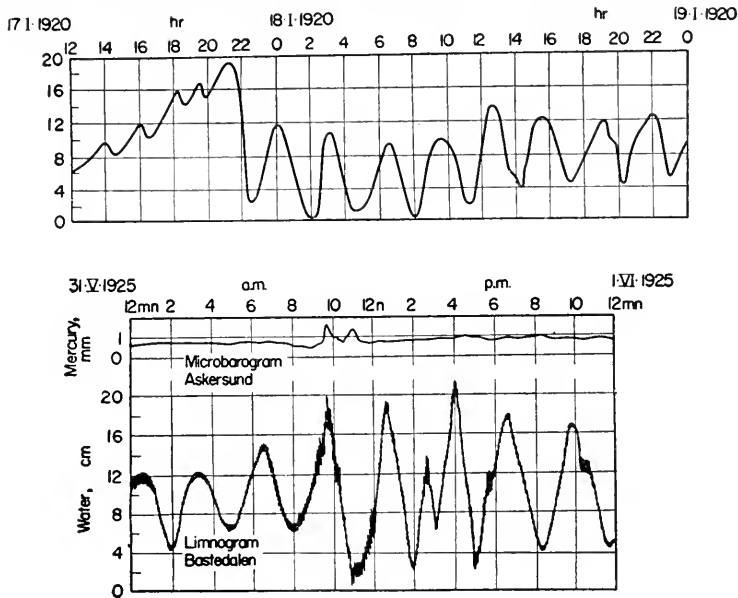


FIG. 94. Seiches in Lake Vättern (Sweden). Records at Bastedalen: above: caused by wind, below: caused by a sudden variation in pressure.

They were able to determine, on the strength of accurate meteorological registrations, that in this instance it was essentially the points 1, 2 and 3 which were responsible for the seiche.

(b) Action of Wind and Atmospheric Pressure on a Lake Surface

Any force acting on the water surface of a lake or a bay will cause the water surface to deviate from its normal position of equilibrium. As long as this force lasts, the water surface will remain in this new position. However, when this force subsides or ceases completely, the water surface tends to resume its former state of equilibrium. The frictional forces being small, this does not happen aperiodically, but in oscillations whose period corresponds to the period of free oscillation of the system. A periodic disturbing force provokes forced oscillations with a period corresponding to the period of the disturbing force. The amplitude will increase if the period of the force approximates the period of one of the natural modes of free oscillation. But these forced oscillations will not last long in a lake which is exactly tuned to certain periods. The forced progressive waves developed in the lake are rapidly dampened by reflection on the shores, and those which correspond to the dimensions of the lake will be least affected.

It is rather simple to examine theoretically and thoroughly the action of changes in atmospheric pressure and wind on the oscillatory processes of water surface in more or less closed basins. One can compute accurately the oscillations already developed if, besides the dimensions of the oscillating mass, we have the atmospheric pressure and wind as functions of locality

and time, as well as the initial state of the surface. The process consists in oscillations around a state of equilibrium, and it is only in taking into consideration these periodical changes in water level that many phenomena related to these disturbances of the normal position of the surface can be correctly understood.

Of the theoretical investigations dealing with the oscillations produced by variations in atmospheric pressure and wind in finite watermasses, the following should be particularly mentioned.

CHRISTAL (1909, p. 455) has given considerable attention to the influence of different atmospheric pressure disturbances in developing seiches in a lake with a parabolical normal curve, neglecting friction and the rotation of the earth. PROUDMAN and DOODSON (1924, p. 140) have, on the contrary, examined the oscillations produced by atmospheric pressure and wind in a basin of constant rectangular cross-section, taking friction into account but neglecting the rotation of the earth. Later on, PROUDMAN (1929) dealt with special cases, neglecting the friction, in which the influence of the earth's rotation is particularly apparent. We are indebted to STENIJ (1932) for an extensive review, in which the problems are treated on a strictly mathematical basis. We will only mention the essential features of these papers, especially stressing the fundamental viewpoints and limiting ourselves to basins of constant rectangular cross-section.

The problem in its most general form is: the general equations of motion and continuity have, with depth of the water h constant, and using the usual symbols, the form

$$\left. \begin{aligned} \frac{\partial u}{\partial t} - fv &= -g \frac{\partial}{\partial x} (\eta - \bar{\eta}) + \nu \frac{\partial^2 u}{\partial z^2}, \\ \frac{\partial v}{\partial t} + fu &= -g \frac{\partial}{\partial y} (\eta - \bar{\eta}) + \nu \frac{\partial^2 v}{\partial z^2}, \\ h \left(\frac{\partial u}{\partial x} + \frac{\partial v}{\partial y} \right) + \frac{\partial \eta}{\partial t} &= 0, \end{aligned} \right\} \quad (\text{VI.130})$$

in which $f = 2\omega \sin \varphi$, ν is the kinematic viscosity coefficient assumed to be constant and $-g\eta$ the variable part of the atmospheric pressure. If l = the length of the basin and the origin of the co-ordinate system is taken in the undisturbed water surface, we have to add as boundary conditions $u = 0$ for $x = 0$ and $x = l$ and for $z = -h$; further an assumption for $\partial u / \partial z$, for $z = 0$ to determine the influence of wind on the surface. Solutions are sought for a given disturbance in the atmospheric pressure and for a given wind.

If the distribution of the atmospheric pressure is stationary the system of equations is satisfied by the "equilibrium solution"

$$\eta = \bar{\eta} + \text{constant}, \quad u = v = 0. \quad (\text{VI.131})$$

Especially interesting are the conditions in an infinitely long, uniform canal. If we neglect in (VI.130) the friction, we find first a solution in the form of Kelvin waves (VI.103); if $\bar{\eta} = 0$, then

$$\bar{\eta} = 0, \quad v = 0, \quad \frac{\eta}{c} = \pm \frac{u}{g} = e^{\mp(f/c)y} F(x \pm ct), \quad (\text{VI.132})$$

in which $c = \sqrt{gh}$ and F is an arbitrary function of the argument $(x \mp ct)$. Proudman, however, has also given a solution for the case that an atmospheric pressure wave with a velocity V travels in the positive direction of the canal. In this case, the solution is

$$\left. \begin{aligned} \frac{\bar{\eta}}{c^2} &= e^{-(fV)y} F(x - Vt) \\ v = 0 \quad \text{and} \quad \frac{\eta}{c^2} &= \frac{u}{Vg} = \frac{1}{1 - \frac{V^2}{c^2}} e^{-(fV)y} F(x - Vt) . \end{aligned} \right\} \quad (\text{VI.133})$$

This is a wave disturbance which travels also in the $+x$ -direction; the factor $1/[1 - (V^2/c^2)]$ shows, however, that large amplitudes are to be expected, when the atmospheric pressure disturbance travels with the same velocity as the free water waves in the canal. The form adopted in (VI.133) for the pressure disturbance in the y -direction is somewhat special; it is difficult to transfer it to arbitrary pressure distributions. But if the canal is not too wide, the e -power in (VI.133) can be disregarded, which means neglecting the earth's rotation. The application is then limited to narrow canals.

Let us now assume that the canal be closed at $x = 0$ and extends infinitely in the x -direction. The wave disturbance generated by a travelling pressure disturbance now must also fulfil the boundary condition $u = 0$ for $x = 0$. This can be done by combining equations (VI.132) and (VI.133) ($f = \omega = 0$) and we obtain:

$$\left. \begin{aligned} \bar{\eta} &= F\left(t - \frac{x}{V}\right) \\ \eta &= \frac{1}{1 - (V^2/c^2)} \left[F\left(t - \frac{x}{V}\right) - \frac{V}{c} F\left(t - \frac{x}{c}\right) \right], \\ v = 0 \quad \text{and} \quad \frac{c}{g} u &= \frac{V/c}{1 - (V^2/c^2)} \left[F\left(t - \frac{x}{V}\right) - F\left(t - \frac{x}{c}\right) \right]. \end{aligned} \right\} \quad (\text{VI.134})$$

A free wave is added to the forced wave. For $x = 0$

$$\eta = \frac{1}{1 + V/c} F(t)$$

and

$$\frac{\eta}{\bar{\eta}} = \frac{1}{1 + V/c} = \text{constant} \quad (\text{VI.135})$$

If V is positive, i.e. when the atmospheric pressure disturbance moves along the canal away from the closed end, the term at the right is always smaller than 1; the amplitude of the forced wave is smaller than the static pressure disturbance. However, if V is negative, i.e. if the pressure disturbance travels towards the closed end of the canal, the ratio can become great and even very great, when the velocity of propagation of the pressure wave nears the velocity of the free waves in the canal. The values of c for depths less than 100 m lie below 30 m/sec, and the velocity of propagation of atmospheric pressure disturbances is also of the order of magnitude of 30 m/sec. Therefore, one can expect a strong impulse to wave disturbances in lakes and bays, when these pressure disturbances travel towards the interior of the bay, and the depth is not too great.

In many cases, the tide gauges have registered this remarkable resonance which is responsible for important variations of the level in lakes and in shallow bays. These theoretical results explain the fact that in oblong lakes extending in the west–east direction there are large variations in the level at the eastern end. The same applies for bays which are shallow and have an opening in the west. In lakes and bays open to the east, there are no such variations in level. These variations occur seldom in lakes and bays extending in a north–south direction. In most cases the pressure disturbances travel approximately in a west–east direction, that is towards the closed end of the canal, which is required to raise the water to a considerable amplitude for the forced oscillations.

CALOI (1938) has been able to prove, for the Bay of Trieste, the correctness of the resonance condition (VI.135), on the strength of gauge registrations made in the northern section of the Adria. Figure 95 can be taken as an example. It shows the deviations from the computed tidal curves and

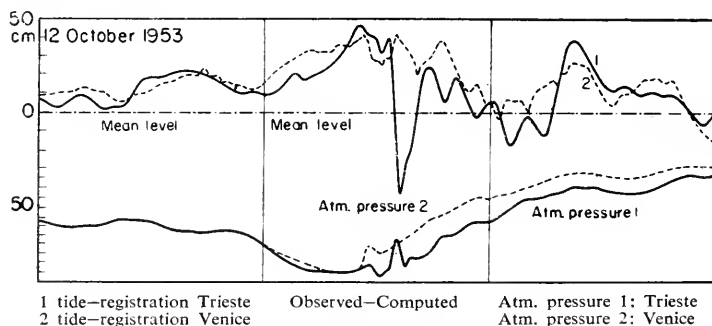


FIG. 95. Registration of atmospheric pressure and water level at Trieste and Venice on 12, 13 and 14 October, 1933.

the curve for the atmospheric pressure for Trieste and Venice for the period 12–14 October 1933 (see p. 189). The low-pressure area which caused the strong fall in pressure on the 12th came from the Po valley and crossed the northern Adria in about 2.2 h. Its velocity of propagation was approximately $50 \text{ km/h} = 14 \text{ m/sec}$. As the average depth of water between Venice and Trieste is about 20 m, the velocity of the free waves will be 50 km/h. The condition for resonance is fulfilled. The

variations in level in Trieste exceed by far those to be expected by the change in pressure. The seiches waves succeeding the large wave are oscillations of the Gulf of Trieste.

An important paper by Proudman and Doodson considers friction but neglects the earth's rotation. The basic equations are identical with those in (VI.40), except that, instead of η , we have $\eta - \bar{\eta}$, according to (VI.130). In accordance with the boundary conditions, η must be proportional to $\cos \kappa x$, and u proportional to $\sin \kappa x$ and $\kappa = (n\pi)/l$, in which n is an integer. If we put

$$\kappa \bar{\eta} = -P \cos \kappa x \quad \text{and} \quad \frac{v}{gh} \frac{\partial u}{\partial z} = W \sin \kappa x, \quad (\text{VI.136})$$

the effect of a stationary change in atmospheric pressure and wind over the basin is determined by the constants P and W . To these stationary influences corresponds, in the basin, a stationary level deformation and a stationary current, which, as can easily be shown, is given by

$$\kappa \eta = -\left(P + \frac{3}{2}W\right) \cos \kappa x \quad \text{and} \quad \frac{v}{gh^2} u = \frac{3}{4} \left(\frac{z}{h} + 1\right) \left(\frac{z}{h} + \frac{1}{3}\right) W \sin \kappa x. \quad (\text{VI.137})$$

We have to add to the statical action of the atmospheric pressure P on the surface deformation a piling up effect by wind in the amount of $\frac{3}{2}W$. The current moves in the upper third part of the water in the direction of the wind, in the lower two-thirds as a compensating current in the opposite direction. The strength of the current is inversely proportional to the water depth and, therefore, the piling up effect of the wind is greater in shallow water than in deep water.

The condition given by (VI.137) is stationary and starts only when the acting forces, atmospheric pressure and wind have acted upon the water-mass steadily for a certain length of time. The final state is attained by oscillations. The simplest case is as follows: Let an atmospheric disturbance (atmospheric pressure and wind) occur suddenly at the time $t = 0$ in the form of (VI.136). At the start, the equations of motion are only satisfied when at the right side of the equations (VI.137) we add

$$\sum_s C_s e^{-(\epsilon_s v/h^2)t} \quad \text{and} \quad \sum_s C_s v(z) e^{-(\epsilon_s v/h^2)t}$$

(p. 157) respectively. We get C_s and the function $v(z)$ from the general solution of the differential equations, considering the boundary conditions. These terms have a certain similarity with those on p. 158, which were derived for the free oscillations of the basin. After a certain length of time, the stationary state (VI.137) will set in. We have now free oscillations superimposed on the stationary state, and these free oscillations are damped by the friction and in time become imperceptible, so that only the stationary state remains.

A similar treatment can be applied to a sudden or gradual appearance of

an atmospheric disturbance, which disappears after a certain time. It will create deformations of the level which attain a maximum and return to its original state of equilibrium by oscillations, when the disturbing forces

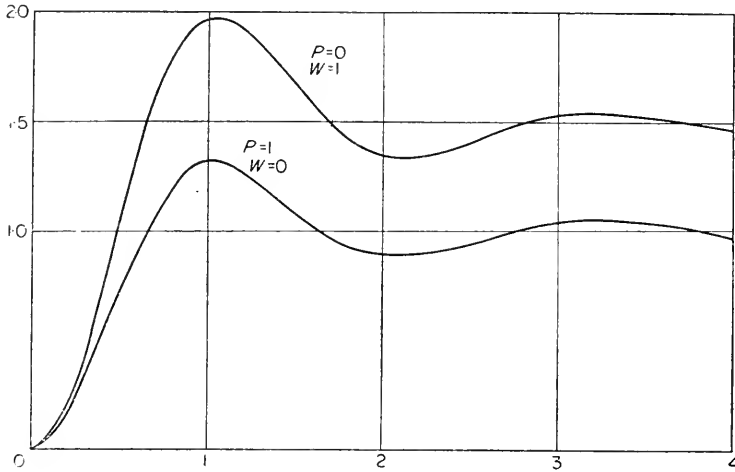


FIG. 96. Surface approaching a steady state at the far end (exposed to the wind) of a rectangular basin for a sudden variation of atmospheric pressure ($P = 1$) and for a sudden wind ($W = 1$). (Proudman and Doodson.)

disappear. Proudman and Doodson have computed numerically two cases which are graphically shown in the Figs. 96 and 97. Figure 96 shows how a sudden atmospheric and wind disturbance respectively affects the level at one end of the basin. In the case of the pressure disturbance ($P = 1$), the

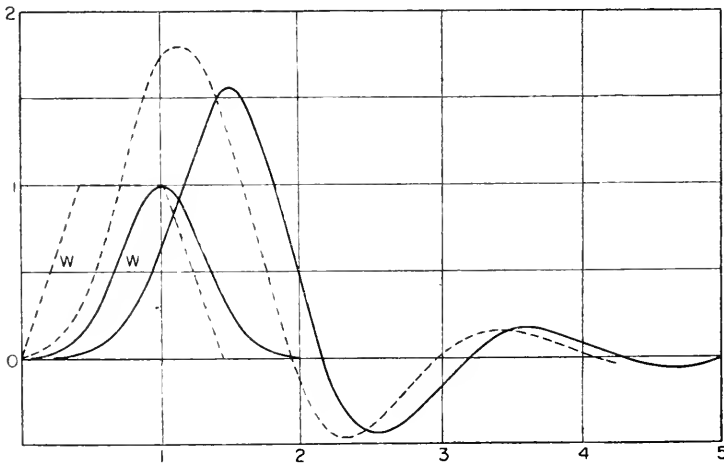


FIG. 97. Deformation of the surface at the far end (wind exposed) of a rectangular basin under the action of a gust of wind. (W gives the course and the length of time of the gust of wind in two cases.) (Proudman and Doodson.)

new state of equilibrium is at 1, in the case of the wind disturbance ($W = 1$), it is at 1.5. In both cases the water level is at the offset higher than the new state of equilibrium. Then, by decreasing oscillations it returns to its new equilibrium position. The second figure shows two kinds of action of a gust of wind on the level at one end of the basin. The gust is followed by a rapid piling up of the water at the closed end of the basin, which decreases by oscillations after the wind gust has ceased. According to Proudman, we find for different values of the depth h , the length of the basin l and a coefficient of viscosity ν , the unit time in the Figs. 96 and 97:

h (m)	20	20	40	40
l (km)	100	200	200	400
ν (cm ² sec ⁻¹)	436	218	1234	617
Time (unit in hours)	2.2	4.4	3.1	6.2

The period of the oscillations is for the first case 4.68 h, whereas that of the free period of oscillations (without friction) would be 3.97 h.

These theoretical computations show that atmospheric disturbances of any nature lead always to seiches in lakes and bays, and are always connected with them.

Of particular interest is the case where a pressure disturbance travels along the length of a uniform canal, so that pressure gradients act only perpendicularly to the canal. This will cause transverse and longitudinal currents in the canal, which must be accompanied by transverse oscillations. As long as the rotation of the earth is neglected, it can be expected that any pressure disturbance will produce transverse oscillations in the canal, whose period is identical with the free oscillations in the canal. Proudman has given a solution for the case where the earth's rotation is considered.

Let us assume that the canal extends in the y -direction and that its shores are at $x = 0$ and $x = 2a$. The depth be constant and equal to h . (Proudman deals also with the case of a canal of variable depth in its cross-sections.) The atmospheric disturbance $\bar{\eta}$ be also only dependent of x . If the friction is neglected, equations (VI.130) take the form

$$\left. \begin{aligned} \frac{\partial u}{\partial t} - fv &= -g \frac{\partial}{\partial x} (\eta - \bar{\eta}), \\ \frac{\partial v}{\partial t} + fu &= 0, \\ h \frac{\partial u}{\partial x} + \frac{\partial \eta}{\partial t} &= 0. \end{aligned} \right\} \quad \text{(VI.138)}$$

Apart from the equilibrium solution as given in (VI.131), there is a stationary solution in the form of the gradient current:

$$\bar{\eta} = 0, \quad \eta = Z(x), \quad u = 0 \quad \text{and} \quad v = \frac{g}{f} \frac{dZ}{dx}, \quad \text{(VI.139)}$$

in which $Z(x)$ is an arbitrary function.

Another solution corresponds to the free oscillations in the transverse direction of the canal, which can be expressed in the form

$$\eta = Z(x)\cos\sigma t, \quad u = U(x)\sin\sigma t, \quad v = V(x)\cos\sigma t$$

By substituting into (VI.138) we obtain

$$U = \frac{-\sigma g}{\sigma^2 - f^2} \frac{dZ}{dx} \quad \text{and} \quad V = \frac{-fg}{\sigma^2 - f^2} \frac{dZ}{dx},$$

$$\frac{d^2Z}{dx^2} + \frac{\sigma^2 - f^2}{gh} Z = 0, \tag{VI.140}$$

with the boundary condition $\frac{dZ}{dx} = 0$ for $x = 0$ and $2a$.

The general solution of the last differential equation gives

$$Z_s = A_s \cos \frac{s\pi}{2a} x,$$

in which A_s is a free constant and s is an integer.

For the frequency of the oscillation s we find:

$$\sigma_s^2 = f^2 + \frac{s^2\pi^2}{4a^2} gh. \tag{VI.141}$$

The result of a sudden pressure disturbance $\bar{\eta} = Z_s(x)$ starting at a time $t = 0$, can be known by combining a disturbance of the equilibrium for $\eta = Z_s(x)$, a steady solution $Z(x) = -(f^2/\sigma^2)Z_s(x)$ and a periodical solution with an adequately selected amplitude. It is shown that the level η in the transverse direction of the canal executes an oscillating motion varying from zero to $2(1 - f^2/\sigma_s^2)Z_s(x)$ and high water will occur at a time $T = \pi/\sigma_s$.

A general solution of the problems will be found by expanding the pressure disturbance $\bar{\eta}$ into a Fourier series, according to $\cos s\pi/2a$. If we assume that the atmospheric disturbance consists in the appearance of a linear pressure gradient across the canal with intensity $2H$ valid for entire width $2a$, we get as the principal oscillation on the banks of the canal

$$\eta = \frac{8}{\pi^2} H \left(1 - \frac{j^2}{\sigma_1^2} \right) (1 - \cos\sigma_1 t), \tag{VI.142}$$

in which σ_1 is given by (VI.141) with $s = 1$.

The period of the s -nodal transverse oscillation of the canal with the earth at rest is $T_r = 4a/s\sqrt{gh}$ and $T_i = 2\pi/f = 12\text{h}/\sin\varphi = \frac{1}{2}$ pendulum day being the period of the inertia oscillations in the latitude φ ; we obtain from (VI.141) for the period of the forced transverse oscillations in the canal

$$T = \frac{T_i}{\sqrt{1 + (T_i/T_r)^2}} = \frac{T_r}{\sqrt{1 + (T_r/T_i)^2}}. \tag{VI.143}$$

For narrow and deep canals, T_r is generally much smaller than the inertia period T_i , so that in a first approximation $T = T_r$, i.e. the effect of the earth's rotation is small and can be neglected in a first approximation. However, the natural period for extensive water-masses with the earth at rest, T_r , is

very large, so that with a rotating earth the period of the forced waves nears rapidly the period of pure inertia oscillations.

It is probable that in narrow, oblong seas (e.g. Adria, Kattegat, etc.) this kind of transverse oscillations is created by atmospheric disturbances, which are particularly favoured by the dimensions of the canal. In the Kattegat there is frequently an approximately 4-hourly oscillation, and LA COUR (1917) and THORADE (1918, p. 234) have explained this in a similar way. Following the storm tide of 15 January 1916, were oscillations of a 4-hourly period with a nodal line in the north-south direction in the southern Kattegat. Fig. 98 gives the variations in the level of the surface for Aarhus and Hornback

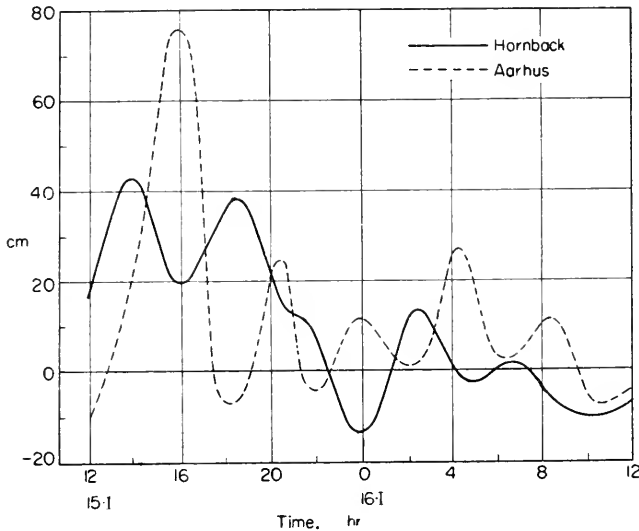


FIG. 98. Variations in the water level at Aarhus and Hornback during the storm flood of 15 January 1916 (La Cour). The curves indicate the variation of the level from 1 h before to 1 h after each time moment.

back; they show clearly the behaviour of the oscillation at both sides of the canal and its period. It also fits quite well the conditions of width and depth existing in the southern Kattegat: $2a = 100$ km and $h = 20$ m, which give $T = 3.97$ h. In this particular case, the rotation of the earth will only be of little importance, as T_i for $\varphi = 55^\circ$ has the value of 14.7 h. As shown by Jacobsen, who analysed tidal currents in this area, the M_6 tide, which has a period of 4 h, is particularly pronounced. The M_6 tide is also quite predominant at Aarhus.

For the transversal seiches and their generation the reader is referred also to SERVAIS (1957).

(c) Storm Surges

The earliest methods to study the meteorological disturbances of sea level are to tabulate the storm effect in terms of barometric pressure, wind

velocity and direction, all at the place where the effect was observed. Such methods are largely statistical in kind and require large numbers of observations to give any kind of precise average effect, and large enough to include all variations in direction and velocity of wind. Thus, it is possible to find for a coast the most effective winds for raising sea level. Such investigations of a more statistical nature have great practical value, as they are the basis for most storm warnings. These studies were mainly concerned with the relations between the generating factors, mostly of meteorological nature, and the changes in water level, without dealing with the actual causes of storm surges. This method of investigating well-developed, single cases was used by DOODSON (1929), in the tabulation of storm surges in the North Sea by CORKAN (1948) and in the Summary by DOODSON (1947). Two especially strong storm surges in the North Sea, namely those of 8 January 1949 and 31 January/1 February 1953, were investigated by CORKAN (1950) and ROSSITER (1954), who associated the changes in water level with the passage of atmospheric disturbances.

As to the theoretical part of the problem, the reader is referred to the previously treated relations between the water level and currents in more or less closed water-masses and the atmospheric disturbances at the surface. These relations form the basis for explaining the occurrence of storm surges. We wish to call attention to the work of GOLDSBROUGH (1954), treating the wind effects on the motion of the sea in an infinite channel and in a rectangular gulf. The basic equations are the equations of motion with the Coriolis force, vertical and lateral friction and the equation of continuity, which can be solved by considering the conditions valid at the boundary of the channel, using infinite series. The results will show only by solving numerical examples. The case of a channel closed at one end is of special interest, in that the dimensions used are an approximate representation of the North Sea. The effect of a transverse and a longitudinal wind, i.e. of a west-east and a north-south wind in the case of the North Sea, has been investigated. Table 28 gives the surface disturbances at the east and west ends of the southern shore, the last two columns give the corresponding surface disturbances in the north where the effects of the southern boundary are evanescent. A transverse wind is much more effective than a longitudinal wind in producing a surface displacement. It has to be mentioned that the surface disturbance at any point diminishes in magnitude with increase in depth, for the same wind strength.

Thus, the following is to be expected: near the southern end of the sea a westerly wind always provides a depression on the English shore and rise on the Continental shore. But in the north, where the effect of the southerly boundary on the motion has disappeared, the displacement depends for both sign and magnitude on the depth. Northerly wind produces a depression on the English shore near the southern end and a rise farther north when depth is 20 or 60 fathoms, but gives the reverse effect at 40 fathoms.

Table 28. Surface disturbances at the east ($x = 0$) and west ($x = a$) ends of the southern shore in a rectangular gulf oriented from North to South (ξ , the displacement of free surface from its undisturbed position; ν , the coefficient of eddy viscosity, T_x the wind stress; a positive T_x will mean a westerly wind and a positive T_y , a wind from the south. According to GOLDSBROUGH, 1954)

Closed end (southern shore)		In the north where the effects of south boundary are evanescent	
$x = 0$	$x = a$	$x = 0$	$x = a$
20 fathoms — 820	696	— 156	156
40 fathoms — 317	287	18.8	— 18.8
60 fathoms — 204	188	— 0.76	0.76

Closed end (southern shore)		In the north where the effects of southern boundary are evanescent	
$x = 0$	$x = a$	$x = 0$	$x = a$
20 fathoms 72.8	5.3	— 360	360
40 fathoms — 2.6	0.07	17.7	— 17.7
60 fathoms 0.06	0.04	— 0.36	0.36

Theoretical investigations of this kind are, without any doubt, of great importance as far as the understanding of the problem of storm surges is concerned; however, one should be careful in applying the results obtained to the actual process in nature because of the simplifications in the models.

In studying the problems suggested by coastal flooding the effects of the interaction between the tide and surge are important. The maxima of the highest surges observed up to the present time have occurred nearer to the time of tidal low water than to the time of tidal high water. Since the timing of the meteorological conditions which generate the surge is independent of the timing of the astronomical tide, it would appear that the characteristic just noted must be of hydrodynamical origin. PROUDMAN (1955*a, b*) and DOODSON (1956) have studied this problem very thoroughly. Proudman has given a theoretical investigation of the distribution, along an estuary, of a combination of tide and surge which have been generated in the open sea. For a single progressive wave, the height of a surge whose maximum occurs near to the time of tidal high water is less than that of a surge whose maximum occurs near to the time tidal low water, and it decreases as the range of tide increases. This is in agreement with the observations; besides, the friction seems to be the cause of these differences. With a standing oscillation on the head of the estuary, when the primary surge rises to its maximum more rapidly than it falls from it, and when this maximum occurs near to the time of tidal high water, the effect of shallow water is to make the surge

increase as the range of tide increases, and the effect of friction is to make the surge decrease as the range of tide increases.

The same problem was tackled by Doodson in a similar manner. He used for a model a long uniform gulf about 100 miles long and about 21 fathoms deep. He had also taken account of the non-linear terms in the equations of motion, which introduces some mathematical difficulties. The numerical methods have been applied to cases where storm surges have been superposed upon the tides, with the maximum of the surge occurring near high water, or near low water, or near one of the two half-tide levels. All four cases demonstrate that the character and magnitude of the interaction are not clear, but it is shown that the apparent surge is dependent upon the coefficient of friction and that the magnitude of this is greatly affected by tides. The actual apparent surge at the mouth of the gulf is affected by the reflexion which takes place at the head of the gulf and thus the correlations of apparent surge with meteorological data are complicated by the reflected oscillation.

In recent times, numerical methods have been used for the solution of the system comprising the equations of motion and the equation of continuity, taking full account of lateral and vertical friction as well as of external forces at the water surface (atmospheric pressure and wind), in order to investigate surges in marginal and adjacent seas and to find their causes. HANSEN (1956) has given a procedure that is based upon boundary and initial values. The differential quotients in the direction of the x - and y -co-ordinates appearing in the equations are approximated by quotients of differences determined according to a grid with a width of mesh l . In this way, a system of common differential equations of time differential quotients is formed, which are all linear. This means: the time variation of the velocity components and the water levels in the grid-points are known if the function values are given. Substituting the time derivation by finite values, it is possible to compute numerically the function values for a subsequent time from the given function values at the initial time.

In the application of this method to the water level in the North Sea at the time of the catastrophic surge on 31 January/1 February 1953 (Holland Storm) the North Sea grid, given in Fig. 98*a*, was used. The meteorological observations were taken from weather maps prepared at 3-hourly intervals. The following boundary conditions were chosen: The water level remains undisturbed at the northern limit of the area, running from Scotland to Norway. The normal component of velocity vanishes along the coasts. This holds also for the entrance to the Skagerrak, which is not treated here. The flow through the Dover Straits is assumed to be proportional to the water level. We wish to point out that no other observations of water level or of water transport were used in the computation. This computation of water levels and mean velocities for the entire duration of the surge was done by the electronic computer BESK. Figure 98*a* gives the isolines of water level on 31 January 1953

at 21:00 G. M. T. The numbers at the heavy dots at the coasts also contained in Fig. 98a give the water levels as derived from observations by ROSSITER (1954). The differences between the observed and computed values along the coast are 0.5 m only at some places and will hardly exceed this amount. Since there are no current observations from the time of the Holland Storm, it is not possible to check the theoretical current values. The

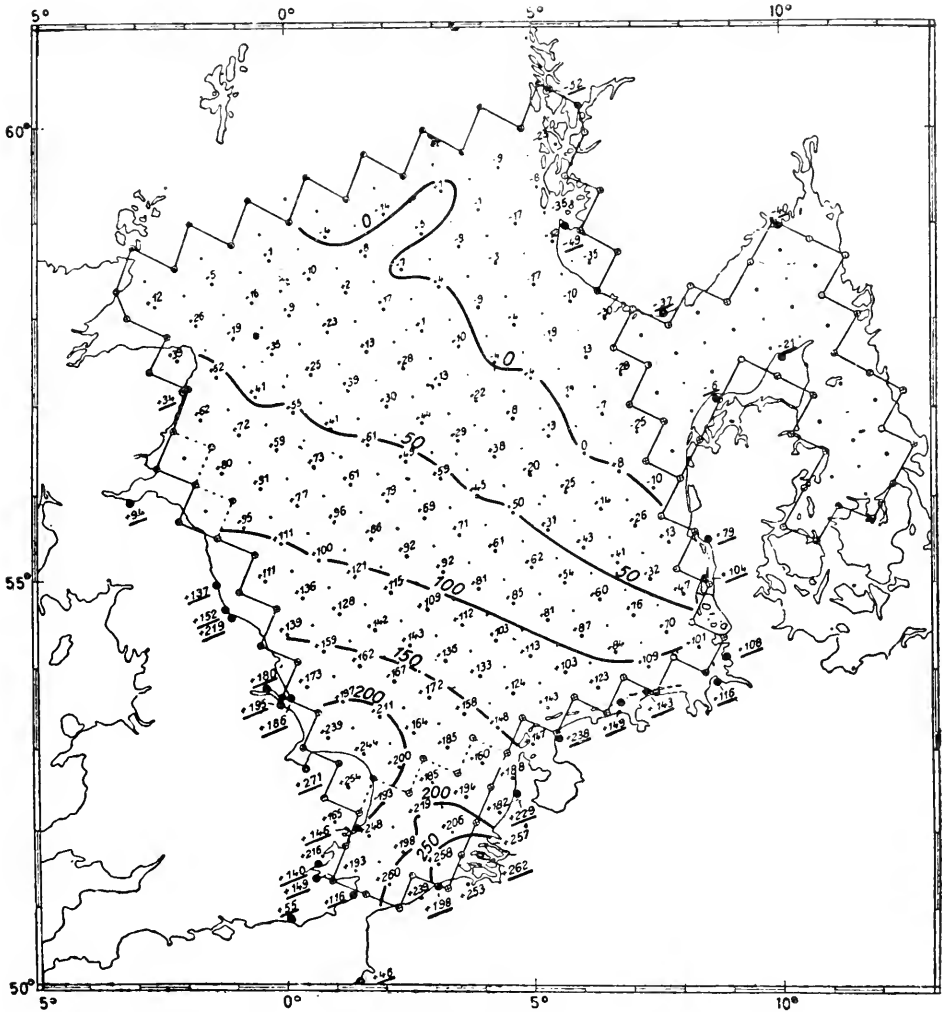


FIG. 98(a). Water level in the North Sea caused by the Holland-orkan (according to Hansen, 1956).

course (progress and intensity) of the surge at the coast of the North Sea is in a generally good agreement with water-level recordings. Although the results of this first computation of a heavy surge in a marginal sea are

not satisfactory in all points, they nevertheless show that the main causes of the generation and development of a surge were considered as correctly as possible and that a successful numerical prediction of sea level can be achieved by further development of the theory and numerical computation methods.

(d) *Oscillations on the Shelf and Meteorological Tsunami*

We have already mentioned previously that tidal recordings on straight coasts include also seiches-like motions of the water surface, which can only be interpreted as being oscillations of the water-masses on the shelf. It is probable that they are developed under certain conditions, which cause a given section of the shelf to behave like an open bay. The period of the oscillations depends in the first place upon the width of the shelf and, as according to the records, varies from a few minutes to 2 h and over. NOMITSU and HABU (1935) and NOMITSU and NAKAMIYA (1937) have continued the work started by Honda and his collaborators. These oscillations are caused by both atmospheric disturbances and submarine earthquakes. The damping of the waves is considerably smaller when they originate from an earthquake. Perhaps this is due to the fact that a storm disturbs the waters to a great extent and, consequently, the coefficient of viscosity is then larger while an earthquake is more distant and the weather and sea remain usually calm.

The agreement between the observed and computed periods for oscillations on the shelf is not bad, even when Merian's formula for bays using the dimensions of the shelf is applied. In most cases, however, there will be a more or less wide range within which to fix the outer limit of the shelf against the open sea, whereas it will not be difficult to take into account the various depths at the shelf, which so far has not been attempted in single cases. A theoretical investigation of seiches which can be produced in the open ocean by a submarine ridge has been made by HIDAHA (1935).

Assume for the depth a curve of the form $h = h_0(1 + x^2/a^2)^{1/2}$, then the bottom configuration characterized by a submarine ridge rising up till the water depth h_0 at $x = 0$; at the distance a the water depth is $h_0 \sqrt{2}$. The possible oscillations are shown in the curves in Fig. 99, in which the longer wave has a node over the ridge; its period is $T_1 = 6.95(a/\sqrt{gh_0})$. The shorter wave has an anti-node over the ridge and the numerical factor in the period is 3.24, instead of 6.95.

Figure 99 contains in its lower part also the possible seiches on a shelf obeying the same law of depth. Here both seiches represented have, of course, anti-nodes at the land end of the shelf, where the depth is h_0 ; the period is $T = 3.21(a/\sqrt{gh_0})$; for the shorter wave the numerical factor is 1.925.

The Japanese shores are frequently the scene of devastations caused by strong, wave like disturbances of the sea surface. Their development is either of a seismic or of a meteorologic origin. On the east coast of the island Hondo

they occur so frequently that the people have named these devastating waves "tsunami". The meteorologic tsunami are nothing but seiches of bays

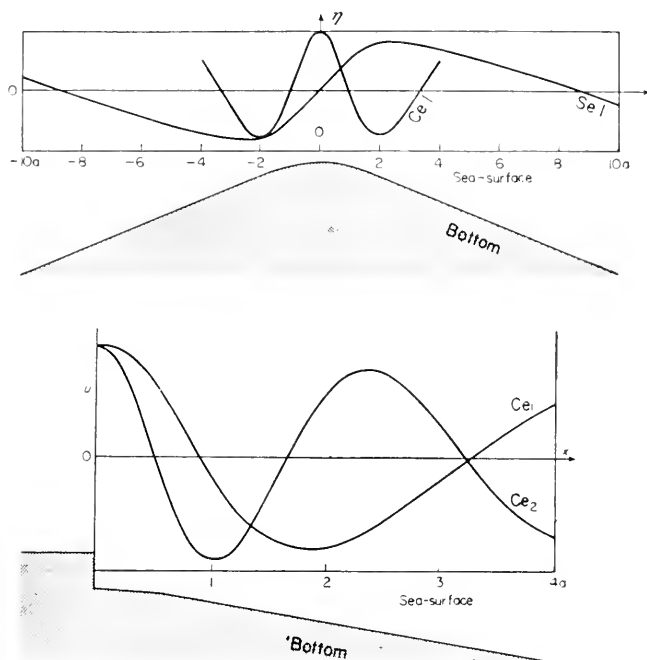


FIG. 99. Upper: seiches over a submarine bank, lower: seiches on the shelf (Hidaka).

and of the shelf, but they exceed in intensity the normally smaller amplitudes of the seiches on the shelf. Consequently, we can refer to the preceding paragraph for their explanation and theory. We have to consider, however, that the amplitude of the variations in level, particularly in the case of tsunami, is no longer small in comparison to the depth. Thereby the equation of continuity has to be adjusted to the change in the surface level. NOMITSU (1935) showed that the corresponding equations have their depth h replaced by $h + \eta$. This has a considerable influence, especially in computing the rise in water level when the sea bottom slopes up towards the coast. If ψ is the slope of the surface, T is the wind stress and ε is a coefficient smaller than $\frac{1}{3}$, we can use for this computation $\sin \psi = -\varepsilon T / g \rho d$, which gives the slope of the surface in relation to the wind (see vol. I, equation XIII. 45). We replace d or h by $h + \eta$, so that we can consider greater amplitudes of the waves:

$$\frac{\partial \eta}{\partial x} = \varepsilon \frac{T}{g \rho (h + \eta)}. \tag{VI.144}$$

Here T is the stress of the wind and ε a numerical factor which, in case of no bottom friction, is equal to 1. With friction and the water sticking to the

bottom (no bottom current) this factor becomes $\frac{2}{3}$ and with an intermediate coefficient of viscosity a value between these two extremes. If the friction is proportional to the bottom velocity u_h , viz. $\rho g u_h$, then we have, as shown by NOMITSU (1935),

$$\varepsilon = \left(1 + \frac{\rho g (h + \eta)}{2\mu}\right) : \left(1 + \frac{\rho g (h + \eta)}{3\mu}\right).$$

If the depth varies irregularly the above-mentioned equation can be used step by step to determine the variation in the piling-up effect, starting from the points where η is negligible up to the beach. If h is a simple function of x (VI.144) can be integrated directly.

If $h = \text{const.}$ at a point x calculated starting from the open ocean, where $\eta = 0$,

$$\eta = h \left[\sqrt{1 + 2\varepsilon \frac{T}{g\rho h^2} x} - 1 \right]. \tag{VI.145}$$

With a uniformly sloping sea bottom (see Fig. 100), $h = h_0 - x \tan \psi = h_0(1 - [x/L])$ and with the condition

$$\int_0^L \eta dx = 0,$$

we obtain

$$\eta = \eta_0 + \bar{\eta}_{h_0} \log \frac{\bar{\eta}_{h_0} - (h_0 + \eta_0)}{\bar{\eta}_{h_0} + (h_0 + \eta - x \tan \psi)}, \tag{VI.146}$$

in which η_0 means the elevation at $x = 0$ and $\bar{\eta}_{h_0} = \varepsilon [T/(g\rho h_0)]L$ the elevation of the water level at the shore with a uniform depth h_0 (according to (VI.144),

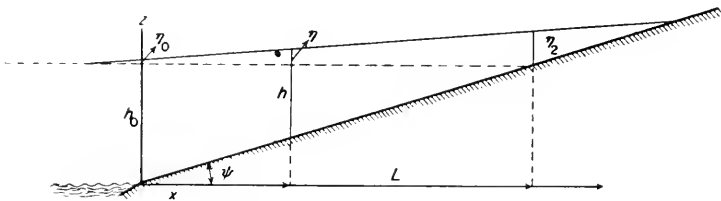


FIG. 100. Computation of the effect of piling up by wind on level shores.

neglecting η); $2\bar{\eta}_0$ is the elevation of the water piled up according to (VI.144) with rising bottom as shown in Fig. 100. If η_0 be small, we obtain at the shore:

$$\frac{\eta L}{\eta_{h_0}} + \log \left(\frac{\eta_h}{\eta_{h_0}} - 1 \right) = \log \left(\frac{h_0}{\eta_{h_0}} - 1 \right). \tag{VI.147}$$

According to this relation, the following values of $\eta_L:\bar{\eta}_{h_0}$ respectively $\eta_L:2\bar{\eta}_{h_0}$ correspond to the values $h_0:\bar{\eta}_0$. The latter values apply, if η at the right in (VI.144) is ignored:

$h_0 : \bar{\eta}_{h_0}:$	0	0.09	1	3.24	8.39	41.2	165	595
$\eta_L : \bar{\eta}_{h_0}:$	0	0.05	1	1.5	2.0	3.0	4.0	5.0
$\eta_L : 2\bar{\eta}_{h_0}:$	0	0.25	0.5	0.75	1.0	1.5	2.0	2.5

Consequently, when approaching the shore it is necessary to consider the increasing values with decreasing depth to obtain more accurate values.

An extensive theory of the formation of tsunami has been given by Nomitsu; however, its fundamentals do not deviate considerably from Proudman's method in his paper on the action of atmospheric disturbances on the sea level (p. 227).

A phenomenon similar to that of tsunami occurs on the Baltic coast and is called "Seebär". The Seebär always sets in quite unexpectedly when the water is calm, often even smooth; out from the sea a high-towering wave rolls on to the beach, and floods it to a height of 1 or 2 m. These waves appear at rhythmic intervals with decreasing height a few times in succession. These Seebärs have been described by DOSS (1907, p. 368), CREDNER (1888), RENQUIST (1926, p. 230) and MEISSNER (1924, p. 14, 63, 76). The phenomenon of the Resaca in the harbours of northern Spain might be related to the Seebär.

The cause of such catastrophic seiches appears to be certainly meteorological, whereas a more precise synoptical explanation of the whole phenomenon is still lacking.

7. Dislocation and Explosion Waves

Besides the waves forced by atmospheric influences, there are in the ocean other wave-like oscillations due to natural catastrophes. First of all a submarine earthquake may cause longitudinal elastic oscillations which travel with the velocity of sound waves. On ships they are felt as shocks which, depending on the force and the distance from the epicenter, may violently rock the ships.

RUDOLPH (1898, p. 273) has made an extensive compilation on the subject of seaquakes, which comprises also observations on dislocation waves. These dislocation waves are of two types, according to their origin. Dislocation waves are waves caused by earthquakes, submarine landslides, etc. Explosion waves are caused by submarine earthquakes which are sometimes accompanied by the release of large amounts of gas that rise toward the surface and may lift the surface up like a dome, thus producing a transverse wave that behaves like any other gravitational wave. At a certain distance from their origin, the variations of the sea surface are similar for both kinds of waves. In KRUEMMEL'S (1911, vol. II, p. 137) text-book there is a whole series of

descriptions of such catastrophic dislocation waves. Destruction waves caused by earthquakes, dislocation waves, or tsunamis are in general associated with submarine landslides which directly create transverse waves.

The central and eastern Mediterranean (Aegæis) has often been the site of such catastrophic events, which were invariably associated with heavy earthquakes. We remember the flood wave that occurred in connection with the terrible Messina earthquake on 28 December 1908, and which destroyed Messina, Reggio and a large number of other places in the Strait of Messina. According to Platania, the height of this wave was at Messina only 2·7 m, it was 8·4 at Giardino and Ali, 8·5 at Briga marina, whereas it amounted to hardly 1 m at Faro and Milazzo. These waves were apparently caused by tectonic changes.

An example from the North Atlantic coast is the disastrous wave in the wake of the Lissabon earthquake on 1 November 1755. Data on this catastrophe were collected by v. Hoff. In Lissabon there appeared, after the second earthquake shock and with simultaneous changes in water depth off the harbour, a wave measuring 5 m in height. Another three waves followed this first one. Along the entire Portuguese coast the waves were much higher. At Cadiz, the wave was still 18 m high and caused heavy damage. On Madeira the sea rose above the high-water mark by 4·5 m, and the oscillations returned, with decreasing intensity, five times. The flood wave spread over the whole Atlantic Ocean, and as far as the Antilles, favoured by local conditions, considerable amplitudes were reached.

The main site of these catastrophic waves is the Pacific Ocean, where they originate in the earthquake centres. They occur relatively often on the Japanese coasts, as a consequence of earthquakes and, as already mentioned, they are designated there by the name of tsunami. When they are caused by tectonic changes at the ocean bottom, they can be designated as "seismic" tsunami, in opposition to the meteorologic tsunami. The damages caused by them to the shores, especially in the shallow ocean bays, are considerable, and the loss of human lives is heavy. Recent studies on the origin of these seismic tsunamis can be found in Ishimoto (1933). HOCHSTETTER (1868, p. 837, 1869, p. 112, 1870, p. 818) has given a description of the waves originated by the earthquake of Arica on 13 August 1868, and GLEINITZ (1878) has described one of Iquique on 9 May 1877. Both "tidal" waves crossed the entire Pacific Ocean. In the immediate vicinity of the origin, there was first a wave crest and then a wave trough, whereas at a great distance from the origin the wave trough was the most important feature and showed itself by a recession of the water on the beach.

In the Indian Ocean we have also such gigantic "tidal" waves. The greatest destructive waves ever witnessed were the ones following the eruption of the volcano Krakatoa in the Sunda Strait on 26 and 27 August 1883. There were several eruptions. The last one on 27 August was the strongest. "Tidal"

waves developed after each explosion, which caused the greatest devastations on the shores of the Sunda Strait (see SYMONS, 1888). The height of the waves varied, but attained at a great distance from the origin 15 m, and in some places even 22 m. In the harbour of Batavia the waves were recorded as a sudden wave crest of 1.8 m height, which was followed by fourteen others with a long period of 122 min. At nearby localities a wave crest preceded the wave trough. The waves did not enter the Pacific Ocean but crossed the Indian Ocean in all directions and also could be traced up the Atlantic Ocean, where they were observed, e.g. by the German Expedition on South Georgia, 13 h 57 min after the great explosion. They were even observed in the European waters (Socoa, in the innermost corner of the Gulf of Biscay: amplitude 8 cm, Rochefort 13 cm, Devonport 15 cm,⁶ and others). These waves, starting from the Sunda Strait, covered a distance of at least 20,000 km in 32 h and 35 min.

These dislocation waves are waves with a long period ranging from 10 min to 2 h, the large values being quite rare. The velocity is of the order of magnitude of about 180 m/sec and upwards. The wave lengths are, therefore, exceedingly large, and one can apply the Lagrangian equation $c = \sqrt{gh}$. A condition for this is that the period of the waves should remain constant. By applying this formula, it was expected to compute the mean depth of the ocean from the travel speed of the waves obtained at various coastal localities. WHARTON and EVANS (1883) did point out that the observed values of c were always smaller than might have been expected, and DAVISON (1897, p. 33) has proved that one obtains systematically too large values of c , if the mean depth is substituted in \sqrt{gh} . As the depth is variable along the path of the wave, the Green-Du Boys equation (VI.32) should be used instead of the simple Lagrangian formula; it is however, questionable whether it can be used for waves starting from one point. Thorade has pointed out these waves are circular waves and not canal waves, and that the Greenian condition, that the depth varies slowly over a distance of a wave length, is hardly fulfilled. When waves follow each other in a rapid succession, one should consider the group velocity.

The propagation of the tsunami of 1 April 1946, from its origin in the Aleutians, south of Unimak island over the eastern Pacific Ocean has been examined thoroughly. It caused large-spread destructions on the Hawaiian islands (MACDONALD, SHEPARD and COX, 1947), and it was recorded by a great number of gauges along the entire American coast (GREEN, 1946). Figure 101 gives the record of the marigraph for Valparaiso, where the wave arrived after a travel time of 18 h and 7 min, with an average velocity of 390 nm/h. The observed travel time agrees very well with the theoretical one, computed from the depth charts after Du Boys's formula. The wave period of the first wave at the station nearest to the origin was 15.0 min and increased gradually to 17.4 min at the more distant stations. At a fixed

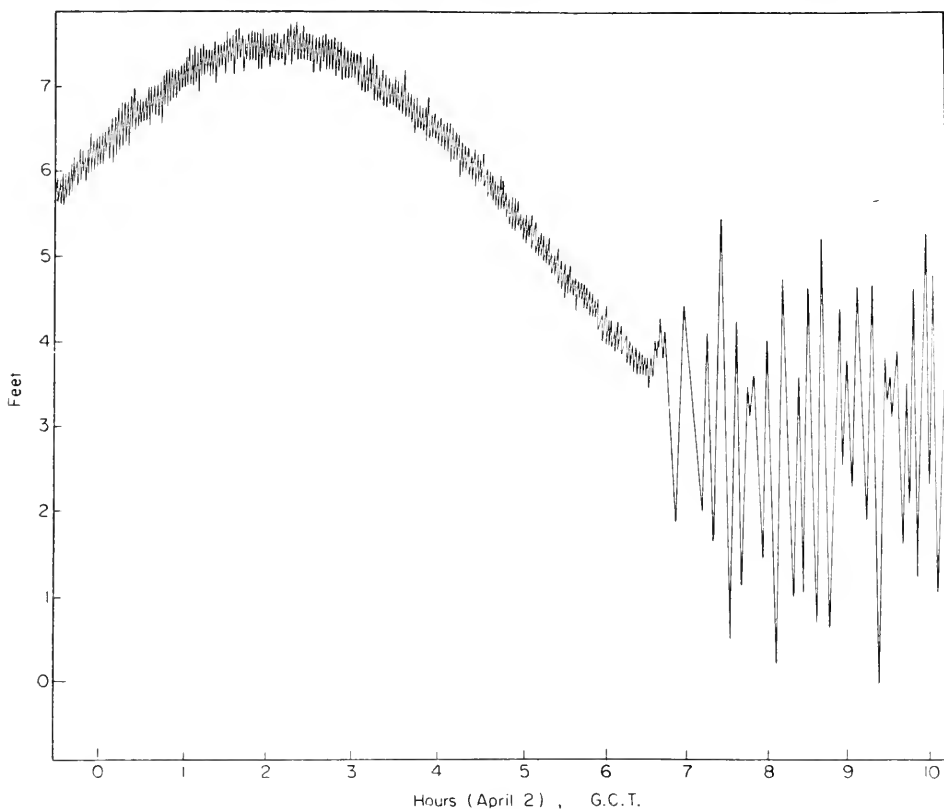


FIG. 101. Tide gauge record at Valparaiso following the earthquake of 1 April 1946.

station, however, the period decreases slowly with time, e.g. in Valparaiso from 17 to 7.5 min. The increase of the wave period with increasing distance from the origin appears to be a general phenomenon. MUNK (1947, p. 198) has solved the problem from a theoretical viewpoint.

If a wave with a wave length λ and a period T travels with a wave velocity c along the $+x$ -axis, its wave length λ changes according to the relation

$$\frac{d\lambda}{dt} = \frac{\partial\lambda}{\partial t} + c \frac{\partial\lambda}{\partial x}. \quad (\text{VI. 148})$$

This change can also be found from the rate at which the wave “stretches” due to the difference in velocity of two adjoining crests. This gives

$$\frac{d\lambda}{dt} = \lambda \frac{\partial c}{\partial x}. \quad (\text{VI. 149})$$

If we add the identity $\lambda = cT$,

$$\frac{\partial T}{\partial t} + V \frac{\partial T}{\partial x} = 0 \quad (\text{VI. 150})$$

can be derived from these relations, in which formula

$$V = c \left(1 + \frac{T}{c} \frac{\partial c}{\partial t} \right).$$

Here we have assumed $c = c(T, h)$ and $h = h(x)$. For an observer travelling at a velocity V , the wave period remains constant. It is to be noticed that the bottom slope $h(x)$ does not enter in this formula. V has not only the character, but is identical with the group velocity when the depth is constant. The wave period of any system of waves in which the crests retain their identity must satisfy the "equation of continuity" (VI.150). A formal solution of (VI.150) is:

$$T = T \left(t - \int_0^x \frac{1}{V} dx \right), \tag{VI.151}$$

in which the limits of integration remain undetermined because no provisions were made to fix the co-ordinate system. It seems convenient to put $x = 0$ for $t = 0$, which designates the time and the position of the initial wave generation; the period at this point would then be $T_0 = T(0)$.

The application of this solution to the tsunami requires the determination of its wave velocity. The velocity of propagation for an infinitely long wave train is

$$c^2 = \frac{g\lambda}{2\pi} \tanh \frac{2\pi h}{cT}.$$

This equation was originally derived for a wave train of constant period, but is also applicable to a wave system of gradually varying period. When $h < 0.05\lambda$, namely for very shallow water, this equation is reduced to the Laplacian equation.

$$c_0^2 = gh. \tag{VI.151a}$$

As the tsunamis fulfil the condition $h < 0.05\lambda$, the Laplacian relation has been successfully applied for computing travel times. This, however, does not explain the secondary phenomenon of the increase of the period, for which (VI.151a) is no longer a satisfactory approximation. The first two terms in the expansion of a hyperbolic tangent are $\tanh a = a - \frac{1}{3}a^3$, and to the same degree of approximation (VI.151a) becomes

$$c^2 = c_0^2(1 - a^2) \quad \text{with} \quad a = \frac{2\pi h}{cT}, \tag{VI.151b}$$

With (VI.150) one obtains the interesting relation $c - V = 2(c_0 - c)$, i.e. for any given wave period the group velocity is smaller than the wave velocity by twice the amount that the wave velocity is smaller than the

Lagrange wave velocity. With this V equation (VI.151) takes the form

$$\left. \begin{aligned} T &= T \left(\Delta t - \frac{J}{T^2} \right), \\ t_0 &= \frac{1}{\sqrt{g}} \int \frac{dx}{\sqrt{h}}, \\ J &= \frac{2\pi^2}{g^{3/2}} \int \sqrt{h} dx, \end{aligned} \right\} \quad \text{(VI.152)}$$

in which $\Delta t = t - t_0$. The two latter values can be computed numerically, when the bottom profile along the path of travel is given. One particular form of the solution (VI.152) is $T = 1/a(\Delta t - J/T^2)$, where a is an arbitrary constant. In this case one has a cubic equation in T . The simplest solution is found by setting $a = 0$, and $T = \sqrt{J/(t - t_0)}$.

The application of these theoretical computations to the tsunami of 1, April 1946, gave a qualitatively good agreement between the theory and observations. Theoretically the wave period must increase with distance of travel, but decreases with time at each station, as the observations actually show. The observed periods seem to be somewhat shorter in the northern Pacific Ocean and somewhat longer in Valparaiso than those computed by the theory. However, in view of the incorrectness in the determination of the periods from marigraphs, one can be satisfied with the quantitative results.

In the development of the "tidal" wave on a shore the configuration of the coast plays a great part. The waves approaching the coasts from the free ocean initiate eigen-oscillations of the bays (seiches) and of parts of the shelf which add to the wave disturbances and confuse in this way the basic

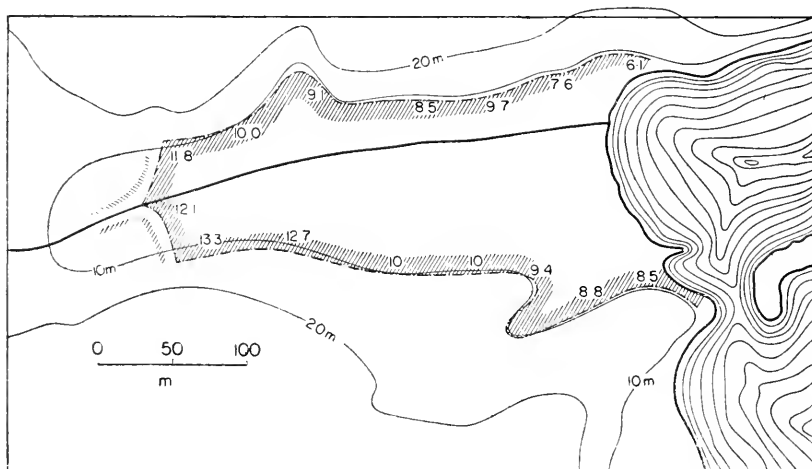


FIG. 102. Area inundated by Tsunami of 3 March 1933 in Bay of Sasu. (Numbers indicate the height of the flood in meters.)

phenomenon. Their interference with the tsunami waves permits only an approximate determination of the time of arrival and of the amplitude of the individual waves. MATUZAWA and his collaborators (1933) have given an accurate analysis of the water motion in the Bay of Sasu (in the innermost part of the Great Toni Bay), for the tsunami of 3, March 1933.

Figure 102 shows the section of the Sasu Bay flooded by the tsunami. This section is almost completely enclosed by the contour line of 10 m depth and has a pronounced trough form. The sudden end of the flood in the innermost part is caused by small hills which produce a partly inward barrier. Figure 103 gives a longitudinal section of the profile close to its right bank and above it the heights of the flood along this profile. The velocity of the "tidal" wave can be determined by considering the inner part of the bay

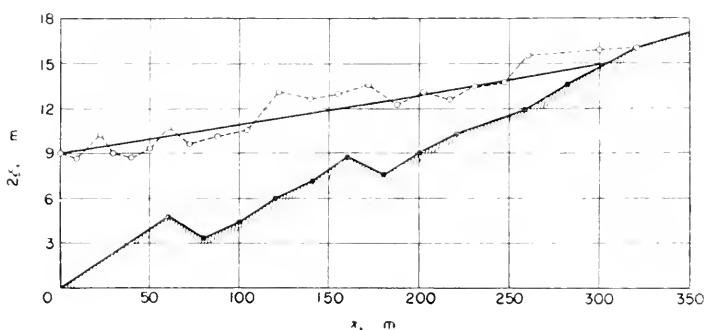


FIG. 103. Longitudinal section of Bay of Sasu (see Fig. 102). Lower line is the bottom profile. Dotted line: observed height of the flood. Full drawn line: computed height of the flood.

with the inundated area as one single oscillating system, co-oscillating with the wave coming from the outside. The assumption that the cross-section is rectangular and that the bottom slopes gently, first less strongly and then stronger in the innermost part, corresponds rather well to the reality. The theoretical computation gives an oscillation time of 224 sec and a distribution of the vertical amplitude as represented in Fig. 103 by the solid line. As the maximum velocity of the tidal wave at the beach, we get around 8 m/sec, all of which agrees very well with the observations. Essentially this tsunami caused a simple co-oscillation of the water-masses of the bay with the strong dislocation wave coming from the open ocean.

Since tsunami are shallow water waves, they are propagated at a speed $c = \sqrt{gh}$. A typical tsunami, one having a period of 20 min for example, has a wave length of 90 miles in water of 5000 ft depth. At the continental slope and walls of deep oceanic trenches, an appreciable depth change takes place over a distance which is small compared with this typical wave length. Therefore a reflection is to be expected.

COCHRANE and ARTHUR (1948) have made a theoretical investigation of such a reflection. The data examined give good evidence that reflections of tsunami do occur. A quantitative treatment shows that the observed wave heights were found to be in good agreement with those calculated on the basis of theory. The theory indicates that the reflected waves can be expected to be considerably smaller than the direct waves. This is also in agreement with observations.

PART II
TIDES AND TIDAL CURRENTS

Chapter VII

Principal Features of Tidal Phenomena

1. Review of the Phenomena

ONE of the most regular and important phenomena is the tides. They manifest themselves by the rhythmic rise and fall of the water, mostly twice a day. It is evident that these vertical displacements of the surface are accompanied by horizontal displacements of the water masses, called tidal currents. The vertical and horizontal displacements are different manifestations of the same phenomenon. The rhythmic rise and fall of the sea is only occasionally disturbed by atmospheric processes. Sometimes these disturbances are quite strong (storm surges), but always does the regularity of the phenomenon return after the meteorological influence has ceased. The perpetuity and regularity of the tides makes an attentive observer realize that a force constantly present, is the cause of the tidal phenomena and governs their course. The fact that on all shores of the oceans and adjacent seas these periodical movements are of the same nature, although different as to their extent, shows that tides are a worldwide phenomenon and must be governed by a system of forces which acts everywhere in the same manner and to which all the water-masses of the earth are similarly subjected. Such a system of forces can only be of a cosmic nature, i.e. it must be related to the position occupied by the earth in space.

The basic phenomenon is the periodical rise and fall of the water surface, which occurs twice in somewhat more than a day. The highest water of a tide is called high water, the lowest water low water, the rise of the water is designated as flood, the fall as ebb. The difference in height between low water and high water is called the range of the tide. As the successive high waters are as different as the successive low waters, one can distinguish a rise of the water during the flood and a fall of the water during the ebb. The arithmetical mean of both is the mean range of the tide.

The average interval between two successive high waters or between two successive low waters is 12 h and 25 min. Consequently, the high and low water is retarded from one day to the next by 50 min. This points to relationship with the motion of the moon, because the moon also is retarded daily by 50 min on its passage through the meridian.

The average duration of two tides is, therefore, 24 h and 50 min, and the duration of one tide corresponds on the average exactly to half an average lunar day. This fact led to relate each meridian passage of the moon to the subsequent high and low water respectively. The difference in time between the time of high water and the transit remains constant, and this is a characteristic value for each locality. It is called the *mean high water lunitidal interval* and it measures, in hours, the mean time difference between the transit of the moon and the occurrence of the next high water. Similarly, the low water lunitidal interval gives the average number of hours and minutes between the transit and the time of low water. The *establishment* is the (apparent) local time of high water occurring at new or full moon, or the high water lunitidal interval when the transit (just preceding the tide) occurs at noon or midnight. At full moon or at new moon (syzygies) the moon and the sun pass through the meridian simultaneously and, as the civil time is counted from the passage of the sun through the meridian, the lunitidal interval indicates at what time, at full or new moon, high water occurs at a given locality.

An exact comparison of the intervals between the transits and high or low water shows that, in general, these intervals deviate from the mean high-water interval by amounts of ± 1 h. When the sun's tidal effects shorten the lunitidal interval, causing the tides to occur earlier than usual, there is said to be a priming of the tide; when from the same cause, the interval is larger than usual, there is said to be a lagging. However, these deviations are not arbitrarily distributed; they return at regular intervals of about half a month. Therefore, this is called the *semi-monthly inequality* in the time of high water, to which corresponds an identical inequality in the time of low water. It is easy to compare these inequalities with each single transit of the moon and to establish that both values are correlated. The semi-monthly inequality is a function of the phase of the moon. The mean semi-monthly inequality is the average value of the inequalities during one year. This mean semi-monthly inequality depends on the phase of the moon, and its period is one-half of a synodic month (29.53 days) = 14.77 days. The upper part of Fig. 104 shows, for an idealized locality with a mean high water lunitidal interval (establishment) of 6 h, this fortnightly inequality. The numbers at the abscissa mean days after new moon (black circle). We can summarize as follows:

High water and low water follow the upper and lower transit of the moon in definite average intervals, which can differ according to localities. However, each interval for a place, has different semi-monthly inequalities and their main period is a half of a synodic month, which shows that these inequalities are related to the phase of the moon.

Neither is the range of the tide a constant quantity, and it varies with the same period of a half of a synodic month. At the times of new and full

moon the relative positions of sun and moon are such that the high water produced by one of those bodies occurs at the same time as that produced by the other; and so also with the low waters; these tides are called spring tides and have a greater range than any others of the lunar month, and at

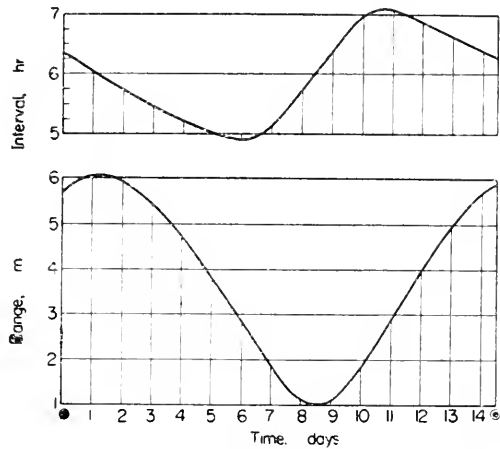


FIG. 104. Semi-monthly inequality in time and in range of high water.

such time we have the highest high tides as well as the lowest low tides, and the tidal range is at its maximum. The time of occurrence of spring tides is called *spring time*. The interval between new or full moon and spring tides is called the *retard* and can be regarded constant for any given place. The minimum *range* (neap tides) occurs with a similar retard after the first and last quarter of the moon (quadratures) at neap time. The time difference between the meridian passage of full or new moon and the occurrence of the spring tide is called the *age of the tide* and is given in days. In the lower part of Fig. 104 the semi-monthly inequality in the range of the tide is illustrated for an ideal locality, where the age of the tide is 1 day, the amplitude (= one-half of the range of the tide) of a spring tide 3 m, of a neap tide 1 m. The chart datum coincides for most European countries with the mean low water of the spring tide. The height of the high water above chart datum will, therefore, be at spring tide 6 m, neap tide $3\frac{1}{2}$ m, that of low water at spring tide (according to the definition) 0 m, at neap tide $2\frac{1}{2}$ m. The mean sea level is in this case 3 m.

The semi-monthly inequality in height and time is introduced by the sun. Apart from these two most important inequalities, there are still others which can be obtained from the residual terms remaining after elimination of the semi-monthly inequalities or from the harmonic analysis (see p. 299). The more important inequalities of this kind are:

(a) *Monthly inequality*. The range of the tide becomes a maximum soon after the moon is in perigee and a minimum soon after she is in apogee.

At these times perigean and apogean tides occur. The cause is the oscillations of the parallax during the period of the lunital interval which is an anomalistic month (27.55 days). This anomalistic month is only about 2 days shorter than the synodic month. The earth lags more and more behind the full moon and the tidal curves change accordingly. The extent of the parallax inequality is generally smaller than that of the semi-monthly inequality; however, there are localities (e.g. at the east coast of North America) where both are equally large, or even where the parallax inequality is larger. In that case, the tides are more governed by the parallax of the moon than by the phase of the moon.

(b) *Declinational inequality* is caused when the moon moves from the celestial equator into the northern and southern hemispheres. The oscillation of the declination of the moon is completed in a tropical month of 27.32 mean solar days. The declinational inequality is dependent only upon the absolute amount of the declination, and not upon its sign, so that its period is only one-half tropical month = 13.66 days. Soon after the moon is upon the equator, the greatest semi-daily range of tide will occur and, soon after the moon's greatest declination, the smallest. Besides this declinational inequality caused by the moon there is also a solar one, which depends upon the sun's declination; declinational inequality is smallest at the time of solstices and greatest at the time of the equinoxes. At that time, the full and new moon are about upon the equator and the range of the spring tide is extremely large and the range of the neap tide extremely small.

(c) *Diurnal inequality* in height is the difference in height between two consecutive high waters or low waters. Diurnal inequality in time or interval is the difference in length of the consecutive high- or low-water intervals. These inequalities, which make the tide curves unsymmetrical, have a period of a half tropical month for the moon and of a half tropical year for the sun. The largest diurnal inequality occurs with a certain lag after the moon's extreme north and south declination and disappears with a same lag when the moon crosses the equator.

The diurnal inequality influences strongly the picture of the tides. Sometimes this influence is so great that the semi-diurnal tides are almost entirely suppressed. The tides then degenerate into an oscillation with a period of one day (see p. 307). In the Atlantic waters, especially in the North Sea and in the English Channel, however, the diurnal inequality is insignificant.

This brief review of the main phenomena of the tides already shows that the tides are an extraordinarily intricate phenomenon obeying definite laws. The tides depend mainly upon the moon and the sun and upon their position relative to each other. A certain position between sun and moon does not recur until a Saros period (18 years) has elapsed. It would be necessary to have a series of observations extending over 19 years to compute exactly the tides for a certain locality. But even a one-year period of observations

is sufficient to determine the principal components, especially if these observations can be tied in to those made at main stations with an extensive record of observations. Figure 105 gives for two successive months (March and April) the tides for Immingham (North Sea, east coast of England) in

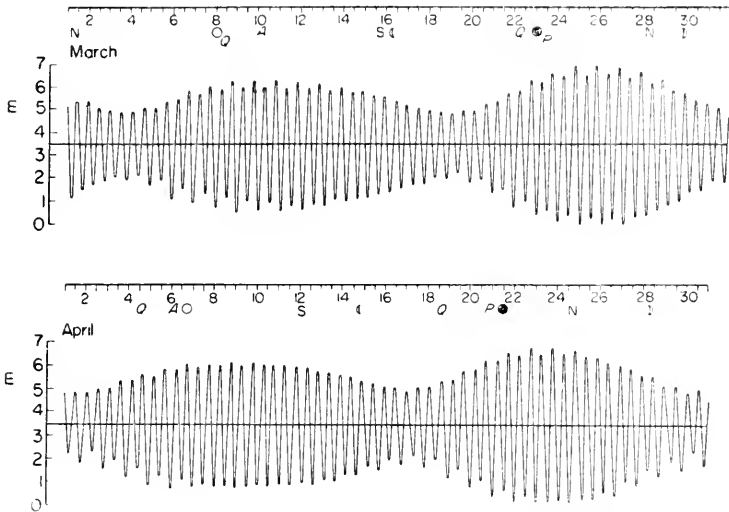


FIG. 105. Tide curves for Immingham (east coast of England) for March and April 1936 (Horn). The *O* of the left-hand scale corresponds to the chart datum. The phases of the moon are below the time scale. *N* and *S* indicate the time of the greatest northern and southern declination; *Q* the time when the moon crosses the equator; *A* and *P*, the time of the Apogee and Perigee.

the form of tidal curves (see HORN, 1943, p. 411). The zero of the height scale at the left side corresponds to the chart datum. The inequalities in time are too small on this horizontal scale to be noticeable. But the variation in height between spring and neap tides is quite clear. The phases of the moon and its other positions are indicated below the time; the difference of the tidal curves from one-half month to the next one shows the influence of the inequalities. The small diurnal inequality is characteristic of the tides at the North Sea.

The essence of tidal phenomena was in part already known to the ancient Greeks and Romans, before the first attempt at a mechanical explanation was successful. In the Mediterranean the tides are not so well developed. However, from the literature on other sea regions it is apparent that the ancient scientists had a certain good knowledge of the tides and were also capable of applying it. The first to write on this subject was Herodotus, who mentioned the tides in the Gulf of Suez. Strabo reports on the views held by Posidonius (deceased in B.C. 51) and Aristotle on the tides near Cadiz and by Seleucus on those in the Red Sea. The spring tides and their

association with the "age" of the moon were also known to Caesar. Plinius wrote about the sun and the moon being the cause of these phenomena. In general, however, the grandeur of this natural phenomenon was looked upon as something sinister and overwhelming by those who had never before experienced it. An example of this feeling, which has become famous, is the description by Curtius Rufus of the mighty tides which were encountered by the fleet of Alexander the Great in the estuary of the Indus River.

It is to be assumed that the sea-faring peoples living on the open coasts were familiar with the tides ever since. Ancient literature lends some support to this assumption. Then, many centuries passed by from which there is no record of any scientific observations of the tides. Only in the sixteenth century were the first attempts made to explain the tidal phenomenon. These were based upon the relations between the sun and the moon with their diurnal, monthly and annual inequalities, which were originally derived to serve the needs of navigation. Important changes in the views as to the causes of the tides were brought about in the Renaissance. After preliminary studies by Kepler, Galileo and others, it was Newton who, in 1687, discovered the correlation between the movements of the moon and sun and the tides. In his book *Philisophiae naturalis principia mathematica*, he published the laws of gravity which still form the base for the theory of the tides.

2. Tidal Observations, Gauges

The methodical analysis of the tides at a coastal locality requires regular observations and recordings of variations of the sea level. Observations of this kind have been gathered for centuries in numerous locations, because it is so essential for coastal navigation. The rise and fall of the sea surface can be easily determined on poles and harbour dams, docks and the like by means of a vertical board (tide staff) divided into feet and tenths of feet. Such observations are, of course, inaccurate, because the water surface is in continuous motion as a consequence of the ever present ocean waves. If one wishes to increase the accuracy and obtain perfectly correct measurements, the level should be determined at a point where the sea has free access, but the canal connecting the gauge with the open ocean should be made so narrow as to dampen short disturbances of the sea surface, like waves, etc. For this purpose, a tape gauge is used (Fig. 106). The rise and fall of the surface due to waves is then largely eliminated. For its description we quote SVERDRUP (1942, p. 360).

The principle of the tape gauge may be adapted for obtaining a continuous automatic record of the tide level. In the standard automatic gauge used by the U.S. Coast and Geodetic Survey (RUDE, 1928), the float, which is suspended in a well, is attached to a wire that turns a pulley mounted on the threaded rod. As the pulley turns, a carriage with a pencil moves back and forth along the threaded rod that is mounted at right angles to a clockwork-

driven roller carrying a sheet of paper. The paper is driven ahead about one inch per hour, and the device thus traces the marigram automatically. Suitable reduction is obtained by varying the size of the pulley and the pitch of the threaded rod. An accurate clock makes a special mark every hour, and a fixed pencil traces a reference line. Short-period waves are largely eliminated

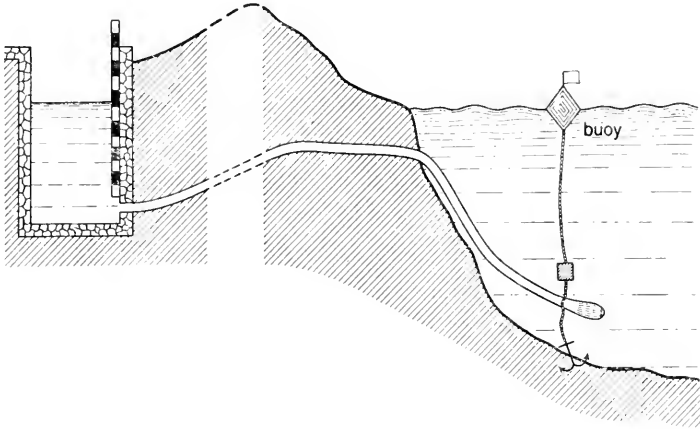


FIG. 106. Construction of a well housing a tide gauge recorder.

because of the damping in the well, but seiches and disturbances of the sea surface lasting several minutes or more are recorded. From the marigram the hourly heights and the levels and times of high and low water are easily read off. The standard gauge carries enough paper for one month, but the clocks must be wound once a week, and each day the instrument must be checked against a staff or tape gauge to ascertain whether it is functioning properly and to make sure that the holes in the float well are free from seaweed and other detritus. A portable recording unit that can be used by field parties is operated on the same principle.

The devices so far described can be used only on shore or where some rigid structure extends above the sea surface. Many types of pressure-recording devices for use on the sea bottom have been designed. In some the pressure element only is placed below the sea surface, with the recording device on land; in others, such as those to be used far from shore, the recording device is an integral part of the instrument, which may be placed on the sea floor or anchored and left in position for a week or more.

A very comprehensive description of high-sea tide recorders can be found in RAUSCHELBACH (1932, pp. 73–129; 1934, p. 177) and GEISLER (1939, p. 12; 1941).

BARTELS (1926, pp. 221 and 270) has drawn attention to the fact that in the tropics, it is possible to derive the semi-diurnal lunar tide M_2 of the

ocean from atmospheric pressure observations made on board of a ship; he has shown how to compute the M_2 component from hourly or 4-hourly ship observations. First, one has to determine the daily pressure curve with a period of a solar day. These values are then subtracted from the hourly observations and the residual values are analysed for a 25 h lunar wave. The lunar pressure wave obtained in this manner is composed of three parts.

(1) Of the atmospheric tide ($\delta_1 p$), which is known with sufficient accuracy from the results of the atmospheric pressure analysis made at land stations and can, therefore, be eliminated.

(2) Of the oscillations of the air-masses generated by the ocean tides, which cause the rise and fall of the isobaric surfaces ($\delta_2 p$). This influence of the ocean waves (also of tides) on the atmosphere, which was formerly disregarded, has been given by CHAPMAN (1919, p. 128) for plane waves in an atmosphere with a uniform vertical temperature gradient. It appears that, for very slow waves (velocity of propagation $c \ll c_0$, the velocity of propagation of free waves in the atmosphere) the disturbances in the atmosphere caused by the ocean waves become negligible, i.e. the isobaric surfaces remain undisturbed. On the contrary, for fast waves ($c \geq c_0$) the atmosphere participates in the wave motion of the water, the isobaric surfaces rise and fall parallel to the sea surface. Generally and in most cases, $c < c_0$. Then the phase of the atmospheric wave is opposed to the phase of the water waves, i.e. the isobaric surfaces lie lower above the crest than above the trough of the wave.

(3) The third part is the variation in pressure ($\delta_3 p$) caused by the rise and fall of the ship by the tide, according to the barometric altitude formula.

If $\delta_1 p$ is eliminated, then only the action of the motion of the sea surface remains in the observed variation. This action is expressed by Bartels in the following relation:

$$\Delta p = \delta_2 p + \delta_3 p = \kappa \delta_3 p,$$

in which

$$\kappa = \frac{1}{1 - (c/c_0)^2}.$$

From the distribution of the co-tidal lines (see charts I and II) one can derive, for instance, the velocity of propagation of the tidal waves in the South Atlantic $c = 1.80 \times 10^4$ cm/sec, whereas with convective equilibrium in the atmosphere one obtains $c_0 = 2.94 \times 10^4$ cm/sec. Then $c : c_0 = 0.61$; the increasing factor becomes $\kappa = 1.6$, with $c = 10^4$ cm/sec (about 1000 m depth) it becomes 1.13, with $c = 6.3 \times 10^4$ cm/sec (depth 400 m) 1.05. Hence, the co-oscillation of the atmosphere with the ocean tides is very important and should be considered in order to obtain a correct value for $\delta_3 p$. From these corrected values the amplitude and the phase of the M_2 tide can then easily be derived.

It has not been attempted thus far to use the enormous amount of observations consisting of barometer readings which were gathered in the ship journals kept in the hydrographic offices, for the purpose of computing ocean tides, despite the fact that the derivation made by Bartels was positively promising in this respect. In view of the circumstance that so far there seems to be no other possibility of obtaining actual measured values of the tides of the free ocean, an attempt of this nature, although requiring a great deal of computing and patience, would certainly be worth while.

Chapter VIII

The Tide-generating Forces

1. Fundamentals for Determining Tidal Forces

THE foundation on which any explanation of the tidal phenomena must be based is the system of tide-producing forces which is exerted by the moon and the sun on the earth. It is necessary to make a sharp distinction between the system of forces producing the tidal phenomena on the earth — not only in the oceans, but also in the atmosphere and in the solid earth — and the effects of this system of forces on the mobile masses in these three layers of the earth. This distinction is of importance for the following reasons. The nature of the tide-producing forces is well known. It was even possible to verify the existence of these forces in laboratory experiments. However, the effects of the tide-producing forces on the oceans, the solid earth and the atmosphere, i.e. the formation of the tides, are not clear in all points, although during the past decades an essential progress has been made (DEFANT, 1942; see also PROUDMAN, 1927; THORADE, 1928). The problem of the tide-producing force of a celestial body — sun or moon — is linked, according to Newton, to the forces of attraction existing between the masses of two bodies. These forces are proportional to the masses of the two bodies and inversely proportional to the square of the distance between them. The forces of attraction regulate in the astronomical system of the sun, the planets and their satellites the annual and monthly motion of the centre body and the secondary body around the common centre of gravity. Considering the system earth–moon, these forces also govern the monthly movement around its centre of gravity.

The mass of the earth is approximately 81 times that of the moon; therefore, the centre of gravity lies about 81 times closer to the centre of the earth than to the centre of the moon. The distance between the centre of the earth and the centre of the moon corresponds to 60 earth radii, and the common centre of gravity lies still inside the earth, viz. at a distance of approximately three-fourths of the earth's radius, 4600 km from the centre of the earth. The monthly orbit of the earth around this point is, therefore, very small compared to that of the moon. If the system earth–moon were only subjected to the forces of attraction, then these would constantly endeavour to reduce the distance earth–moon. The monthly motion of the two bodies around

the common centre of gravity generates centrifugal forces, which counter-balance the centripetal attracting forces giving the system a stable equilibrium. This equilibrium requires that, for instance, for the system earth-moon the resultant of all forces of attraction between the earth and the moon is equal and directly opposite in direction to the resultant of all centrifugal forces. The origin of this resultant is in the centre of the earth.

How large is the centrifugal force for an element of mass which moves around common centre of gravity? The motion in question is a simple translation without rotation. In the case of a so-called *revolution*, each particle of mass of a body travels the same orbit around a central point. Figure 107

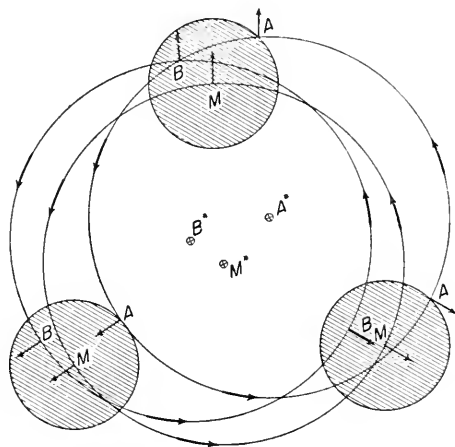


FIG. 107. Centrifugal forces when a body M rotates around M^* .

explains such a motion. The body with its centre in M accomplishes a revolving motion around the central point M^* , and all points of M , for instance, A and B , go through the same circle. The centres of these orbits A^* and B^* are in the same position to each other as the corresponding points in the body M . The arrows then indicate the direction of the centrifugal forces. The magnitude of the force Z is given by V^2/a , if V is the velocity of the body and a the radius of her orbit. The centrifugal forces of all particles of mass of a body participating in a revolving motion are equal and have the same direction. If T_0 is the time of a revolution of the body on its orbit and a is the radius, then the centrifugal force will be for a unit of mass $Z = 4\pi^2 a/T_0^2$ and is directed along the radius towards the outside.

If M is the mass of the moon concentrated in its centre, and if an element of unit mass of the earth is at a distance ρ from the centre of the moon, this element of mass is attracted by the moon with the force $\kappa(M/\rho^2)$ where $\kappa =$ coefficient of gravitational force distance apart. The stability of the system earth-moon requires that

$$\sum \frac{4\pi^2 a}{T_0^2} = \sum \propto \frac{M}{\rho^2} \quad (\text{VIII.1})$$

and the summation should extend over all the particles of mass of the earth.

Although this relation is always fulfilled for the earth considered as a whole, this does not prove that for each point of the earth there is equilibrium between the attractive forces and the centrifugal forces acting at the point in question. In fact, this could hardly be expected, because the two forces obey different physical laws. Comparing these forces at any arbitrary point of the earth, we find residual forces, and these are the *tide-producing forces*. When the moon stands in the zenith, the forces of attraction are greater than the centrifugal forces in a point *Z* on the earth closest to the centre of the moon; both act in the direction of a line joining the centre of the earth with the centre of the moon. The resultant is the tide-producing force at the point *Z*; here it is directed against the moon (see Fig. 108). At the opposite

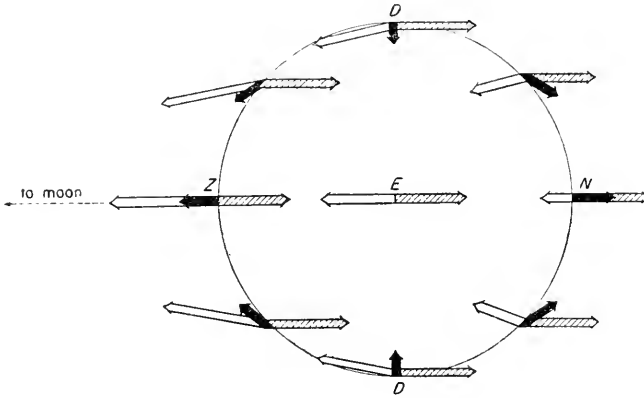


FIG. 108. Determination of intensity and direction of the tide generating forces resulting from the difference between attractive and centrifugal forces. \longrightarrow , open arrows: attractive forces; $\overline{\text{|||||}}$, hatched arrows: centrifugal forces; \blackrightarrow , black arrows: tide generating forces.

point *N*, where the moon stands in the nadir, the force of attraction is smaller than in *Z* and smaller than the centrifugal force. For this reason, the tide-producing force is directed away from the moon. Consequently, in both cases there is a force directed from the centre of the earth towards the outside. Thus, for any point on the earth's surface, we can compute the direction and the intensity of the resultant between the forces of attraction and the centrifugal force. The total sum of all these resultants all over the earth is zero, but at no point does this tide-generating force become zero, and it has everywhere a definite direction and force. A schematic drawing of the distribution of the tide-generating force in a meridional section in the direction earth-moon is shown in Fig. 108.

The tide-generating force can easily be computed for the zenith and nadir point. The forces of attraction and the centrifugal forces act in this case in the same direction and their resultants can be simply obtained by adding and subtracting their magnitudes respectively. The direction of the force towards the moon shall be positive. If R is the radius of the earth and a the distance between the centre of the earth the centre of the moon, M is the mass of the moon, μ an element of mass of the earth at the point under consideration, we obtain for the points

	Zenith	Centre of the earth	Nadir
The forces of attraction:	$+\varkappa \frac{\mu M}{(a-R)^2}$	$+\varkappa \frac{\mu M}{a^2}$	$+\varkappa \frac{\mu M}{(a+R)^2}$
The centrifugal force*:	$-\varkappa \frac{\mu M}{a^2}$	$-\varkappa \frac{\mu M}{a^2}$	$-\varkappa \frac{\mu M}{a^2}$
The tide-producing force:	$+\varkappa \mu M \left[\frac{1}{(a-R)^2} - \frac{1}{a^2} \right]$	0	$-\varkappa \mu M \left[\frac{1}{a^2} - \frac{1}{(a+R)^2} \right]$
or †	$+\varkappa \mu M \frac{2R}{a^3}$	0	$-\varkappa \mu M \frac{2R}{a^3}$. (VIII.2)

It is easy to see that these values are the maxima tide-producing forces which can be found on the earth's surface. Consequently, the tide-producing forces is proportional to the mass of the disturbing body and inversely proportional to the cube of the distance of the earth to the disturbing body. In the hemisphere facing the moon, the forces act in the direction towards the disturbing body, in the other hemisphere they act in the opposite direction, i.e. away from the moon.

It is easy to compare the tide-producing forces of the moon with those of the sun. For a point of the earth, the tide-producing force of the sun, according to (VIII.2), is given by $\varkappa \mu S(2R/s^3)$, in which S is the mass of the sun and s the distance sun-earth. When E is mass of the earth, the ratio of this force to that of the moon is then

$$\frac{S}{M} \cdot \frac{a^3}{s^3} = \frac{333,200E}{1/81.5E} \cdot \frac{(60R)^3}{(23,360R)^3} = 0.460 \sim \frac{4}{9} < \frac{1}{2}.$$

The mass of the sun being 27 million times that of the moon, the tide-producing force of the sun should be 27 million times that of the moon. However, the sun's distance from the earth is 389 times the moon's distance. Consequently, the sun's tide-generating force is to that of the moon in the ratio of 27×10^6 to 390^3 or 1:2.17, less than half that of the moon. This definitely explains why the influence of the moon is preponderant in ocean tides.

* The centrifugal force, according to (VIII.1), has been equalized in the centre of the earth with the negative attractive force.

† If R^2/a^2 is neglected against $2R/a$ then

$$\frac{1}{(a \mp R)^2} = \frac{1}{a^2} \left(1 \pm \frac{2R}{a} \right),$$

R/a being equal to $1/60$, this means neglecting $1/3600$ against $1/30$.

It is interesting to compare the tide-producing force with a force familiar to us, e.g. the force of gravity. If E is the mass of the earth, the gravity for a mass element μ on the earth's surface is in sufficient approximation

$$\kappa\mu(E/R^2)$$

and the ratio

$$\begin{aligned} \frac{\text{maximum tide-producing force of the moon}}{\text{force of gravity}} &= 2 \frac{M}{E} \frac{R^3}{a^3} = \\ &= 2 \frac{1}{81.5} \cdot \frac{1}{60^3} = \sim \frac{1}{9 \text{ million}} \end{aligned}$$

i.e. the tide-producing force of the moon is approximately a nine-millionth part of the force of gravity; it reduces gravity by that amount at the points N and Z and, therefore, this reduction of gravity is extraordinarily small.

One may get an idea of its minuteness considering that, under its action, the end point of a spiral spring, which is extended one meter by a 1 kg weight suspended to it, is displaced by the tide-producing force as little as

$$\frac{1}{9 \text{ million}} m = \frac{1}{9} 10^{-3} \text{ mm} = \frac{1}{9} \mu .$$

In the considerations put forth thus far on the tide-generating forces, the rotation of the earth around its axis in 24 h has been disregarded, since it does in no way influence the derivation of the tide-producing forces. It causes only relatively small changes in the shape of the earth's surface (revolution ellipsoid instead of a sphere) and a small change in the apparent weight of the individual unit of mass. Gravity is now the resultant of the attractive force and the centrifugal force of the rotation, but there is no modification in the magnitude and the direction of the tide-generating forces. The derivation of the tide-producing forces, as done here, was made by considering the "revolution" of the bodies around their common centre of gravity. This derivation seems to be the most simple and at the same time the most logical. Incorrect derivations, which are mainly due to a wrong interpretation of the influence exerted by the revolution or rotation of the two interacting bodies and which lead to forces of a different order of magnitude, have appeared in literature but soon disappeared. (see MÜLLER, 1916).

On the untenable flood theory by Galileo, developed before Newton, which regarded the tides as an effect of the relative motion between the solid earth and the oceans, see MACH (1904).

2. The system of Tide-producing Forces as a Function of the Zenith Distance

The distribution of the tide-generating forces can be derived for any arbitrary point on the earth, by extending the considerations given above for the points Z and N . Let B be such a point with the unit mass ($\mu = 1$) (see Fig. 109), E the centre of the earth and M the centre of the moon. Then

the force of attraction $A = \kappa(M/\varrho^2)$ acts in the direction BM , the centrifugal force $Z = (4\pi^2 a/T_0^2)$ in the direction parallel to EM . According to the third law of planetary motion by Kepler, which states that the squares of the

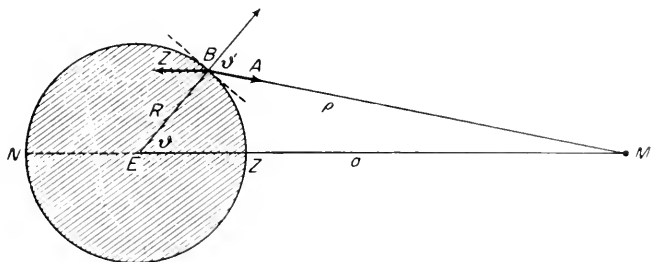


FIG. 109. Determination of the potential of the tide generating forces.

periods of revolution of the planets around the sun are in the same ratio as the cubes of their mean distances from the sun ($a^3/T_0^2 = \text{const.} = \kappa M/4\pi^2$) we can also write for $Z : Z = \kappa(M/a^2)$ and we obtain in the point B with the zenith distance of the moon ϑ for the horizontal and vertical components of the forces of attraction:

$$A_h = \kappa \frac{M}{\varrho^2} \sin \vartheta' \quad A_v = \kappa \frac{M}{\varrho^2} \cos \vartheta' ;$$

and of the centrifugal force:

$$Z_h = \kappa \frac{M}{a^2} \sin \vartheta, \quad Z_v = \kappa \frac{M}{a^2} \cos \vartheta .$$

It can easily be found from the triangle EBM that

$$\cos \vartheta' = \frac{a \cos \vartheta - R}{\varrho}, \quad \sin \vartheta' = \frac{a \sin \vartheta}{\varrho}, \quad \varrho = a \left(1 + \frac{R^2}{a^2} - \frac{2R}{a} \cos \vartheta \right)^{1/2} .$$

If, in developing $1/\varrho^3$ into a series, we neglect the term of a higher order, then we have

$$\frac{1}{\varrho^3} = \frac{1}{a^3} \left(1 + \frac{3R}{a} \cos \vartheta \right)$$

and we obtain for the two components

$$\left. \begin{aligned} K_h &= A_h - Z_h = \frac{3}{2} \kappa \frac{MR}{a^3} \sin 2\vartheta, \\ K_v &= A_v - Z_v = 3\kappa \frac{MR}{a^3} \left(\cos^2 \vartheta - \frac{1}{3} \right). \end{aligned} \right\} \quad (\text{VIII.3})$$

These forces have a potential

$$\Omega = \frac{3}{2} \kappa \frac{MR^2}{a^3} \left(\frac{1}{3} - \cos^2 \vartheta \right) = MR \left(\frac{1}{3} - \cos^2 \vartheta \right) \quad (\text{VIII.4})$$

if $\frac{m}{g} = \frac{3}{2} \frac{M}{E} \left(\frac{R}{a}\right)^3$. Then, if we take the horizontal component positive in the direction towards the point of the earth's surface lying perpendicular beneath the moon (against the point Z) then

$$K_h = \frac{1}{R} \frac{\partial \Omega}{\partial \vartheta} = m \sin 2\vartheta, \quad K_v = -\frac{\partial \Omega}{\partial R} = -\frac{m}{2} (\cos 2\vartheta + \frac{1}{3}). \quad (\text{VIII.5})$$

The quantity m is characteristic of the tide-generating force:

$$\frac{m}{g} = \frac{3}{2} \frac{M}{E} \left(\frac{R}{a}\right)^3 \quad (\text{VIII.6})$$

and one obtains:

$$\left. \begin{aligned} \text{for the moon } m/g &= 8.57 \times 10^{-8}, \\ \text{for the sun } m/g &= 3.78 \times 10^{-8}. \end{aligned} \right\} \quad (\text{VIII.7})$$

If a more correct value for the tide-producing potential Ω is required, we have to keep more terms in the development in series of $1/\varrho$, and then the best way is to develop $1/\varrho$ according to spherical functions of the zonal type $P_n(\vartheta)$. These P 's are functions of ϑ alone and are called zonal harmonics or Legendre coefficients. We obtain

$$\left. \begin{aligned} \frac{1}{\varrho} &= \frac{1}{a} \sum_{n=0}^{\infty} \left(\frac{R}{a}\right)^n P_n(\vartheta), \\ P_0(\vartheta) &= 1, \\ P_1(\vartheta) &= \cos \vartheta, \\ P_2(\vartheta) &= \frac{1}{2}(3 \cos^2 \vartheta - 1), \\ P_3(\vartheta) &= \frac{1}{2}(5 \cos^3 \vartheta - 3 \cos \vartheta), \\ P_4(\vartheta) &= \frac{1}{8}(35 \cos^4 \vartheta - 30 \cos^2 \vartheta + 3) \quad \text{etc.} \end{aligned} \right\} \quad (\text{VIII.8})$$

We then have

$$\Omega = -\varkappa \frac{MR^2}{a^3} \left[P_2(\vartheta) + \frac{R}{a} P_3(\vartheta) + \frac{R^2}{a^2} P_4(\vartheta) + \dots \right] = \Omega_2 + \Omega_3 + \Omega_4 + \dots \quad (\text{VIII.9})$$

As both P_2 and P_4 are symmetrical to the great circle $\vartheta = 90^\circ$, the same applies for the parts of Ω , which originate from these terms. An asymmetry between the two hemispheres with the moon above or below the horizon can only come from the terms Ω_3, Ω_5 , etc. The term Ω_3 reinforces the Ω_2 -part on the hemisphere where the moon is in the zenith and weakens it on the hemisphere where the moon is in the nadir. The most important term by far is Ω_2 , which corresponds to (VIII.4).

Equation (VIII.3) describes the distribution of the tide-producing forces by a body on the surface of the earth. The distribution of the total force is shown in Fig. 110. The circle represents a cut through the earth and the moon is at a great distance in the direction M . The arrows indicate the direction and the strength of the total force which result from the conflicting

attractive and centrifugal forces. The numbers indicated give the intensity, with the assumption that $m = \frac{1}{2}$. Over the entire hemisphere of the earth which faces the moon, the forces of attraction are greater than the centrifugal

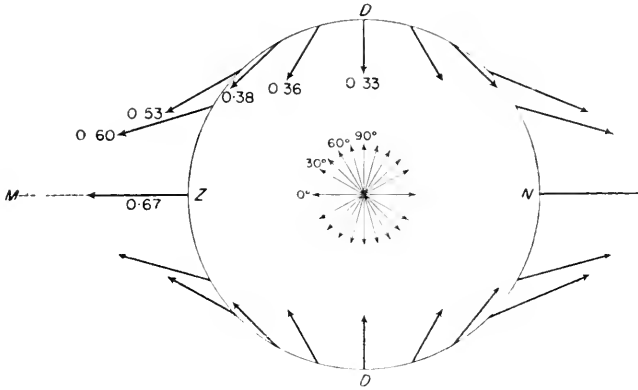


FIG. 110. Distribution of the total tide generating force of a celestial body in a meridional section of the earth.

forces; on the other hemisphere, the predominance is reversed. It has been found easier to consider separately the distribution of the two components given in equation (VIII.3).

The *radial component* has the same direction as gravity and its intensity is increased and decreased respectively, by very small amounts. It can, therefore, be considered as a tidal disturbance of the gravity, and it is then advisable to count it positively downwards (same as the force of gravity). From the second part of (VIII.3) then follows:

$$\delta g = -\frac{1}{2}m(\cos^2 \vartheta + \frac{1}{3}). \tag{VIII.10}$$

Its largest negative value is found in the zenith and nadir point, the largest positive value on a great circle 90° distant from the zenith point, and the ratio of these values is 2:1. The force disappears on the circles which are at a distance of $54^\circ 43'$ from the zenith, and the nadir point (nodal lines), respectively. This vertical component of the tidal force causes also an extraordinarily small periodical change in the density of the water-masses; however, this change contributes so little to the motion of the water that it can generally be completely disregarded.

Whereas the radial component can only influence the magnitude of the gravity very slightly, the *horizontal component* causes a slight change in its direction. Its main significance for the motions of the water-masses on the earth lies in the fact that its intensity equals the order of magnitude of other forces acting in the horizontal direction, which are mainly gradient forces. Its distribution, according to the first term of (VIII.3), is expressed by

$$K_h = m \sin 2\vartheta. \tag{VIII.11}$$

It is quite apparent that the horizontal component vanishes in the zenith and the nadir point, as well as on the great circle 90° distant therefrom and attains a maximum value on circles 45° distant from these points. On the hemisphere facing the moon, this horizontal force is directed concentrically towards the zenith point; on the other hemisphere it is directed towards the nadir point. This system of forces has a fixed position in regard to the tide-producing body; if the latter shifts, the system of forces follows this movement. Figure 111 shows, at the left, the distribution of the horizontal

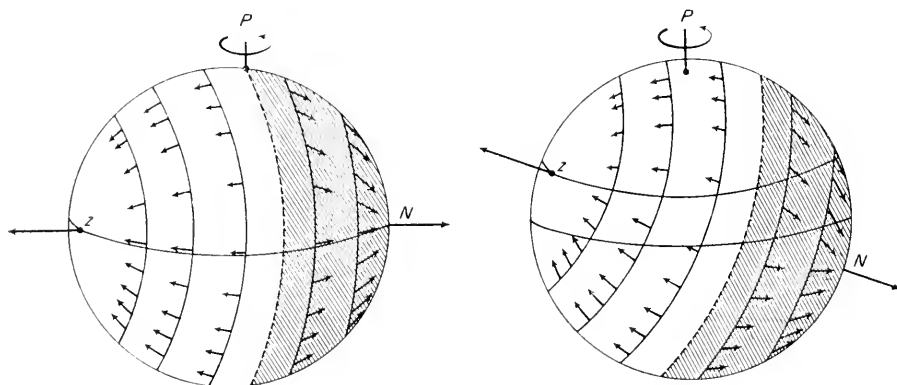


FIG. 111. Left: distribution of the horizontal component of the tide generating force when the moon is in the equator. Right: same when the moon has a positive declination of 28° N.

components when the disturbing body is located in the equatorial plane of the earth; at the right when it stands 28° above same on the northern hemisphere.

This system of forces is fixed in relation to the direction of the moon, meanwhile the earth rotates once a day around its axis, and these cause the entire system of tide-producing forces to become periodical for a given point of the earth's surface. If, for example, the moon's orbit is in the plane of the equator (see Fig. 112), it will appear to somebody who looks at the earth from the outside as if the observer is first in A_1 . The rotation of the earth moves him to A_2 . The tide-producing force is directed towards the south just before reaching A_2 and reaches its maximum value after three lunar hours in a point A_3 . Then the force decreases to zero at a point A_4 , where the moon sets. The force then changes its direction, reaches a maximum after 3 lunar hours, etc. The tidal force, therefore, changes its direction and force, with a period equivalent to a half lunar day. Both components have obviously the same period, but we can derive from the relations (VIII.9 and 10) that the phase of the horizontal component lags one-quarter period (3 h) behind the vertical component.

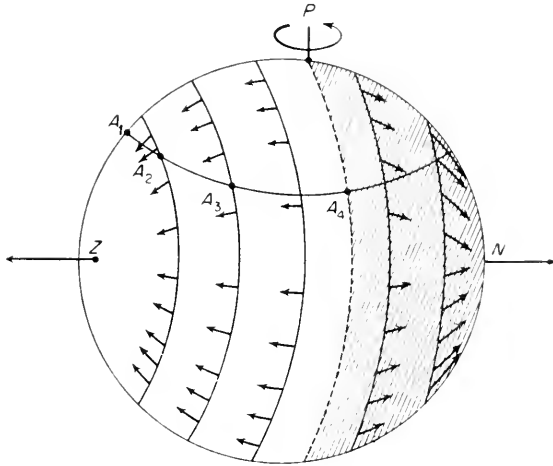


FIG. 112. The system of the horizontal component of the tide generating force at the surface of the earth. The disturbing body is in the zenith of the point Z.

3. The Harmonic Analysis of the Tidal Potential

As a consequence of the orbital motion of the disturbing body and of the diurnal rotation of the earth, the system of the tide-producing forces relative to the earth is changing constantly. The distance of the disturbing

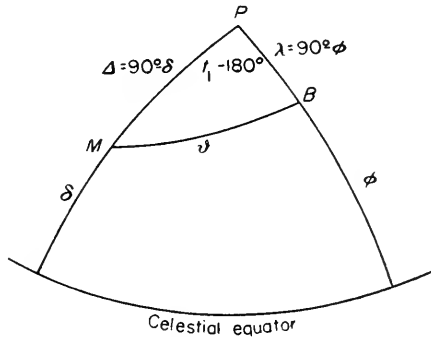


FIG. 113.

body *M* from the zenith depends upon its declination δ and upon the geographical co-ordinates ϕ and λ of the point *B* on the earth. In a spherical triangle in the sky *MPB* (*M* = disturbing body, *P* = celestial pole, *B* = observed point; see Fig. 113),

$$\cos \delta = \sin \phi \sin \delta + \cos \phi \cos \delta \cos(t + \lambda - 180^\circ)$$

if *t* is the real hour angle of the disturbing body (moon) in Greenwich, counted from the lower culmination. If we introduce the complementary angle (polar distances of *M* and *B*)

$$\Delta = 90^\circ - \delta \quad \text{and} \quad \zeta = 90^\circ - \phi$$

this relation can be written

$$\cos\theta = \cos\chi\cos\Delta + \sin\chi\sin\Delta\cos(t + \lambda - 180^\circ). \quad (\text{VIII. 12})$$

If we introduce this expression in (VIII.4), we obtain, if $\frac{1}{2}mR = A$

$$\begin{aligned} \Omega = A(\cos^2\Delta - \frac{1}{3})(3\cos^2\chi - 1) - A\sin 2\delta\sin 2\phi\cos(t + \lambda) + \\ + A\cos^2\delta\cos^2\phi\cos 2(t + \lambda). \quad (\text{VIII. 13}) \end{aligned}$$

Each of these terms can be considered as representing a partial tide (LAMB, 1932, p. 359).

(1) The first term does not contain the hour angle. As the declination varies only very slowly, it can be regarded for a short time as constant. In regard to χ , i.e. the geographical latitude ϕ , it represents (see $P_2(\delta)$ in VIII.8) a zonal harmonic of the second order and gives a tidal spheroid symmetrical with respect to the earth's axis having as nodal lines the parallels for which $\cos^2\chi = \frac{1}{3}$ or $\phi = \pm 35^\circ 16'$. The amount of the tidal elevation in any particular latitude varies as $\cos^2\Delta - \frac{1}{3} = \frac{1}{2}(\cos 2\Delta + \frac{1}{3})$.

The main declinational inequality has, in case of the moon, a period of one-half of the period of the variation of the declination, i.e. one half tropic month. We have here the origin of the lunar fortnightly or 'declinational' tide. When the sun is the disturbing body, we have a solar semi-annual tide.

(2) The second term is a spherical harmonic. The corresponding tidal spheroid has as nodal lines the meridian of which is distant 90° from that of the disturbing body, and the equator ($\phi = 0$). The disturbance of level is greatest in the meridian of the disturbing body, at distances of $45^\circ N.$ and $S.$ of the equator (Tesseral harmonic P_2'). The oscillation at any one place goes through its period with the hour angle, i.e. in a *lunar or solar day*. The amplitude is, however, not constant, but varies slowly with Δ , changing sign when the disturbing body crosses the equator. This term accounts for the lunar and solar 'diurnal' tides.

(3) The third term is a sectorial harmonic P_2^2 and gives a tidal spheroid having as nodal lines the meridians which are distant $45^\circ E.$ and W from that of the disturbing body. The oscillation at any one place goes through its period with 2χ , i.e. in *half a (lunar or solar) day*, and the amplitude varies as $\cos^2\delta$, being greatest when the disturbing body is on the equator. We have here the origin of the lunar and solar 'semi-diurnal' tides.

The expression (VIII. 13) shows the essential properties of the tide potential which varies with time, but it is not entirely satisfactory. Both the declination δ and the amplitude A are variable with time, because also the fluctuations in the distance between the earth and the disturbing body enter in the value m . A complete harmonic analysis of the tide potential requires Ω to be expanded in a series of simple cosine or sine-functions, with constant amplitudes and constant periods. The actual periods (e.g. lunar day and solar day) are not integer multiples of one fundamental period, but are incommensurable, and such an expansion is most intricate. The derivation of each expansion requires long and extensive computations. We will give here the fundamental idea.

Let us assume that a simple term in Ω has the form

$$\Omega_1 = U\cos(\sigma t - \alpha), \quad (\text{VIII. 14})$$

where U is not constant, but varies around an average value u with the frequency σ' , so that

$$U = u + u' \cos(\sigma' t - \alpha'); \quad (\text{VIII.15})$$

generally σ' is much smaller than σ (e.g. if U contains the fortnightly variation of declination, the period in σ' is approximately 14 days for the moon, and 6 months for the sun, whereas the period in σ is $\frac{1}{2}$ day for the moon and 1 day for the sun). Substituting in (VIII.14), we obtain

$$\Omega_1 = u \cos(\sigma t - \alpha) + \frac{1}{2} u' \cos[(\sigma + \sigma') t - (\alpha + \alpha')] + \frac{1}{2} u' \cos[(\sigma - \sigma') t - (\alpha - \alpha')]. \quad (\text{VIII.16})$$

Besides the variation with the frequency σ , which is to be considered as the fundamental one, there are two other oscillations with the amplitude $\frac{1}{2} u'$ which depends upon the variations of U , and with frequencies equal to the sum and difference of the two frequencies. The same can be done with two or more terms. The variables which determine the true motions of the sun and the moon, and which follow from such a development in sine and cosine terms are the following.

If θ is the sidereal time (hour angle of the vernal equinox), the hour angle of the sun is $\theta - h_1$, if h_1 is the real longitude of the sun eastward along the ecliptic. Whereas θ increases practically uniformly, h_1 increases irregularly in easterly direction. The sun is replaced by a fictitious sun supposed to move steadily around the ecliptic at a rate which is the average rate of the true sun and its longitude (h) is said to be the mean longitude of the sun, which increases also steadily. Then

$$t = \theta - h$$

is the *mean solar time*.

The same procedure is followed for the moon; if s is the mean longitude of the moon, then

$$\tau = \theta - s$$

is the *mean lunar time*.

From these relations follows:

$$\tau = t + h - s, \quad \text{where } D = s - h,$$

is the angular difference between the mean moon and the mean sun.

The other quantities appearing in Ω , like distance, declination, real hour angle, etc., can all be expressed by h and s and three other angles increasing uniformly. These are: p , the mean longitude of the lunar perigee, p_s , the mean longitude of the solar perigee, and $N' = -N$, in which N is the mean longitude of the ascending lunar node. These variables increase during a mean solar day by the following amounts, whereas the length of their period (time of a full revolution of 360°) is indicated beside:

τ	$360^\circ - 12.91^\circ$	24 h 50.47 min (lunar day)	p	0.1114°	8.847 years
s	13.176°	27.32 days (sidereal month)	N	0.0529°	18.61 years
h	0.986°	1 year	p_s	0.000047°	20940 years

DOODSON (1922, p. 305) and RAUSCHELBACH (1924) have given a full development of the tidal potential of the kind indicated above, whereas the earlier classical developments of DARWIN (1883, p. 49) and BOERGEN (1884, p. 305) have only taken into account the influence of the slow motion of the lunar node by slow variations in the amplitude and phase of the corresponding terms. For the rest, the fundamental idea is the same; it emanated from KELVIN (1872), who was the first to substitute fictitious celestial bodies for individual terms of the tide potential.

It is not possible to give here in all its details a harmonic analysis, (see for example BARTELS, 1936, p. 309; and, 1957, p. 734). We will only mention briefly the final result. Each term of the series corresponds to the equation (VIII.14) and Ω is the sum of all terms of this equation, which have the form:

$$\begin{aligned} \text{Partial tide} &= \text{numerical coefficient} \times \\ &\text{geodetic coefficient} \times \begin{cases} \cos \\ \sin \end{cases} (\text{argument}). \end{aligned} \quad (\text{VIII.17})$$

The geodetic coefficients are only dependent upon the geographical latitude ϕ ; the most important are those derived from Ω_2

$$G_0 = \frac{1}{4} mR(1 - 3\sin^2\phi),$$

$$G_1 = \frac{1}{2} mR\sin 2\phi,$$

$$G_3 = \frac{1}{2} mR\cos^2\phi.$$

The argument or the phase ($\sigma t - \kappa$) is an aggregate composed of the above-mentioned six variables; they determine the frequency of the term and, hence, its period. Thus, for instance, τ represents lunar time, $(\tau + s)$ sidereal time, $(\tau + s - h)$ solar time, 2τ the semi-diurnal lunar wave, etc. Abbreviating, the partial tides are designated according to their argument, and this is given symbolically by the "argument number". The argument $(2\tau - 3s + 4h + p - -2N + 2p_s)$ is given by the argument number (229.637): the first figure gives the factor of τ , whereas the following figures are the factors of the other variables increased by 5. The most important are the first 3 figures, inasmuch as they give positions which repeat themselves within a year. The last figure is generally left out. The first figure also gives the main distribution of the partial tides: 0 long periodical, 1 diurnal, 2 semi-diurnal, 3 the third diurnal partial tides.

The argument in (VIII.17) is composed of two parts: the variable part t (frequency \times time) and the phase, which is the non-variable part of the argument, which is given at the origin of time, usually the 1st of January of a year at 00.00 h.

The complete list of all components established by Doodson lists approximately 390, of which about 100 are long periodic, 160 diurnal, 115 semi-

diurnal and 14 one-third diurnal terms. Table 28a contains a selection of the more important components with their basic values, and it also indicates the symbol by which they are designated. The numerical coefficient of the largest component M_2 is put equal to 100. The amplitude ratios (refer to $M_2=100$) listed in Table 28a under column coefficient ratio are the most exact

Table 28a. Principal harmonic components

Name of partial tides	Symbol	cos sin	Argument	Speed per mean solar hour	Period in solar hours	Coefficient ratio $M_2 : 100$
Semi-diurnal components						
Principal lunar	M_2	cos	255.55	28.98410°	12.42	100.0
Principal solar	S_2	cos	273.55	30.00000	12.00	46.6
Larger lunar elliptic	N_2	cos	245.65	28.43973	12.66	19.2
Luni-solar semi-diurnal	K_2	cos	275.55	30.08214	11.97	12.7
Larger solar elliptic	T_2	cos	272.55	29.95893	12.01	2.7
Smaller lunar elliptic	L_2	cos	265.45	29.52848	12.19	2.8
Lunarelliptic second order	$2N_2$	cos	235.75	27.89535	12.91	2.5
Larger lunar evectional	ν_2	cos	247.45	28.51258	12.63	3.6
Smaller lunar evectional	λ_2	cos	263.65	29.45563	12.22	0.7
Variational	μ_2	cos	237.55	27.96821	12.87	3.1
Diurnal components						
Luni-solar diurnal	K_1	sin	165.55	15.04107°	23.93	58.4
Principal lunar diurnal	O_1	sin	145.55	13.94304	25.82	41.5
Principal solar diurnal	P_1	sin	163.55	14.95893	24.07	19.4
Larger lunar elliptic	Q_1	sin	135.65	13.39866	26.87	7.9
Smaller lunar elliptic	M_1	sin	155.65	14.49205	24.84	3.3
Small lunar elliptic	J_1	sin	175.45	15.58544	23.10	3.3
Long-period components						
Lunar fortnightly	Mf	cos	075.55	1.09803°	327.86	17.2 8.6
Lunar monthly	Mm	cos	065.45	0.54437	661.30	9.1 4.6
Solar semi-annual	Ssa	cos	057.55	0.08214	2191.43	8.0 4.0

according to the latest analysis of Doodson and differ slightly from previous computations by other authors. The signs refer to the equilibrium tide $\bar{\eta}$ (see p. 273). If we select from the complete list those whose relative numerical coefficient is ≥ 0.5 , we obtain 63 components, of which, however, quite a few are almost insignificant. In practice, one uses mainly the following 7 components:

- 4 semi-diurnal components: $M_2, S_2, N_2, R_2^{K_2}$, and
- 3 diurnal components: K_1, O_1, P_1 .

It is to be noticed that the luni-solar partial tide K_1 and K_2 are each composed of a lunar and a solar part. The ratio of these parts is the same as for the ratio of the total tidal forces of moon and sun (100:46). Hence, for K_1 $57.4 = 39.9 + 18.5$, for K_2 $12.7 = 8.7 + 4.9$.

The combination of the components K_1 (lunar part) $+ O_1$ which have almost identical numerical coefficients (39.9 and 41.5) gives the diurnal lunar tide. Neglecting the slight difference in the numerical coefficient, we have

$$\sin(\tau - s) - \sin(\tau + s) = -2\sin s \cos \tau :$$

this is a diurnal lunar tide with an amplitude varying monthly. The maxima occur at $s = 90^\circ$ and 270° , i.e. when the moon is in its greatest northern and southern declination respectively. The combination of P_1 and K_1 (solar part) with 19.4 and 18.5, will give, because

$$\tau + s - h = t = \text{solar time} ,$$

$$\sin(\tau + s - 2h) - \sin(\tau + s) = \sin(t - h) - \sin(t + h) = -2\sin h \cos t .$$

This is a diurnal solar tide with yearly variable amplitude; maxima occurs at $h = 90^\circ$ and 270° , respectively, which is at the time of the solstices and the zero values at the time of the equinoxes. This presentation, which can be extended to the K_2 -values, shows it makes equal sense to interpret K_1 and K_2 either as seasonal variable solar tides or as monthly variable lunar tides. This is because $\tau + s = t + h$.

4. The Experimental Proof of the Tide-generating Forces

If one had in the laboratory an absolutely rigid base, one could measure the horizontal component of the tide-generating forces by means of the oscillations of a pendulum, which coincides with the plumb-line when at absolute rest (variations in the direction of the plumb-line). The vertical component of this force could be measured by means of the time variations in the weight of a small body (variations in gravity). These observations should give the exact amount of the variations of these components, which were derived theoretically from the system of tide-generating forces. The variations in the plumb-line and in gravity observed in this manner are denoted as tidal oscillations and these should fully agree, in case of an entirely rigid earth, with the theoretical ones.

The maximum value of these variations can easily be derived from the equations (VIII.10 and 11), along with the numerical values in (VIII.7). For the maximum acceleration in the horizontal and vertical direction relative to gravity, we obtain

	in the horizontal	in the vertical
for the moon:	8.57×10^{-8}	11.43×10^{-8}
for the sun:	3.78×10^{-8}	5.04×10^{-8}

The maximum deflection of the plumb-line then becomes $\Delta\psi = \varrho''$ times horizontal acceleration, which is 0.0177'' for the moon and 0.0078'' for the sun, whereas the maximum disturbance of the gravity is 0.114 mgal for the moon and 0.050 mgal for the sun.* It is obvious that only extremely sensitive

* ϱ'' is $\frac{180^\circ}{\tau} = \frac{1}{\sin 1''}$, and 1 gal = 1 cm sec⁻², 1 mgal = 0.001 gal.

instruments are able to determine such extraordinarily small variations and that first a very advanced measuring technic should be developed, in order to obtain perfect results.

Horizontal pendulums are used for measuring small periodical disturbances of the plumb-line. Such a pendulum consists in principle of a rod movable in horizontal direction and which can turn around an *almost* perpendicular axis (see Fig. 114). If this axis were exactly perpendicular, such a pendulum

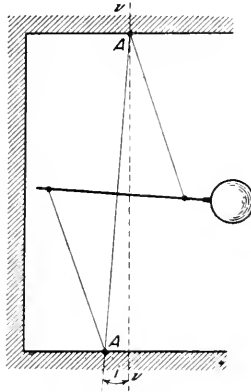


FIG. 114. Basic idea of Zollner horizontal pendulum.

could be swung by any lateral force, however small, but it would soon be immobilized in this position after the force ceases to act (indifferent equilibrium). However, if the axis AA of the pendulum is slightly inclined against the vertical line VV (by a small angle i), small lateral forces still can move the pendulum out of its position of rest; however, when the force ceases, it returns automatically to the initial position of rest by a component of the force of gravity. The amount of the deviation from the position of rest is an indication as to the intensity of the force. Bifilar suspension of the rod and photographic registration strongly reduce frictional influences. As only forces transverse to the plane of the pendulum cause the latter to rotate, two horizontal pendulums placed perpendicularly to each other are needed for measuring the west-east and the north-south component of the tide-generating force. Great precautions are to be taken in these measurements, because the apparatus, of course, reacts upon any inclinations of the base supporting it. Such inclinations can also, by all kinds of external circumstances (e.g. temperature variations of the upper layers of earth, etc.), easily take such proportions as to cause deflections which are greater than those of the tidal forces. For a review of measurements on gravity, see Schweydar (1921). A long series of measurements was made by Schweydar (1921) in a mine gallery (depth 189 m) in Freiburg (Saxony), and by SCHAFFERNICHT (1937, p. 349); (see also TOMASCHEK and SCHAFFERNICHT, 1932, p. 787) in a 25 m deep cave

in Marburg a. L. The most important features can be found in Fig. 115. It shows the variation of the direction and force of the tide-generating force with time for the principal lunar component M_2 in Freiburg and Marburg, derived by harmonic analysis. The results are similar for the other semi-

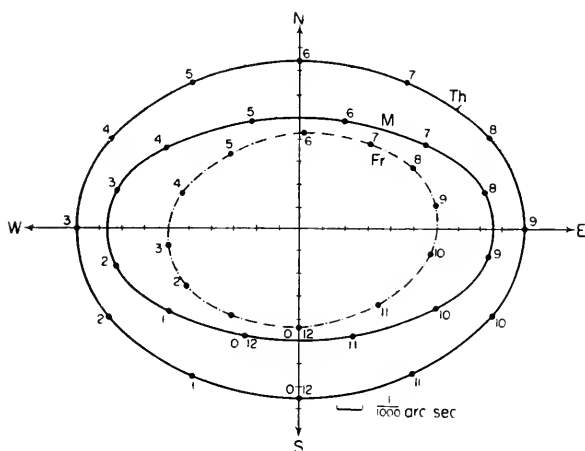


FIG. 115. Variation in direction and intensity of the horizontal component of the tide generating force for the principal lunar tide M_2 . *Th*: computed values for a rigid earth; *M* and *F*: observed values at Marburg a. L. and Freiburg i. S. (Tomaschek and Schaffernicht).

diurnal and diurnal components. There is no doubt that the plumb-line deviates through the action of the tidal forces. This proves the presence of the horizontal components of the tidal forces. However, the ellipses are considerably smaller than they should be theoretically, and there also appear slight deviations in the phase. Mean values from several components give as ratio of the amplitudes 0.6, but here a difference between semi-diurnal and diurnal terms cannot be established for sure. There is also a phase shift of about $1\frac{1}{4}$ h, which may be somewhat smaller for diurnal components. The decrease of the amplitudes can only be explained if the earth is not completely rigid, but that it yields somewhat to the tide-generating forces; hence, that there are tides of the solid earth.

This result has been fully confirmed by measurements of the periodic variations of gravity caused by the vertical component of the tide-generating forces.

In recent times Tomaschek and Schaffernicht were successful in constructing an instrument which provides useful results, namely, the Bifilargravimeter.

The discussion of the long series of measurements made in Marburg and in Berchtesgaden has shown that the observed periodical variations in gravity are only about two-thirds of the value computed for a rigid earth and that there are also small phase displacements. Figure 116 gives for the principal lunar tide M_2 the curves from observations made simultaneously at both

localities during two months. The decrease in amplitude as compared to the theoretical value is approximately identical at both localities, except that Marburg lags behind the moon by 1 h, whereas Berchtesgaden precedes it by

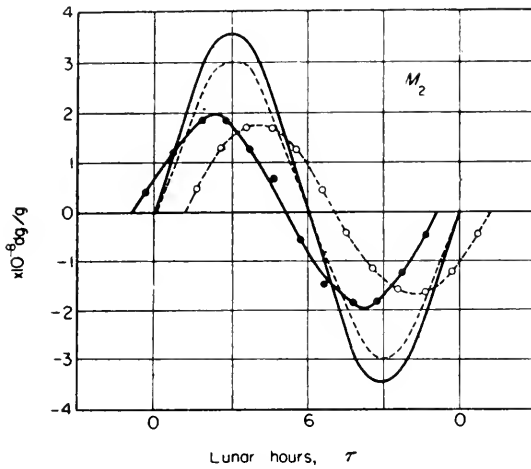


FIG. 116. Variation in the force of gravity for the lunar tide M_2 at Marburg a. L. (—o—o—) and Berchtesgaden (—•—•—) compared with the values computed for a rigid earth (---- for Marburg, — for Berchtesgaden). Passage of the moon through the meridian at 9 h.

approximately 1 h. Hence, it is proven that there are also variations of the vertical components of the tidal forces.

In connection with the results of the measurements with horizontal pendulums, it has become possible to get an idea of the elastic tides of the solid earth, which is of great importance for geophysics.

For further details we refer to the textbooks on geophysics.

Chapter IX

Theory of the Tides

1. The Equilibrium Theory

IN order to visualize the effect of the tide-generating forces on an ocean covering uniformly the whole earth, we can use the presentation of the horizontal components given in Fig. 111. Under the action of this system of forces, the water tends to flow towards the points Z and N and accumulation of water occurs at these convergence points, while at the great circle with a distance of 90° from these points the sea level lowers. These flood protuberances originating in the zenith and nadir increase only until there exists an equilibrium between the tide-generating forces and the horizontal forces provided by the differences in pressure. Then the flood protuberance at the surface has a fixed position in the direction of the moon (Fig. 117).

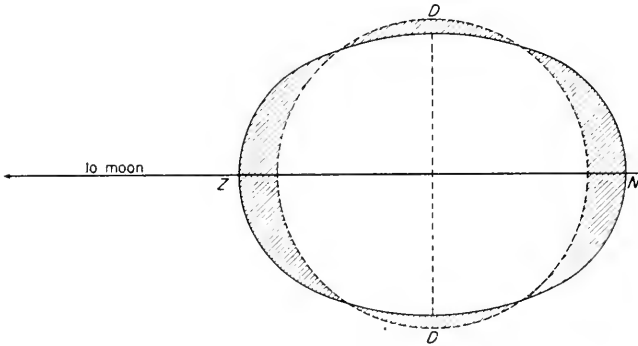


FIG. 117. Flood protuberance caused by the action of the tide generating forces on an ocean covering the entire earth.

Newton, who developed the equilibrium theory of tide, was conscious of the fact that treating the tides as a *static problem* was only a rough approximation of the phenomenon. The equilibrium theory of the tides was completed 50 years later when the Paris Academy of Science asked for the best mathematical and physical explanation of the tides. BERNOULLI, EULER and MACLAURIN (1741) were among the contestants. The work of Bernoulli is of quite some interest still today.

In the equilibrium theory of the tides, the free surface is assumed to be

a level surface under the combined action of gravity, and of the disturbing force. The sum of the potentials of these forces must be constant at this surface. Then no work will be performed when a particle of water is moved along the surface. This can also be expressed by saying that the pressure force and the tide generating force must be in equilibrium at any point. If $\bar{\eta}$ denotes the elevation of the water above the undisturbed level, then gravity potential is $g\bar{\eta}$, and the above condition requires that $g\bar{\eta} + \Omega = \text{constant} = C$, or

$$\bar{\eta} = -\frac{\Omega}{g} + C$$

when Ω denotes the disturbing potential.

If we put $mR/g = H$, we obtain with (VIII.4)

$$\bar{\eta} = H(\cos^2\theta - \frac{1}{3}) + C, \quad (\text{IX.1a})$$

$$H = \frac{3}{2} \frac{M}{E} \left(\frac{R}{a}\right)^3 R \quad (\text{IX.1b})$$

in which M = mass of the moon; a = distance moon-centre earth; E = mass of the earth; R = earth's radius, θ = moon's zenith distance.

The equilibrium form of the free ocean surface is a harmonic spheroid of the second order, of the zonal type, whose axis passes through the disturbing body. If we consider first a disturbing body alone, its equilibrium flood $\bar{\eta}$ attains a maximum for $\theta = 0^\circ$ and 180° , i.e. when the disturbing body is in the zenith or the nadir and $\bar{\eta}_{\max} = \frac{2}{3}H$ and a minimum for $\theta = 90^\circ$, which is when the disturbing body is on the horizon and $\bar{\eta}_{\min} = -\frac{1}{3}H$; the amplitude of the oscillation is, therefore H .

If we put $R = 6370$ km, we have

$$H = \frac{\text{lunar tides}}{0.55 \text{ m}} \quad \frac{\text{solar tides}}{0.24 \text{ m}} \quad \frac{\text{combined effect of both}}{0.79 \text{ m}}.$$

Owing to the diurnal rotation of the earth and to the orbital motion of the disturbing body, there are periodic variations in $\bar{\eta}$ for a given point of the earth's surface; their periods are exactly the same as those of the tide potential discussed on page 263. We have for $\bar{\eta}$ the same developments as in (VIII.13); only we now have to substitute $\frac{1}{3}H$ for A . Consequently, there are three kinds of partial tides in the equilibrium theory: long period, diurnal and semi-diurnal tides, and all that was discussed on the subject that the harmonic analysis of the tide potential can be applied without restriction to the partial tides of the equilibrium theory. The different terms constituting the tide-potential Ω can be expressed in the quantity $\bar{\eta}$, and this is the usual form in which it is presented.

We will discuss the combined action of the moon and the sun in connection with the semi-diurnal tides. If we introduce in the equation (VIII.13)

the amplitude varying with declination, $A = \frac{1}{2}H\cos^2\phi\cos^2\delta$ then we can consider this variation for a short time to be constant for a point on the earth. If, we introduce the sidereal time θ and the right ascension a instead of the hour angle of the disturbing body, (see p. 265) we obtain for the combined semi-diurnal lunar and solar tide, the equilibrium tide

$$\bar{\eta}_3 = A\cos 2(\theta - a) + A'\cos 2(\theta - a') \quad (\text{IX.2})$$

in which the quantities marked with a prime refer to the sun. The superposition of these two waves can be imagined to give a single wave with variable amplitude and phase. If we put: $\theta - a' = \theta - a + (a - a')$

$$\bar{\eta}_3 = A_3\cos 2(\theta - a + \alpha_3) \quad (\text{IX.3})$$

in which

$$A_3 = \sqrt{A^2 + A'^2 + 2AA'\cos 2(a - a')} \quad \text{and} \quad \tan 2\alpha_3 = \frac{\sin 2(a - a')}{A + A'\cos 2(a - a')}.$$

The amplitude A_3 will have a maximum when $a = a'$ and $a = a' + 180^\circ$. This happens at the conjunction and opposition of moon and sun, e.g. at the time of the syzygies or at full and new moon. These are the spring tides. At the same time, $\alpha_3 = 0$, i.e. the spring tides appear at the moment $\theta = a$ and $a + 180^\circ$, which is at the upper and lower culmination of the moon, which for full and new moon coincides with midnight and noon.

The minimum of A_3 occurs when $a - a' = 90^\circ$ and 270° , which is at the time of the quadratures (first and last quarter of the moon respectively). $\bar{\eta}_3$ then becomes smallest; these are the neap tides. In this case too $\alpha_3 = 0$, and $\bar{\eta}_3$ is reached when $\theta = a$, i.e. again at the upper and lower culmination of the moon, which at this time occurs approximately at 6 h and 18 h. At any other time α_3 is different from zero and high water does not occur at the moon's transit, but this phase displacement is not very large (semi-monthly inequality in the time of occurrence).

The combined action of the principal lunar and solar tides as seen by an observer at the equator is illustrated in Fig. 118 drawn by BIDLINGHANGER (1908). The upper part shows the conditions at full and new moon. At noon both bodies are in the zenith, the water level is $1\frac{1}{2}$ times as high as for the lunar tide alone (spring tide). The next figure shows the position for the first and the last quarter. At 6 a.m., when the sun rises, the moon is at the zenith, lunar and solar tide oppose each other (neap tide). The following figures show halfway between spring and neap tide, neap and spring tide respectively. In the first case, the moon is in the 1st and 5th octant and reaches its highest point at 9h, whereas the sun and its tide are still rising. High water is retarded by about an hour against the culmination of the moon. In the second case (3rd and 7th octant) the moon goes through the meridian at 3 a.m., whereas the nadir flood of the sun passed three hours earlier. Hence, high water appears approximately an hour before culmination of the moon.

The *daily* inequality in height and time can be easily understood from the illustrations of Figs. 119 and 120. If the disturbing body is not upon the equator, the axis of rotation of the spheroid does not coincide any more with the axis of the earth (see Fig. 117). In Fig. 119 are shown isohypses of the spheroid for both hemispheres, when the disturbing body (moon) stands in 28° N. latitude in the zenith above the centre meridian. The corresponding point then lies on the other hemisphere

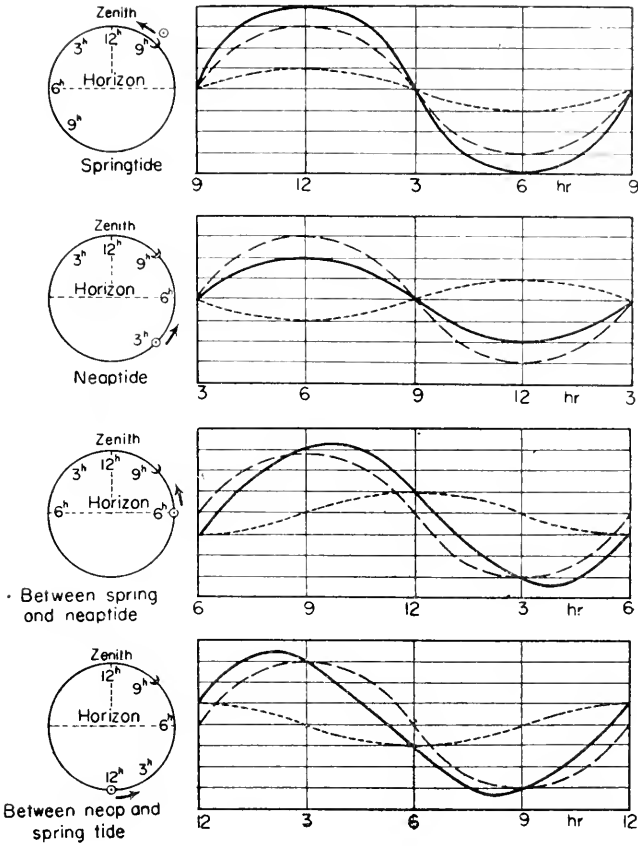


FIG. 118. Interaction between principal lunar and solar tides for different positions of the sun and moon. Schematic apparent course of the sun (☉) and moon (☾) in the sky. At the start of the tide curve (left) both sun and moon occupy the indicated positions in the apparent orbit. They have travelled 180° at the right end of the curves. Indicated time given the position of the sun at that particular time. The --- line shows the principal lunar tide, the - · - · - ·, the principal solar tide, the ———, the combination of both tides. Sun and moon are assumed to occupy during 12 h the same position with respect to each other (Hann-Bidlingmaier).

in 28° S. latitude. During the diurnal rotation of the earth around its axis, a point at the equator has no daily inequality, as can be readily seen from Fig. 120; at 10° N. latitude a zenith tide of 24 cm corresponds with a nadir tide of 14 cm. At 30° S. lat. conditions are still more extreme, the zenith tide having only a range of 5 cm, whereas that of the nadir tide is 28 cm; the former remains permanently below the mean water level.

The equilibrium theory of the tides is able to explain many facts related to the ocean tides but, on the other hand, a comparison with the observations shows its insufficiency. There is agreement insofar as spring tide always appears at full moon and new moon, neap tide at the quadratures; furthermore, the height of spring tide is at least three times that of neap tide. How-

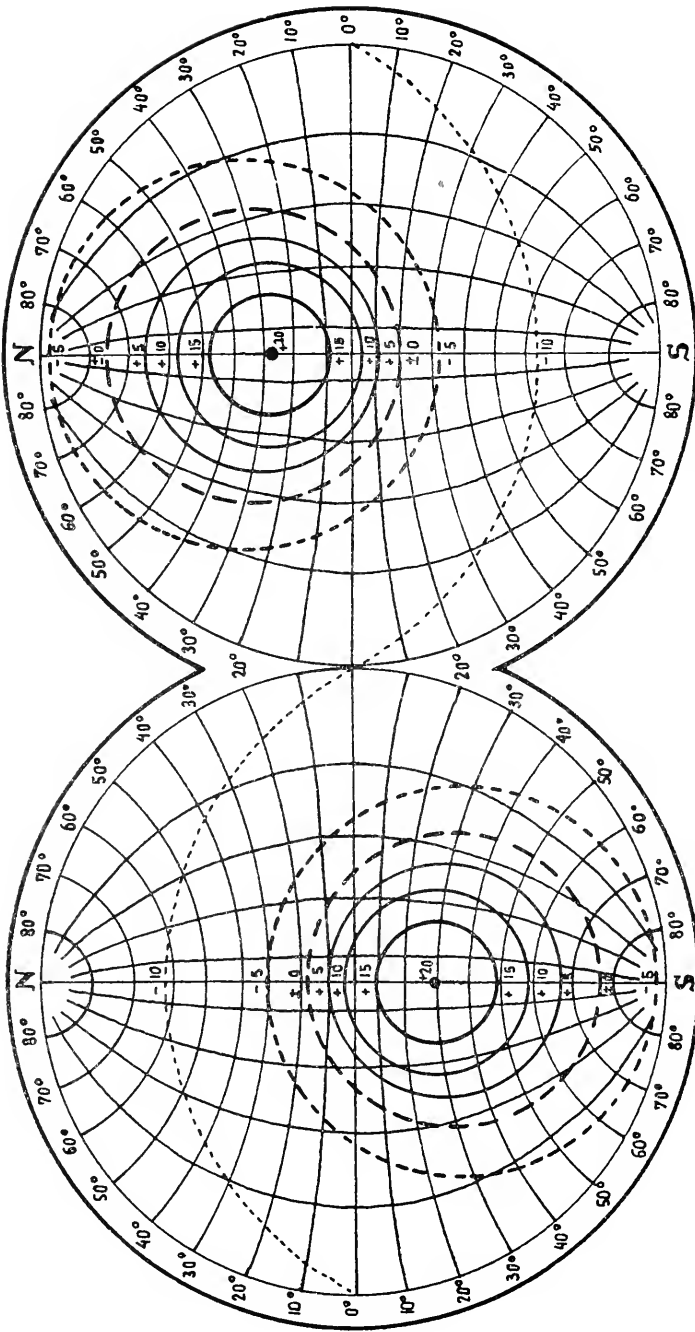


FIG. 119. Planispheric map showing the daily inequality.

ever, the observed tides are generally much greater than those derived from the equilibrium theory. On the other hand, the daily inequality of the theory agrees with the observations insofar as it will disappear when the tide-generating body is at the equator and will reach a maximum at the times of greatest northerly and southerly declination. The magnitude of the daily inequality does not agree with the theory, and in many localities the tide is largest when it should be the smallest according to the theory and vice versa. Furthermore, the theory requires that at the syzygies (full and new moon) high water occurs

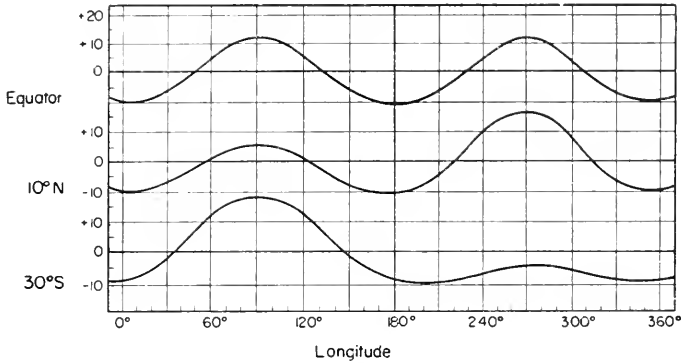


FIG. 120. Profile for three circles of latitude from Fig. 119.

exactly at noon and at midnight; hence, that the lunar tidal interval is zero for all localities. According to experience, this interval can have any value between zero and 6 h, and it is apparent that we have here a downright contradiction between the observations and the theory.

The equilibrium theory, therefore, is unfit to explain the actual tides of the oceans. The main reason is, no doubt, that it attributes certain properties to the water which it definitely lacks. The theory requires that, at any moment, there is equilibrium between the tide-producing forces and the gradient forces of the zonal spheroid. Inasmuch as the tide-producing celestial bodies change their position to the earth so rapidly after all, tremendous displacements of water-masses should take place within the ocean with great velocities which never occur in nature, and the water-masses would go beyond their position of equilibrium because of its inertia. Hence, the equilibrium theory requires that the water be deprived of its inertia, whereas its gravitational properties should be kept. Such an assumption, however, has no basis and can only give approximate results, if the tidal forces vary very slowly. This theory, therefore, can be applied at the most to the long-period partial tides.

Despite this bad agreement, it has frequently been attempted to improve the noticeable difference between the time of occurrences of high water and the time of maximum tide potential. The constant C in (IX. 1a) is determined

by the condition, that the volume of the ocean is constant and the integration must extend over the entire ocean surface S . If the ocean covers the whole earth, then $C = 0$, by the general property of spherical surface harmonics. However, in case of a limited ocean C depends on the distribution of land and water on the globe. If the tide-producing potential according to (VIII. 17) consists of terms of the form $A_s G \cos(\sigma t + s\lambda)$ where A is the numerical coefficient and G the Goedic coefficient and S is an integer and if we abbreviate

$$P = \int_S G \cos(s\lambda) dr, \quad Q = \int_S G \sin(s\lambda) dr$$

we obtain for the partial tide produced by this term

$$\eta_s = \frac{A_s}{g} \left\{ \left[G \cos(s\lambda) - \frac{P}{S} \right] \cos \sigma t - \left[G \sin(s\lambda) - \frac{Q}{S} \right] \sin \sigma t \right\}. \quad (\text{IX. } 3b)$$

The integrals P , Q and also S , the surface of the oceanic area, can be computed by mechanical quadratures, and certain corrections are added to the previous values, which also depend upon the relative motion of the disturbing body. These corrections were primarily derived by THOMSON and TAIT (1883 para. 808) and, later on, they were examined more closely by DARWIN and TURNER (1886), and it was then found that they are quite unimportant with regard to the actual distribution of land and water. However, it became apparent that, in this improved equilibrium theory "corrected for the continents", the time of high water does no longer coincide with the maximum of the tide potential, i.e. that there is an "establishment" which is different for each locality.

A further improvement consists in considering the mutual attraction of the water particles. To the tide potential of the disturbing body comes the gravitation potential of the elevated water-masses in the tidal spheroid. If the ocean covers the entire earth Ω is increased by

$$-\frac{3}{5} \frac{\varrho}{\varrho_m} g \bar{\eta}$$

in which ϱ is the density of the water, ϱ_m the mean density of the earth and $\varrho/\varrho_m = 0.18$. Thereby the amplitude H increases in the proportion

$$\frac{1}{1 - \frac{3}{5} (\varrho/\varrho_m)}$$

which factor is 1.12. The consideration of the gravitation potential of the elevated water increases the equilibrium tide by 12%. In addition to this, POINCARÉ (1910, p. 60) has taken into account the distribution of land and sea. The calculations then became very intricate and the resulting improvement seems to be so important that the above-mentioned formulae are no longer accurate, even approximately.

2. The Dynamical Theory of the Tides

A century after NEWTON (1774), Laplace substituted for the equilibrium theory, which considers the tides hydrostatically, a dynamical theory. According to this theory, the tides are considered as waves induced by rhythmical forces and, therefore, have the same periods as the forces. The problem of the tides thus becomes a problem of the motion of fluids. In the development of these forced tide waves, various factors other than the periodic forces play a decisive part, like the depth and the configuration of the ocean basin (its morphologic configuration), the Coriolis force and frictional influences of various kinds. The tide generating forces are known with great accuracy, so that there is no difficulty in establishing the hydrodynamical equations for the corresponding motion of the water particles. The first equations of this kind were derived by Laplace. The general equations of the dynamical theory have not been solved yet insofar as the tides of the oceans are concerned: we need simplifications to solve the equations. These simplifications are based in the first place on the fact that the tide waves belong to the group of the "long waves", for which reason the latter are also designated as tidal waves.

The tidal motion belongs, insofar as it is generated and maintained by external periodical forces, to the forced waves; however, it is obvious that, especially when fulfilling the boundary conditions, "free waves" will also appear. The importance of these free waves, which fix the natural periods of the oscillatory system, becomes particularly evident if one considers that the amplitude and the phase of the forced oscillation are determined (see p. 8) by the difference between the free oscillation period of the system and the period of the force. However, perfect resonance occurs only very seldom and when it does, a closer consideration of the frictional influences is necessary.

The dynamical theory of the tides is extremely intricate in its details and requires, even if ideal conditions are assumed for the depths and the contours of the oceans, considerable mathematical work. LAPLACE (1775-76, 1799) succeeded in computing the theoretical tides of a homogenous ocean covering uniformly the entire earth, but the results are, in general, very poor and without much importance for the comprehension of the terrestrial tides of the seas. Only in recent times have they gained importance in connection with atmospheric tides. It appears that only lately, methods have been developed which to some extent take into account the complicated contours of the oceans and which, therefore, promise more success.

(a) *The Theory of Laplace*

The hydrodynamical equations of motion in polar co-ordinates (R radius of the earth, ϑ pole distance, λ geographical longitude) are:

$$\frac{du}{dt} - 2\omega v \cos \vartheta + 2\omega w \sin \vartheta = -\frac{1}{R+z} \frac{\partial}{\partial \vartheta} \left(\Omega + \frac{p}{\rho} \right),$$

$$\frac{dr}{dt} + 2\omega v \cos \theta = -\frac{1}{R \sin \theta} \frac{\partial}{\partial \lambda} \left(\Omega + \frac{p}{\rho} \right),$$

$$\frac{dw}{dt} + 2\omega u \cos \theta = -\frac{\partial}{\partial z} \left(\Omega + \frac{p}{\rho} \right).$$

The external force X, Y, Z has a potential Ω if it can be represented by

$$X = -\frac{1}{R} \frac{\partial \Omega}{\partial \theta}, \quad Y = -\frac{1}{R \sin \theta} \frac{\partial \Omega}{\partial \lambda}, \quad Z = -\frac{\partial \Omega}{\partial z}.$$

In these equations the frictional terms have been neglected. If we neglect the vertical acceleration which is small compared to the acceleration of gravity and neglect also the vertical component of the Coriolis force, which is for all practical purposes without importance, the third equation of motion is reduced to the hydrostatic equation. If we put $\rho = 1$ and substitute R for the depth $R+z$ assuming z is small in comparison with the earth's radius and, further, if we consider that $p \sim g\eta$ and $\bar{\eta} = -\Omega/g$ the two first equations of motion can be written:

$$\left. \begin{aligned} \frac{\partial u}{\partial t} - 2\omega v \cos \theta &= -\frac{g}{R} \frac{\partial}{\partial \theta} (\eta - \bar{\eta}), \\ \frac{\partial v}{\partial t} + 2\omega u \cos \theta &= -\frac{g}{R \sin \theta} \frac{\partial}{\partial \lambda} (\eta - \bar{\eta}). \end{aligned} \right\} \quad (\text{IX.4})$$

To this we have to add the equation of continuity for variable water depth h ,

$$\frac{\partial \eta}{\partial t} + \frac{1}{R \sin \theta} \left\{ \frac{\partial h u \sin \theta}{\partial \theta} + \frac{\partial h v}{\partial \lambda} \right\} = 0.$$

If the tide-producing potential is of a periodical nature, u, v and η will be also, and we can assume that all these quantities contain the time factor $\exp \{i(\sigma t + s\lambda + \epsilon)\}$, where s is an integer. These equations become, if the depth h is only a function of θ , and if the boundaries to the sea coincide with parallels of latitude:

$$\left. \begin{aligned} i\sigma u - 2\omega v \cos \theta &= -\frac{g}{R} \frac{\partial}{\partial \theta} (\eta - \bar{\eta}), \\ i\sigma v + 2\omega u \cos \theta &= -\frac{igs}{R \sin \theta} (\eta - \bar{\eta}), \\ i\sigma \eta &= -\frac{1}{R \sin \theta} \left\{ \frac{\partial h u \sin \theta}{\partial \theta} + i s h v \right\}. \end{aligned} \right\} \quad (\text{IX.6})$$

u and v can be computed as functions of η from the two first equations and if these values are introduced into the third equation, we obtain a differential equation for η alone, whose solution gives the tide waves generated and

forced by the tide-producing forces in an ocean covering the entire earth. According to the selection of s , there are various kinds of these waves.

(1) $s = 0$ gives, according to the designation of Laplace, the “oscillation of the first species”. These oscillations are independent of the rotary motion of the earth and depends wholly upon the motion of the disturbing body in its orbit. The periods of these oscillations are very long and to these belong particularly the fortnightly lunar tide and the semi-annual solar tide.

(2) $s = 1$ gives the “oscillations of the second species”, the most important of which is the diurnal lunar and solar tides.

(3) $s = 2$ are the “oscillations of the third species”: which include the semi-diurnal lunar and solar tides.

We can only explain here the fundamental solutions for these three types of oscillations, following the simplified explanations of KELVIN (1875, p. 279); AIRY (1845); DARWIN (1886, p. 377); LAMB (1932, p. 330).

If we put

$$\begin{aligned} \eta - \bar{\eta} &= \eta', & \frac{\sigma}{2\omega} &= f, & \frac{\omega^2 R}{g} &= m, \\ \beta &= \frac{4mR}{h} = 4 \frac{\omega^2 R^2}{gh} & \text{and} & & \mu &= \cos\theta \end{aligned} \quad (\text{IX.7})$$

a simple computation in the case $s = 0$ gives as the differential equation for η

$$\frac{\partial}{\partial \mu} \left(\frac{1 - \mu^2}{f^2 - \mu^2} \frac{\partial \eta'}{\partial \mu} \right) + \beta \eta = 0. \quad (\text{IX.8})$$

If, in this equation, we assume $\eta' = \eta$ we obtain the free oscillations of the ocean. If there were no rotation ($f = \infty$ and $\beta f^2 = \sigma^2 R^2 / gh$), the free oscillations would be given by $\sigma^2 = n(n+1)gh/R^2$ (n an integer); the simplest oscillations have the form of spherical surface harmonic functions. In the case of rotation, Laplace introduces in (IX.8) a solution of $\bar{\eta}$ in series of increasing powers of μ and determines their coefficients from the boundary conditions. This leads to their determination in the form of infinite continued fraction. This famous solution of Laplace has led to controversies between AIRY (1842), FERREL (1874) and KELVIN (1875, p. 227); however, the latter has given the proof of its correctness and has developed it.

Under natural conditions, these continued fractions, and the series for η , converge rapidly. For the shortest period of this oscillation, for which the elevation of the free surface behaves like a zonal spherical harmonic function of 2nd order $P_2(\cos\theta)$ we obtain, e.g. for a depth of 17,700 m and 2210 m the values 11 h 35 min and 32 h 49 min respectively.

The *forced oscillations* of the first species ($s = 0$) start with the potential

$$\bar{\eta} = A_1 \left(\frac{1}{3} - \cos^2\theta \right) \cos(\sigma t + \epsilon).$$

The determination of the coefficients to solve η is made in a similar way as

for the free oscillations. In the case of the fortnightly lunar tide, f is the ratio of a sidereal day to a lunar month and is 0.0365. Thus, f^2 becomes = 0.00133 and we obtain a very good approximation in putting $f = 0$, which shortens the computation considerably. The same applies for the other tides with a long period. The result can be found in the first lines of Table 29 under

Table 29. Ratio of the polar and equatorial tides to their respective equilibrium values

		$\beta \dots$	40	20	10	5	g/g_0
Depth (ft)...			7260	14,520	29,040	58,080	
(m)...			(2210)	(4430)	(8850)	(17,700)	
Long-period tides	Equator	Laplace	0.455	—	0.708	0.817	0
		Hough	0.426	0.551	0.681	0.796	0.181
	Pole	Laplace	0.154	—	0.470	0.651	0
		Hough	0.140	0.266	0.443	0.628	0.181
Semi-diurnal tides (uniform depth)	S_2 Equator	Laplace	-7.434	-1.821	+ 11.259	+1.924	—
		Hough	-7.955	-1.502	-234.87	+2.139	—
	M_2 Equator	Hough	-2.419	-1.800	+ 11.07	+1.922	—
		$[\sigma/2\omega = 0.96350]$					

Laplace. They give the ratios of the range of these partial tides to the range of the corresponding tides of the equilibrium tide at the equator and at the pole, for four different depths of the ocean. These ratios show that the long-period tides, at the considered depths, are everywhere direct, i.e. high water always occurs simultaneously with that of the equilibrium tide though; the position of the nodal lines will, of course, shift somewhat from the positions given by the equilibrium theory. For a depth corresponding to the actual mean depth of the oceans this tide is less than half that of the equilibrium value and it approximates this equilibrium value more and more when the water depth becomes very large, with consequent decrease of β .

The forced oscillations of the second species ($s = 1$) which include the lunar and solar diurnal tides, have a disturbing potential corresponding to a tesseral harmonic of the second order. This gives

$$\bar{\eta} = A_2 \sin \vartheta \cos \vartheta \cos(\sigma t + \lambda + \epsilon),$$

in which σ does not differ very greatly from ω . Here also the computation is considerably simplified if we select $\sigma = \omega$, which means that the proper motion of the disturbing body is neglected and therefore $f = \frac{1}{2}$. With this

assumption, the equations have a solution and we can calculate the forced oscillations, if the depth of the ocean follows the law $h = h_0(1 - c \cos^2 \theta)$, where c is any given constant. From this follows that, if the water depth is h_0 at the equator, it will be $h_0(1 - c)$ at the pole. We obtain by simple computation

$$\eta = \frac{2ch/mR}{1 - 2ch/mR} \eta = -\frac{8c}{\beta - 8c} \eta \quad \text{when} \quad \beta = \frac{4mR}{h}.$$

This relation shows first of all that the ratio of the tidal ranges is everywhere constant in relation to those given by the equilibrium tide; further, that $\eta = 0$, when $c = 0$, i.e. *in the case of uniform water depth, there are no diurnal tides in the ocean* so far as the rise and fall of the surface is concerned. However, although there is no rise and fall of the surface, there are, nevertheless, diurnal tidal currents. Laplace derived this remarkable result from his theory, and considered it very important, in view of the fact that the diurnal partial tides are almost completely absent in the European waters; in fact, he wanted to show by this that the dynamic theory is able to do away with the discrepancy between the observations and the results of the equilibrium theory. However, the diurnal tides having proved to be large at many points of the ocean, this conclusion had to be discarded.

With the *oscillations of the third species* ($s = 2$), which includes the lunar and solar semidiurnal tides, the disturbing potential of the tidal force is a sectorial harmonic of the second order, hence

$$\eta = A_3 \sin^2 \theta \cos(\sigma t + 2\lambda + \varepsilon)$$

in which σ is nearly equal to 2ω . The computation can be considerably simplified, assuming that the orbital motion of the disturbing body is very slow, so that $\sigma = 2\omega$ and therefore $f = 1$. This approximation is rough for M_2 , but there is a "luni-solar" semi-diurnal tide whose speed is exactly 2ω if we neglect the changes in the planes of the orbits. If here the depth is assumed to change according to $h = h_0 \sin^2 \theta$, (at the equator the water depth h_0 , at the pole zero) there is a solution

$$\eta = -\frac{8}{\beta - 8} \eta = -\frac{2h/mR}{1 - (2h/mR)} \eta.$$

In this case too, the ratio of the tidal range to that of the equilibrium tide is constant, but as $\beta > 10$ for depths existing actually in the ocean, the tide is everywhere inverted, i.e. there where the equilibrium tide is high, low water occurs, and vice versa. It should be noted that at the pole the depth becomes zero ($\theta = 0$) and consequently the velocity at the pole becomes infinite.

Laplace has also derived the semi-diurnal tide ($s = 2, f = 1$) for a sea of uniform depth. In this case, there are again continued fractions for the de-

termination of the coefficient of the series. For these a separate procedure of computation is given. The result for the equator can be found in Table 29 in the line "semi-diurnal tides, Laplace". It is found at once that the tides at the poles are direct for all depths. They are also direct at the equator, when the depth of the ocean is greater than 26,250 ft (8000 m); the range becomes practically equal to the equilibrium value when the depth becomes larger. Between 29,000 ft (8850 m) and 14,500 ft (4430 m) there must be a *critical depth*, for which the tide at the equator changes from direct to inverted. Not far below 7250 ft (2210 m) there seems to be soon a second critical value; with smaller depths the tide is again direct. With inverted tide at the equator and direct tide at the poles, there must be one or more pairs of nodal circles $\eta = 0$ symmetrically situated on both sides of the equator. With $h = 7250$ ft (2210 m), this nodal line is at a geographical latitude of about $\pm 18^\circ$.

(b) *Hough's Theory*

120 years after the theory of Laplace, HOUGH (1897, p. 201; 1898, p. 139; see also HILLEBRAND, 1913) has given a further development and an improvement of the Laplace theory. He substituted expansions in spherical harmonics for the series of powers of $\cos \vartheta$ and $\sin \vartheta$; these expansions offer the advantage of converging more rapidly, otherwise the computations are similar to those of Laplace, but he succeeds in considering also the mutual attraction of the particles of water. In Table 29, the values of Laplace have been compared with those of Hough, for the long-period tides. The influence of the mutual attraction consists in a decrease of the amplitude, however this decrease is not especially large except in the periods of the free oscillations, which for ocean depths of 58,100 ft (17,700 m) and 7250 ft (2210 m) are reduced to 9 h 52 min and 18 h 4 min respectively (see previous reference).

The free oscillations of the second and third species ($s = 1$ and $s = 2$) have been especially analysed by Hough. Two waves of equal amplitude travelling around the earth in opposite directions (with and against the rotation) will give by their superposition on a non-rotating earth standing oscillations in a form of spherical harmonic functions. On the rotating earth the waves will have different velocities of propagation, so that normal standing oscillations are split up into waves having the character of tesseral ($s = 1$) and sectorial ($s = 2$) spheric harmonics travelling westward and eastward. The waves travelling westward are more important, as they are faster than those travelling eastward and because they have the same direction as the tidal forces. Table 30 gives the period in sidereal time for these oscillations "of the first class" which are of most importance in relation to the diurnal and semi-diurnal tides, for different depths. At the same time certain steady motions which are possible without change of level, where there is no rotation are converted into long-period oscillations with change of level. The corresponding moves are called as "of the second class". The quickest oscillation of the

Table. 30. Periods of oscillations of "the first class" on a rotating earth in sidereal time

	$\beta \dots$	40	20	10	5
	Depth (ft)...	7260	14,520	29,040	58,080
	(m)...	2210	4,430	8,850	17,700
No rotation $\omega = 0$	—	32 h 49 min	23 h 12 min	16 h 25 min	11 h 35 min
Second species $s = 1$	Westward	14 h 41 min	12 h 51 min	11 h 5 min	9 h 8 min
	Eastward	24 h 24 min	19 h 16 min	14 h 50 min	11 h 6 min
Third species $s = 2$	Westward	17 h 59 min	14 h 52 min	12 h 1 min	9 h 24 min
	Eastward	38 h 34 min	26 h 54 min	18 h 40 min	12 h 55 min

second class has in each case a period of over a day and the periods of the remainder are very much longer (LAMB, 1932, p. 350).

As regards the *forced oscillation of the second species* ($s = 1$), Laplace's conclusion that when $\sigma = \omega$, the diurnal tide vanishes in the case of uniform depth, still holds. The computation for the most important lunar diurnal tide, for which $\sigma/\omega = 0.92700$, shows that with such depths as we have considered the tides are small compared with the equilibrium heights and are in the main inverted.

Of the *forced oscillations of the third species* ($s = 2$) we note first the solar semi-diurnal tide, for which $\sigma = 2\omega$ with sufficient accuracy. In Table 29 we have listed under S_2 the ratio of the dynamical tide height to the equilibrium tide height at the equator. A comparison with Laplace's values in this table shows that the influence of the attractive forces of the flood protuberance is to increase the ratio of the tide to the equilibrium tide. The very large coefficient for $\beta = 4\omega^2 R^2/hg = 10$ indicates that for this depth the period of the free oscillation of semidiurnal type differs but slightly from half a day, which means we have nearly resonance. Table 30 shows, in fact, that when $\beta = 10$, the period is 12 h 1 min. We see then that though, when the period of forced oscillations differs from that of one of the types of free oscillations by as little as 1 min, the forced tide S_2 may be nearly 250 times as great as the corresponding equilibrium tide; whereas a difference of 5 min between these periods will be sufficient to reduce the tide to less than 10 times the corresponding equilibrium tide. It seems then that the tides will not tend to become excessively large, unless there is very close agreement with the period of one of the free oscillations. The critical depths for which the forced tides become infinite are those in which a period of free oscillations coincides exactly with 12 h. They may be computed by putting $\sigma = 2\omega$ in the period equation for the free oscillations and solving this equation for the determination of h .

The corresponding critical depths for the solar semi-diurnal tide are about 28,182 and 7375 ft (8894 and 2248 m). For the depths between these two values the tide is inverted.

Hough has also computed the lunar semi-diurnal tides for which $\sigma/2\omega = 0.96350$. The ratios for the same four depths have been entered in Table 29. One can see that the critical depths are now somewhat displaced; they lie near 26,050 and 6450 ft (7938 and 1965 m). However, for the mean ocean depths existing on the earth all semi-diurnal tides are always inversed.

(c) *Tides in Bounded Ocean Basins*

GOLDSBOROUGH (1913, p. 31, discussion by DOODSON, 1928, p. 541) has given a solution for a polar basin of uniform depth bounded by one or two parallels of latitude. The difficulties, in this case as in all similar cases, are in the fulfilment of the boundary conditions (transverse velocity zero at the limiting parallel of latitude). Table 31 gives the amplitude of the tide for

Table 31. *Component tides in a polar basin limited at 60° latitude*

(Ratio of the amplitudes to the amplitudes given by the equilibrium theory)

Depth (ft)	At the Pole (long-period tides)	At the 60 lat. boundary		
		Long-period tides	Diurnal tides	Semi-diurnal tides
7260 ft (2210 m)	0.100	-0.216	-2.86	1.070
14,250 ft (4430 m)	0.133	-0.247	-1.16	1.030
29,040 ft (8850 m)	0.158	-0.269	-0.194	1.014
58,080 ft (17,700 m)	0.176	-0.276	+0.386	1.003

a polar basin limited at 60° latitude. Similar conditions are to be found for a limit of $\phi = 75^\circ 30'$. The long-period tides are unimportant and the semi-diurnal tides are practically equal to those of the equilibrium theory. The diurnal tides vary considerably with the size of the basin and the depth and are as a rule large, whereas in a uniform ocean covering the globe they are negligible. This will show very clearly the great influence of limitation. The large ratios for a small depth indicate an intensification of the diurnal tides in the polar waters, which actually occurs in the observed tides. The diurnal tides are quite prominent, as the semi-diurnal tides are weak. Goldsborough found that the greatest critical depth for a resonance of the semi-diurnal tides is about 160 m when the basin is limited at 60° latitude, and about 12 m when the boundary is at 75½°. The smallness of these depths against the real ones excludes completely stronger semi-diurnal tides. GOLDSBOROUGH (1914, p. 207;

1928, p. 692) has also treated the case of an ocean extending from pole to pole and bordered by two meridians (bi-angle on the sphere). The mathematical difficulties become greater and require working with an infinite number of functions, in order to meet the condition that, for the semi-diurnal tides, the velocity perpendicular to the equator be zero, same as at the shores of the ocean. Goldsborough has further given a solution for the case that the depth varies with the square of the cosine of the latitude and is bordered by two meridians which are 60° apart. The mean depth has been selected at 15,500 ft (5200 m). The conditions are roughly like those of the Atlantic Ocean. He had found previously that large semi-diurnal tides cannot develop in a polar basin for the given depths, from which he inferred that the Atlantic Ocean cannot get its large semi-diurnal tides from the Polar Ocean through simple propagation; they must be increased through resonance. This seems to be confirmed by the fact that the critical depth in the case under consideration is about 16,880 ft (4800 m), whereas the mean depth of the Atlantic Ocean is about 12,700 ft (3900 m). The condition of resonance would be fulfilled at this depth by a bi-angle with an opening of 53° .

PROUDMAN and DOODSON (1928, p. 32) have contributed important papers to the problem of tides in bounded oceans. The former has extended Taylor's method, which he used for the computation of the tides in a rectangular basin and which was discussed on p. 210, to ocean basins with a different configuration. He reduced it in a general way to an infinite system of linear equations, which can be solved according to the method of the infinite determinants. He thus was successful in deriving the tides of a semi-circular ocean of uniform depth. An application of this solution is given in the discussion of the tides of the Black Sea, which can be approximately compared with a sea of this form. Much more difficult is the computation of the tides of a *hemispheric ocean bordered by a complete meridian*. Doodson has developed a numerical method of integration of his own, which, however, has not yet been applied in practice. GOLDSBOROUGH (1931, p. 689; 1933, p. 241) has also dealt with this problem, but his method is rather complicated and there are no numerical results. PROUDMAN (1916, p. 1; 1931, p. 294) has recently shown that a solution of an infinite series of simultaneous equations takes care of the problem, but that the solution of a finite number of equations can already give a quite sufficient approximation. The mathematical developments are very difficult and the work in connection with the numerical computation, even for one single depth, is most extensive. Such computations have been made by DOODSON (1936, p. 273; 1938, p. 311) for the partial tide K_1 ($\sigma = \omega$) and K_2 ($\sigma = 2\omega$) for various depths. The essential results of these important investigations are given summarily as follows.

In the following figures the tide is represented by lines of equal phase (co-tidal lines) and by lines of equal amplitude (co-range lines). The numbers on the co-tidal lines represent the phase in degrees. The zero-value is the phase

given by the equilibrium theory for the central meridian. The amplitude for K_1 is given in a ratio to the amplitude of the equilibrium theory. For the semi-diurnal tide K_2 , on the contrary, the maximum amplitude has been taken equal to one and the lines 0.8, 0.6, 0.4, 0.2 have been drawn "solid". For each case, the amplitude can be computed relative to the maximum value of the equilibrium theory H with the aid of a coefficient. Only a quadrant of the entire ocean has been described, as there is always symmetry to the equator and to the central meridian.

It is shown that, for the diurnal tide K_1 , there is resonance for the depths of 26,510 ft (8080 m) and 9449 ft (2880 m). Figure 121 illustrates the tide for the cases $\beta = 0, 20$ and 30.63 , which corresponds to the depths $\infty, 14,520$ ft (4420 m), and 9449 ft (2880 m). $\beta = 0$ gives the equilibrium tide. Tide ranges at zero occur at the equator and at the pole, and the tide wave travels from east to west in the shape of co-tidal lines converging towards the pole. Decreasing depth influences especially the tide at the pole. Whereas here the amplitude was previously zero, it now reaches there the maximum, and the co-tidal lines do not converge any longer towards the pole; at the boundary meridian there is a constant variation of the phase from the equator to the pole. The changes in the tidal picture beyond the first resonance depth are not great, but a point where the amplitude is zero, namely, an amphidromy, can be spotted in the central meridian. This form then appears clearly with the second resonance depth of 9449 ft (2880 m); this amphidromy governs the entire picture of the ocean, while, in a most characteristic way, the large amplitudes remain in the vicinity of the pole. In the equatorial section of the ocean, the variations in phase are only slight, with very small amplitudes. With further decreasing depth, the central amphidromy splits up apparently in two parts; one lies in the western, the other one in the eastern quadrant, but the amplitudes are very small. Large amplitudes only occur in the polar regions where the whole phenomenon of the diurnal tide is concentrated.

Figure 122 shows three cases of the semi-diurnal tide K_2 . The first case applies again for $\beta = 0$ and gives the equilibrium tide. We notice a star-shaped distribution of the co-tidal lines around the pole with a regular propagation of the tide from east to west with maximum amplitudes at the equator. If the depth becomes smaller, the amphidromic distribution of the co-tidal lines moves southward (northern hemisphere) on the central meridian and at $\beta = 2$ (depth 44.3 km) a well-developed amphidromy appears at approximately 52° . With further decreasing depth this amphidromy splits in two; with $\beta = 6$ (depth 14.8 km) each quadrant is governed by an amphidromy with a positive direction of rotation (counter-clockwise). The picture becomes more and more complicated with further decreasing depth, so that with $\beta = 18$ (depth 4.92 km) each hemisphere has already 3 amphidromies (two in the positive, one in the negative sense of rotation), as shown by the centre picture in Fig. 122. With a depth of 14,500 ft (4430 m)

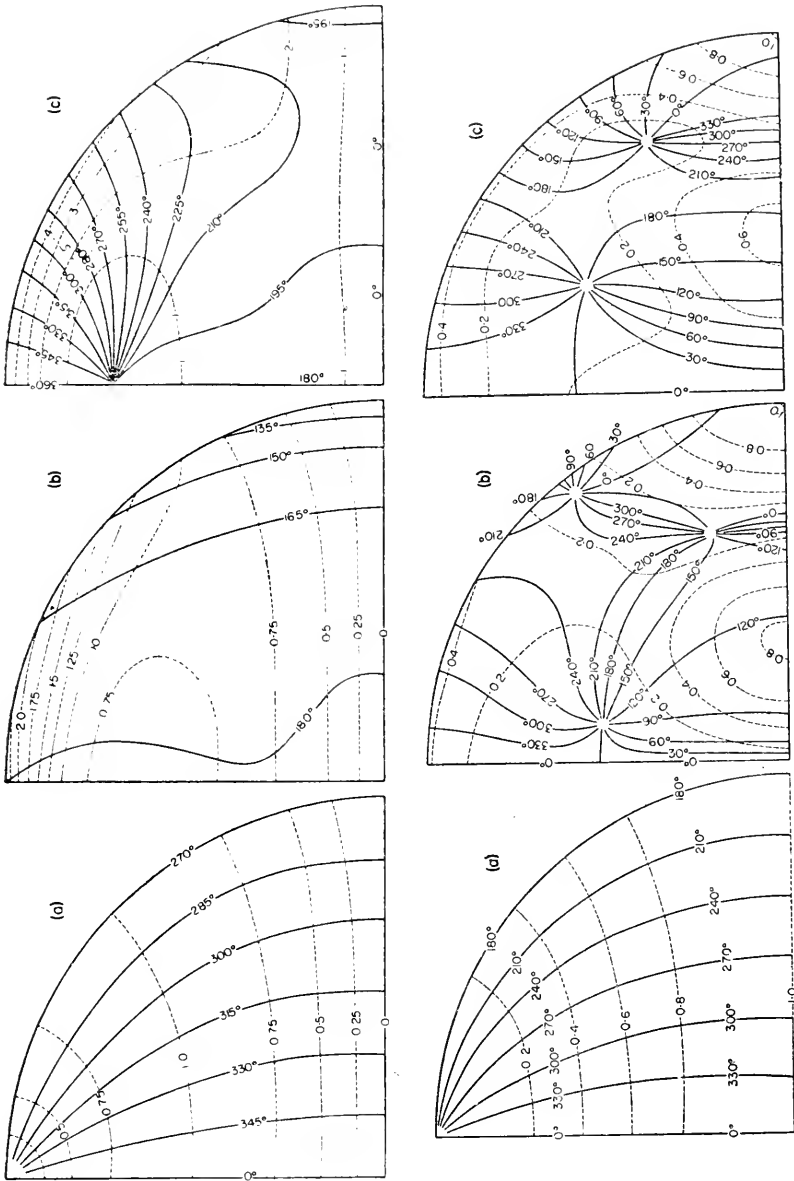


FIG. 121. Diurnal component K_1 : co-tidal lines (dotted lines); for $\beta = 0$ (infinite depth, equilibrium tide); for $\beta = 20$ (depth 14,498 ft, 4420 m); and for $\beta = 30.63$ (depth 9446 ft, 2880 m, resonance) (Doodson).
 FIG. 122. Semi-diurnal component K_2 : co-tidal and co-range lines. $\beta = 0$ (equilibrium tide-factor = H); $\beta = 18$ (depth 16,138 ft, 4920 m, factor = $-6.03H$); $\beta = 20$ (depth 14,498 ft, 4420 m, factor = $+6.57H$) (Doodson).

approaching the real depths of the oceans, there remain in each quadrant two positively rotating amphidromies. The tidal range is largest at the boundary with the maximum occurring at the equator at the western and the eastern points.

These investigations of Proudman and Doodson are undoubtedly of great importance for the future tidal research. Surveying the theory of the tides, we recognize how, starting from the simple equilibrium theory and progressing by way of the Laplacian dynamic theory of the tides in an ocean covering uniformly the whole earth, it arrives at the study of the tides of bounded seas. These studies lead to results that are comparable to the tides in the actual seas bounded by the continents. So far, the most important knowledge is the occurrence of *systems of amphidromies*, which sometimes may comprise the whole or parts of an ocean. When a large number of such theoretical tidal pictures have been computed for different depths and limits of the oceans, they will form a good basis for the understanding of the observed tidal features.

3. Canal Theory of the Tides

The Laplacian theory started from the assumption of an ocean covering the entire earth and considered only recently the land masses bounding the seas. AIRY (1845) has attempted to solve the phenomena of the tides by a study of the oscillatory processes in narrow canals covering the whole earth or parts of it (see LAMB, 1932, p. 267). He thus became the founder of the "canal theory of the tides"; he has treated this theory exhaustively in his famous paper "Tides and waves". Although, in many respects, it can hardly claim today the same significance it had previously, it still offers many interesting features, especially for the explanation of the tides in narrow sections of the oceans, in straits and estuaries.

(a) Canal of Uniform Depth Extending all over the Earth

In chapter VI, paragraph 1 we discovered the tide waves in a canal of constant rectangular cross-section. The pertaining equations of motion (VI.8) were expressed in the horizontal and vertical displacements of the water particles ξ and η . On account of the assumed narrowness of the canal, the transverse motions and the influence of the Coriolis force are neglected. For a continuous canal of a uniform depth h coincident with the earth's equator, it is appropriate to introduce the geographical longitude λ (counted from a fixed meridian eastward) instead of the x -co-ordinate. The equations then take the form ($c^2 = gh$, R the radius of the earth):

$$\frac{\partial^2 \xi}{\partial t^2} = c^2 \frac{\partial^2 \xi}{R^2 \partial \lambda^2} \quad \text{and} \quad \eta = -h \frac{\partial \xi}{R \partial \lambda}. \quad (\text{IX.9})$$

The free oscillations of such a canal can be easily derived therefrom: one obtains

$$\xi = (A_s \cos s\lambda + B_s \sin s\lambda) \cos(\sigma_0 t + \varepsilon) \quad (\text{IX.10})$$

in which s is an integer and $\sigma_0 = S(c/R)$. These normal oscillations are simple harmonic with the period $T_0 = 2\pi R/sc$. The free waves all travel with the velocity c and travel around the circumference of the earth in a time T_0 . The most important free wave for the theory of the tides is the one which needs 24 h to travel around the equator. The necessary velocity is 900 nm/h or 1670 km/h, and to it corresponds an ocean depth of 72,160 ft (22 km). For smaller ocean depths the waves travel slow (e.g. for $h = 16,400$ ft (5000 m), $c = 432$ nm/h or 800 km/h, and $T = 50$ h), for greater depths more rapidly. The free wave can only keep pace with the sun when the depth is 13 nm or 22 km; for the free wave moving with the moon the critical depth is 12.5 nm or 20.5 km.

For the oscillations forced by a periodic horizontal tidal force, the force K_h has to be added to the right term of the first equation in (IX.9). This force is $K_h = m \sin 2\theta$, according to equation (VIII.11), if θ is the zenith distance of the tide-producing body.

The simplest case is, when the disturbing body (moon) describes a circular orbit in the equatorial plane of the earth with the apparent angular velocity $n = \omega - n_1$ when $\omega =$ angular velocity of the earth's rotation and $n_1 =$ angular velocity of the moon in her orbit. Then, according to (VIII.12), $\theta = nt + \lambda + \varepsilon$ and the equation of motion can be written

$$\frac{\partial^2 \xi}{\partial t^2} = \frac{c^2}{R^2} \frac{\partial^2 \xi}{\partial \lambda^2} - m \sin 2(nt + \lambda + \varepsilon). \quad (\text{IX.11})$$

For the tides or forced waves we have, if we put

$$\begin{aligned} \frac{nR}{c} &= p, \\ \xi &= -\frac{mR^2}{4c^2} \frac{1}{1-p^2} \sin 2(nt + \lambda + \varepsilon), \\ \eta &= \frac{H}{2} \frac{1}{1-p^2} \cos 2(nt + \lambda + \varepsilon) = \frac{H}{2} \frac{1}{1-(\sigma^2/\sigma_0^2)} \cos 2(nt + \lambda + \varepsilon). \end{aligned} \quad (\text{IX.12})$$

According to (VIII.18), we have $H = mR/g$ (for the moon 55 cm, for the sun 24 cm) and $\sigma = 2n$ is the frequency of the forced oscillation, $\sigma_0 = 2c/R$ the frequency of the free oscillation ($s = 2$). $\frac{1}{2}H$ is the amplitude of the tide producing force, so that $\frac{1}{2}H \cos 2(nt + \lambda + \varepsilon)$ represents the tide according to the equilibrium theory.

The tide is therefore semi-diurnal (the lunar day being of course understood), and, when $p > 1$ or $c < nR$ and $\sigma > \sigma_0$ it is inverted; on the contrary when $p < 1$ or $c > nR$ and $\sigma < \sigma_0$ it is direct. The second form of the equation for the amplitude of η corresponds to the equation (I.9) and one sees

that, when the period of the force corresponds to the period of the free wave, there is *resonance*. This is the case for the sun, when the depth of the canal is 22 km or 13 nm, and for the moon when the depth is 20.5 km or 12.5 nm. In the actual case of the earth we have

$$\frac{\sigma_0^2}{\sigma^2} = \frac{g}{n^2 R} \cdot \frac{h}{R} = 311 \frac{h}{R}.$$

For the oceans h/R is about $\frac{1}{6000}$ at its maximum, and σ will always be larger than σ_0 so that the tides of the ocean will be inverted at the equator. The tides which are caused by the disturbing bodies are not large; their amplitude for a depth of 1300 ft (4000 m) is only 6 cm. For greater depths the tide becomes larger, but the tides remain inverted until the critical depth of 22 km or 13 nm; for depths beyond this limit the tides become direct and approximate more and more values of the equilibrium theory.

If the canal is not in the equator, but parallel to a circle of latitude ϕ , whereas the orbit of the disturbing body remains in the equatorial plane, then

$$\cos \vartheta = \cos \phi \cos(nt + \lambda + \epsilon)$$

and we have

$$\eta = \frac{H \cos^2 \phi}{2} \frac{1}{1 - p^2 \cos^2 \phi} \cos 2(nt + \lambda + \epsilon). \quad (\text{IX.13a})$$

If $c < nR$, the tides will be direct or inverted, depending on whether $\cos \phi \geq c/nR$. Therefore, it is possible that in higher latitudes the tides are opposite to the tides in lower latitudes.

If the moon be not in the plane of the equator, but has the pole distance Δ , we have to use for $\cos \vartheta$ the equation (VIII.12) in which $\chi = 90^\circ - \phi$

$$\begin{aligned} \eta = & \frac{1}{2} \frac{c^2 H}{c^2 - n^2 R^2 \sin^2 \chi} \sin 2\chi \sin 2\Delta \cos(nt + \lambda + \epsilon) \\ & + \frac{1}{2} \frac{c^2 H^2}{c^2 - n^2 R^2 \sin^2 \chi} \sin^2 \chi \sin^2 \Delta \cos 2(nt + \lambda + \epsilon). \quad (\text{IX.13b}) \end{aligned}$$

It is then seen that the first term is a diurnal tide of period $2\pi/n$ which is added to the semi-diurnal tide. The diurnal tide vanishes, when the declination of the disturbing body is zero, i.e. when the moon crosses the equator, i.e. twice a month. The amplitude of the semi-diurnal tide with a period π/n , however, is smaller than before in the ratio of $\sin^2 \Delta : 1$.

In the case of a canal coinciding with a meridian we should consider the fact that the undisturbed figure of the free surface is one of relative equilibrium under gravity and centrifugal force, and is therefore not exactly circular. We will assume by anticipation that in a narrow canal the disturbances are sensibly the same as if the earth were at rest, and the disturbing body were to revolve round it with the proper relative motion. If the moon be supposed to move in the plane of the equator $\cos \vartheta = \cos \phi \cos(nt + \epsilon)$ if $nt + \epsilon$ is the hour angle from the meridian of the canal.

The fluctuations above and below the disturbed mean level are given by

$$\eta = \frac{H}{4} \frac{1-p^2}{1} \cos 2\phi \cos 2(nt + \varepsilon) \quad (\text{IX. 14})$$

The tide is semi-diurnal and if, as in the actual case of the earth, $c < nR$, there will be high water at latitudes above 45° , and low water at latitudes below 45° , when the moon is in the meridian of the canal and vice versa. These circumstances would all be reversed if the moon is 90° from that meridian.

(b) *Canals of Limited Extent* *

In the case of a canal which does not extend over the entire earth, but is of limited extent, there is no more exact agreement or exact opposition between the tidal force and tidal elevation. The boundary condition $\xi = 0$ for the ends of the canal $\lambda = \pm \alpha$ is added to the equation of motion. In the case of an equatorial canal, the equation of motion has the same form as (IX. 11). ε can be left out in its cos term if the origin of time is the passage of the moon through the meridian in the center of the canal ($\lambda = 0$).

If we neglect the inertia of the water ($\partial^2 \xi / \partial t^2 = 0$), we find

$$\eta = \frac{1}{2} H \left\{ \cos 2(nt + \lambda) - \frac{\sin 2\alpha}{2\alpha} \cos 2nt \right\}. \quad (\text{IX. 15})$$

This solution is designated as the elevations on the "corrected equilibrium theory". At the centre of the canal ($\lambda = 0$) we have

$$\eta = \frac{1}{2} H \left(1 - \frac{\sin 2\alpha}{2\alpha} \right) \cos 2nt. \quad (\text{IX. 16})$$

If α is small, the range is here very small, but there is not a node in the absolute sense of the term. The time of high water coincides here with the transit of the moon through the meridian. At the ends of the canal $\lambda = \pm \alpha$ we have according to LAMB and SWAIN (1915)

$$\eta = \frac{1}{2} H R_0 \cos 2(nt \pm \alpha \mp \varepsilon_0); \quad (\text{IX. 17})$$

* Let us take the case of forced oscillations in a canal of small dimensions closed at both ends (inland sea) generated by a uniform horizontal force $X = m \cos(\sigma t + \varepsilon)$. The lake which is outstretched in a west-east direction has a length l ; $v = T_t : T_K$ (ratio of the period of the free oscillations to the period of the force) and ϕ the geographical latitude, then the range at the end of the land-locked sea is then

$$2\eta = \frac{m}{g} l \cos \phi \frac{\tan \pi}{\arcsin \frac{\pi}{2}} v.$$

For the semi-diurnal tide, the phase (referred to the centre meridian of the lake) is at the west end $9h$, at the east end $3h$, if $v < 1$ (direct tides); with $v > 1$ we have the inverted (indirect) tides, (see LAMB, 1932, p. 226).

in which

$$R_0 \cos \varepsilon_0 = 1 - \frac{\sin 4\alpha}{4\alpha} \quad \text{and} \quad R_0 \sin 2\varepsilon_0 = \frac{\cos 4\alpha - 1}{4\alpha}.$$

If α is small, then

$$R_0 = 2\alpha \quad \text{and} \quad \varepsilon_0 = -\frac{1}{4}\pi + \frac{2}{3}\alpha \quad (\text{IX.18})$$

approximately apply.

High water starts at the eastern end at the time $(-a - \varepsilon_0)/15^\circ$ h, with small α , therefore, at the time $(9^{\text{h}} - \alpha/45^\circ)$ at the western end, on the contrary, at the time $+(a - \varepsilon_0)/15^\circ$, with smaller α at the time $(3^{\text{h}} + \alpha/45^\circ)$ h. If the canal is of finite length, these times are reduced to about 9^{h} at the eastern end and 3^{h} at the western end, and the tide has the simple character of a standing wave, which character it loses more and more the longer the canal is.

Taking the inertia of the water into account, it is easy to find that the tide in the canal will be

$$\eta = -\frac{H}{2} \frac{1}{p^2 - 1} \left[\cos 2(nt + \lambda) - \frac{p}{\sin 4p\alpha} \{ \sin 2(nt + a) \cos 2p(\lambda + a) - \sin 2(nt - a) \cos 2p(\lambda - a) \} \right]. \quad (\text{IX.19})$$

If p tends to the limit 0 we obtain (IX.15) of the equilibrium theory. In all cases which are at all comparable with oceanic conditions p is considerably greater than unity. At the ends of the canal we find

$$\eta = \frac{1}{2} HR_1 \cos 2(nt \pm a \mp \varepsilon_1),$$

where

$$R_1 \cos 2\varepsilon_1 = \frac{p \sin 4\alpha - \sin 4p\alpha}{(p^2 - 1) \sin 4p\alpha}$$

and

$$R_1 \sin 2\varepsilon_1 = \frac{p(\cos 4p\alpha - \cos 4\alpha)}{(p^2 - 1) \sin 4p\alpha}. \quad (\text{IX.20})$$

When α is small (IX.18) applies again, as with the corrected equilibrium theory. The value of R_1 becomes infinite (resonance) in (IX.20), also when $\sin 4p\alpha = 0$. This determines the critical lengths of the canal, for which there is a free period of the canal equal to π/n , i.e. 12 lunar hours or half a lunar day. In fact, the free oscillation period of a canal of the extension 2α is $4\alpha R/c$, and if this should be

$$\pi/n, \quad 4p\alpha = \pi.$$

If the canal is not at the equator, but in the geographical latitude ϕ , the

equation (IX.19) changes only insofar as H is replaced by $H\cos^2\phi$ and $p = (nR/c)\cos\phi$.

For a series of zonal canals which can be imagined to exist in the oceans between the continents, PRÜFER (1936) and DIETRICH (1944) have computed the distribution of heights and phases along these canals for the M_2 and the K_1 tide. An example is given in Table 32; it refers to the transverse oscillation in a zonal canal of the Atlantic Ocean at 10°S . latitude. The forced

Table 32. Forced transverse oscillation of the Atlantic at 10°S . Lat., 35°W .– 13°E . long. (between South America and Africa)

(Depth = 4.52 km. Phase referred to Greenwich)

λ°	35°W .	31°W .	26°W .	21°W .	16°W .	11°W .	6°W .	1°W .	4°E .	9°E .	13°E .	
M_2	Phase ($^\circ$)	75	72	72	65	58	338	258	251	244	244	241
	Amplitude (cm)	63	62	55	41	22	5*	22	41	55	62	63
K_1	Phase ($^\circ$)	235	239	246	253	269	337	45	61	68	75	79
	Amplitude (cm)	30	27	23	15	8	4*	8	15	23	27	30

transverse oscillations of a semi-diurnal and diurnal character have in the entire Atlantic Ocean (with the exception of 30°N . for the semi-diurnal, where the ocean has its largest zonal extension) one “pseudo” nodal line, at which the amplitude is reduced to a minimum and the phase changes by about 180° over a short distance. In the Pacific Ocean, the number of nodal lines increases when going from the pole towards the equator. For M_2 there is one nodal line at 50°N ., two in 40° and 30°N ., three in the equatorial sections. In the Southern Pacific Ocean there are two nodal lines, when the Tasman Sea and the Coral Sea are excluded. In the Indian Ocean, the M_2 tide shows a nodal line for a canal at 5°N ., and two for canals at 10° and 30°S . The K_1 -tide, in the Indian Ocean, as well as in the Pacific, has only one nodal line in each zone; only in the latter are there two nodal lines at 10°N . in the region of the largest zonal extension.

These computations are supposed to give only indications as to the approximate behaviour of these oceans in respect to the oscillation in a west-east direction. It is obvious that transverse motions may alter essentially the actual tidal picture resulting from the tide-generating forces, and, as we have seen, there will be a development of amphidromies. However, there will be little change in the number and position of the nodal lines, which become nodal points through the development of amphidromies. Thus, the canal theory of Airy also contributes towards a better comprehension of the ocean tides.

4. Remarks Concerning the Dynamic Theory of Tides

The dynamic theory of the tides of Laplace starts out from the general dynamic principle of the wave theory, according to which in an oscillating system the motions forced by an external disturbing force have the same period as this force, but that the amplitudes and phases of these motions are also influenced by the possible free oscillations of this system. This influence is the stronger, the more the periods of the free oscillations approach those of the disturbing force. For the completeness of such a dynamic theory, it is necessary to know and to consider *all the free oscillations* of the system. According to V. Bjerknes, however, this has not always been done. He has proven that a kind of possible free oscillations, which he calls "gravid-elastoidic" oscillations, have been disregarded, which, if taken into account, will possibly modify the results. He, therefore, designates the Laplacian theory as a "semi-dynamic" method, to explain the theory of ocean tides. However, the complete theory in the exact form has not yet been applied hitherto.

The elastoidic waves occur in rotating fluids as oscillating motions under the influence of forces which originates by the variation of the centrifugal force in the case of radial displacements of the water particles. These are forces acting like the elastic forces on a solid body, for which reason they are called "elastoidic". This kind of waves can appear both as standing and as progressive waves, and it is preferable to start from the elastoidic free oscillations in a tube bent to return in itself. It can be shown that, in case of a slightly bent tube of rectangular cross-section, the length of the period of the free oscillations depends only upon the ratio of the lateral side to the radial side of the cross-section. Such elastoidic waves must, of course, also occur, for instance, in a canal along the equator of the rotating earth; only in this case the action of gravity must be added, which is also directed towards the vortex axis of the rotating water ring. These gravid-elastoidic waves have the same character as those of the purely elastoid oscillations. If the water ring has a free surface, as in the case of an equatorial canal, and if T' is the period of the orbit of the oscillating motion, L the width of the tube (canal) and h the thickness of the layer in which the wave disturbance occurs, the equation $h = 4L^2/gT'^2$ applies both for standing and for progressive waves of a gravid-elastoidic character.

The wave disturbance appears as an oscillatory motion between the side walls of the open canal. When all particles move in the same phase, the disturbance has the character of a standing oscillation; if the phase varies along the cross-section, the disturbance propagates along the canal.*

* It is noteworthy that the above formula is identical with the simple Merian formula for oscillations for a rectangular basin of the length L and the depth h . The oscillations would then only be gravitational waves between the walls of the canal. Has the "elastoid" of the oscillations not disappeared by neglecting?

If we select for $T' = T_0 = 1$ sidereal day = 86,164 sec, it appears that the "gravoid-elastoidic" surface waves only occur in an extremely thin surface layer; if we imagine an ocean of a constant depth of 5 km or divided in tubes (canals) of 8.5 km width, the top layer influenced by the waves would be only 4 mm thick. This shows that the inner elastoid oscillations of the sea are without any importance for the variations of the surface. This changes however, if we consider the "gravoid-elastoidic" surface disturbances in thicker layers. The equation gives the following correlated values of the depth h and the width L of the canal, when $T' = T_0$, hence for diurnal waves:

h	(m)	...	492	873	1360	2000	5500
L	(km)	...	3000	4000	5000	6000	10,000.

For a canal extending in width between the northern and the southern tropics for instance, the water layer occupied by the gravoid-elastoidic waves would be 2000 m deep, like oceanic depths. With these diurnal waves, the water, in case of a standing wave, flows everywhere in the canal during 12 h to the north, then during 12 h to the south, or in case of a wave with a wave length equal to the circumference of the earth, the current will be directed northward on one hemisphere and southward on the other hemisphere.

There is no doubt that "gravoid-elastoidic" surface waves may possibly occur in the oceans, also in the preference of diurnal tide generating forces. Inasmuch as in the existing dynamic theory this kind of free oscillations has not been considered, it might easily happen that the diurnal tidal phenomena mentioned therein are not complete, and particularly that the theory of Laplace concerning the disappearance of the diurnal tide in a sea of constant depth is not tenable, because the possible "gravoid-elastoidic" inertia waves have not been considered. V. Bjerknes is of the opinion that the great success encountered by the existing "semi-dynamic" method can only be attributed to the favourable circumstances that the "gravoid-elastoidic" disturbances can only in an extreme case have a period approaching the semi-diurnal period which is most important for the tides. Bjerknes also proves that the inaccuracy of the prevailing presentation lies in the fact that in the equations of motion the vertical acceleration of the water particles and the vertical component of the Coriolis force have been neglected. Only when they are taken into account we will have together all possible free oscillations of the systems necessary for the comprehension of the phenomenon. However, only the application of the exact theory in all its details will show in how far the objections of Bjerknes mean a serious improvement of the theory of the tides.

SOLBERG (1936, p. 237) has made a thorough investigation regarding the free oscillations of a homogeneous water layer on a rotating earth in connection with the dynamic theory of the ocean tides, and has shown that their character changes completely when $1 - 4\omega^2/\sigma^2$ passes through zero. For

longitudinal oscillations which are identical in all longitudes and for which $\sigma^2 > 4\omega^2$, i.e. the period is smaller than 12 h, he obtains results which do not show any essential difference with those obtained by Laplace and Hough. With $\sigma^2 < 4\omega^2$, i.e. for periods larger than 12 h, Solberg expects results differing widely therefrom. A second part of the research in connection herewith is still lacking. PROUDMAN (1942, p. 261) has recently broached the question of the validity of the Laplacian theory and, comparing its results with those of a more accurate theory, discussed thoroughly their discrepancies. He has been able to show that the cellular oscillations with the semi-diurnal components can only be of any importance in the vicinity of the poles, whereas the long period components acquire importance only in the vicinity of the equator. Diurnal cellular oscillations are only possible if their horizontal wave length is of the same order of magnitude as the water depth. This, however, is not the case for the actual oceans. Generally speaking, the necessary improvements made to the solution of the simpler Laplacian theory seem to be only very slight for the ocean as a whole.

Chapter X

The Harmonic Analysis of Tidal Observations

(1) The Preparation of Sea-level Recordings and their Scientific Use

THE dynamic theory of the tides teaches that the tide waves caused by the tide-generating forces must have the period of these forces. However, due to the complicated bottom configuration of the oceans and of the contours of the continents, it is not possible to derive theoretically the amplitude and the phase of these waves for the various points of the oceans with sufficient accuracy. There is, however, no doubt that the tides obey laws. So, whereas the periods of the occurring tides are determined theoretically, once for all, by the harmonic analysis of the tide potential (see p. 263), their amplitudes and phases remain unknown. They can, however, be computed for a locality where a series of extended observations of the sea level is available. Inasmuch as the tidal phenomenon constantly repeats itself within a certain interval, it is to be expected that the amplitudes and phases of the tide waves derived from the observations are for each locality constants, which are characteristic for the tidal process in that particular locality. The method used for this reduction is called the harmonic analysis of the tides, and since it was introduced by Thomson and Darwin, it has developed into an exceedingly important method of analysing tidal observations. The most important part of the very extensive literature on this subject has already been given in discussing the harmonic analysis of the tide potential. Important contributions have been made by Børgen, and later by RAUSCHELBACH (1924) and especially by DOODSON (1928, p. 223).

The procedure is based on the principle that any periodic motion or oscillation can always be resolved into the sum of a series of single harmonic motions.

To a harmonic term of the tide potential as given in (VII.17) and which in general the form $\Omega = C \cos(\sigma t + V_0)$ corresponds according to the dynamic theory, a component of the form

$$\eta = H \cos(\sigma t + V_0 - \kappa) \quad (\text{X.1})$$

σ is the frequency (angular velocity) of the potential component and equally of the forced partial tide, V_0 is the argument of the tide for 0^h of the first day of the series of observations to be subjected to the harmonic analysis; it can be

computed from the orbital elements of the tide-generating bodies, which vary in relation to the mean time. κ/σ is the lag between the tide and the tide potential, respectively, the time of the high water interval. κ is called the phase of the partial tide in the locality in question or kappa number. H is the mean value of the amplitude or semi-range of the component or partial tide. The epoch κ is the difference between the theoretical and actual phase as determined from the tidal observation. H and κ are functions of localities on the earth and are different for each harbour. It is these constants which must be derived from the tidal observations. They are called the harmonic tidal constants of a locality. If they are known, together with the diurnal part of the partial tide V_0 , the above-mentioned formula permits computation of, for any time t of the day, the deviation η of the surface from mean level and, if the height of mean level above chart datum is known, the water depth at that time.

The main purpose of the harmonic analysis consists in deriving from the heights of the observed tides in a locality over a great length of time (sea-level recordings or hourly observations) the harmonic constants H and κ for each component of the tides. The observations should be considered as the superposition of a large number of waves of the form (X.1), each with different H , σ and κ . Each one of these waves repeats itself in the same way in the time interval $T = 2\pi/\sigma$. Let us consider such a wave with the period T_0 and let us divide the tidal curve into equal parts of this length T_0 . For instance in the case of the M_2 tide, in two periods of 12 and 24 lunar h respectively (counted from the transit of the moon through the meridian in the locality) high and low water will always occur in each of these equal parts at the same hour. We read from the tidal curve the height of the sea level for each lunar hour, and if we take for each particular hour the average height over a very long series of lunar days, the average variation in the sea level of such a lunar day will be particularly apparent. At the same time, all other components which have different periods check and counteract each other; therefore, if the series of observations extends over a large number of lunar days, these different components balance each other out. Thus, we can eliminate all other waves, with the sole exception of the one under consideration, and the mean variation in sea level obtained in this manner can be regarded as that of the considered partial tide for one single day of observation. One-half of the range is the amplitude, whereas the interval between the transit of the fictitious "moon" through the meridian and the high water gives the phase of the partial tide.

The observations show the sea level η as a function of time which can be written in the form

$$\begin{aligned} \eta &= H_0 \cos(\sigma_0 t - \kappa_0) + \sum_{n=1}^r H_n \cos(\sigma_n t - \kappa_n) = \\ &= B_0 \cos \sigma_0 t + C_0 \sin \sigma_0 t + \sum_{n=1}^r H_n \cos(\sigma_n t - \kappa_n). \quad (\text{X.2}) \end{aligned}$$

The partial tide has the index 0 (amplitude H_0 , phase z_0 , period $T_0 = 2\pi/\sigma_0$), whereas the other tides are together under the summation sign; $H_0 \cos z_0 = B_0$ and $H_0 \sin z_0 = C_0$.

If we multiply (X.2) once by $\cos \sigma_0 t$, another time by $\sin \sigma_0 t$, and if we integrate these expressions from $t = 0$ to $t = pT_0$, where p is a large number, hence over a large number of periods of the partial tide σ_0 , we obtain

$$\int_0^{pT_0} \eta \frac{\cos \sigma_0 t}{\sin \sigma_0 t} dt = \frac{B_0}{C_0} \frac{p}{2} T_0 \pm \sum_{n=1}^r H_n \frac{\sigma_n}{\sigma_n^2 - \sigma_0^2} \left[\frac{\cos \left(\frac{\sigma_n}{\sigma_0} 2p\pi - z_n \right) + \cos z_n}{\sin \left(\frac{\sigma_n}{\sigma_0} 2p\pi - z_n \right) - \sin z_n} \right] \quad (\text{X.3})$$

These relations show that the computation of B_0 and C_0 , which determine the amplitude H_0 and the phase z_0 of the partial tide σ_0 , become more accurate when pT_0 increases, i.e. the accuracy increases with the number of full periods of the partial tide σ_0 which are used to compute averages. We then obtain with a good approximation

$$H_0 \frac{\cos z_0}{\sin z_0} = \frac{2}{pT_0} \int_0^{pT_0} \eta \frac{\cos \sigma_0 t}{\sin \sigma_0 t} dt. \quad (\text{X.4})$$

It is also possible to determine the smallest number of complete periods which are necessary to eliminate a certain partial tide to have the expression (X.4) become valid. The influence of other partial tides on a selected partial tide which is to be obtained as clearly as possible, becomes important when the frequencies approach each other. Thus, for instance, the S_2 tide will prove to be particularly disturbing in computing the M_2 tide. However, this influence will vanish when in (X.3) the term below the summation sign for this partial tide becomes zero. This happens for the disturbing σ_n component, when

$$\frac{\sigma_n}{\sigma_0} 2p\pi \text{ approximates } 2s\pi.$$

Consequently

$$\frac{\sigma_n}{\sigma_0} = \frac{s}{p}. \quad (\text{X.5})$$

In which both s and p should be large integers.

If we take, for instance, the S_2 tide, then $\sigma_n = 15^\circ$, whereas for the M_2 tide $\sigma_0 = 14.492051^\circ$; therefore, in this case,

$$\frac{\sigma_n}{\sigma_0} = 1.03505 \text{ average solar hours.} \quad (\text{X.6})$$

If observations are available extending over a period of about one year, and if this complete material is to be used, then pT_0 is approximately 360 days, and with $T_0 = \frac{1}{2}$ day p is approximately 720. The ratio of two whole

numbers s and p nearest to this figure which satisfy (X.6) is obtained when $p = 738$ and $s = 713$. This means that $pT_0 = 369$ days, is the most favourable length of time to be selected for the harmonic analysis of the M_2 tide. The periods of the tide being incommensurable, it is possible to analyse to the fullest extent only *one* tide at a time, by selecting the proper interval, and the influence of the other tides will become smaller, the greater the interval. The time of 369 days proves to be the most favourable interval for a great number of component tides with a short period, so that this interval has generally been selected for the reduction of the tides. In case the observations extend over a shorter period of time, the procedure has to be changed somewhat; however, this depends essentially upon the form in which the material is available.

The numerical computation of the average variation in sea level caused by a partial tide, requires the division of the whole tidal curve into equal intervals of one period (component days), whose lengths are the periods of the various diurnal components or twice the periods of the semi-diurnals. Such component days are divided into twenty-four equal parts called component hours. The tidal curve is read at the component hours. Then follows the averaging of all hourly values, in order to obtain the average variation during a component day. By repeating this procedure for other periods, it is possible to separate all partial tides from each other. However, such an analysis would require extremely extensive, laborious and time-consuming computations and only the observations made with a self-recording tide gauge could be used, with the exclusion of observations consisting in hourly readings of the sea level. Roberts and Darwin have therefore given the following important simplification of the procedure.

The tidal curve is tabulated in mean solar hours, so that one obtains 24 sums of the water height which will serve all components. Then one distributes the solar hourly heights among the component hours as nearly as possible. The speed or periods of the components determine where the various component hours fall upon the solar hours. If s_1 is the hourly speed of the mean sun ($= 15^\circ$) or diurnal solar component, c_1 the speed for any other diurnal component, then $c_1/s_1 = c_1/15$ represents the portion of any component hour corresponding to a solar hour. A half component hour will be lost or gained accordingly as c is less or greater than s , when $\frac{1}{2}s_1/(s_1 \sim c_1) = 15/(30 \sim 2c_1)$ solar hours shall have elapsed from the beginning. At subsequent regular intervals of $s_1/(s_1 \sim c_1) = 15/(15 \sim c_1)$ solar hours, a whole component hour will be lost or gained, that is, the difference between component and solar hours will increase one at such time. If $c_1 < s_1$ as is usually the case, two adjacent solar hours at one of these times fall upon the same component hour, i.e. within a half component hour of the time aimed at; but if $c_1 > s_1$ a component hour will be skipped because no solar hour occurs within a half component hour of it. If the maximum divergence allowed be

assumed to be a half solar hour, then all solar hours are not represented by component hours when $c_1 < s$; and when $c_1 > s_1$ a solar hour may occasionally be taken to represent each of two consecutive component hours. For each partial tide printed blanks can be used, in which is indicated at certain spots by special marks where the hourly heights are to be entered. These blanks do indicate the places where an hourly height has to be entered in two successive columns, or where two successive hourly heights have to be entered in the same column. The labour of writing still remains considerable. Excellent forms for this computation can be found in HANN (1939, p. 85) and POLLACK (1926 or 28). Each variation in mean sea level given by the mean values for each component hour is then developed into a series of simple, double, etc., speed of the considered tide. We finally obtain, according to the usual procedure of the Fourier Series

$$\eta = P'_0 + P'_1 \cos(\sigma_1 t - \alpha'_1) + P'_2 \cos(2\sigma_1 t - \alpha'_2) + \dots + P'_n \cos(n\sigma_1 t - \alpha'_n) + \dots \quad (X.7)$$

The hourly values of the separate component hours of a partial tide obtained by the above-mentioned method do not give exactly the sea level at the indicated full tidal hour, but the mean sea level at all times during an interval of a half hour before and a half hour after the full tidal hour. Therefore, the resulting mean value will be a trifle smaller (numerically) than the true ordinate. To obtain the true value, we need to introduce an augmenting factor. If the correct presentation of η is given by

$$\eta = P_0 + P_1 \cos(\sigma_1 t - \alpha_1) + P_2 \cos(2\sigma_1 t - \alpha_2) + \dots + P_n \cos(n\sigma_1 t - \alpha_n) + \dots \quad (X.8)$$

we obtain (X.7) by substituting each value in (X.8) by the average value for the interval from a half hour before until a half hour after the full hour. As an hour is given by $T/24$, this means the integration of (X.8) extends $(t-T)/48$ to $(t+T)/48$ and subsequent division by the entire interval $T/24$. As we seek P_n , we generally obtain

$$P_n = P'_n \frac{n\pi/24}{\sin(n\pi/24)}$$

so that the fraction to the right is the corrective factor which is to be applied to each term of equation (X.7) in order to obtain corrected augmented values. The phases remain unchanged ($\alpha = \alpha'$) These augmenting factors are for

$f \dots$	P_0	P_1	P_2	P_3	P_4
	1	1.00286	1.01152	1.02617	1.04720

They are to be applied to all short period components, excepting the *S*-tides, where no augmentation is required, because the hourly values used were derived from the value at that particular full solar hour. Therefore, in the analysis of the *S*-tide, each hourly height of the original tabulation is used once and once only.

If the term $P_1 \cos(\sigma_1 t - \alpha_1)$ represents in (X.7) the considered partial tide, the following terms give the overtides in the same way as the upper harmonics in the theory of acoustics; their frequencies are integer multiples of the frequencies of the fundamental tide. This frequency agrees with that of the tide potential. The occurrence of such overtides is due to the fact that, in

the vicinity of the shores and in shallow water, the amplitude of the tides cannot be regarded any longer as small in comparison with the water depth. Frictional influences will cause deformations of the purely harmonic form of the tide curve, in the form of overtides.

BÖRGEN (1894) (see HESSEN, 1928, p. 1) extended DARWIN'S method, whereby a great deal of computation work is eliminated and which needs less observations. It is based upon a special way of grouping the material which permits to emphasize each time one of the partial tides, whereas the others remain completely repressed. The reduction of the tide curve is first made in ordinary mean solar time, so that for each day we have a horizontal series of 24 values. If we add up a series of n days, the S_1 and S_2 -tide which conform to solar time, will be added, whereas the other components will cancel each other to a certain extent. A certain period of n days can now be found, in which the influence of a given tide, for instance of M_2 attains a positive maximum; then another period of n days in which the influence of this tide M_2 has a negative maximum, whereas S_1 and S_2 are present in both series in equal intensity. If we form the difference of the sums of the two series, S_1 and S_2 will vanish and the effect of M_2 appears to be doubled. This procedure is repeated m times and the result of the m series summarized. If m is selected correctly, the influence of all other components, with the exception of the one which is wanted, can be repressed to the greatest possible extent. According to this method, we need 92 selected days to determine M_2 accurately, whereas Darwin's method requires observations over a full year.

This Börger method is most elegant, but nevertheless it proves very difficult in practice, because the calculation, etc. cannot be left to untrained help. This is, in effect, the reason why it is seldom used.

Another reduction factor should be mentioned which should be incorporated into the methods of Darwin and Börger in order that the results of the harmonic analysis of different intervals may be compared with each other. Contrary to the more accurate evaluations of the tide potential by Doodson, the influence of the regression of the nodes of the moon's orbit is not incorporated in the earlier classical methods as an independent component tide, but rather as a slow variation of the amplitude and phase of the other components. The amplitudes $P_1, P_2, \dots, P_n \dots$ in (X.8) derived from observations contain functions: (a) of the angle J between the moon's orbit and the equator, (b) functions of the obliquity (ϵ) of the ecliptic; and (c) functions of the inclination i of the moon's orbit to the ecliptic. Darwin proposed to reduce P to the average value of these functions. He takes a certain point of reference of the moon's orbit and then applies to the amplitude a factor f . Then $P = fH$ and H is the average amplitude of the tide. H and κ are the harmonic constants of the considered tidal constituent. Tables of these factors f or $1/f$ can be found for different values of J in Darwin and Börger, respectively.

The harmonic constants of the most important components can also be derived with a fair accuracy from shorter periods of observation. For this purpose, one requires at least 15 or 29 days of observation. DOODSON (1938) has given instructions for working up the observations for such short periods

(see also MIYAHARA, and NIIMI, 1939). For the complete analysis of observations extending over one year, see also, the papers written by HARRIS (1897) and SCHUREMAN (1924) and those of STERNECK (1923, p. 39).

The procedure is somewhat different for deriving the harmonic constants of the long-period tides. It starts with the daily sums of the hourly heights, which are freed from the influence of the short-period components by simple reduction factors. For the rest, one proceeds according to the same principles as previously; only the execution is simpler and clearer. For more detailed information we refer to the papers of DARWIN and HESSEN (1920, p. 441).

2. Characteristics of the Tides as Shown by their Harmonic Constants

The amplitudes and kappa numbers of the harmonic analysis are particularly well suited to define more clearly a number of properties of the tides. As stated already, each component or partial tide varies as to its importance. A few determine the essential features of the tidal process. The 7 most important component tides are: M_2 , S_2 , N_2 , K_2 and K_1 , O_1 , P_1 and, among these, the two largest semi-diurnal and diurnal tides M_2 , S_2 and K_1 , O_1 respectively, stand out as the most important ones. The κ -value of M_2 gives, for semi-diurnal tides, the approximate time of occurrence of the high water after the transit of the moon through the meridian (high water lunital interval, establishment). At full and new moon the sun and the moon pass through the meridian simultaneously at noon; however, the two components have a lag which are given by the κ -values κ_M and κ_S . The difference of the angular velocities or speeds of $30^\circ - 28.984^\circ = 1.016^\circ/\text{h}$ or 24.384° in a day which makes the M_2 tide lag daily by $0.84 \text{ h} = 50 \text{ min}$ behind the S_2 tide. At the syzygies both waves have the same phase and their amplitudes are to be added $M_2 + S_2$; the time of this spring tide is determined by the κ -value of the S_2 -tide which is $\kappa_S/30$ hours in civil time. The interval between the spring tide and full moon and new moon is given by $\kappa_S - \kappa_M$; $(\kappa_S - \kappa_M)/24.384 = 0.04(\kappa_S - \kappa_M)$ is then the quantity which is called the "age of the tide". The difference between the amplitudes $M_2 - S_2$ gives the amplitude of the neap tides. The effect of a small diurnal tide on a large semi-diurnal tide is to increase the heights of alternate high water and decrease the heights of the intermediate high waters with similar effects in the heights of low water. Similarly, alternate high waters may be accelerated in time and the intermediate high waters may be retarded with similar effects in the times of low water. These effects are referred to as the "diurnal inequality". The diurnal inequality, therefore, is mainly governed by the amplitude of S_2 .

For the diurnal tides the phase of the K_1 tide, together with the phase of the O_1 tide, determines the time of high water. This high water does not show any relationship any more with the transit of the moon through the meridian. The phase of the principal tide K_1 conforms to sidereal time and

it can, therefore, be said that high water occurs within a constant time interval from the transit of a certain star through the meridian. Without considering the O_1 tide, the κ -number of K_1 will give in local time the high water on 21 June; on each following day it occurs 4 min earlier, for each month 2 h earlier, so that (always in a rough approximation) with such tides the high water will occur at each hour of the day in the course of a year. For instance, if high water occurs on 21 June at 2 p.m., it can be expected on 21 December at 2 a.m. The O_1 tide causes a periodical increase and decrease in the amplitude of K_1 , as does the S_2 tide for the M_2 tide. The contrast between spring tides and neap tides occurs with the diurnal tides every 13.66 days, whereas they do occur every 14.765 days for the semi-diurnal tides. The relative speed is here $\kappa_K - \kappa_O = 15.041^\circ - 13.943^\circ = 1.098^\circ/\text{h}$, or 26.3528° per day. The spring tides occur every $360:26.353^\circ = 13.66$ days, which is 26.74 times during the course of a year. For the semi-diurnal tides, such spring tides occur only 24.74 times in a year. The difference $\kappa_K - \kappa_O$ which corresponds to the "age of the tide" gives the delay of the spring tide. $\kappa_K - \kappa_O : 26.3528^\circ = (\kappa_K - \kappa_O)0.038$ is the lag in days after the greatest declination of the moon.

A further complication, in the case of diurnal tides, is caused by the P_1 tide, whose high water occurs 4 min later each day; hence, its relative motion against the K_1 tide is 8 min/day, 4 h/month. K_1 and P_1 have the same phase at the time of the summer solstice; at that time, both tides reinforce each other. The same is the case for the winter solstice, where the difference in phase is $6 \times 4 = 24$ h. At the equinoxes (March and September), the difference in phase is 12 h; the two components counteract each other. The P_1 tide causes the diurnal tides to have a maximum not at the equinoxes but at the solstices. This is a remarkable feature of this type of tide, distinguishing it from the semi-diurnal tides.

In order to classify the tides of a locality, P , VAN DER STOK (1897) has adopted three principal types of tides based on the ratio of the sum of the amplitudes of the diurnal components $K_1 + O_1$ to the sum of the amplitudes of the semi-diurnal components $M_2 + S_2$. This ratio increases when the diurnal inequality of the tides increases. It attains a maximum when there is only one high water a day. Therefore $F = \frac{K_1 + O_1}{M_2 + S_2}$ is designated as the "Formzahl" of the tides. COURTIER (1938) (see also DIETRICH, 1944, p. 69, who increased the number from 3 to 4) has given the following classification.

F : 0–0.25 *semi-diurnal* type; two high waters and two low waters daily of approximately the same height. The interval between the transit of the moon and high water at a locality is nearly constant. The mean range at spring tide is $2(M_2 + S_2)$.

F: 0.25–1.5 mixed, mainly semi-diurnal type. There are daily two high and two low waters which, however, show inequalities in height and time, which attain their maximum when the declination of the moon has passed its maximum. The mean spring tide range is $2(M_2 + S_2)$.

F: 1.5–3.0 mixed, mainly diurnal type. Occasionally only one high water a day, following the maximum declination of the moon. At other times there are two high waters in the day, which show, however, strong inequalities in height and time, especially when the moon has passed through the equator. The mean spring tide range is $2(K_1 + O_1)$.

F: 3.0–∞ diurnal type. Only one high water daily, and the semi-diurnal almost vanishes. At neap tide, when the moon has passed through the equatorial plane, there can also be two high waters. The mean spring tide range is $2(K_1 + O_1)$.

Table 33. Harmonic constants of the principal component tides for four ports.

Characteristic of the different types of tides

Place...	Immingham (east England)		San Francisco (California)		Manila (Philippines)		Do Son (Indo China)	
ϕ ...	53° 38' N.		37° 48' N.		14° 36' N.		20° 43' N.	
λ ...	0° 11' W.		122° 27' W.		120° 57' E.		106° 48' E.	
Period of observation...	1 year		10 years		2 years		2 months	
Component tide	Phase (z°)	Ampl. (cm)	Phase (z°)	Ampl. (cm)	Phase (z°)	Ampl. (cm)	Phase (z°)	Ampl. (cm)
M_2	161	223.2	330	54.2	305	20.3	113	4.4
S_2	210	72.8	334	12.3	338	6.8	140	3.0
N_2	141	44.9	303	11.5	291	3.8	(99	0.8)
K_2	212	18.3	328	3.7	325	2.1	140	1.0
K_1	279	14.6	106	37.0	320	29.7	91	72.0
O_1	120	16.4	89	23.0	279	28.3	35	70.0
P_1	257	6.4	104	11.5	317	9.3	91	24.0
$2(M_2 + S_2)$	252.2 cm		133.0 cm		54.2 cm		14.8 cm	
$2(K_1 + O_1)$	62.2 cm		120.0 cm		116.0 cm		284.0 cm	
$F = \frac{K_1 + O_1}{M_2 + S_2}$	0.11		0.90		2.15		18.9	

In order to illustrate the influence of the type of tides in a harbour, Fig. 123 shows the tidal curves of four harbours with different types of tides calculated in advance for the month of March 1936 according to the tidal constants (see German tide tables, 1940). Table 33 contains the harmonic constants

of the principal tides of these four harbours. Immingham has a semi-diurnal type of tides with a ratio $F = 0.11$; San Francisco has the mixed type, mainly semi-diurnal tides with a ratio $F = 0.90$; Manila shows a mixed, but mainly diurnal type of tides $F = 2.15$, whereas Don Son in the Gulf of Tonkin has a pronounced diurnal tide with the very high ratio $F = 18.9$. These four main tides (M_2, S_2, K_1, O_1) are responsible for the tidal picture because they account for about 70% of the total amplitude in all four harbours. When we take into account the other important components N_2, K_2 and P_1 this percentage is increased to about 83%.

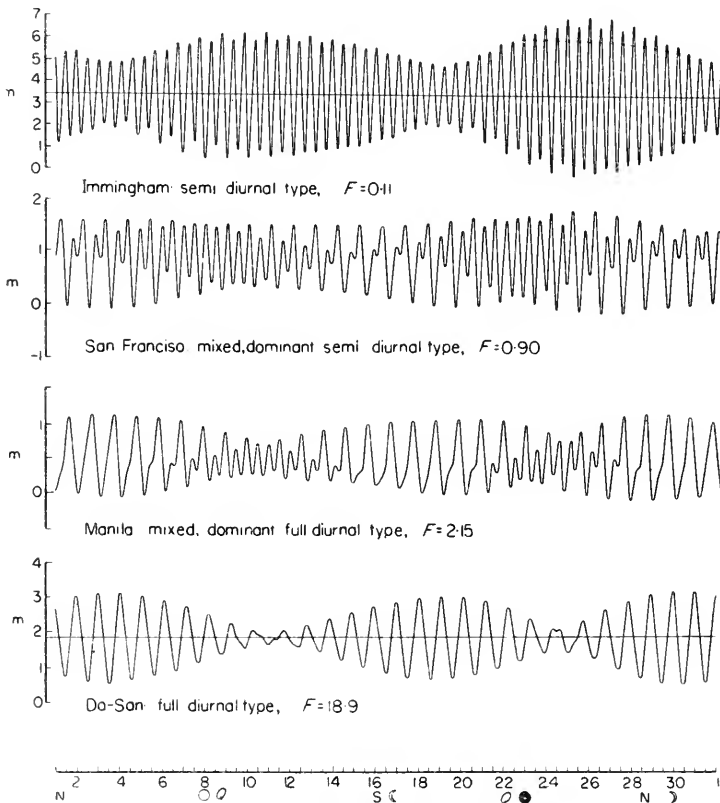


FIG. 123. Tide curves for March 1936 \bigcirc $\left(\frac{\bullet}{\bullet}\right)$, phases of the moon. N and S are the largest northern and southern declination of the moon; Q passage of the moon through the Equator.

3. Variations in the Harmonic Tidal Constants

When tidal records extending over a number of years are available for a locality the harmonic constants of the main constituents can be computed for each period of one year. Contrary to what would be expected, they are not constant, but show small variations from year to year, both in the

amplitudes and in the phases, even when the above-mentioned reduction to average conditions is made. As an example, Table 34 gives a summary of the variations in amplitude and phase of the seven most important components M_2 , S_2 , N_2 , K_2 and K_1 , O_1 , P_1 , for Bombay for the years 1906–15. It shows that the variations from one year to another are relatively small for am-

Table 34. Variations in tidal constants of Bombay 1906–15

Component tide	Amplitude (cm)					Phase	
	Maximum	Minimum	Difference	Average amplitude (cm)	Average deviation (cm)	Maximum difference	Average deviation
M_2	122.5	120.0	2.5	121.08	0.64	1.51°	0.49°
S_2	47.8	47.2	0.6	47.58	0.21	2.94°	0.78°
N_2	30.8	28.8	2.1	29.77	0.71	4.67°	1.69°
K_2	13.7	11.4	2.3	12.32	0.58	9.60°	2.99°
K_1	42.5	42.0	0.5	42.27	0.18	1.19°	0.34°
O_1	20.2	19.6	0.6	19.92	0.21	1.31°	0.40°
P_1	13.1	12.3	0.8	12.57	0.24	3.07°	1.00°

plitudes and phases, but they, nevertheless, show that the differences increase with decreasing amplitude of the component. Even more so, when one considers the other, less important constituents. For these PROUDMAN (1920, p. 328) has shown that in some years the amplitude is ten times larger than in other years, whereas the phase values show great deviations from the average value.

There is hardly any doubt that the yearly variations of the harmonic constants are partly caused by the methods of analysis that are used; however, it seems that there are also systematical variations attributable to specific causes. DOODSON (1924, p. 573) has closely checked the harmonic constants of Bombay and St. John, Bay of Fundy, and has dealt probably for the first time with such questions more thoroughly. In the case of the most important semi-diurnal component M_2 , he found three definite kinds of disturbances. The first one has a period of approximately 19 years, corresponding to the regression of the node of the moon, the second one has a period of about 4 years and is supposed to be based chiefly upon insufficiencies of the analytical methods, whereas the third kind is of a secular, unknown origin.

Figures 124 and 125 show the variations of the harmonic constants of M_2 for St. John and Bombay, according to Dawson and Roberts. In both harbours the variations are very large. In St. John H varies from 291.3 to 307.1 cm; if the reduction factor f is considered, these values are reduced to 288.2 and 304.7 cm. It is obvious that the reduction factor f , which is applied for the purpose of reducing H to average conditions, makes no sense, for which reason Dawson wants it no more to be used. The main variation in H and α is, at any rate, the period of 19 years. It also appears in Bombay,

although much weaker, but here there is a particularly evident period of approximately 4 years with a large amplitude. Doodson proves that part of this variation is due to the influence of the N_2 on M_2 , whereas the period of 19 years can be eliminated, when the variation in the ascending node of the moon's orbit is taken into account. If these two reductions are made,

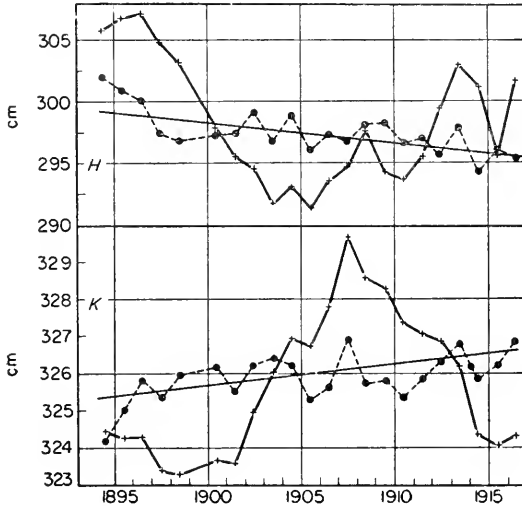


FIG. 124. Harmonic constant M_2 for St. John (Bay of Newfoundland). +—+—, original values; ---•---, reduced values; —, average secular variation (Doodson).

there remains in both cases under consideration a secular variation, which for St. John is a decrease of the amplitude of about 3 cm and increase in the phase of 1° over a period of 20 years. In Bombay, the decrease of the amplitude is constantly 0.085 cm per year, whereas in the period 1880–1900 the phase increased from 329.2° to 331.5° , and then decreased again. The harmonic constants of N_2 and S_2 show similar variations; the amplitude of K_1 decreases constantly since 1890. Karachi, on the contrary, shows variations in the opposite direction (amplitude M_2 in 1870, 75.3 cm; in 1920, 79.3 cm), whereas the phase does not show a steady variation.

The variations of the mean sea level in Bombay, Karachi and Aden show the following values:

Decade ...	1880–90	1890–1900	1900–10	1910–20
Bombay (cm)	312.0	311.9	310.6	312.4
Karachi (cm)	218.8	219.3	219.6	224.4
Aden (cm)	177.7	178.3	178.6	178.3

Karachi shows the greatest variations with about 3.6 cm within 30 years; however, the increase seems to be accelerated. These variations in the mean sea level are not sufficiently important to explain the observed secular

variations in M_2 . It seems that these can only be explained by variations in the bottom configuration (sand banks, etc.) in the immediate vicinity of the harbours.

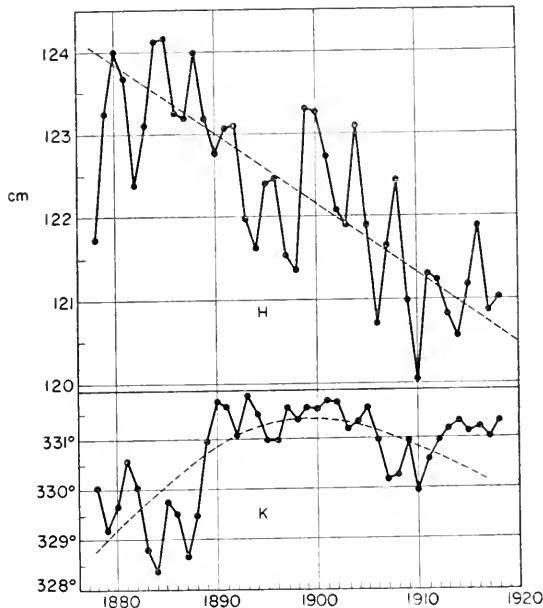


FIG. 125. Harmonic constant M_2 for Bombay. — · — · —, original value; · · · · ·, corrected value (Doodson).

4. Prediction of the Tides. Tide Tables, Tide-predicting Machines

The knowledge of the laws governing the tides makes it possible to compute in advance their occurrence for a certain harbour and thus to predict the tides. Since ocean liners running according to a fixed time-table have replaced the old sailing ships, there has been an ever increasing need for exact tidal data, and the prediction of the tides as contained in the tide tables constitutes one of the most important tasks of the hydrographic offices, in all countries. For the prediction of the heights and times of tides in a harbour one must, of course, refer to the tidal observations made previously in this locality from which the basic constants of the tides characteristic of the harbour must be derived.

The detailed computations for the tides can be executed according to two different methods; the so-called non-harmonic methods and the harmonic methods.

(a) The Non-harmonic Method

This was first developed by LUBBOCK (1839) (1830–50). It uses mainly the time and the heights of high and low waters, and to a lesser extent the

hourly readings. Especially the luni-tidal intervals are taken into account, and the procedure varies according to whether the different "establishments" are used. It is, therefore, based principally upon the semi-diurnal components and can only be used to advantage for harbours in which the diurnal inequality is small. If this inequality is great, an additional number of corrections is required to obtain usable results. The method fails completely where diurnal tides prevail. The method is based on equation (IX.2), where we have the superposition of the semi-diurnal lunar tide with the semi-diurnal solar tide for the equilibrium theory. In reality, each tide lags against the position of the celestial body in the sky which is considered by introducing \varkappa numbers. The equation (IX.2) is, therefore, replaced by

$$\eta = A \cos[2(\theta - a) - \varkappa] + A' \cos[2(\theta - a') - \varkappa']. \quad (\text{X.9})$$

The values with the prime are for the sun. θ is the sidereal time, a and a' the right ascensions of the moon and sun respectively. $\tau = \theta - a$ and $\tau' = \theta - a'$ are the hour-angles of the moon and the sun and we have $\tau = \tau' - \psi$, if $\psi = a - a'$ is the difference in hour angles of the moon and sun. We still wish to mention that $2\tau = \sigma_M t$ and $2\tau' = \sigma_S t$ in which σ_M and σ_S are the frequencies of the semi-diurnal lunar and solar tide respectively. $\tau/15^\circ$ is the time expressed in lunar hours, $\tau'/15^\circ$ are solar hours = t hours.

In this way (X.9) becomes

$$\eta = A \cos[2(\tau' - \psi) - \varkappa] + A' \cos[2\tau' - \varkappa']. \quad (\text{X.10})$$

The two terms on the right can be contracted into a cos member with a somewhat variable amplitude and phase and we obtain

$$\eta = C \cos \left[2 \left\{ (\tau' - \psi) - \frac{\varkappa}{2} + \beta \right\} \right], \quad (\text{X.11})$$

$$\left. \begin{array}{l} \text{in which} \\ C = [A^2 + A'^2 + 2AA' \cos 2\psi']^{1/2}, \\ \tan 2\beta = \frac{A \sin 2\psi'}{A + A' \cos 2\psi'}, \quad \psi' = \psi + \frac{\varkappa - \varkappa'}{2}. \end{array} \right\}$$

When the moon goes through the local meridian, the angular distance of the sun is ψ and the time $\tau'/15^\circ$ but the angular distance of the high water caused by the sun and the moon is $\psi + \frac{1}{2}(\varkappa - \varkappa')$. \varkappa and \varkappa' are constant, but ψ varies $0.5080^\circ/\text{h}$ and 12.192° or $0.81^\circ/\text{h day}$

$$\psi = \tau' - \tau = \frac{1}{2}(\sigma_M - \sigma_S) = 15^\circ - 14.492^\circ = 0.508^\circ.$$

The variation of $2\psi'$, which makes β periodical, becomes

$$2\psi' = (\sigma_S - \sigma_M) \left[t - \frac{\varkappa' - \varkappa}{\sigma_S - \sigma_M} \right] = \frac{2\pi[t - \varepsilon]}{14.77 \text{ days}} \quad (\text{X.12})$$

if $\varepsilon = 0.041(\varkappa' - \varkappa)$ represents the age of the tide.

From (X.11) we obtain for the time of the high water

$$\frac{1}{15^\circ} \left[\psi' + \frac{\varkappa}{2} - \frac{1}{2} \arctan \frac{A' \sin 2\psi'}{A + A' \cos 2\psi'} \right]. \quad (\text{X.13})$$

The third term in the brackets is a semi-monthly inequality. At the time of full and new moon $a - a' = \psi = 0$ and the

$$\text{time of high water} = \frac{1}{30^\circ} \left[\varkappa - \arctan \frac{A' \sin(\pm \varkappa - \varkappa')}{A + A' \cos(\varkappa - \varkappa')} \right]. \quad (\text{X.14})$$

This is the approximate true local time of the high water at full and new moon and is called the "vulgar establishment". To the contrary,

$$\frac{\varkappa}{\sigma_M} = \frac{\varkappa}{30^\circ} \quad (\text{X.15})$$

is the "corrected" establishment or the mean high water lunitidal interval.

Determining the vulgar establishment is very simple and, consequently, it is known for many harbours. On the contrary, the computation of the corrected establishment requires continuous observations of the sea level (determination of the \varkappa -number of M_2). The corrected establishment still deviates from individual values of the lunitidal interval by considerable amounts. Greater accuracy is obtained if, for each day of the lunar period, one computes the specific lunitidal interval according to (X.13) or derives it statistically from lengthy observations.

The expression for C in (X.11) gives at spring time (time of occurrence of the spring tide)

$$C = A + A', \quad 2\psi' = 0; \text{ from which follows that spring time} = \text{day} \\ \text{before full and new moon} - \text{age of the tide}. \quad (\text{X.16})$$

If Z_0 is the height of the mean sea level above chart datum, the height of the high water = $Z_0 + C$ = approximately

$$\left. \begin{aligned} & Z_0 + (A + A' \cos 2\psi'). \\ \text{height of the low water} = Z_0 - C & = \text{approximately} \\ & Z_0 - (A + A' \cos 2\psi'). \end{aligned} \right\} \quad (\text{X.17})$$

It can be seen from equations (X.11) to (X.17) that if the lunitidal interval and the true solar time of the transit of the moon through the meridian for one day are known, one has all the factors necessary to determine the semi-diurnal tide, insofar as they are dependent on the simple orbital motion of the disturbing body in the equatorial plane. However in order that the basic values computed therefrom can be compared with the actual ones, they must be corrected, for the influence of the declination and the parallax of moon and sun and then also for the daily inequality; these corrections themselves vary with the declination of the disturbing bodies. For this reason, this procedure can only be applied, where the diurnal inequality is small

(like in the North Atlantic Ocean). Consequently the following rules can be applied for the computation of time and height of the high water:

Time of the high water = true solar time of the culmination of the moon +
 + lunitidal interval + correction for declination + correction for
 parallax + diurnal inequality - equation of time.

Height of the high water = height of the high water above chart datum +
 + correction for declination + correction for parallax + diurnal
 inequality.

The corrections should only be taken for the moon whereas those for the sun being small can be neglected. The lunitidal interval is equal to the mean lunitidal interval + the semi-monthly inequality; likewise the height of the high water above chart datum = the mean height of the high water + the semi-monthly inequality. For a certain harbour tables and graphs are made up in advance, which facilitate considerably the actual computation.

As an example, we refer to the curves of the lunitidal intervals for Portsmouth and Aden given in Fig. 126. The former harbour is characteristic

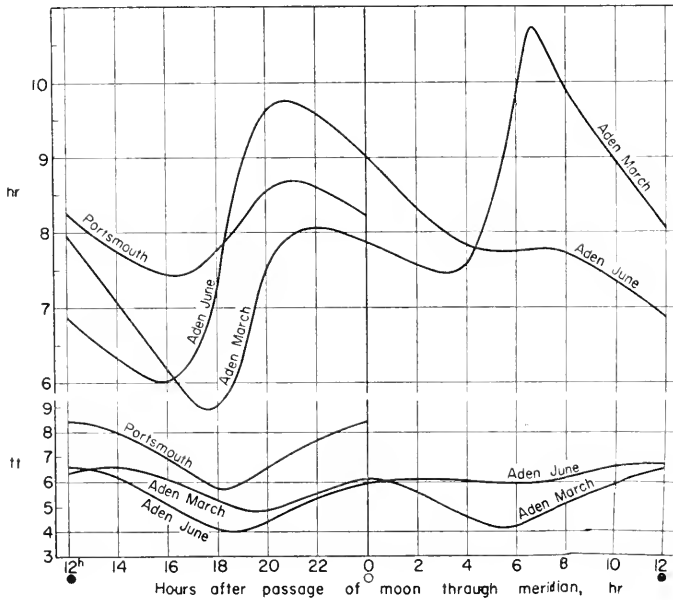


FIG. 126. Curves for the lunar tide interval and range for Portsmouth and Aden. (For Portsmouth 28 h have been deducted (Darwin).)*

for its semi-diurnal tides, in the latter the diurnal inequality is strongly noticeable, wherefore a difference has to be made between day and night. Let us try to find time and height of the high water in Aden, for instance, on 17 March 1889. At that particular date, the moon passes through the local

* The curve for Aden, March must be shifted upwards by 0.3 hours.

meridian at 11 min after noon, viz. 12·11 p.m. The curve gives a lunital interval of 8 h 4 min the correction for the lunar parallax was 2 min so that the high water will occur at 20·17 h. The table gives for the height of the high water 6·89 ft (210 cm), the correction was 5 cm so that the corrected height of the high water will be 2 m 15 cm.

Not many tide tables of this kind are being used, although they would be very practical.

(b) *Method of the Reference Stations*

Instead of computing extensive tables for the time and height of the high and low waters for all coastal localities, which may be very numerous and for which detailed tidal observations are generally not available, this is only done for a certain number of selected harbours. The tide tables contain only detailed predictions of all high water and low water times and heights for such "reference localities". If synchronous observations of the tide are available over a certain period of time for two localities lying in the same tidal area, the average *tidal differences* in time and height between these localities can be ascertained, and it will be seen that these differences remain somewhat constant. The tidal curve at the subordinate station is similar to that at the reference station, i.e. the differences in time and the difference between the high and low waters are almost constant between the two stations. One station can serve as a reference for a great number of more or less neighbouring coastal localities, and the tidal difference of a certain locality is the difference in time between the establishment of the subordinate station as compared with the establishment of the reference station corrected by the difference in longitude expressed in time.

The computation of the tides for the subordinate station is then simply made by adding the tidal difference to the tidal values of the reference station valid for that particular day, which can be found in the tables computed in advance. In practice the tables will give all high waters, low waters and times. Then there is a table for each subordinate station giving the difference in amplitude and in time for the high waters and low waters between the subordinate and reference station. Furthermore, there is a table giving the corrections for amplitude and time to be applied to spring and neap tides. This method is particularly suited for tides which are of the semi-diurnal and diurnal type, and less suited for the mixed type, where errors up to several hours occur; the errors in height are correspondingly large.

(c) *The Harmonic Method*

The common tide table gives generally only the height of the tide at the time of high and low water and complicated computations are necessary to determine with some accuracy this height for other hours. In view of the increasing need for accurate knowledge of the water depth, they are insufficient to solve correctly a great number of problems. The harmonic method of computing the tides eliminates this deficiency. The dynamic theory and

the harmonic analysis of the tides show that the tide, in a given locality, can be considered as a combination of a great number of constituent tides with constant amplitude and constant phase. These constants have been computed by harmonic analysis from good tidal records for coastal localities for the most important components, and they are characteristic and valid for the tide in a locality without any changes for a long period of time. Nothing prevents then the computation of any component tide for a given day of the year, and the sum of all these partial tides then gives the tidal process of the whole day under consideration, i.e. for each hour the expected height of the water above chart datum. If Z_0 is the height of the mean sea level above chart datum, the height of the water H (above chart datum) at the time t is given by $H = Z_0 + \sum A_i \cos U_i$. A_i is the amplitude of the partial tide i and $U_i = \sigma_i t + T_i + P_i$ in which σ_i is the frequency of the partial tide, T_i is the angle which the tide i has reached in the locality, on the day concerned at 0^h (T_i increases every day by $24\sigma_i$) and P_i is the phase of the tide, i.e. the negative α number of the component tide (corrected for the local time); $P_i + T_i$ is the total angle of the tide in the locality on the day under

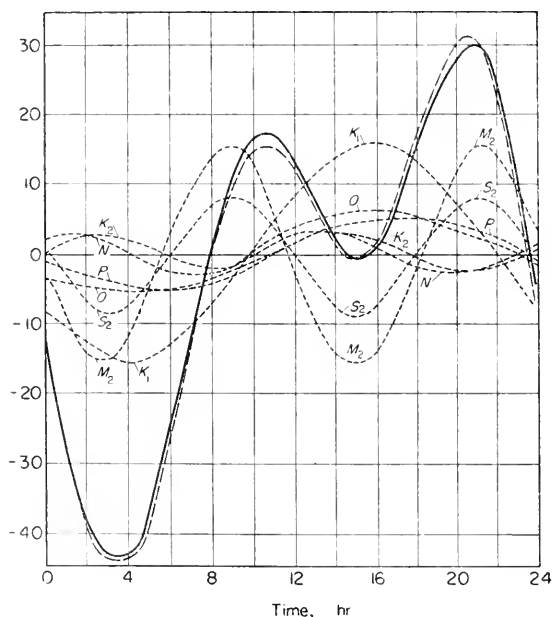


FIG. 127. Computation of the tide of Pola for 6 January 1909 (Full moon close to the winter solstice, very low water). — computed, ---- observed tides.

consideration at 0^h. If A_i and P_i are given as constants by the harmonic analysis, then H can be computed for any day, as a function of time, especially since T_i can be easily determined and tabulated for every day of a year.

These computations for a great number of days are very extensive (see tide-prediction machines), when many constituents are considered, but they

offer the great advantage of permitting the comparison of the predicted tide with the actual tide, and are, therefore, very instructive. These comparisons make it further possible to examine thoroughly the influence of air pressure and wind on the sea level in a harbour with strong tides. Figure 127 gives such a comparison for Pola, on 6 January, 1909; it shows a tidal curve at full moon with calm weather and a very strongly developed first low water. One can see how well the prediction corresponds to the tidal process, although only seven partial tides were used for the prediction (KESSLITZ, 1900).

The practical use of the harmonic method has only been carried through in recent times, although there is no doubt that it is the most accurate method. Especially for localities where the amplitudes of the diurnal tides are large it is far superior to all other methods. Of course, it presupposes the knowledge of the harmonic constants. However, with time the number of coastal localities for which these constants are known increases rapidly. The German tide tables of 1939 contain the harmonic constants of about 1800 localities for as many as ten tides, the Admiralty tide tables (1938) has these constants for 2650 reference localities; besides for 3500 subordinate stations the constants for M_2 , S_2 , K_1 and O_1 have been derived from the reference stations by means of differences (Admiralty tide tables, part II, London, 1938),

A practical procedure of predicting the height of the tide in a locality at any arbitrary time has been given by the German Tide tables starting in 1940. The following 10 components are used:

Tides	M_2	S_2	N_2	κ_2	μ_2
Periods in hours	12.42	12.00	12.66	11.97	12.87
Tides	K_1	O_1	P_1	M_4	MS_4
Periods in hours	23.93	25.84	24.07	6.21	6.10

To the usual 7 main components (4 semi-diurnal and 3 diurnal), they have added the so-called shallow-water tides $\mu_2 = 2MS_2$, M_4 and MS_4 . They are of some importance in regions of very shallow water, as is often found off harbours. The M_4 , as an overtide or harmonic of M_2 , causes an asymmetry of the semi-diurnal tidal curve, and combined with MS_4 also a slight variation of spring and neap time. An example will illustrate the computation. (Table 35). The first and the second lines contain the tidal constants for the indicated components for a locality. They can be taken from the list of harmonic constants. T_i is listed under "speed" σt under the hour angle which can be found, for all days of the year and all hours of the days, in the tide tables. The sum of the last three lines gives the angle U , which is to be reduced by entire multiples of 360, for the computation of $\cos U$. The values of $A \cos U$, which can also be taken directly from tables, are in the vertical column at left. Their sum together with Z_0 gives the height of the tide H at the hour in question.

If the other partial tides are neglected, there will be an error which will seldom be important enough to interfere with navigation. If the constants are not known for the other components, or if a lesser accuracy is sufficient, these constants must be left out in the forms. The error then is at the most equal to the sum of the amplitudes of the neglected tides.

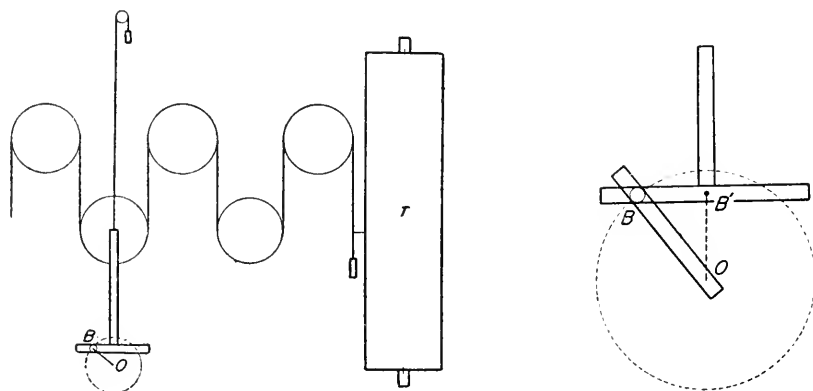
(d) Tide-predicting Machines

The computations for the tide tables for a complete year would represent a most laborious and expensive work, if it were accurately done every year for a great number of harbours. In each coastal locality there are yearly

Table 35. Computation of the range of the tide at Casablanca on 29 March, 1939, at 11 h 30 min G. M. T.

		Z_0	M_2	S_2	N_2	K_2	μ_2	K_1	O_1	P_1	M_4	MS_4	
Tides	$A \cos U$	+214	104	37	21	7	5	6	5	2	2	2	Amplitude (cm)
M_2	.	+ 30	304°	278°	323°	280°	351°	312°	53°	323°	193°	322°	Phase
S_2	- 5	.	156°	0	179	23	311	102	52	265	313	156	Speed T_i
N_2	- 7	.	333°	345	327	346	322	173	160	172	307	318	σt
K_2	.	+ 2											
μ_2	- 1	.	793°	623	829	649	984	587	265	760	813	796	Sum
K_1	- 4	.	720°	360	720	360	720	360	0	720	720	720	-n. 360°
O_1	- 0	.	73°	263	109	289	264	227	265	40	93	76	U
P_1	.	+ 2	.	180°	180	360	180°	180	180°	.	180°	.	
				+	-	-	+	+	+	.	-	.	
M_4	- 0	.	.	83°	71°	71°	84°	47°	85°	.	87°	.	
MS_4	.	0											
Sum	-17	+248	Height of the tide: 2.3 m										
Height (cm)		+231											

about 1400 high and low waters and an experienced computer, considering only the most important partial tides, can at the most in one year complete the predictions of only a few harbours. Therefore, for the sake of economy



FIGS. 128, 129. Schematic drawing of a tide-predicting machine.

as well as accuracy, the idea was conceived, only a few years after the introduction of the harmonic analysis, to use a machine for these predictions. KELVIN (1887) was the first to devise such a machine for computing the tides, which later on was improved by ROBERTS (1879). The first machine built in

1876 is in the South Kensington Museum in London. Similar machines have been built later by the Government of the Indies, by France (MICHEL-MOROT, 1908, p. 394), by the USA (1918) and by Germany (RAUSCHELBACH, 1924, p. 285). The latest machine, which can take care of 62 partial tides, has been completed in Germany in 1938. The construction of all these machines is based essentially upon the following features. System of gearing by means of which shafts representing the different components are made to rotate (see Figs. 128 and 129) with angular speeds proportional to the actual speeds of the components; then, a system of cranks and sliding frames for obtaining harmonic motion. Then, summation chains connecting the individual component elements, by means of which the sums of the harmonic terms are transmitted to the recording device. Furthermore, there is a system of dials and pointer for indicating in a convenient manner the height of the tide for successive instants of time and also the time of the high and low waters. Furthermore, a tide curve of graphic representation of the tide automatically constructed by the machine. To set the harmonic constants, the registration of the time and height of about 1400 high and low waters in print for a year requires approximately 10–15 h according to the complexity of the tides in the locality concerned (see SHUREMAN, 1924, p. 123).

Chapter XI

Tides and Tidal Currents in the Proximity of Land

1. Preliminary Remarks

THE following paragraphs are part of the more recent developments in the tidal theory. It is not so much intended to consider the tides of the oceans as a whole, but rather to explain the actual tides in certain adjacent seas. Starting out from the dynamical theory, the phenomena are treated from a geophysical viewpoint. Above all, the important relations between the vertical tide and the tidal currents are studied in detail.

In studying the tides synthetically, it was found best to proceed from the elementary to the more complicated questions and to study separately the modifying effects of single factors, amongst which the most important are the influences of the configuration of shore and bottom, the change caused by the earth's rotation and the distortion caused by friction. The results were applied first to the tidal phenomena of shallow parts of the ocean communicating with the vast expansions of the open oceans by straits and channels. The tides of these adjacent seas seem often to be independent and, apparently, their relationship with the tides of the open oceans is often very limited. These shallow waters are located without exception on the wide continental shelf; shallow water and complicated orographical coastal contours can strongly influence the tides. The friction caused by the sea bottoms is so powerful here that it is able to influence the motions of the entire water layer up to the surface. In this sense we then speak of tides "in the proximity of land".

2. General Considerations on the Influence of the Earth's Rotation and of the Friction on Tides and Tidal Currents

(a) Influences Due to the Earth's Rotation

In Chapter VI, 1/a (p. 142) is explained the form of the progressive tide waves in a non-rotating canal of uniform depth, if friction is neglected. The vertical tide and the tidal currents are given by the equations (VI.3 and 6); they have the form

$$\eta = \eta_0 \sin(\sigma t - \alpha x),$$

$$u = \sqrt{\frac{g}{h}} \eta_0 \sin(\sigma t - \kappa x),$$

with

$$c = \frac{\sigma}{\kappa} = \sqrt{gh}. \tag{XI.1}$$

The tidal current, in the direction of propagation of the wave, is purely alternating and attains its maximum velocity at high and low water. The motion is uniform from the surface to the bottom. The velocity of propagation is $c = \sqrt{gh}$.

If the canal has a rotating motion, these tide waves are changed into Kelvin waves (p. 206, equation VI.103). The only difference with conditions in a non-rotating canal is that the amplitude of the vertical tide, and also that of the alternating tidal currents varies across a section of the canal. The amplitude decreases from right to left, referred to the direction in which the wave progresses if the rotation is counter clockwise (*contra solem*) and from left to right if clockwise (*cum sole*). These conditions are clearly illustrated in Fig. 130, according to SVERDRUP (1926).

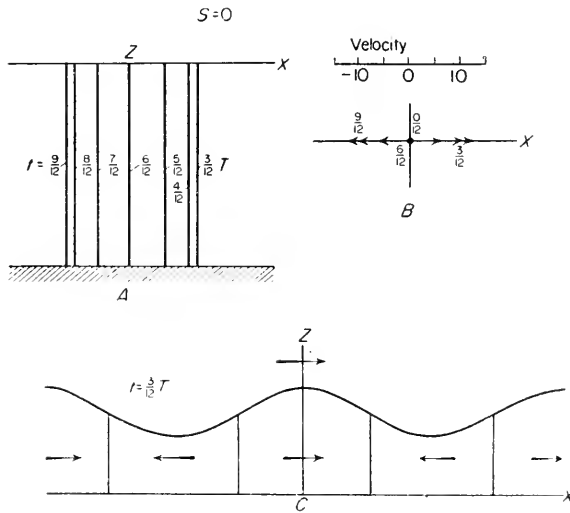


FIG. 130. Tide wave in a rotating canal of uniform depth (without friction). *A*: vertical line of particles at different phases; *B*: current diagrams; *C*: wave form and distribution of the current in the direction of propagation of the wave (Sverdrup).

The equations of tide waves on a rotating disk of infinite dimensions are derived from the differential equations (VI.100 and 101). Sverdrup showed that progressive tide waves of a simple form are only possible if the period of the tide is shorter than one-half pendulum day. These tide waves have the form ($f = 2\omega \sin\phi$).

$$\begin{aligned} \eta &= \eta_0 \sin(\sigma t - \kappa x), \\ u &= \sqrt{\frac{g}{h}} \sqrt{\frac{1}{1-s^2}} \eta_0 \sin(\sigma t - \kappa x), \\ v &= \sqrt{\frac{g}{h}} \sqrt{\frac{s^2}{1-s^2}} \eta_0 \cos(\sigma t - \kappa x), \\ s &= \frac{f}{\sigma}, \quad c = \sqrt{gh} \sqrt{\frac{1}{1-s^2}}. \end{aligned} \tag{XI.2}$$

In contrast to the Kelvin waves, the amplitude of the wave is constant along the wave-front. To the motion in the direction of progress, which may be called the longitudinal, is now added a motion along the wave-front which may be called transversal, and there is a phase difference of quarter period length between the longitudinal and the transversal motion. If the velocities of the fluid particles are represented by a central vector diagram, the end-points of the vectors lie on an ellipse, or we can say with Sverdrup that the configuration of the motion is an ellipse. The direction in which the velocities rotate is negative or *cum sole*, if the rotation of the disk is positive (*contra solem*) or vice versa. The direction of the maximum velocity of the current (major axis of the current ellipse) coincides with the direction of progress of the waves and is reached when the wave reaches its maximum height. The ratio between the axes of the ellipse, i.e. the ratio between the minimum and maximum velocity, is $s = f/\sigma$. The current ellipse is the same for all depths and maximum velocity occurs at the time of high or low water as was mentioned before. The velocity of propagation is $c = \sqrt{gh}/\sqrt{1-s^2}$, which is greater compared with the velocity of a wave of the same period length on a non-rotating disk. One can see that, when $s = 1$ or $\sigma = f$, the velocities become infinite, i.e. the wave degenerates into a simple circular motion at $\eta = 0$ (inertia motion; see vol. I/2, Chapter VI/6). Consequently, tide waves are only possible in this case if $s < 1$ or $\sigma > f$. This means that the period of the tide wave must be larger than the period of the inertia wave. Figure 131 shows conditions when $s = 0.6$.

In a very wide rotating canal a tide wave might perhaps be expected to be characterized by a rotary motion of the fluid particles in the middle of the canal and alternating motion along the walls. A wave of this kind, however, could not exist in an infinitely long canal, because the velocity of progress would vary with the distance from the walls but it seems possible that such a wave could exist on a short stretch. A solution of the fundamental equation which satisfies the boundary conditions in this case seems impossible, but a formal solution which does not agree with any fixed boundary conditions may be of value in future applications, because it represents a wave of an intermediate character compared with the two kinds of waves treated previously. According to Sverdrup, this wave has the form:

$$\eta = \eta_0 e^{-(m/c)y} \sin(\sigma t - \kappa x), \quad r = \sigma \frac{f-m}{\sigma^2 - fm}$$

$$u = \sqrt{\frac{g}{h}} \left[\frac{1}{1-r^2} \eta_0 e^{-(m/c)y} \sin(\sigma t - \kappa x) \right] \text{ with } c = \sqrt{gh} \left[\frac{1-r^2}{(1-sr)^2} \right], \quad (XI.3)$$

$$v = \sqrt{\frac{g}{h}} \left[\frac{r^2}{1-r^2} \eta_0 e^{-(m/c)y} \cos(\sigma t - \kappa x) \right].$$

These equations have for u and v the same form as (XI.2), except that s is replaced by r . According to (XI.3) the configuration of the motion is an ellipse with the ratio r between the axes. When $r = 0$, we have $m = f$ and $c = \sqrt{gh}$ and this corresponds to a tide wave of the Kelvin type (narrow canal); if, on the contrary, $m = 0$, $r = f/\sigma = s$, we obtain the conditions prevailing on the rotating disk

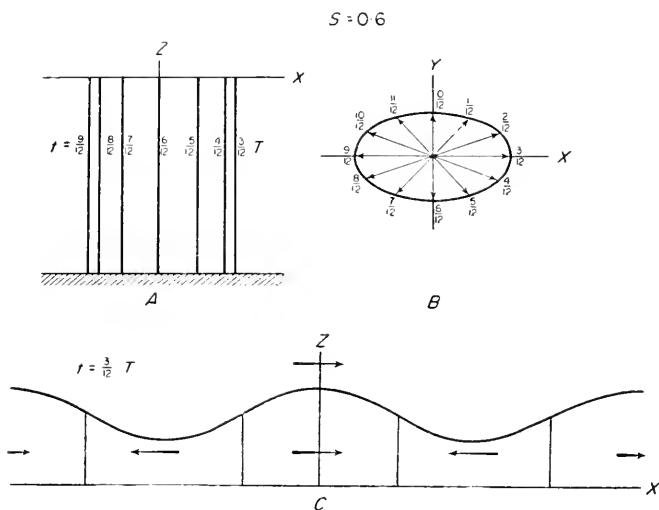


FIG. 131. Tide wave in a rotating unlimited frictionless layer. A, B and C as in Fig. 130.

of infinite dimensions, equation (XI.2). Generally $0 < m < f$, and the wave is of an intermediate character; the motion is rotary, but the ratio between minimum and maximum velocity is smaller than on an infinite disk. The amplitude decreases along the wave-front, but less rapidly than in a channel and the velocity of propagation is greater than in a channel but smaller than on an infinite disk. When $r = 1$, $\sigma = f$, the wave degenerates into a simple inertia motion.

(b) Relations Between the Tide and Tidal Currents

THORADE (1928–29, p. 290) has studied the relation between the current and tide level variation, not by solving the corresponding differential equations, but in a different manner. If friction is disregarded, the tides can be designated, after Thorade, as “frictionless tides” (“Nulltiden”), and their corresponding tidal currents as “frictionless currents” (“Nullströme”). The equations (XI.3) for instance, give the frictionless tides and currents for a very large body of water. According to the theory of ocean currents of Ekman (see vol. II, Chapter VI), the effect of the bottom friction makes itself felt only up to a relatively small height above the ocean bottom (lower frictional depth); it can be assumed that the frictionless tidal current is practically similar to conditions existing in the upper layers of deep oceans.

The forces which cause the tidal motions are, on the one hand, the tide-generating forces, and on the other hand, the gradient forces; their components along the axes of the co-ordinates are given by

$$\left. \begin{aligned} +g \frac{\partial \bar{\eta}}{\partial x} & \quad \text{and} \quad +g \frac{\partial \bar{\eta}}{\partial y}, \\ -g \frac{\partial \eta}{\partial x} & \quad \text{and} \quad -g \frac{\partial \eta}{\partial y}, \end{aligned} \right\} \quad (\text{XI.4})$$

to which correspond the frictionless tides and frictionless tidal currents of the form

$$\left. \begin{aligned} u &= u_1 \cos \sigma t + u_2 \sin \sigma t = U \cos(\sigma t - \alpha), \\ v &= v_1 \cos \sigma t + v_2 \sin \sigma t = V \sin(\sigma t - \beta), \\ \eta &= \eta_1 \cos \sigma t + \eta_2 \sin \sigma t = \eta_0 \cos(\sigma t - \varepsilon). \end{aligned} \right\} \quad (\text{XI.5})$$

The two forces (XI.4) can be combined into one single force of the form

$$\left. \begin{aligned} G_x &= G_{x,1} \cos \sigma t + G_{x,2} \sin \sigma t, \\ G_y &= G_{y,1} \cos \sigma t + G_{y,2} \sin \sigma t. \end{aligned} \right\} \quad (\text{XI.6})$$

Since the tide-generating forces in small seas are small compared to the gradient force, $G_{x,1}$, $G_{x,2}$ and, similarly, G_y are represented by $-g(\partial \eta_1 / \partial x)$ and $-g(\partial \eta_2 / \partial x)$, respectively and similarly by $-g(\partial \eta_1 / \partial y)$, $-g(\partial \eta_2 / \partial y)$ respectively. The end-point of the vectors representing the frictionless tidal current (u, v) and the total force (G_x, G_y) lie on an ellipse (current ellipse and diagram of forces). According to the theory, frictionless tidal current and tidal force are in a mutual adjustment to each other: To the force (XI.6) belongs a frictionless tidal current (XI.5) and vice versa.

The Coriolis force is directed perpendicularly to the direction of the motion. If all other forces, acting upon a body that was moving with a horizontal velocity c , referred to the rotating co-ordinate system, suddenly ceased to act, the body, under the influence of this force of inertia, would continue in an orbit which in the rotating co-ordinate system would be a circle with the radius of $r = c/f$. If the rotation is positive (*contra solem*), the direction of revolution in the circle of inertia is negative (*cum sole*) and vice versa. Consequently, rotations *cum sole* are favoured on the rotating earth. If a water particle completes a circle with the radius l and the angular velocity σ , its orbital velocity is $s_0 = \sigma l$ and, when the rotation is *cum sole*, $u = s_0 \cos \sigma t$ and $v = s_0 \sin \sigma t$. The current diagram is then a circle. The corresponding centrifugal force is $\sigma^2 l = \sigma s_0$, the Coriolis force acting inward is $f s_0$. If these forces are in equilibrium ($\sigma = f$), the water particle moves on the circle of inertia. For tide waves $2\omega \sin \phi = f < \sigma$ (the most important case), so that a tidal force S must be present to compensate for the difference $(\sigma - f)s_0 = S$. Relative to the motion of the particle, the components of the force will then be: $G_x = -S \sin \sigma t$, $G_y = -S \cos \sigma t$ and it is

apparent that to a current diagram which is a circle and whose sense of rotation is *cum sole* belongs a circular diagram of forces *cum sole*, whose phase is 90° "ahead of" the phase of the velocity, here we have $s_0 = S/(\sigma - f)$.

It can also be proven that a circular current diagram *contra solem* $u = r_0 \cos \sigma t$, $v = r_0 \sin \sigma t$ requires a tidal force *contra solem* with

$$G_x = -R \sin \sigma t, \quad G_y = R \cos \sigma t \quad \text{and} \quad r_0 = \frac{R}{\sigma + f}.$$

A comparison of the two cases shows that equal tidal forces ($R = S$) produce very different tidal current velocities, depending on whether they rotate *cum sole* or *contra solem*; at 54° N. lat. (southern North Sea) we have for M_2 $\sigma - f = 0.229 \times 10^{-4}$ and $\sigma + f = 2.58 \times 10^{-4}$, so that on the Northern Hemisphere a frictionless tidal current rotating to the right subject to the action of the Coriolis force is eleven times stronger than a current rotating to the left, all other conditions being alike.

If two of these circular motions are superimposed, we can derive the general case of a force rotating in an ellipse. To a tidal force

$$G_x = -(R+S) \sin \sigma t, \quad G_y = (R-S) \cos \sigma t, \quad (\text{XI.7})$$

to which corresponds a diagram of forces which has the form of an ellipse with the semi-axes $(R+S)$ and $(R-S)$, belongs a tidal current

$$\left. \begin{aligned} u_0 &= \left(\frac{R}{\sigma + f} + \frac{S}{\sigma - f} \right) \cos \sigma t = A \cos \sigma t, \\ v_0 &= \left(\frac{R}{\sigma + f} - \frac{S}{\sigma - f} \right) \sin \sigma t = B \sin \sigma t. \end{aligned} \right\} \quad (\text{XI.8})$$

The current diagram is an ellipse with the semi-axes

$$\frac{R}{\sigma + f} \pm \frac{S}{\sigma - f}.$$

The discussion of the equations (XI.7 and 8) leads to very important conclusions. If R and S are equal, then the *cum sole* current is definitely preponderant among the frictionless tidal currents, because $\sigma - f < \sigma + f$. Further we have

- if $S > R$: B always negative; with a diagram of forces *cum sole*, frictionless tidal current always *cum sole*;
- if $S = R$: $G_y = 0$: with alternating force, frictionless tidal current *cum sole*, axis ratio of the current ellipse σ ;
- if $S < R$: with a diagram of forces *contra solem*, frictionless tidal current *cum sole*, as long as $R/S < (\sigma + f)/(\sigma - f)$;
- if $\frac{R}{S} = \frac{\sigma + f}{\sigma - f}$ or $\frac{R-S}{R+S} = \frac{f}{\sigma}$: force *contra solem*, frictionless tidal current alternating;

if $\frac{R-S}{R+S} > \frac{f}{\sigma}$: force *contra solem* (small axis of the ellipse of force more than f : σ times the large axis), frictionless tidal current *contra solem*, with very weak velocities.

This compilation shows the extreme preponderance of the frictionless tidal currents *cum sole* on the rotating earth. Thorade has compiled in Fig. 132 a few cases of diagrams of forces with corresponding current diagrams. The

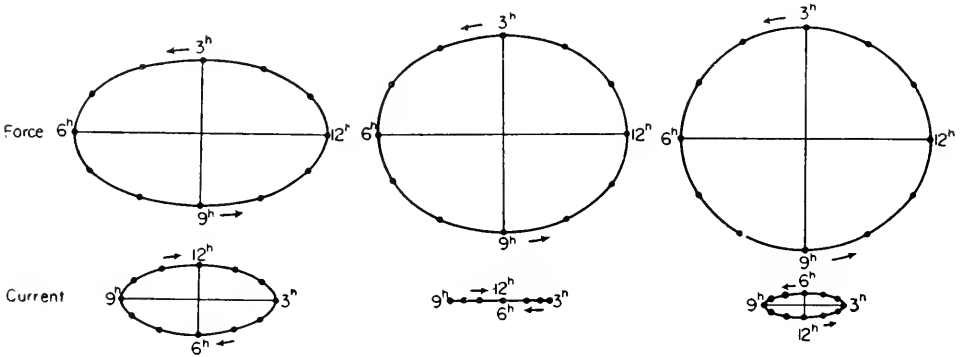


FIG. 132. Three examples of diagrams of tidal forces and corresponding current diagrams. The vectors of the force originate at the centre of the dotted ellipse and go to the points indicated by the hours of the tide. The corresponding vectors of the 'frictionless' current connect the centre of the full drawn ellipse and the corresponding hours of the tide (Thorade).

results are in full agreement with those found by Sverdrup in the analytical way. Their importance and utilization are limited by the fact that in shallow seas, where current measurements are easier, the frictional influences extend from the bottom to the surface layers.

(c) Influence of the Friction

The influence of the friction on tidal currents has been the subject of papers by Sverdrup and Thorade, and also by FJELDSTAD (1929), after Lamb had already treated the subject in a very elementary form in his *Textbook of Hydrodynamics* (1932). It is important to ascertain the influence of the friction caused by the bottom which, through turbulence will make itself felt in a more or less extensive bottom layer. The conditions, in this case, are similar to those for stationary ocean currents, except that here the tide waves are of a periodic nature. The assumptions regarding the friction are the same in both cases. Sverdrup and Fjeldstad have found integrals for the equations of wave motion, whereas Thorade treats the problem in a more synthetical way, which is more elementary, very clear and it gives a good insight in the way friction works. We will follow essentially THORADE'S method (1931 p. 152).

As shown previously, a circular tidal force S rotating *cum sole* commands a circular frictionless current *cum sole* with the radius $s = S/(\sigma - f)$. It is to be expected that frictional influences will decrease the radius of this current diagram (ellipse) with increasing depth until it becomes zero at the sea bottom. The water particles of thin individual layers describe circles with the radius s/σ , which decrease with depth, until the motion vanishes at the bottom, whereby at the same time a retardation of the phase occurs increasing with depth. For deriving the laws governing this decrease of the radius and increase of the retardation of phase, Thorade uses the same idea which has been used by Ekman for his elementary derivation of the stationary gradient current, which is explained in vol. I/2, Chapter V. Let us give the entire water layer and the sea bottom an additional circular motion s_0 , with a phase difference of 180° ($-u_0 = -s_0 \cos \sigma t$, $-v_0 = +s_0 \sin \sigma t$). If the water is sufficiently deep, both movements will equalise each other at the surface, which will be at rest, whereas at the bottom ($z = 0$) we will have the velocity components $-u_0$ and $-v_0$. This circular motion of the bottom is transmitted by friction to the superimposed water layers decreasing gradually in intensity until it vanishes at great height ($z = \infty$). Thorade calls this system of motion the "differential current" ("Differenzstrom"); u, v at the bottom it is $-u_0, -v_0$, at a large height above the bottom ($z = \infty$) it is zero. It must satisfy the equations of motion ($\nu = \mu/\rho$, the kinematic coefficient of viscosity) (see vol. I/2).

$$\begin{aligned} \frac{\partial u}{\partial t} &= +fv + \nu \frac{\partial^2 u}{\partial z^2}, \\ \frac{\partial v}{\partial t} &= -fu + \nu \frac{\partial^2 v}{\partial z^2}, \end{aligned} \tag{XI.9}$$

with the boundary conditions $u = -u_0, v = -v_0$ for $z = 0$ and $u = v = 0$ for $z = \infty$.

If the constant frictionless current (u_0, v_0) is then added again to this solution, we obtain the tidal current with friction, which satisfied its boundary conditions

for $z = 0, u - u_0 = 0, v - v_0 = 0$ and for $z = \infty, u + u_0 = u_0, v + v_0 = 0$.

The integration of (XI.9) gives

$$\left. \begin{aligned} u &= -s_0 e^{-(\pi/D_1)z} \cos\left(\sigma t - \frac{\pi}{D_1}z\right), \\ v &= +s_0 e^{-(\pi/D_1)z} \sin\left(\sigma t - \frac{\pi}{D_1}z\right), \\ D_1 &= \pi \sqrt{\frac{2\nu}{\sigma - f}}. \end{aligned} \right\} \tag{XI.10}$$

If the original motion was *contra solem*: $-u_0 = r_0 \cos \sigma t, -v_0 = -r_0 \sin \sigma t$, the "differential current" has the form

$$\left. \begin{aligned}
 u &= -r_0 e^{-(\pi/D_2)z} \cos\left(\sigma t - \frac{\pi}{D_2}z\right), \\
 v &= -r_0 e^{-(\pi/D_2)z} \sin\left(\sigma t - \frac{\pi}{D_2}z\right), \\
 D_2 &= \pi \sqrt{\frac{2\nu}{\sigma+f}}
 \end{aligned} \right\} \quad (XI.11)$$

The quantities D_1 and D_2 have a meaning similar to that of Ekman's depth of frictional resistant $D = \pi \sqrt{2\nu/f}$ (see vol. I/2, equation XIII. 24). However, in (XI.21) they are also dependent on the frequency σ of the tide wave, and for currents rotating to the right (Northern Hemisphere) D_1 is considerably larger than D_2 for currents which rotate to the left. At 54° N. lat. (southern North Sea), for instance, $D_1 = 3.36 D_2$. Both "differential currents" (XI. 20 and 21) s and r are represented vectorially by a logarithmic spiral; in Fig. 133

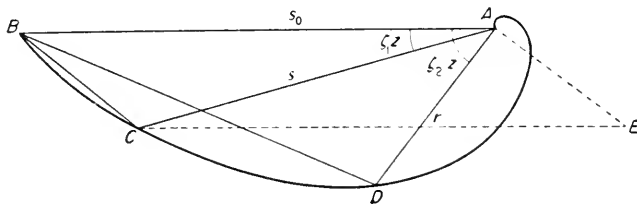


FIG. 133. Behaviour of the differential current in the presence of tidal currents (Thorade).

$AC = s$ and $AD = r$, for a height z , are two vectors of the rotary motion and $AB = -s_0$ and $-r_0$ respectively. In order to obtain the actual tidal current, the frictionless current s_0 and r_0 is added geometrically to s and r respectively. $CE = BA = s_0$ is added geometrically to AC ; in the height z above the bottom, this will give a current with the vector

$$AE = BC = s = s_0 \sqrt{1 + e^{-(2\pi/D_1)z} - 2e^{-(\pi/D_1)z} \cos(\pi/D_1)z} \quad (XI.12)$$

for the current rotating to the right,

$$BD = r = r_0 \sqrt{1 + e^{-(2\pi/D_2)z} - 2e^{-(\pi/D_2)z} \cos(\pi/D_2)z} \quad (XI.12)$$

for the current rotating to the left. Figure 134 gives for $\phi = 54^\circ$ and for the main lunar tide M_2 , s and r as a function of $z/\sqrt{\nu}$; the curves are similar to those of the stationary gradient current (vol. I/2, equation XIII.4c).

Through adequate superposition of s_0 and r_0 , we can obtain all kinds of frictionless current at the sea surface and equations (XI.9 to 12) give the current diagrams with friction. For the Northern Hemisphere, the following cases are possible:

(a) *Alternating frictionless current*: then $s_0 = r_0$ and in the case illustrated by Fig. 134 the current above the height of approximately $z = 460/\sqrt{\nu}$ is very weakly rotating to the right, almost alternating; below this height we have $r > s$, the current figures become an ellipse rotating to the left and this the stronger, the closer to the bottom.

(b) Frictionless current rotating to the right: $r_0 < s_0$. In Fig. 134 the solid curve s must be moved to the right according to s_0 . In most cases there will then still be a point of intersection with the dotted curve r . Above it the current rotates elliptically to the right, downwards elliptically to the

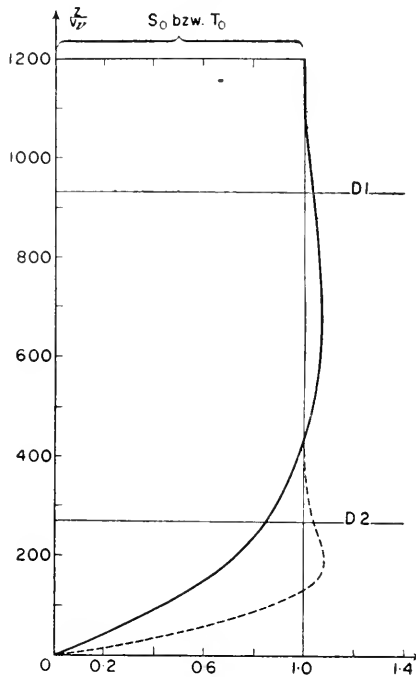


FIG. 134. Current in the presence of tidal currents close to the bottom which rotate to the right (—) and to the left (---). ($\phi = 54^\circ \text{N.}$, M_2 -tide, according to Thorade).

left. Only when $s_0 : r_0 > D_1 : D_2$, the rotary motion to the right reaches down to the bottom, while the current ellipse narrows gradually.

(c) Frictionless current rotating to the left: $r_0 > s_0$. The current ellipse remains an ellipse rotating to the left down to the bottom, and the ratio of the axis increases constantly.

The investigations made by Sverdrup and Fjeldstad deal particularly with the dynamics of a free progressive tide wave. For a wide canal the solution of the differential equations is:

$$\left. \begin{aligned} u &= \sqrt{\frac{g}{h}} C \left[M \cos \sigma \left(t - \frac{x}{k} \right) + N \sin \sigma \left(t - \frac{x}{k} \right) \right] e^{-\mu x - m y}, \\ v &= \sqrt{\frac{g}{h}} C \left[P \cos \sigma \left(t - \frac{x}{k} \right) + Q \sin \sigma \left(t - \frac{x}{k} \right) \right] e^{-\mu x - m y}, \\ \eta &= C \cos \sigma \left(t - \frac{x}{k} \right) e^{-\mu x - m y}. \end{aligned} \right\} \quad (\text{XI.13})$$

M, N, P, Q are quantities depending in a complicated way upon the water depth, the quantity $s = f/\sigma$, the damping of the wave μ , the decrease m of the wave amplitude transversely to the direction of propagation x , as well

as upon the coefficient of friction ν . The vector diagram of the current is an ellipse, the ratio of the small axis to the large axis is smaller than in the case of an infinite ocean, where the ratio is exactly equal to s . The effect of the Coriolis force is partly compensated by the slope of the wave crest transversely to the direction of propagation. Under these circumstances, such a wave cannot travel without changing its form; however, the solution will remain valid for a relatively long distance. The velocity of propagation is no longer as it was in (XI.2), but will be

$$c = n \sqrt{gh} \sqrt{\frac{1}{1-s^2}},$$

in which the factor n depends in a complicated way upon the depth h , the frequency σ and f . The factor n is the ratio of c/c_0 , when $c_0 = \sqrt{gh} \sqrt{1/(1-s^2)}$ or the velocity of the wave in absence of turbulence. Sverdrup has given the following Table 36 for n .

Table 36. The ratio c/c_0 as function of $h \sqrt{\sigma/2\nu}$ and s

$h \sqrt{\frac{\sigma}{2\nu}}$	$s = f/\sigma$			
	0.0	0.3	0.6	0.9
0.4	0.43	0.41	0.36	0.18
0.8	0.72	0.70	0.58	0.30
1.2	0.84	0.82	0.71	0.40
1.6	0.88	0.87	0.80	0.51
2.0	0.90	0.89	0.86	0.61
2.5	0.92	0.91	0.88	0.72
3.0	0.93	0.92	0.90	0.78
4.0	0.94	0.93	0.92	0.84
5.0	0.95	0.95	0.93	0.88
∞	1.00	1.00	1.00	1.00

The last line gives the values without friction ($\nu = 0$). It is apparent that the friction retards the waves, and much more so at the pole ($s = 0.9$) than at lower latitudes. But the velocity of propagation also depends very much upon the frequency σ of the waves, so that for long distances there must be a dispersion of the waves.

The motion at a depth h can be fully described by the following four quantities (Fig. 135).

- (1) V = the scalar value of the maximum velocity in the direction of the main axis of the current ellipse.
- (2) αV = the minimum velocity in the direction of the small axis; α is the ratio between the scalar values of minimum and maximum velocity.

- (3) χ = the angle of orientation which the major axis of the ellipse forms with the positive axis; it is positive, when the maximum velocity (corresponding to the maximum wave height) is to the left of the $+x$ -axis.
- (4) The angle τ (in time τ/σ) which gives the phase difference expressed in degrees between the time of the maximum velocity and the time of maximum wave height.

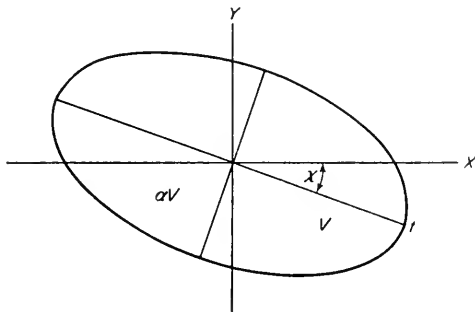


FIG. 135.

All these quantities can be computed in a simple way with (XI.24) from the values M, N, P, Q , as shown by WERENSKIÖLD (1916, p. 360)

$$\left. \begin{aligned}
 2V &= \sqrt{\frac{g}{h} \frac{C}{2} \left[\sqrt{\{(M+Q)^2 + (N-P)^2\}} + \sqrt{\{(M-Q)^2 + (N+P)^2\}} \right]}, \\
 2\alpha V &= \sqrt{\frac{g}{h} \frac{C}{2} \left[\sqrt{\{(M+Q)^2 + (N-P)^2\}} - \sqrt{\{(M-Q)^2 + (N+P)^2\}} \right]}, \\
 \tan 2\chi &= \frac{2(MP+NQ)}{(M^2-Q^2) + (N^2-P^2)}, \\
 \tan 2\tau &= \frac{2(MP+NQ)}{(M^2-Q^2) - (N^2-P^2)}.
 \end{aligned} \right\} \quad \text{(XI.14)}$$

Table 37 contains two cases computed according to the equations (XI.23); both are for the M_2 tide ($\sigma = 1.4052 \times 10^{-4}$). In both cases the current diagram is an ellipse *cum sole*, with the greatest velocities at the surface. The minimum velocity decreases more rapidly with depth than the maximum velocity. This causes the ellipse to become narrower in approaching the bottom. The maximum velocity occurs before the high water, the difference increases with depth. The conditions in cases of friction can be represented schematically in Fig. 136, according to Figs. 130 and 131. A discussion of the equation (XI.23) by Fjeldstad gives the same conclusions and results as found by Thorade and Sverdrup in a different way.

Sverdrup and Fjeldstad deal also with the case which is important for the polar regions, when a sea is covered by a layer of ice (pack-ice) which dampens the movement of the water through friction. In that case the boundary

Table 37. Current data for tide waves, taking the friction into account

$$(\sigma = 1.4052 \times 10^{-4})$$

Case 1: Polar Sea, $\phi = 72^\circ \text{N.}$, $f = 1.387 \times 10^{-4}$, $s = 0.987$, depth 50 m, coefficient of eddy viscosity $\nu = 182$.

Depth(m)...	0	20	40	45
V	3.28	2.87	1.56	0.78
aV	-2.22	-1.76	-0.73	-0.26
a	-0.68	-0.61	-0.47	-0.34
χ°	-20°	-18.4°	-7.5°	-3°
τ°	-5°	-6.3°	-17.0°	-22.6°
$t(\text{min})$	-10	-13	-35	-46

Case 2: Southern Kattegat, $\phi = 56^\circ 20' \text{N.}$, $f = 1.213 \times 10^{-4}$, depth 30 m, coefficient of eddy viscosity $\nu = 100$.

Depth(m)...	0	10	20	27.5
V	3.38	3.08	1.79	0.67
aV	-2.06	-1.76	-0.61	-0.20
a	-0.61	-0.57	-0.34	-0.30
χ°	-15.1°	-13.3°	-7.8°	1.7°
τ°	-0.4°	-3.4°	-7.2°	-19.4°
$t(\text{min})$	-0.7	-6.9	-14.5	-38.8

conditions change and the maximum velocities of the tide wave are then greatest in the middle layers, while the velocities at the surface and bottom, are zero. In nature, however, the vertical structure of the sea, for a case like this, consists of three layers: the upper layer is almost homogenous and has strong turbulence, a bottom layer with little turbulence, and the middle layer between these two is a stable, relatively thin water layer with nearly no friction. The tide waves then take the character of internal tide waves (see p. 517).

(d) Results of Current Measurements

There are not many observations available to test the above-mentioned theoretical results. In making such a comparison, it should be remembered first of all that the theory is based on a frictional coefficient which is assumed constant, whereas in reality this coefficient varies with depth, according to the vertical density distribution. This circumstance can cause considerable deviation, especially if several horizontal strata are present. The assumption that there is on slipping motion along the bottom is perhaps not accurate in all cases. For shallow water only the lower parts of the curves in Fig. 134 are to be considered, where the coefficient of friction is most noticeable, but generally

speaking, comparisons have shown that the principal phenomena are correctly represented by the theory. Sverdrup and Fjeldstad tested mainly the current observations obtained during the "Maud" expedition, from 1918

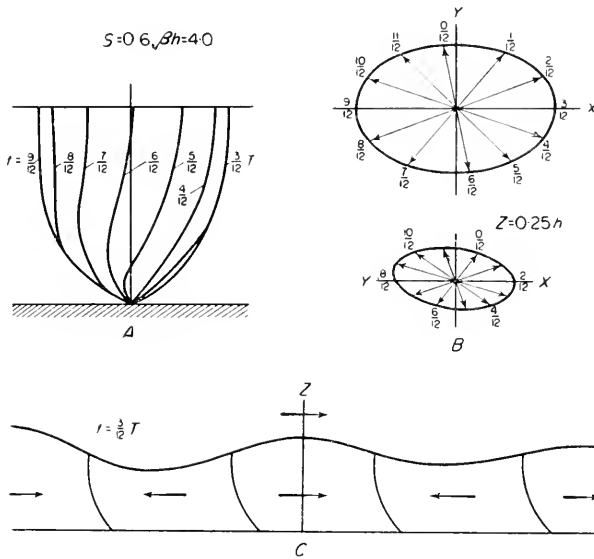


FIG. 136. Tide wave in a rotating, ($s = 0.6$) unlimited canal (Sverdrup). In upper figure of *B*, current diagram at the surface; lower figure current diagram in $3/4$ depth; otherwise the same as in Fig. 130.

to 1925, on the North Siberian shelf, which were made mostly in the presence of a more or less thick layer of pack-ice. Figure 137 reproduces graphically the observations of St. 8 (18 July, 1924, 76.5° N., 141.5° E., depth 22 m).

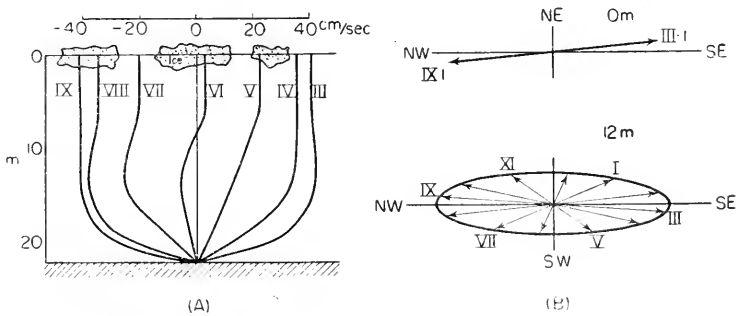


FIG. 137. Tide currents on the Siberian shelf. Station 8 (18 July, 1924) (Sverdrup).

The vertical section *A* has been placed in the direction of propagation of the wave (NW. to SE.), the component of the current in the direction of progress is represented for every Greenwich lunar hour. *B* gives the vector diagram for the currents for 0 and 12 m depth. There are three circumstances

pointing to great resistance: The maximum velocity is not at the surface, but below it and is reached 2 h before high water; the velocity of propagation of the wave is only 10 m/sec, whereas \sqrt{gh} gives 14.7 m/sec. Since the currents are practically alternating, we can assume $s = 0$ and $\mu = \nu \rho = 690 \text{ cm}^{-1} \text{ g sec}^{-1}$, but then the agreement with the observations is not good. The observed currents in the upper layers change more slowly with depth than those computed, but more rapidly close to the bottom. The computed currents reach a maximum velocity about 1.1 h before high water, but the observed difference is 2 h. Fjeldstad has also taken into account the resistance offered by the ice and has thus obtained a better agreement. For the entire layer 0–12 m the observations give in the vector diagram for the currents $V = 38.0 \text{ cm/sec}$, $\alpha V = -5.0 \text{ cm/sec}$ and a priming of the phase of $t = -2 \text{ h}$, whereas the theory gives $V = 38 \text{ cm/sec}$, $\alpha V = -1.56$ and $t = -1.2 \text{ h}$.

The discussion made by Thorade of the current and tide observations in the Deutsche Bucht shows that the agreement with the theory is only partially satisfactory. Figure 138 gives a comparison and it shows that the observed

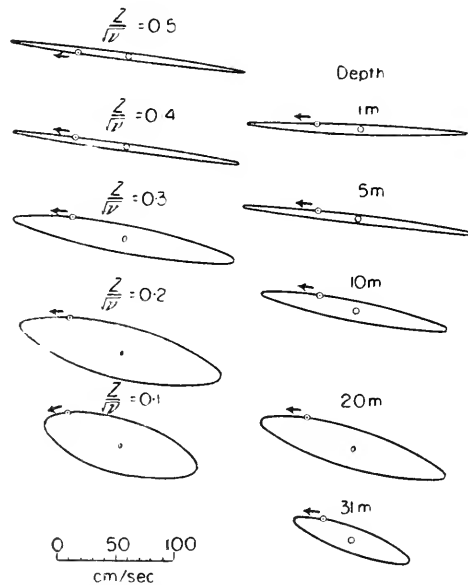


FIG. 138. Tide currents in the Deutsche Bucht of the North Sea. $\varphi = 54^{\circ}.0' \text{ N.}$, $\lambda = 7^{\circ}30'$ 18–21 June, 1924, (Thorade). Left: according to theory; right: according to the observations.

current ellipses are not in bad agreement with the theory. It is quite apparent that, with an alternating tidal current at the surface (frictionless current), there will be a rotation to the left approaching the bottom, and the ellipses will grow wider and wider. Observations made at the Wester Sill show also that, with a surface current rotating to the right, there is an alternating current

in the layers above the bottom and then a rotation of the current to the left at the bottom as required by the theory. However, when going into details, deviations become noticeable which render the interpretation difficult. Figure 139 shows a section through stream filament according to the observations

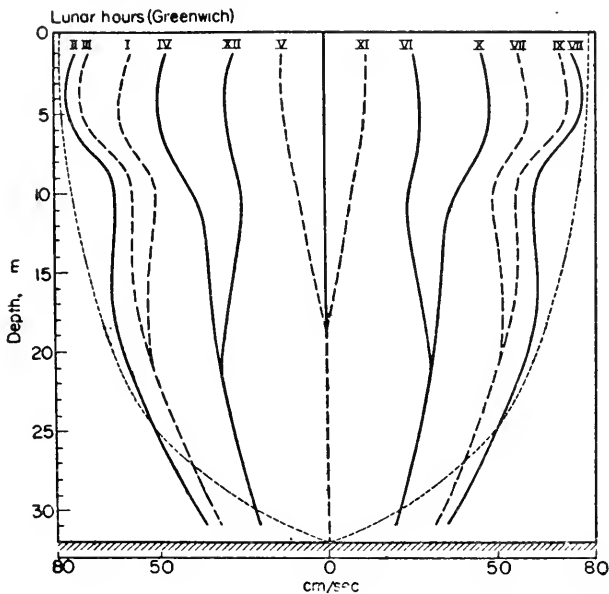


FIG. 139. Section through stream filament in tide current in the Deutsche Bucht, 18-21 June, 1924, (Thorade). — and ---, observed; ·······, computed.

on which Fig. 138 is based. In the bottom layers, the increase in velocity is much less than required by the theoretical curve. The reason for this might be found in the presence of a thin boundary layer at the bottom, over which the upper watermasses glide. Disturbances appear also at the surface; the maximum velocity is found at 5 m depth, below this there is a rapid decrease down to 10 m, although there were no singularities in the disturbance of the density. Thorade has endeavoured to compute also the coefficient of friction for single cases; however, the results were unsatisfactory. Acceleration, pressure force, Coriolis force and friction, being connected to each other in the equations of motion, he tries, for a case with particularly good observations to determine the friction, when the first three quantities are given. Apparently, the frictional resistance is not proportional to the momentary differences in velocity, but, depending upon depth, to those velocity differences which prevailed more or less long before. Such an inertia of the turbulence would not be improbable, but the differences in phase which were found were indeed too great as compared with the differences in velocity. It is possible to gain an idea of the order of magnitude of the coefficients of friction by forming mean values over an entire tidal period. Thorade finds the following values:

Depth (m)	1	5	10	20	30
ν in $g\text{ cm}^{-1}\text{ sec}^{-1}$	1140	1720	1250	952	75

The order of magnitude agrees with the values found by Sverdrup.

The current observations published by DEFANT and SCHUBERT (1934) made during 7 tidal periods by four ships of the Kattegat expedition in August 1931 were used for the study of the vertical distribution of the tidal currents. One

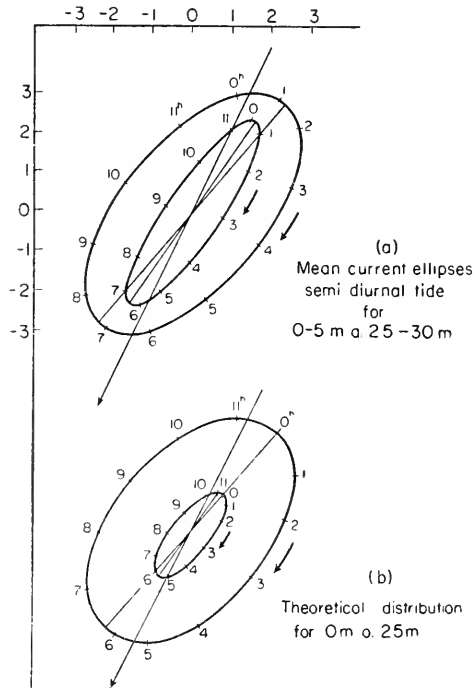


FIG. 140. Current diagrams in the southern Kattegat, August 1931.

obtains a better picture by computing mean values for all periods and all ships. The current ellipses, in all depths, rotate *cum sole*. Neglecting the ellipse at 17 m depth, they become narrower with increasing depth; at 5 m the ratio of the axis was 0.51, at 25-30 m about 0.24. There is also the priming of the phase with increasing depth, which conforms with the theory. The main results are given in Table 38, whereas in Fig. 140 are reproduced the two middle diagrams. Below is the theoretical distribution of the current computed for a coefficient of friction $\nu = 100$. The similarity of these two figures is apparent; the size of the current diagrams in the lower layer is, according to the observations, approximately twice the size of the computed one. The cause of this might be the discontinuity layer between 13 and 17 m.

GRACE (1929, p. 150) has investigated the influence of the friction by other

Table 38. Tidal currents in the Kattegat, August 1931

Layers	Main direction	Main axis of ellipse referred to the Direction of Propagation		Maximum velocity (cm/sec)	
		Observed	Computed	Observed	Computed
0-5 m	N. 40 E.	-15	-15	3.7	3.4
25-27 30 m	N. 33 E.	-8	-5	2.9	1.95
Phase h		Priming of phase (min)	Sense of rotation	Ratio of axis	
				Observed	Computed
0-5 m	1.2	54 38	cum sole	0.50	0.61
25-27/30 m	0.3			cum sole	0.24

methods, in the current observations made on the light ships *Varne*, *Smith's Knoll*, *Horn's Reef*, etc. The results are in a generally good agreement with those given above. For further investigations on the effects of friction on the tides see also p. 326.

3. Tides in Adjacent Seas

In the preceding paragraph we discussed mainly the relations between the vertical tide and the pertaining tidal currents in their vertical distribution. In the following paragraphs we will examine the tides in adjacent seas, which are enclosed seas and communicate with the open ocean only by means of openings. It will facilitate the discussion to treat first the case of a rectangular ocean basin neglecting the earth's rotation and friction (see DEFANT 1919, 1925). The influence of complicated shore and bottom configurations, as well as the Coriolis force and the friction will be discussed next.

(a) Independent and Co-oscillating Tide

If we consider a water mass of which the greatest part is enclosed, we find that the tides occurring herein are of a twofold origin. The tide-generating forces cause periodical horizontal water displacements which produce the *independent tides*. On the other hand, the tides of the open ocean in front of the opening cause the partly enclosed water masses of the adjacent sea to co-oscillate with the same period as the tides in front of the opening. As the latter is originated by the tide generating forces, these co-oscillating tides have also the periods of the generating force.

(a) *Rectangular basin* of the length l with a depth h ; closed end is at $y = x/l = 0$, opening into the ocean is at $y = x/l = 1$. It is necessary to add on the right-hand side of the equation of motion (VI.5 and 8) a periodic force $X = m\cos(\sigma t + \epsilon)$ which causes an *independent tide*, for which the boundary conditions are to be fulfilled: at the closed end $\xi = 0$, at the opening

$\eta = 0$. If we put: $\nu = T_f : T_\infty = \sigma l / c\pi$ in which $T_f = 2l / \sqrt{gh}$ is the period of the basin if it would be completely closed and $T_\infty = 2\pi / \sigma$ the period of the force, we obtain for this independent tide:

$$\left. \begin{aligned} \xi &= \frac{2m}{\sigma^2 \cos \nu\pi} \sin \frac{1}{2} \nu\pi y \sin \nu\pi (1 - \frac{1}{2} y) \cos(\sigma t + \epsilon), \\ \eta &= \frac{mT_\infty \sqrt{gh}}{2\pi g \cos \nu\pi} \sin \nu\pi (y - 1) \cos(\sigma t + \epsilon). \end{aligned} \right\} \quad \text{(XI.15)}$$

It has the character of a *standing wave*. If ν becomes $\frac{1}{2}, \frac{3}{2}, \frac{5}{2}$, etc., ξ and η become infinite. This means *resonance*, which, in the absence of friction, means that the amplitude of the motion increases so rapidly that the solution becomes unapplicable. If $\nu\pi$ is very small, i.e. if the period of the generating force is large compared with the period of the slowest free oscillation of the basin, we obtain for η in first approximation:

$$\eta = \frac{m}{g} l (y - 1) \cos(\sigma t + \epsilon).$$

This is a simple oscillation with a nodal line at the opening, as if the water were without inertia.

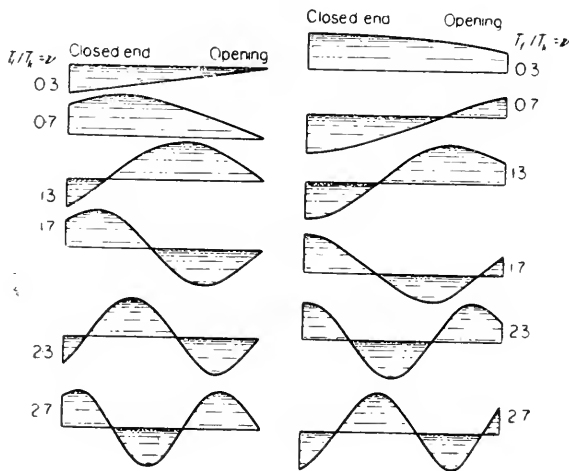


FIG. 141. Distribution of the amplitude in a longitudinal section of a rectangular basin of uniform depth for the independent tide (left) and the co-oscillating tide (right).

The left part of Fig. 141 gives the distribution of the amplitude in a basin, for different values of ν , assuming that the factor $mT_\infty c / 2\pi g = 1$ cm. The amplitudes of the independent tides increase, when the basin becomes deeper. According to (VIII.7) $m/g = 1.235 \times 10^{-7}$ for the combined lunar and solar tides at the equator, so that the factor becomes $0.0273 \sqrt{h}$ in cm. In the latitude ϕ we must multiply m/g by $\cos \phi$.

$h =$	36	64	100	144	196	m
Factor =	1.6	2.2	2.7	3.3	3.8	cm.

It is obvious that the independent tides are small, except when the period of the free oscillation comes close to the period of the forced oscillation and resonance occurs. It is only in this case that this kind of tide becomes important in the more or less closed water masses of the adjacent seas. For a basin which corresponds approximately to the dimensions of the North Sea ($l = 800$ km, $h = 80$ m, $\phi = 53^\circ$ N. lat.), we have $T_f = 15.86$ h, $\nu = 1.29$. Consequently, the independent tide for M_2 will show two nodal lines: one at the opening, the other one approximately 200 km distant from the inner end. But the amplitude, at this end, will only reach about 2 cm. Things are very different, when the condition of resonance is nearly fulfilled. If we select the free oscillation period of the basin $T_f = 18.9$ h (for instance, like the Red Sea with the Gulf of Suez and the gulf of Akaba), then for the semi-diurnal tide $\nu = 1.52$, and with $h = 450$ m the amplitude at the closed end will be 91 cm and there will be a nodal line of the standing wave in the centre of the basin.

For the *co-oscillating tide* the basic equations are the same as in (VI. 5 and 8), and the boundary conditions require that at the closed end ($y = 0$) $\xi = 0$, whereas at the opening ($y = 1$) we must always have $\eta = Z \cos(\sigma t + \epsilon)$, i.e. the tide must always correspond with the tides of the open ocean. Then the co-oscillating tide has the form

$$\left. \begin{aligned} \xi &= Z \frac{l}{\nu \pi h} \frac{\sin \nu \pi y}{\cos \nu \pi} \cos(\sigma t + \epsilon), \\ \eta &= Z \frac{\cos \nu \pi y}{\cos \nu \pi} \cos(\sigma t + \epsilon). \end{aligned} \right\} \quad (\text{XI.16})$$

This part of the tide also has the character of a *standing wave*. There will be resonance for the same values of ν as in the case of the independent tide. Figure 141, right, gives the distribution of the amplitude in a longitudinal section of the basin for various values of ν ; here $Z = 1$. As the range of the tide in front of the opening of the ocean basin can, in most cases, attain very large values, it is apparent that the co-oscillating tide will be decisive for the tides of the adjacent seas.

The origin of the co-oscillating tide can be imagined to be the superposition of an incoming tide wave and of the totally reflected wave at the closed end. It is obvious that only the *total* reflection at the closed end produces a co-oscillating tide in the form of a standing wave.

(β) *Ocean basins with a complicated configuration.* For ocean basins with complicated orographical conditions the same methods can be used for determining the independent and the co-oscillating tides as are used to determine their free oscillation period (see Chapter VI/2, p. 154). The equations of motion

and of continuity are the same as there: (VI.5 and 47). The solution for certain simple cases, in which both the width and the depth of the canal vary proportionally to the distance from the closed end, has already been given in Lamb's *Hydrodynamics* (2nd edition, 1931, para. 186). Defant has made other applications, using the Chrystal theory of seiches. Other theories of seiches can also be used; however, the simplest one seems to be the method of the step-wise numerical integration of the hydrodynamical equations (p. 165). It can be applied also, when the cross-sections along the valley vary very irregularly and gives at once the entire form of oscillation of the basin (position of the nodal lines, amplitude of the horizontal and vertical displacements and the tidal currents respectively).

To compute the *co-oscillating tide* one uses the equations (VI.54 and 55) and starts the computation at the closed end of the basin where must be $\xi = 0$ and selects for η an arbitrary value, for instance 100. The period of the co-oscillating tide is given by the selection of the component tide. Therefore, ξ and η can be computed step-wise from cross-section to cross-section. Finally, one obtains at the end of the basin which opens into the ocean ($x = l$) a certain value $\eta = \eta_1$. However, according to the boundary condition indicated above, the amplitude of the tide for this point in the open ocean is Z . In order to obtain the correct distribution of the amplitude of this tide, it will suffice to multiply each value by the ratio Z/η_1 . The equations remain satisfied, inasmuch as the proportionality factor in ξ and η eliminates itself from them.

For the *independent tide*, which is generated directly by the tidal forces, it is necessary to add to the equations a term for a periodic force $X = m\cos(\sigma t + \varepsilon)$. The equations for the step-wise computation of ξ_2 and η_2 from the values ξ_1 η_1 , of the preceding cross-section will then be

$$\xi_2 = -\frac{1}{S_2[1 + (ar_2)/(4S_2)]} \left[\varrho_1 + \left(\eta_1 + \frac{a}{4}\xi_1 + \frac{1H}{2} \right) v_2 \right], \quad (\text{XI.17})$$

$$\eta_2 = \eta_1 + a \frac{\xi_1 + \xi_2}{2} + \Delta H,$$

$$\varrho_2 = \varrho_1 + \frac{\eta_1 + \eta_2}{2} v_2$$

in which $\Delta H = (m/g)\Delta x$. The boundary conditions to be fulfilled are: at the closed end ($x = 0$) $\xi = 0$ and at the open end ($x = l$) $\eta = 0$. η_0 at the cross-section 0 (closed end) must be selected in such a way that the second condition is fulfilled at the end of the computation. One varies the values of η -which necessitate a repetition of the computation, until the correct value is sufficiently narrowed down between two limits. This tedious calculation can be considerably shortened by the following artifice. One selects for η_0 a value resulting from the equation (XI.15) for $y = 0$ for a canal of equal length

and constant cross-section (corresponding to the mean depth of the basin). Then one proceeds with the computation according to (XI.17) until the last cross-section (opening). One obtains here a definite value for η' , which, if it were correct, would be zero. If this is not the case, one adds to the computed distribution of amplitude another one, corresponding to a *co-oscillating tide*, which at the last cross-section (opening) gives an amplitude $-\eta'$. The total sum of the two satisfies the differential equations of the independent tide and also the boundary condition at the opening. In this way, one can compute the independent tide nearly as rapidly as the co-oscillating tide.

A condition for these methods is that the tide-generating force in the considered region of the ocean is synchronous everywhere along the "Talweg". If this is not the case, for instance, for long and curved canals, one must divide the tide-generating force into two periodic components with prescribed phase, and make the computation for each component separately. Such a division is always possible. The results added again with their respective phases will give the longitudinal oscillation of the ocean basin, whereby all orographic factors are taken into consideration.

(b) Effects of the Rotation of the Earth

As regards the influence of the Coriolis force on standing waves of the independent tide and the co-oscillating tide in adjacent and boundary seas, see particularly the explanations given in Chapter VI, 5th para. (p. 204), which can also be applied in this instance. To consider in first approximation the Coriolis force, it is sufficient to compute the horizontal tidal currents of both kinds of tides from the corresponding values of ξ and, as explained on pp. 143, 154, to determine the transverse oscillations caused by the deflecting force of the earth's rotation. The superposition of the longitudinal oscillation and the transverse oscillations transforms the nodal lines into amphidromies, which rotate *contra solem*. The alternating tidal currents change into rotary currents and their vector diagrams are ellipses, in this case there is not a complete equilibrium between the transversal gradient and the Coriolis force (same as for the Kelvin waves).

Taylor has given an accurate solution of the kind of co-oscillation which can be expected of a rectangular bay of uniform depth with the external tide before its opening into the open ocean. The result is explained on p. 210. At some distance from the inner end, the co-oscillating tide has the simple form of the superposition of the incoming and the reflected Kelvin wave with alternating currents. In the part of the bay closest to the end, however, there appear transverse oscillations which make it possible that the boundary condition $\xi = 0$ at the closed end is fulfilled. Figures 91 and 92 show the distribution of the co-tidal lines and co-range lines and the current diagrams of the tidal currents for a bay whose length is twice its width. The case discussed corresponds approximately to the North Sea 53° N. lat., width 465 km, depth 74 m. The northern amphidromy shows the superposition of

the incoming and the outgoing Kelvin wave; the southern amphidromy is somewhat disturbed compared to the northern. The co-oscillating tide takes the aspect of a tide wave travelling anti-clockwise (*contra solem*) along the shore; the tidal ranges are always largest at the shore and drop to zero towards the centres of the amphidromies.

These investigations give valuable indications as to the extent to which the earth's rotation influences the tidal phenomena. There where the influence of the Coriolis force is small (narrow basins, small velocities and low geographical latitudes) both the independent and the co-oscillating tide have the character of standing waves with very pronounced nodal lines; there where the Coriolis force can develop more fully, both tides rather have the character of waves travelling along the coast *contra solem*, with rotary currents in the inner part of the bay.

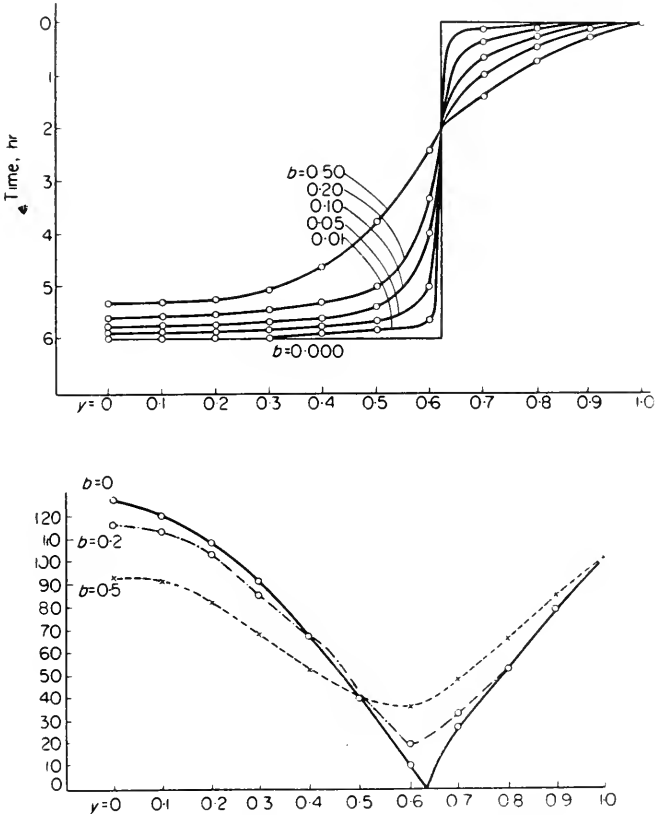
(c) Influence of Friction

The influence of friction on the tidal motions in adjacent seas can be explained by referring to the influence of friction on seiches (see Chapter VI, para. 2/b, p. 155). In the case of these periodical motions, the wave energy is reduced primarily by the *eddy viscosity*, which is caused by the irregularities of the ocean bottom and of the coasts. The simplest way of considering this viscosity is, as was already pointed out in the afore mentioned chapter, to introduce into the differential equations for the horizontal water displacements a term of the form $\beta(\partial\xi/\partial t)$. It means that, if β is constant, the friction is proportional to the velocity of the motion. This assumption does not quite correspond to our knowledge as to how the friction is related to the velocities in case of a turbulent state of motion; however, it has the advantage that the calculations can be completed until the end, thus permitting one to survey better the frictional influence. The quantity β is not a constant, as we know already from the damping curves of the seiches, but depends upon the depth and the nature of the bottom. In the theory β generally appears in the relation $\beta/\sigma = \beta T/2\pi$, and it was shown that its order of magnitude, in relation to the mean depth, is given approximately by the following quantities:

$$\begin{array}{cccccc} h = & 100 & 50 & 30 & 10 & m \text{ and below} \\ b = & 0.1-0.2 & 0.5 & 0.5-1.0 & 1.0-2.0 & \text{sec}^{-1} \end{array}$$

With this assumption for the friction, the differential equations of the horizontal and vertical displacements of the water particles for independent and co-oscillating tides can be integrated for a rectangular basin and uniform depth, see DEFANT (1919). The changes in amplitudes and phases around the bay shores, become larger when the friction increases. The horizontal velocities are greatest in the vicinity of the nodal lines, and consequently the friction is particularly noticeable there. The friction causes the abrupt change of phase of half a period to be replaced by a gradual change. The

standing wave of the independent and of the co-oscillating tide takes the character of a progressive wave, which travels apparently from the opening of the bay to its closed end. If friction does not become too great, the position of the nodal lines continues to be clearly perceptible by the crowding of the co-tidal lines. The node where the amplitude of the tide is zero disappears and instead we find a region with minimal range. This minimum is smaller if the friction is greater. The Figs. 142 and 143 show clearly the



FIGS. 142, 143. Distribution of the phase and amplitude of the semi-diurnal co-oscillating tide of a rectangular bay of uniform depth ($\nu = 0.8$) for various values of b . Opening at $y = 1$, where amplitude = 100 cm, phase 0 h.

distribution of the phase and the amplitude of the semi-diurnal co-oscillating tide of a bay with $\nu = 0.8$ and various values of b . The amplitude at the opening ($y = 1$) is assumed to be 100 cm, the phase at 0 h.

For adjacent seas with an irregular configuration and with the same assumption for the friction, there is a method similar to the step-wise computation of the independent and co-oscillating tide.

We assume for the differential equations of the horizontal and vertical displacements a solution in the form

$$\left. \begin{aligned} \xi &= \xi_1 \cos \sigma t + \xi_2 \sin \sigma t, \\ \eta &= \eta_1 \cos \sigma t + \eta_2 \sin \sigma t \end{aligned} \right\} \quad (\text{XI.18})$$

and replacing the differential quotients by difference quotients, one obtains the system of equations

$$\left. \begin{aligned} \Delta \eta_1 &= a(\xi_1 - b\xi_2), \\ \Delta \eta_2 &= a(\xi_2 + b\xi_1), \\ \xi_1 &= -\frac{1}{S_1} \int \eta_1 b dx, \\ \xi_2 &= -\frac{1}{S_1} \int \eta_2 b dx. \end{aligned} \right\} \quad (\text{XI.19})$$

By means of this system we can compute step wise the quantities ξ_1 , ξ_2 , and η_1 , η_2 , and their combination in (XI.18) gives the tidal motion within the bay. The equation for $\Delta \eta_1$, is similar to the one without friction, except that another term is added which contains the coefficient for friction. Generally, it is small and acquires some importance only there, where ξ_2 is large, i.e. at the nodal lines.

An example is given in Table 39. It concerns the co-oscillating tide of the Gulf of Bristol with the external tide in the Irish Channel, as given by DEFANT (1920, p. 253). The computation was started at the cross-section 0 with the boundary values $\xi_1 = \xi_2 = 0$ and the arbitrary values $2\eta_1 = +100$ and $2\eta_2 = +20$ cm. The table gives the correlated values of $2\eta_1$, and $2\eta_2$ for all eight cross-sections. According to the observations, the range at the open end is 7.6 m, the phase 5.5 h. We then have for $y = 1$ the equation

$$34.16 \cos \frac{2\pi}{T}(t - \varepsilon) - 46.01 \sin \frac{2\pi}{T}(t - \varepsilon) = p \cos \frac{2\pi}{T}(t - 5.5 \text{ h})$$

This gives $\varepsilon = 7.3 \text{ h}$ and $1/p = 0.174$, and the co-oscillating tide at the various cross-sections; in the next column are the observed values of establishment and range at coastal localities. The agreement is very good.

Table 39. Co-oscillating tide in gulf of Bristol

Cross-section	y	Mean depth (m)	b	$2\eta_1$	$2\eta_2$	2η (min)	Phase lunar hours	Observed	
								Range (m)	Establishment h
0	0	0	—	+100	+20.0	13.6	7.64	—	—
1	1:7	12	2.0	95.8	+ 4.5	12.8	7.4	12.7	7.4
2	2:7	15	1.5	88.8	- 7.9	11.9	7.1	11.8	7.0
3	3:7	16	1.2	76.2	-22.4	10.6	6.7	10.6	6.6
4	4:7	21	1.0	61.4	-34.1	9.4	6.3	9.4	6.3
5	5:7	32	1.0	51.5	-40.0	8.7	6.0	8.5	5.9
6	6:7	35	1.0	43.2	-43.4	8.2	5.8	7.9	5.8
7	1	45	1.0	34.16	-46.0	7.6	5.5	7.6	5.5

The development of the co-oscillating tide into a standing wave requires that the incoming wave is totally reflected at the inner end of the bay. If this is not the case, the reflected wave is not exactly like the incoming one and

the superposition of the two gives a progressive wave, which differs the more from a standing wave, the greater the amount of tidal energy is lost inside the bay. Many bays and adjacent seas become very shallow in their inner regions, where a considerable portion of the tidal energy is absorbed and thus lost for reflection (see DEFANT 1928, p. 274). In such adjacent seas the co-oscillating tide loses its character of a standing wave, even when the depth is very large elsewhere. The case of a rectangular bay of constant depth, at whose inner end tidal energy gets lost, can be computed mathematically. Let the bay at $y = l$ open into a sea where the tide is

$$\eta = Z \cos \sigma t.$$

The time is counted from the time of high water at the open end. The amplitude of the incoming wave (in the negative x -direction) is a . The reflected wave, however, has the amplitude b , so that the quantity of energy $(a^2 - b^2)/a^2$ has been lost by the reflection at the inner end of the canal. $b = a$, means total reflection. The horizontal and vertical displacements of the water particles along the bay ($v\tau = \sigma l/c$) can be written

$$\left. \begin{aligned} \xi &= a \sin(\sigma t - \varepsilon + v\tau y) - b \sin(\sigma t - \varepsilon - v\tau y), \\ \eta &= -\frac{h\sigma}{c} [a \cos(\sigma t - \varepsilon + v\tau y) + b \cos(\sigma t - \varepsilon - v\tau y)]. \end{aligned} \right\} \quad \text{(XI.20)}$$

a/b is given by the loss of energy; the amplitude a and the phase ε must be given by the only boundary condition at the opening. We obtain

$$\eta = Z \left[\frac{\cos \varepsilon}{\cos v\tau} \cos v\tau y \cos(\sigma t - \varepsilon) - \frac{\sin \varepsilon}{\sin v\tau} \sin v\tau y \sin(\sigma t - \varepsilon) \right] \quad \text{(XI.21)}$$

in which $[(a - b)/(a + b)] \tan v\tau = \tan \varepsilon$

and $a = -\frac{cZ}{h\sigma} \frac{\sin(v\tau + \varepsilon)}{\sin 2v\tau}$.

For $a = b$ the equation (XI.21) changes into a standing wave as given by (XI.16) for a *total* reflection. In the case a/b the co-oscillating tide is the superposition of two orthogonal waves (phase difference = one-quarter period). Along the bay the phase retards gradually against the phase at the opening by increasing amounts, until it reaches the full amount ε at the inner end. For *one* nodal line the phase difference then is no longer 180° but, according to the value of v , $180^\circ \pm \varepsilon$.

When an adjacent sea has in itself an orographical configuration such that its tides are only little disturbed by the friction, its co-oscillating tide with the open sea will no longer have the form of a simple standing wave, when in its inner end a portion of the wave energy is lost. This is also the case, when for instance the inner end of a more or less closed sea becomes a very shallow one, where the dissipation of tidal energy is large. The co-oscillating

tide in the main section will then seem to be the superposition of two orthogonal standing waves. This simple case, which can also be computed, is important in dealing with an actual sea (see p. 368).

It is far better to assume that the friction is proportional to the square of the average velocity of the tidal current (see vol. I/2, p. 499). Taylor's assumption for the frictional force has the form

$$F = k\rho u^2, \quad (\text{XI.22})$$

if u is the mean velocity, ρ the density of the water and k a constant between 0.002 and 0.0016, based on values observed in natural channels. If the bottom configuration is irregular, this constant can have far higher values. The work done by the frictional force is then

$$\kappa \rho u^3 = k\rho U^3 \cos^3 \frac{2\pi}{T} t.$$

The mean value of $\cos^3(2\pi/T)t$ for a full period is $\frac{1}{3}\pi$, so that the amount for the dissipation of the energy is

$$4 \frac{k\rho}{3\pi} U^3.$$

TAYLOR (1919) was the first to compute, using this relation, the loss of energy of the tidal motion in the Irish Channel. According to observations, the average $U = 2\frac{1}{2}$ knots = 114 cm/sec, and we obtain as the mean loss of energy for this sea 1300 erg per cm²/sec. Taylor has also applied another method to determine the loss of energy for the same sea. He computes the quantity of energy which this section of the sea receives on one hand through its southern entrance (Arklow-Bardsey Island) and, on the other hand, through its northern entrance (Red Bay-Mull of Cantire). To this quantity of energy E_a has to be added to the quantity of energy E_i which the tide generating force transmits to the water-masses of the Irish Sea. The only loss of energy R is caused by friction. As the tidal energy during a full period neither increases nor decreases, $R = E_a + E_i$. The numerical computation, in the case of the Irish Sea, gives a loss of energy through friction of 1530 erg cm⁻² sec⁻¹ which agrees with the above-mentioned value as to the order of magnitude.

The principle of the conservation of energy teaches that, in every physical process, the transformation of kinetic and potential energy of a system T and V always equals the work Q done by the external force and to the loss of energy through friction E . If the first three quantities are known, the fourth quantity can be computed. The kinetic and potential energy are given by the equations

$$T = \frac{1}{2} \rho h \left(\frac{\partial \xi}{\partial t} \right)^2$$

and

$$V = \frac{1}{2} \rho g \eta^2,$$

whereas $Q = \rho h X(\partial \xi / \partial t)$, when X represents the external force. The above-mentioned relation

allows, through comparison with the corresponding differential equation for ξ , the computation of the dissipation of the energy E per unit time and unit surface. We have

$$E = \frac{2\pi}{T} \rho h b u^2.$$

For a full period of 12 lunar hours, the mean value of $u^2 = \frac{1}{2}U^2$ and if we assume again $U = 114$ cm/sec, $\rho = 1.03$ and for the Irish Sea $h = 68$ m, and if we take $b = 0.2$ and according to the previous table (p. 342) then E is nearly exactly 1300 erg per cm^2/sec in good agreement with Taylor's value.

Another way of evaluating the friction of tides in adjacent seas has been used by GRACE (1931, 1936, 1937). If we assume that, in an oblong-shaped ocean, the tidal motion is completely longitudinal, we can compute from the equation of continuity the mean velocity u at each cross-section for the M_2 tide, and the equation of motion gives then, the only unknown factor, the frictional force F . The action of the tide-generating force can be neglected, being very small. The corresponding equations are

$$\left. \begin{aligned} \frac{\partial u}{\partial t} &= -g \frac{\partial \eta}{\partial x} - F, \\ fu &= -g \frac{\partial \eta}{\partial y}, \\ \frac{\partial Su}{\partial x} &= -b \frac{\partial \eta}{\partial t}, \end{aligned} \right\} \quad (\text{XI.23})$$

if S is the area of the cross-section and b the width at the surface of a cross-section at the point x of the "Talweg". The second equation is used to reduce the values η observed on the shores to the "Talweg". If we put

$$\left. \begin{aligned} \eta &= A \cos(\sigma t - \gamma) = \eta_1 \cos \sigma t + \eta_2 \sin \sigma t, \\ u &= \bar{u} \cos(\sigma t - \alpha) = u_1 \cos \sigma t + u_2 \sin \sigma t \end{aligned} \right\} \quad (\text{XI.24})$$

we can compute from the third equation $\Delta S u_1 / \sigma$ and $\Delta S u_2 / \sigma$ for the intervals between each cross-section. If we know \bar{u} at *one* cross-section (light-ship), the values u_1 and u_2 can be determined for all cross-sections. Now everything is given in the first equation except

$$F = \bar{F} \cos(\sigma t - \beta) = f_1 \cos \sigma t + f_2 \sin \sigma t.$$

This method has been applied by Grace to the tides of the Gulf of Bristol and of the English Channel between Le Havre — Brighton and Ramsgate — east of Calais, and he obtained for \bar{F} and β the values shown in Tables 40 and 41. The result is that the phase of friction is in first approximation the same as that of the tidal current, but we see that the frictional constant varies in an irregular way. The mean value for the Bristol Channel is 2.6×10^{-3} , which is in good agreement with the value 2.4×10^{-3} found by Taylor. This value of k corresponds to a $b = 1.3$, which is also in good agreement with the value assumed by Defant. In the English Channel the phase of the

Table 40. Tides in Bristol Channel

Cross-section	Vertical tide		Current		Friction		Coefficient of friction $k = \frac{hF}{u^2}$
	H (cm)	Phase (ϵ°)	\bar{u} (cm/sec)	α	\bar{F} (cm/sec ²)	β°	
0							
1	389	200					
2	375	194	145	280	0.041	296	3.0×10^{-3}
3	361	192	153	281	0.018	308	1.4
4	351	187	168	281	0.030	307	2.4
5	331	178	164	280	0.048	277	4.1
6	317	172	134	279	0.026	277	3.5
7	304	170	105	276	0.011	270	2.5
8	292	169	99	274	0.004	—	1.4

Table 41. Tides in the English Channel

Cross-section	Vertical tide		Current		Friction		Coefficient of friction $k = \frac{hF}{u^2}$
	H (cm)	Phase (ϵ°)	\bar{u} (cm/sec)	α	\bar{F} (cm/sec ²)	β°	
0							
1	212	337					
2	243	333	107	192	0.0073	187	2.4×10^{-3}
3	279	328	77	182	0.0122	141	6.3
4	305	326	52	162	0.0112	160	12.1
5	316	326	37	123	0.0083	172	19.4
6	307	324	47	92	0.0021	76	3.2
7	252	318	62	78	0.0215	—12	21.3
8	235	312	75	72	0.0069	53	5.1
	225	308	73	66	0.0058	86	4.8

friction corresponds also roughly to the phase of the current, but here the variations are larger; the average is 9.3×10^{-3} , corresponding to a value $b = 1$. A strict correlation apparently exists between the difference between the phase of the current and the phase of the friction, and the values of k ; the latter increases with the former values. Grace uses a similar method to determine the friction in the shallow Gulf of Suez. He finds $k = 3.6 \times 10^{-3}$ or $b = 0.11$; this latter value is smaller than would be expected for a mean depth of 44 m. On the other hand, the frictional influences prove to be very great, so that they cannot originate from the ordinary bottom friction alone; it is probable that they are increased by the existence of numerous cliffs and banks.

All investigations show that Taylor's assumptions of the friction are capable of giving its most essential effects on the tides, but as long as the friction-produced changes in the tidal current are not more exactly considered, only a rough approximation can be obtained.

Investigations of this kind have been made in more recent times by BOWDEN (1947), BOWDEN and PROUDMAN (1949) and BOWDEN and FAIRBAIRN (1952*a, b*). Records of fluctuations in the speed of the tidal current (in the Mersey estuary) near the bottom were obtained and compared with other records taken with the current meter suspended freely at various depths. The fluctuations covered a wide range of periods but could be separated into two main types: "short period", having periods of the order of a few seconds, and "long period", with periods from 30 sec to several minutes. The short-period fluctuations correspond approximately in period to the waves, and their amplitudes are of the same order of magnitude as the calculated wave-particle velocities. From an exact analysis of the fluctuations it is concluded that the fluctuations observed near the bottom are evidence of the turbulence associated with bottom friction. It is believed to be the first time that the presence of turbulent velocity fluctuations of this time-scale in the sea has been established experimentally. The long-period fluctuations show amplitudes, which increase with the basic current and with depth and sometimes attain 0.4 of the basic current; their features are consistent with their being turbulent in origin also, although turbulence of the time-scale involved in this case would probably be mainly horizontal.

Later the component of turbulent velocity in the direction of the basic current and across has been studied by means of several current meters placed in the direction of the mean flow and across. The periods of the turbulent fluctuations recorded varied from a few seconds up to several minutes, and it appears that, as in other types of turbulence, a *continuous spectrum of fluctuations* is present. It was found that the integral scale of the turbulence in the direction of flow is of the order of 7 m, compared with 14 m, the mean depth of water, whereas scales in the vertical and lateral directions are of the same order of magnitude and of the order of one-third of the scale in the direction of the mean flow.

In order to study the internal structure of a tidal current in relatively shallow water, where frictional effects, originating at the sea bed and communicated through the water by internal stresses, will occur, measurements were made of all factors in tidal currents a few miles from the coast (off Red Wharf Bay, Anglesey). The results shall be briefly outlined as follows: Expressing the amplitude of the frictional force at the bottom in the form $F = k\rho U^2$, where U is the amplitude of the mean current from surface to bottom, and ρ is the density of the water (see XI.22), the results give the coefficient k an average value of 1.8×10^{-3} , which agrees with the value given on p. 346. The internal frictional stress in the water was found to increase approximately linearly with depth from the surface to the bottom, and the corresponding values of the mean eddy viscosity covered a wide range of values (from 130 to 500 $\text{cm}^2 \text{sec}^{-1}$). Previous estimates of the eddy viscosity in tidal currents give a similar range.

4. The Tidal Phenomena in Narrow Embayments

The tides of coastal embayments derive their energy from the ocean tides and are considered to be part of co-oscillating systems in which the period is determined by the tide in the outer sea, while the detailed character of the motion depends on the size and form of the enclosed water-masses. In these small embayments the influence of the earth rotation is insignificant, while the influence of friction cannot be neglected. REDFIELD (1950) has recently given a method to analyse the tidal phenomena in these small embayments. This method starts from the theory of free waves, which are subjected to damping as they advance towards a coast on which they are reflected, which theory was developed by FJELDSTAD (1929; see also SVERDRUP *et al.*, 1946). The actual tide in the narrow embayment may be considered to be due to two progressive waves of the same period travelling in opposite directions. The tide is treated a single cos-wave. One of these is the primary wave originating in the open sea; the other is the reflected wave originating at the closed end of the embayments, which can be considered as a barrier. At the barrier the two waves are equal in elevation and are in phase. In a uniform channel the elevation of the primary wave is given by

$$\left. \begin{array}{l} \eta_1 = A \cos(\sigma t - \kappa x) e^{-\mu x}, \\ \text{that of the reflected wave by} \\ \eta_2 = A \cos(\sigma t + \kappa x) e^{\mu x}, \end{array} \right\} \quad (\text{XI. 25})$$

A is the amplitude of the waves at the barrier, σ the change of the phase per unit of time and t will be measured from the time of high water (H.W.) at the barrier, when $t = 0$. κ is the change in phase per unit of distance and x is the distance measured from the barrier, where $x = 0$, μ is the damping coefficient.

The elevation of the water η at any time and place along the channel is

given by $\eta = \eta_1 + \eta_2$ and H.W. occurs when $\partial\eta/\partial t = 0$. Letting t_H denote the local time for H.W. this equation gives

$$\sigma t_H = \tan^{-1}(-\tan \kappa x \tanh \mu x). \tag{XI.26}$$

This function gives the time of H.W. at any position along the channel for any chosen coefficient of damping.

Equation (XI.26) can be used to find the relative height of H.W. at any point — the ratio of height of H.W. at the point under consideration to the

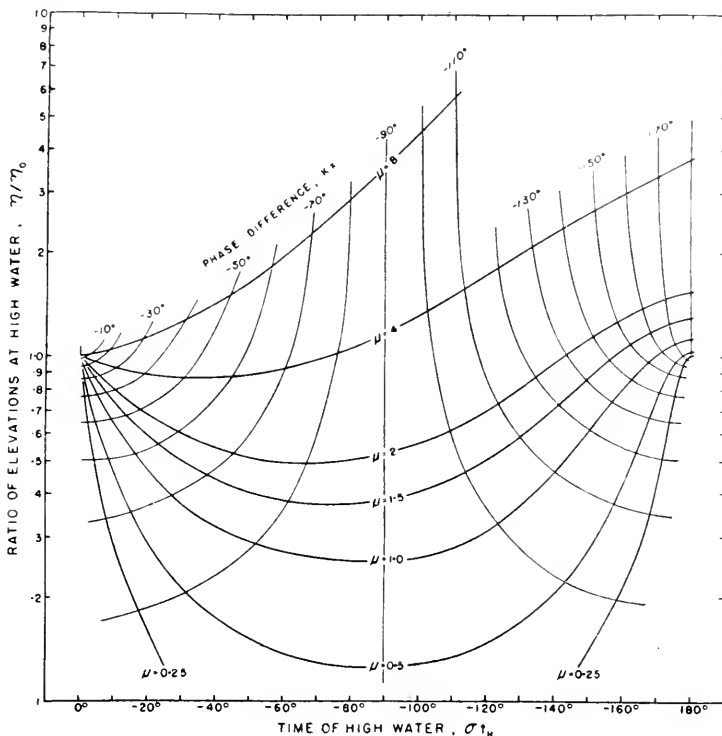


FIG. 144. Relations between the ratio of height of high water at any point to the height of high water at the barrier η/η_0 , the time angle of high water σt_H , the phase difference of a primary wave at that point relative to the barrier κx , and the coefficient of damping μ . Reflection occurs where $\eta/\eta_0 = 1.0$ and $\sigma t_H = 0$.

height at the reflecting barrier — along the channel. Restricting η and η_0 to the elevations at H.W. the ratio η/η_0 can be written

$$\eta/\eta_0 = \sqrt{\frac{1}{2}(\cosh 2\mu x + \cos 2\kappa x)}. \tag{XI.27}$$

This function relates the height of H.W. at any position along the channel to the height at the barrier for any chosen coefficient of damping. Redfield derives in the same way the time of slack water or maximum current at any point. Letting t_S denote the local time of slack water, σt_S is given by

$$\sigma t_s = \tan^{-1} \frac{\tanh \mu x}{\tan \kappa x} - \tan^{-1} \frac{\mu}{\kappa} \tag{XI.28}$$

This function relates the time of slack water to any position along the channel for any chosen coefficient of damping. The time of maximum current will precede or follow the time of slack water by one-quarter period or 90°.

Tidal data are available in the form of records of the time of H.W., the elevation at H.W. and the time of slack water or maximum current at various positions along the channel. We have now the possibility to test these equations on the tidal data. This will give us indications to the effect of a given channel on the primary or reflected wave; information on the distribution of phase differences along the channel and on the damping which is required. These applications are to be tested with the same restrictions as discussed previously in this chapter. By combining these relations defined by equations (XI.26 and 27) Fig. 144 was constructed in which the observed variables (the

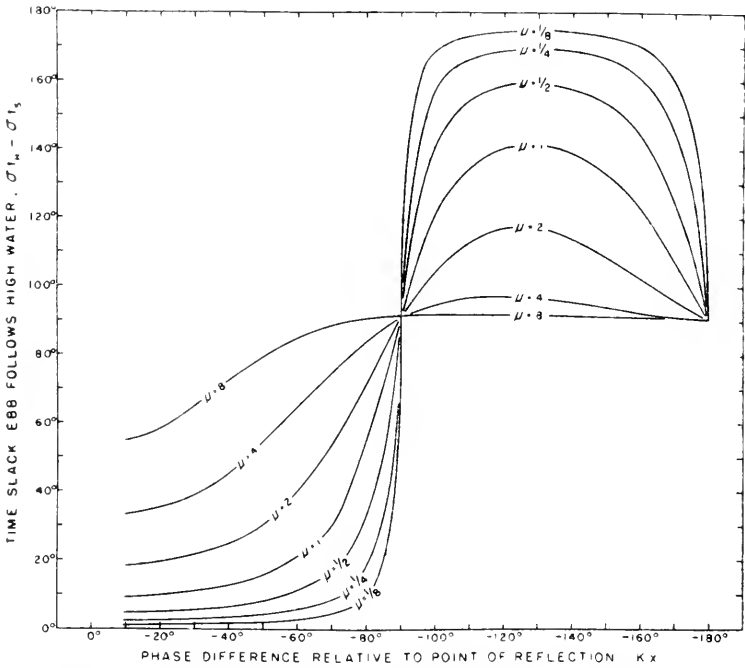


FIG. 145. Relations of the time angle between high water σt_H , and slack water σt_s at any point along a channel, the phase difference of a primary wave at that point relative to the barrier κx and the coefficient of damping μ , when reflection occurs at a barrier where $\kappa x = 0$.

ratio of the H.W. elevations η/η_0 on a logarithmic scale and the local time of H.W. σt_H) are represented by the rectangular co-ordinates and the desired properties of incoming wave (the phase relations and the coefficients of damping) are represented each by a series of curves. This nomogram is

completely general being independent of the actual dimensions of the basin or of the period of the wave. It is consequently a simple matter to plot a series of tidal data giving the elevations and time of H.W. in Greenwich time on a similar semi-logarithmic co-ordinate system and by superposing the curves on Fig. 144 to determine whether a satisfactory fit can be obtained. If this is the case, the properties of the primary wave as determined by the position

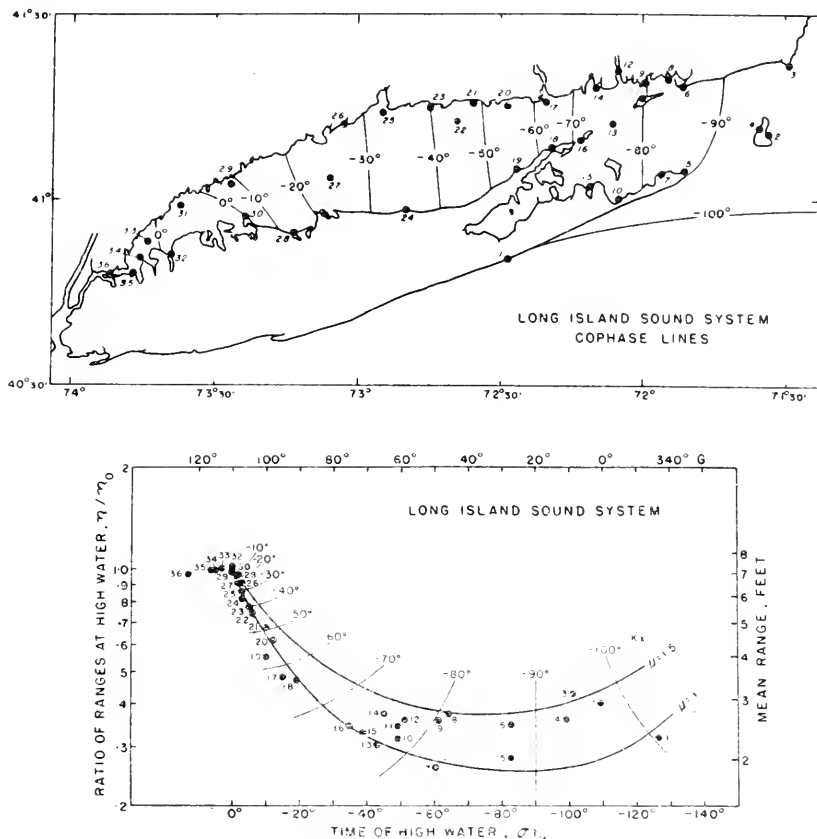


FIG. 146. Upper part: chart of Long Island Sound showing stations and co-phase lines.
Lower part: analysis of Long Island Sound system.

of the points on the nomogram may be transferred to charts or diagrams in which the geographical position of the points are indicated, and these may be used to determine the distribution of phase differences of the primary and reflected wave in the channel.

In an entirely similar way the relations of equations (XI.26 and 28) may be combined to construct a graph in which the local time of H.W. σ_{t_H} is related to that of slack water σ_{t_S} , as in Fig. 145. This figure may be used to check the adequacy of the theoretical treatment and to predict the expected time of slack water from data of the time of H.W.

Redfield has tested this very practicable method of analysis on three embayments: Long Island Sound, the Bay of Fundy and the system formed by the Strait of Juan de Fuca and the Strait of Georgia. In all these cases Redfield proves that the assumptions underlying the equations are valid. He obtains a detailed description of these systems in terms of the distribution of phase differences for the primary and reflected waves along the channel, the velocity of their propagation and the coefficient of damping. An excellent example of the application of this method is found in Redfield's analysis of the Long Island Sound illustrated in Fig. 146 in which the data of mean range of tides and time of H.W. are plotted on the co-ordinate system of Fig. 144. The best fit of the data to the co-ordinate system is obtained by assuming that the reflection occurs from stations 30 to 32 where the mean tidal range is maximal at 7.2–7.4 ft. The observations made within Long Island Sound proper, along the south side of Block Island Sound and including Station 1 on the outer coast of Long Island fall closely along the co-ordinate for a damping coefficient $\mu = 1.0$. The phase difference of the primary wave at each station relative to the point of reflection may be determined from this diagram and the "co-phase" lines representing the advance of the primary wave into Long Island Sound have been drawn in the upper part of Fig. 146. The velocity of the primary wave is about 27 knots. In Fig. 146 a number of stations appear where the range is greater than would be expected if the value of μ is 1.0. These stations are all on the right-hand side of the direction of propagation of primary waves and is an effect which may be attributed to the rotation of the earth. The Bay of Fundy and the system formed by the Strait of Juan de Fuca and the Strait of Georgia have been analysed in a similar way. This simple method has proven its advantages (see also REDFIELD, 1953).

5. Relations Between Tidal Current and Co-tidal and Co-range Lines

The differential equations of motion give the most important relations between the tides and tidal currents. From these relations we can deduct the influence of islands and coastlines on the tides. PROUDMAN (1914, p. 89; 1925, p. 243) has investigated these relations; however, he did not treat the structure of the tidal current.

The tide in a locality can be represented by

$$\eta = H \cos(\sigma t - \varepsilon) = \eta_1 \cos \sigma t + \eta_2 \sin \sigma t$$

in which η_1 and η_2 are independent of time and high water occurs at the time $t = \varepsilon/\sigma$.

Here

$$\eta_1^2 + \eta_2^2 = H^2$$

and

$$\frac{\eta_2}{\eta_1} = \tan \varepsilon .$$

If $\varepsilon = 0$ or $\eta_2 = 0$, the tide wave is a progressive wave; the maximum of the flood occurs simultaneously with high water. If $\varepsilon = 90^\circ$ or $\eta_1 = 0$, the tide wave is a standing wave; the maximum flood occurs at half tide. Let us designate the angles formed by the co-tidal lines ($\tan \varepsilon = \text{const}$) and the co-range lines ($H = \text{const}$) with the x -axis by ψ and ψ' .

We find that

$$\tan \psi = \frac{\eta_1 \frac{\partial \eta_2}{\partial x} - \eta_2 \frac{\partial \eta_1}{\partial x}}{\eta_1 \frac{\partial \eta_2}{\partial y} - \eta_2 \frac{\partial \eta_1}{\partial y}} \quad \text{and} \quad \tan \psi' = \frac{\eta_1 \frac{\partial \eta_1}{\partial x} + \eta_2 \frac{\partial \eta_2}{\partial x}}{\eta_1 \frac{\partial \eta_1}{\partial y} + \eta_2 \frac{\partial \eta_2}{\partial y}}. \tag{XI.29}$$

The general equations of motion are

$$\left. \begin{aligned} \frac{\partial u}{\partial t} - fr &= -g \frac{\partial \eta}{\partial x} - \frac{F}{h}, \\ \frac{\partial v}{\partial t} + fu &= -g \frac{\partial \eta}{\partial y} - \frac{G}{h} \end{aligned} \right\} \tag{XI.30}$$

in which F and G are the components of the frictional force for the unit surface of the ocean bottom. If at a locality the x -axis is put in the direction of the maximal flood current and the time is counted from its start, then ε/σ is the time of high water relative to this time, and we can substitute

$$\left. \begin{aligned} u &= U \cos \sigma t, \\ v &= V \sin \sigma t, \\ F &= \frac{F_1}{h} \cos \sigma t, \\ G &= \frac{G_2}{h} \sin \sigma t. \end{aligned} \right\} \tag{XI.31}$$

From the equations (XI.39) results

$$\left. \begin{aligned} g \frac{\partial \eta_1}{\partial x} &= -F, \\ g \frac{\partial \eta_2}{\partial x} &= \sigma U + fV, \\ g \frac{\partial \eta_2}{\partial y} &= -(\sigma V + fU), \\ g \frac{\partial \eta_2}{\partial y} &= -G \end{aligned} \right\} \tag{XI.32}$$

$$\tan \psi = - \frac{(\sigma U + fV) + F \tan \varepsilon}{(\sigma V + fU) \tan \varepsilon - G},$$

and

$$\tan \psi' = \frac{(\sigma U + fV) \tan \varepsilon - F}{(\sigma V + fU) + G \tan \varepsilon}. \tag{XI.33}$$

If there is no friction ($F = 0$, $G = 0$), these equations are reduced to

$$\begin{aligned}
 gH \frac{\partial H}{\partial x} &= \eta_2(\sigma U + fV), & gH \frac{\partial H}{\partial y} &= -\eta_1(\sigma V + fU), \\
 gH^2 \frac{\partial \varepsilon}{\partial x} &= \eta_1(\sigma U + fV), & gH^2 \frac{\partial \varepsilon}{\partial y} &= \eta_2(\sigma V + fU), \\
 \tan \psi &= -\frac{\sigma U + fV}{\sigma V + fU} \cotan \varepsilon \\
 \tan \psi' &= \frac{\sigma U - fV}{\sigma V + fU} \tan \varepsilon
 \end{aligned} \quad \left. \vphantom{\begin{aligned} \tan \psi \\ \tan \psi' \end{aligned}} \right\} \quad \text{(XI.34)}$$

from the latter equation it follows that $\psi' = \frac{1}{2}\pi + \psi$; in the absence of friction, the co-tidal lines and co-range lines are always perpendicular to each other.

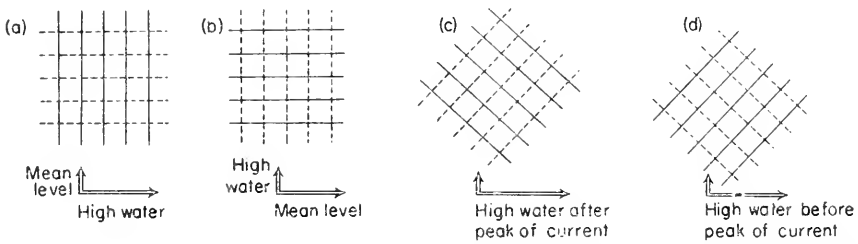


FIG. 147. ———, co-tidal lines; ----, co-range lines, (a) for a progressive tide wave ($\varepsilon = 0^\circ$), (b) for a standing tide wave ($\varepsilon = 90^\circ$), (c) when high water occurs $\frac{1}{4}$ period after current maximum $0 < \varepsilon < \frac{1}{2}\pi$, (d) when high water occurs $\frac{1}{4}$ period before current maximum $-\frac{1}{2}\pi < \varepsilon < 0$.

If we take a progressive tide wave, then $\varepsilon = \eta_2 = 0$, i.e. $\partial H/\partial x = 0$ and $\partial \varepsilon/\partial y = 0$. Conditions will be as illustrated in Fig. 147a. The co-tidal lines have the direction of the current at half tide, the co-range lines the direction of the current at high and low water respectively.

For a standing wave, $\varepsilon = 90^\circ$ and $\eta_1 = 0$, i.e. $\partial H/\partial y = 0$ and $\partial \varepsilon/\partial x = 0$, and conditions are as in Fig. 147b. For this case also we find that the co-tidal lines follow the direction of the current at half tide, the co-range lines the direction of the current at high and low water respectively, so that this rule applies in general.

For an example, Proudman cites the distribution of the co-tidal and co-range lines in the northern part of the Irish Sea (see p. 384). The minimum velocity here is practically zero ($V = 0$) and high water occurs with slack water. The co-tidal lines must follow the stream-lines, the co-range lines must be perpendicular to these. This is, in fact, largely the case.

For general conditions, we have mostly $\sigma > f$ and $U > V$, so that $(\sigma U + fV)/(\sigma V + fU)$ is positive. If high water occurs within one quarter period after the maximum in the current, we have $0 < \varepsilon < \frac{1}{2}\pi$ and $\frac{1}{2}\pi < \psi < \pi$, $0 < \psi' < \frac{1}{2}\pi$, i.e. the co-tidal lines make an obtuse angle, the co-range lines

an acute angle with the direction of the current maximum (Fig. 147c). If on the contrary, H.W. precedes by one quarter period the maximum current we have $\frac{1}{2}\pi < \varepsilon < 0$ and $0 < \psi < \frac{1}{2}\pi$ and $\frac{1}{2}\pi < \psi' < \frac{1}{2}\pi$, the position of the isolines is exactly the reverse of the previous one (Fig. 147d).

If there is friction, the systems of curves are no longer perpendicular to each other, and the essential point is whether or not frictional terms are predominant in the equations for $\tan \psi$ and $\tan \psi'$ in (XI.33). Both for the progressive and the standing tide wave we get $\tan \psi \cdot \tan \psi' = -F/G$. When the friction is small, F will not be very different from G ; and $F:G$ will not deviate considerably from 1; the angle enclosed by the two systems of curves will not deviate much from 90° ; with other conditions, there can be strong deviations from 90° .

6. Conditions Along Shores and Disturbances on Account of Bays and Islands

If the current runs parallel to a shore (x -direction) we have in its proximity $V = 0$, and we obtain from (XI.34)

$$\left. \begin{aligned} \tan \psi &= -\frac{\sigma}{f} \cot \varepsilon, \\ \tan \psi' &= \frac{\sigma}{f} \tan \varepsilon. \end{aligned} \right\} \quad \text{(XI.35)}$$

If we consider a short stretch of shore, the variations in the time of the maximal current and in the occurrence of the high water will be small, although the variations in the magnitude and in the direction of the currents are large.

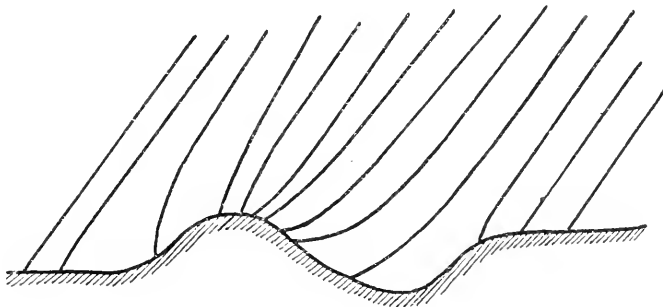


FIG. 148. Co-tidal lines in the vicinity of a Cape and in a Bay.

In (XI.35) ε is to be considered as nearly constant, i.e. the slope of the co-tidal and co-range lines towards the shore line will be almost constant. Although this seems to be the case, great variations show up in the direction of the slope. Figure 148 illustrates the course of the co-tidal lines in the immediate vicinity of a cape and of a small bay. Both the time of high water and the range vary much more rapidly around the cape and much slower in front of the bay than farther outside, where they have a more uniform course.

An example of this can be found in the western part of the North Sea, off the coast between Forth and Humber. Here high water occurs at the time of the maximum of the current, which runs parallel to the coast, so that the co-tidal lines are perpendicular, the co-range lines parallel to the coast. It shows clearly that where the coast is convex to the sea, ϵ of M_2 tide varies rapidly, whereas this value varies slowly if the coast is concave to the sea. This can be observed particularly well at Flamborough Head between Whitby and Brindlington. Further examples can be found at the south-east coast of Ireland (described by TAYLOR, 1919, p. 32). At Wicklow Head there is a considerable retardation in the progress of the tide wave. In Wicklow, a few miles north of the cape, high water occurs at 10 h 53 m, which is 2 h 30 m later than in Arklow, 11 miles south of the cape. There is another example at Greenore Point (south-east corner of Ireland). The time of high water at Saltees, about 10 miles south-west of Carnsore Point, is 6 h 6 m, at Carnsore Point (4 miles south of Greenore Point) at 6 h 25 m, however at Tuskar Rock (4 miles off Greenore Point) at 6 h 10 m, and in Wexford South Bay, on the northern side of the cape, at 6 h 5 m. The disturbance north of the cape in the Wexford Bay is apparently so great that here the co-tidal lines run for a short distance in the opposite direction.

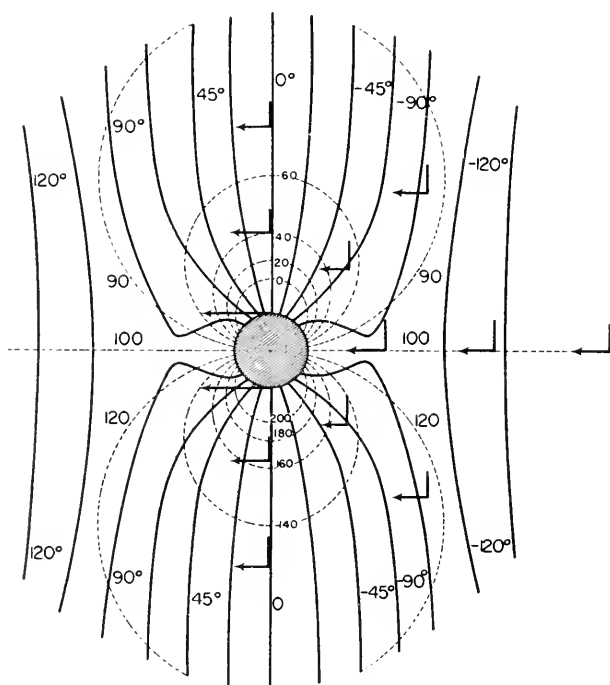


FIG. 149. Tide wave travelling from the right to the left, diffracting on a small island.
 —, co-tidal lines ----, co-range lines.

Proudman has also studied how different coastal configurations influence the tide waves. In this case one deals with diffraction of the waves at these irregularities of the coast, whereby the ocean depth is supposed to be constant (vertical shores). Although in nature these conditions apply only approximately, yet one gets an idea as to how the co-tidal and co-range lines are changed by such orographical coast disturbances. The corresponding mathe-

mathematical developments are not simple, for which reason we will only discuss here the most important results. Figure 149 illustrates the case of a wave with a straight wave crest progressing from right to left, which is confronted with a small island, whose dimensions are small compared to the wave length. The current ellipses rotating to the right are indicated on the right side of the picture by the two semi-axes of the ellipse. We see that the tide wave travels slower on both sides around the island than farther outside (in the manner of Fig. 148), whereby the ranges on the left side are increased, those on the right side reduced. This can be so strong that a curved nodal line is formed, within which the tide proceeds inversely.

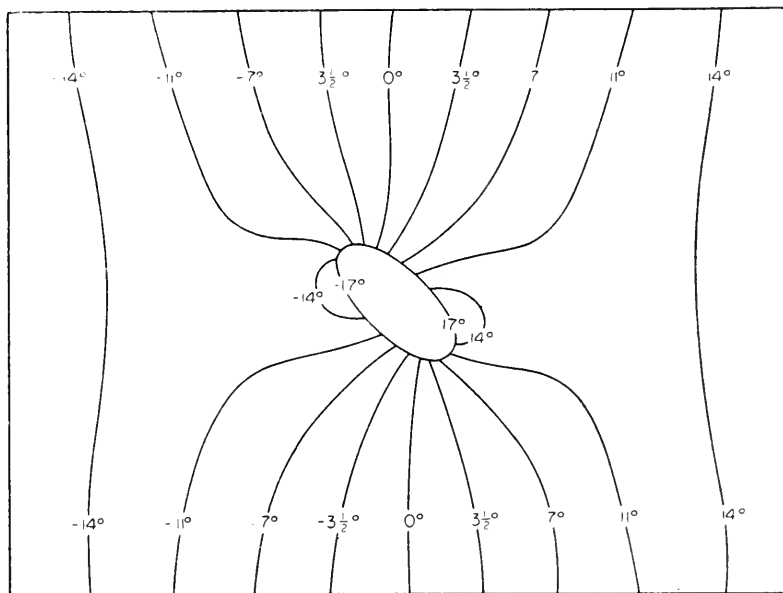


FIG. 150. Disturbance of co-tidal lines by an island elliptically shaped (Proudman).

Figure 150 shows the co-tidal lines in the immediate vicinity of an elliptic island, whereas Fig. 151 indicates how the co-tidal lines are changed when the tide wave passes from right to left in front of the opening of a bay. This disturbance corresponds exactly to the conditions in Fig. 148, where the co-tidal lines diverge within the bay and converge at the corners. Proudman has also dealt with the case of a straight coast where another sea is connected through an opening. In the undisturbed state there is an antinode at a straight coast. According to whether $\sigma \gtrless f$, the passing of the tide wave through this opening is different.

7. Computation of the Tide from Tidal Current Measurements

The equations of motion and of continuity form a link between the tidal currents and the vertical displacement caused by the tide. Therefore, it must

be possible to determine the extent of the vertical tide if we have a sufficient number of tidal current measurements. The adjacent and boundary seas extend mostly on to the shelf, and their depth seldom exceeds 200 m; therefore, current measurements can be made without any difficulty. This enables us to determine the distribution of the tide over the entire area of the adjacent

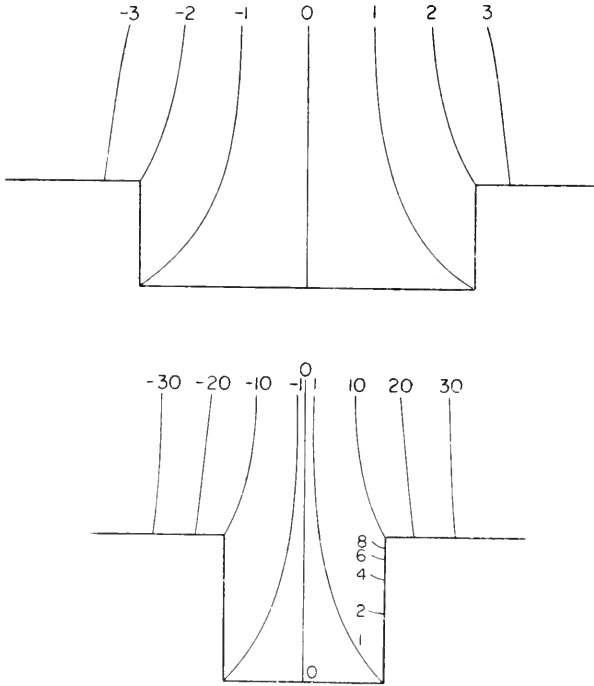


FIG. 151. Disturbance of co-tidal lines by a Bay.

sea. There exist nowadays for many adjacent seas and canals representations of the currents, which give for every hour of the tide a picture of the actual currents. Although these tidal current charts serve only practical purposes, and their basic data cannot always be too accurate, they can, nevertheless, be used in drawing conclusions as to the vertical tide within these seas. It can be expected that the increasing number of current measurements and the improvement of their accuracy will make such current charts a reliable aid also in purely scientific questions in the near future.

Two different methods have been used for determining the tide from tidal current measurements. One of these is based on a study of the tides in the North Sea by DEFANT (1923); it is mainly based on the equation of continuity and constitutes principally a differentiation process. The other method was used by PROUDMAN and DOODSON (1924, p. 185) in their study of the tides of the North Sea, and it uses only the equations of motion; therefore it is

essentially a process of integration along certain lines from coast to coast, right across the North Sea.

(a) *Defant's Method*

Defant uses the simple equation of continuity in the form (VI.100). If we introduce therein

$$\left. \begin{aligned} \eta &= \eta_1 \cos \sigma t + \eta_2 \sin \sigma t, \\ u &= u_1 \cos \sigma t + u_2 \sin \sigma t, \\ v &= v_1 \cos \sigma t + v_2 \sin \sigma t, \end{aligned} \right\} \quad (\text{XI.36})$$

it is split up into the two equations:

$$\left. \begin{aligned} \eta_1 &= \frac{1}{\sigma} \left(\frac{\partial hu_2}{\partial X} + \frac{\partial hv_2}{\partial Y} \right), \\ \eta_2 &= - \frac{1}{\sigma} \left(\frac{\partial hu_1}{\partial X} + \frac{\partial hv_1}{\partial Y} \right). \end{aligned} \right\} \quad (\text{XI.37})$$

If the area of an adjacent sea is divided into a great number of equal area squares by means of orthogonal lines and if the length of the sides of these squares is taken so small that, in first approximation, all quantities along it can be considered to vary linearly then the two values η_1 and η_2 can be computed for the centre of each square, when the velocities of the current u_1, u_2 and v_1, v_2 are known at all corner points. Within such a small area the depth can be taken as constant. The determination of these quantities which, combined, give the range and the phase of the tide at this point, is independent of the values in the vicinity and likewise independent of the coastal values.

THORADE (1924, p. 63) has given a generalization of this method, in case the currents at the surface and also in greater depths are sufficiently well known. The usual assumptions of a simple harmonic function for the currents and for the tide, as well as for the friction must not be considered. One has only to compute for each hour the water-masses going in and out of each layer in a prismatic space. From these values it is then possible to calculate the rise and fall of the surface. In this way one can obtain, by a somewhat laborious but not difficult calculation, step by step the tidal curve at a certain point. However, at the present time, our knowledge of the currents is limited to only a few stations, so that, for the time being, an application of this refined procedure cannot be considered.

(b) *The Method of Proudman-Doodson*

We introduce in the equations of motion (XI.30) the values of (XI.36) for η, u , and v ; for the frictional forces F and G we take Taylor's assumption that both are proportional to the square of the velocity

$$ku \{ (u^2 - v^2) \quad \text{and} \quad kv \{ (u^2 - v^2)$$

respectively. If u_1, u_2, v_1, v_2 are known, these equations can then be subjected to a harmonic analysis.

$$\left. \begin{aligned} F &= F_1 \cos \sigma t + F_2 \sin \sigma t, \\ G &= G_1 \cos \sigma t + G_2 \sin \sigma t. \end{aligned} \right\} \quad (\text{XI.38})$$

If, furthermore, we put

$$\left. \begin{aligned} a &= 10^7 \frac{\sigma}{g} = 1.432, \\ b &= 10^7 \frac{f}{g} = 1.487 \sin \phi, \\ c &= 10^7 \frac{g}{h} = \frac{1.019}{h : 10^4}, \end{aligned} \right\} \quad (\text{XI.39})$$

in which the numerical values apply for the M_2 — tide, the equations (XI.30) take the form

$$\left. \begin{aligned} 10^7 \frac{\partial \eta_1}{\partial x} &= -au_2 + br_1 - cF_1, \\ 10^7 \frac{\partial \eta_1}{\partial y} &= -av_2 - bu_1 - cG_1, \\ 10^7 \frac{\partial \eta_2}{\partial x} &= au_1 + bv_2 - cF_2, \\ 10^7 \frac{\partial \eta_2}{\partial y} &= av_1 - bu_2 - cG_2. \end{aligned} \right\} \quad (\text{XI.40})$$

If good and reliable tidal current measurements are available for a certain stretch, we can compute the gradients of η_1 and η_2 for the single intervals of this stretch. If these gradients are connected to known values of η_1 and η_2 at the coastal points where the section starts or where it ends, then we have the tide along the entire curve. The accuracy of the method depends upon the number of the current measurements used and when these become insufficient to make reliable interpolations, or if the current values vary too strongly, interpolations should not be attempted.

Both methods have given good results in determining the tides of the North Sea and at present they are the only methods which permit the computation of the tides of an adjacent sea based on shore values.

HANSEN (1940, p. 41; 1942, p. 65; 1943, p. 135; 1948, p. 157) has shown recently that, when the tides and tidal currents are given for any arbitrary line of demarcation of an area, the tide in the whole region can be clearly defined by solving a system of linear equations. If we introduce in the equations (XI.30) for the frictional forces βu resp. βv and eliminate the time by introducing $e^{-i\sigma t}$ we get with $i\sigma + \beta = \lambda$ and using the equation of continuity the following equations (the derivation with respect to x and y is indicated by their indices)

$$\left. \begin{aligned} \lambda u - fv + g\eta_x &= 0, \\ fu + \lambda v + g\eta_y &= 0, \\ i\sigma \eta + (hu)_x + (hv)_y &= 0. \end{aligned} \right\} \quad (\text{XI.41})$$

By eliminating u and v , we obtain the differential equation for η

$$\Delta\eta + \eta_x \left(\frac{h_x}{h} - \frac{f}{\lambda} \frac{h_y}{h} \right) + \eta_y \left(\frac{h_y}{h} + \frac{f}{\lambda} \frac{h_x}{h} \right) - \frac{i\sigma(f^2 + \lambda^2)}{gh\lambda} \eta = 0. \quad (\text{XI.42})$$

It can be mathematically proven that this equation has a solution for an entire area, when the vertical displacement η or the normal components of the velocity are given for an arbitrary line of demarcation. This is also correct, when this line demarcation separates an ocean from an adjacent sea. In order to solve the problem, the equation (XI.42) is transformed into an equation of differences, the area under consideration is divided up in small squares and for the centre of each square we establish an equation of differences. The resulting system of equations must then be solved. The numerical computation is, however, very laborious.

Chapter XII

Tides in the Mediterranean and Adjacent Seas. Observations and Discussion

WE intend to give, in this chapter, a survey of the tidal phenomena of several Mediterranean and adjacent seas, based on observations. We will only deal with the principal, most important and characteristic features of the respective seas. Furthermore, the attempts made to interpret these features will be briefly outlined. For complete descriptions, we refer to the literature quoted.

1. The Tides of the North Sea

The first attempts to represent the tides of the North Sea in charts started in the beginning of the last century. On these charts the tide wave penetrates through the Strait of Dover and, from the north, through the wide opening between Scotland and Norway. These were the first trials at all, after the theory of the tides had been founded, to approach the tidal phenomenon by means of geographical representations. Ever since, the tides of the North Sea have remained a test for the various tidal theories (see THORADE, 1930, p. 195). We can distinguish three periods in the development of the theory of the North Sea tides. The first period includes Young, Whewell and Airy. Young recognized that the tides of smaller ocean basins can hardly be a direct effect of the tide-generating forces, but that the tide penetrates into these basins from the open ocean. By drawing co-tidal lines (referred to the transit of the moon) for the areas off the British Island, he was able to show the penetration of the tidal wave into the North Sea from the north, as well as from the English Channel. WHEWELL (1836, p. 289) has given a detailed map with co-tidal lines for the North Sea (Fig. 152) in which he indicated the presence of an amphidromic point in the Hoofden and suggested also a second one in the Deutsche Bucht. Although he considered his first attempt at a co-tidal chart as tentative, he recognized already that the tide wave progresses at the English coast from north to south, at the Belgian and the Dutch coast from south to north and at the German coast from west to east. He explained these conditions as being the result of interferences of standing oscillations.

The comparison of this chart with later ones based on far more extensive observations shows how good Whewell's picture of the North Sea tides was already at such an early period.

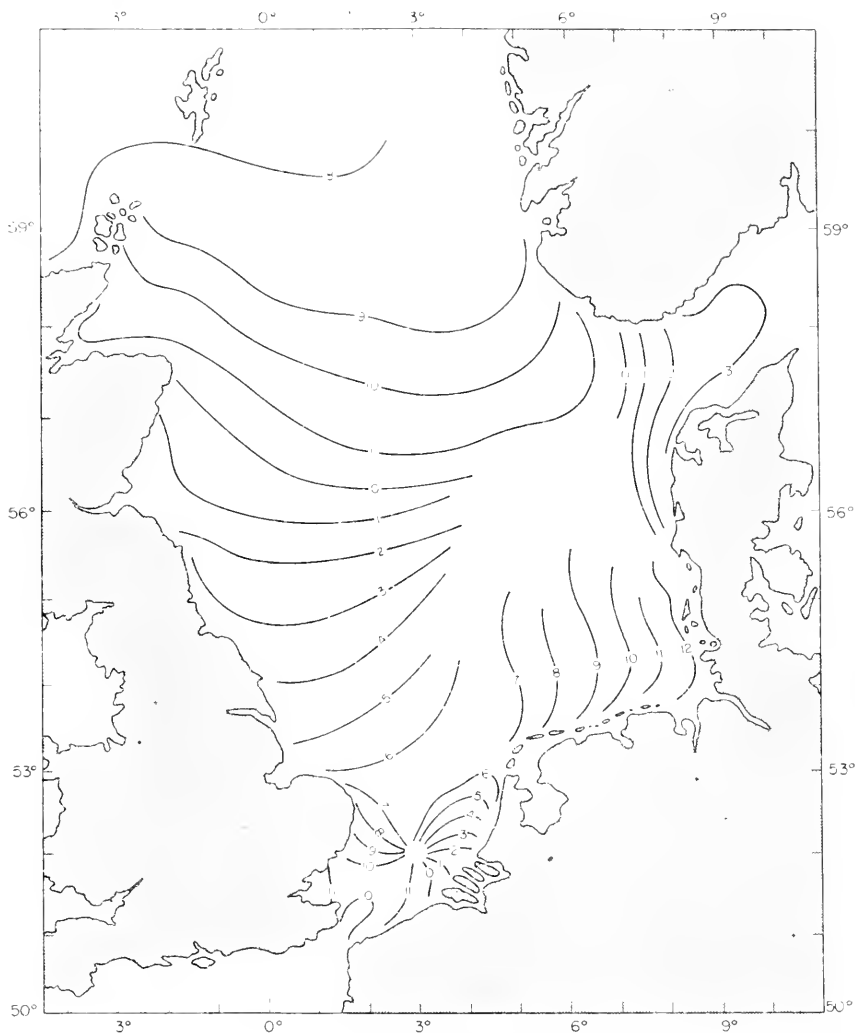


FIG. 152. Co-tidal lines of the North Sea according to Whewell. (The numbers indicate approximately the corrected establishments in lunar hours.)

This accurate conception was, however, forgotten later on, when Airy, in his book *Tides and Waves* (1845) denied the existence of amphidromies and rotary tides and expressed the opinion that the distribution of the tides in the North Sea is mainly determined by progressive waves, whose propagation was influenced above all by the depth (see p. 148). The chart given by Airy, compared to that of Whewell, must be considered as a step back.

although for a long time it was regarded as the best presentation of the North Sea tides. The rejection of Whewell's chart was principally based upon the opinion first expressed that the co-tidal lines are similar to the crest-line of the tide wave. This erroneous view was retracted later on by himself and corrected in so far as these co-tidal lines connect only the geometrical localities, where high water occurs simultaneously. This difference has been well described by THORADE (1924, p. 27) and SCHUMACHER (1924, p. 35).

The conception that several systems of waves coming from different directions were responsible for the tides of the North Sea was prevalent during the second period. BÖRGEN (1898, p. 414) considered for the first time the observations on tidal currents, but arrived at the same conclusion that all essential tidal phenomena could be explained by two systems of progressive waves. A similar opinion was expressed by KRÜMMEL (1911, p. 350). He however, considers as a given feature an amphidromy in the Hoofden, which had already been proven hydrodynamically by HARRIS (1904). Krümmel tries to explain the tidal picture by several progressive waves that are influenced by the bottom configuration and interfere with the direct waves. The co-tidal lines are very much curved and this curvature was based upon the supposition that the tide will be earlier in deep water than in shallow water, as the rate of travel of a progressive wave increases with the square root of the depth. It is obvious that no satisfactory results can be obtained by such purely qualitative discussions.

During the third period, research is based on the hydrodynamical theory of the tides. The great width of the North Sea does not permit a more exact direct application of the methods described in the previous chapters, which apply mainly to narrow, channel-like adjacent seas. However in a first approximation, we can consider the North Sea as a wide channel, open against the open ocean at its northern end and which receives from this side strong impulses to co-oscillate with the external tide. The opening at the southern end is not of great importance. The tidal energy entering the North Sea through the Strait of Dover is small, and as KELVIN (1891, p. 201) pointed out already in 1878, its influence does not go beyond the island of Texel. One can consider, as far as the tides are concerned, the region south of 53° N. lat. as belonging to the English Channel.

If we consider the North Sea as a bay open on one end, the character of its semi-diurnal co-oscillating tide is defined by the value of ν . The average depth of a great number of west-east cross-section show in rough approximation that the depth increases linearly from the south towards the north. The period of the free oscillation of such a basin gives $\nu = 1.47$ and the co-oscillating tide with the external tide in the north has, according to DEFANT (1923, p. 57), two nodal lines, one located not far from the northern opening, the other one a little less than one-third of the total length from the inner end. As the phase at the northern end is approximately 9.5 h, the centre section

of the North Sea between the nodal lines should have a phase of 3.5 h and the innermost part again the phase of 9.5 h. These nodal lines are transformed into amphidromies by the rotation of the earth. If we keep these conditions in view, the agreement between the observations and these assumptions is not bad. The schematic presentation of the co-tidal lines of the North Sea

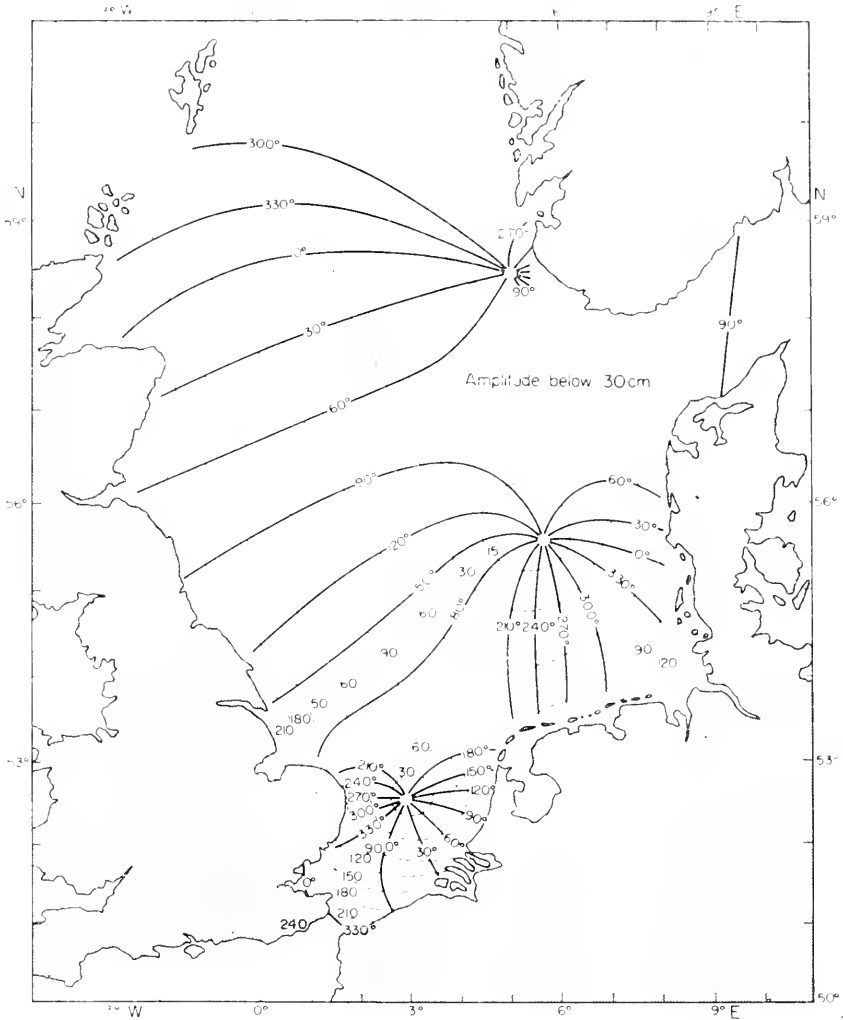


FIG. 153. Co-tidal lines (in degrees) and co-range lines (amplitudes in cm) of the M_2 tide in the North Sea (Proudman and Doodson).

given by STERNECK (1920, p. 131), in his paper on the tides of the oceans based on the "vulgar establishment", shows also these two amphidromies; one in the northern part at approximately 56° N. lat., the second in the southern part, and which is slightly moved in the direction of the Deutsche Bucht.

It is possible to explain the distribution of the co-tidal lines by using Taylor's theory on oscillations in a rectangular basin, open at one end. It can be shown that the two amphidromies and the changes in the tidal currents during a full tidal period are caused by the superposition of an incoming Kelvin wave and its reflection on the southern end. Fundamentally, the North Sea tides can be considered as tides co-oscillating with the external tide at its wide northern opening.

DEFANT (1923, p. 177) and PROUDMAN and DOODSON (1924, p. 185) published almost simultaneously their theories in which they attempted to derive the distribution of the vertical tide over the entire area of the North Sea from the numerous observations on tidal currents. Defant used as basis the charts of the tidal currents published by the DEUTSCHE SEEWARTE (1905) and, by means of the equation of continuity, derives the periodic variations of the vertical displacements of the sea level during the tide; Proudman and Doodson, on the contrary, start out from the equations of motion and, with the aid of reliable current measurements taken on profiles across the North Sea, they compute the variations of the vertical displacements of the sea surface. Defant's and Proudman-Doodson's distribution of the co-tidal and co-range lines are very similar and correspond to the distribution found by Sterneck. Figure 153 gives an example of Proudman and Doodson's map. Both tidal presentations were based on the relation between the vertical tides and the tidal currents and are, therefore, not a result of a theory.

Another set of co-tidal lines was given by MERZ (1923, p. 30; 1921, p. 393), based on coastal data and the numerous tide curves obtained at sea. It contains only the amphidromy in the southern part of the North Sea; the northern amphidromy is lacking and is replaced by a dense crowding of co-tidal lines. STERNECK (1925, p. 147) has proven that, according to recent Norwegian observations, the tide wave progresses southward along the Norwegian coast, which is incompatible with a rotary tide. The apparent lack of this second amphidromy must perhaps be attributed to the effect of friction. The Kelvin wave penetrating from the north is not totally reflected on the shallow coast of Germany, a large part of its energy is lost because of the small depths off the southern coast and complicated configuration (islands, sand banks and wadden). The reflected wave, although still sufficient to cause the formation of the amphidromy in the Deutsche Bucht, is perhaps too weak to produce a second one at a greater distance. It should also be considered that part of the incoming tidal energy makes its way through the Kattegat, is used up for the greater part in the Belt and then in the Baltic, and does not return any more into the North Sea. The superposition with the incoming wave gives only a narrow and dense crowding of co-tidal lines and in the wide area of the North Sea the impression of a progressive wave travelling southward. Figure 154 gives the best and most recent picture of the tides of the North Sea taken from the German Tide Tables. There is no doubt that

the explanation just given of the tides of the North Sea, which is based principally on the M_2 tide, is correct and it seems that the criticism by Sterneek against this mode of interpretation is unjustified (see DEFANT 1925 p. 231). There still are, of course, many questions which need explanation, which will become possible when we have more and better tide observations, especially by means of gauges in the open ocean.

A problem still waiting for a solution is the interpretation of the spring

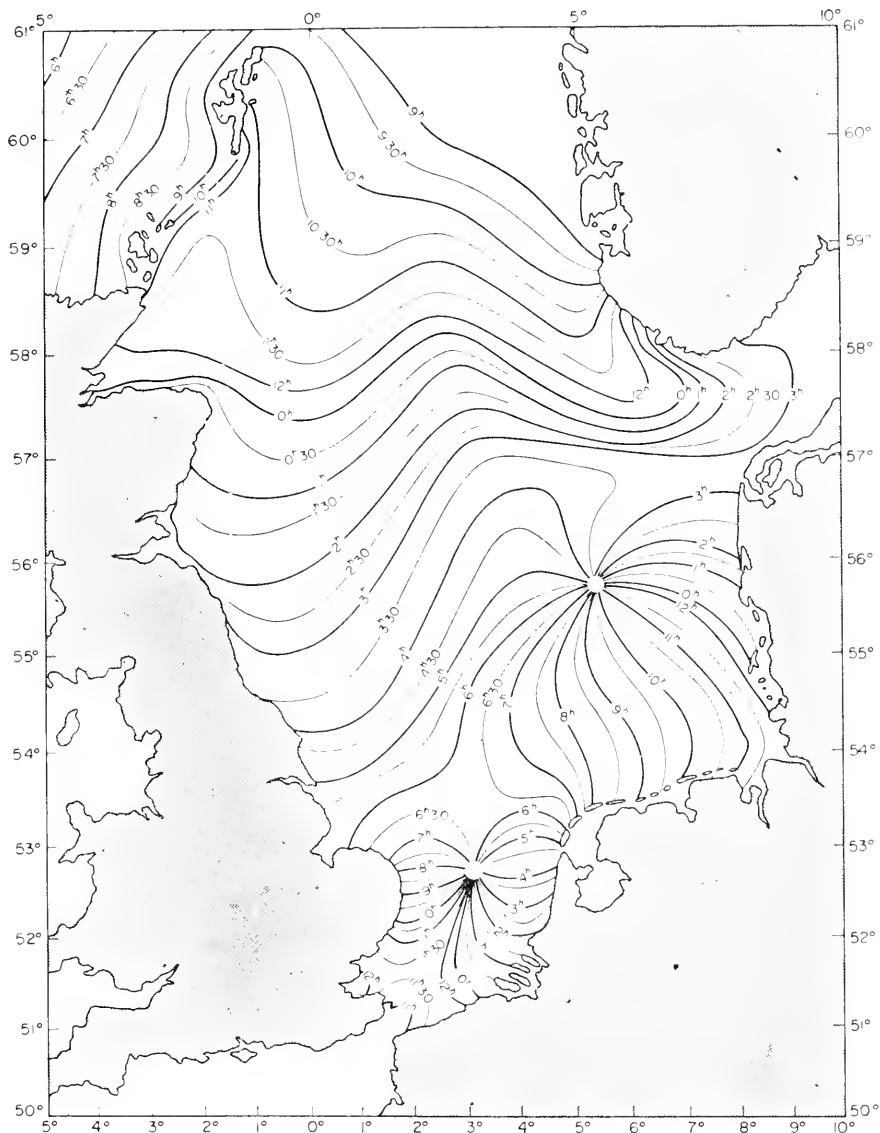


FIG. 154. (a) Lines of the same time interval between upper culmination of the moon in Greenwich (solar hours) and high water.

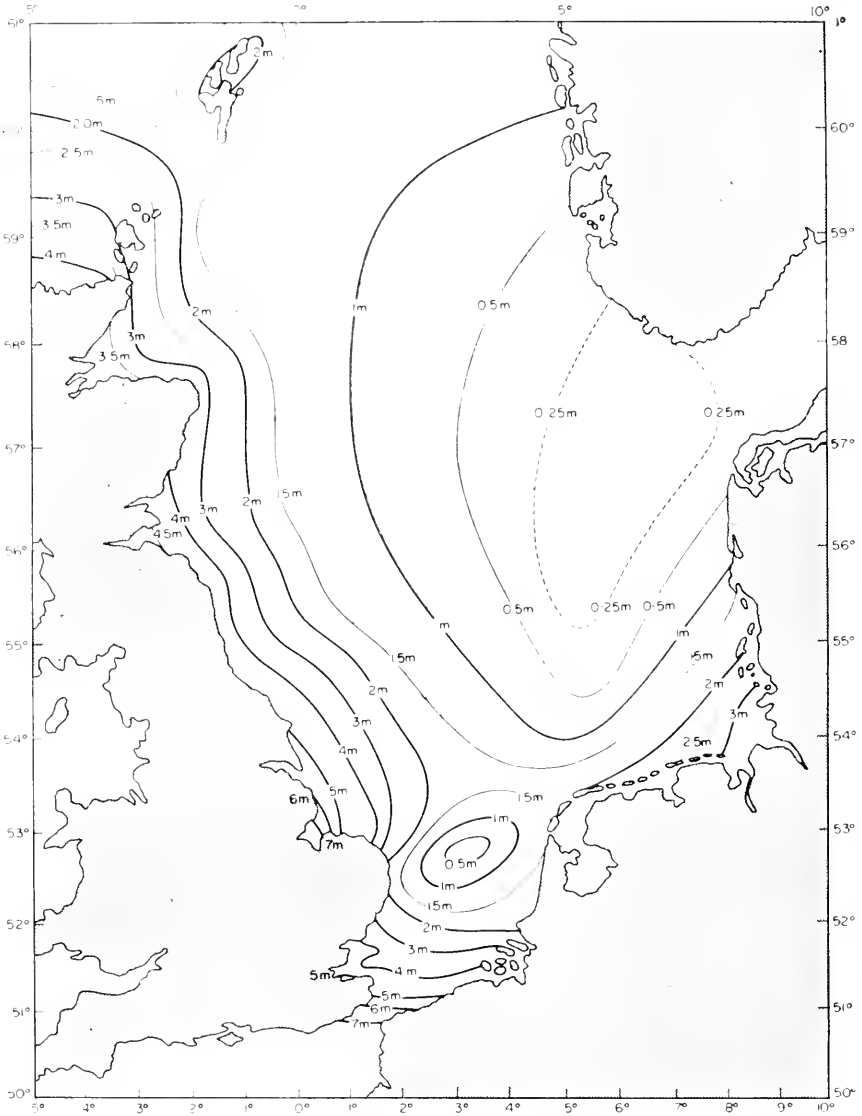


FIG. 154. (b) Lines connecting the same average spring tide range in the North Sea.

retardation and of the ratio of the neap range to the spring range for which Merz has published the map shown in Fig. 155. It can be seen that both distributions are determined by geographical factors. The spring retardation increases in the corner of the Deutsche Bucht up to nearly 3 days, whereas in the Kattegat there is an extraordinarily rapid change from a lag of about 30 h to a priming of about 40 h. The ratio of the neap tide and the spring tide ranges, which should be theoretically 36%, increases regularly from north to southeast up to 89% in Hamburg. It is not possible to establish the real

cause of this discrepancy; it will presumably be due to the fact that the North Sea basin responds differently to each partial tide frequency, and thus the

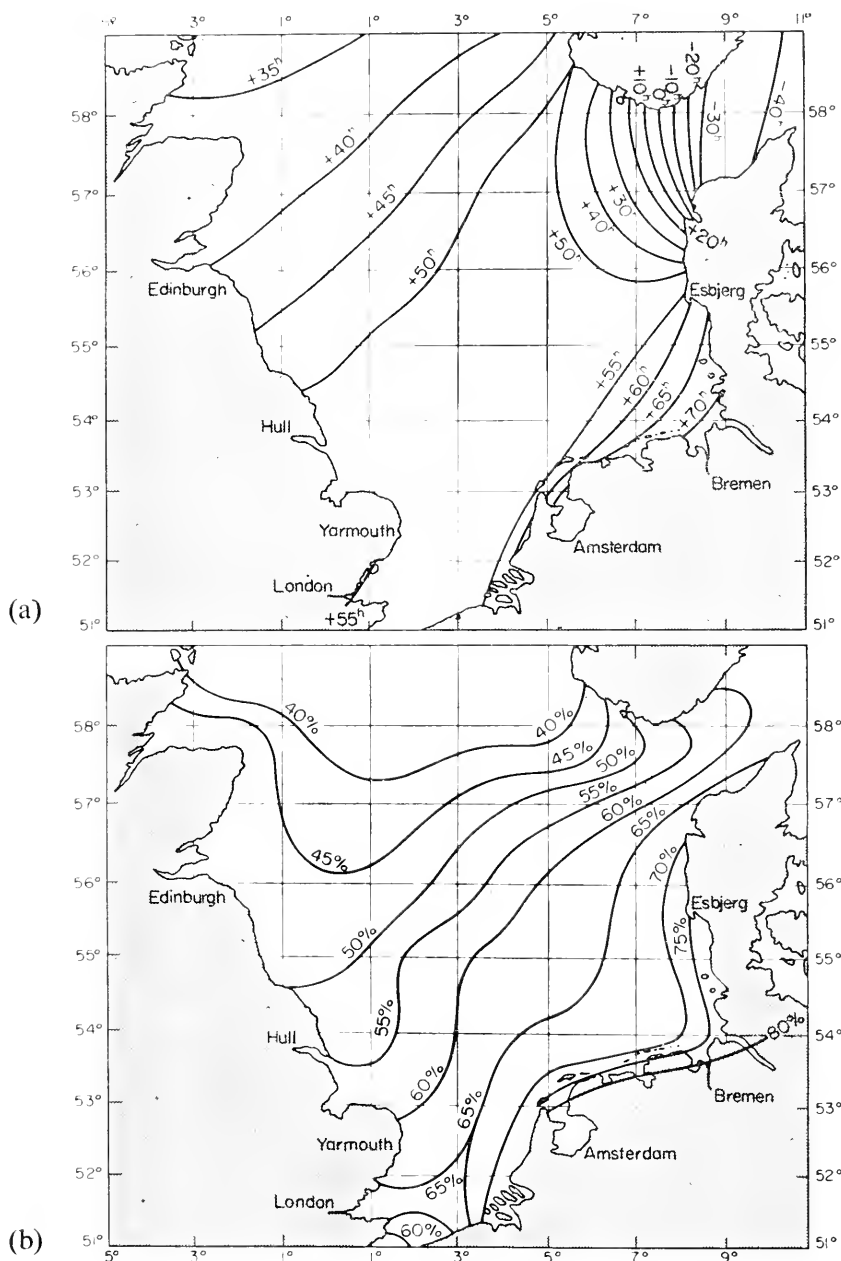


FIG. 155. Properties of the tides in the North Sea (Merz). (a) Lines of equal retardation at spring tide in hours, (b) lines of equal ratio of the range at neap tide to spring tide in per cent.

individual waves can be shifted with respect to each other. HANSEN (1938, p. 429) has given detailed explanations regarding the ratio of the amplitude and the difference in phase of the harmonic components in the North Sea. For details of the tides in the Deutsche Bucht see also the paper of MÖLLER (1933). Table 42 gives a compilation of the harmonic constants for a series of coastal localities of the North Sea (north of 53° N. lat.).

In all following tables, unless indicated otherwise, the amplitudes are expressed in cm, the phases \varkappa in degrees. The origin of time is local time of the maximum value of the corresponding term of the tide-generating potential (referred to the upper transit of the tide generating "fictive" moon through the meridian).

A comparison between the phases and a presentation of the tides by co-tidal lines, require a reduction of the phases to a reference meridian. It is useful to give the equations necessary for this reduction, because often in the literature we find that incorrect equations have been applied. Let in a locality (geographical longitude λ , positive towards the east) the considered partial tides have the form $H \cos(\sigma t_0 - \varkappa)$, t_0 is the local time in hours, \varkappa the phase referred to local time. According to equation (VIII. 13), this same partial tide, in Greenwich time, has the form $H \cos(\sigma t_{GR} + p\lambda - \varkappa)$, in which t_{GR} is the Greenwich time in hours and p is 1 or 2, according to whether the tides are diurnal or semidiurnal. If we designate the phase referred to the meridian of Greenwich by g_0 , then we have $g_0 = \varkappa - p\lambda$ (λ positive towards the east).

If we select as reference meridian the meridian of S° , Greenwich time must still be changed into t_S time. As $t_{GR} = t_S - S^\circ/15$ (S positive towards the east), then $H \cos(\sigma t_S + p\lambda - \sigma(S^\circ/15) - \varkappa)$ and the phase of the tide referred to the meridian of S° will be $g_S = \varkappa - p\lambda + \sigma S^\circ/15$ (λ and S positive towards the east). The last equation is particularly used to reduce \varkappa values of a small area of an ocean to a central meridian; like, for instance, the \varkappa values of the Mediterranean to the meridian of 15° E., which divides this sea nearly in half.

A reduction of the phase to mean solar hours is obtained by dividing the phase values by the angular velocities (per hour) of the respective tide (for instance, $M_2 = 28.984^\circ$, $S_2 = 30^\circ$, $K_1 = 15.041^\circ$, $O_1 = 13.943^\circ$, for further partial tides see Table 28a, p. 267).

2. The Tides of the Kattegat and the Baltic Sea

The narrow and shallow communication between the North Sea and the Baltic through the Kattegat and the Sound does not allow a good transmission of tidal energy into the Baltic, the more so as the tides in the Skagerrak are not very developed. The Kattegat has the form of a narrow, shallow canal opening at its northern end into the Skagerrak and the North Sea, and at its southern end there are three openings (Lillebelt, Storebelt and Öresund) into the Baltic. The tide wave penetrates into this channel from the north, is reflected partly in the south, and a part of the tidal energy penetrates into the Baltic. Thus the tide wave in the Kattegat takes the form of a progressive wave travelling southwards with somewhat larger amplitudes at the east coast of Jutland (12–30 cm) and smaller amplitudes at the Swedish coast (4 cm). DEFANT (1934) has given an accurate analysis of the M_2 wave, using the observations gained during the international Kattegat expedition of 1931. He was able to show that the observations (tides and corresponding currents) can be represented, according to the theory previously developed (p. 345), as the superposition of two standing waves which are shifted against each other. The

Table 42. Harmonic constants for the North Sea

Position	M_2	S_2	K_1	O_1	$\frac{K_1+O_1}{M_2+S_2}$	$M_2+S_2+K_1+O_1$
Bergen 60° 24' N. 6° 18' E	$H(\text{cm})$ 43.9 φ° 295.0	15.9 334.0	3.2 171.0	3.2 18.0	0.11	66.2
Stavanger 58° 58' N. 5° 45' E.	14.5 282.0	6.6 332.0	1.5 180.0	1.6 15.0	0.15	24.2
Mandal (Tregde) 58° 00' N. 7° 34' E.	8.3 109.0	2.5 64.0	0.4 40.0	1.1 286.0	0.14	12.3
Hirtshals 57° 36' N. 9° 57' E.	10.8 116.0	3.5 70.0	0.7 333.0	1.3 263.0	0.14	16.3
Esbjerg 55° 29' N. 8° 27' E.	65.7 58.6	16.0 122.3	4.9 80.8	8.6 288.2	0.17	95.2
Heligoland 54° 11' N. 7° 53' E.	96.8 332.0	24.0 39.8	5.8 32.2	7.6 245.2	0.11	134.2
Cuxhaven 53° 52' N. 8° 43' E.	134.6 1.9	34.3 69.5	7.1 45.8	8.8 257.8	0.09	184.8
Rotersand-Leuchtturm 53° 51' N. 8° 05' E.	128.5 331.9	33.2 52.7	6.6 25.9	8.3 233.1	0.09	176.6
Bremerhaven 53° 34' N. 8° 34' E.	152.9 12.5	38.4 85.6	6.8 62.6	10.0 265.4	0.09	208.1
Wilhelmshaven 53° 31' N. 8° 09' E.	158.1 1.9	40.4 70.9	7.0 44.7	9.4 250.8	0.08	214.9
Emden 53° 21' N. 7° 12' E.	131.1 339.1	32.6 48.3	8.1 40.7	9.2 249.6	0.11	181.0
West-Terschelling 53° 22' N. 5° 13' E.	73.3 236.6	19.3 299.2	6.7 14.9	9.1 215.6	0.17	108.4
Vlieland 53° 18' N. 5° 03' E.	69.0 236.7	16.0 292.4	5.0 8.2	6.0 211.5	0.13	96.0
Den Helder 52° 58' N. 4° 45' E.	61.7 178.7	17.2 246.1	7.0 1.3	9.8 198.1	0.21	95.7
Lowestoft 52° 29' N. 1° 46' E.	71.0 264.0	21.3 324.0	17.7 334.0	14.0 167.0	0.34	124.0
The Wash, Skegness 53° 09' N. 0° 21' E.	213.1 170.0	74.7 220.0	10.7 304.0	13.4 114.0	0.08	311.9
Humber, Immingham 53° 38' N. 0° 11' W.	223.3 161.1	72.8 209.5	14.6 278.6	16.4 120.0	0.10	327.1
Whitby 54° 29' N. 0° 37' W.	164.6 102.0	52.1 146.0	11.3 256.0	12.5 102.0	0.11	240.5
Hartlepool 54° 41' N. 1° 12' W.	157.4 96.0	53.0 137.0	11.6 246.0	13.2 84.0	0.12	235.2
Berwick 55° 46' N. 2° 00' W.	160.3 57.0	50.6 118.0	4.3 202.0	7.0 88.0	0.05	222.2
Aberdeen 57° 09' N. 2° 05' W.	130.9 20.7	45.0 57.8	11.0 202.8	12.7 50.2	0.13	199.8
Invergordon 57° 41' N. 4° 10' W.	138.7 328.0	47.9 5.0	11.6 167.0	12.2 35.0	0.13	210.4
Wick 58° 26' N. 3° 05' W.	110.6 320.0	32.6 353.0	6.7 180.0	10.7 9.0	0.12	160.6
Fair Isle 59° 33' N. 1° 38' W.	63.1 301.0	20.7 328.0	12.2 188.0	11.0 28.0	0.28	107.0

tides can be considered essentially as co-oscillating tides of a channel where the incoming tidal energy is reflected partly at the inner, not completely closed end; a part is lost directly in the channel. GUSTAFSON and OTTERSTEDT (1930), and JACOBSEN (1913) have analysed the current measurements for several depths for the Kattegat and the Danish waters, respectively.

WITTING (1911) has tried a synthesis of the tides of the Baltic, on the basis of the harmonic constants of a great number of localities which are summarized in Table 43 (for Danish localities see CRONE, 1906). It shows that the

Table 43. Harmonic constants for Kattegat and Baltic

Place	Amplitude (cm)				Phase α in degrees				$K_1 + O_1$	$M_2 + S_2 +$
	M_2	S_2	K_1	O_1	M_2	S_2	K_1	O_1	$M_2 + S_2$	$+ K_1 + O_1$
Frederikshavn	12.2	3.4	0.8	2.6	161°	113°	282°	296°	0.22	19.0
Aarhus	13.6	4.2	0.9	3.2	305	271	80	339	0.23	21.9
Fredericia	11.6	3.3	0.8	1.6	335	296	241	0	0.16	17.3
Korsör	10.7	3.3	0.9	1.5	10	349	228	20	0.17	16.4
Slipshavn	12.0	4.1	0.9	2.1	2	337	217	19	0.19	19.1
Hornbæk	6.8	2.3	0.8	2.9	260	224	347	337	0.41	12.8
Copenhagen	6.0	2.7	0.5	2.0	279	250	37	7	0.29	11.2
Marienleuchte	3.3	0.7	2.2	(0.3)	167	154	218	(295)	(1.07)	(6.5)
Warnemünde	2.7	0.8	1.8	(0.2)	216	213	219	(218)	(1.00)	(5.5)
Gjedser	3.6	0.8	1.6	1.8	192	207	180	143	0.77	7.8
Arkona	0.9 ₅	0.5	1.4	(0.2)	265	272	168	(221)	(1.95)	(3.0)
Karlskrona	0.6	0.3	1.1	1.4	119	136	137	213	2.85	3.4
Pillau	0.6 ₅	0.4	0.5	(0.3)	11	46	286	(272)	0.88	(1.8)
Memel	0.5	0.4	1.0	(0.5)	30	52	292	(296)	(2.25)	(2.4)
Libau	0.1	0.2	0.6	0.6	128	110	297	277	3.71	1.5
Landsort	0.8 ₅	0.3	0.7	0.5	180	199	103	97	1.06	2.4
Hangö	1.3	0.5	0.7	1.2 ₅	217	244	6	39	1.13	3.8
Reval	0.4	0.2	1.0	1.0	301	266	348	347	4.15	2.6
Helsinki	0.4	0.1 ₅	1.7	1.8	186	240	33	16	6.38	4.1
Kronstadt	1.7	0.8	1.9 ₅	4.8	335	129	23	253	2.68	9.2
Björn	0.7	0.4	0.2	0.3	77	147	150	42	0.43	1.6
Draghällan	0.7	0.3	0.4	0.3	41	121	125	171	0.75	1.7
Raten	0.2	0.1	1.4	1.1	15	346	7	321	7.54	2.8

The values in brackets refer to P_1 , instead of O_1 .

tides of the Baltic are very small. The sum of the amplitudes of the principal constituents $M_2 + S_2 + K_1 + O_1$ is about 100 cm in the North Sea and decreases in the Skagerrak and Kattegat to below 20 cm, in the Belts to about 10, in the Baltic to between 5 and 2 in the Gulf of Bothnia mostly below 2 cm. In the Gulf of Finland there seems to be a gradual increase to nearly 10 cm. The table shows also that, whereas in the Skagerrak and the Kattegat the

tides are definitely semi-diurnal, they are of a mixed type in the Belts and become diurnal in the entire Baltic. This is most pronounced in the central Baltic (Libau, Karlskrona) and in the Gulf of Finland. An attempt to represent the co-tidal lines has been made in Figs. 156 and 157. The semi-

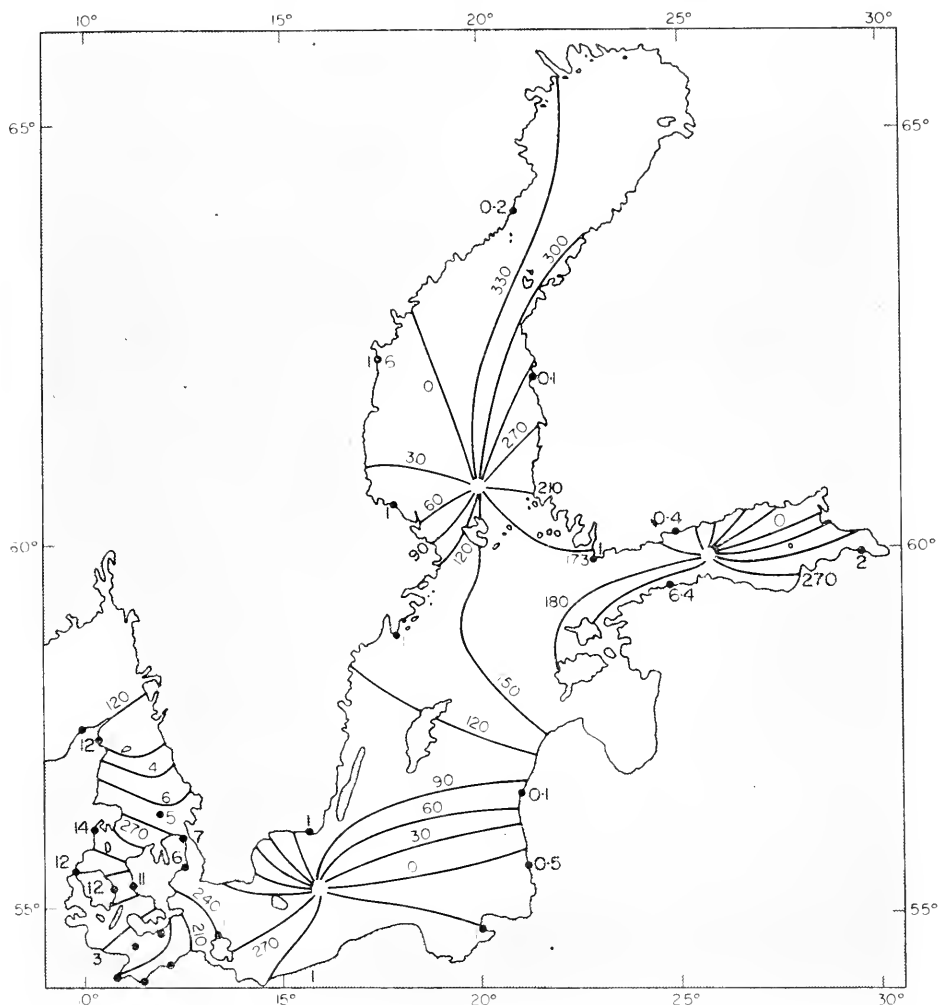


FIG. 156. Co-tidal lines of the M_2 tide for the Kattegat and Baltic. (Phase in degrees and amplitude in cm.)

diurnal tide shows three amphidromies, namely, one in the south-western Baltic, one in the Gulf of Finland and the third one in the Gulf of Bothnia (all *contra solem*). The central basin shows a transition from the south-western amphidromy to the others; there is no reason to consider it as a separate amphidromy, as Witting did. The amplitudes show a decrease in the Danish waters and then remain below 1 cm everywhere, except in the south-western

part where they reach 3–4 cm. The diurnal tide (Fig. 157) has a large amphidromy *contra solem* in the central basin; it includes the two gulfs in the north and the north-east. The amplitudes of this wave are of the same order of magnitude, mostly even greater than in the Kattegat and in the Danish waters. This points to the fact that the diurnal tides are generated in the Baltic itself, whereas it can be assumed that the semi-diurnal tides are

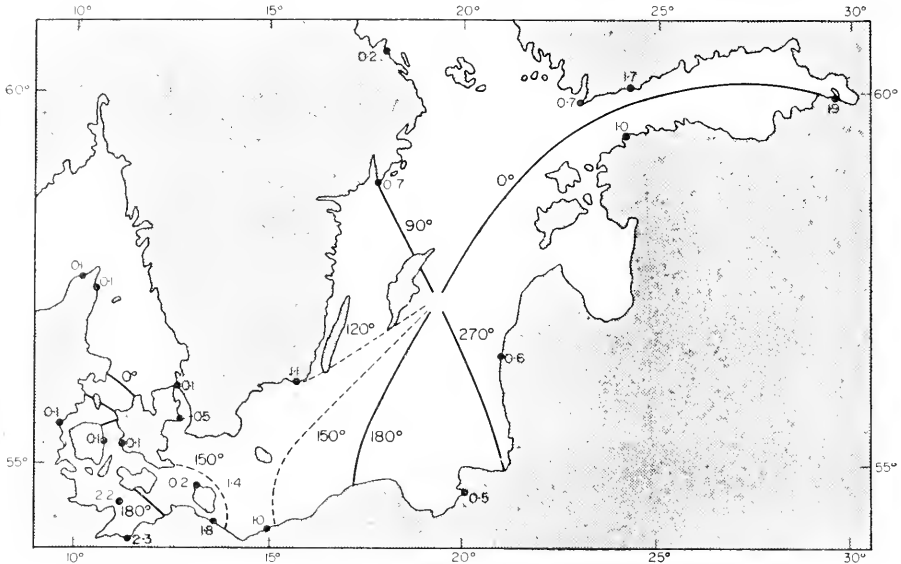


FIG. 157. Co-tidal lines of the K_1 tide (0° , 90° , 180° and 270° correspond to 0 h, 6 h, 12 h and 18 h sidereal time; amplitude in cm) (Witting).

influenced through the Belts and the Sund. According to the considerations on page 194, the period T_f of the principal free oscillating system Kieler Bucht-Mecklenburger Bucht, Darsersill, Baltic, Gulf of Finland, is 27.6 h. From this follows that for the semi-diurnal tides $\nu = T_f:T_x = 2.2$ and for the diurnal tides around 1.15. This means that:

(1) if the Baltic is imagined to be closed in the south-west (the Baltic being considered as a lake), the semi-diurnal tides, having very small amplitudes, must have three nodal lines, the diurnal tides, with somewhat larger amplitudes, one nodal line;

(2) for the tides co-oscillating with the tides in the Danish waters, the semi-diurnal tides must have two, the diurnal tides one nodal lines.

Witting has computed the tides generated directly by the tide-generating forces as listed under (1), as well as the transverse oscillations of this type (periods of the free oscillation at about 2.5–5.5 h). The amplitudes of the M_2 tide came to 0.6–0.9 cm, those of the K_1 tide to 3–4 cm. When the ratio of the natural period to the period of the force is favourable, the amplitude

of the transverse oscillations may reach 0.5 cm, but generally they are smaller. Longitudinal and transverse oscillations produce corresponding amphidromies *contra solem*. Comparing with the observations, we can conclude that the diurnal tides must be generated directly in the Baltic; the semi-diurnal tides, on the contrary, should be considered as the superposition of the directly generated and co-oscillating tides, the latter predominating by far. For the tides of the Finnish and Bothnian bay, see LISITZIN (1943, 1944).

3. The Tides of the English Channel and the South-western North Sea

These two regions represent interconnecting channels between two tide-carrying oceans; the boundaries in the west are a line from Isle d'Ouessant to the Scilly Islands; in the east, a line connecting the Wash (south of Grimsby) to the Island of Ameland off the Dutch coast. Hence, this includes the entire English Channel and the Hoofden and connects the Atlantic Ocean with the North Sea.

Ranges and establishments for a great number of coastal localities are given in Table 44. In the English Channel the establishment increases on both the French and English coast from 4.5 h at the opening in the Atlantic Ocean to 11 h in the Strait of Dover. However, the co-tidal lines do not advance uniformly over the entire Channel. In the western part there are rather great distances between the individual co-tidal lines, whereas they are crowded in the narrow section of the Channel at the Cotentin Peninsula. East of this region there are only very small differences in establishments over a large area. This distribution of the co-tidal lines has no correlation with the existing water depths. The ranges of the tides at the French coast are considerably larger than at the English coast, which can be attributed to the rotation of the earth (see p. 206). Disregarding the enormous range at the inner end of the gulf of St. Malo (which are of a different origin) the range decreases on both coasts until Cape De la Hague and St. Albans Head, where the co-tidal lines are crowded as mentioned before. Then it increases to a maximum off the Strait of Dover, where at spring tide, Hastings has a range of 7.3 m, Treport in the south a range of 9.3 m. The minimum range and the crowding of the co-tidal lines in the central narrow section of the Channel would indicate the presence of a pseudo-nodal line of a standing wave, especially since the difference in establishment between the western part and the Strait of Dover is about 6 h. The distribution of the establishment and of the range in the area east of the Strait of Dover (Hoofden) points to a well-developed amphidromy *contra solem*, which was already assumed by HARRIS (1904).

The extraordinarily high tides occurring in the Gulf of St. Malo are due to the effect of resonance between co-oscillating water-masses of the Bay of Normandy and the tide in the Channel. This was proven by a simple computation of the co-oscillating tides of this bay, which gives an increase in the range from about 5.8 m at the channel islands to about 12 m inside the Gulf.

Table 44. Harmonic constant for English Channel and south-west part of the North Sea

Position	M_2	S_2	K_1	O_1	$\frac{K_1+O_1}{M_2+S_2}$	$M_2+S_2+O_1+K_1$
West-Terschelling 53° 22' N. 5° 13' E.	$H(\text{cm})$ 73.3 λ° 236.6	19.3 299.2	6.7 14.9	9.1 215.6	0.17	108.4
Den Helder 52° 58' N. 4° 45' E.	61.7 178.7	17.2 246.1	7.0 1.3	9.8 198.1	0.21	95.7
Ijmuiden 52° 28' N. 4° 35' E.	66.0 113.3	17.1 180.8	8.3 351.2	11.5 184.7	0.24	102.9
Hoek van Holland 51° 59' N. 4° 07' E.	75.3 70.6	18.6 130.8	7.9 351.4	11.2 181.3	0.20	113.0
Brouwershaven 51° 44' N. 3° 54' E.	113.9 67.0	28.5 127.1	7.6 5.4	11.0 189.8	0.13	161.0
Zierikzee 51° 38' N. 3° 53' E.	138.9 61.7	35.2 121.5	7.6 8.5	10.9 192.0	0.11	192.6
Vlissingen 51° 27' N. 3° 36' E.	172.1 41.4	47.8 98.3	7.2 4.7	10.9 182.5	0.08	238.0
Zeebrugge 51° 21' N. 3° 12' E.	164.3 20.6	46.5 75.0	6.0 352.1	10.6 178.3	0.08	227.4
Nieuport 51° 09' N. 2° 44' E.	188.0 5.7	55.4 58.4	5.3 344.6	9.2 170.4	0.06	257.9
Dunkerque 51° 03' N. 2° 22' E.	206.8 357.7	62.2 49.9	3.9 355.4	6.5 170.0	0.04	279.4
Dieppe 49° 56' N. 1° 05' E.	303.7 314.6	98.2 4.1	7.6 128.6	4.0 35.8	0.03	413.5
Fécamp 49° 36' N. 0° 23' E.	266.7 298.9	87.2 346.0	8.6 125.2	4.5 23.3	0.04	367.0
Le Havre 49° 29' N. 0° 06' E.	261.5 285.2	87.7 331.9	9.8 117.5	5.1 9.1	0.04	364.1
Cherbourg 49° 39' N. 1° 37' W.	186.6 227.3	69.0 270.2	9.3 107.1	6.9 357.1	0.06	271.8
Jersey, St. Hélier 49° 11' N. 2° 07' W.	346.9 186.0	125.9 236.0	11.0 103.0	7.9 349.0	0.04	491.7
St. Malo 48° 38' N. 2° 02' W.	374.6 175.6	148.9 225.2	9.3 91.4	8.0 342.2	0.03	540.8
Lezardrieux 48° 47' N. 3° 06' W.	318.5 160.5	121.5 208.3	10.1 84.0	6.9 354.8	0.04	457.0
Brest 48° 23' N. 4° 30' W.	203.5 100.4	74.3 139.1	6.4 71.9	6.7 323.4	0.05	290.9
Humber, Immingham 53° 38' N. 0° 11' W.	223.3 161.1	72.8 209.5	14.6 278.6	16.4 120.0	0.10	327.1

Position	M_2	S_2	K_1	O_1	$\frac{K_1+O_1}{M_2+S_2}$	$M_2+S_2+K_2+O_1$
The Wash, Skegness 53°09'N. 0°21'E.	$H(\text{cm})$ 213·1 ≈ 170·0	74·7 220·0	10·7 304·0	13·4 114·0	0·08	311·9
Lowestoft 52°29'N. 1°46'E.	71·0 264·0	21·3 324·0	17·7 334·0	14·0 167·0	0·34	124·0
Harwich 51°57'N. 1°17'E.	129·8 328·2	36·2 19·9	9·8 354·1	12·1 178·2	0·13	187·9
Southend 51°31'N. 0°43'E.	200·7 355·0	57·5 50·4	11·0 5·6	12·4 192·9	0·09	281·6
Sheerness 51°27'N. 0°45'E.	191·9 0·5	53·3 56·0	11·5 14·0	13·7 193·0	0·10	270·4
Margate 51°23'N. 1°23'E.	166·4 345·0	54·3 39·0	9·1 1·0	11·6 192·0	0·09	241·4
Ramsgate 51°20'N. 1°25'E.	187·3 344·0	57·2 36·0	6·8 19·0	10·4 181·0	0·07	261·7
Dover 51°07'N. 1°19'E.	223·4 333·0	70·9 24·0	4·2 40·0	7·0 176·0	0·04	305·5
Folkstone 51°05'N. 1°11'E.	243·5 332·0	83·8 21·0	3·7 59·0	3·4 169·0	0·02	334·4
Newhaven 50°47'N. 0°03'E.	218·2 321·0	66·8 9·0	8·5 103·0	2·7 281·0	0·04	296·2
Nab Tower 50°40'N. 0°57'W.	143·5 315·4	44·8 359·0	9·3 112·0	0·9 340·9	0·05	198·5
Portsmouth 50°48'N. 1°07'W.	142·9 323·9	44·1 8·8	8·7 109·9	2·6 343·0	0·06	198·3
Southampton 50°54'N. 1°24'W.	135·9 326·4	40·7 12·3	8·7 112·8	3·4 3·8	0·07	188·7
Hurst Point 50°42'N. 1°53'W.	62·4 308·0	21·6 328·0	12·5 134·0	6·7 6·0	0·23	103·2
Christchurch 50°43'N. 1°44'W.	43·3 289·0	14·9 304·0	7·9 106·0	4·3 31·0	0·21	70·4
Poole-Harbour 50°40'N. 1°56'W.	37·2 267·0	18·0 289·0	9·1 111·0	4·9 328·0	0·25	69·2
Swanage 50°37'N. 1°57'W.	37·8 258·0	19·5 276·0	7·9 95·0	1·2 285·0	0·16	66·4
Portland 50°34'N. 2°26'W.	63·0 189·1	32·4 238·1	8·8 110·6	5·3 341·6	0·15	109·5
Dartmouth 50°21'N. 3°34'W.	139·0 158·0	56·4 213·0	8·5 98·0	5·8 349·0	0·07	209·7
Devonport 50°22'N. 4°11'W.	167·3 145·0	64·0 203·0	7·9 109·0	5·5 330·0	0·06	244·7
Penzance (Newlyn) 50°06'N. 5°33'W.	171·3 124·7	56·9 168·5	6·1 102·0	5·5 334·0	0·05	239·8

According to coastal observations, we have in the Channel between the Atlantic Ocean and the North Sea a tide wave with two pseudo-nodal lines, one north of the Cotentin Peninsula and one in the Hoofden. The rotation of the earth causes the tidal range to be greater on the French coast and to transform the nodal line in the Hoofden into an amphidromy.

The tidal currents in the English Channel have been described extensively by STOK, 1905; DALHUISEN, 1907 and in a publication by the DEUTSCHE SEEWARTE (1905). BÖRGEN (1898) has discussed these currents. The lines of convergence and divergence which shift during a tidal period are especially well suited to characterize the current. Børgen distinguishes three boundary lines: the "Atlantic", which is west of the Greenwich meridian, the "Channel line" east thereof and south of $52\frac{1}{2}^{\circ}$ N. lat., and the "North Sea line" which

Table 45. Position of lines of convergence and divergence in the English Channel

Time		Lines of convergence and divergence		
		Con. } Div. } Atlantic	Con. } Div. } Channel	Con. } Div. } North Sea
1 h after } 5 h before }	High water at Dover	— —	Hastings, Eastbourne to Fécamp, Dieppe	Hoek van Holland Ijmuiden toward NNW.
2 h after } 4 h before }	High water at Dover	Lands End to Isle of Bas	Hastings to Treport, Cayeux	Ijmuiden, Helder and Cromer, Washbucht to NNE.
3 h after } 3 h before }	High water at Dover	Falmouth, Plymouth Entrance to Bay of Normandy	Ryebay to Estuary of Somme	Washbucht to NE. and Terschelling to WNW.
4 h after } 2 h before }	High water at Dover	Start Point to Casquets	Dungeness to Authie Bay	Outside eastern outlet
5 h after } 1 h before }	High water at Dover	Lyme Regis to Cap de la Hague	Margate to Gravelines	—
Low water } High water }	at Dover	Large area with no currents south of Isle of Wight	Thames Estuary to Ostende	—

belongs already more to the system of the North Sea currents. Table 45 gives information concerning the position of these boundaries for all tidal hours. One can see how each of them apparently travels from west to east through the entire channel. The "Atlantic" and the "North Sea" boundaries

are lines of convergence for all phases after high water near Dover (including low water at that point), and lines of divergence for the phases at or before high water near Dover. The opposite holds for the channel boundary. In the vicinity of the boundary lines there is, of course, no current. The velocities of the current are in the vicinity of the pseudo-nodal lines between St. Albans Head and Cape de la Hague, always greater than east and west thereof (3.5 knots in the centre of the channel up to 5 knots at the French coast). A second place where the current velocities are greater is located in the Strait of Dover, where at times velocities of 5–6 knots are attained. (For flow of water through the Strait of Dover related to wind and differences in sea level, see BOWDEN, 1956). The French coast of the English Channel has higher current velocities than the English side; east of the Strait of Dover (Hoofden) conditions are reversed, but the velocity here is reduced to $1\frac{1}{2}$ –3 knots.

Most tidal charts of the Channel are based upon the assumption that the tide wave travels faster in the central part of the Channel because of the greater depths, so that the co-tidal lines across the channel seem to be curved. According to whether the bottom influence was given more or less importance, the co-tidal lines are more or less convex towards the east. As explained previously (p. 148), this assumption, however, is absolutely false and, therefore, such charts should be discarded. Modern methods in *Hydrodynamics* did not substantiate such curvature in the co-tidal lines and as a matter of fact the curvature, if any, would be in the opposite direction. Hydrodynamical investigations were made by DOODSON and CORKAN (1932), who used the Proudman method which has already given satisfactory results for the North Sea. The small number of current observations and of stations with harmonic constants in the Channel required the use also of somewhat less accurate coastal tidal constants which were previously reduced. The computations refer to the M_2 tide. The result for the English Channel is given in Fig. 158. The course of the main partial tide along the entire Channel is readily seen from this figure, and it is shown that the previously given results, based on coastal observations only, apply also to the central parts of the Channel.

BÖRGEN (1898) has tried to explain the tidal phenomena in the English Channel. He assumed that two progressive waves, one coming from the Atlantic Ocean, the other one from the North Sea, cross each other after repeated reflections in the Channel. According to recent views on the behaviour of tide waves in the vicinity of land, it is obvious that a hydrodynamical theory of the tides of the Channel must start with the fact that the water-masses co-oscillate with the tides of the oceans in front of the two openings. Airy had already assumed this, but did not explore it further. Börger denies this explanation, probably because in his time there were no methods to verify it by means of computations. DEFANT (1919, see also

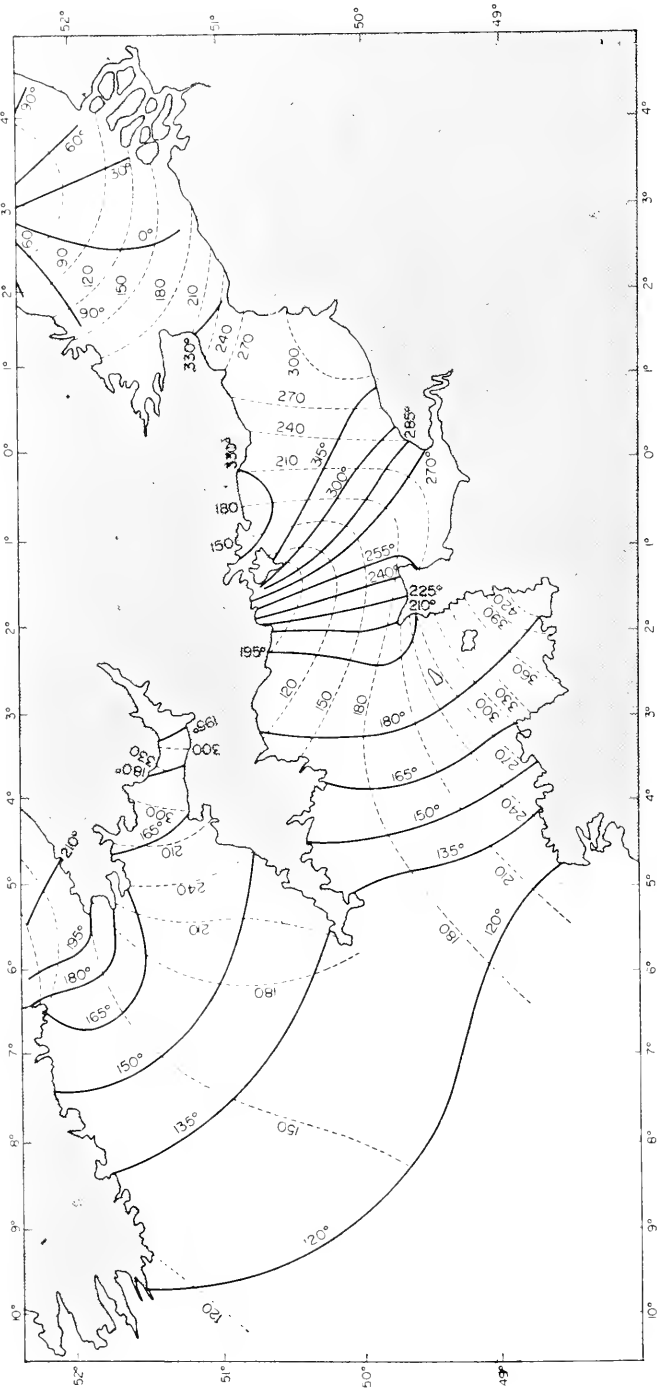


FIG. 158. Co-tidal and co-range lines of the M_2 tide in the English Channel and south west North Sea. —, phase in degrees referred to the upper culmination of the moon in Greenwich; - - - - -, amplitude in cm.

THORADE, 1921, p. 105) has developed this method to compute the tidal phenomena, and it agrees very well with the observations.

The period of the free oscillation of the Channel supposed to be closed at both ends is 29.5 h and, therefore, the independent tides are absolutely unimportant in respect to the co-oscillating tides. The latter can be assumed to be composed of (a) the co-oscillation of the water-masses of the Channel with the Atlantic Ocean if the North Sea is supposed to leave no tides, and (b) co-oscillation with the North Sea if the Atlantic Ocean is supposed to be free of tides at the western opening of the Channel. Both parts can be computed step-wise, according to the methods already explained. If at first the friction is neglected, both are standing waves which, ν being = 2.4, have two nodal lines inside the Channel. Of course, they do not coincide; besides, these standing waves have a phase difference of $1\frac{1}{2}$ h, so that their superposition

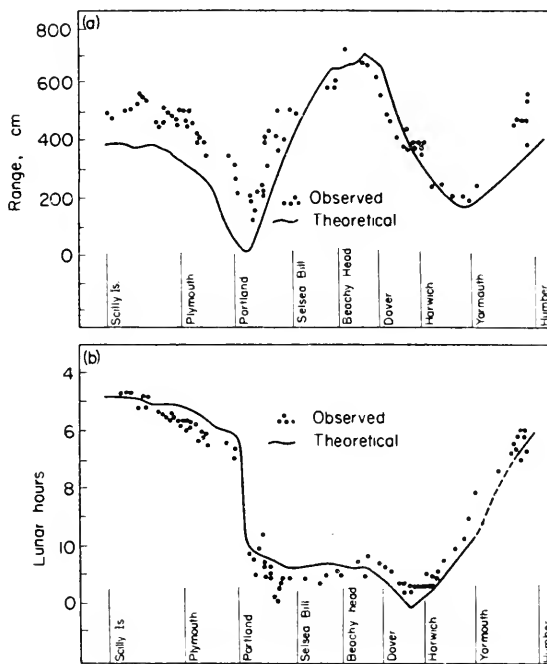


FIG. 159. Semi-diurnal tide in the English Channel and in the Hoofden. (Spring tide values from the tide tables.) (a) shows the range, (b) shows the establishments in lunar hours.

gives the picture of a wave travelling from west to east. If friction is considered, it causes the transformation of the nodal lines of each co-oscillating tide into a crowding of the co-tidal lines, but this does not essentially modify the picture. The computed horizontal water movements permit the approximate determination of the influence of the Coriolis force. A noticeable fact is that the rotation of the earth is not able to transform the crowding of the co-tidal lines into an amphidromy in the narrow part of the Channel

north of the Cotentin peninsula but only increases the crowding on the northern side whereas on the southern side they are more spaced. However, in the Hoofden we have the picture of a well-developed amphidromy.

The combination of the longitudinal and transverse oscillations gives finally the theoretical tides, and it must be admitted that they agree very well with the observations, especially if one considers that the theory bases itself only on the tidal observations at the ends of the connecting channel. Figure 159 gives a comparison between the observations and the theory for the northern coast of the channel. Figure 160 shows a comparison for four hours of the tidal

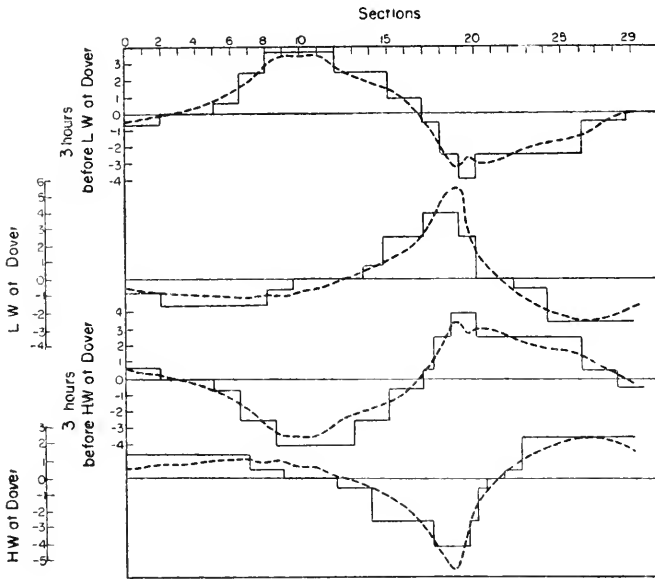


FIG. 160. Tidal currents in the English Channel and Hoofden (nm/h). +, direction North Sea; —, direction Atlantic Ocean; ----, computed; \square — \square —, observed.

period; the same conditions prevail for the other hours. There is no doubt that the tides of the English Channel and of the south-western North Sea result from the impulse which their water-masses receive from the Atlantic Ocean and from the North Sea. It can also be shown that the diurnal tides in the Channel are small because the diurnal tides in the ocean off the openings are also small.

4. The Tides of the Irish Sea

In the Irish Sea, the oscillating area is situated between the line Cape Clear — Scilly Islands in the south and the line Tory Island — Hynish Point in the north; consequently, it comprises the St. George Channel, the Irish Sea and the North Channel.

The Irish Sea can be treated in exactly the same way as the English Channel.

The computation made by DOODSON and CORKAN (1932, see also PROUDMAN and DOODSON, 1923) of the tides of the Irish Sea is shown in Fig. 161. Airy had already found that the tides in the central part of the Channel, the actual Irish Sea, have almost the character of a standing wave. The tidal current changes nearly everywhere simultaneously, and the currents are strongest

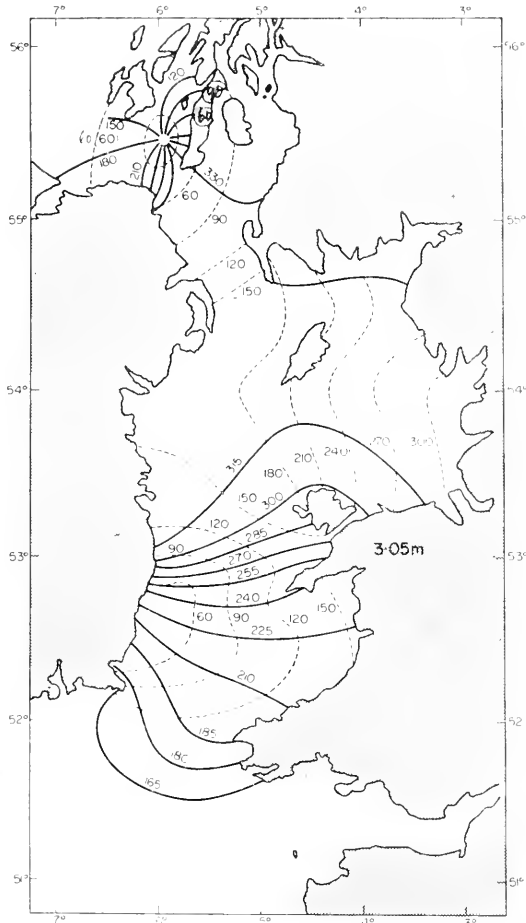


FIG. 161. Co-tidal and co-range lines of the M_2 tide in the Irish Sea. —, phase in degrees referred to upper culmination of the moon in Greenwich; -----, amplitude in cm.

where the range is smallest (in the St. George Channel and in the North Channel), whereas the currents are smallest, even almost imperceptible, where the range is largest (Isle of Man). This points unmistakably to standing waves. The distribution of the co-tidal lines shows in the south an incoming wave from the Atlantic Ocean, then a crowding of these lines, particularly in the northern part of the St. George Channel; in the Irish Sea a large area with nearly uniform time of high water (homochromy), which still persists

Table 46. Harmonic constants for the Irish Sea

Position	M_2	S_2	K_1	O_1	$\frac{K_1+O_1}{M_2+S_2}$	$M_2+S_2+K_1+O_1$
Cardiff	$H(\text{cm})$ 409.0	142.0	9.4	6.7	0.03	567.1
51°27'N. 3°10'W.	\approx° 191.0	239.0	144.0	6.0		
Milford-Haven	229.2	84.7	4.9	6.7	0.04	325.5
51°42'N. 4°57'W.	164.0	208.0	144.0	5.0		
Holyhead	177.1	62.8	11.0	10.4	0.09	261.3
53°19'N. 4°37'W.	282.0	319.0	169.0	16.0		
Liverpool	305.5	97.1	11.9	11.1	0.06	425.6
53°25'N. 3°00'W.	320.4	5.4	190.0	42.0		
Workington	274.3	76.8	13.4	8.8	0.06	373.3
54°39'N. 3°34'W.	328.0	6.0	189.0	24.0		
Douglas (Isle of Man)	227.4	75.6	9.8	15.9	0.08	328.7
54°09'N. 4°28'W.	317.0	0.0	177.0	34.0		
Ramsey (Isle of Man)	262.4	92.4	13.7	6.1	0.06	374.6
54°19'N. 4°22'W.	317.0	4.0	196.0	58.0		
Greenock	132.8	31.6	5.0	7.3	0.07	176.7
55°57'N. 4°46'W.	337.0	42.0	224.0	54.0		
Loch Fyne,						
East Loch Tarbert	109.4	32.6	14.0	10.7	0.17	166.7
55°52'N. 5°24'W.	329.0	27.0	202.0	53.0		
Sound of Gigha	18.9	16.2	9.4	8.2	0.50	52.7
55°41'N. 5°44'W.	70.0	145.0	195.0	31.0		
Sound of Sura,						
Carsaig Bay	46.0	25.0	8.5	8.2	0.24	87.7
56°03'N. 5°38'W.	98.0	132.0	183.0	33.0		
Islay, Port Askaig	51.2	30.8	8.2	7.9	0.20	98.1
55°51'N. 6°06'W.	137.0	176.0	176.0	23.0		
Portrush	50.9	22.3	8.5	7.0	0.21	88.7
55°12'E. 6°39'W.	177.0	198.0	170.0	8.0		
Londonderry	78.6	29.8	8.5	8.0	0.15	124.9
55°00'E. 7°19'W.	217.8	242.5	183.8	37.9		
Belfast	122.5	29.0	7.9	12.8	0.14	172.2
54°36'E. 5°55'W.	303.0	345.0	175.0	30.0		
Dublin	133.5	36.9	8.6	11.1	0.12	190.1
53°21'E. 6°13'W.	314.0	356.0	164.0	4.0		
Dun Laoghaire						
(Kingstown)	136.3	40.4	4.5	5.5	0.06	186.7
53°18'E. 6°08'W.	313.0	357.0	190.0	49.0		
Wexford Harbour	48.8	22.6	6.7	7.0	0.19	55.1
52°20'E. 6°22'W.	175.0	241.0	185.0	47.0		
Queenstown	136.7	42.6	1.9	4.2	0.03	185.4
51°50'E. 8°18'W.	133.3	177.0	160.0	37.0		

in the southern part of the North Channel. The opening in the north has an amphidromy, as a transition to the oceanic tides.

The extensive bays and sounds on the east coast of the Irish Sea have a great influence on the development of the tides. The tides of the Bristol Channel have been discussed by TAYLOR (1921, p. 320). The water-masses in the area off Liverpool and in the Solway Firth, as well as in the Firth of Clyde, co-oscillate with those of the Channel outside the opening and a considerable part of the penetrating tidal energy is used up through friction.

BÖRGEN (1894, p. 395) has also in this case tried to explain the Irish tides by assuming two progressive waves travelling in opposite directions; this explanation, however, agrees only partly with the observations. The later used hydrodynamical methods as applied by Defant have permitted the numerical computation of the tides and tidal currents. On the basis of eighteen cross-

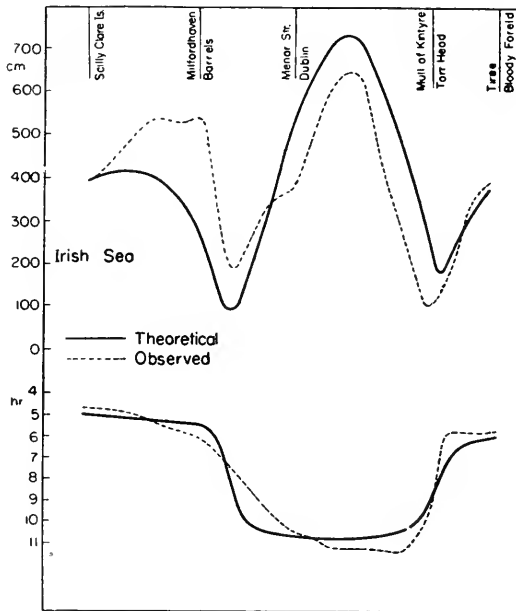


FIG. 162. Semi-diurnal tide in the Irish Sea (spring tide values of the tide tables).

sections, DEFANT (1919) computed the co-oscillating tides of the water-masses of the entire channel with the tides at the north and south openings, taking into account all adjacent bays. As the difference in phase at these openings is less than one hour and, as the amplitudes there are almost the same, the superposition of the two co-oscillations does not essentially change the character of a standing wave, and there are two places where the range is small and the variation in the phase is rapid. Here again, as in the English Channel, the rotation of the earth is not able to transform the nodal line into an amphidromy; the crowding of the co-tidal lines, especially on the Irish side in the

St. George canal, subsists. In the northern part of the North Channel, there is an amphidromy (exactly as in the Hoofden). Figure 162 gives a comparison between the observations and the theoretical computations. The Irish tides can be explained by the impulses received by their water-masses from the Atlantic Ocean. There is also very good agreement between theory and observations on the tidal currents. For the tidal currents in the North Channel see also PROUDMAN (1939).

DOODSON, ROSSITER and CORKAN (1954) have made a rather interesting investigation of the tides of the Irish Sea, in which they used methods similar to the so-called "relaxation methods", using finite differences in all variables and attempting to satisfy all the conditions of motion within the sea, proceeding by successive approximations. Only coastal observations of tidal elevations are supposed to be known. There are many difficulties, peculiar to the tidal problem, in the application of these methods, due to the very irregular coast lines and depths, gaps in the coasts, shallow water near the coasts, frictional forces, and the very serious complication due to the fact that the tides are oscillating and thus require two phases to be investigated simultaneously owing to their reactions one upon the other.

The resulting chart is shown to be very closely the same as the existing chart, thus proving the validity of the method.

5. The Tides of the Mediterranean

The tides of the Mediterranean, including the adjacent seas, have been investigated exhaustively in more recent times, although they are comparatively weak. A satisfactory explanation was found, but it took numerous new observations to arrive at a basic theory of these tides.

A compilation has been made of all the available coastal observations on establishments and tidal ranges of the western and eastern basin, and of the Strait of Gibraltar and the Strait of Tunis (where the 15° E. meridian, which divides the Mediterranean in two, has been taken as a reference). In Fig. 163, drawn by STERNECK (1915, p. 905) (see also DEFANT, 1916, p. 462) is shown schematically the distribution of the establishments; not considering the Straits of Messina and of Tunis. The majority of the establishments fall in two groups, namely, 3.3 and 9.3 h. At the ends of the various basins we have entered the average establishment of the stations located there. The lines of demarcation between the areas with the establishments 3 and 9 h are to be considered as nodal lines of standing oscillations. This indicates that the tides in the Mediterranean can be represented by two standing waves, one covering the western, the other the eastern basin. The arrows in the figure indicate the direction of the tidal currents from 3 to 9 h at the time of the syzygies. In the Straits of Messina and Tunis, the rotation of the earth causes strong transverse oscillations which, according to the observations, transform the nodal lines into amphidromies *contra solem*. The other nodal lines are

likewise according to observations transformed into amphidromies; this is particularly the case for the one in the eastern basin. The Mediterranean can be considered to be divided by these three nodal lines of the longitudinal oscillations in six sections, each of which extends from an antinode to a node and vice versa.

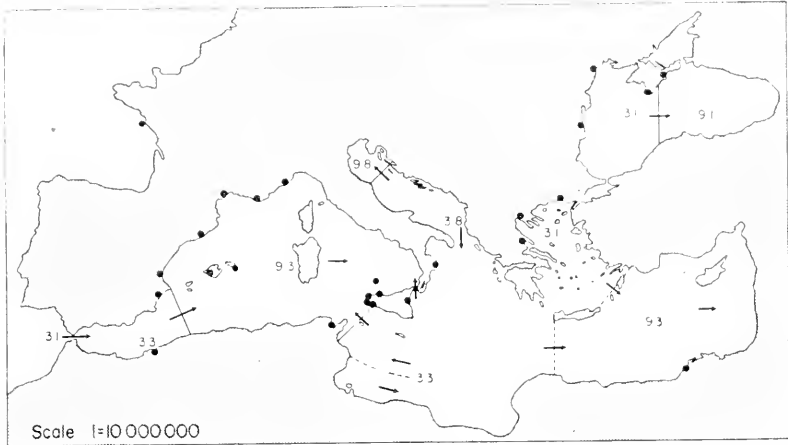


FIG. 163. Oscillating areas of the Mediterranean (numbers indicate average establishments in central European time, those in the Black Sea in Eastern European time) (Sterneck).

The interpretation of these basic facts, which were found rather early (see GRABLOVITZ, 1909, p. 191) goes back to two different fundamental ideas (see MERZ, 1914). One is based on an assumption expressed by Darwin that the Mediterranean is so completely closed by the Strait of Gibraltar that only independent tides can develop in this sea, like in a large lake, so that in each basin only forced oscillations are possible. STERNECK (1912, p. 1245), who at first accepted this conception, has explained the equal establishments in the large basins of the western Mediterranean (between the Balearic Islands, Corsica and Sardinia, on the one hand, and in the Thyrrenian Sea on the other hand) by assuming forced oscillations, such that in the coastal regions of these basins high water occurs simultaneously, while at the same time the central parts of the basins have low water, and vice versa. For such oscillations the nodal lines would be closed in themselves. DE MARCHI (1908, p. 12) has proven, however, that such oscillations caused by the vertical component of the tide-generating forces can only be very small and that they cannot deserve any consideration; unless the period of the impulses coincide with the period of the basin, which is not the case. Later on, Sterneck has found that these oscillations, which would require a constant water volume in the individual basins, do not exist. A great amount of tidal energy penetrates through the Strait of Gibraltar into the western Mediterranean and influences conditions in the western basin.

A second mode of interpretation of the observations denies in advance

the possibility of independent tides and attempts to explain the existing ones by an Atlantic wave penetrating through the Strait of Gibraltar into the Mediterranean. WEGEMANN (1913, p. 555) has developed this theory and tries to make it agree with the observed data through interferences between the penetrating wave and the reflected wave on the Italian coasts and which leads partly to standing waves. In the eastern Mediterranean basin he assumes, like HARRIS (1904), an amphidromy *contra solem* around Crete, which he thinks results from the superposition of the Atlantic wave penetrating through the Strait of Tunis with its reflection on the coasts of Syria.

STERNECK (1913–15, see also, DEFANT, 1913, p. 361; 1916, p. 462; 1922) attempted in several papers to explain the tidal phenomena of the Mediterranean by computation based on hydrodynamics. He developed this theory further and it agrees with the harmonic constants observed at coastal localities. He examines first the direct effect of the tide-generating forces for each of the two Mediterranean basins, assuming that these basins are completely closed on all sides. The natural period is 5·96 h for the western basin and 8·54 h for the eastern basin, and he finds in each basin a nodal line placed almost exactly in the middle of the Mediterranean with establishments of 3 h in the western and 9 h in the eastern part.

The eastern basin has no other tidal components than this independent tide. This seems astonishing, as it is connected with the other basins of the Mediterranean (the Adriatic and Aegean Sea, and the Straits of Messina and Tunis). However, Sterneck pointed out that, at the time of the syzygies from 3 to 9 h, the eastern basin receives from the Adriatic 13·1 km³, from the Aegean Sea 35·1 km³ of water, in all 48·2 km³, whereas during the same time it loses 11·0 km³ through the Strait of Messina, 41·9 km³ through the Strait of Tunis, totalling 52·9 km³, so that but for the small quantity of 4·7 km³ the total water-mass of the eastern basin remains constant during one tidal period. In first approximation the co-oscillating tides with the other basins will be negligible compared to the independent tidal component.

Sterneck gives an exceptional position to the Syrtis Minor, which features small water depths and in its central part a considerable increase in tidal ranges. He treats this region as a closed one, separating it from the water masses in the eastern section of the Strait of Tunis, which is a rather arbitrary decision. It would seem more simple to regard the Syrtis Minor as a bay extending from the estuary of Ras Kapudia (tidal range 22 cm) in the north to a point a little west of Tripoli (tidal range 20 cm) in the south. The free period of this region is about 6 h, so that ν will be about $\frac{1}{2}$. This points to a co-oscillation of the water-masses in this bay with the outer tides magnified by resonance. It is for this reason that there are the great tidal ranges of nearly 200 cm at Gabes and Skhirra.

The western basin has, beside its independent tide, co-oscillating tides with the Atlantic Ocean through the Strait of Gibraltar and, with the eastern

basin through the Straits of Tunis and Messina. These co-oscillating tides can be accurately determined by the method of the step-wise integration of the hydrodynamical equations (p. 339), because we know the water-masses which pass through the straits within a half-tidal period. According to the current observations of Captain N. S. Nares there is from 3 to 9 h an inflow of 69.8 km^3 into the western basin, which enables one to compute the co-oscillating tide for all cross-sections. The co-oscillating tide is larger than the independent tide (a little east of Gibraltar about at the ratio 5:3) and it is evident that the influence of the tides of the Atlantic Ocean on those of the Mediterranean is considerable. The nodal line of the oscillation in the western section of the basin is between Cape de la Nao (between Valencia and Alicante) and a point of the Algerian coast between Alger and Oran.

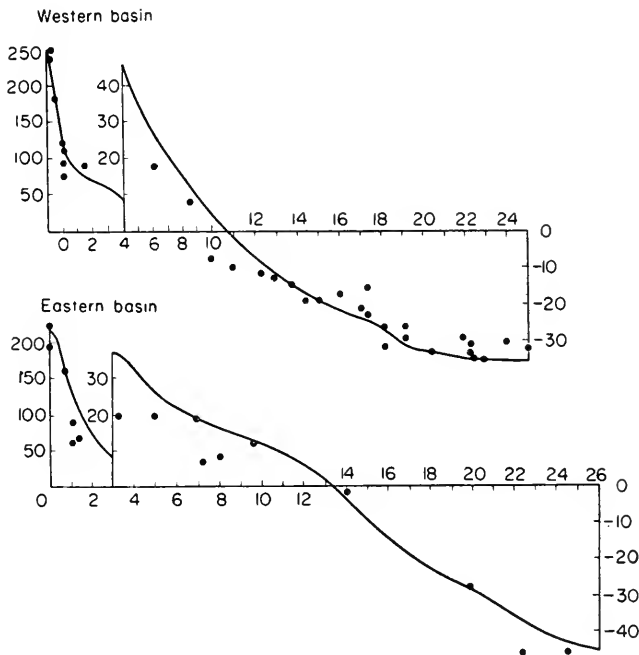


FIG. 164. Longitudinal oscillations of the semi-diurnal tides in the western and eastern basins of the Mediterranean. —, theoretical distribution of the springtide ranges; •••••, observed values; positive values: phase around 3 h; negative values: phase around 9 h Central European Time.

For the co-oscillation of the western basin with the eastern basin, we can consider first the Strait of Messina. One can use the same cross-sections as for the co-oscillation with the Atlantic Ocean and obtain at the western end of the basin a range of only 3 cm; the nodal lines lie in the centre of the Tyrrhenian Sea. Somewhat greater is the influence of the co-oscillation through the Strait of Tunis. On account of the position of this opening, it was necessary to select another arrangement of the cross-sections. One

obtains a range of about $7\frac{1}{2}$ cm for the western end near Gibraltar, where it nearly comes to a periodical parallel displacement of the entire surface without a nodal line.

All these separate parts of the tides can simply be added together to obtain the theoretical tide of the western Mediterranean basins, since all are almost synchronous: namely, the independent and the co-oscillating tide with the Atlantic Ocean in the west with the phase 3 h; the independent and co-oscillating tide with the eastern basin with the phase of 9 h. Figure 164 shows the good agreement between the theory and the observations, both for the western and the eastern basin. This is remarkable, when one bears in mind that the theory is solely based on the fact that the tides at the western

Table 47. Harmonic constants for the Mediterranean

Place	Amplitude (cm)					λ in degrees				
	M_2	S_2	N_2	K_1	O_1	M_2	S_2	N_2	K_1	O_1
Cadiz	92.8	32.3	16.4	6.1	6.1	41°	69°	34°	28°	294°
Gibraltar	38.3	14.1	7.4	3.0	1.1	36	65	23	122	154
Alicante	1.8	1.0	0.4	3.7	2.2	59	81	29	163	110
Toulon	5.9	2.7	1.5	3.5	1.8	247	250	227	188	118
Marseille	6.7	2.4	1.3	3.5	2.1	230	247	223	188	97
Genoa	9.0	3.1	2.0	3.2	1.2	240	256	232	188	190
Civita Vecchia	11.2	4.3	2.3	2.9	1.5	257	284	237	208	110
Naples	11.0	4.0	2.0	2.6	0.8	268	282	246	216	128
Cagliari	8.5	3.6	1.8	3.2	1.6	255	273	248	200	121
Palermo	10.9	4.5	3.1	3.1	1.1	264	285	259	213	135
Malta	6.1	3.7	1.0	1.0	0.7	95	100	116	52	72
Catania	6.6	3.8	1.0	1.6	1.2	95	95	111	60	66
Taranto	6.5	3.7	0.6	1.8	0.8	105	107	118	59	51
Tripoli	11.1	5.4	—	2.0	0.6	85	101	—	26	135
Beirut	13.4	9.1	—	2.1	1.5	304	319	—	328	326
Port Said	11.7	6.9	2.0	2.1	1.7	304	319	303	305	275
Alexandria	7.2	4.1	1.2	1.7	1.3	305	319	308	303	271

end of the basin corresponds to the tides of the Strait of Gibraltar. The well-developed nodal lines are transformed by the rotation of the earth into amphidromies which should influence the establishments in their vicinity. There are indeed indications to that effect, but sufficiently accurate observations are lacking.

Some years ago, a harmonic analysis of the tidal observations has been made for a large number of Mediterranean localities. Table 47 gives a compilation of the constants for the most important tidal components. Sterneck has used them to test his theory. The phase of each component after being

reduced to the 15° E. meridian proved to be nearly constant and this applies in part to the amplitude, so that we can group the separate localities and obtain average values for the Tyrrhenian, Ligurian and Ionian Sea. The result is tabulated in Table 48.*

Table 48. Harmonic constants for separate oscillating areas in the Mediterranean
(α' referred to 15° E.)

		M_2	S_2	N_2	K_1	O_1
Cadiz	H	92.8	32.3	16.4	6.1	6.1
	α'	82°	111°	74°	49°	314°
Gibraltar	H	38.3	14.1	7.4	3.0	1.1
	α'	77°	106°	64°	142°	174°
Alicante	H	1.8	1.0	0.4	3.7	2.2
	α'	89°	112°	58°	179°	124°
Ligurian Sea	H	7.0	2.8	1.4	3.5	1.8
	α'	255°	267°	245°	199°	118°
Tyrrhenian Sea	H	10.4	4.1	1.8	3.0	1.2
	α'	266°	287°	253°	212°	126°
Ionian Sea	H	6.4	3.7	0.8	1.5	0.9
	α'	97°	100°	114°	57°	62°
Eastern Mediterranean Sea	H	10.8	6.7	1.5	2.0	1.5
	α'	268°	284°	270°	290°	260°

From one group to another the phase of the semi-diurnal tide varies by nearly 180° , so that one has three nodal lines in the longitudinal oscillation of the entire Mediterranean which is in accord with the theory. Figure 165 shows this in the form of a graph for the M_2 , S_2 and K_1 tides. The amplitudes also correspond to the values derived previously for the various semi-diurnal tides. Therefore, this theory can be regarded as complete.

The data gained by harmonic analysis are also useful for the investigation of the diurnal tides of the Mediterranean. The reduced phases of the diurnal components like K_1 , P_1 and O_1 show a steady increase from west to east. This points to an interference of two non synchronous standing waves, one of which originates from the co-oscillation of the Mediterranean with the external tide through the Strait of Gibraltar, whereas the other one

* Sterneck reduced the phase to the 15° E. meridian by using the equation $g_{15^\circ} = \alpha + \sigma/15^\circ(15^\circ - \lambda)$ which is wrong. He did the same for the Adria (see p. 400). The Mediterranean being small, the deviation from the values according to the correct formula is not great (although in Alexandria it is 2°), but this equation cannot be used for greater distances.

is the independent diurnal tide of the entire Mediterranean. If we assume for the latter at an arbitrary locality a range $\eta_1 = a_1 \cos(\sigma t - \kappa'_1)$, for the co-oscillating tide $\eta_2 = a_2 \cos(\sigma t - \kappa'_2)$, then $\eta = \eta_1 + \eta_2 = H \cos(\sigma t - \kappa')$ in which

$$a_1 = H \frac{\sin(\kappa' - \kappa'_2)}{\sin(\kappa'_1 - \kappa'_2)} \quad \text{and} \quad a_2 = H \frac{\sin(\kappa' - \kappa'_1)}{\sin(\kappa'_2 - \kappa'_1)}.$$

Table 48 gives us H and κ' and with κ'_1 which for the independent tide (reduced to the central meridian of 15° E.) is approximately 90° , and κ'_2 which

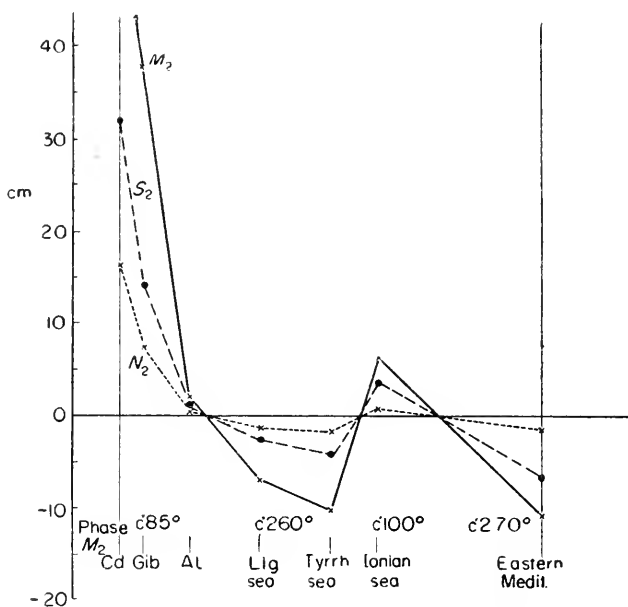


FIG. 165. Distribution of the amplitudes and phases of the semi-diurnal partial tides in the Mediterranean.

is the reduced κ -number of Cadiz, we can compute the amplitudes of the two components for every locality. The result can be found in Fig. 166. For the co-oscillation there are two nodal lines, one between Cadiz and Gibraltar, i.e. in the Strait of Gibraltar itself, the second one between the Tyrrhenian and the Ionian Seas, probably in the Straits of Tunis and Messina. The independent tide shows, beginning at Cadiz where it must be zero, an increase towards the east, then a decrease to the only nodal line in or east of the Ionian Sea.

The distribution of the nodal lines and amplitudes of the semi-diurnal and diurnal tides allow a complete explanation of the observed variations in the character of the tide in the Mediterranean. The small ratio of 0.10 in Cadiz is opposed by the large value of 2.13 at Alicante. This can be

explained by the position of the nodal line of the semi-diurnal tides in the western part of the western basin, where at the same time the diurnal tides have an antinode. The Ligurian Sea, which is not close to a nodal line neither of the semi-diurnal nor of the diurnal tides, has an ratio of 0.56, which does not deviate essentially from the normal value of 0.49. In the

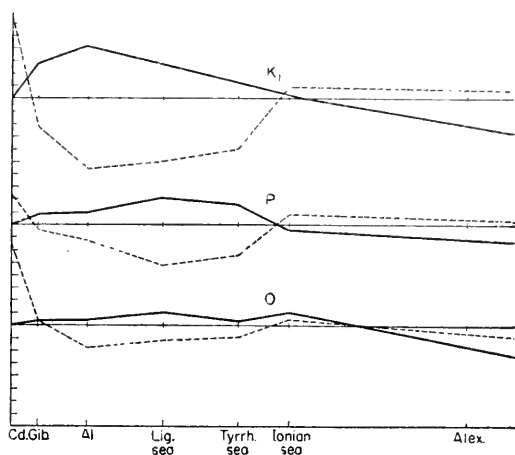


FIG. 166. Distribution of the amplitude of the diurnal partial tides in the Mediterranean (Sterneck). -----, co-oscillation with Atlantic ocean, ——— independent tide.

Tyrrhenian Sea with an antinode of the semi-diurnal tides there is a decrease of the ratio to 0.30, which continues in the Ionian Sea to 0.24, because here lies the nodal line of the diurnal tides. In Alexandria the ratio is also not much greater, as the amplitudes of the semi-diurnal tides increase towards the east.

6. The Tides in the Strait of Messina

There are in the Strait of Messina strong currents which have the rhythm of the tides and which are known since antiquity by the Homeric description of Scylla and Charybdis. It was already known to Aristotle that these currents are associated with the tides in neighbouring seas. The first compilation of the basic facts (1824) is due to the French Vice-Consul in Messina, RIBAUD. A detailed description of the current conditions throughout the whole strait was given by MARINI in 1917. Later on, these phenomena were investigated from a biological viewpoint without dealing with the geophysical process as such. A first extensive oceanographical survey of the entire phenomenon was made by VERCELLI (1925) aboard the research ship "Marsigli" in 1922–23. These observations were the basis of a geophysical explanation given by DEFANT (1940, p. 145). An extensive description of the eddies and currents within the strait has been given recently by MAZZARELLI (1938). The stationary currents at the narrowest point of the strait flow in a southward direction,

down till 30 depth and from this depth to the bottom at about 106 m in a northward direction corresponding to the vertical density distribution of the Tyrrhenian Sea in the north and of the Ionian Sea in the south (see vol. 1/2). Their velocities in both layers are of the order of magnitude of 10 cm/sec, but can increase to considerably greater values, through wind and piling up effects. Superposed on these stationary currents are the tidal currents originating from the co-oscillation of the water-masses of the strait with the tides of the adjacent seas. As we have seen, these tides have a nearly opposite phase with equal amplitudes, i.e. when the Ionian Sea off the strait has high water, then the Tyrrhenian Sea has low water and inversely. If the tides at the opening of the strait in the north and the south are known, the tides and the tidal currents within the strait can be computed according to the method of the step-wise integration of the equations of motion (p. 339), taking into consideration the morphologic conditions of the connecting canal. If at first, the frictional influences are neglected we obtain the picture as represented in Fig. 167. The tides of the area of the strait south of the nar-

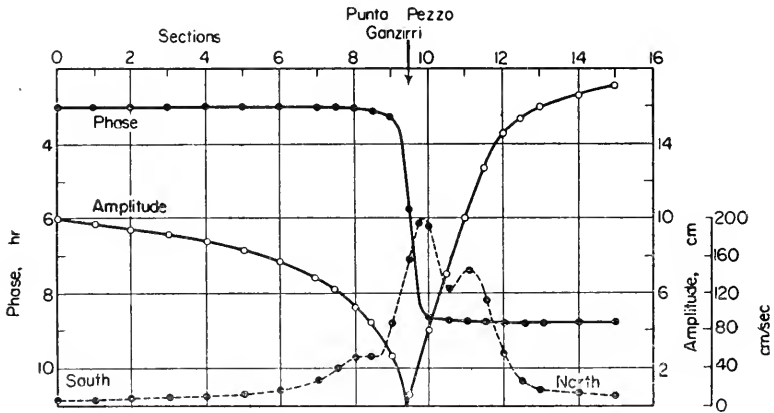


FIG. 167. Phase and amplitude of the tide in the Messina Straits. ---, intensity of the tidal current (friction neglected).

rowest cross-section (Punta Pezzo–Ganzirri) behave essentially like the Ionian Sea, except that the amplitude of the tide gradually decreases to zero approaching the first location. The same applies for the section north of this cross-section, which is governed by the tides of the Tyrrhenian Sea. Within a very short distance of a little more than 3 km, the phase of the tide varies by nearly 6 h. At this point occur the greatest slopes of the sea surface. At 3 h the difference in elevation of the sea surface over this short distance is 1.7 cm/km from south to north. At 9 h it is reversed from north to south and at 0 h and 6 h the surface is nearly level. The velocities of the current related with the maximum gradients are shown in the figure: between 3 h and 9 h the current is directed northward; this is the so-called “rema mon-

tante"; at the narrowest point it attains at 6 h its maximum of nearly 200 cm/sec. Between 9 h and 3 h the current is directed southward, which is called the "rema scendente"; at 0 h it has the same maximum value of 200 cm/sec. These currents computed theoretically can be compared with observations made by Vercelli on an anchor station of 15 days in the cross-section Punta Pezzo-Ganzirri, and which were submitted to the harmonic analysis. He found the following surface values.

Table 49. Harmonic constants of the tidal current
in the Strait of Messina

(H in cm/sec, reduced to the transit of moon through the meridian in central European time.)

	M_2	S_2	N_2	K_2	K_1	O_1	P_1	M_3
Surface								
Punta Pezzo-Ganzirri H	164	46	25	15	41	20	15	15
(38°2' N., 15°6' E.) α	129°	122°	122°	147°	73°	56°	73°	82°

In the lower layers down to the bottom the phase is almost constant, but the velocity decreases slightly. The mean phase of the entire tidal current is approximately 4.7 h, its intensity around 200 cm/sec. The theory gave 5.9 h, so that the observations show a priming of 1.2 h. It can certainly be attributed partly to the friction on the rough ocean bottom and partly to the strong turbulent mixing of the Tyrrhenian and Ionian Sea which takes place in the narrowest section of the straits. In a very narrow canal, where the compensation between the different levels on the surface takes place like a river, the phase of these currents should be about 2.9 h. In the case of a very wide canal, on the contrary, the tide would flow undisturbed and, according to the theory, its phase would be 5.9 h. The actual case probably lies between these two extremes; the average is 4.4 h, which is very close to the observed value. Using the observed phases, we obtain along the strait the average current conditions represented graphically in Fig. 168. Naturally, the three-dimensional distribution over the entire cross-section of the strait will be much more complicated. In the section after the sharp bend of the strait to the north-east between Punta Pezzo-Ganzirri and C. Peloro-Scilla we notice the occurrence of stream convergences, for the first time between 2½ h and 4 h when the current turns from north to south, the second time between 6½ h and 8 h when the current changes from south to north. These stream convergences must be the seat and the source of current disturbances, whose turbulent nature is still increased by the meeting of the two different bodies of water which are never in equilibrium next to each other. The Ionian water coming from the south is more saline and therefore heavier than the water coming from the Tyrrhenian Sea which is lighter. This is the point where eddies with vertical and horizontal axes develop and which

can acquire large dimensions. The circumstance that in this part of the strait the upper water layer in its steady position travels southwards, whereas the lower layer moves northwards, plus the tidal currents, contributes to the development of dynamical instabilities, which dissolve into eddies. This is substantiated by the observations. Around 3 h, when the “rema montante”

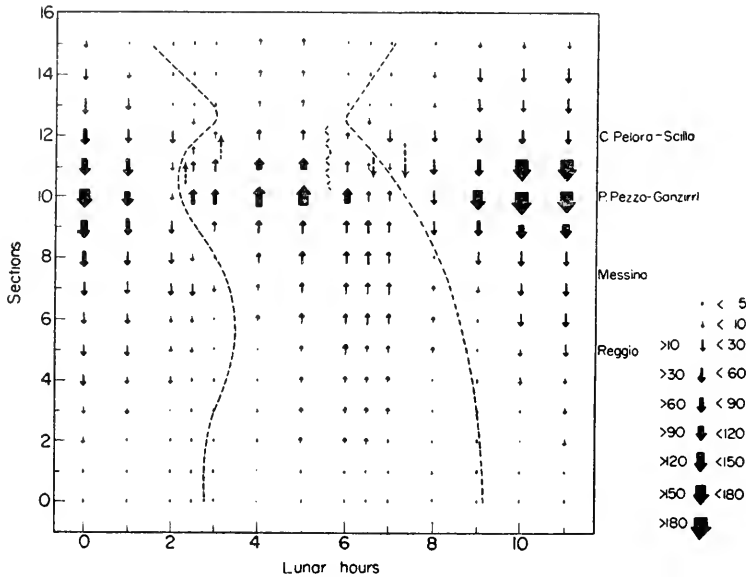


FIG. 168. Average current for each lunar hour along the N. S. longitudinal axis of the Strait of Messina.

starts, a disturbance of the current develops in the form of a bore called “primo taglio della rema montante” near Ganzirri, which travels to C. Peloro in 45 min. At 4 h there is a second wave in the vicinity of Torre Faro which travels in 35 min to Scilla; this is called the “secondo taglio”. According to Vercelli, these waves are like a bore in estuaries (p. 464), the heavy water of the Ionian Sea rushes head on against the slowly receding lighter water of the Tyrrhenian Sea.

The “rema scendente” is also accompanied by “tagli”; the first one, rather weak, is formed near Pezzo at about $6\frac{1}{2}$ h to 7 h and travels up to Messina; the second one, the largest, the “taglio grande”, develops near C. Peloro and travels southwards down the entire strait. The lighter Tyrrhenian water glides rapidly over the heavier Ionian water in the form of a bore. The “tagli” or “scale di mare”, which are particularly important at the time of syzygies, have been described extensively by Vercelli and Mazzarelli, to whose papers the reader is referred. However, they develop into large-scale phenomena when strong winds pile up one kind of water against the other.

In connection with the convergences of currents, we must mention the

eddies with a vertical axis. There are three points where they develop: (1) in front of C. Peloro, i.e. the Charybdis; (2) in front of Scilla, i.e. the Scilla eddies; and (3) near the Punta San Ranieri in front of the harbour entrance of Messina. The eddies off Charybdis and in front of Messina are the most important and they develop through the rotational movement in the eddies, whereby the heavier water sinks under the lighter water; the direction of rotation is mostly cyclonic. There are, however, also anticyclonic eddies, in which the water rises in the centre. They are visible by a smooth, apparently oily area in the centre of the eddy (*macchie d'oglio*). The eddies off Scilla are nowadays insignificant. In earlier days their intensity and extension must possibly have been greater. This decrease in intensity might be connected with morphological modifications of the bottom relief off Scilla.

7. The Tides of the Adriatic

The Adriatic Sea has the form of a canal about 500 miles (820 km) long penetrating far into the continent and ending in the Ionian Sea, through the Strait of Otranto. The mean width is 100 miles (166.5 km), the opening is about half this width and its cross-section has a surface of around 37 km². The depth chart shows two different kinds of basins; the bottom in the northern basin slopes down regularly towards the south, up to a cross barrier which separates it from the southern basin. The latter has the shape of a kettle with maximum depths of a little over 3900 ft (1200 m) in the centre. The mean depth of the cross-section of the opening is only 1457 ft (444 m), whereas at the cross-section the maximum depth is nearly twice this figure, 2516 ft (767 m). Table 50 contains a compilation of the amplitudes and phases of the principal components (referred to 15° E.). [KESSLITZ (1919), TENANI (1929)].

The distribution of the harmonic constants of the semi-diurnal tides along the coasts indicates the presence of a well-developed amphidromy. It results from the superposition of a longitudinal oscillation with a nodal line south of Punta Bianche (Dugi) and the transverse oscillations caused by the rotation of the earth. The ratio of the amplitudes of M_2 and S_2 is smaller than 2 for all the adriatic stations, and, consequently, reaches nowhere the theoretical value of 2.3. There is practically no difference between the phases, so that in the Adria there is no "age of the tide".

The diurnal tides show a quite different picture. Their amplitude decreases uniformly to the south-east and seems to become nearly zero near the Strait of Otranto. The differences in phase are small and form the northern part of a weak amphidromy, whose centre is in the vicinity of the Strait of Otranto. The amplitude of the K_1 component exceeds that of the other diurnal tides very strikingly.

As the phases of the semi-diurnal tides vary very much in the different sections of this sea and those of the diurnal tides differ only slightly, there

must be a great variety in the tide-form in the Adria. Particularly characteristic is the distribution of the ratio $(K_1+O_1)/(M_2+S_2)$. In the southern section up till the line Vieste–Dubrovnik, it has the value 0.47, the semi-diurnal tides dominating slightly. The northern section has values near 0.6,

*Table 50. Harmonic constants for the Adriatic Sea **

(*H* in cm; *g* in degrees referred to the 15° E.L. meridian)

Place		M_2	S_2	N_2	K_2	K_1	P_1	O_1
Brindisi	<i>H</i>	8.7	4.8	1.6	1.3	4.7	1.7	1.7
	<i>g</i>	104	116	102	87	73	60	51
Vieste	<i>H</i>	7.9	5.1	1.9	1.9	4.2	1.6	1.5
	<i>g</i>	89	113	76	104	80	84	66
Ancona	<i>H</i>	6.7	3.6	1.5	1.5	12.9	4.2	4.2
	<i>g</i>	329	354	333	335	85	72	68
Pesaro	<i>H</i>	12.8	6.8	3.2	1.8	15.4	5.1	4.2
	<i>g</i>	311	313	279	313	84	84	56
Venice (Malamoco)	<i>H</i>	23.5	14.0	4.1	4.0	18.3	5.8	5.3
	<i>g</i>	296	305	295	299	82	70	65
Trieste	<i>H</i>	26.3	15.8	4.3	5.2	17.5	4.8	5.0
	<i>g</i>	277	285	286	281	70	74	57
Fiume	<i>H</i>	10.4	5.7	1.9	1.7	14.0	4.2	4.0
	<i>g</i>	249	250	240	243	65	64	54
Pola	<i>H</i>	15.1	8.7	2.3	2.5	15.6	4.9	5.0
	<i>g</i>	265	273	272	271	69	70	62
Porto Cigale	<i>H</i>	8.5	4.4	—	2.4	15.5	—	3.7
	<i>g</i>	246	248	—	244	67	—	63
Porto Pantera	<i>H</i>	4.5	3.3	—	1.2	11.9	3.3	3.7
	<i>g</i>	194	204	—	197	69	51	67
Sibenik	<i>H</i>	6.3	4.4	—	1.4	93	—	3.0
	<i>g</i>	135	132	—	127	57	—	4.2
Cosima	<i>H</i>	7.4	5.2	1.3	1.4	7.8	2.4	2.8
	<i>g</i>	108	119	109	116	57	51	40
Dubrovnik	<i>H</i>	9.3	5.8	1.5	1.7	5.1	1.7	2.1
	<i>g</i>	103	108	90	104	59	55	44
Pelagosa Isl.	<i>H</i>	10.3	5.9	3.0	3.0	6.0	3.0	3.0
	<i>g</i>	103	115	104	103	71	48	58
Antivari	<i>H</i>	9.2	5.6	1.3	1.7	4.8	1.9	1.4
	<i>g</i>	105	110	114	108	57	63	33
Durazzo	<i>H</i>	9.3	5.5	0.6	1.5	5.0	1.6	1.4
	<i>g</i>	102	104	123	114	48	48	27

* Tenani, 1940.

but in the central section the ratio increases to more than 1.5, and in the immediate vicinity of the nodal line of the semi-diurnal tides it exceeds 2, so that the tides are almost of the diurnal type. This distribution is fully explained by the behaviour of the Adria in regard to the semi-diurnal and diurnal impulses from the Ionian Sea.

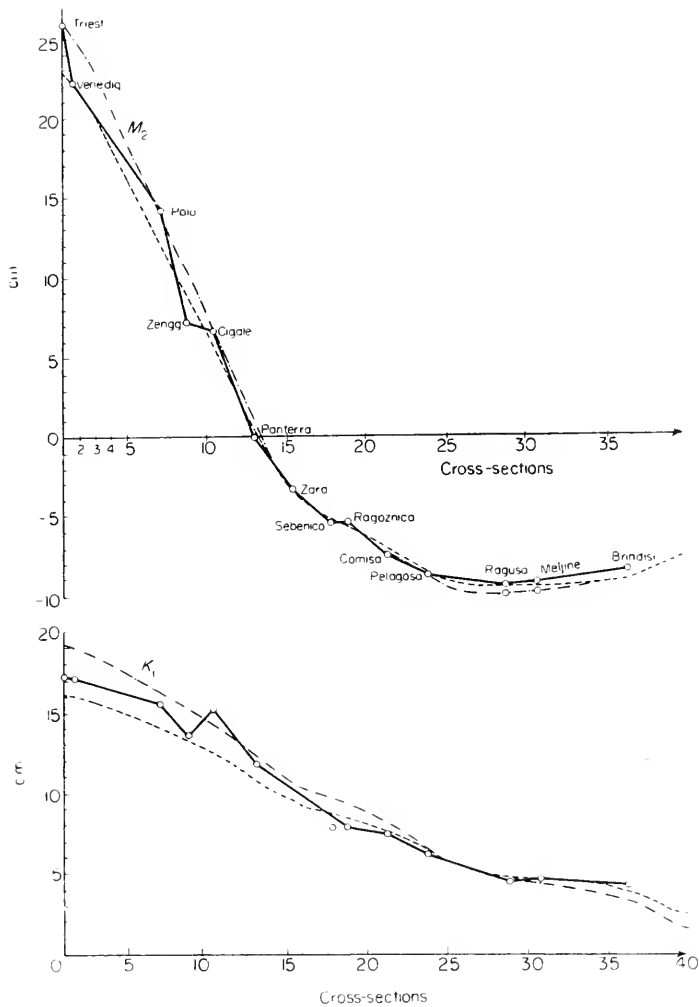


FIG. 169. Distribution of the amplitudes of the M_2 and K_1 tides of the longitudinal co-oscillation of the Adria with Ionian Sea. —, observed; ----, theoretical distribution of co-oscillation with Ionian Sea, - · - · -, considering the independent tide.

For the purpose of explaining the tides, the Adria was first considered as a canal open at one end, co-oscillating with the tidal motion of the Ionian Sea, [DEFANT (1914, p. 270), STERNECK (1914) and DEFANT (1914, p. 556;

1915, p. 147)]. The agreement thus reached between the theory and the observations was already very good. But STERNECK (1919) has tried to have theory and observations agree even better. He used forty cross-sections and, according to the usual method, he calculated the co-oscillating tides and the distribution of the amplitudes of the longitudinal oscillation for all the semi-diurnal and diurnal components. He took into account the influence of the tide-generating forces and he attempted to fulfil the boundary conditions by assuming the coincidence with the amplitudes on certain stations in the centre of the Adria. Figure 169 gives the distribution of amplitudes for the M_2 and K_1 tide along the Adria. The full line represents the observed values, the dashed line the theoretical values if only the co-oscillation tides, the dot-dashed line the theoretical values when the co-oscillating and the independent tides are considered. The latter distribution corresponds a little better to the observed one; however, it is obvious that the co-oscillating tide is the major influence. The theory places the nodal line exactly at the same point as observed. The good agreement in phases and amplitudes leads to the assumption that the frictional forces are negligible, which should be attributed to the great depths of the central and southern sections of the Adria.

The diurnal tides do not show a nodal line; the tide consists in a rise and fall coinciding with the external tide, whereas the amplitude increases slightly towards the inner closed end of the canal, corresponding to the natural period and the reduction of the cross-section.

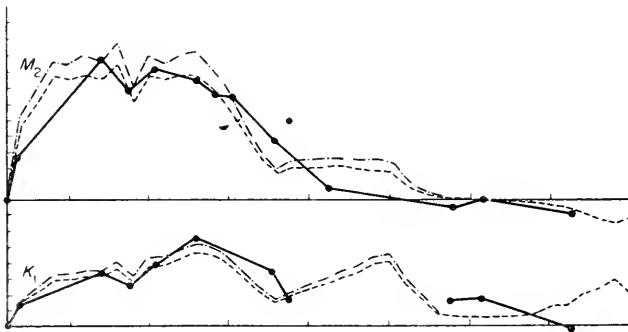


FIG. 170. Transverse oscillations in the Adria of the M_2 and K_1 tides caused by the Coriolis force. For explanation of curves see Fig. 169.

The Coriolis force acts upon the horizontal water displacements of the longitudinal oscillations and causes transverse oscillations. These can be calculated accurately but, if the phase and the amplitude of the theoretical longitudinal wave are known, they can also be derived from the observations. The comparison (Fig. 170) shows an entirely satisfactory agreement. It is remarkable that the transverse oscillations in the southern part of the Adria have a phase opposite to the phase of the transverse oscillation in the central

and northern section. This is explained by the fact that in this southern section, the amplitude of the longitudinal oscillations reaches a maximum towards the open end in the south, and then decreases which requires a change in the sign of the horizontal displacement of these oscillations.

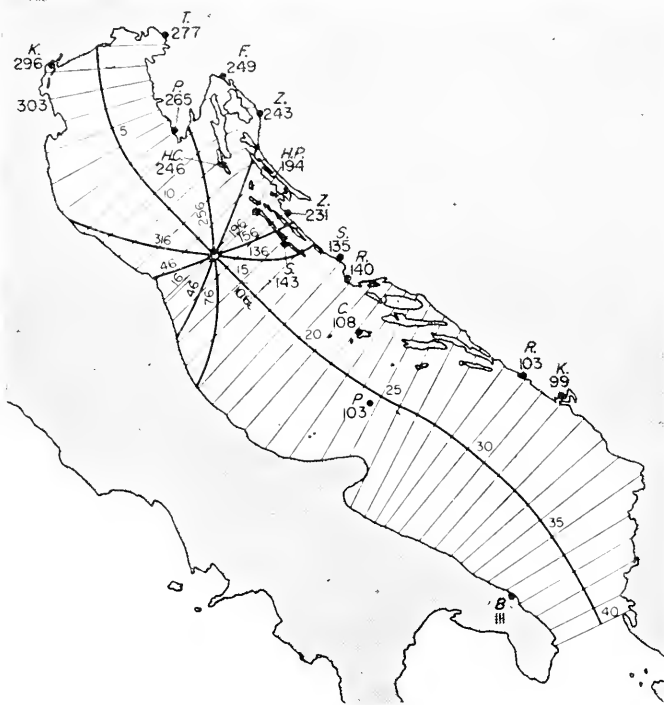


FIG. 171. M_2 tide in the Adria. Numbers at stations are the g values according to Sterneek. Transverse lines correspond to the sections used for the theoretical computation.

The combined longitudinal and transverse oscillations give the tidal picture of the Adria represented in Fig. 171. The agreement with the tidal constants of the coastal localities is excellent for both the semi-diurnal and the diurnal tides.

8. The Tides of the Aegean Sea

This sea, which has a very intricate configuration, can be considered as a bay of the eastern Mediterranean basin and is connected with the latter by means of the two straits west and east of Crete. The areas of the cross-sections are respectively 25 and 55 km², so that the eastern strait is to be considered as the more important opening. The entire bay, on account of its bottom relief is divided in two basins which are fairly well separated from each other: (1) the Cretan basin, which is bordered in the north by the Cyclade Islands and in the south by Crete, and which has a good

communication with the Ionian Sea through the strait between the Peloponnese and Crete; and (2) the actual Aegean basin, which east thereof communicates directly with the eastern Mediterranean basin. It seems that these two basins have different tidal forms.

The Aegean basin seems to co-oscillate with the eastern Mediterranean. The natural period, according to STERNECK (1915, p. 936), with a length of 403 miles (651 km) and a mean depth of 1188 ft (362 m) and with a correction for the shape and the opening (considered as a bay) is 11.42 h. We have for M_2 $\nu = 0.44$. This value is very close to the condition for resonance and, therefore, according to Fig. 141, one can expect a nodal line near the opening. This results also from the computation of the co-oscillating tides, if the Aegean is considered in its entirety. With amplitudes of about $1\frac{1}{2}$ cm at the opening between Rhodes and Crete, we obtain at Salonika 15 cm. But at Rhodes the establishment is 10.6 h (eastern European time, 30° E.), against 4.0 h for Salonika, so that a nodal line somewhere north of Rhodes may be assumed. Table 51 gives for various localities the harmonic constants for M_2 and S_2 . Complete analyses by Tenani (1930) are now available for

Table 51. *Harmonic constants for the Aegean Sea*
(H in cm; $g_{30^\circ E}$ in degrees.)

Tide	Salonika	Volos	Bay of Kephalos	Aiwali	Leros	Cos	Stampalia	Lindos (Rhodes)
M_2 H	14.6	22.9	10.0	10.7	2.8	3.6	3.1	5.9
g	128	100	89	106	2	329	353	307
S_2 H	6.1	10.7	4.9	4.6	1.4	2.3	2.3	3.9
g	130	105	90	110	8	347	349	329

the islands of the Dodecanes. As we can see from the table, the nodal line of the co-oscillating tide may lie somewhere north of the island Leros. The amplitude there is below 3 cm and the ratio determining the character of the tide is nearly 1 against 0.45 farther south which shows that here the semi-diurnal components must decrease. Near Rhodes the phase is 10.7 h, in the north at the Macedonian-Bulgarian coast around 4.4 h (Salonika 4.4 h, Dede Agach 4.3 h) according to STERNECK (1914) so that the required difference in phase of 6.2 h is almost fulfilled. However, this oscillation seems to be confined to the Aegean basin. The Sea of Candia (Crete) has other values for the establishment, which do not fit in here. Gulf of Corinth 5.5 h Khania 2.6 h (with an amplitude of only 2 cm), which is better suited to a co-oscillation with the Ionian Sea (establishment 4.3 h).

9. The Tides of the Black Sea

As far as tides are concerned, the Black Sea should be considered as a completely enclosed water-mass and, consequently, its tides can only be considered

as caused directly by the tide-generating forces. Any influence from the Bosphorus is hardly to be expected. Under these circumstances, its tides will be very small, the more so as its natural period of around 5 h (see p. 200) differs considerably from that of the tidal forces. STERNECK (1912, 1915, 1926) determined for four localities the phase and amplitude for the principal components listed in Table 52. The observations reveal for the semi-diurnal

Table 52. Harmonic constants for the Black Sea
(H in cm; α in degrees).

Place		M_2	S_2	N_2	K_2	K_1	P_1	O_1
Odessa	H	3.5	1.9	0.5	0.8	0.9	0.6	0.4
	α	142	148	136	155	79	109	112
Sevastopol	H	0.4	0.3	0.1	0.1	0.35	0.4	0.1
	α	110	90	126	100	79	23	61
Poti	H	2.9	1.2	0.7	0.5	1.2	0.35	1.0
	α	293	299	280	297	299	291	277

tides the presence of an amphidromy *cum sole* (clockwise). This amphidromy cannot be caused by the rotation of the earth acting on a longitudinal oscillation in the west-east direction. The amplitudes of these tides are very small: in the centre of the west and east coast they are about 9 cm, in the centre of the north coast (Crimea) about 3–2 cm.



FIG. 172. Amphidromy of the semi-diurnal tides in the Black Sea. Establishments of the stations (according to Sterneck).

STERNECK (1922, p. 81) has given a schematic theory of the tides of the Black Sea, in order to explain this remarkable amphidromy. He assumes that the tidal forces act synchronously upon the entire water-mass and he

substitutes for the entire sea a rectangular basin of a length of 600 miles (1000 km), a width of 310 miles (500 km), and a constant depth of 4130 ft (1259 m), so that its natural period becomes exactly equal to that of the Black Sea (see Fig. 172). It would then be easy to reproduce the tides by superposition of the following four oscillations which can be determined theoretically: (1) the east-west oscillation forced by the west-east component of the tidal forces; (2) the north-south oscillation forced by the north-south component of these forces; (3) and (4) north-south and west-east oscillations which are caused by the action of the Coriolis force on the oscillations under (1) and (2) respectively. This theory was first applied to the combined M_2 and S_2 tides at the time of the syzygies and gave at the west and east coast the amplitude 4.6 cm, in the centre of the north and south coast 1.1 cm and a distribution of the co-tidal lines as shown in Fig. 172. The establishments of Constanta, Odessa, Sevastopol, Feodosiya and Poti are also entered in the figure; one can see that both the amplitudes and the establishments fit very well the theoretical picture. Even the approximate establishments and amplitudes of Novorossisk and Tuapse as given by ENDRÖS (1932, p. 442) fit well. The distribution of the tidal forces for such a basin is such that the action in the north-south direction always lags in its phase by one-quarter period to the action in the east-west direction, so that the superposition must produce an amphidromy rotating to the right (*cum sole*). The oscillations caused by the Coriolis force are negligible and are only able to weaken slightly the amphidromy, but not to suppress it.

Later on, Sterneck has replaced his schematic theory by an "exact" theory, in which he took fully into account the morphological conditions for the computation of each separate oscillations. The assumption of synchronous action of the tide-generating forces was dropped and he took into account the small differences in phase of the force in the various sections of the sea. For the computation of the four components of the oscillation he used the method of step-wise integration. He obtained the amplitude and the phase of the tide ($M_2 + S_2$) for the northern and southern points and the centres of the fourteen cross-sections. The result does not deviate considerably from his schematic theory.*

A hydrodynamical theory of the tides of the Black Sea which in a more exact way takes into account the effect of the deflecting force of the rotation of the earth should be based on Taylor's theory of the oscillations in a rotating basin (p. 216). GRACE (1931) has computed accurately for a basin of uniform depth of similar dimensions as the Black Sea, the oscillations forced by the tide-generating forces and compared his results to those of Sterneck. He finds first of all that for a rectangular basin having approximately the dimensions of

* The diurnal K_1 tide, on the contrary, has a counter-clockwise amphidromy; however, its amplitudes are very small (1.6-0.1 cm). The harmonic constants confirm this result.

the Black Sea, both the accurate dynamical solution and the one found by Sterneck differ very little from the solution according to the equilibrium theory, where the Coriolis force is neglected, so that the deviations therefrom should be considered as small corrections. Sterneck's solution, however, shows in certain parts greater deviations than Grace's solution. Anyway, the good agreement with the observations is to be attributed exclusively to the circumstance that the equilibrium theory is by far preponderant. In so far the "exact" computations of Sterneck are useless. This is also shown clearly by the compilation given by Grace in Table 53. The differences between

Table 53. Comparison between observed and computed values of the tides of the Black Sea

Place	Observed		Computed from equilibrium theory		Vector difference		Computed from Sterneck's theory		Vector difference	
	H(cm)	Phase	H(cm)	Phase	H(cm)	Phase	H(cm)	Phase	H(cm)	Phase
Constanza	3.9	96°	3.6	100°	0.4	57°	4.5	102°	0.7	315°
Odessa	5.4	150°	2.9	135°	2.7	166°	3.0	126°	2.9	175°
Sevastopol	0.7	102°	0.9	152°	0.7	22°	1.1	141°	0.7	359°
Feodosia	1.1	237°	1.4	218°	0.5	353°	1.1	216°	0.4	316°
Poti	4.1	279°	5.1	277°	1.0	89°	5.6	270°	1.7	68°

the results from the simple equilibrium theory and the observations (after Sterneck) are smaller than those between the former and the values computed by Sterneck. In this case the rotation of the earth need not be considered. The tides of the Black Sea, owing to its great depth, are nothing else than the forced oscillations of these water-masses by the tidal forces.

10. The Tides of the Red Sea

The shape of the Red Sea makes it especially fit for a test of the dynamical theories of the tides. It is, namely, a simple longstretched basin with steep walls in the direction S. 30° E., which communicates at its southern end through the narrow strait of Bab el Mandeb (smallest cross-section somewhat north of the Island Perim is only 1.7 km²) with the Gulf of Aden and the Indian Ocean. It ends in the north into two narrow canals, namely, the Gulf of Suez and the Gulf of Agaba. The Gulf of Suez is shallow and interspersed with small isles and cliffs (mean depth 118 ft, 36 m), whereas the Gulf of Agaba is deep (average depth 2132 ft, 650 m). Correspondingly, the natural period of the former is 6.7 h, that of the latter 0.9 h. For this reason alone there must be marked differences between the tides in these northern extensions of the Red Sea among themselves and those in the main basin.

HARRIS (1904, Part IV, A, p. 649 and Part IV, B, p. 363) was the first to

attempt an explanation of the tides of the Red Sea; he regarded them as the superposition of a standing wave produced in this sea by the tide-generating forces and a progressive wave penetrating through the Strait of Bab el Mandeb. BLONDEL (1912), following a suggestion of POINCARÉ (1910), has used a special method of the calculus of variations for the computation of the tides of this sea; however, due to an error, he did not obtain a good agreement between the theory and the observations. This mistake was corrected by CHANDON (1930), with the result that the agreement was improved. DEFANT (1919, p. 110) has given a theoretical discussion of the spring tides by applying the step-wise integration of the equations of motion. The tides were considered as the superposition of a tide co-oscillating with the Gulf of Aden and an independent tide. The observations available at that time consisted only of the establishments and mean heights of the spring tides $2(M_2+S_2)$ given by the *Admiralty Tides Tables* which were not very accurate. The agreement was quite good and it showed that the tidal motion is due in equal parts to the independent tide and to the co-oscillating tide.

One result of the cruise of the "Ammiraglio Magnaghi" was the harmonic constants of eleven coastal localities in the Gulf of Suez and in the Red Sea computed by VERCELLI (1925). He also analysed a 15 days' anchor station in the Strait of Bab el Mandeb and got the harmonic constants of the tidal current at the open end in front of the Gulf of Aden. Table 54 gives a compilation of these values, on which are based all further theoretical investigations of the tides of this sea.

From the distribution of the amplitudes and phases along the longitudinal axis of the sea it can be concluded that the semi-diurnal tides have three nodal lines: one south of Assab, a second one near Port Sudan and a third one in the Gulf of Suez between Tor and Ashrafi Island. Generally the tide has the nature of a standing wave with a rapid transition of the phase in the vicinity of the nodal lines. The Gulf of Agaba oscillates, according to the rough values of the tide tables, with the tides of the main basin without a nodal line ($\nu < 0.5$). The diurnal tides, on the contrary, show only one nodal line, namely, for K_1 between Kamaran Island and Massaua, for O_1 somewhat more south of the former locality; here also it is essentially a standing wave.

The character of the tides is given by the ratio $(K_1+O_1)/(M_2+S_2)$ (see Table 54). In the areas outside the nodal lines it is definitely semi-diurnal; however, the nodal lines of the semi-diurnal tide stand out as areas with an extreme diurnal type; this is especially the case in the Red Sea. It is also remarkable that the elliptic tide N_2 is remarkably great in the entire sea, which also applies to the Gulf of Aden.

The tidal currents in the Strait of Bab el Mandeb are very strongly developed and, essentially, of the same nature over the entire cross-section of the strait. The type of the current can be designated (see p. 307), as "mixed,

Table 54. Harmonic constants of the Red Sea
(H in cm; ε in degrees).

Place		M_2	S_2	N_2	K_2	K_1	P_1	O_1	$\frac{K_1+O_1}{M_2+S_2}$
Suez	H	56	14	18	—	5	—	1	0.09
	ε	342°	7	313	—	190	—	216	—
Zafarana	H	42	13	14	3.5	—	—	1	—
	ε	345°	4	315	4	—	—	232	—
Ras Gharib	H	18	7	6	2	3	1	2	0.19
	ε	340°	8	310	8	—	—	190	—
Tor	H	8	2	2.5	0.5	4	1	1.5	0.55
	ε	271°	296	242	296	197	197	192	—
Ashrafi	H	13	4	4	1	2	1	2	0.22
	ε	184°	212	155	212	201	201	187	—
Shadwan Islands	H	25	4	8	1	2	1	1	0.16
	ε	185°	212	155	212	202	202	212	—
Quiseir	H	22	5.5	7	1.5	2	1	2	0.15
	ε	180°	205	150	205	192	192	226	—
Jidda	H	7	1	2	0	4	1	2	0.69
	ε	202°	236	182	236	226	226	183	—
Port Sudan	H	1	1	0	0	2	1	2	2.31
	ε	278°	330	248	330	207	207	215	—
Massaua	H	34.5	12	10	3	2	1	2	0.09
	ε	42°	51	14	51	206	206	213	—
Kamaran Islands	H	33	9	9	2	2	0.5	1	0.06
	ε	28°	56	8	56	76	76	182	—
Assab	H	8	3	2	1	18	6	6	2.25
	ε	358°	257	352	257	18	18	28	—
Perim	H	36.5	17	—	—	—	—	—	—
	ε	226°	243	—	—	—	—	—	—
Djibouti	H	35	23	—	—	41	13	20	0.80
	ε	220°	239	—	—	30	30	35	—
Aden	H	47.8	20.9	13.4	6.0	39.8	12.0	20.0	0.87
	ε	226°	247	221	239	35	31	37	—

Current in the Strait of Bab-el Mandeb
(12°42'30"N., 43°17'40"E.)

Positive to the North cm/sec	H	38.4	11.0	11.0	3.0	38.2	12.7	21.9	1.22
	$g_{45} E.$	308°	333	304	333	128	128	144	—

preponderantly semi-diurnal”, but it comes already close to the diurnal type.* The tidal current, with rapidly decreasing amplitude and gradual shifting in the phase maintains the same form till about 16° N.; south of the Dahalach Archipelago there seems to be a “nodal line”.

DEFANT (1926, p. 185) has made a new computation of the tides of the Red Sea for M_2 and K_1 which can be expected theoretically on the basis of the more accurate data obtained from the harmonic analysis. The agreement with the observations was again very good. The difference with the first computation was, however, that now the co-oscillating tides dominated, whereas the tide generating forces should only cause slight modifications. STERNECK (1927, p. 129) has been induced by this contradiction with the first attempt to make a mathematical segregation between the co-oscillating tide and the independent tide according to his “Zerlegungs” method. He concluded that, for the larger part of the Red Sea, the ratio of the two tides is for M_2 1:3, for S_2 1:4. In the Gulf of Suez this ratio becomes considerably larger. For K_1 the amplitude of the two tides is approximately equal.

As we will explain later on (see p. 508) Proudman has expressed the thought that the co-oscillation with the water-masses of the Gulf of Aden and the independent tides, the tides of the Red Sea are influenced by the tides of the solid earth. He has shown how the tides of the solid earth influence those

Table 55. Comparison between observed and theoretical values of M_2 tide in Red Sea

Place	H (cm)	γ°	Corrected values		Theoretical values		Computed H_1/H_2	Observed H_1/H_2
			H (cm)	γ°	H (cm)	γ°		
Suez	56.1	277	56.1	277°	48.3	300°	0.28	0.79
Zafarana	42.4	280	42.5	279	37.8	300	0.28	0.73
Ras Gharib	18.2	274	18.8	268	16.4	301	0.27	1.07
Tor	7.8	204	4.1	208	6.2	118	0.32	-3.45
Ashrafi	13.4	117	13.4	119	23.2	120	0.28	0.30
Shadwan Island	25.1	117	25.1	117	25.4	120	0.28	0.34
Quiseir	21.9	112	22.0	110	24.8	119	0.30	0.48
Jidda	7.4	124	7.9	139	5.6	110	0.48	-0.05
Port Sudan	0.9	204	1.6	30	1.0	3	-1.11	-3.97
Massaua	33.4	327	34.8	330	25.5	299	0.30	-0.25
Kamaran Island	32.8	303	32.5	303	30.0	297	0.34	0.23
Assab	7.8	273	9.8	259	8.5	201	-2.32	1.46
Perim	36.5	139	36.4	138	35.9	138	-0.03	-0.03

* The measurements made by Gedge (1898, see vol. 1/2) according to which there are only diurnal tidal currents in the strait, are based on too short a series of measurements, where, at the time of the equinoxes and quadratures, the semi-diurnal variation becomes of less importance.

of small bodies of water like canals, and he has also given methods to compute numerically this influence. We will discuss this problem of the ocean and earth tides later on more thoroughly (p. 506). Here we will mention only the results obtained by GRACE (1930, p. 274) who was the first to apply Proudman methods to the M_2 tide of the Red Sea. For this purpose, it is necessary to have tidal data as accurate as possible along the central axis of the sea, for which reason a reduction of the harmonic constants of the coastal localities to the centre line of the Red Sea should be made. Under certain conditions, such a reduction is feasible and Grace obtained for certain points on the centre line the constants of the M_2 tide listed in Table 55 (see "corrected" values). With these values one obtains, by numerical integration of the hydrodynamical equations, provided appropriate factors are selected to satisfy the boundary conditions, the theoretical M_2 tide. Then, from the factors one obtains also the proportionality factor of the motion of the earth to the tide generating force (see p. 508). The comparison between the theoretical tides and the observations shows that in the Gulf of Suez the agreement is not good, perhaps for the reason that transverse motions and friction are more disturbing here. In the Red

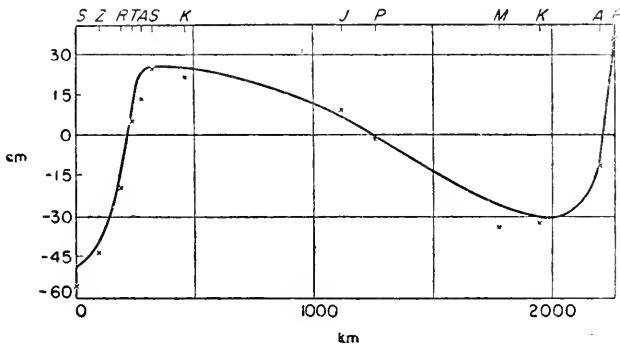


FIG. 173. Distribution of amplitude along the Gulf of Suez and the Red Sea. —, computed by Grace; x: observed values, reduced to the centre axis.

Sea the values for Massaua, which are locally disturbed, do not agree; otherwise, the agreement is in general somewhat better than by Defant's method. In Fig. 173 the theoretical distribution of the amplitudes of the longitudinal oscillation is represented by the full-drawn curve, whereas the observed values are indicated by dots.

For determining the ratio of the co-oscillating tide to the independent tide, the theoretical and the observed values of Table 55 can be divided into two parts, one of which will have the phase of the tide-generating potential on the central axis of the sea in its principal direction (Phase: 44° or 224° from Greenwich), the other one the phase of M_2 in Aden 136° from Greenwich. We, therefore, put $H\cos(\sigma t - \gamma) = H_1\cos(\sigma t - 44^\circ) + H_2\cos(\sigma t - 136)$ in which

$$H_1 = H \frac{\sin(136^\circ - \gamma)}{\sin 88^\circ}$$

is the amplitude of the independent tide and

$$H_2 = H \frac{\sin(\gamma - 44^\circ)}{\sin 88^\circ},$$

the amplitude of the co-oscillating tide. The two components are graphically shown in Fig. 174; the full-drawn curve gives the co-oscillating tide, the dashed curve indicates the independent tide. The observed values are entered for

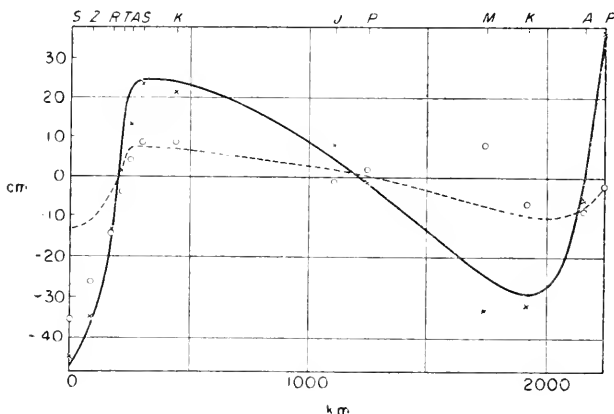


FIG. 174. Distribution of amplitude along the Gulf of Suez and the Red Sea for the co-oscillating tide (—) and for the independent tide (----); x, observed values of the co-oscillating tide; : observed values of the independent tide.

comparison. The agreement between the observations and the theory is still not very good in the Gulf of Suez; it is a great deal better in the Red Sea, with the exception of Massaua and in the vicinity of the nodal lines. Table 55 gives in the last column the ratio H_1/H_2 , both for the theoretical and for the observed values. For the largest part of the Red Sea this ratio is about 3:10, in agreement with the findings of Sterneck.*

These recent papers have proven that the M_2 tides of the Red Sea are the superposition of an independent tide and a tide co-oscillating with the Gulf of Aden. However, the amplitude and phase can only be fully explained when the tides of the solid earth are taken into consideration: their action is of about the same order of magnitude as that of the tide-generating potential. For their determination very accurate tidal observations are required, more accurate than those which are presently available. The frictional influences

* The deviations in Defant must be mainly attributed to the fact that, when determining the independent tide, he did not take into account a canal section in the south about 190 miles long, north of Perim, which omission is not justified.

should not be neglected, especially in the Gulf of Suez, which influences react on the tides in the Red Sea. This can cause a shift in the phases which, although small, should not be ignored for such computation as pointed out by DEFANT (1928, p. 274).

11. The Tides of the Persian Gulf

In considering the tides in this area, we should consider the Persian Gulf, the Strait of Hormuz and the Gulf of Oman as a unity. Their orographical conditions are quite intricate, because the longitudinal axis of the area of

Table 56. Tidal data at spring tide in the Persian Gulf and Narrows of Hormuz and in the Gulf of Oman

Gulf of Oman	Range (m)	Establishment ref. to 56°15'E. (h)	Persian Gulf	Range (m)	Establishment ref. to 56°15'E. (h)	
Ras-al Hadd	2.8	9.0	East coast	Lingeh	—	0.0
Chahbar	2.6	9.2		Qais Island	2.3	0.6
Masqat	2.1	9.1		Tahiri	—	5.3
Jask	2.7	9.5		Bushire	1.8	8.1
				Fao Fort	3.0	0.0
Narrows of Hormuz			West coast	Kuwait	2.7	0.8
Chor Kawi	3.0	9.5		Bahreim	1.7-2.0	6.4
Djesiret Larek	(3.6)	10.3		El Bida (Doha)	1.8	8.8
Qishm	3.7	10.9		Abu Thabi	2.1	0.1
				Ras al Khaima	(2.1)	11.7

oscillation must be considered as a canal with two nicks in it. This circumstance, in fact has hardly any effect on the co-oscillating tides, but all the more on the independent tides, where the phase of the tide-generating force depends upon the longitudinal direction of the basin. There is still another reason for which the formation of the tide in the Persian Gulf will differ from that in the Red Sea, which has a more simple configuration. The Persian Gulf, at its entrance, has a cross-section of 4.0 km² in the Strait of Hormuz, whereas the Red Sea has as its entrance (Bab el Mandeb) a cross-section of 1.7 km². But the volume of water of the Persian Gulf is only 5910 km³, whereas in the Red Sea this volume is 223,810 km³. Mean depth of the Gulf is 131 ft (40 m), against 1571 ft (476 m) in the Red Sea. Therefore, the large incoming tidal energy will cause considerable tide ranges.

For the entire area we have only the harmonic constants of two harbours (Masqat in the Gulf of Oman and Bushire inside the Persian Gulf). Then for a relatively large number of their localities we know the vulgar establishment and the ranges at spring tide from the tide tables. They permit only

a rough picture of the semi-diurnal tide. For a series of localities these values are compiled in Table 56; Table 57 gives the harmonic constants of the two afore-mentioned localities, together with those of Karachi, on the Indian Ocean. The tidal picture resulting from these observations is briefly the following (Fig. 175).

Table 57. Harmonic constants

		M_2	S_2	N_2	K_1	O_1	$\frac{K_1 + O_1}{M_2 + S_2}$
Karachi	$H(\text{cm})$	77	29	18	39	20	0.56
	$\alpha(^{\circ})$	294 $^{\circ}$	322	277	46	47	—
Masqat	$H(\text{cm})$	63	24	16	39	20	0.68
	$\alpha(^{\circ})$	276 $^{\circ}$	306	258	39	41	—
Bushire	$H(\text{cm})$	31	12	7	29	20	1.14
	$\alpha(^{\circ})$	210 $^{\circ}$	261	183	280	244	—

High water occurs simultaneously over the entire area of the Gulf of Oman, whereas the range increases slightly inside the Gulf. Consequently, the water surface rises and falls almost simultaneously up till the opening off the Strait of Hormuz. In this Strait there is then a regular increase of the establishment from 9.5 h till 0.0 h at the southern end of the Persian Gulf; the tidal range increasing in the middle of the Strait up till 12 ft (3.7 m), then decreasing again to 7.2 ft (2.2 m). The establishment in the Persian Gulf itself can be explained by assuming two amphidromies rotating to the left, one in the southern section, the other one in the northern section of the Gulf. The distribution of the ranges is then also in agreement.

Beside the important semi-diurnal tides, the diurnal tides must also be well developed in the Persian Gulf, according to the harmonic constants of Bushire.

The explanation given by KRÜMMEL (1911, vol. II, p. 384) of the tides of this adjacent sea is entirely based on the previous conception of the explanation of the tides by progressive waves. The tide wave penetrates through the Strait of Hormuz and, clinging to the land on the right side, it travels counter-clockwise around the entire gulf. This is the only way to explain, in agreement with the water depths, the "otherwise incomprehensible establishments". The tidal ranges do fit this picture less well. DEFANT (1919) has given a hydrodynamical theory which explains from the orographical configuration of the sea area the two amphidromies as the main feature within the Gulf, and also the remarkable distribution of the establishment and the range in the Strait of Hormuz.

The natural period of the Persian Gulf, including the Strait of Hormuz,

is 22.6 h according to the Japanese method, 21.7 h according to the Chrystal method. The ratio r for the semi-diurnal tides is, therefore, about 2.3, which for both tidal components causes the development of two nodal lines. The step-wise computation gives these two nodal lines for the co-oscillating tide, the first off Qais, the second a little south of Bushire. In the Gulf of Oman, the tidal range is about 6.6 ft (200 cm), it increases in the Strait of Hormuz to 8.2 ft (250 cm), and at the antinodes of the stand-

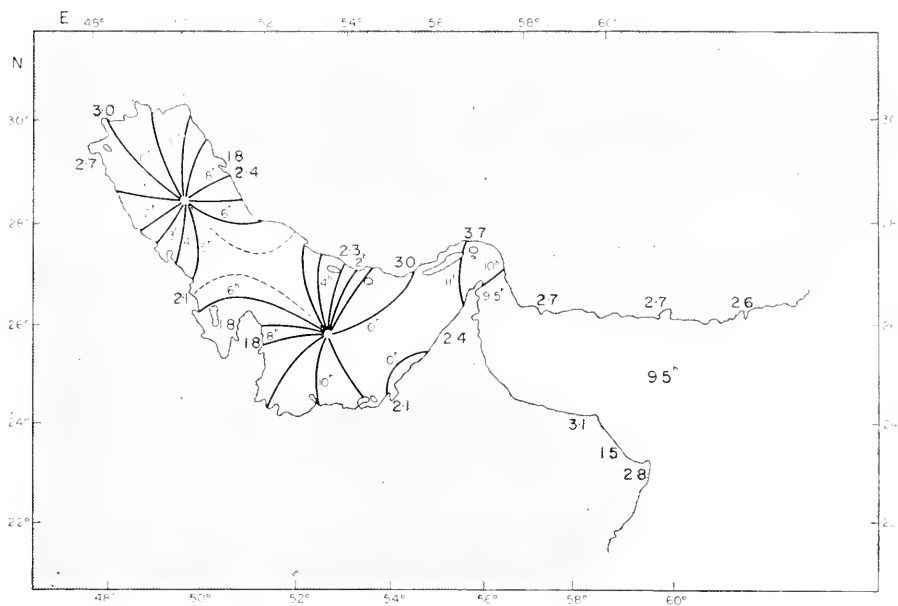


FIG. 175. Phases (lunar hours) and amplitude (cm) of the spring tides in the Persian Gulf derived from observations.

ing wave it attains values of about 5.6 ft (170 cm) at the southern end and 8.2 ft (250 cm), at the northern end of the gulf.

The computation of the independent tide is somewhat complicated, due to the bend of the longitudinal axis of the area of oscillation. According to Fig. 176 the entire area can be schematized in three canal sections: (I). The actual Persian Gulf with its main direction NW.-SE. (II). The south-eastern shallow section of the Gulf, together with the Strait of Hormuz, the main direction being SW.-NE. (III). The Gulf of Oman, whose longitudinal direction is essentially similar to that of the first section. The tide generating forces for $(M_2 + S_2)$ can then be computed for each of the different sections and we obtain:

$$\text{section I} \quad K_1 = 7.875 \times 10^{-7} \cos \frac{2\pi}{12} (t - 10 \text{ h});$$

$$\begin{aligned} \text{section II} \quad K_{II} &= 10.103 \times 10^{-7} \cos \frac{2\pi}{12}(t - 8.6\text{h}) \\ &= K_1 + 6.82 \times 10^{-7} \cos \frac{2\pi}{12}(t - 7\text{h}); \end{aligned}$$

$$\begin{aligned} \text{section III} \quad K_{III} &= 7.875 \times 10^{-7} \cos \frac{2\pi}{12}(t - 10\text{h}) \\ &= K_1 + 6.82 \times 10^{-7} \cos \frac{2\pi}{12}(t - 7\text{h}) - 6.82 \times 10^{-7} \cos \frac{2\pi}{12}(t - 7\text{h}). \end{aligned}$$

For the component of the independent tide “of the first kind” the same force K_1 acts along all three sections; it can be computed numerically according to the methods previously described (p. 339). For the first part of the component of the independent tide “of the second kind”, the force

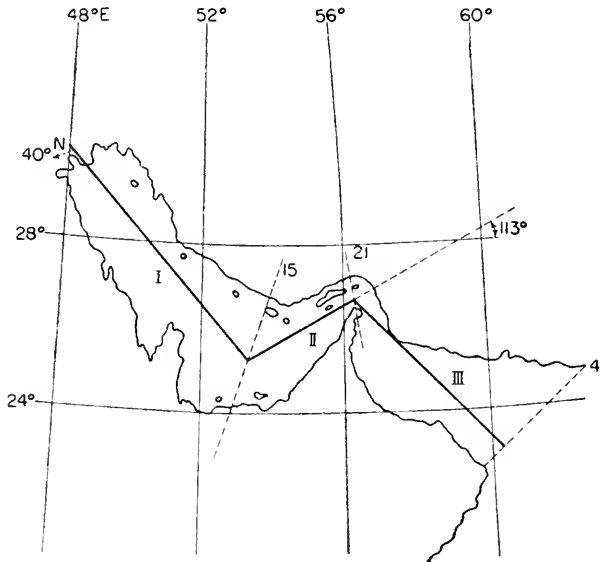


FIG. 176. Division of the oscillating areas of the Persian Gulf in three canals.

$6.82 \times 10^{-7} \cos(2\pi/12)(t - 7\text{h})$ acts in the canal sections II and III; it has a nodal line at the opening into the free ocean and its form must be such that the section I can co-oscillate freely. For the second part of the component “of the second kind” of the independent tide, the force $-6.82 \times 10^{-7} \cos(2\pi/12)(t - 7\text{h})$ only acts in the canal section III; it has again the amplitude zero at the opening into the Indian Ocean and the canal sections I and II must co-oscillate with it at the end.

All these components can be computed by a numerical integration. It appears that the component of the independent tide of the first kind, as well as the first part of that of the second kind have such small amplitudes that their contribution to the tides of the Persian Gulf is insignificant. The second

part of the component of the second kind, on the contrary, has a substantial range, i.e. the water-masses co-oscillate vigorously with the independent tide in the Gulf of Oman. The nodal lines of this pseudo co-oscillating tide coincide with those of the real co-oscillating tide; however both standing waves have a phase difference of $3\frac{1}{2}$ h.

The superposition of all these components gives the tides of the entire area of oscillation. To this has to be added the effect of the deflecting force of the rotation of the earth, which transforms the nodal lines into amphidromies *contra solem*; these, however, are very well developed, because large amplitudes over small depths command great velocities in the horizontal displacements. The theoretical picture resulting from the superposition of the longitudinal and transverse oscillations, does not deviate very much from that of Fig. 175 neither as to phases nor as to ranges, so that the theory in question can be considered to give a satisfactory explanation of the tides of this adjacent sea. A more detailed investigation must be postponed until such time when we have a sufficient number of harmonic constants of coastal localities. It should be mentioned that frictional influences have not been taken into account by this theory. In view of the small depths this omission might perhaps not be justified.

As the natural period of the Gulf lies close to 24 h, it is to be expected that the diurnal tides are well developed. For these diurnal tides ν is about 0.95, and the co-oscillating tide of the diurnal tides will have a nodal line somewhere in the centre of the Persian Gulf and will show in the antinodes amplitudes which might be quite large. This explains that, in the Persian Gulf, and particularly in the vicinity of the nodal lines of semi-diurnal tides, the tides become almost of the diurnal type. In this case more and newer values of the harmonic constants for adequately situated localities will give a better insight.

12. The Tides of the East Indian Archipelago

The only description of the tidal phenomena in this entangled system of straits in the East Indian Archipelago has been given by VAN DER STOK (1897, 1910, 1911, p. 354). Thanks to him, the harmonic constants of a very great number of coastal localities in the Indonesian Archipelago are known, so that there is a good basis for explaining the tidal phenomena. However, it has hitherto not been attempted to make an accurate hydrodynamical investigation based on modern methods. A description of the tidal picture has been given by KRÜMMEL (1911, vol. II, p. 384), in which he makes reference to charts of the co-tidal lines of the M_2 and K_1 tide designed by him. He bases himself entirely on the viewpoint that the tides penetrate as progressive waves from the open ocean into the various basins, and that they travel according to the depths and that by mutual interferences they create the actual tidal picture. We wish to direct the attention to the more recent charts of Van

der Stok, in which he has only drawn short fragments of the co-tidal lines protruding from the coast into the ocean, without trying (except in very few cases) to connect these co-tidal lines from coast to coast. He too is firmly convinced that progressive waves alone are responsible for the picture of the phenomena. DIETRICH (1944, p. 69) has recently given a presentation of the

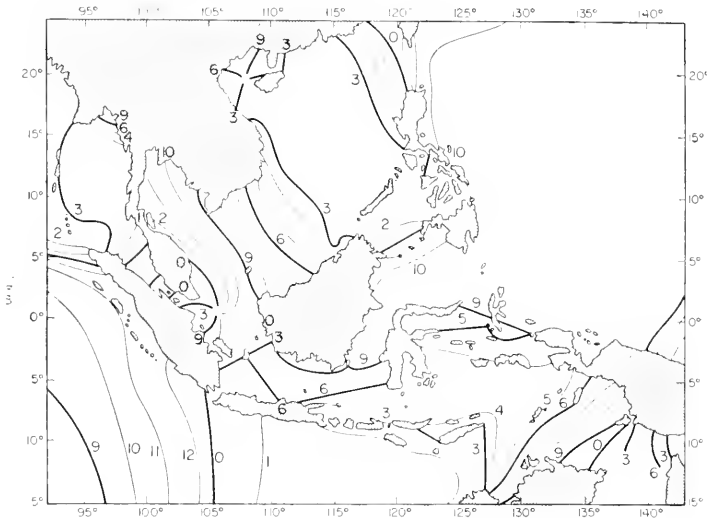


FIG. 177. Co-tidal lines of the M_2 tide in the Indonesian Archipelago (referred to the upper culmination of the moon in Greenwich), according to Dietrich.

co-tidal lines for the M_2 and K_1 tide which is part of his presentation of the tides of the oceans without, however, accompanying it by any further discussion. His two charts (the scale of which has been slightly enlarged) are reproduced in the Figs. 177 and 178, but we cannot agree on all points with his drawing of the co-tidal lines, nor with his interpretation of the observed values. Table 58 gives a summary of the most important harmonic constants of this area.

The semi-diurnal M_2 tide penetrates from all sides into the Basins of Indonesia; there seem, however, to be three points which are particularly important for the development of the tides. (a) The wide strait to the north between Formosa and Luzon, leading into the South China Sea. (b) The areas between Mindanao and Halmahera, leading to the Celebes and Molukkes Sea. (c) In the south, the straits between Timor and the Aroe Islands, connecting the Timor and Arafura Sea with the Banda Sea. The other entrances between the group of Islands in the south and through the Strait of Malacca seem to be only of minor importance.

These three large straits who function as entrances are connected with each other by three complicated "canals".

Table 58. Harmonic constants in the Indonesian Archipelago

Place	ϕ°	λ	Amplitude (cm)						Phase α (degrees)					$O_1 + K_1$
			M_2	S_2	N_2	K_1	O_1	M_2	S_2	N_2	K_1	O_1	$M_2 + S_2$	
Singapore	1-3 N.	103-9 E.	66	27	11	24	24	300	348	272	100	53	0-52	
Trandjon Buton (Lingga)	0-2 S.	104-6 E.	20	12	4	61	48	35	136	2	152	74	3-42	
Trandjon Kalean	2-0 S.	105-1 E.	25	12	5	95	55	186	216	166	159	93	4-06	
Poeloe Langkoeas	2-5 S.	107-6 E.	2	3	—	64	38	237	16	—	141	86	20-40	
Thousand Is.	5-6 S.	106-3 E.	1	6	1	28	7	266	11	314	165	138	5-00	
Edam Is.	6-0 S.	106-8 E.	5	6	2	27	8	294	308	322	141	129	3-18	
Java Sea	Boompjes Is.	5-9 S.	108-4 E.	11	6	3	14	7	324	218	285	102	118	1-24
Karimon Djawa Is.	5-9 S.	110-4 E.	2	5	1	23	4	246	344	42	357	262	3-87	
Bawean Is.	5-9 S.	112-7 E.	4	4	3	43	25	72	16	116	326	300	8-50	
Surabaya	7-2 S.	112-6 E.	44	26	9	47	27	351	355	337	318	284	4-06	
Flores Sea	Boelelong	8-1 S.	115-1 E.	29	15	—	31	21	334	348	—	311	267	1-18
Bima	8-4 S.	118-7 E.	34	10	4	30	10	9	52	350	302	263	0-91	
Saleier	6-1 S.	120-5 E.	39	10	9	32	21	4	67	339	300	281	1-08	
Banda Sea	Banda	4-5 S.	129-9 E.	57	22	11	29	18	36	103	8	314	298	0-60
Ambon	3-7 S.	128-2 E.	47	17	10	29	21	36	95	4	316	314	0-78	
Fak-fak	3-0 S.	132-3 E.	40	22	8	19	14	36	124	32	348	290	0-53	
Ternate	0-8 N.	127-4 E.	27	22	4	14	10	169	197	149	261	249	0-49	
Gorontalo	0-5 N.	123-1 E.	14	20	2	25	10	115	173	85	284	227	1-03	
Kema	1-4 N.	125-1 E.	21	27	2	17	11	161	190	186	260	252	0-58	
Makassar Str.	Tontoli	1-0 N.	120-9 E.	42	35	6	14	14	161	199	131	285	227	0-36
Tandjong Seilor	2-8 N.	117-4 E.	32	19	6	10	11	235	306	223	339	284	0-41	
Aroe Bank	2-2 S.	116-6 E.	17	17	1	7	6	147	199	126	291	253	0-38	
Makassar	5-1 S.	119-4 E.	8	11	3	28	17	70	194	347	300	278	2-37	
Bandjermasin	3-3 S.	114-6 E.	31	5	8	59	32	187	125	157	354	300	2-53	
Kampung Koemai	2-8 S.	112-5 E.	24	6	—	41	21	180	53	—	318	276	2-10	
Tambelan	1-0 N.	107-6 E.	5	9	—	23	23	155	114	—	82	35	3-29	
Borneo	Pemangkat	1-2 N.	109-0 E.	26	4	7	14	16	111	177	86	54	7	1-00
Laoet (N. Natoena)	4-7 N.	107-9 E.	9	4	—	35	19	73	45	—	323	289	4-16	
Labuan	5-2 N.	115-2 E.	27	12	6	41	33	321	359	293	315	266	1-90	
Kudat	6-9 N.	116-8 E.	24	11	4	36	30	305	342	290	321	267	1-89	
Sandakan	5-9 N.	118-1 E.	37	15	6	36	27	309	345	292	323	281	1-22	
Cebu	—	—	42	23	7	30	28	334	22	324	330	294	0-89	
Halsey (Calamian)	11-8 N.	119-9 E.	24	10	7	30	30	311	4	289	318	276	1-76	
Manila	—	—	17	5	3	32	26	326	356	310	321	288	2-64	
Bolinao	—	—	10	4	—	26	21	278	313	—	313	276	3-36	
Toko (Formosa)	—	—	18	7	—	18	16	243	233	—	294	256	2-27	
Gyo-oto (Pescad.)	—	—	90	23	—	24	23	332	20	—	271	245	0-42	
Amoy	—	—	187	41	24	27	20	1	57	332	274	252	0-21	
Hong Kong	—	—	44	17	8	36	26	266	292	255	297	248	1-02	
Haiphong	—	—	4	4	—	69	70	83	121	—	81	32	17-38	
St. Jacques	—	—	80	32	—	70	44	54	95	—	309	274	1-02	

(1) *a* with *c* through the South China Sea, the area between Sumatra and Western Borneo, the Java—Flores Sea and the Banda Sea.

(2) *b* and *c* through the Celebes Sea, the Strait Makassar, the Flores Sea to the Banda Sea.

(3) *b* and *c* also through the Molukkes Sea direct to the Banda Sea.

The water-masses of these three canals with their intricate widths and depths co-oscillate, on one hand, with the tides of the open ocean at their openings *a*, *b* and *c*. On the other hand, certain basins with great depths

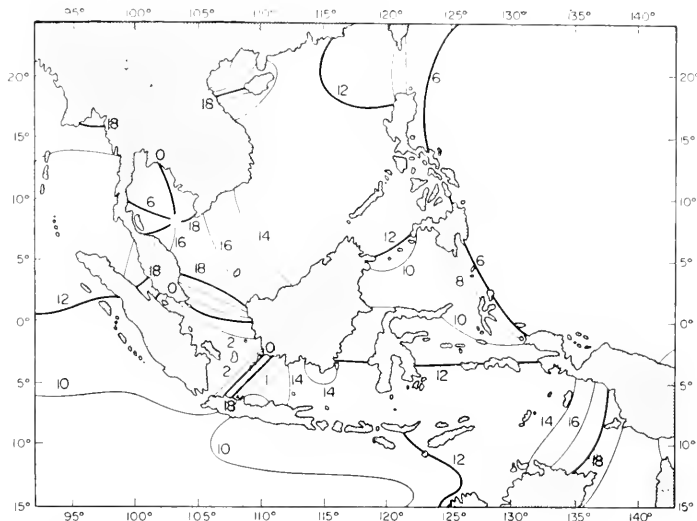


FIG. 178. Co-tidal lines of the K_1 tide in the Indonesian Archipelago (referred to Greenwich) (according to Dietrich).

can have large independent tides. An accurate computation of these tidal components is not yet available but, nevertheless, we are able to describe roughly the aspect of the tidal picture of the semi-diurnal and diurnal tides.

Canal 1 has a natural period of about 33 h; for the semi-diurnal tides ν is about 2.7, and it is to be expected that each co-oscillating tide will have three nodal lines. They can be supposed to lie: (1) in the northern section of the South China Sea; (2) near the Nautoena islands at the southern end of this adjacent sea; and (3) in the Java Sea. Inasmuch as the co-oscillation at the two openings occurs almost exactly with opposite phases (in the north $g = 130^\circ$, in the south $g = 340^\circ$, referred to the meridian of Batavia), there will be no strong shifting of the standing waves, so that the nodal lines should be well developed. In fact, we find in the co-tidal lines of Fig. 177 near the northern outlet of the South China Sea, on one hand, and between southern Indo China and north-west of Borneo, on the other hand, a great crowding of the co-tidal lines, which can be interpreted as a pseudo-nodal line accompanied by a decrease in amplitude; in between there is a large area with

a phase of about 310° . There is a second area with a nearly uniform phase of about 150° between Western Borneo and Sumatra. At the end of the Strait of Malacca there might be a small amphidromy rotating to the left, with its center north of the Lingga Islands. It would seem that its area on the Dietrich chart has been assumed too large. It is probably caused by the interference of the tide wave progressing south-eastward through the Strait of Malacca.

Along the main canal, the phases and amplitudes show a pronounced, outstretched amphidromy rotating to the left in the Java Sea with its center near Bawean Island. From this centre to Southern Celebes (Macassar) many co-tidal lines are crowded together in a small space, so that they form almost a nodal line with a change of phase from 320° to 140° . The amphidromy is particularly well indicated by the decrease of the amplitudes to 5 cm and below, which in this area results in an almost diurnal tide. The canal section of the Flores and Banda Sea has nearly uniform phases between 330° and 350° .

Canal section 2 has again the phases at its opening of about 130° in the north and 340° in the south, consequently again almost opposite phases, so that with a natural period of about 12 h and $\nu = 1$, one nodal line should occur in the middle, i.e. at the southern entrance into Strait Macassar. This is exactly the point where there is a nodal line extending, from the amphidromy in the Java Sea to Southern Celebes. In accordance with this interpretation, the observations made in the Celebes Sea and in the entire Strait of Macassar show phases near 130° .

Canal section 3 also has the same phases at its openings. With an approximate natural period of 7.1 h and $\nu =$ about 0.6, one nodal line can be expected and, in fact, a dense crowding of the co-tidal lines is noticeable near the group of islands extending from Celebes to Halmahera.

On going over these rough outlines of a theory of the M_2 tide, in which the independent tides have been neglected, one must admit that the characteristic features of the theoretical tidal picture are in good agreement with the observed facts. But only an accurate computation by the theory can show how much the independent tides can change the picture. The influence of the deflecting force of the rotation of the earth is probably small, inasmuch as we have to deal with regions near the Equator.

In the case of the diurnal tides, which appear to be very well developed in this entire area, conditions are more complicated, although here the picture of the co-tidal lines is simpler. The direct influence of the tide-generating forces might be far more apparent with these partial tides, as the ν values for the two first canals come very close to the corresponding resonance values. Thus, the superposition of the two components creates a picture of the co-tidal lines which is not easy to disentangle. In the South China Sea the phase over a large area (referred to Batavia) is 310° , then the co-tidal lines crowd in the south-western section, and in the western section of the Java Sea there

appears to exist an amphidromy, and towards the Banda Sea the phase remains almost constant at 290° .

In the second and third canal, the distribution of the co-tidal lines look as if the main influence comes from the Pacific Ocean, whereas the Banda Sea would only co-oscillate with the Indian Ocean. In neither of the two cases is there any indication of a nodal line which, as a matter of fact, could not be expected in view of the value of r .

The high values of the ratio indicating the character of the tides in the entire Indonesian Archipelago indicate the part which the diurnal tides play in here. Figure 179 gives a presentation of this ratio. Particularly apparent

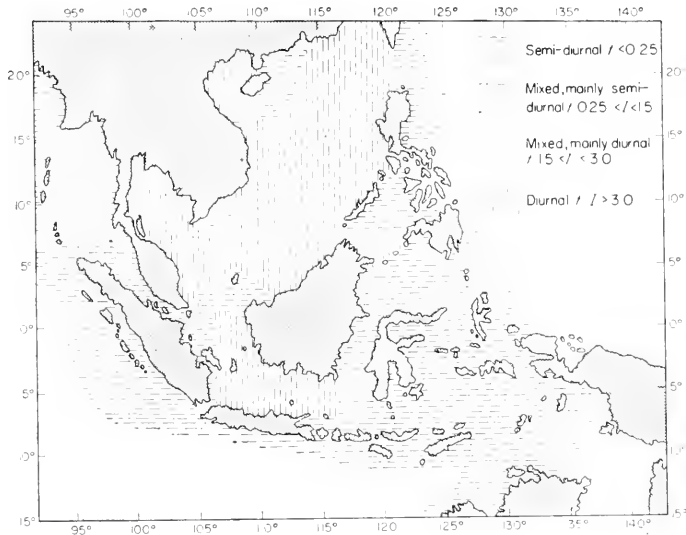


FIG. 179. Ratios indicating the character of the tides in the Indonesian Archipelago.

are the nodal lines of the M_2 and S_2 tides, where this ratio exceeds everywhere the high value of 3. The entire area of the central Java Sea belongs to it, equally the area between Indo China and North-west Borneo. An area of a relatively low value of this ratio extends east of 120° E., where it does not reach 1.

The ratio of the M_2 tide to the other semi-diurnal tides like S_2 and N_2 is abnormal and points to the fact that the tides of the entire Indonesian Archipelago are dependent upon the natural periods of the various basins. Especially the age of the semi-diurnal spring tides is very irregular. Localities situated close to each other show very great differences; thus, the Thousand Islands have a lag of 4.3 days, the Edam Island (Bay of Batania) a priming of -0.9 days; near Samarang it increases to -5.0 days. On the contrary, Karimon Endjawa has again a lag of 4 days which eastwards increases to

Table 59. Harmonic constants for the East China Sea

Place	ϕ° (N.)	λ° (E. lat.)	Amplitude in cm			Phase α in degrees					$\frac{K_1 + O_1}{M_2 + S_2}$
			M_2	S_2	K_1	M_2	S_2	K_1	O_1		
									M_2	S_2	
Ryukyu Is.	29.6°	129.6°	58	24	23	15	196°	226°	198°	173°	0.46
			58	24	20	16	199	224	212	190	0.44
			19	5	19	15	295	285	232	208	1.42
Formosa	31.4°	121.5°	95	31	20	14	30	77	207	149	0.27
			59	18	22	13	315	2	311	267	0.45
			74	22	18	13	306	6	325	280	0.32
China	37.6°	122.8°	20	6	23	16	291	351	321	276	1.50
			83	29	14	10	63	103	302	262	0.21
			94	24	25	18	95	164	146	114	0.36
			117.7°								
Liaotung	40.6°	122.2°	117	33	33	26	153	208	103	65	0.39
			99	29	27	20	300	348	1	329	0.37
Korea	37.5°	126.6°	292	113	37	26	131	181	298	267	0.16
			213	74	31	25	92	140	279	245	0.20
			76	29	31	18	304	329	207	188	0.38
Nagasaki	32.7°	129.8°	78	34	23	18	230	256	203	189	0.37
			75	33	25	20	204	234	200	174	0.42

5 days. All over the north and the west, phase lags of 2 days are common. Also in the ratio of K_1 to O_1 , there are frequent irregularities.

13. The Tides of the Eastern China Sea

The Eastern China Sea consists of three parts: the Eastern China Sea (Tung Hai), with which the Yellow Sea (Hwang Hai) is connected, which, in its turn, communicates through the Strait of Chili, with the Po Hai (Gulf of Chili) and the Gulf of Liaotung. The East China Sea is bordered in the

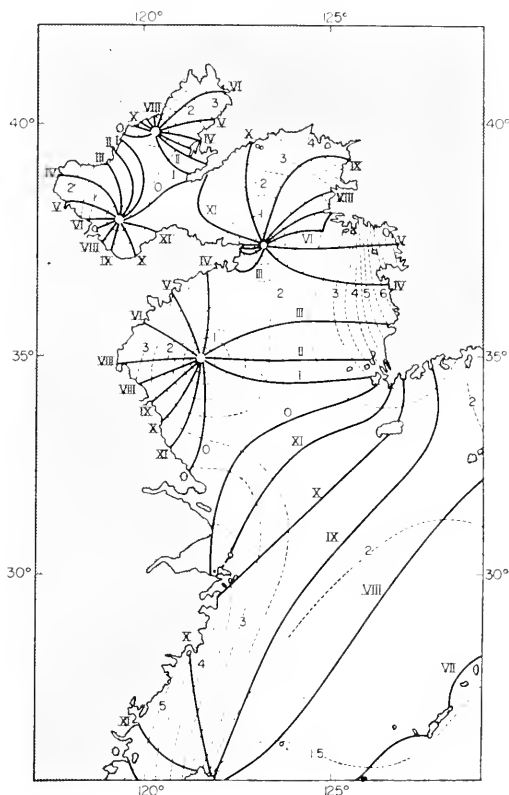


FIG. 180. Co-tidal lines of the M_2 tide and range of the semi-diurnal tide in the Eastern China Sea. (Phases referred to the 135° E. L. meridian and co-range $2(M_2 + S_2)$ in m.)

east, by the Ryu-Kyu-Retto (Nansei Islands), in the north it is connected by the Strait of Tsushima with the Sea of Japan and in the south by the Formosa Strait with the South China Sea. From the Ryu-Kyu Islands, the ocean bottom rises rapidly from 6560 ft (2000 m) to 656 ft (200 m) and the depths of the entire north-western sections of the boundary sea are less than 328 ft (100 m).

The number of tidal stations is very large on the coasts of Japan, Korea and the Peninsula of Liaotung, but small at the Chinese coast. A compilation

of the harmonic constants can be found in OGURA (1933), who made a thorough research of the tides and the tidal currents of this boundary sea. Table 59 gives a summary for a series of selected localities. The distribution of the stations on the coasts is so good that it is possible to draw for the entire boundary sea co-tidal and co-range lines for the semi-diurnal and diurnal tides. Furthermore, a great number of tidal stations have been made by the Japanese Navy in the Po Hai (Gulf of Chili) and in Hwang Hai far from the coast, for which the tidal constants could be determined by wire soundings,

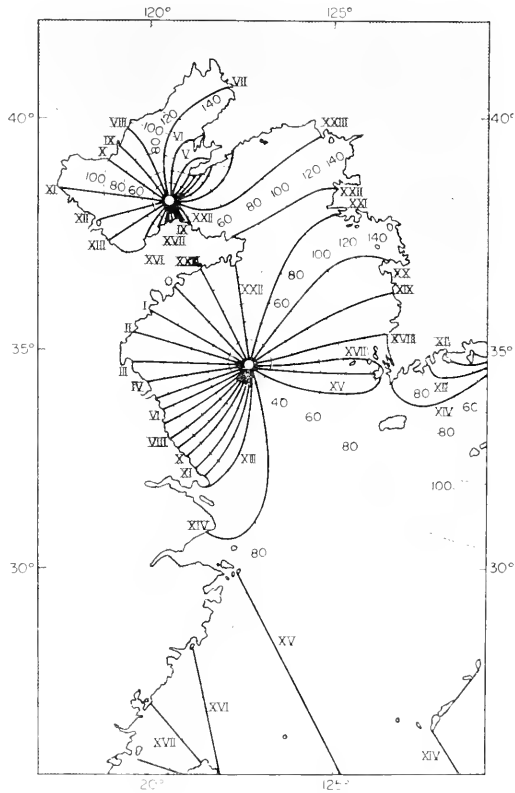


FIG. 181. Co-tidal lines of the K_1 tide and co-range lines $2(K_1 + O_1)$ in cm.

and recently also by means of high-sea gauges. The observations of the vertical tide in the open ocean are complemented by a large number of current measurements as given by OGURA (1933, pp. 47, 89, 91, 133, 137, 179 and 1934, pp. 431, 471). On the basis of the complete available observations and using the method of Proudman and Doodson (see p. 361), OGURA (1936, pp. 147-81) has drawn charts of the M_2 and K_1 tide which seem to be very reliable. Especially for the northern section of the Hwang Hai, for the Po Hai and for the Gulf of Liaotung there is a sufficient number of observations and tidal

stations in the open ocean to guarantee the course of the co-tidal and co-range lines. This is not true for the southern section of the Hwang Hai and the Tung Hai. In Figs. 180 and 181 the most recent results have been compiled in a chart covering the entire South China Sea.

The crest of the semi-diurnal wave, coming from the Pacific Ocean, reaches the chain of islands of the Ryu-Kyu almost simultaneously at about 7 h (referred to the meridian of 135° E.). The range at spring tide $2(M_2 + S_2)$ is about 180 cm near the north-eastern islands, and about 125 cm near the south-western islands. The tide wave penetrates with a wide front into the East China Sea and till the opening into the Yellow Sea (from Shanghai to the southern tip of Korea) it has apparently the nature of a progressive wave. It reaches this line with the phase 0 h, while the amplitude increases to nearly 8.2 ft (250 cm). The interior sea, up to the central section of the Gulf of Liaotung, can then be regarded as a canal with many curves, with a length of about 1600 km and a mean depth of about 50 m. The natural period with an opening correction will be of the order of magnitude of about 46 h, so that for the semi-diurnal tides the $\nu = 3.7$ and for the diurnal tides $\nu = 1.8$. We can, therefore, expect for the semi-diurnal tides four nodal lines for the diurnal tides two nodal lines. The rotation of the earth will transform them into amphidromies. This is, in fact, the tidal picture shown in Figs. 180 and 181. For the M_2 tide, the southern section of the Yellow Sea oscillates with the phase 0 h at the opening in such a way that at the south coast of the Shantung Peninsula the phase is 6 h. The northern section of the Yellow Sea and the Strait of Chilli co-oscillate with the co-tidal line $3\frac{1}{2}$ h (south-east coast of the Liaotung Peninsula $9\frac{1}{2}$ h). The Po Hai (Gulf of Chili) then oscillates with the phase $11\frac{1}{2}$ h and, finally, the Gulf of Liaotung, with the co-tidal line 0 h, so that in the central section there is again the phase 6 h.

The K_1 tide behaves similarly. Here the entire East China Sea has the phase $14\frac{1}{2}$ h with ranges $2(K_1 + O_1)$ of 70–80 cm. The entire Yellow Sea is then covered by a large amphidromy, the northern section oscillating with the phase 22 h. The second amphidromy lies at the western end of the Strait of Chili and covers the entire Po Hai and the Gulf of Liaotung.

An accurate hydrodynamical theory of the tides of the entire East China Sea has not yet been given. Analyses of separate parts can be found in OGURA (1926, p. 167; 1933, p. 269), who has studied the oscillations of the Gulf of Liaotung, considering the Coriolis force and friction, and who was able to obtain a very good agreement with the observations. The tidal phenomenon of the entire East China Sea is almost exclusively conditioned by those water-masses which penetrate through the canals between the Ryu-Kyu islands within a half-tidal period and then flow out again within the following half tidal period. The straits between Formosa and the Continent, and also the Strait of Tsushima, are less important, as is shown by the following table.

Water transport during 6 h of the M_2 tide through:

the canals of the Ryu-Kyu islands	350 km ³
the northern entrance of the Formosa Strait	130 km ³
the south-western entrance into the Strait of Tsushima	20 km ³

This proves that the tides of the boundary sea are essentially of Pacific origin. Concerning the tidal currents in the different sections, see Ogura (p. 424). Table 59 gives the ratio of the diurnal to the semi-diurnal tides. The ratio indicating the character of the tide is generally smaller than 0.5; the tides, therefore, are mixed, preponderantly semi-diurnal, increasingly so with a further penetration into the boundary sea, where they become almost exclusively semi-diurnal. Excepted are only the areas in the vicinity of the centres of the amphidromies, where of course, the diurnal tides are predominant.

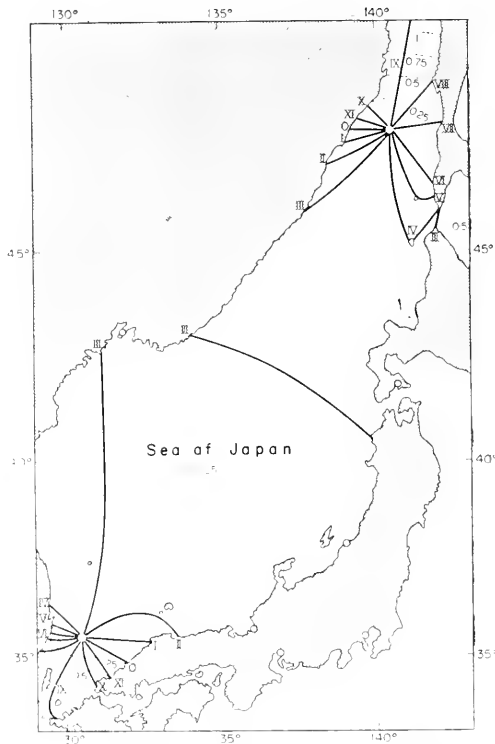


FIG. 182. Co-tidal lines of the M_2 tide (referred to the 135° E. L. meridian) and range $2(M_2+S_2)$ in m for the Sea of Japan (Ogura).

14. The Tides of the Sea of Japan and the Sea of Okhotsk

The Sea of Japan is connected with other seas by four straits, the most important of which is the Strait of Korea or of Tsushima, whereas the Strait of Tsugaru between Honshu and Hokkaido and the Strait of Soya (La Perouse Strait) are of lesser importance, and still less so is the Gulf of Tatar between

Sakhalin and the continent. This deep adjacent sea will, therefore, receive its principal impulse for the tidal motion through the Strait of Tsushima. Table 60 contains a compilation of the tidal constants of the most important coastal localities, for numerous other localities they can be found in the above mentioned paper of Ogura. Figures 182 and 183 represent the co-tidal and co-range lines, according to the latter.

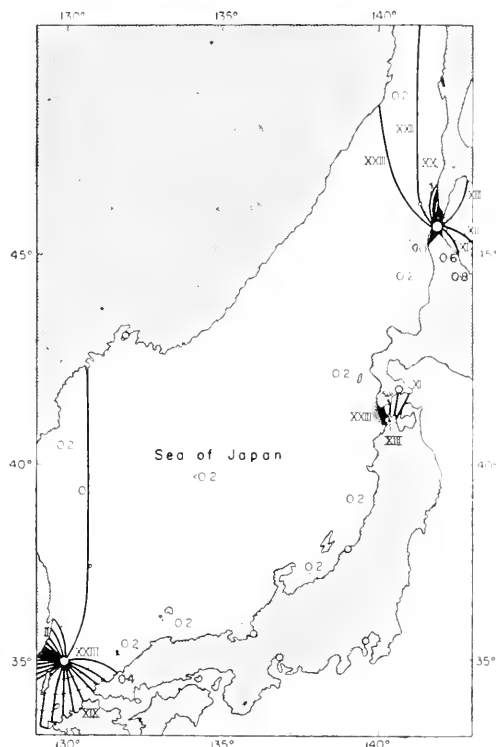


FIG. 183. Co-tidal lines of the K_1 tide and range $2(K_1 + O_1)$ in m for the Sea of Japan (Ogura).

The semi-diurnal tidal wave penetrating from the south shows a well-developed amphidromy at the northern outlet of the Strait of Tsushima, which has already been assumed at this point HARRIS (1900, 1904). The length of the entire strait is estimated to be 280 miles (450 km), its mean depth around 328 ft (100 m) this gives a natural period of 8.1 h and $\nu = 0.65$. As the difference in phase at both ends of the strait is exactly 180° , the distribution of the amplitudes along the same is according to DEFANT (1919, p. 105) given by

$$\eta = \frac{1}{\sin \nu \tau} [a \sin \nu \tau (1 - y) - b \sin \nu \tau y] \cos(\sigma t + \epsilon),$$

a and b are the amplitudes at the southern end ($y = 0$), and at the northern

Table 60. Harmonic constants for the Sea of Japan

Place	ϕ° (N.)	λ (E. Lat.)	Amplitude in cm			Phase α in degrees			$\frac{K_1 + O_1}{M_2 + S_2}$		
			M_2	S_2	K_1	O_1	M_2	S_2		K_1	O_1
Kyushu Tsushima	33.6	129.9	59	28	16	15	263	286	248	231	0.36
	34.6	129.4	45	22	7	7	248	276	210	227	0.21
Honshu	34.9	132.1	8	4	7	8	354	6	352	325	1.25
	36.2	133.3	6	2	5	5	61	87	347	323	1.25
	37.4	136.9	6	2	5	5	80	107	346	320	1.25
	38.8	139.7	5	2	6	6	88	128	350	328	1.72
Hokkaido	41.4	140.1	7	3	5	5	132	161	258	262	1.00
	45.4	141.7	3	2	7	7	109	143	13	350	2.80
Sakhalin	46.7	141.9	5	2	6	7	201	208	347	323	1.86
	49.8	142.2	40	14	6	5	264	298	334	309	0.20
Yanina Tetyukle	49.6	140.3	18	6	6	5	298	336	357	321	0.46
	44.4	135.9	6	2	4	1	117	130	352	352	0.62
Korea	39.4	127.5	9	4	5	5	82	101	359	323	0.77
	37.5	130.9	4	2	4	4	96	90	353	322	1.33
	35.1	129.0	39	19	4	2	234	263	138	104	0.10

end ($y = 1$) respectively. As a is roughly 60 and $b = 6$ cm, it appears that there is a nodal line near $y = 0.95$, which is very close to the northern outlet of the Strait of Tsushima into the Sea of Japan. The rotation of the earth transforms it into an amphidromy which will be well developed, inasmuch as the tidal currents are rather strong (see Table 61 and NISIDA (1927, 1928, 1930)). This has also been observed. In the entire Sea of Japan, up to

Table 61. Currents in the western and eastern canal of the Tsushima Strait

Depth	Average current		Semi-diurnal current			Diurnal current			
	Velocity (cm/sec)	Direction (°)	Velocity (cm/sec)	Direction (°)	Phase (h)	Velocity (cm/sec)	Direction (°)	Phase (h)	
Western canal: 25-26 April 1928; (age of moon, 5-6 days; declination 25.7-24.4 N.).									
5m	Max	20	18	34	209	4.6	39	204	4.3
	Min			11	299	7.6	10	294	10.3
100m	Max	16	7	24	217	4.3	28	204	3.1
	Min			3	127	7.3	1	294	9.1
Eastern canal: 19-20 October 1929; (age of moon, 16-17 days; declination 11.8-17.4 N.).									
5m	Max	45	85	65	211	5.9	34	231	5.6
	Min			5	301	8.9	8	321	11.6
100m	Max	23	27	53	224	5.0	17	201	5.0
	Min			6	314	8.0	2	111	11.0

about 45° N. lat., high water occurs at the same time (around 3 h), and the range is very small (spring height along the coasts of Honshu and Hokkaido about 16 cm, at the coast of Korea about 20 cm). In the northern outlet of the Sea of Japan, in the Gulf of Tartary, there is another well-developed amphidromy whose centre is located in the southern section, not far from the passage to the open sea. Here also its existence is confirmed by theoretical considerations by OGURA (1923, p. 89). With a length of the Gulf of about 750 km (465 miles) and a mean depth of 250 m (820 ft), the natural period is 8.3 h and $\nu = 0.68$, so that there is a nodal line very close to the opening. The increase in amplitude towards the north is a result of the orographical configuration of the Gulf, but also of the fact that ν is close to the resonance value.

The diurnal tide also shows an amphidromy in the Strait of Tsushima, with its centre displaced unsymmetrically towards the coast of Korea. The range $2(K_1 + O_1)$ is in the south about 80 cm, and decreases towards the north, on the Japanese side as far as 40 cm, on the Korean side to about 12 cm. It maintains this order of magnitude all over the Sea of Japan, and high water occurs for K_1 in the east almost simultaneously at 23 h, in the west

at about 0 h. The Gulf of Tartary co-oscillates with the diurnal tides with the Sea of Japan without a nodal line, and the phase lags somewhat because of frictional influences.

Whereas the character of the tide in the Strait of Tsushima is still semi-diurnal, it becomes in the entire Sea of Japan of a diurnal type with a value of the ratio between 1.00 and 1.50 and then it resumes its semi-diurnal character in the Gulf of Tartary. This phenomenon is not a consequence of a greater prominence of the diurnal tides, but rather of the decrease of the semi-diurnal tides in the large and deep interior sea.

MURAMOTO (1932, p. 227) has made a survey of the ocean currents in the Strait of Tsugaru on the basis of the current observations on two stations, and has also tested the results on models.

A hydrodynamical theory of the tides of the entire Sea of Japan including the Strait of Tsushima and the Gulf of Tartary has been given by Ogura on the basis of the canal theory. The computations by means of sixty six cross-sections perpendicular to the "Talweg" resulted for the semi-diurnal tides in almost complete agreement with observations; the amphidromies result of the co-oscillation of the water-masses of the Sea of Japan with the tide in front of the Strait of Tsushima; the other communications with the adjacent seas are unimportant. The diurnal tides do not agree as well and Ogura is of the opinion that this is due mainly because we cannot neglect the transport of 16.5 km^3 of water through the Strait of Tsugaru in 12 h whereas the transport through the Strait of Tsushima is 32 km^3 . However, it is not impossible that the independent tidal component of the diurnal tides makes itself felt even though the amplitudes are small. OGURA (1932, p. 1) has treated the tides of the Strait of Tsugaru theoretically and has obtained a good agreement with the observations made by Muramoto.

The Sea of Okhotsk communicates with the Pacific Ocean by the numerous passages between the various Kuril islands; it also communicates with the Sea of Japan by the Soya Strait (La Perouse Strait) between Sakhalin and Hokkaido, and by the Gulf of Amur through the Gulf of Tartary, on the other hand. The two latter communications, however, are of far less importance than the former. Inside the chain of the Kuril Islands there is a basin more than 3000 m (9800 ft) deep, but then the ocean bottom rises rapidly up to 200 m (600 ft) towards the centre of the sea. The north-eastern section of the Sea of Okhotsk is the Gulf of Penhinskaya which ends in a narrow arm.

The number of tidal stations on the Kuril Islands and along the coast of Sakhalin is sufficiently large to give an outline of the tides. At the north and north-west coast there are only few values available; at the west coast of Kamchatka there are none. Table 62 gives the harmonic constants for a series of localities and Fig. 184 shows, according to Ogura, for the M_2 tide the co-tidal lines and the ranges $2(M_2 + S_2)$.

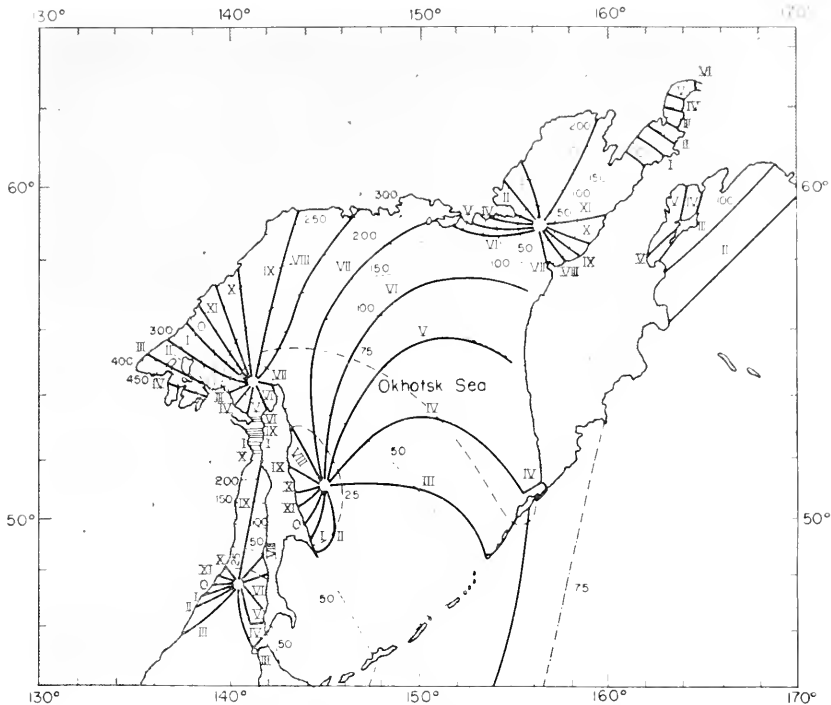


FIG. 184. Co-tidal lines of the M_2 tide and range $2(M_2 + S_2)$ in m for the Sea of Okhotsk. (Phase referred to the 135 E. L. Meridian) (Ogura).

This presentation is not very reliable, but they contain all that can be derived from the coastal observations.

The semi-diurnal tide wave progresses from the Pacific Ocean through the Kuril Islands; along the islands the phase retards $1\frac{1}{2}$ h going from the south-west to the north-east, the amplitude increases in the same direction from 50 to 80 cm. Consequently, the co-oscillation of the water-masses of the adjacent sea does not have the same phase, which complicates conditions somewhat. The rectangular shape of the whole sea reminds one of North Sea, but its dimensions are far larger. With a length of about 1600 km (1000 miles) an opening around 700 km (440 miles) wide, and an average depth of 200 m (660 ft), the period of the free oscillations is approximately 24 h, so that ν has the value of about 2. This means that the semi-diurnal tides have two nodal lines which the rotation of the earth transforms into amphidromies. In fact, the map of Ogura shows two amphidromies, both displaced to the west, one with its centre in front of Sakhalin, the other one in the shallow north-western bay. STERNECK (1922, p. 145) has assumed only one amphidromy in the central part of the sea. The decrease in range in the vicinity of the amphidromies shows that their presence is real. Only new observations on the coast of Kamchatka will decide whether the center of the outer amphidromy is not located farther out at sea.

Table 62. Harmonic constants for the Sea of Okhotsk

Place	ψ (N.)	λ (E. Lat.)	Amplitude in cm			Phase α in degrees			$\frac{K_1+O_1}{M_2+S_2}$		
			M_2	S_2	K_1	O_1	M_2	S_2		K_1	O_1
Gulf of Penghina	62.4	164.5°	133	26	252	161	230	278	332.2	299	2.6
			88	30	197	109	40	93	242	216	2.6
			27	5	123	83	123	336	256	224	6.4
Sakhalin	59.5	150.7	122	45	52	35	238	289	229	203	0.52
			87	32	45	39	23	84	227	205	0.71
			154	48	48	46	99	161	251	218	0.47
			9	2	16	17	230	332	312	271	3.0
Kuril Is.	45.4	148.8	24	9	18	14	102	172	197	172	0.97
			25	9	25	18	99	149	162	143	1.26
			21	7	36	27	114	167	170	145	2.25
			24	10	42	30	141	192	170	143	2.11

Tidal observations in the Gulf of Penzhinskaya are very scarce. With $l = 600$ km and a mean depth of about 50 m, ν will be about 1.5, which is close to the resonance value. Therefore, if the amplitudes are large there will be two nodal lines (amphidromies) for the semi-diurnal tide; one near the opening, the other one near the closed end. The former is indicated in Ogura's map, whereas he has transformed the latter in the narrow arm into a progressive wave. Whether this corresponds to the reality can only be decided by observations. The range $2(M_2 + S_2)$, which is 64 cm at the opening, increases at the first antinode to a little above 200 cm, at the closed end to 318 cm, which shows how strongly these water-masses co-oscillate with the external tide.

The diurnal tide wave has a phase of about 10 h at the northern end of the Kuril Islands and of $14\frac{1}{2}$ h at the north coast of the adjacent sea. According to the ν value, one should expect an amphidromy; but according to the available observations, there seems to be none. The range $2(K_1 + O_1)$ is very great and increases from the outside to the inside. The value of the ratio determining the character of the tides in the vicinity of the semi-diurnal amphidromies is quite high. Chaivo on Sakhalin has a ratio of over 6.

The diurnal tides in the Gulf of Penzhinskaya are excessively large. They are considerably intensified by resonance; at the closed end, Cap Astronomicheskii $2(K_1 + O_1)$ attains the value of 826 cm, which is the largest value ever known for diurnal tides. Point Matugin has still 612 cm. However, the ratio decreases from the opening into the Gulf of Penzhinskaya towards the closed end from 6.4 to 2.6; this shows that the semi-diurnal tides, become stronger relatively to the diurnal tides, which can also be concluded from the ν value.

The tidal picture of the Sea of Okhotsk is still very uncertain. Moreover, throughout a great part of the year, the central part of this sea is covered with a thick layer of ice and the pack- and drift-ice masses do influence the tide wave through friction (see vol. I). Whether this causes seasonal variations in the harmonic constants and how this effects also the ranges on the coasts, is still completely unknown.

15. The Tides of the Bering Sea

HARRIS (1904) part IV, p. 394 has made a first attempt to represent the tides of this sea, basing himself on a very small number of observations. Since then only few new tidal values have been added (see Table 63). The establishments permit the following conclusion; the Pacific tide wave progresses westward, past the Alaskan Peninsula; then it penetrates north-westward through the wider and deeper passages between the Aleutians, especially between 170° and 175° west of Greenwich into the deep [3000 m (9840 ft) to 4000 m (13,100 ft)] area of the Bering Sea and reaches the coast of Asia almost simultaneously with an establishment of 4 h. The wave is retarded against the shallower shelf area towards the north-east, and it seems as if

Table 63. Harmonic constants in the Bering Sea

Place	ϕ° (N.)	λ° (W. Lat.)	Amplitude in cm				Phase α in degrees				K_1+O_1	
			M_2	S_2	K_1	O_1	M_2	S_2	K_1	O_1	M_2+S_2	
Aleutians	Sanak-Peterson	54.4	162.6	59	22	41	24	355	18	124	97	0.80
	Dutch Harbour	54.0	166.2	19	4	32	22	105	304	148	131	2.40
	Port Clarence	65.2	166.4	14	1	8	4	213	346	115	289	0.74
	St. Michael	63.5	162.0	16	2	40	32	235	216	295	248	3.47

this shallow section north-east of the line from Cape Navarin to the Pribilof Islands simply co-oscillates with the tide in the deep sea in the south-west. According to Harris, the island of St. Lawrence would be the starting point of a node going south-eastwards to Cape Romanzof, and there would be a counter clockwise amphidromy in the adjacent wide Norton Sound. Only observations can give evidence as to actually prevailing conditions. According to the harmonic constants of St. Michael, there are in the Norton Sound extreme diurnal tides, whereas for the other areas the ratio governing the character remains below 1. Remarkable are the small amplitudes of the S_2 tide, and also the age of the tide appears to be very much disturbed. In Port Clarence (Cape Prince of Wales) the semi-diurnal tides have been shifted to such an extent that the semi-diurnal spring tides occur almost at the time of quadratures and the diurnal spring tides at the time the moon is in the equator.

16. The Tides of the Gulf of California

The simple orographical configuration of this outstretched gulf would make us expect tides of a simple nature. The gulf has the form of a canal closed at one end 1100 km (660 st. miles) long, whose depth decreases regularly from an average depth of 1670 m (5470 ft) at the opening to very small depths at the closed end. The cross-section narrows near the islands Tiburon, San Esteban and San Lorenzo, at a distance of about two-thirds of its length from the opening. The few available values for establishments and range indicate that in the larger southern section up to the narrowing just mentioned, high water occurs nearly simultaneously (Guaymas, 27.90 N.; 3 h 28 min G.M.T., range 1.2 m (3.9 ft)), whereas in the shallow section high water occurs about 6 h later, Colorado estuary 9 h 54 min (range at spring tide 8 to 9 m (26–29 ft), at neap tide 5 to 6 m (16–19 ft)). This points to a standing wave with a nodal line at the narrow section of the gulf. The period of the free oscillation of the entire gulf is computed at 7.66 h, so that $\nu = 0.62$. The nodal line will be at a distance of approximately two thirds of the length, which corresponds to the observations. For the inner shallow section alone which has a length of 390 km (240 land miles) mean depth 160 m (480 ft), Krümmel computes a period for the free oscillation of 12.14 h (using a correction for the opening).

This value is sufficiently close to the period of the semi-diurnal tides for explaining the strong increase of the ranges at the closed end of the gulf. However, the very shallow depth of this area is also partly responsible for this increase.

17. The Tides of the Gulf of Mexico

In the entire American Mediterranean Sea the tides are weakly developed. This is not only true for the Caribbean itself, but also for the entire Gulf of Mexico, in which the tidal ranges nowhere exceed 0.7 m (2.3 ft). A particularly characteristic feature is the conspicuous weakening of the semi-diurnal tides, so that in this adjacent sea the establishment becomes practically unusable. The tide is governed by the extreme lunar declinations instead of by the semi-monthly variation of the spring and neap tides. In most localities the tides are diurnal and the amplitudes and phases of the semi-diurnal wave show up only in the results of the harmonic analysis. However, their amplitudes are small compared to those of K_1 and O_1 , so that the ratio determining the character mostly exceeds 1 and will even attain, at the northern side of the gulf, a maximum of >9 . In the Caribbean the diurnal tides are still predominant and the contrast in amplitudes between the Atlantic side and the Caribbean side of the islands which separate these seas is sharp (e.g. on Puerto Rico, Ponce has 8.40, San Juan 0.91).

Table 64. Harmonic constants for the Gulf of Mexico

Place	Amplitude in cm				Phase α in degrees				$K_1 + O_1$
	M_2	S_2	K_1	O_1	M_2	S_2	K_1	O_1	$M_2 + S_2$
Key West	17.1	5.2	8.2	8.8	260°	280°	274°	273°	0.77
Tortugas	14.6	5.2	11.3	11.0	278	292	275	271	1.12
Cedar Keys	32.3	12.8	16.2	14.9	24	51	314	309	0.69
St. Mark's	34.1	13.4	17.7	15.5	44	73	319	308	0.70
Pensacola	1.8	0.9	12.5	12.5	317	315	320	310	9.11
Mobile	2.1	1.2	11.6	11.3	301	313	318	308	6.82
Cat Island	3.7	2.1	15.9	14.6	11	24	325	315	5.26
Mississippi									
South P.	1.8	1.2	13.4	10.1	317	298	321	312	7.70
Galveston	6.7	1.2	10.7	10.1	125	134	321	312	2.62
Tampico	2.4	—	10.6	—	—	—	—	—	—
Vera Cruz	6.1	1.8	16.5	19.2	75	355	282	320	4.50
Campeche	22.0	—	26.6	—	—	—	—	—	—

For thirteen localities of the Gulf of Mexico, more or less evenly distributed around the Gulf, the harmonic constants are known (Table 64) but, unfortunately, only for few localities of the Caribbean. Therefore a detailed investigation of the tides in the Caribbean cannot be performed.

FERREL (1874, p. 245) mentioned the diurnal nature of the Mexican tides. HARRIS (1900, Part IV A, p. 661) has expressed the opinion that, for the diurnal tide, the Gulf of Mexico and the Caribbean form one single oscillating system with a nodal line extending from Western Haiti to Nicaragua. The consequence of this would be that the tides of the Gulf are essentially simultaneous. ENDRÖS (1908, p. 86) has shown that, with a nearly convex parabolic normal curve the period of the free oscillation of the system comes close to 24 h, which would explain the prominence of the diurnal components. WEGEMANN (1908, p. 532) has also assumed a resonance effect of the diurnal components in the Gulf of Mexico. He computed as period of the free oscillation 24.8 h for a west-east oscillation of the Gulf (Cuba–Vera Cruz $l = 1650$ km = (1000 land miles) mean depth 875 m (2625 ft) with an opening correction of $1\frac{1}{4}$. $\nu = 0.4$ and when the water-masses of the Gulf co-oscillate with the diurnal tides of the Atlantic Ocean, there will be a simultaneous rise and fall of the water surface in the Gulf which conforms to the observations. For the semi-diurnal tides, $\nu = 0.8$, i.e. the semi-diurnal tides co-oscillating with the Atlantic Ocean will have one nodal line approximately on a line Mississippi River delta – Yucatan peninsula which, is transformed into a weak amphidromy rotating to the right by the rotation of the earth. STERNECK (1920, p. 131; 1921, p. 363) has assumed for the semi-diurnal an amphidromy rotating to the left having its centre in the middle of the Gulf, and for the diurnal tides a co-oscillation with the Atlantic Ocean but with an opposite phase (see also DEFANT, 1925).

GRACE (1932, p. 70; 1933, p. 156) has developed an entirely new method to investigate the tides in deep adjacent and boundary seas, which he tested for the first time for the Gulf of Mexico. It consists essentially in dividing the sea under consideration into a number of rectangular basins of approximately uniform depth; some of these are closed at one or more of their sides, whereas the other sides are open. Grace then applies his solutions of the tidal motion in a deep rectangular basin (GRACE, 1931, p. 385) to this system of regularly shaped basins. For such a basin open on one side, he assumes a tidal current of the tidal period under consideration entering through this side and computes theoretically the average range on each side of the basin; that is the part directly generated by the tide-producing forces (independent tide) in a basin imagined to be closed, as well as the part generated by the assumed tidal current at the open end (opening). After all the computations have been made for all partial basins, we obtain the theoretical tide at each coastal point as the total sum of all the influences of all adjoining partial basins, and a comparison with the observed values makes it possible to compute the unknown tidal currents at the opening. The totality then should give the tidal picture for this sea as it is formed by the independent and co-oscillating tides. Figure 185 shows how the Gulf of Mexico is schematized by a succession of lines A, B, C, \dots, K , the sides CD, DE, FG being considered

as "open". The tidal motion of the entire basin was computed in four steps, viz.: (a) the independent tides with basins imagined to be completely closed; (b) the co-oscillating tide with only one side open *FG*, at which there is a uniform tidal current *U*; (c) the co-oscillating tide at the opening *DE* with

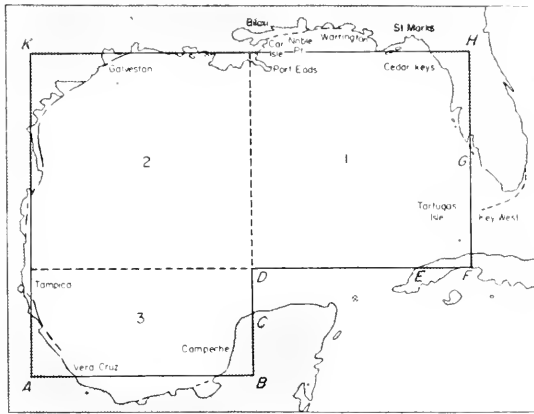


FIG. 185. Schema of the division of the Gulf of Mexico for the theoretical computation of the tides. Position of the tide stations around the Gulf.

a tidal current *V*; and finally (d) the co-oscillating tide at the opening *CD* with the tidal current *W*. The tides of the entire Gulf are regarded as the superposition of these 4 partial tides, and the comparison with the observations gives the tidal currents *U*, *V*, *W* at the openings.

Table 65. Comparison between theory and observations in Gulf of Mexico

Place	K_1 tide				M_2 tide			
	Computed		Observed		Computed		Observed	
	cm	Phase*	cm	Phase*	cm	Phase	cm	Phase
Key West	9.9	268°	8.5	268°	14.4	254°	17.1	251°
Tortugas	8.8	276	11.3	268	12.9	258	14.6	264
Cedar Keys	11.8	312	16.3	307	11.7	280	32.3	10
St. Mark's	12.7	311	17.6	313	10.1	279	34.2	33
Warrington	14.8	307	12.5	317	5.5	276	1.9	312
Mobile P.	14.8	308	11.7	316	4.6	279	2.2	297
Biloxi	15.0	310	17.3	318	3.5	284	3.4	9
Cat Island	15.0	310	16.0	324	3.2	287	3.5	10
Port Eads	15.1	310	13.4	292	1.8	311	1.8	315
Galveston	16.5	318	11.1	325	6.2	70	8.0	127
Tampico	14.8	319	10.6	301	9.1	76	2.4	79
Vera Cruz	17.5	304	16.4	288	14.1	89	6.2	87
Campeche	18.0	305	26.6	315	15.8	98	22.0	91

* Phase referred to the centre meridian of the Gulf, 89.9° west of Greenwich.

The theoretical fundamentals can be found in the paper of Grace already mentioned and its practical application causes no further difficulties. The comparison between the results of the theory and the observations for the two partial tides K_1 and M_2 is given in Table 65. For the K_1 tide the agreement is better; the average error, without considering the sign, amounts to 10° for the phase and 3.3 cm (23%) for the amplitudes. The tidal currents computed for the cross-sections at the openings are of the same order of magnitude as the observed ones, which date from 1887 and probably are very inaccurate, but in the phases there are considerable differences. In making such a comparison, it should be borne in mind that the theory gives an average current for the entire cross-section, but that the observations are values at a certain point, which were obtained intentionally at the point where the current is strongest. Besides, they are based on measurements extending only over a few days and can be considerably disturbed by wind and stowing. Figure 186 gives

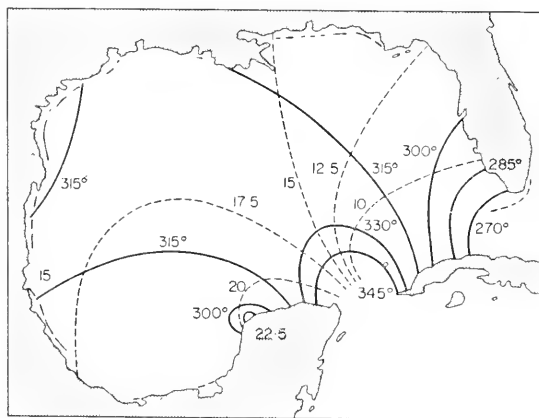


FIG. 186. Co-tidal lines and amplitudes of the K_1 tide in the Gulf of Mexico. —, phases referred to the centre meridian 89.9° W.; ---, amplitude in cm (Grace).

the co-tidal and co-range lines of the K_1 tide constructed from the theoretical values. With the exception of the areas in the vicinity of the opening, this tide occurs almost simultaneously in the entire Gulf. The amplitude increases from 10 cm in the east in a counter-clockwise revolution, to about 20 cm in the south. The wave apparently penetrates through the Strait of Florida and circulates around the Gulf in the positive sense, leaving it in the Strait of Yucatan. It can be concluded from the tides of the single components that the diurnal tides are almost exclusively co-oscillating tides, whereas the independent tide becomes of less importance.

The computations for the M_2 tide are more difficult. It was necessary to reject the observations at the north-east coast, which has high amplitudes of more than 30 cm (1 ft) because these stations are apparently disturbed by local influences (extensive, shallow areas off the coast). There was an average

error in the phase of 4° and in the amplitude of 3.0 cm. Here also there was agreement between the computed currents at the opening of the cross-sections and the observed currents only as to the order of magnitude, but the phases do not agree. Figure 187 gives the picture for the M_2 tide. The co-tidal lines

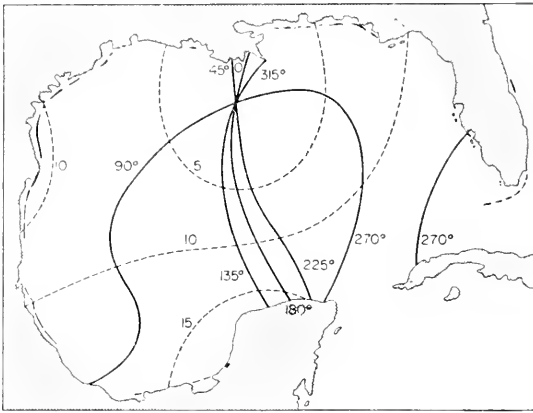


FIG. 187. Co-tidal lines and amplitudes of the M_2 tide in the Gulf of Mexico (see Fig. 186).

show a positive amphidromic point in the north-western section of the Gulf with a strong crowding of the co-tidal lines in the north-south direction, so that the tide comes close to a simple oscillation. Here also the co-oscillation with the tide in front of the Strait of Florida seems to be the most important. The independent tides by themselves would give a negative amphidromy, and this might be the reason why the amphidromy of the co-oscillating tide appears to be so little developed.

18. The Tides of the Gulf of St. Lawrence

The tidal picture of this adjacent sea has been given by DAWSON (1920). Current observations are available in sufficient quantity (DAWSON 1907, 1913, 1920), so that nothing would prevent a complete hydrodynamical theory of these tides. However, its orographical configuration is very intricate. In the south-east it has a good communication with the ocean through the 56 nm wide Cabot Strait; in the north-east the narrow Strait of Belle Isle leads into the Labrador Sea. In the north-west the Gulf is separated by Anticosti Island from the St. Lawrence River estuary, and in the south-west Prince Edward Island shields Northumberland Strait. These irregularities of the coastal configuration on three sides make it difficult to compute accurately the conditions of oscillation.

Already Harris found that the essentially semi-diurnal tides of the Gulf can be represented by an amphidromy rotating to the right which he assumes to be formed by the effect of the rotation of the earth on the co-oscillating tides coming through the Cabot Strait. Basing on the observations of

Table 66. *Tidal data for the Gulf of St. Lawrence*

(according to Krümmel)

	Place	ϕ° N	λ° W. Lat.	Establishment*		Range (m)
				(h)	(min)	
Cabot Strait	Cape North	47.1	60.4	0	2	1.2
	St. Paul's Island	47.2	60.2	0	0	1.5
	Port-au-Basques (N. F.)	47.6	59.2	0	51	1.8
West coast Newfoundland	Codroy	48.9	59.6	1	13	1.8
	Cow Head	49.9	57.8	2	39	1.9
	St. Genevieve Bay	51.1	56.8	2	30	1.5
Belle Isle Strait	Pistolet Bay	51.5	55.8	11	21	1.0
	Red Bay	51.7	56.5	11	31	1.0
North coast of the Gulf	Bonne Esperance	51.6	57.7	1	06	1.5
	Cape Mecatina	50.5	59.3	2	28	1.5
	Wapitaqun	50.2	60.0	2	30	1.5
	Natashkwan	50.2	61.8	3	07	1.5
	Betchewun	50.2	63.2	3	45	1.5
	Mingan	50.3	64.0	5	32	1.8
	Seven Island	50.2	66.5	6	06	2.7
	Egg Island	49.7	67.2	6	29	3.4
St. Lawrence River	Pointe des Monts	49.3	67.4	6	40	3.7
	Cape Chat	49.1	66.7	6	40	4.0
	Bersimis Pt.	48.9	68.6	6	34	3.7
	Father Pt.	48.5	68.5	6	48	4.0
	Green Island	48.1	69.4	7	23	4.9
	Grosse Island	47.0	70.6	10	06	5.8
Anticosti	Quebec	46.7	71.2	11	23	5.5
	West Pt.	49.9	64.5	6	18	1.8
	South-west Pt.	49.4	63.6	5	44	1.8
	East Pt.	49.1	61.7	5	07	1.5
West coast	Bear Bay	49.5	62.4	5	21	1.5
	Cape Magdalen	49.2	65.3	5	36	2.2
	Cape Gaspé	48.7	64.2	6	43	1.5
	Miscou	48.0	64.5	6	45	1.5
Magdalen Island	Escouminac Pt.	47.1	64.8	8	29	1.2
	Amherst	47.2	62.0	0	28	0.9
Prince Edward Island north coast	Cascumpeque	46.7	64.0	9	56	0.9
	Richmond	46.6	63.7	10	15	0.9
	St. Peter's	46.5	62.7	10	41	1.1
	East Pt.	46.5	62.0	0	38	1.1
Northumberland Strait	Egmont Bay	46.6	64.2	7	14	1.2
	Crapaud	46.2	63.5	2	14	2.4
	Bay Verte	46.0	64.0	2	16	2.7
	Charlottetown	46.2	63.1	2	57	2.9
	Pictou	45.6	62.5	2	11	1.8
	Port Hood	46.0	61.5	1	06	1.4

* Establishment after Greenwich.

Dawson (see Table 66) KRÜMMEL (1911, vol. II, p. 328) has given a new presentation of the co-tidal lines, which are essentially the same as the chart of Harris. Springstube (1934) has given a hydrodynamical analysis of the entire tidal phenomena of this adjacent sea based on revised observations. Figure 188 shows the co-tidal lines (referred to 60° W.) and co-range lines

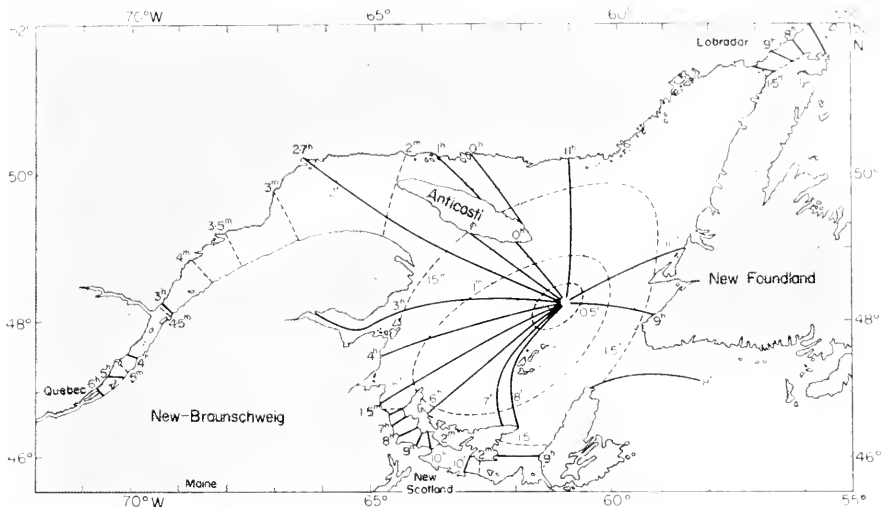


FIG. 188. Co-tidal lines (— referred to 60° W.) and ---- co-range lines for spring tide in m.

of the spring tide (in m). They are intended to give only an approximate picture of the tidal process in the interior part of the Gulf; especially the distribution of the range remains very hypothetical. The chart shows the centre of the amphidromy near 61°W. and 48½°N., north-west of the Magdalen Islands. The vast areas of the narrow north-east canal have almost synchronous tides with establishments between 10 h and 11 h. This entire north-eastern section probably co-oscillates with the tides of the middle of the Gulf. The same is the case for the funnel formed by the river estuary. After the junction with the Saguenay River, the tide wave is changed into a progressive wave moving up the St. Lawrence River. Near Grosse Isle the wave attains its largest amplitude 5·8 m (19 ft) at spring tide; it travels up to 67 nm (135 km) beyond Quebec in 4¾ h with retarding phase and even farther till Lake St. Peter. In Trois Rivières, at the lower outlet of the lake, there is still 30 cm spring tide range (according to Krümmel).

In the south-western section of the Gulf, the co-tidal lines are very much crowded and this part of the amphidromy is probably of the character of a standing wave. The Northumberland Strait behaves like a canal open at both ends, whose water-masses can be made to oscillate from both sides. The entire south-eastern section of the Gulf behind the Cabot Strait has an establishment of approximately 8½ h. At this point the influence of the

external ocean tides on the Gulf tides is greatest. It is remarkable that the range of the spring tides along all the coasts is rather uniform between 1 m (3 ft) and 1½ m (5 ft). The Magdalen Islands have 0.9 m (3 ft) which indicates a decrease towards the centre of the amphidromy.

In the Strait of Belle Isle there is a transition of the establishment from about 10 h at the Gulf opening to about 7 h in front of the opening into the open ocean, whereas the range decreases slightly.

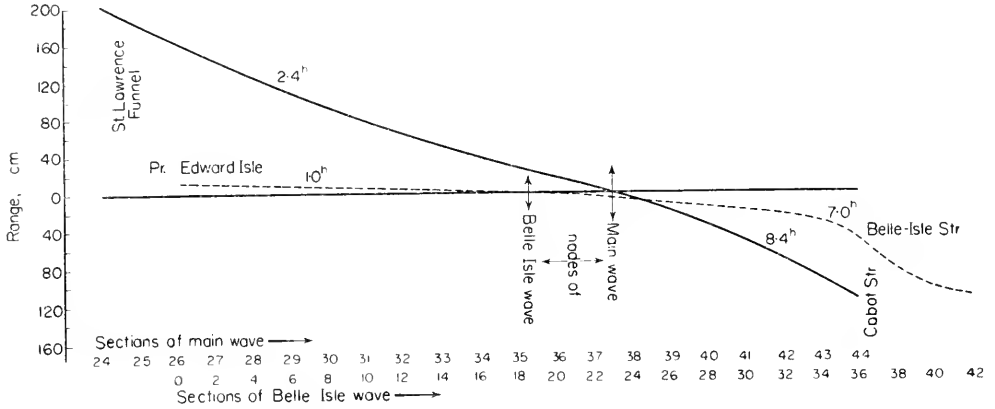


FIG. 189. Tides of the Gulf of St. Lawrence co-oscillating with the tides of Cabot Strait and the Strait of Belle Isle.

The analysis of the Gulf tides given by Springstubbe shows that they are almost pure co-oscillating tides. Figure 189 shows the distribution of the ranges of these tidal components along the main axis when co-oscillating at the Cabot Strait and at the Strait of Belle Isle. The nearly complete disappearance of the latter component, which formerly was only assumed or even used in the explanation of the amphidromy, is thus proved clearly. The superposition of these two parts of the co-oscillating tides will give an amphidromy rotating to the left and not one rotating to the right, as the observations show. Springstubbe proves mathematically that the latter is an effect solely due to the deflecting force of the rotation of the earth on the tides co-oscillating through the Cabot Strait. The observations on tidal currents agree well with the theoretically computed ones; especially the tidal currents in the Strait of Belle Isle are fully explained.

For the Gulf of St. Lawrence there are very few harmonic constants available. The few data of Table 67 show that the ratio for the character of the tides is 0.44 near St. Paul in the Cabot Strait and steadily decreases going towards the centre of the Gulf; Quebec has a genuine semi-diurnal type.

In accordance with the period of the free oscillation of the basin (Cabot Strait — north coast) of approximately 7 h and the small amplitudes of the

diurnal tidal components in front of the Cabot Strait, the diurnal tides will only be very little developed. As $r = 0.3$, we will only be very little developed. As $r = 0.3$, we will have a simultaneous rise and fall of the water surface of the entire Gulf. The harmonic values seem to confirm this. According to Dawson, the daily inequality in the Northumberland Strait increases from

Table 67. Harmonic constants for the Gulf of St. Lawrence

Place	Amplitude in cm				Phase g in degrees (referred to 60 W. Lat.)				$K_1 + O_1$
	M_2	S_2	K_1	O_1	M_2	S_2	K_1	O_1	$M_2 + S_2$
St. Paul Island	31	10	8	10	246	286	236°	205°	0.4
Forteaubay (Belle Isle Strait)	41	14	10	8	285	308	180	162	0.34
Father Point	126	42	22	22	78	118	217	191	0.26
Quebec	180	43	23	21	207	256	284	255	0.20

east to west; the tidal currents also show irregularities here which, according to Springstube, can be explained from the co-oscillation of the water-masses in the canal with the tides at the openings in the west and in the east. Dawson also points out the surprising reversal of the daily inequality between the opening in the Cabot Strait and the opposite coasts in the west, i.e. if on a certain day the morning tide is higher in the east, the evening tide will be higher in the west. Krümmel sees correctly in this the effect of the standing (semi-diurnal) wave.

19. The Tides of the Bay of Fundy

The Bay of Fundy has the largest tides of the earth and, therefore is of great interest. The bay forms a narrow bend extending to the north-east off the wide Gulf of Maine which in its centre has a depth of more than 200 m (650 ft). It is bordered on both sides by high, rocky, steep banks, and its width varies only little until it bifurcates into two canal-like arms. The Advocate Peninsula separates the Chignecto Basin from the Minas Basin. The water depths are still more than 100 m (320 ft) at the opening, then gradually decrease to 50 m (160 ft) in front of the bifurcation. In the Minas Basin, the depth decreases to 20 m (65 ft) and less, and the Basin ends in sand and rock banks. Table 68 gives a survey of the variations of the establishments and tidal ranges at spring tide along the entire bay. One notices that in the outward section high water occurs almost simultaneously; the lag up till the bifurcation is only 24 min and this happens only in the last section. In the Chignecto Basin there is a further lag of 26 min up to Sackville; it is greater in the shallower Minas Basin. Near Noel high water occurs around 1 h 40 min after high water at the opening. The tidal ranges at the opening are not very

Table 68. Tidal data at spring tide for the Bay of Fundy
 Tidal hours given in difference with the establishment at St. John, N. B.:
 3 h 42 m Greenwich time

Place (outer part of the bay)	Tidal hours difference h min		Range (m)	Place	Tidal hours difference h min		Range (m)
<i>East coast</i>				<i>Chignecto Bay</i>			
Pubnico	-1	56	3.7	Spicer's Cove	+0	12	11.3
Yarmouth	-1	07	4.9	Grindston Island	+0	21	12.5
Grand Passage	-0	31	6.4	Folly Pt.			
Petit Passage	-0	34	6.7	Estuary of the	+0	24	13.7
Weymouth	-0	26	7.3	Peticodiac River			
Digby	-0	18	8.4	Moncton	+0	46	Bore
Port George	-0	07	9.8	Sackville	+0	30	13.9
<i>West coast</i>				<i>Minas Basin</i>			
Machias Seal Island	-0	08	5.5	Haut Island	-0	04	10.1
Gr. Manan, Seal Cove	-0	22	6.1	Black Rock Pt.	+0	03	11.0
Campobello	+0	02	7.2	Spencer Island	+0	17	11.9
Lepreau Bay	-0	01	7.5	Parrsborough	+0	53	13.1
St. John, N. B.	0	00	8.2	Horton	+1	05	14.7
Quaco	-0	12	9.1	Noel	+1	14	15.4

large, about 3 m (9.5 ft), but increase rapidly inward. St. John, about in the middle, has already more than 8 m (25 ft); in the Chignecto Basin the range increases near Sackville to 14 m (46 ft). At Noel, at the end of the Minas Basin, there is a normal spring tide range of 15.4 m (50.5 ft).

All these facts prove definitely the presence of a standing wave, which must be considered as a co-oscillating tide. The strong increase of the tidal range points to an intensification of the amplitude through resonance. In fact, with a length of the Bay of 250 km (162 miles), a mean depth of 70 m (225 ft) and a ratio of length to width at the opening of 0.23, the period of the free oscillation of the Bay assumed to be closed in 6.29 h. This gives $\nu = 0.505$ which means that the resonance condition is almost completely fulfilled. The lag of the phase is a consequence of the frictional influences in the innermost shallow sections. The tidal ranges in the south (the northern coast of Nova Scotia) are always somewhat larger than in the corresponding localities to the north (which is the southern coast of New Brunswick), which is an effect of the rotation of the earth. According to the relation $2\omega \sin\phi \cdot u = -g(\partial\eta/\partial y)$ (see p. 204) one obtains with a u of 1.8 knots in the main canal and a width of 58 km (37.8 miles), an increase of the tidal range of 56 cm at the southern coast; the observations give an increase between 0.7 and 0.3 m.

DAWSON (1905) investigated the current in front of and at the opening of the Bay of Fundy into the Gulf of Maine. The observations show a nearly

alternating current with velocities averaging 1·8 knots. The average time of the reversal of the current is at the opening 35 min after high water at St. John. This speaks also in favour of a standing wave as co-oscillating tide. Towards the end of the bay the velocity increases somewhat with narrowing cross-sections; in the Minas Basin velocities of 9 knots have been measured; this, however, can only occur in a very limited region.

In the Petit Coudiac (in the centre of the Chignecto Basin) a bore follows the larger tidal ranges existing there, which impedes the practical use of the waterway and requires very expensive constructions on the banks and at the landing points (p. 469). Furthermore, with storms from the south-west water-masses in the canal pile up so that storm tides can still increase the tidal range by 2 m (6 ft) and more. Famous is the "Saxy" tide of 5 October, 1869, when the water level in the Coudiac River was as high as 8·9 m (29 ft) above and 7·2 m (23·6 ft) below the normal sea level; so the range was 16·1 m (52·5 ft) (see DAWSON 1902, p. 85). Older reports mention tidal ranges of 21·3 m (70 ft) in the Coudiac River, according to HERSCHEL (1875, p. 756), even as high as 36·5 (120 ft). Dawson is of the opinion that these figures are very much exaggerated.

20. The Tides of the White Sea and of the Gorlo

The orographical configuration of the White Sea seems very intricate; it can be divided into three sections: The main basin with its greatest depths of 350 m (1180 ft) extending from the north-west (Kandalakshskaya Bay) to the south-east divided into the Dvinskaya Bay and the Bay of Onezhskaya, 20 m (65 ft)–40 m (130 ft) deep. This main basin communicates with the Barents Sea by way of the bow-form Gorlo and later through the Woronka funnel. There are a large number of tidal observations, with establishments and ranges, for a number of localities. At the outer opening of the Gorlo the establishments are about 7 h (Greenwich time), the tidal ranges at spring tide vary between 2–3 m. The tide wave retards little at first and then rapidly, to 8 and 9 h, and attains about 1 h at the inner opening while the range decreases. The entire north and north-west coast of the main basin has a phase of 1 h. At the south coast the establishment becomes 3½ h up to the opening into the Bay of Onezhskaya. The same phase applies to the Bay of Arkhangelsk, whereas in the Bay of Onezhskaya we find 6 h 40 min.

SHOULEJKIN (1926, p. 321) has tried a hydrodynamical explanation of these tides based on Airy's canal theory. He based his chart of co-tidal lines on Airy's viewpoint that the crest of the tide wave has a different velocity of propagation perpendicularly to the cross-section, which viewpoint, however, proved to be erroneous (p. 148). Therefore, his presentation cannot be expected to agree with actual conditions. In interpreting the tides in the White Sea, it should be borne in mind that the period of the free oscillation of the entire basin is about 10 h or $\nu = 0·8$ (see DEFANT, 1925, p. 71). This means

that with a phase of 7 h at the opening, the inner basin will have a phase of 1 h. There will be a nodal line in the Gorlo, i.e. the channel which leads to the Barents Sea; owing to the increased friction at small depths and the great current velocities, the standing wave phenomenon ends and changes into a progressive wave. This seems to be confirmed by the observations.

In the principal inner basin, there are beside the co-oscillating tides, still independent tides, which, according to the main direction of the basin, should have a phase of around 7.5 h. With $\nu = 0.5$ the independent tide of a closed basin becomes indirect, the northern basin will have the phase of 1.5 h, the southern basin a phase of 7.5 h. The superposition with the co-oscillating tide in the northern section of the basin will then give a phase between 1.0 h and 1.5 h. In the southern section the phase will be either $3\frac{1}{2}$ h in the Bay of Arkhangelsk or 6–7 h in the Bay of Onezhskaya depending on the amplitudes of the components. The amplitudes will be small. This is also in agreement with the observations; however, only an accurate computation of each component and its superposition will tell whether this provides a foundation sufficient for the explanation of the tidal picture.

21. The Tides of the North Polar Basin or Arctic Ocean

The tides of this deep sea, which has a wide shelf extending in front of its coasts — especially in northern Siberia — with depths below 200 m and mostly even below 50 m have aroused interest since early days. Already WHEWELL (1833, p. 147) assumed that the tide wave enters the Arctic Ocean between Greenland and Norway, travels as a progressive wave to the coasts in the vicinity of the Bering Strait. HARRIS (1904–11) basing himself on the very scarce observations available at that time, drew a chart of co-tidal lines for the Arctic Ocean, which he completed and partly changed in 1911 in his paper “Arctic Tides”. This later chart of Harris shows the tide wave travelling from the European North Sea between Spitzbergen and Greenland towards the north-east keeping to the right side of the entire Arctic Ocean as a progressive wave up till the Bering Strait and then farther on to the Beaufort Sea. It needs 20 h to cover the whole distance. A second weaker off-shoot turns north of Greenland westwards, interferes with the wave coming from the Davis Strait and Baffin Bay and forms, just in front of the northern coast of Greenland, a small amphidromy rotating to the right. A vast area, however, remains uncharted; it may be the area where there was supposed to be land.

FJELDSTAD (1923), using partly the observations gathered during the “Maud” Expedition in the area of the north Siberian shelf, has made a new map of the co-tidal lines. He too assumes a progressive wave coming from the Atlantic Ocean between Greenland and Spitzbergen, and travelling to the east coast of Siberia, thereby maintaining its direction. He leaves open a strip immediately north of Canada for lack of usable observations. In the eastern

section his chart looks like Harris's, in the western section it shows less crowded co-tidal lines, in accordance with a deep central polar basin, which was assumed by Nansen. The crossing of the entire polar basin takes about 12 h, against 18 h assumed by Harris.

DEFANT (1924, pp. 153, 177) includes the Arctic Ocean in his first picture of the tides of the Atlantic Ocean, considering the former a bay with one closed end and part of the Atlantic Ocean. The tides of the Arctic Ocean are considered partly as co-oscillating tides with those of the Atlantic Ocean through the opening Greenland-Spitzbergen, and partly as independent tides. Both components are computed following the method of the step-wise integration of the equations of motion. The influence of the rotation of the earth is taken care of through superposition of transverse oscillations. In this way one obtains for semi-diurnal tides two positive amphidromies, one with its centre in the vicinity of Spitzbergen, the other one somewhat beyond the Pole. On the whole, the agreement with the observations is not bad. For the diurnal tides, there is an amphidromy south of Spitzbergen, and the largest part of the polar basin is covered by a progressive wave which covers the distance Greenland-Bering Strait in 12 h.

The small tidal amplitudes at the north coast of Alaska and East Siberia induced STERNECK (1928, p. 81) to abandon his assumption of a single oscillating area in the entire Arctic Basin. He divides this area into a very deep central basin and a shallow shelf zone. He then assumes that the tides of the central basin are developed independently of the shelf and are composed of the independent and co-oscillating tides. He found that the M_2 tide is essentially a co-oscillating tide with an amphidromy rotating to the right with its centre in the vicinity of the pole, whereas the K_1 tide seems to be almost a pure independent tide, with an amphidromy rotating to the left and with very small amplitudes. The co-tidal lines of the M_2 tide are extended from the central basin into the shelf zone in the form of a progressive wave and brought into agreement with the observations on the coast. He assumes also that this dissipates tidal energy, but the effect of this dissipation upon the main wave in the central basin is not considered.

Sterneck's conception of a different tidal behaviour for the two separate areas of the Polar Basin is no doubt justified and logical. But his computations are not representative of the actual conditions. The energy lost by friction on the shelf is lost for good and is also a loss for the central basin and, therefore, it is not possible for the co-oscillating tide in this basin to be a standing wave. Beside this loss of energy of the principal wave, STERNECK does not consider the fact that the Arctic Ocean is almost constantly and completely covered by a layer of ice and that, the incoming tide wave suffers another important loss of energy by friction against this layer of ice. It is, therefore, to be expected that the co-oscillating tide of the Arctic Ocean will rather appear as a progressive wave coming from the European North Sea

and travelling towards the Bering Strait. The independent tide is insignificant, because the semi-diurnal tide-generating forces are very small in the vicinity of the pole. One then approaches the presentation given by Fjeldstad of the co-tidal lines, which reproduces the observations correctly. However, the lack of observations precludes an actual tidal picture of the central basin. See DEFANT (1928, p. 274) and TENANI (1931, p. 879).

The case is different for the shelf areas, and for its North Siberian section we have the excellent work by SVERDRUP (1926) on the observations made principally during the "Maud" Expedition in 1924-25. The area comprises the largest continental shelf of the earth, extending from Point Barrow (Alaska) to Cape Chelyuskin (Taimyr Peninsula). The co-tidal lines of the entire area are based on the observations of the tides on coastal stations, and on current observations made on a large number of anchor stations of the "Maud". Sverdrup's presentation has been reproduced in Fig. 190, which shows how the tide wave enters this area from the north (see Table 69). We see that

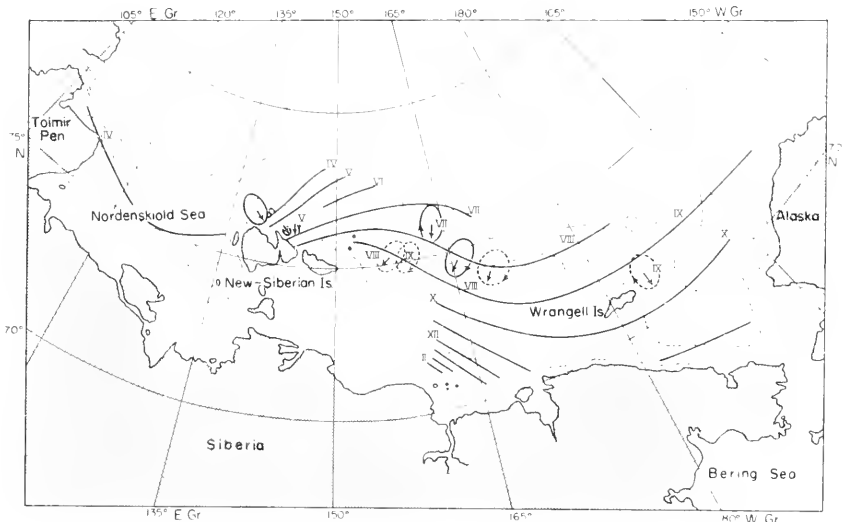


FIG. 190. Co-tidal lines and range at spring tide for the North Siberian Shelf. ····, curves indicate the depth contours for 25, 50, 75 and 100 m; the roman numerals indicate the time of the co-tidal lines and the time of high water at each station (Sverdrup).

the co-tidal lines have a tendency to be parallel to the bottom contour lines and to run directly towards the coast. The progressive character of the wave becomes thus apparent. Sverdrup draws special attention to the following points, which result from the discussion of the observations:

(1) The tidal currents are not alternating in the direction of progress of the wave, but throughout the area the currents rotate *cum sole* (see Table 70). The large and small axes of the current ellipses are about the same for all

Table 69. Tidal data at spring tide for points at the North Siberian Shelf
(according to Sverdrup)

Location (old and new names are given)	Geographical positions		Spring tide		$\frac{S_2}{M_2}$	$\frac{K_1 + O_1}{M_2 + S_2}$	Age of spring tide (in days)
	Lat. ϕ	Long. λ	Range (cm)	Establish- ment (h)			
Point Barrow	71.3 N.	156.7 W.	15	9.65	0.40	0.46	1.6
Cape Serdze Kamen (Cape Dezhneva)	66.9 N.	171.8 W.	14	6.73	0.70	0.44	—
Pitlekaj	67.0 N.	173.5 W.	7	11.71	0.38	0.73	2.3
Ajon Island (Aion)	69.9 N.	167.7 E.	5	12.33	0.48	0.26	2.0
Bear Island							
Medvezhi O.)	70.7 N.	162.4 E.	3	3.2	0.4	0.6	1.7
Station 3	74.7 N.	166.4 E.	18	8.2	—	—	—
Station 7	76.5 N.	144.0 E.	92	5.4	—	—	—
Station 8	76.5 N.	141.7 E.	210	5.0	—	—	—
Bennett Island	76.7 N.	149.1 E.	105	6.6	—	—	—
Cape Chelyuskin	77.6 N.	105.7 E.	34	3.88	0.42	0.40	1.5

stations on the open shelf, but are quite different for stations in the vicinity of the coast, where the currents become almost alternating and parallel to the coast.

(2) The currents are not uniform in the layers between the surface and the bottom of the ocean and show a definite correlation with the vertical density distribution (see p. 451). The time of the greatest velocity does not correspond exactly to the high water, but it occurs about 1 or 2 h earlier.

(3) The velocity of propagation of the wave differs considerably from the value $\frac{1}{2}gh$; when the current is rotating in a circle, the velocity is too large in comparison with the velocity of the formula, and too small when the current is more alternating.

(4) The tidal range varies from 210 cm (7 ft) directly north of the New Siberian Islands to only 3 cm (1 in.) at Bear Island. The amplitudes of the waves decrease along the co-tidal lines from right to left (taken in their direction of propagation) and also in the direction of propagation of the wave itself. The amplitude drops from 210 cm (7 ft) at the New Siberian Islands to 14 cm (1 ft) near Point Barrow, and in the direction of propagation they drop from 18 cm (1.5 ft) at a point 400 nm off the coast to 5 cm (2 in.) near the Aion Island and to 3 cm (1½ in.) near Bear Islands.

All these characteristics can be explained theoretically, if one considers the tide wave as a progressive wave affected by gravity, and takes into account the friction at the boundary and caused by turbulence. In connection therewith

Table 70. Current measurements on the North Siberian Shelf

No.	Date	Geographical positions		Bottom depth (m)	Depth in which tidal current measurement (m)	Maximum tidal current			Minimum tidal current	Ratio min. max.
		Lat. ϕ	Long. λ			cm/sec	Against true direction	Phase tidal hour		
1	8-10 Aug. 1922	71.3°N.	175.0°W.	76	0-20	16.5	S	9.5	13.0	0.79
2	20-21 March 1923	74.2°N.	169.7°E.	50	40	20.0	S. 45°W.	8.4	18.0	0.90
5	24-27 Nov. 1923	75.2°N.	159.7°E.	38	28	9.5	S. 55°W.	9.1	7.5	0.78
6	6-9 Feb. 1924	75.2°N.	157.7°E.	38	28	9.5	S. 55°W.	8.9	5.0	0.58
3	17-20 May and									
4	29 May-2 June 1923	74.7°N.	166.2°E.	56	0-56	3.8	S. 55°W.	8.2	3.0	0.79
7	27 Aug.-2 Sept. 1923	76.2°N.	164.0°E.	64	0-64	6.5	S. 15°W.	7.5	4.2	0.65
	30 June-3 July 1924	76.5°N.	144.0°E.	35	0-35	16.5	S. 10°E.	4.8	5.5	0.33
8	18 July 1924	76.5°N.	141.5°E.	22	0-22	38.0	S. 45°E.	3.0	5.0	0.13
9	1 Aug. 1924	76.6°N.	138.5°E.	22	0-22	22.5	S. 50°E.	2.2	13.0	0.58
Current measurement at St. 3										
3	17-20 May and 29 May-2 June 1923	74.7°N.	166.2°E.	56	0-30					
									Too weak to be measured	
					35	6.2	S. 50°W.	8.9	5.4	0.87
					42	15.4	S. 73°W.	8.9	12.9	0.84
					46	11.0	S. 29°W.	7.2	8.8	0.80
					50	5.4	N. 87°W.	6.8	2.8	0.52

Direction of rotation of current in all cases *cum sole*.

we refer to Fig. 136, which contains a schematic presentation of all important points.

Of particular interest is the vertical distribution of the tidal currents at the various stations. The conditions at a normal station were discussed on p. 333 (Fig. 137). If there is an uninterrupted layer of ice on a station, the distribution of the current becomes very much complicated. Fig. 191 illustrates the typical case of Station No. 3 (see Table 70). *A*, shows the graphical presentation of the component of the tidal current in the direction of progress of the wave in the form of a vertical section. The

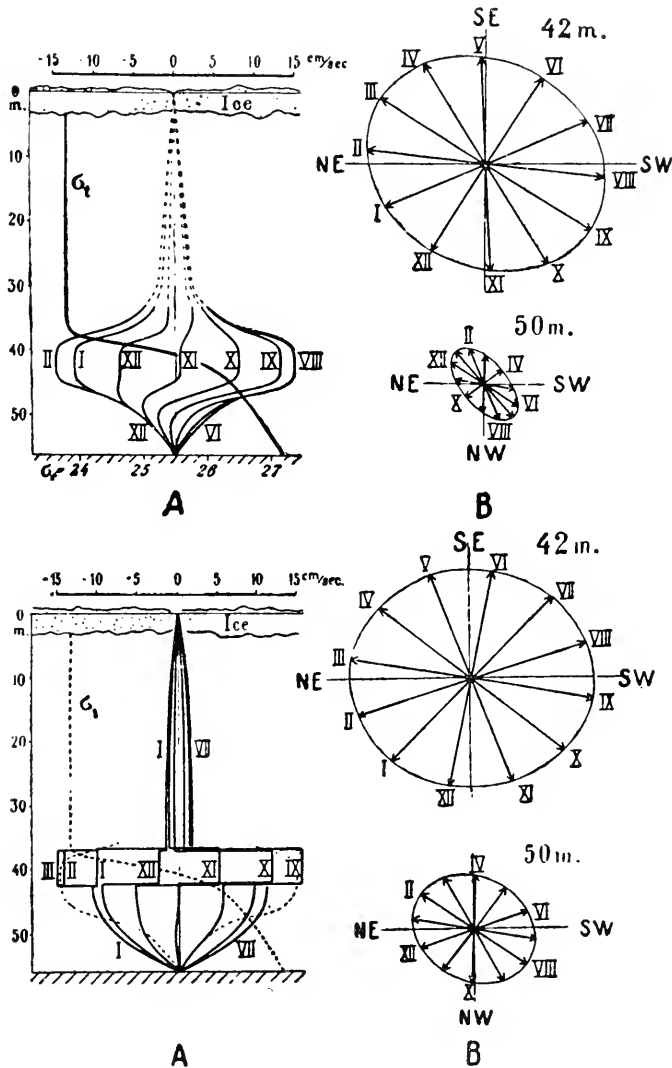


FIG. 191. Upper. A: Graphical presentation of the observed component of tidal currents in the direction of progress of the wave in the form of a vertical section, for Station 3 on the North Siberian Shelf. B: Current diagrams in 42 and 50 m depth. Lower: theoretical computation of these tidal currents (according to Sverdrup).

ice does not participate in the tidal motion and down to a depth of 35 m the velocity of the current is too weak to be measured. Below this depth there is a rapid increase of the velocity of the current; the maximum occurs in the discontinuity layer of the density at 42 m (see the vertical distribution of the density σ_t); then the velocity decreases towards the bottom. The current figures to the right under *B* show a rotation *cum sole* in all depths, but towards the bottom the ellipse becomes narrower and is turned to the right in comparison with the upper layers and maximum current occurs earlier.

The lower presentation of Fig. 191 refers to a theoretical computation of these currents, assuming that the upper and bottom layer had a constant eddy viscosity separated by a layer of no-eddy viscosity, which coincided with the discontinuity layer, which has great stability. The computed currents deviate, of course, from the observed ones, because the discontinuity layer is replaced in nature by a gradual density increase. But there is agreement as to the main features, so that there is no doubt that the rotation of the earth and the turbulence varying in the vertical direction determine the character of the currents at the observed station.

22. The Tides in Inland Seas

In order to determine the order of magnitude of the tides in inland seas of various dimensions, let us refer to the equations in Chapter IX, para. 3, (b); (p. 293). Table 71 shows that in small, shallow seas the tidal ranges can be expected at spring tides to be of the order of magnitude of 2–3 mm, which can increase to 10 cm and more for large seas with a long period of free oscillation.

Table 71. Range of the tides in lakes

Natural period T_f (h)	Length (km)	$r = T_f : T_\alpha$	$\beta = \frac{\tan \pi}{\text{arc } 2} r$	Range of	
				M_2 (mm)	$M_2 + S_2$ (mm)
$\frac{1}{2}$	25	0.04	1.00	1.5	2.2
1	50	0.08	1.006	3.0	4.4
3	150	0.24	1.05	9.6	13.9
6	300	0.48	1.24	22.5	32.4
9	450	0.72	1.88	51.4	74.7

High water	{ western end	3 h	centre meridian time
	{ eastern end	9 h	

The amplitude and the phase of such forced tidal oscillations in inland seas have only some value if it is possible to subject a long series of observations collected by very sensitive limnographs to a harmonic analysis; otherwise the result will be inaccurate, because the influences caused by the free oscillations (seiches) and other unperiodical variations like those caused by wind and air pressure will be large compared to the small tidal amplitude. The problem is the same as the analysis of the atmospheric tides from ordinary barometric registrations, which was solved successfully, even for stations at higher latitudes, where the unperiodical disturbances in atmospheric pressure are larger than the very small atmospheric tides (see BARTELS, 1928, p. 163).

The oldest observations of tides in inland seas are those of the large North American lakes. HARRIS (1908, p. 483) has published the results of the harmonic analysis of observations for four localities at Lake Michigan and Lake Superior and has compared them with the results of the improved equilibrium theory. The complete agreement shows that we have to do with actual astronomical tides. Later on, ENDRÖS (1930, p. 305) has analysed the curves of Lake Erie published in a paper of Henry. He found, besides the free oscillations, both the M_2 and the S_2 tide in the observations at Buffalo at the eastern end and in Amsterburg at the western end. High water occurred in Buffalo at 3 h, in Amsterburg at 9 h, so that we have here *indirect tides*. This had to be this way, because ν is for M_2 and S_2 , 1.15 and 1.19 respectively.

Table 72. Tidal data observed in lakes and inland seas

(1) Harmonic constants for the Great Lakes (Harris, 1907).

Components	Lake Michigan (Milwaukee)		Lake Superior (Marquette)		Lake Superior (Duluth)			
	$\phi = 43\ 02'N.$ $\lambda = 87\ 54'W.$		$\phi = 46\ 32'N.$ $\lambda = 87\ 23'W.$		$\phi = 46\ 47'N.$ $\lambda = 92\ 05'W.$			
	H (ft)	K (°)	H (ft)	K (°)	H (ft)	K (°)	H (ft)	K (°)
K_1			0.0066	263.03	0.0297	85.04	0.0035	99.37
M_2	0.0247	37.4	0.0130	298.84	0.0631	71.05	0.0658	72.22
S_2	0.0103	48.3	0.0086	349.33	0.0336	87.91	0.0337	87.70

(2) Lake Erie (Endrös). Amsterburg, west end: time of high water (local time for centre meridians) for M_2 ; 8.5 h; for S_2 ; 8.6 h.

Amplitude (mm)	M_2	S_2	N_2	K_2
Observed	52	19	12	5
Computed	54	19	13	5.3

(3) Lake Balaton (Endrös). Time of high water at the Syzygies: east end Kenese, 9 h; west end Keszthely, 3 h; amplitude 5-6½ cm for both ends.

(4) Lake Baikal (Sterneck). Penschannja Bay (52°15'N., 105°43'E.).

Component		M_2	S_2	N_2	K_2	K_1	P_1	O_1
Amplitude H (mm)	Observed	4.5	2.9	0.8	0.7	3.5	0.8	2.2
	Computed	8.6	4.0	1.7	1.1	4.8	1.6	3.4
Phase α (degrees)	Observed	47°	65°	53°	56°	74°	73°	63°
	Computed	50°	50°	50°	50°	70°	70°	70°

The amplitudes resulting from the analysis of the various components are given in Table 72; underneath these are the theoretically computed values, and one can see the complete agreement between the observations and the theory. In HAYFORD'S paper (1922) which deals with the variations in the sea level of Lake Erie there are also definite indications of the presence of the tide wave, which is, however, concealed by the strong free oscillations of the lake.

Endrös has also proven the semi-diurnal tide wave for Lake Balaton (Hungary) from the limnographic registrations of CHOLNOKY (1897) for the period 1892-96. He showed that the western end has high water at 3 h, the eastern end at 9 h. The tidal ranges at the time of the syzygies were between 10 and 13 mm. The uninodal period of the free oscillation of the lake has a duration of 9.4-10 h, so that ν lies between 0.75 and 0.85. The theory gives tidal ranges of 13-15 mm for the semi-diurnal tide wave, which come very close to the observations.

ENDRÖS has proven that in smaller seas there are occasionally tide waves contrary to the opinion expressed by Forel. The Lake of Geneva has semi-diurnal waves which were observed at its western end (Secheron) with a high water between 2 and 3 h and a low water between 8 and 9 h. The tidal range is only 1.9 mm. Superimposed to these semi-diurnal waves is a stronger diurnal wave with a 2.8 mm tidal range and which is probably of meteorological origin. These tide waves can only be found with any certainty from the limnograms on days when seiches are non-existent, but the comparison with the expected tides from the theory proves beyond doubt that we have to do with pure tides. As, in such cases ν is very small one can apply the simple equilibrium theory. We find for the semi-diurnal tides a tidal range of 5.1 mm and, considering also the north-south oscillation at the western end, an establishment of 2 h. This agrees very well with the observations; the observed tidal range is only one-third of the theoretical value. Frictional influences can hardly cause such a strong decrease of the tidal ranges, but perhaps we attribute this decrease to the tides of the solid earth (see Chapter XV).

The question as to whether tide waves can be detected in *every* lake by means of properly made observations must be answered affirmatively.

The deep Baikal Lake (about 615 km (380 miles) long) has been thoroughly investigated. JERIMOV and KRAWETZ (1926, p. 54) have computed the first reliable tidal constants of the main lunar tide of the lake from two year's registrations made in the Penrtschannja Bay ($\phi = 52.15^\circ\text{N}$, $\lambda = 105.43^\circ\text{E}$). Later on, STERNECK (1926, p. 316; 1928, pp. 147, 221) has made a more complete analysis of these observations, whose results agree with those obtained by the Russian scientists. Sterneck computed for the two components M_2 and K_1 as principal representatives of the semi-diurnal and diurnal tides respectively, the distribution of the tidal ranges and phases for sixteen cross-

sections along the lake, according to the canal theory. Figure 192 shows a clockwise rotation of the M_2 high water around Lake Baikal, but with extraordinarily rapid transitions in the centre of the lake. Therefore, the tide wave corresponds almost exactly to a standing wave with the phase 2.1 h at the south-west end and a phase of 7.0 h at the north-east end. A com-

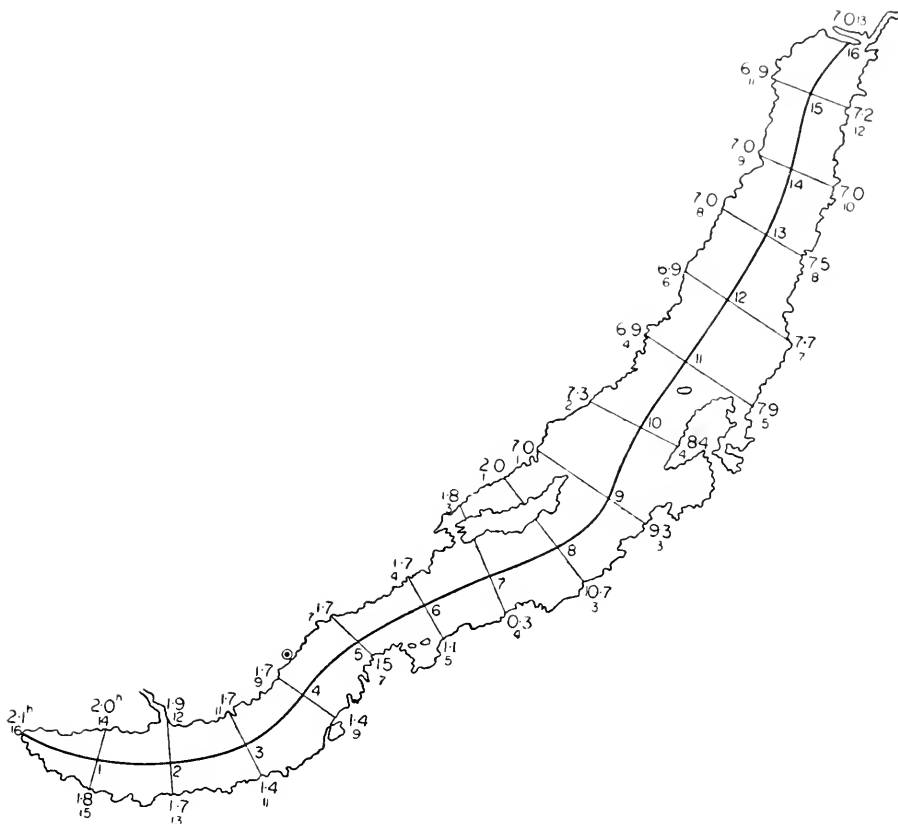


FIG. 192. Theoretical M_2 tide wave in Lake Baikal. At each end of each cross-section is indicated the time of high water in lunar hours referred to the centre meridian of the lake; and the numbers below indicate the amplitude in mm. \odot is the position of Penrtschannja Bay.

parison of the theoretical amplitude with the amplitude derived from the harmonic analysis shows (see Table 72) that the former is nearly twice as large, whereas the phases are almost exactly the same. The difference between the times of high water for M_2 at both ends of the lake is not 6 but 5 lunar hours, which can be considered as a consequence of the bend in the lake. Similar conditions exist for the K_1 tide; only the amplitudes here are in better agreement with the observed values. The fact that the observed amplitudes

are smaller than those computed theoretically should be attributed, according to Sterneck, to frictional influences which might perhaps be stronger between cross-sections 4 and 6 (see Fig. 192), where the lake is relatively shallow. GRACE (1931, p. 301) has, however, expressed the opinion that the effect of the tides of the solid earth might manifest themselves, and he has been able to prove that this assumption can explain perfectly the decrease of the amplitudes (see Chapter XV, p. 508).

Chapter XIII

Tides in Estuaries

1. Observations

THE tides of the open ocean cause oscillations in estuaries which make the water level rise and fall with the tides. The place up to where the effect of the tides is noticeable is called *the tide mark*.

That part of the river which is subject to the tides of the oceans and which stretches from the estuary to the tide mark is here called the river tide zone or briefly tide zone. The Amazon River seems to have the longest tide zone. According to La Condamine, the tidal mark lies near Obidos, i.e. 850 km from the opening; however, BATES (1863, p. 133; see also SCHICHEL, 1893, p. 100) still found tidal effects in the Cupari, a minor tributary of the Tapajoz ending near Santarem, which is at a distance of 870 km from the ocean. In the case of the Congo River the tide mark is only 170 km from the Atlantic Ocean, because the rapids near the estuary prevent a further extension of the tide zone. In the Yangtse Wuhu River the length of the tidal zone is 500 km; in summer, the tidal effects are completely suppressed by the high current velocities in the swollen river (HOFMEIER, 1901).

The tidal wave penetrating into the river is subjected to some characteristic modifications especially by the decrease in depth and the ensuing increased friction and by the river flow itself. These influences must be considered chiefly as being of a hydraulical nature and are much more subjected to the external conditions than the purely hydrodynamical occurrences.

Systematic investigations of the tide zone were made for a few European rivers only, and not all observational data have the reliability one would desire. The most important feature is the shape of the tidal curve. Whereas it is still entirely symmetrical in the open ocean in front of the estuary, the curve becomes asymmetrical in the river. The water-level shows a quicker rise and a slower fall, so that the duration of the flood is shorter than that of the ebb. Table 73 gives a series of data for the Elbe and the Weser, according to FRANZIUS (1880, p. 299); for the Gironde and Garonne according to COMOY (1881); for the St. Lawrence River according to BELL DAWSON (1824, p. 141). Figure 193 gives as examples tidal curves of the Elbe for three periods of 12 lunar hours, whereas Fig. 194 shows tidal curves for Father Point and Quebec at the St. Lawrence River for the period from 6 to 9 October, 1896, which illustrated clearly the asymmetry.

This increasing asymmetry can only occur when the velocity with which the peak of the tide wave (high water) travels differs from the velocity of the foot of the wave (low water). Table 74 gives for the same rivers these velocities

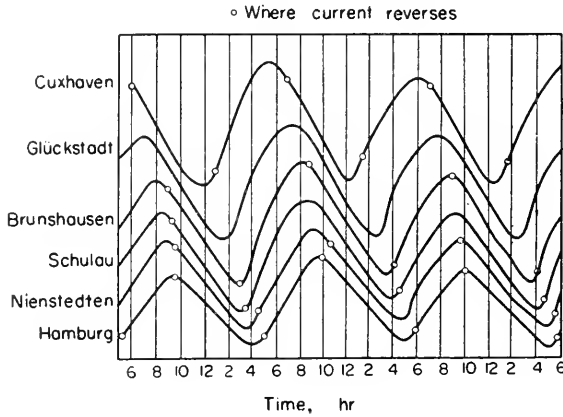


FIG. 193. Tide curves in the "River tide zone" of the Elbe; ◦ indicates slack water. Height scale about 1 : 170.

according to the same sources. In fact, they are different according to the depth of the rivers, but the high-water values are everywhere considerably

Table 73. *Asymmetry of the flood wave in estuaries*

	Rising flood hours	Falling ebb hours
Elbe (1-2 August, 1854)		
Cuxhaven	5 h 42 min	6 h 42 min
Brunshausen	5 h 30 min	6 h 54 min
Nienstedten	4 h 54 min	7 h 30 min
Hamburg	4 h 24 min	8 h 0 min
Weser (25 December, 1877)		
Bremerhaven	5 h 18 min	7 h 12 min
Vegesack	4 h 12 min	8 h 12 min
Bremen (Börsenbrücke)	3 h 30 min	8 h 54 min
Gironde (spring tide — 19 September, 1876)		
Pointe de Grave (Estuary)	6 h 10 min	6 h 8 min
Pauillac	4 h 41 min	7 h 37 min
Bordeaux (Garonne)	3 h 45 min	8 h 33 min
Castets (limit of flood in the Garonne)	2 h 10 min	10 h 8 min
St. Lawrence River (mean values)		
Father Point	6 h 13 min	6 h 12 min
Rivier du Loup	6 h 9 min	6 h 16 min
Orignaux Point	6 h 0 min	6 h 25 min
Grosse Isle	5 h 22 min	7 h 3 min
Quebec	5 h 2 min	7 h 23 min

greater than the low-water values. According to Comoy, the velocity of the foot of the wave in the French rivers seems to correspond to the formula $v = \sqrt{gh} - U$, in which h is the depth at low water and U the velocity of the river water (head water) downstream.

Table 74. *Velocity of the crest (high water) and of the trough (low water) of the flood wave in rivers*

	Velocity (m/sec)	
	Crest (H.W.)	Trough (L.W.)
Elbe between:		
Cuxhaven and Brunsbüttel	7.45	6.02
Brunsbüttel and Glückstadt	6.59	6.59
Glückstadt and Brunshausen	5.41	4.58
Brunshausen and Lühe	8.02	5.73
Lühe and Hamburg	6.30	4.58
Hamburg and Buntehaus (North Elbe)	4.87	2.29
Weser between:		
Bremerhaven and Brake	9.50	4.30
Brake and Farge	7.02	2.55
Farge and Vegesack	6.66	2.81
Vegesack and Bremen	2.73	1.77
Bremer Sicherheitschafen and Börsenbrücke	1.00	0.90
Gironde and Garonne between:		
Pointe de Grave and La Maréchale	15.70	5.72
Bec d'Ambès and Bordeaux	7.66	4.85
Langon and Castets	3.25	2.36

The data in Table 74 apply for normal tide waves. At spring and neap tide conditions can be different; especially at neap tide the foot of the wave seems to travel faster upstream, in the lower section of the tide zone, than at spring tide. Thus, this velocity was, on 26 September 1875, in the Gironde between Pointe de Grave and La Maréchale, 17.95 m against only 5.72 at spring tide on 19 September. However, upstream the difference soon became smaller and the velocity at neap tide was already somewhat smaller than at spring tide (near Bordeaux 4.51 against 4.85). The cause of this remarkable difference is that at neap tide the low water is not so well developed as at spring tide and that the water depth is greater at neap tide than at spring tide. However, v adjusts itself according to h . The range of the river tides in most cases first increases somewhat up stream. Then, from a certain point, it decreases again slowly to the tide mark; see as an example Table 75.

Another characteristic feature of the tide zone is that the peak of the tide wave along the tide zone (the high-water mark) maintains almost the same *absolute* height from the ocean to the tide mark or rises slightly only in the upper section of the tide zone. Irregularities are due to local widenings or narrowings of the cross-section of the river. Table 75 shows, after Comoy, the elevations of the wave crest above normal datum (NN) of the French general levelling for the various points along the Gironde and the Garonne

for the spring tide of 19 September, 1876. The high water line rises slowly but continuously from the mouth to the tide mark by somewhat more than 2 m, i.e. there is a rise of 2 m over a distance of 150 km, which must probably

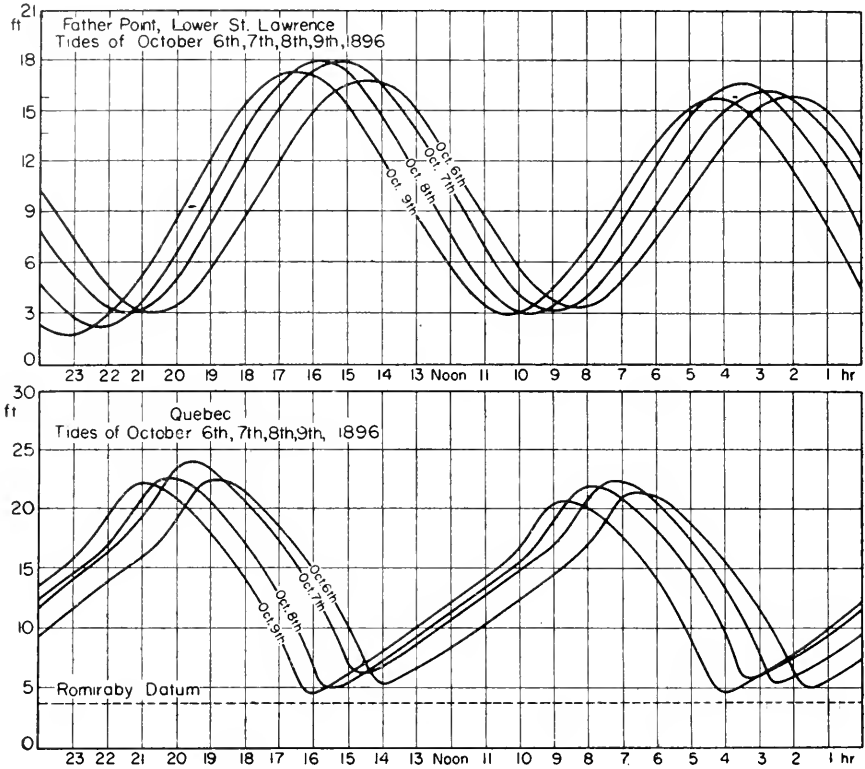


FIG. 194. Tide curves of Father Point and Quebec at the St. Lawrence River from 6-9 October, 1896.

be attributed to the slope of the river water (head water). For other French rivers (see Table 76) this slope is not so well developed and, over some distance, its direction is reversed. The variations, however, are very small.

According to Franzius, the same applies for the Elbe and the Weser, as is shown in Table 77 for tides with an average range. The difference in level between the mouth and tide mark is at high water for the Elbe +1.28, for the Weser +1.68 m, so not very large.

On the contrary, the level of the low water (low-water line) deviates considerably from the horizontal and shows everywhere a strong slope downstream (for the Elbe +4.14, for the Weser +5.06 m). A difference between spring and neap tide is very obvious, as Table 75 shows for the Gironde-Garonne. The low-water line in the lower section of the tide zone lies deeper at spring tide than at neap tide, and in the upper section it is higher at spring

tide than at neap tide. This is an essential difference between the river tides and the ocean tides, whose low waters are, always and everywhere, lower at spring tide. A graphic presentation of the values of Table 75 shows that

Table 75. Tides in the Gironde and Garonne Rivers *

Place	Distance from mouth (km)	Range (m)	Height of high water above NN (m)	Difference between low water and NN at		Height of mean sea level above NN at	
				Spring tide (m)	Neap tide (m)	Spring tide (m)	Neap tide (m)
Gironde							
Pointe de Grave	0	4.75	2.80	-1.96	-0.05	0.42	0.12
La Maréchale	38	4.95	3.22	-1.76	-0.45	0.74	0.60
Pauillac	51	5.06	3.35	-1.72	-0.56	0.82	0.58
Blaye	61	5.27	3.40	-1.89	-0.66	0.76	0.51
Bec d'Ambès	72	4.97	3.52	-1.48	-0.73	1.03	0.54
Garonne							
Bordeaux	95	4.78	3.72	-1.04	-0.81	1.33	0.57
Portets	116	4.12	4.02	-0.10	-0.38	1.96	0.96
Cadillac	131	2.48	4.16	+1.68	+0.99	2.92	1.72
Langon	142	1.04	4.42	+3.38	+2.81	—	—
Castets	149	0.24	4.98	+4.74	+4.11	—	—

* According to M. Comoy, spring tide 19 September, 1876.

the connecting line between the low waters of the spring tide cuts the one of the neap tides in the upper section of the tide zone. For the Garonne, this point of intersection lies between Bordeaux and Portets. This, however,

Table 76. Level of high water of rivers in France
(According to M. Comoy)

Loire		Charente		Seine		
Distance from mouth (km)	Height of high water (m)	Distance from mouth (km)	Height of high water (m)	Distance from mouth (km)	Height of high water (m)	
					1st H.W.	2nd H.W.
0	3.480	0	3.21	0	3.92	3.46
13.5	3.307	19	3.24	24	4.33	3.61
35.5	3.657	68	2.71	96	3.21	3.50
51.5	3.237	80	2.82	136	3.71	3.93
55.5	3.267					

holds only when the head water is equally large at spring and neap tides. When the head water increases at spring tide, this point of intersection moves downstream; if the head water decreases, the point moves upstream. In case of great drought and correspondingly little head water, the surface level lines for neap and spring tide do not intersect at all.

Table 77. Tides in Elbe and Weser *

Elbe				Weser			
Place	Distance (km)	Low water (m)	High water (m)	Place	Distance (km)	Low water (m)	High water (m)
Cuxhaven	0	0.03	2.89	Bremerhaven	0	0.66	4.12
Brunsbüttel	28.1	0.16	2.87	Nordenham	10.3	0.88	4.26
Glückstadt	46.9	0.14	3.01	Brake	27.4	1.30	4.40
Brunshausen	70.7	0.29	3.06	Elsfleth	34.7	1.46	4.43
Lühe Estuary	80.3	0.87	3.10	Farge	42.0	1.86	4.44
Blankensee	91.8	1.18	3.15	Vege sack	50.5	2.40	4.44
Hamburg	102.2	1.36	3.24	Hasenbüren	59.0	2.80	4.54
Buntehaus	115.2	2.59	3.35	Bremen (Free Port)	64.0	2.96	4.62
Hoopte	126.3	3.49	3.69	Bremen (Large Weser Bridge)	68.0	3.94	4.68
Elbstorf	135.6	4.17	4.17	Habenhausen	74.9	5.72	5.80

* According to L. Franzius. The heights for the Elbe refer to "Cuxhaven Zero". The heights for the Weser refer to a plane which is 5 m below "Bremen Zero".

Whereas for localities on ocean shores the mean sea level (average value of the ordinates of the tide curve) has a constant value and varies only very little locally, the line connecting the mean water levels for the localities along the tide zone is a curve varying very much from one locality to another; the mean water at spring tide lying definitely higher than that at neap tide. A decided slope downstream develops only in the upper part of the tide zone (see Table 75).

Particularly remarkable in the river tides are the tidal currents within the tide zone. There, the flow of the river will be reversed for several hours, which is the most striking feature to the "islander". We can take as a simple example, the Elbe near Cuxhaven, as shown in Fig. 195. The flood current starts about 1 h 30 min after low water, and the ebb current about 1 h 25 min after high water. The currents alternate after (and not *at*) the water has reached its maximum and minimum heights. The lag after low water seems to maintain itself up stream approximately with the same amount. According to Franzius, this lag is in the Elbe near Cuxhaven 1 h 20 min, near Brunshausen 20 min, near Nienstedten equally 20 min, near Hamburg 25 min. According to Comoy, the lag of the ebb current after low water is of the same

order of magnitude in the French rivers (Charente near Taillebourg 30 min, 12 km upstream near Saintes 40 min, Ardour near Urt 25 min, 13.4 km upstream near Lannes 30 min). It seems that upstream the head water feeds the ebb current for a longer period of time than could be expected from the wave motion alone, probably because of its gradient.

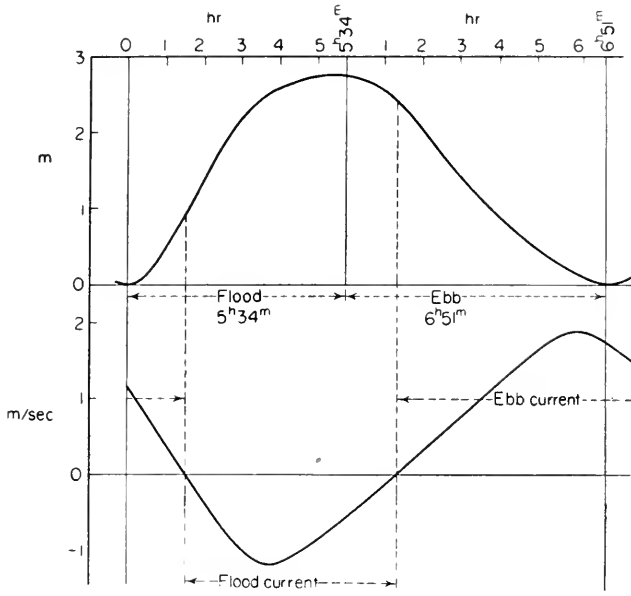


FIG. 195. Tide curve and tidal current at Cuxhaven.

The flood current, on the contrary, alternates more close to high water the more we get upstream; thus, near Cuxhaven it is 1 h 30 min after high water, near Brunshausen and Nienstedten 30 min, near Hamburg 12 min after high water. Table 78, gives the velocities of the tidal current of the Elbe and Weser. The flood current, near the entrance, is generally stronger than the ebb current. In the Elbe the slope of the upper stream starts to make itself felt close to Hamburg; in the Weser no flood stream is noticeable above Vegesack, only a stowing of the water by the tidal wave from 1 to 2 min; to the contrary, the ebb current has a velocity up to 0.7 m/sec.

The velocity of propagation of the high water (crest of the flood wave) upstream is for the lower Elbe, according to Table 73 of the order of magnitude of 6 m/sec; the velocity of the flood current, according to Table 78 does not quite reach one-tenth thereof. If c is the mean velocity of the flood current, V the mean velocity with which slack water at the end of the flood current progresses up stream (average velocity of propagation of the flood wave) and T the duration of the flood, then TV is the length of the wave crest. According to Comoy, the water travels upstream during time $(TV)/(V-c)$, so that the distance covered during that time is $S = (TVc)/(V-c)$. This equation has been used to compute how far saline sea water will penetrate up the river. For the Gironde we have $T = 22,200$ sec, $V = 12$ and $c = 1.9$ m/sec, so that $S = 50.2$ km. The observations showed that sea-water was still present near Pouillac, 51 km from the mouth. For the Elbe near Cuxhaven

we have $T = 5 \text{ h } 30 \text{ min} = 19,800 \text{ sec}$, $V = 7.45$ and $c = 1.08 \text{ m/sec}$, which gives $S = 25 \text{ km}$, a point still below Brunsbüttel. According to the observations, with normal head water and tidal range, the Elbe water has no seawater at low water at Brunsbüttel, at high water near Glückstadt. This equation should, however, be used cautiously, for it ignores the stratification of fresh water and sea water within the river current. In reality, the tide causes a mixing of the two kinds of water, through which fresh water is transported more rapidly downstream, and sea water further upstream than if the streamlines of the separate layers were completely parallel.

Table 78. Tidal currents in the Rivers Elbe and Weser
(According to Franzius)

Elbe			Weser		
Place	Velocity (m/sec)		Place	Velocity (m/sec)	
	Flood	Ebb		Flood	Ebb
Below Brunsbüttel	0.59	0.57	Bremerhaven	0.76	0.63
Above Brunsbüttel	0.65	0.58	Dedesdorf	0.77	0.55
Brunshausen	0.48	0.41	Brake	0.55	0.36
Lübe	0.33	0.31	Elsfleth	0.74	0.51
Hamburg	0.17	0.35	Vege sack	0.20	0.60
			Bremen	0.00	0.70

The tidal curves of the tidezone often show irregularities caused by the important shallow water tides (harmonic and combined tides); often there is a double, in rare cases a triple high water. The latter case is known to happen in the Forth River up to Stirling and is called "Leaky". The tidal curve of Southampton also shows three secondary maximas which for 3 full hours keep the high water level which is so very useful for navigational purposes. In the Seine there are also two secondary high waters, even a third one near Isigny, and at Le Havre. Similar phenomena occur in the estuary of the Sao Francisco and of the Paranagua at the coast of Brazil, where there are four high waters in 24 h, two higher and two lower, which are called "meias marés". Such irregularities are always connected with particularly shallow water.

2. Theoretical Considerations Regarding River Tides

If a channel with a uniform cross-section and a level bed opens up into a sea with tides, its water-masses will be forced by these tides to co-oscillate at the mouth. As in estuaries the water depth is small and decreases gradually upstream, the periodical variations in water level in the river will hardly be of the form of a standing wave, as is the case with deeper, canal-like adjacent seas. The effect of the friction will give it the character of a progressive wave travelling up the river. As the velocity of propagation with small water depth is very small, it can happen, in the case for great, long rivers, that, before a tide wave reaches the tide mark, a new wave has already arrived in the

estuary. According to FRANZIUS (1901, p. 229), this happens on the Elbe and the Weser, where there are at the same time two tide waves; on the Amazon River, whose tide zone is nearly 1000 km long, there are sometimes even seven or eight tide waves present at the same time. Assuming that the tidal curve at the mouth is represented by a simple sinus curve, we have in

$$h + \eta = a + b \sin \frac{2\pi}{T} t \quad \text{or} \quad \frac{\eta}{h} = \frac{a-h}{h} + \frac{b}{h} \sin \frac{2\pi}{T} t, \quad (\text{XIII. 1})$$

which h is the height of the undisturbed water-level of the river, η the elevation above this level and a can only be slightly different from h . The water surface behaves like a "bore" and according to (VI.13) and (V.12) respectively its water volume travels upstream with velocity: $c = \sqrt{gh} (1 + \frac{3}{4} \eta/h)$.

During a full period T , the amount of water $\int_0^T c \eta dt$ penetrates into the river. If we neglect the small term $(a-h)^2$, the integral gives

$$ha = \frac{3}{8} (b^2/a). \quad (\text{XIII. 3})$$

This means that the mean water level does not correspond to the sea level at the mouth of the estuary, but is lower by $\frac{3}{8} (b^2/a)$. This difference is noticeable; for $a = 6$ m below the mean sea level and an elevation of 3 m above it, this difference in level is 0.25 m. This is, in fact, what the observations show (see LEVY, 1898).

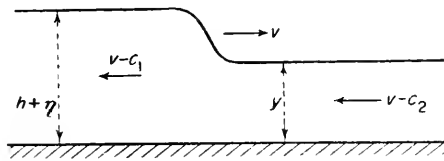


FIG. 196. Relationship between velocity of progress V , velocity of current c and height η of a bore.

The retarding influence of the friction appears particularly, according to M. MÖLLER (1896, p. 479), in the correlation between the velocity of propagation V of the flood wave, the velocity of the current c and the tidal range η . If there is a "bore" out at sea with a velocity of propagation V which travels upstream (see Fig. 196), and the velocity of the current is c_1 out at sea and c_2 in the river, the relative velocities compared to the bore are $V - c_1$ and $V - c_2$. Möller now imagines the bore to be fixed and applies Bernoulli theorem to the current; then

$$(V - c_2)^2 - (V - c_1)^2 = 2g\eta, \quad (\text{XIII. 4})$$

and the equation of continuity gives

$$h(V - c_2) = (h + \eta)(V - c_1), \quad (\text{XIII. 5})$$

if h is the water depth in front of the bore. From these two equations we obtain

$$\frac{2\eta h}{h^2} (V - c_1)^2 \quad \text{and} \quad \frac{2\eta(h + \eta)}{(h + \eta)^2} (V - c_2)^2 = 2g\eta \quad (\text{XIII.6})$$

respectively, and substituted into (XIII.4) when the height of the bore is small,

$$V - c_1 = \mathbf{J}(gh) \quad \text{and} \quad (V - c_2) = \mathbf{J}[g(h + \eta)]$$

respectively, which is in excellent agreement with the equation found by Scott Russell for the propagation of wave disturbances with an elevation η above the undisturbed water level over a depth h (see (V.14) on p. 118). With the small current velocities in the river in front of the bore (XIII.4) becomes

$$c_1 = V - \mathbf{J}(V^2 - 2g\eta). \quad (\text{XIII.7})$$

The changes in the form of the waves when they pass from deeper into shallower water have been discussed in more detail in the chapter concerning shallow water waves (see p. 109). With a gradual change of the width b and the depth h of a canal in which a flood wave travels, the amplitude of the wave varies according to GREEN (1837) according to $b^{-1/2}h^{-1/4}$. When a flood wave approaches the coast, there is no variation in b , but h does vary and, for this reason, the wave amplitude increases approaching the shore. In a river in which b varies also, there is another increase of the amplitude. Besides the decrease of the water depth causes the waves not to travel any more with the same constant velocity of propagation, but with each rise and fall of the surface the wave will travel with a velocity depending on the existing depth. If h is the depth before the wave has arrived and η the actual water depth when the wave is there, then this special velocity is $c = g^{1/2}(3\eta^{1/2} - 2h^{1/2})$.

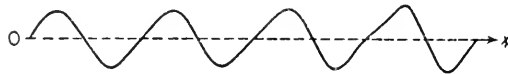


FIG. 197. Progressive changes of wave profile in shallow water.

For waves with small amplitude η is approximately equal to h , and the velocity of propagation is equal to that of the long waves: $\mathbf{J}(gh)$. However, if the amplitude becomes comparable with h , parts of the wave crest move faster than those of the wave trough. The flood waves then cannot propagate without changing their profile. With decreasing water depth, the slope of the waves becomes steeper and steeper on the front side and gentler on the rear side, until finally a state develops in which the wave breaks and surges. Equation (V.21 (p. 122)), which was developed by Airy, gives the curve of Fig. 197. It shows a succession of profiles of a single flood wave which travels up a river. The steepening of the front side of the progressing wave adopts finally the form of a bore, as shown in Fig. 196. FJELDSTADT (1941) has

given a mathematical solution for the change in profile of a breaking flood wave, which reproduces exactly all the stages a wave goes through.

The changes in shape which the waves undergo in a river are also influenced by the fact that the river water flowing downstream forces the sea water back, which increases the steepness of the wave.

POINCARÉ (1910, p. 409), following computations by Saint-Venant, has given a mathematical most extensive theory of the river tides, taking into account all important factors. Furthermore, KREY (1926) has given a survey of the tide waves in estuaries with applications of a hydraulic nature. The tide in channel-like bays and estuaries are characterized by the same basic equations, as apply to the co-oscillating tides in adjacent seas (p. 143). As for small channels and estuaries the Coriolis force is of no importance, the general equations reduce to the one-dimensional case. Taking account of the friction at the bottom and designating by \bar{u} , η and τ the mean values of velocity, vertical motion and bottom stress, respectively, over the entire cross-section S of the width b , we obtain the equations of motion and the continuity equation in the following form:

$$\left. \begin{aligned} \frac{\partial \bar{u}}{\partial t} + \bar{u} \frac{\partial \bar{u}}{\partial x} + g \frac{\partial \eta}{\partial x} &= \frac{b}{S} \tau, \\ \frac{\partial \eta}{\partial t} + \frac{1}{b} \frac{\partial}{\partial x} (S \bar{u}) &= 0. \end{aligned} \right\} \quad (\text{XIII. } 7a)$$

The bottom stress (friction at the bottom) τ can be considered proportional to the square of the mean current velocity:

$$\tau = k \bar{u} |\bar{u}|,$$

where $k = 2.6 \times 10^{-3}$ (see p. 346, XI. 32). HANSEN (1956) has used these equations to compute for the estuary of the Ems River the total tide distribution up to about 100 km upstream (Herbrum) from the boundary values at the mouth into the North Sea (near the Island of Borkum; heights of the water level on (25 June 1949) and from the freshwater transport of the Ems near Herbrum. The method of boundary values was applied, which was also developed by HANSEN (pp. 372 and 362) to compute the tides of the North Sea. The section of the Ems between Borkum and Herbrum, measuring 102 km in length, was subdivided into intervals of 2 km each; the variations of the water levels were numerically determined for points 4, 8, 12, ..., 100 km from the mouth and the current velocity for points 2, 6, 10, ..., 98 km. In Fig. 197a, the estuary of the Ems is shown on the left-hand side, while to the right there are given the observed and computed water levels and current velocities in this river (25 June 1949) for some points of the estuary as shown to the left. The agreement between the observed and computed water levels and between the current velocities is quite remarkable and even shows details of the curve shape. Much earlier, hydraulic specialists have developed several methods to compute

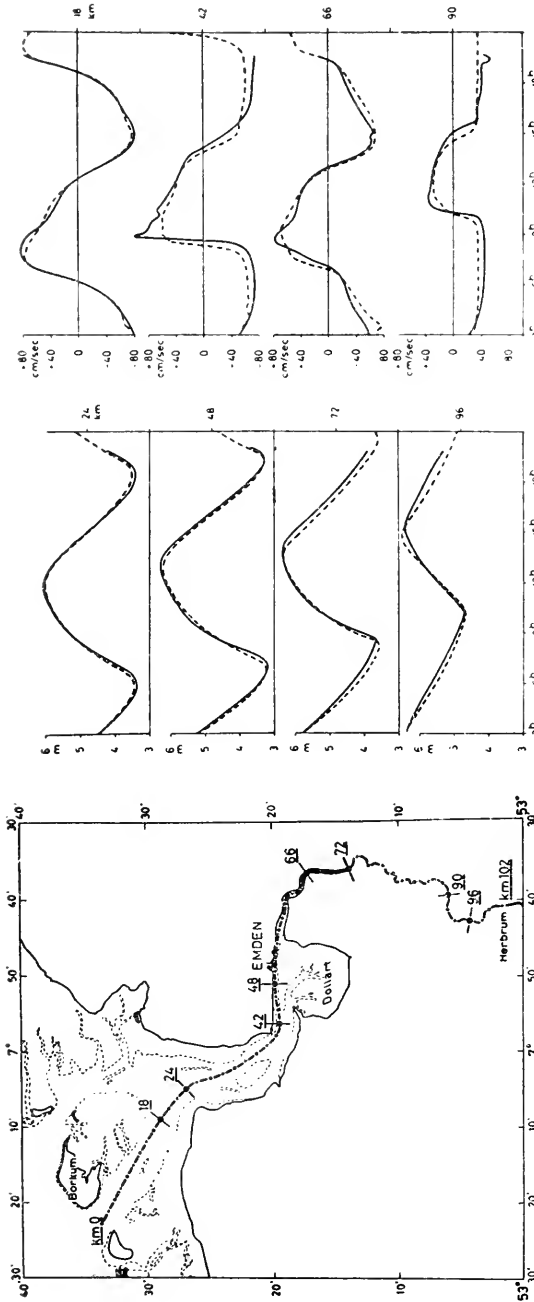


FIG. 197a. Left: Tide estuary of river Ems. The grid coincides with the axis of current. The numbers give the distance in km, upstream from the mouth at Borkum. Center and right: observed (—) and calculated (-----) water-levels and velocities of current of Ems on 25/6/1949. For comparison are given the water-levels at 18, 42, 66 and 90 km distance from the estuary (after HANSEN, 1956).

tides estuaries and have also obtained good results; Hansen's method is a purely numerical one and is a special case of the common two-dimensional case given on page 362. It goes without saying that these methods are of great practical importance.

3. Bores

In a large number of rivers the wave profile of the tide wave travelling up the river changes into what is called a "bore" (in French: *mascaret*). A wall of water with a steep front over the entire width of the river gushes upstream. This phenomenon is characteristic of most funnel-shaped estuaries with shallow depths at low water. In the larger German rivers there is no bore; it is said that there was one in the Ems before its regulation. It is

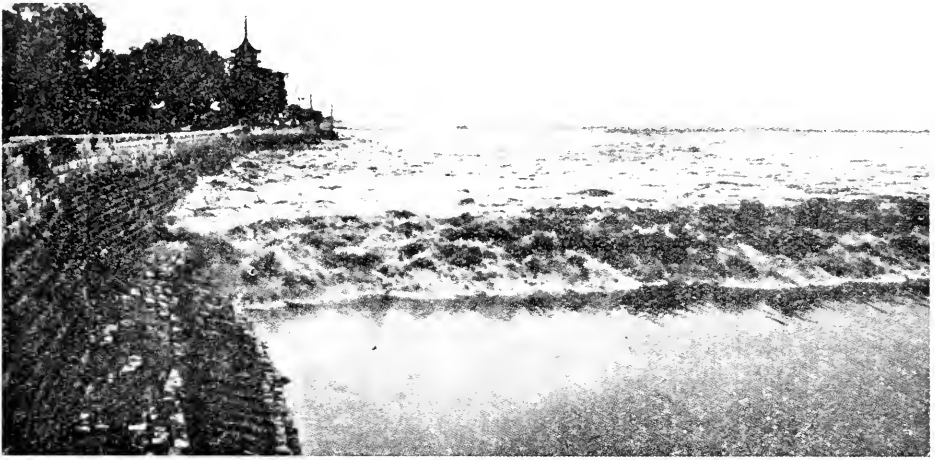


FIG. 198. Bore on the Chien-tang-kiang.

generally found in the French river estuaries and it is particularly well developed in the Seine, where PARTIOT (1861, p. 71) has made the most thorough study of it, farther in the Orne near Caen, in the Couesnon (designated as Barre, Bay of St. Malo), in the Vilaine and Charente, in the Gironde, but not in the Loire and in the Adour. Of the English rivers which have a bore we will mention the Severn, which was described by Airy and, subsequently by CORNISH (1900, p. 44); (1934, p. 101). Furthermore, for the bore of the Trent, CHAMPION and CORKAN (1936, p. 158) have published an exhaustive survey; the bore occurs regularly when the River Trent flows into the Humber, past Torksey and appears in the peculiar form of numerous short waves up to 2 m high, it is called here *the eager*. In U.S.A. the bore is known to exist in the Petitcodiac River at the northern end of the Bay of Fundy, and BELL DAWSON (1899, p. 22) has given an excellent description of it; further, on the mouth of the Colorado River into the Gulf of California. In South

America the phenomenon in the estuary of the Amazon River has gained great fame; it is called there *Pororoca*. This *Pororoca* originates in the mouth of river and in many of the numerous tributaries and canals, where it makes the Canal do Norte sometimes absolutely unnavigable. For a good description of a *Pororoca* see KRÜMMEL (1911, vol. II, p. 301). Large bores occur in the estuary of the Narbada River into the Gulf of Barygaza (Cambay), in the Hugli near Calcutta, in the Menga, in numerous rivers of the East Indian Islands. Particularly famous is the bore in the Chien-tang-kiang, which was studied by Admiral MOORE (1888, 1893). The bore in the Amazon River is perhaps the greatest one, and it frequently attains heights of 25 ft (8 m). Seen from the high dykes, it has the appearance of a several-mile long waterfall which travels upstream with velocities of 12–13 knots (6.5 m/sec) and produces a roar which is audible at a distance of 22 km. Figure 198 gives a picture of a bore on the Chien-tang-kiang which we owe to Prof. G. Schott.

The principal characteristic of a bore is the quick rise in level. This wall of water, sometimes a straight wall, sometimes curved concave, rushes upstream; the water in the back overtakes the water at the front side of the wave. The height of the bore varies a great deal: we have already mentioned that it attains 8 m (25 ft) in the Chien-tang-kiang, in the Amazonas and the Ganges it attains 5–6 m, in the Trent $1\frac{1}{2}$ –2 m, in the French rivers it remains

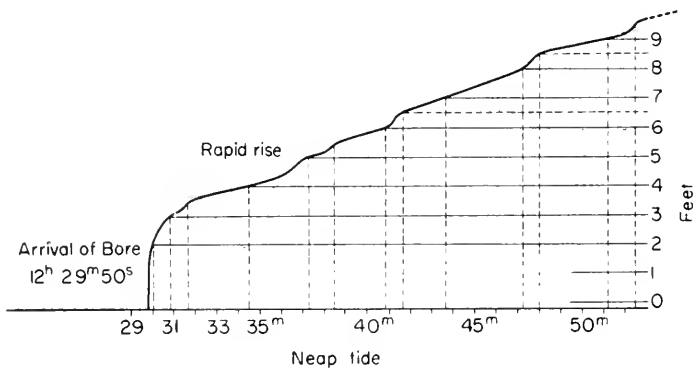


FIG. 199. Longitudinal profile of a bore in the vicinity of Moneton on the Petit-codiac River. 6 August 1898 (5th tide after spring tide).

normally below 1 m. The bore occurs at the time of the syzygies (spring tides), but there are also cases in which it occurs at every tide (as for instance in the Chien-tang-kiang). According to Comoy, the formation of a bore seems to be dependent on the fact that the capacity of the channel is too small to take care of the extra influx of water. If a bank is located at the mouth of the river (as for the Seine), the tide enters only slowly, the banks, which were dry at ebb, become covered with water and a large water-mass

gets into the river. As the foot of the wave progresses only slowly and the water in front of it rises very rapidly, the bore soon develops. Head winds can increase the stowing of the water in front of the foot of the wave. If the bank is located in front of the entrance, then, according to Comoy, the opening is narrow and the cross-section of the river increases upstream. In this case, no bore appears, as for instance like in the Loire.

Figure 199 gives an example of a longitudinal profile of a bore, which has been taken from a survey made by BELL DAWSON, on the Petit-codiac River in Moneton. It shows the bore of 6 August 1898 (fifth tide after spring tide, full moon on 2 August). The wave travelled with a velocity of 14.4 km/h upstream and the picture shows how the water level changed until 23 min after the passage of the bore. If we change the succession in time into a succession of places, the picture represents from the start of the bore on the left to the right edge a distance of $5\frac{1}{2}$ km. The heights are indicated at the right in feet. Champion has obtained interesting automatic registrations of the bore in Flixborough on the River Trent. Figure 200 gives these regis-

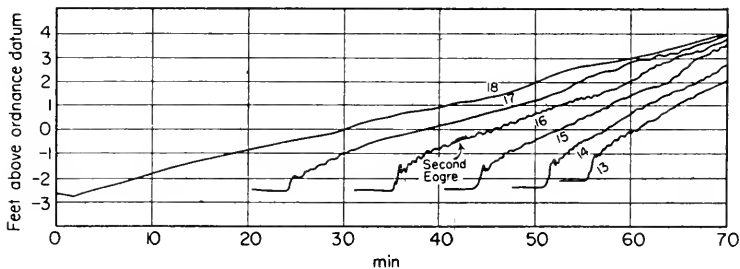


FIG. 200. Automatic records of a bore at Flixborough 13–18 September 1931 (Champion and Corkan).

trations of the beginning of the bore for 6 successive days; they clearly show the difference of the bore at spring and neap tide. At spring tide the passage is sharp and within about 10–20 sec the water surface rises nearly $\frac{1}{2}$ ft, followed by waves of about 1 min period. At neap tide the bore is hardly noticeable and the rise goes on continuously for 20 min and more. The thorough investigations made on the River Trent have also revealed the variations of the profile of the water surface along the entire river during a whole tidal period and have thus shown the propagation of the bore form. Figure 201 gives these profiles at spring tide for eleven successive intervals. It appears that the bore starts to develop in the River Trent and then runs up to Torksey with nearly uniform velocity and increasing intensity. Between Walkerith and Torksey the bore seems to disintegrate. Unfortunately, no observations are available for this interesting area.

It is easy to see that the increasing asymmetry in the wave profile of the river tides must finally lead to the development of a bore. The front slope

of the wave becomes almost vertical and the passage of this wall manifests itself by an almost sudden variation of the water level. The raised water-masses move rapidly onward, overtake and flood constantly the shallow water-masses in front of this wall. The wave has adopted the form of the breakers and, henceforth, is more like a travelling eddy with a horizontal

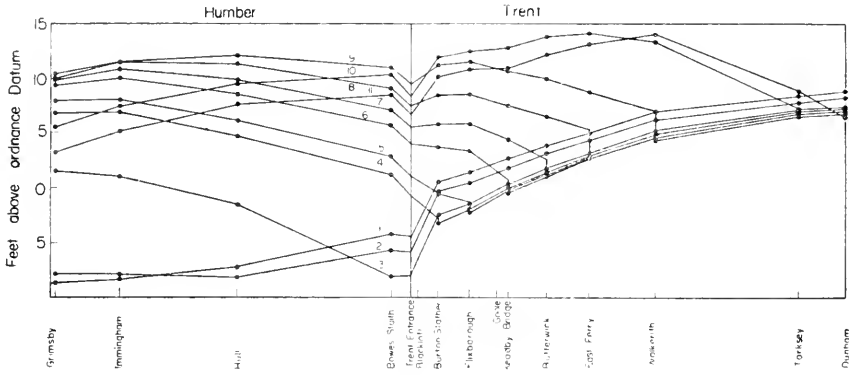


FIG. 201. Profile of the water surface in Humber and in the River Trent during a complete tidal period at springtide. Low water 1 at Grimsby, 2 at Hull, 3 at Bowes Staith, 4 at Burton Stather, 5 at Flixborough, 6 at Keadby Bridge, 7 at Butterwick, 8 at East Ferry, 9 at Walkerith, 10 at Torskey, 11 at Dunham.

axis than like a periodical variation of the water surface. The bore thus becomes similar to the phenomenon which occurs when a water-mass is piled up in a canal and suddenly freed and then moves down through the canal in the form of a translation wave. BAZIN (1865, p. 495) has been able, in this way, to create experimentally a bore in a wave tank. It showed there that those secondary waves which develop frequently behind the actual bore in deeper water (les "éteules" in the Seine, the "whelps" in the Trent) occur also in the experiments and are, therefore, characteristic in the development of this phenomenon.

From a mathematical view, the bore can be treated as a discontinuity wave. If there is a transition from one uniform level to another where the heights of the water surface above the bottom at the deep and shallow side of the wave are h_1 and h_2 , and if the low water is at rest, we have for the velocity of propagation of this discontinuity (bore) against the low water

$$u_1 = \sqrt{\left(gh_2 \frac{h_1 + h_2}{2h_1}\right)}. \tag{XIII.8}$$

If h_1 is not very different from h_2 , this velocity is reduced to the velocity of propagation of long waves \sqrt{gh} . If the process takes place in a river with a velocity U directed downstream, then we have to add $-U$ to the right.

According to Rayleigh (1914) (see also LAMB, 1932 para. 187 or Forchheimer, 1924, p. 182) equation (XIII.8) can be derived in the easiest way by means of the artifice of steady motion. If Q denotes the volume per unit width which crosses each section in unit time we have for reasons of continuity $u_1 h_1 = u_2 h_2 = Q$. (XIII.9). If we consider the mass of fluid which is at a given instant contained

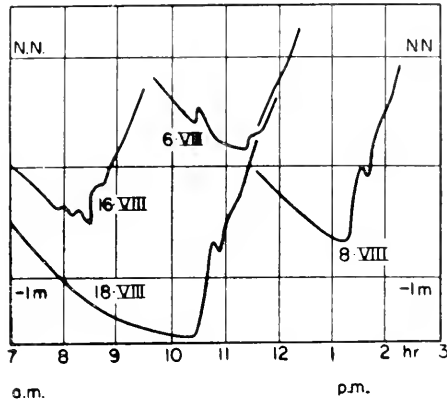


FIG. 202. Bore-like rise of the surface in sea-shore rills (*Prielen*) of German North Sea coast (Watten meer). Coast (Thorade-Schumacher).

between two cross-sections, one on each side of the transition wave (bore) we see that in unit time it gains momentum to the amount $Q(u_2 - u_1)$, the second section being supposed to lie to the right of the first. Since the mean pressure over the two cross-sections are $\frac{1}{2}g\varrho h_1$ and $\frac{1}{2}g\varrho h_2$, we have

$$Q(u_2 - u_1) = \frac{1}{2}g(h_1^2 - h_2^2). \tag{XIII.10}$$

and from (XIII.9) we obtain

$$Q^2 = \frac{1}{2}g h_1 h_2 (h_1 + h_2). \tag{XIII.11}$$

If we impress on the entire system a velocity $-u_1$, we get the case of a bore invading still water with the velocity of propagation

$$u_1 = \sqrt{\left(gh_2 \frac{h_1 + h_2}{2h_1}\right)}$$

in the negative direction; the particle velocity in the advancing wave is $u_1 - u_2$ in the direction of propagation of the bore. Rayleigh proves also that a positive discontinuity wave (wave above the mean water level) can only continue to progress unchanged if there is a dissipation of energy with the transition from one level to another. To the contrary, a negative discontinuity wave (depression below the mean water level) can progress unchanged when additional energy is supplied. It follows that a negative bore of finite height cannot in any case travel unchanged.

As pointed out by JEFFREYS (1934, p. 157), there does not seem to be an essential difference between a tidal bore in a river and the normal beach surf. Both depend, in the first place, upon the increase of the wave height due to reduction of the cross-section (decrease in depth, reduction of width), secondly upon the circumstance that, when the wave height becomes of the same size as the undisturbed water depth, the wave crests travel more rapidly than the wave troughs, overtake these troughs and break and, in the third place, upon

the possibility of the progress of a wall of water on the water surface. All these circumstances are of the same nature for both phenomena, only the dimensions differ correspondingly.

Phenomena like that of the bore are not limited to estuaries and rivers. SCHUMACHER and THORADE (1923, p. 48) have shown that bore-like rises of the water level occur at low tide in the *Prielen* (sea shore-rills) of the shallow seashore waters of the German North coasts (Watten meere) (see Fig. 202). Bores appear also in shallow straits, when different types of tides at the mouths can cause similar phenomena, as for instance the remarkable currents and eddies in the Strait of Messina (see p. 395).

Chapter XIV

Tides of the Oceans

1. First Co-tidal Chart of the Oceans

ONE could get a better picture of the tidal processes in the oceans if the distribution of the phase and amplitude of the tidal wave would be given for all points of the oceans. We would then have maps with co-tidal lines, and maps with co-range lines places for the various parts of the oceans. We have seen that from a pure mathematical standpoint, this problem cannot be solved now. The theory can only tell us how various factors affect the development of the tidal wave in the oceans and how they try to force certain forms on the co-tidal lines and on the distribution of the amplitudes. At the present time it seems fit to look at the observations from a geophysical viewpoint, based on the harmonic constants of the principal tides which are available for coastal localities and islands, and to connect these constants into an oscillating system extending all over the oceans. The main problem is then to select from the large number of possible oscillating systems, the system which is geophysically the most probable one on the basis of the theory of the tides. The degree of reliability of such a picture depends, of course, upon the number of available observations from coastal localities and islands far away from the coast. It is very important to obtain reliable tidal constants of islands if we want to further our knowledge of the ocean tides.

Up to 1911 only two attempts had been made to present the tides of the oceans in a map. WHEWELL (1833, 1836) has made a map for the Atlantic Ocean, which he based on new data collected by himself for this purpose. Whewell realised that his map could only be considered as rough approximation to the real conditions. It was limited to the semi-diurnal tides, as he could only base it on the establishments. BERGHAUS (1845, 1892) incorporated this map in an extended form in his atlas, thus giving it wider distribution though WHEWELL (1848), had retracted his presentation of the ocean tides because of the many criticism. Nowadays Whewell's map retains only an historical interest.

Whewell's map of the co-tidal lines indicates that the tidal wave in the ocean is mostly a progressive wave and since that time this viewpoint was adopted by the geographers. This is also the viewpoint taken by Krümmel in his textbook of oceanography. He was not very successful in trying to

make the velocity of propagation of the waves computed from the establishments agree with the known depths. In order to explain many discrepancies Krümmel assumed interferences of waves travelling in opposite directions which are very improbable.

HARRIS (1904, Part IV B, p. 315) in his general treatment of the oceanic tides started from a different viewpoint. He used for the first time the harmonic constants of a large number of coastal stations. He followed a thought expressed by Ferrel that the ocean tides are not progressive waves, but standing waves. These theoretical assumptions were, in many instances, based on not sufficiently secured fundamentals, so very soon the reliability of his results was questioned. Harris divides arbitrarily the oceans into areas of oscillation, adapting their dimensions to the period of oscillation and the depth of the area. Each area oscillates then independently. DARWIN (1902, p. 145) has rejected these assumptions, pointing out that the complicated co-tidal maps of Harris is inducive to find a simpler solution which will be representative of all the facts. Harris should be given credit for having been the first to include the diurnal tides in his considerations. STERNECK (1920, 1921, 1922) has given a different presentation of the co-tidal lines of the oceans. He had at his disposal a greater number of harmonic constants; furthermore, he referred his maps of the semi-diurnal tides to the high water at spring and he used numerous data of the establishments found in the tide tables of the various countries. His method is based upon the simple principle of splitting the tidal motion observed in each locality into two orthogonal oscillations, whose phases thus differ by a quarter period. Each of the oscillations is a standing wave in itself. For the semi-diurnal tides he chose as basic phases 0 and 3 h in such a way that

$$\eta = H \cos \sigma(t - \varepsilon) = H_1 \cos \sigma t + H_2 \cos \sigma(t - 3h),$$

$$H_1 = H \cos \sigma \varepsilon, \quad H_2 = H \cos \sigma(\varepsilon - 3h).$$

The first term of the decomposition with the amplitude H_1 represents a system of synchronous oscillations covering the entire ocean and which is nothing else than a standing wave with the phase 0 and 6 h respectively. The points $H_1 = 0$ will fall on certain lines which are to be considered as nodal lines of this standing oscillation. Along these lines we will observe exclusively establishments of 3 or 9 h because only the second term of the equation will then be instrumental in determining the establishments in these points. Similarly, the second term represents a system of synchronous oscillations covering also the entire ocean and whose phase is 3 and 9 h respectively. At points where $H_2 = 0$ we will have the nodal lines of this system and here the establishments will be 0 and 6 h. Establishing these nodal lines is most important, because these nodal lines form the frame of the whole system of co-tidal lines. The establishments of the coastal localities give the position of the nodal points on the coasts, and their connection across the oceans from coast to coast gives the position of the nodal lines on the open ocean.

The fact that the depths of the oceans are not considered, that is, their effect on the shape of the co-tidal lines, produces a certain simplification. The procedure in itself is very simple, but requires an intimate knowledge of the tides.

According to this method STERNECK (1920, p. 131; 1921, p. 363; 1922, p. 145) has drawn co-tidal lines for all three oceans for the semi-diurnal and the diurnal tide waves.* These maps are the first attempt at cartographical presentation based on a uniform principle. Progressive tide waves have not been considered and, wherever they appear, they are to be regarded as an interference of two standing wave systems. In theoretical support of Sterneck's method, it should be noted that this splitting up into two orthogonal oscillating systems is in itself of a purely formal nature. According to the basic phase selected, it can be solved in an infinite number of ways. Physically the method means that although he considers the tides of the oceans as oscillations of a closed basin, they do not appear as a simple standing wave; but can always be considered as the superposition of two systems of orthogonal standing waves (see DEFANT, 1928, p. 274; 1929, p. 209). This is important because the tides of the different oceans act upon each other and dissipate a great amount of energy on the shelf and on the ice in the polar regions.

2. Methods used to Incorporate the Observations Presently Available in Maps of the Tides of the Oceans

The number of coastal localities for which harmonic constants have been computed has increased lately to such an extent that it has become possible to map the oceanic tides, based on many reliable data.

The International Hydrographic Bureau in Monaco has published, from 1930 to 1940 for 2650 localities a list of their harmonic constants, the location of the tide gauges, duration of the observations, highest high water and lowest low water and mean sea level during the period of observation. The British tide tables (1938, Part II) supplement these data by giving for 3500 other localities the constants of the

$$M_2, S_2, K_1 \text{ and } O_1$$

tides. However, these constants are not as accurate because they have not been computed from the harmonic analysis but are obtained by applying tidal differences between these stations and the reference stations (see p. 311). The German tide table published in 1940 contain the harmonic constants of the ten principal tides for a large number of coastal stations as they are

* The first term of this split-up equation for the diurnal tide has a phase 0 h and the co-tidal lines for 6 h and 18 h are nodal lines of this oscillating system. The second term has the phase 6h and high water occurs along the nodal lines at 0 and 12 h.

used for the prediction of the tides (p. 317, see also SHUREMAN, 1924). DIETRICH (1944, p. 69; 1943, p. 123) used all these data to map the tides of the ocean, which is much more reliable than previous attempts. The map was limited to the oceans, omitting the adjacent and boundary seas, which require a different approach. Table 79 shows the increase in the number of constants used by Dietrich compared to those used by HARRIS in 1904 and STERNECK in 1920. The distribution of the data over the different oceans

Table 79. Number of localities used for the study of the tides of the oceans

Ocean	Harris (1904)	Sterneck (1920-21)	Dietrich		Total
			Harm. analysis until Monaco, 1940	Admiralty tide tables, 1938	
Atlantic	58	61	278	316	594
Indian	66	70	167	253	420
Pacific	59	73	397	254	651
Total	183	204	842	823	1665

is still very irregular and by no means uniform. There are coasts which are covered with localities for which harmonic constants have been computed and, on the other hand, there are hundreds of miles of coastline for which no constants are available at all. Many more data are needed for the coasts of Africa, Australia and on the Pacific side of Central and South America; also for the coasts of the Antarctic and for islands in the oceans which would be of special importance for this problem. Very few data are available from islands in the Pacific. The hydrographical work done by the Japanese has provided us with data for the main islands, but we have only very few constants for the islands of the eastern Pacific Ocean. It is easy to see that the progress of our knowledge in the geographical distribution of the tides over the ocean depends upon new observations of this kind.

The published phase and amplitude values can only be used after scrutinizing them closely. Discrepancies in the phases must be rectified. These discrepancies are mostly sudden variations of the phase by 180° or 90° in neighbouring localities were this cannot be explained orographically, and Dietrich has taken great pains in eliminating dubious values. He specially refers to his list of dubious harmonic constants. The corrected phases which are mostly referred to the local or zone time (α or g values) must be changed into Greenwich Time. In this connection see p. 372. The data entered in geographical maps show the phase at the coast and for the few islands, but to connect these data across the oceans, the author needs a vast knowledge

of the behaviour of the tides on the open oceans. Therefore, the maps will always remain quite subjective and will give at their best the probable system of oscillation of the partial tide under consideration.

Still more difficult than the presentation of the distribution of the phase is the cartographical presentation of the distribution of the amplitudes. It is very difficult to bridge the vast expanses of the oceans by interpolation between the amplitudes given along the coasts, due to the disturbing influence of the varying slope of the continental shelf.

Dietrich restricted himself to give a distribution of the amplitude along the coasts in the form of a diagram, or to enter its value for a large number of coastal localities. It is true that, in this way, no picture of the distribution of the amplitudes over the entire ocean is given but in using the map of the phase one can roughly visualize the principal features of the distribution of the tidal ranges; this is perhaps preferable to lines, which simulate only an accuracy not existing in reality.

3. The Charts of the Tides in the Various Oceans

Charts I and II are, according to DIETRICH (1944), the presentation of the co-tidal lines of the semi-diurnal and diurnal tides of the ocean. The M_2 tide has been chosen as representation for the semi-diurnal tide and the tide K_1 for the diurnal tide. Another kind of representation of the amplitudes of the semi-diurnal and diurnal tides along the coast of all oceans has been chosen here. It is presented in the charts III and IV. The average tidal range of the ocean surface is indicated by straight lines in these diagrams for the west and east coast of each ocean (ordinates) and with the latitude along the coast as abscissa. Chart III contains the range of the semi-diurnal tide $2(M_2 + S_2)$ and chart IV that of the diurnal tide $2(K_1 + O_1)$. An immediate and excellent impression of the distribution of the tidal amplitude along the ocean coast is obtained in this way. This allows a much better insight into the distribution of the amplitudes than any plot of the amplitude values at corresponding coastal places on an ocean chart. The distribution of the characteristic number $F = (K_1 + O_1)/(M_2 + S_2)$ along individual coasts has been indicated in the diagram III by different forms of the vertical lines (full, dashed, dashed-dotted or dotted, see text to chart III).

The principal features of the tides in the total ocean are well explained by these four charts I–IV can be found in the previously mentioned paper of Dietrich. Moreover the co-tidal lines of the two next important tides S_2 and O_1 have in general the same aspects as the co-tidal lines of the M_2 and K_1 tides. This is evidenced by the fact that for vast areas the differences in phase between $S_2 - M_2$ and $K_1 - O_1$ remain constant. Large discrepancies in this difference in phases for the diurnal tides $K_1 - O_1$ occur only occasionally (for instance on the European and South African coasts); however, this happens generally when the amplitude is very small and therefore it can probably be attributed to uncertainty in the constants.

The main pictures of the M_2 - and K_1 -co-tidal lines are, with a few exceptions, that of rotary waves (amphidromies *contra solem*), in both hemispheres. In most cases, their development is unsymmetrical; often there is a more or less pronounced crowding of the co-tidal lines and, in extreme cases they degenerate into real nodal lines with opposite phases on both sides. Mostly there is no discontinuity, but we have narrow bands in which the phase changes rapidly from one locality to another. For instance, the amphidromies of the semi-diurnal and diurnal tides of the North Atlantic Ocean are symmetrical, nearly pure nodal lines are found for the semi-diurnal tides in front of the Gulf of Bengal and between Japan and New Guinea. Sometimes a compact group of co-tidal lines starts out from the centre of the amphidromy running into only one direction; then it is difficult to judge in how far it is better to represent the observations by a nodal line or by an amphidromy.

Theoretically the amplitude becomes zero in every centre of an amphidromy and on every nodal line. In practice one finds a minimum of the amplitudes in the vicinity of the amphidromy and the range increases with the distance from the centre of the amphidromy and the same holds true for the nodal line. The maximum values of the tidal ranges are found on the coasts, even if one allows for the increase in amplitude caused by the shelf. But this is not the case on the coasts of islands, inasmuch as these are usually closer to the centre of the amphidromy. Thus, according to Dietrich, in the immediate vicinity of the pseudo-nodal line between Japan and New Guinea the smallest mean spring tide range of the semi-diurnal tide is only 16 cm; west of this point it reaches with increasing distance from the nodal line to 44, 100, 120 and 150 cm. Towards the east there is an increase from 16 to 60, 89, 116, 136, 152, and up to 176 cm. The distribution of the amplitudes is also quite characteristic for amphidromies if there are sufficient data of localities available. Thus, in the centre Solomon Islands the amphidromy of M_2 lies near Nusosonga ($8^{\circ}25'S.$, $157^{\circ}14'E.$ lat.) which has an amplitude of 0 cm. The small spring tide range of 12 cm must be attributed to the S_2 tide. The tidal ranges increase rapidly with the distance from this centre. The spring tide range of the eastern Solomon Islands is 121 cm; to the south-west in the Louisiade Archipelago it is 75 cm, on the border of the Great Barrier Reef of Australia it is 172 cm and on the Australian continent in Queensland, under the influence of the shallow coral coast, it increases to 476 cm. There is always a close correlation between the co-tidal lines and the amplitudes; one-sided crowding of the co-tidal lines extending to the coast is reflected there in a decrease in the range of the tide, so that such minima in range can always be regarded as a characteristic sign of a rapid variation in the phase.

In judging the amplitudes along the coast one should consider the increase in the amplitude through the co-oscillation of the shelf sea with the tides

of the open ocean. A sufficient number of cases illustrating this fact, can be found in the maps. An accurate analysis of the entire phenomenon is still lacking. The research on the tides of shelf regions along selected lines will be facilitated after high-sea gauges will have been constructed and tried.

The distribution of characteristic number of tide $F = (K_1 + O_1)/(M_2 + S_2)$ along the ocean coast is given in Chart III. Contrary to other oceans, the coasts and islands of the Atlantic Ocean show a marked predominance in the semi-diurnal tidal form, nearly everywhere the ratio determining the type of the tide remains below the theoretical value of

$$\frac{K_1 + O_1}{M_2 + S_2} = 0.68 ;$$

along the European and African coasts it seldom exceeds 0.10. This special position the Atlantic Ocean is not the result of high amplitudes of the semi-diurnal tides, but rather of the smallness of the diurnal tides, for the spring tide range of the diurnal tide remains below 40 cm generally disregarding local exceptions.

In other oceans the diurnal tides are much stronger; in the Pacific Ocean the mixed type is predominant; in the Indian Ocean we find in equal quantities both semi-diurnal and mixed, predominantly semi-diurnal type. The purely diurnal type of tides are restricted to locally, very limited areas, considering the wide expanses of the ocean. They can of course be found in the centre of the semi-diurnal amphidromies and along the nodal lines, where the amplitudes of the semi-diurnal tides decrease very much. The remarkable occurrence of high characteristic tide numbers (Formzahl) is thus explained very easily.

We will now discuss as briefly as possible in some detail, the main phenomena of the tides of the three oceans. In Tables 80, 81 and 82 can be found a compilation of the harmonic constants of selected coastal localities and islands. They were selected according to their importance for the character of the tides.

4. The M_2 Tide as the Typical Tide Wave of the Semi-Diurnal Tides

(a) Atlantic Ocean (Table 80)

In the Southern Atlantic Ocean the tide wave travels from south to north over the entire width of this ocean. Large disturbances appear on the Patagonian Shelf. From a line running from the Falkland Islands to the north-eastern tip of Tierra del Fuego then north of the Golfo San Jorge the phase increases by a full 360° and then there is a further increase by the same amount up to east of Bahai Banca. This is due to two amphidromies caused by the co-oscillation of the wide shelf extending out of the southern part of the South American with the open ocean. North of these areas there is over a relatively short distance an increase in the phase of more than 150° which, coinciding

Table 80. Harmonic constants of the Atlantic Ocean

Position	M_2	S_2	K_1	O_1	$\frac{K_1+O_1}{M_2+S_2}$	$M_2+S_2+K_1+O_1$
Godthaab, $H(\text{cm})^*$	135.9	46.9	21.0	9.1	0.16	212.9
64°11'N. 51°45'W. λ° *	193	229	127	81		
St. John (N. F.),	35.7	14.6	7.6	7.0	0.29	64.9
47°34'N. 52°41'W.	210	254	108	77		
Halifax,	63.1	14.4	9.7	5.1	0.19	92.3
44°40'N. 63°34'W.	223	254	56	34		
Sandy Hook,	65.4	13.8	9.7	5.2	0.19	94.1
40°28'N. 74°01'W.	218	245	101	99		
Fernandina,	87.0	15.5	10.5	7.7	0.18	120.7
30°41'N. 81°28'W.	228	258	127	129		
St. George (Bermudas),	35.5	8.2	6.4	5.2	0.27	55.3
32°22'N. 64°42'W.	231	257	124	128		
Nassau (Bahama Is.),	37.9	6.4	8.7	6.5	0.34	59.5
25°05'N. 77°21'W.	213	237	120	124		
Port of Spain (Trinidad),	25.2	8.0	8.8	6.7	0.47	48.7
10°39'N. 61°31'W.	119	139	187	178		
Pernambuco,	76.3	27.8	3.1	5.1	0.08	112.3
8°04'S. 34°53'W.	125	148	64	142		
Rio de Janeiro,	32.6	17.2	6.4	11.1	0.35	67.3
22°54'S. 43°10'W.	87	97	148	87		
Buenos Aires,	30.5	5.2	9.6	15.4	0.70	60.7
34°36'S. 58°22'W.	168	248	14	202		
Port Louis (Falkland Is.),	47.1	15.0	10.9	13.7	0.40	86.7
51°33'S. 58°09'W.	157	195	37	4		
Moltkehafen (South Georgia),	22.6	11.7	5.2	10.2	0.45	49.7
54°31'S. 36°00'W.	213	236	52	18		
Capetown,	48.6	20.5	5.4	1.6	0.10	76.1
33°54'S. 15°25'E.	45	88	127	243		
Takoradi,	45.9	15.4	11.8	2.0	0.23	75.1
04°54'N. 01°45'W.	100	127	347	321		
Freetown,	97.7	32.5	9.8	2.5	0.09	142.5
08°30'N. 43°14'W.	201	234	334	249		
Puerto de la Luz (Las Palmas),	76.0	28.0	7.0	5.0	0.12	116.0
28°09'N. 15°25'W.	356	19	21	264		
Funchal (Madeira),	71.2	26.7	6.1	4.5	0.11	108.5
32°38'N. 16°55'W.	10	31	29	285		
Ponta Delgada (Azores),	49.1	17.9	4.4	2.5	0.10	73.9
37°44'N. 25°40'E.	12	32	41	292		
Lisbon,	118.3	40.9	7.4	6.5	0.09	173.1
48°42'N. 09°08'W.	60	88	51	310		
Brest,	206.1	75.3	6.3	6.8	0.05	294.5
48°23'N. 04°29'W.	99	139	69	324		
Londonderry,	78.6	30.1	8.2	7.8	0.15	124.7
55°00'N. 07°19'W.	218	244	181	38		
Stromness (Orkney Is.),	90.0	35.3	11.4	10.2	0.17	146.9
58°58'N. 03°18'W.	265	297	153	3		

* In each case the figures on the top line are H cm and the figures on lower line λ° .

with a minimum of amplitude (Rio Grande do Sul only 5 cm), indicates a pseudo-nodal line. North thereof the variations in phase are small with large tidal ranges up to Cape Sao Rogue and even farther along the entire north-east coast of South America (disregarding the wide shelf of this coast). This distribution along the coast becomes less definite towards the open South Atlantic Ocean, so that the distinct nodal line on the coast (according to the observations on the islands) changes into a gradual variation of the phase, which becomes more pronounced in a north-eastern direction towards the African coast. While the increase in the phase is gradual, the amplitudes remain constant between 40 and 50 cm; only in the inner part of the Gulf of Guinea they increase to 75 cm after crossing a wide shelf.

North of the equator there seems to exist an antinode which extends over the entire width of the ocean from Pernambuco to West Africa. This anti-node is joined northward by a well-developed pseudo-nodal line. The increase in phase in the western part between Martinique and Puerto Rico is 165° and the phase in the eastern part between Cape Verde and the Tropic of Cancer vary by the same amount. In the west the crowding of co-tidal lines seems to originate from an amphidromy, whose centre is located in the eastern part of the Caribbean (Ponce on Puerto Rico where amplitude of $M_2 = 1$ cm). In the western part of the Atlantic, north of this nodal line up to the south coast of New Foundland the phase varies but little and decreases slightly. At the coast of the eastern N. Atlantic, on the contrary, the phases increase continuously from N.W. Africa, to the Canary Islands, Madeira, the Azores and farther along the European coast, so that this entire northern section of the North Atlantic Ocean is occupied by a very well-developed amphidromy.

The transition to the European North Sea takes place by a well-developed nodal line in the Denmark Strait and by a narrow amphidromy with a sudden change in phase of 150° over a short distance between the Hebrides and the Shetland Islands in the east and a corresponding decrease in the phase on the east coast of Iceland. The centre should lie north-west of the Faeroe Islands where the amplitude is only 10 cm against a minimum of 33.5 cm on the east coast of Iceland and 39.5 cm on the Shetland Islands.

The tidal picture of the Atlantic Ocean is clearly shown by the co-tidal lines on Chart I, and will not be changed essentially by new observations. This is proven by the fact that the presentation of the Atlantic Tides (see Fig. 203) given by STERNECK (1920) does not deviate essentially from Dietrich's newer map. The divergence from Harris's map is, however very great. Harris assumed a very remarkable pattern of the co-tidal lines, particularly in the region of the Northern Atlantic Ocean; but he had already found the amphidromy in the North Atlantic.

(b) *Indian Ocean (Table 81)*

Dietrich points out as a particular feature in the Indian Ocean the very

small variation in phase in the following five vast regions when again the disturbances caused by the shelf are neglected:

(1) Western Region: the entire African coast from the Southern Atlantic Ocean via Cape of Good Hope up till north of Ras Hafun in Italian East

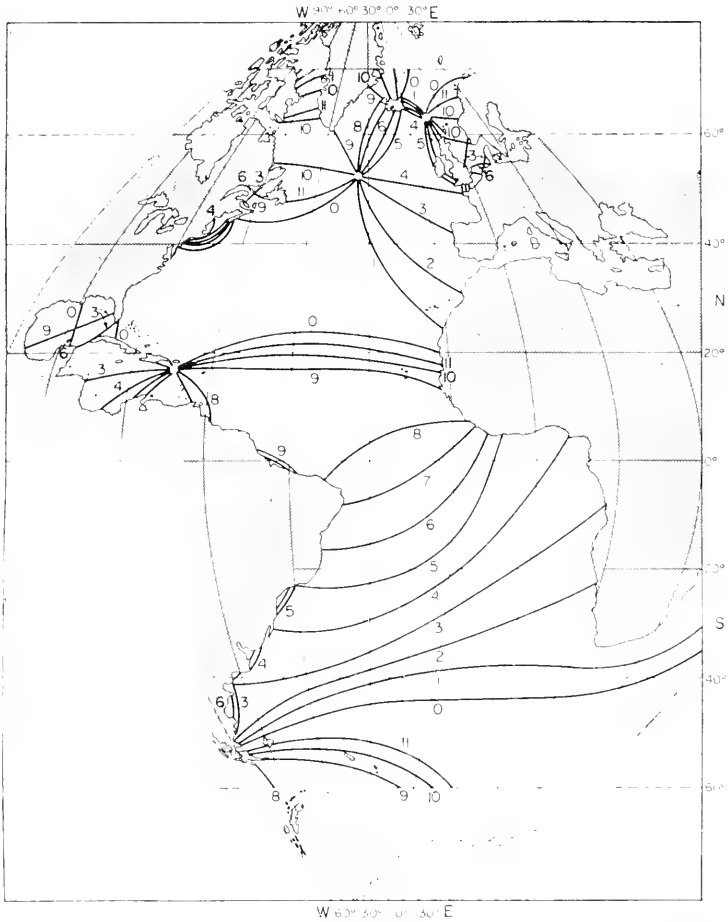


FIG. 203. Co-tidal lines for the Atlantic Ocean for the semi-diurnal tides (M_2 and S_2 together; referred to Greenwich) (STERNECK, 1920).

Africa, including the west coast of Madagascar, the Comoro Islands, Amirante Island, and Seychelles. The phases all lie near 0° .

(2) Eastern Region: the west coast of Australia north of Fremantle across the entrance of the Timor sea to the centre of Java; the phases are about 45° .

(3) Between the western and eastern regions in the middle of the ocean there seems to be a wide band, in the north-south direction along which the phase remains constant at about 240° . It starts in the north near the southern Maldivé Island and runs across the Chagos Arch, Rodriquez, St. Paul,

Table 81. Harmonic constants of the Indian Ocean

		M_2	S_2	K_1	O_1	K_1+O_1 M_2+S_2	M_2+S_2 $+K_1+O_1$
Mergui Is., 12°26'N. 98°36'E.	$H(\text{cm})^*$	167.5	89.2	16.0	6.4	0.09	279.1
	α° *	310	349	334	315		
Port Blair (Andaman Is.), 11°41'N. 92°46'E.		61.0	29.3	12.2	4.8	0.19	107.3
		280	315	327	302		
Baras (East Sumatra), 2°01'N. 98°21'E.		25.0	16.0	12.0	6.0	0.44	59.0
		167	200	281	246		
Emma Haven (Padang), 0°58'S. 100°20'E.		35.0	14.0	13.0	8.0	0.43	70.0
		177	218	277	265		
Java's 4te Punkt, 6°04'S. 105°53'E.		24.0	12.0	7.0	3.0	0.28	46.0
		210	280	226	216		
Tjilatjap, 7°44'S. 109°00'E.		50.0	25.0	19.0	12.0	0.41	106.0
		249	311	279	268		
Bonjuwangi, 8°12'S. 114°24'E.		49.0	24.0	24.0	13.0	0.51	110.0
		292	349	289	265		
Koe pang, 10°10'S. 123°34'E.		46.0	26.0	16.0	10.0	0.36	98.0
		317	18	314	328		
Darwin, 12°28'S. 130°51'E.		199.9	104.9	58.2	34.7	0.30	397.7
		144	193	336	313		
Port Hedland, 20°18'S. 118°35'E.		174.9	105.7	24.9	14.9	0.14	320.4
		315	16	294	282		
Freemantle, 32°03'S. 115°45'E.		4.8	4.4	19.4	11.3	3.34	39.9
		286	292	300	291		
Albany, 35°02'S. 117°53'E.		4.8	8.0	19.0	12.7	2.48	44.5
		339	342	330	312		
Thevenard, 32°09'S. 133°39'E.		30.0	37.2	19.0	13.2	0.48	99.4
		353	29	14	360		
Port Lincoln, 34°43'S. 135°52'E.		22.9	26.0	23.4	15.5	0.80	87.8
		32	74	22	5		
Adelaide, 34°51'S. 138°30'E.		51.8	51.2	25.3	15.9	0.40	144.2
		120	181	52	32		
Melbourne, 37°51'S. 144°54'E.		24.6	3.1	9.0	6.6	0.56	43.3
		69	164	132	95		
Betsy Cove (Kuguelen), 49°09'S. 70°12'E.		43.6	24.5	4.4	6.6	0.16	19.1
		9	52	289	292		
Durban, 29°52'S. 31°03'E.		54.9	30.9	5.1	1.5	0.08	92.4
		106	138	176	330		
Port Louis (Mauritius), 20°09'S. 57°29'E.		13.2	10.1	7.4	4.3	0.50	35.0
		23	26	121	98		

		M_2	S_2	K_1	O_1	$\frac{K_1+O_1}{M_2+S_2}$	M_2+S_2 $+K_1+O_1$
Reunion, 20°55'S. 55 17'E.	$H(\text{cm})^*$	14.4	6.9	5.4	2.7	0.38	29.4
	κ° *	79	77	159	103		
Tamatave, 18°09'S. 49°26'E.		20.5	9.5	2.5	4.1	0.22	36.6
		55	54	79	64		
Zanzibar, 6°10'S. 39°11'E.		118.6	57.0	18.9	11.0	0.17	20.55
		102	140	38	40		
Kilindini, 4°05'S. 39°39'E.		106.0	51.4	18.7	11.2	0.19	187.3
		107	147	36	41		
Aden, 12°47'N. 44°49'E.		47.5	20.6	39.7	20.1	0.88	127.9
		227	245	35	37		
Maskat, 23°37'N. 58°36'E.		63.3	23.7	33.8	20.2	0.68	146.0
		277	307	40	41		
Karachi, 24°48'N. 66°58'E.		78.2	29.2	39.9	20.1	0.56	167.4
		294	323	46	47		
Port Albert Victor, 20°57'N. 71°32'E.		87.4	34.2	49.5	22.3	0.59	193.4
		59	83	66	67		
Bombay, 18°55'N. 72°50'E.		122.2	48.3	42.5	20.1	0.37	233.1
		331	4	46	49		
Mormugao, 15°25'N. 73°48'E.		55.2	19.5	31.2	15.9	0.63	121.8
		300	332	46	49		
Cochin, 9°58'N. 76°15'E.		22.2	8.0	18.0	9.4	0.91	57.6
		332	29	52	58		
Colombo, 6°57'N. 79°51'E.		17.6	11.9	7.3	2.9	0.35	39.7
		50	95	33	62		
Minicoy, 8°17'N. 73°03'E.		26.3	10.7	21.0	10.2	0.84	68.2
		329	20	51	59		
Trincomali, 8°33'N. 81°13'E.		17.7	6.4	6.6	2.0	0.36	32.7
		241	265	331	309		
Madras, 13°06'N. 80°18'E.		33.2	13.9	9.1	2.9	0.25	59.1
		240	270	337	325		
Dublat (Hugli), 21°38'N. 88°08'E.		140.5	64.2	15.1	5.8	0.10	225.6
		291	328	352	338		
Chittagong, 22°20'N. 91°50'E.		135.5	47.9	18.1	8.8	0.15	210.3
		35	69	22	12		
Diamond Is., 15°52'N. 94°17'E.		66.8	30.4	12.9	4.9	0.18	115.0
		281	314	340	324		
Rangoon, 16°46'N. 96°10'E.		170.1	61.1	20.8	8.9	0.13	260.9
		132	171	34	24		

* In each case the figures on the top line are H cm and the figures on lower line κ° .

Kerguelen Island to the Antarctic (Gauss Station, phase 229°). With high amplitudes everywhere it seems to be an oscillation opposite in phase to the western and eastern sections of this ocean.

(4) From the Gulf of Aden to the coast of Baluchistan and then to the 12° N. parallel on the coast of southern India there is a very small change in phase.

(5) The entire inner part of the Bay of Bengal, including the Andaman Sea, is characterized by a nearly constant phase of 75° .

The transitions between these regions are clearly defined by the coastal values, but the drawing of the co-tidal lines is, however, only possible in a few cases and is left to subjective interpretation. The best defined conditions are at the entrance of the Bay of Bengal. From the east coast of Ceylon a crowded bunch of co-tidal lines to the northern point of Sumatra with a sudden transition in the phase of 180° , while the amplitudes are reduced to small values for M_2 (in the western section 13 cm, in the eastern section 4 cm). This points clearly to a well-developed nodal line and a uniform oscillation of the entire bay with a phase opposite to that of the open Indian Ocean, in the south.

The other transitions have the forms of amphidromies of which the one in front of the Arabian sea is rotating to the right and is supported by the amplitude distribution in the west and the east. The two other amphidromies are located at about 30° S. the western one, with its centre south of the Mascarenes (amplitude here only 13 cm) rotating to the left; the one in the eastern part, with its centre west of south-west Australia (amplitude only 5 cm) rotating to the right.

The co-tidal lines given by Dietrich for this southern section of the Indian Ocean are not as reliable and accurate as those in the northern region, but they fit in with the available observations and permit an interpretation. They agree with the map of Sterneck, whereas PRÜFER (1939) in working up almost the same observations, had a different conception. Prüfer completely omits the western amphidromy in the southern Indian Ocean and draws the co-tidal lines down to the Antarctic Continent and moves the eastern amphidromy much farther to the north. The more recent observations rather seem to confirm Dietrich's conception. Harris's map does not indicate any amphidromy at all in the south whereas in the northern Indian Ocean there is good agreement with Dietrich's map.

An excellent representation, also on a theoretical basis, of the diurnal tides along the equator in the Indian Ocean was given by FAIRBAIRN (1954). The distribution of the semi-diurnal tidal constituent K_2 along the equator has been calculated with the aid of known harmonic constants at approximately fifty coastal stations in the northern part of the Indian Ocean. This has been achieved by use of a theorem in tidal dynamics, which connects integrals involving the tidal elevations and currents along the boundaries of an oceanic region and the equilibrium elevation over its surface (see p. 362).

In the equatorial distribution the variations of phase give supporting evidence for recent co-tidal charts of the ocean. In addition, however, an estimate for the amplitude of the constituent is given for any point on the equator. The tidal chart for the region studied by Fairbairn is given in Fig. 203a.

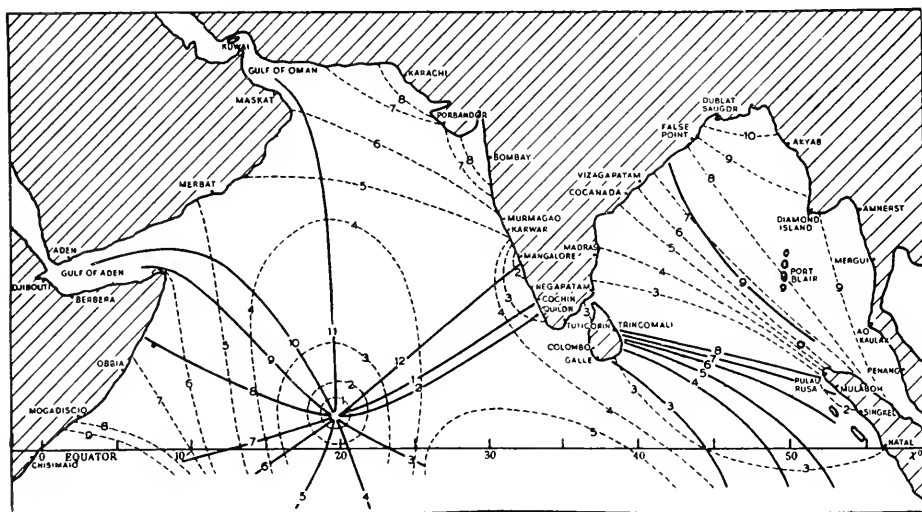


FIG. 203a. Co-tidal and co-range lines for constituent K_2 . The numbers on the full lines give the time of high water in hours which are one-twelfth of the period, the time origin being on the standard meridian where $\lambda = 32^\circ$ ($x = 0$ being at 43° E., where the equator strikes the coast of Africa). The numbers on the broken lines give the amplitude H in cm.

(c) *Pacific Ocean* (Table 82)

Condition in this vast ocean are more complicated than in the Atlantic and Indian Ocean. The expanse of the Pacific Ocean and the unsatisfactory distribution of the observations are cause for uncertainties. Harmonic constants in sufficient number are available for the north-western and northern regions. In the other areas, except the western part of the South Sea, harmonic constants are scarce. One can, therefore quite well understand that Dietrich looks at his distribution of the phases in the central and southern part of the Pacific as an attempt and he does not consider it definite.

In the western region there is a pseudo-nodal line extending from Japan to New Guinea. The line is quite narrow, amplitudes are at a minimum. The transition of the phase is about 180° between the territory west of this line, Western Carolina Islands Palau (Moluccas, Phillipines, Formosa, Riu-Kiu and Japan) and east of this line (east coast of New Guinea to Southern Kamchatka). OGURA (1933) already assumed such a line at this place.

Another phenomena well established is that the phase completes a full 360° circle with a rotation to the left around New Zealand. It could be taken for an amphidromy, but the sense of rotation is unusual for the southern

Table 82. Harmonic constants of the Pacific Ocean

	M_2	S_2	K_1	O_1	K_1+O_1 M_2+S_2	M_2+S_2 $+K_1+O_1$
Orange B., Cape Horn, H cm*	58.9	9.2	21.5	17.9	0.58	107.5
53°31'S. 68°05'W. \approx	104	134	36	347		
Puerto Monto, Chile,	217.0	111.0	6.0	4.0	0.03	338.0
41°28'S. 72°57'W.	146	54	7	2		
Valparaiso,	43.0	14.2	15.2	10.0	0.44	82.4
33°02'S. 71°38'W.	279	300	330	286		
Balboa, Panama,	184.6	48.9	13.5	3.6	0.07	250.6
8°57'N. 79°34'W.	89	145	342	352		
Mazatlan,	32.8	22.6	19.6	13.8	0.60	88.8
23°11'N. 106°27'W.	265	254	72	75		
Magdalena B., California,	48.5	30.8	24.1	17.1	0.52	120.5
24°38'S. 112°09'W.	244	253	71	77		
San Juanico B., California,	52.4	31.1	12.5	8.8	0.26	104.8
26°15'N. 112°28'W.	246	252	93	55		
San Diego,	55.3	22.3	33.6	21.2	0.71	132.4
32°43'N. 117°10'W.	276	273	94	79		
San Francisco,	54.3	12.3	36.9	23.0	0.90	126.5
37°48'N. 122°27'W.	330	334	106	88		
Victoria, Vancouver Is.,	36.8	9.8	63.0	37.2	2.15	146.8
48°26'N. 123°23'W.	70	85	146	124		
Prince Rupert,	194.7	63.8	50.7	31.2	0.32	340.4
54°19'N. 130°20'W.	6	38	129	114		
Sitka, Alaska,	109.7	34.6	45.6	27.8	0.51	217.7
57°03'N. 135°20'W.	4	34	124	108		
Cape Whitshed,						
Prince William Sound,	134.8	47.5	46.1	32.3	0.43	260.7
60°28'N. 145°55'W.	8	44	130	118		
Unalga B., Aleutians,	18.6	3.8	32.2	21.9	2.24	76.5
54°00'N. 166°10'W.	105	304	148	131		
Petropavlovsk, Kamchatka,	30.8	8.5	37.5	27.7	1.66	104.5
53°01'N. 158°38'E.	94	162	131	132		
Taraku, Kurile Is.,	27.0	12.0	27.0	20.0	1.21	86.0
43°35'N. 146°21'E.	98	139	160	133		
Miyako,	28.4	13.1	22.7	18.6	1.00	82.8
39°38'N. 141°53'E.	114	150	170	154		
Yokohama,	46.7	22.7	24.9	19.3	0.64	113.6
35°27'N. 139°38'E.	155	185	180	160		
Nagasaki,	78.0	34.0	23.0	18.0	0.37	153.0
32°43'N. 129°51'E.	230	256	203	189		
Naha Ko,	57.5	24.3	20.4	15.7	0.44	117.9
26°12'N. 127°40'E.	199	224	212	190		
So-o,	44.0	19.0	18.0	18.0	0.57	99.0
24°35'N. 121°52'E.	181	207	226	201		

	M_2	S_2	K_1	O_1	$\frac{K_1+O_1}{M_2+S_2}$	$M_2+S_2+K_1+O_1$
Finsch = hafen, New Guinea, 6°35'S. 147°50'E.	6.8 75	9.6 124	25.5 204	7.0 272	1.98	48.9
Thursday Is., Torres Str., 10°35'S. 142°13'E.	35.8 51	34.9 320	56.1 197	29.2 148	1.21	156.0
Cairns, 16°55'S. 145°47'E.	59.7 282	34.1 245	26.6 190	12.4 166	0.42	132.8
Brisbane, 27°20'S. 153°10'E.	67.8 290	18.8 309	21.2 174	11.9 143	0.38	119.7
Port Denison, Sydney, 33°51'S. 151°14'E.	51.8 251	13.1 266	14.7 121	9.6 94	0.37	89.2
Auckland, 36°51'S. 174°46'E.	116.4 206	17.7 268	7.2 169	1.6 145	0.07	142.9
Wellington, 41°17'S. 174°47'E.	49.1 139	3.0 330	2.5 85	3.1 37	0.11	57.7
Bluff, 46°36'S. 163°20'E.	87.1 36	15.3 50	1.8 116	3.4 73	0.05	107.6
Amoy, 24°23'N. 118°10'E.	186.7 1	40.8 57	26.5 274	19.5 252	0.20	273.5
Toko (Formosa), 22°28'N. 120°26'E.	20.0 238	7.0 236	20.0 298	17.0 254	1.37	64.0
Manila, 14°23'N. 120°36'E.	17.3 321	5.4 355	32.0 321	26.2 288	2.56	80.9
Tabaco, 13°22'N. 123°44'E.	53.4 175	23.4 199	16.0 203	11.8 190	0.36	104.6
Santa Elena (Phillip.), 11°21'N. 124°59'E.	14.9 312	10.4 30	22.1 316	20.1 270	1.67	67.5
<i>Islands in the Pacific Ocean</i>						
Saipan Ko, Marianas Is., 15°12'N. 145°43'E.	16.7 226	4.7 248	14.3 215	10.2 190	1.17	46.4
Yaruto Ko, Marshall Is., 5°55'N. 169°39'E.	46.4 104	26.4 129	9.0 241	5.8 212	0.20	87.8
Honolulu, Hawaiian Is., 21°18'N. 157°52'W.	16.0 106	5.1 102	14.9 70	8.2 58	1.09	44.2
Ponape Ko, Caroline Is., 6°59'N. 158°13'E.	25.1 81	19.5 104	16.1 224	9.7 200	0.58	70.4
Natusima, 7°22'N. 151°53'E.	6.4 73	9.9 95	17.8 219	11.5 196	1.80	45.6
Bungana, Solomon Is., 9°11'S. 160°13'E.	11.3 94	8.2 140	20.7 207	11.3 183	1.64	51.5
Apia, Samoa Is., 13°48'S. 171°46'W.	37.7 188	8.8 174	4.7 257	3.1 246	0.17	54.3
Tahiti, 17°45'S. 149°22'W.	8.9 351	7.8 20	1.1 278	1.5 293	0.16	19.3
Gambier Is., 23°07'S. 134°58'W.	27.5 86	9.4 38	1.9 184	1.0 276	0.08	39.8

* In each case the figures on the top line are H cm and the figures on lower line α° .

hemisphere and the high amplitudes do not support this interpretation. The phases from the Tasman Sea and Coral Sea to New Guinea and New Caledonia remain constant at about 300° . The transition to the previously mentioned large area of nearly constant phase of $120\text{--}150^\circ$ takes place in the western part by a well-developed amphidromy in the vicinity of the Solomon Islands with its centre located at Nusosonga which has an amplitude of 0 cm.

In the north-east Pacific Ocean, the coast of the Gulf of Alaska, between the eastern Aleutians up to Vancouver Islands, is a region with a relatively constant phase of $240\text{--}270^\circ$, there is a crowding of co-tidal lines in the north near the central Aleutians, and again north of Lower California. This distribution of the phase would fit an amphidromy with its centre south of the Gulf of Alaska. The 60° lacking for a full revolution can be distributed between Lower California and the Hawaiian Islands. For a further portion of the eastern boundary of the Pacific Ocean Dietrich assumes two other amphidromies: one in front of the Gulf of Panama and another one in front of Chile with its centre south of Easter Island. Both amphidromies are indicated by phases and amplitudes observed at coastal localities, but their position and form is uncertain in the open oceans due to lack of observations. The few harmonic constants at present available for the central Pacific are insufficient for an accurate drawing of co-tidal lines. The few constant of places bordering this region seem to point to a rotation of the phase of 360° to the left. The phase of several islands in this region would fit very well in this picture. Dietrich assumes, therefore, a large amphidromy in the Central Pacific with its centre north of the Samoa, Tahiti and Gambier Island. The decrease in the amplitude of the semi-diurnal tides in the centre of the amphidromy would explain why the establishment and the differences in time of the occurrence of high water in the Tahiti region (approximately between 140° and 160° W. and between 25° S. and the equator) show such an inextricable confusion.

Including another amphidromy in the Southern Pacific Ocean at about 50° S. which actually belongs to the belt girding the Antarctic between 70° and 50° S. lat. Dietrich's map shows for the entire Pacific Ocean six amphidromies and two pseudo-nodal lines. A comparison with v. Sterneck's presentation shows considerable differences both in the northern and in the southern sections. The differences with Harris's map are still greater. Even though the increased number of observations has eliminated many uncertainties, Dietrich's map should still be regarded as provisional, and only more observations will prove its reliability.

5. The K_1 Tide as the Typical Tide Wave of the Diurnal Tides. (See Chart II)

It is to be expected that the diurnal tides will show a simpler picture than the semi-diurnal tides because of their longer period. This circumstance will compensate for the disadvantage that there are fewer harmonic constants for

the diurnal tides. Comparing Chart II with Chart I there is quite a simplification characterized by the smaller number of amphidromies.

In the Atlantic Ocean there are two large amphidromies. One covering the entire Northern Atlantic Ocean has its centre at approximately 30° N. lat., and is symmetrical towards all sides, whereas the second one covers the Southern Atlantic Ocean and seems to have a definite crowding of the co-tidal lines in its western part. The distribution of the amplitudes of the K_1 tide is very uniform in the entire Atlantic Ocean, except that in the extensive shelves and in large bays it remains mostly below 10 cm.

In the Indian Ocean we find an amphidromy in the form of two bundles of crowded co-tidal lines, supported by the constants on the coast and Islands. Its centre is located east of the Chagos Archipelago. The distribution of the amplitudes support well the drawing of the co-tidal lines with a minimum of 5–10 cm along a line extending from north-west Sumatra to southern Ceylon, the Chagos Archipelago, the Mascarenes, and to South Madagascar. In the antinode in the north-western part the tidal ranges exceed 20 cm on the Seychelles and Laccadives, and more than 40 cm on the south coast of Arabia.

According to Dietrich there seems to be a small amphidromy rotating to the right at the southern opening of the Mozambique channel.

In the Pacific there are, similar to the Atlantic, two distinct regions with regard to the distribution of the phase which lie opposite one another. In the east the coasts of Peru and northern Chile have a minimum of about 30° ; from there on the phase increases to the north and to the south. In the west there is a maximum with approximately 90° in the region of the Philippines and Formosa and from this point the values decrease rapidly to the north and to the south. Judging by the values in between, both regions lie on a wide anti-node which extends across the entire Pacific Ocean. The values north and north-west of this zone can be grouped into a large, unsymmetrical amphidromy; its centre seems to be located between the South Sea Islands in the south, the Hawaiian Islands in the north and the Marshall Islands in the west. According to the K_1 phases its location is probably south of Fanning Island.

In the Southern Pacific Ocean we have the remarkable case of an island appearing as the centre of an amphidromy. All constants on New Zealand point a complete rotation of 360° to the right around both islands, and at the same time the K_1 amplitude decreases to below 3 cm. The observations on distant islands and on the coast of Australia do support this amphidromy.

The amplitudes of the K_1 wave are relatively small in the Pacific Region, but they exceed 10 cm, at the coasts of this ocean (except in a small strip along Equador). Around the Antarctic these amplitudes reach 30 cm and more, while in the Gulf of Alaska they amount to 40 cm and above. In general the diurnal tide in the Pacific, as well as in the Indian Ocean, is greater

Table 83. Semi-diurnal tidal currents in the Atlantic

Station	Latitude	Longitude	Depth (m)	Mean tidal current				Direction of co-tidal lines			
				Mean direction	Velocity (cm/sec)	Phase lunar hours* Greenwich	Ratio of minor to major axis	Sense of rotation	Theory	According to Sterneck	Difference ψ
"Mich. Sars" 58	37.6 N.	29.4 W.	15	N. 16 E.	24	11.4 h	0.791	Cum sole	N. 55 W.	N. 31 W.	+24
"Pillsbury" 5	35° N.	74° W.	6-238	S. 7 W.	13.2	11.8 h (0.2 h)	0.349	Cum sole	N. 27° E.	N. 4 E.	-23
"Arm. Hansen" D	30.2° N.	14.0° W.	100-600	N. 4° W.	10.0	2.3 h	0.550	Cum sole	N. 78° W.	N. 60 W.	+18°
"Meteor" 438	30.0 N.	43.8° W.	5-50	N. 12 E.	6.6	3.9 h	0.544	Cum sole	N. 73 W.	N. 65 W.	+ 8°
"Arm. Hansen E	29.7 N.	16.9° W.	100-600	N. 42° E.	10.3	0.7 h	0.386	Cum sole	N. 52 W.	N. 50 W.	+ 2°
"Meteor" Pre-Exp.	28.6° N.	15.6° W.	100	N. 9 E.	19.6	2.6 h	0.735	Cum sole	N. 85 E.	S. 55 E.	+40°
"Pillsbury" 31	28° N.	77° W.	55-110	S. 7 W.	12.0	10.6 h (11.1 h)	0.159	Cum and contra s.	N. 55 E.	N. 3° W.	-58°
"Meteor" 385	16.8° N.	46.3 W.	5-50	N. 12 W.	9.1	6.6 h (11.0 h)	0.367	Cum sole	N. 70° E.	E.	+20°
"Pillsbury" 5B	13° N.	60° W.	27-238	N. 27° W.	16.2	10.9 h (10.9 h)	0.282	Cum sole	N. 71° E.	N. 54 W.	+55°
"Meteor" 288	12.6 N.	47.6° W.	0-150	N. 10° W.	12.7	10.0 h	0.302	Cum sole	N. 54° E.	E.	+36°
"Meteor" 229	4.0° N.	1.0° W.	100-700	N. 47° W.	5.8	4.9 h	0.345	Contra solem	N. 48° E.	N. 14 E.	-34°
"Meteor" 214	3.7° N.	25.9° W.	0-1000	N. 57° W.	7.4	10.9 h (6.8 h)	0.429	Cum and contra s.	N. 78 E.	N. 61 E.	-17
"Meteor" 254	2.5 S.	35.0 W.	0-50	N. 4 W.	5.9	9.8 h (0.1 h)	0.223	Cum sole	N. 48 W.	N. 52 E.	+84
"Meteor" 241	3.8 S.	1.1° E.	0-25	N. 23° W.	7.3	10.0 h (6.0 h)	0.364	Cum sole	N. 37° E.	N. 35 E.	- 2°
"Meteor" 186	9.0 S.	10.9 E.	0-1100	N. 7 E.	7.9	7.9 h (2.8 h)	0.194	Cum and contra s.	N. 63° W.	N. 50 E.	-67
"Meteor" 147	14.9 S.	0.1° W.	0-2500	N. 41 W.	9.9	2.0 h (2.7 h)	0.310	Cum sole	N. 50 E.	N. 53° E.	+ 3
"Meteor" 176	21.5 S.	11.7° W.	0-500	N. 8° W.	8.8	5.7 h (4.3 h)	0.450	Cum sole	(N. 7 W)	N. 55 E.	(+62°)
"Meteor" 36	28.1° S.	19.4 W.	0-2500	N. 38° W.	10.6	3.2 h (3.7 h)	0.176	Cum sole	N. 50 E.	N. 63° E.	+13°

* Values in brackets refer to the lower layers.

than in the Atlantic Ocean, where they sporadically exceed 10 cm. The tidal picture of the antarctic belt remains questionable until new observations are available. Dietrich's presentation can only be considered as provisional.

6. Tidal Currents in the Atlantic Ocean

The Atlantic Ocean is at present the only ocean for which we have current measurements obtained at a fair number of anchor stations; they permit the formation of an approximate picture of the distribution of these currents in the centre of this ocean, but of course, this can only be considered as an attempt. Current measurements from an anchored ship present some difficulties, and their results contain errors which are difficult to eliminate. In view of their limited number, the few existing stations do not permit one to give a detailed picture of the distribution of the currents. But in conjunction with the co-tidal lines of the vertical tide we can get a good general idea. Most of these anchor stations have been made by the "Meteor" Expedition and their results have been published by DEFANT (1932) (see also THORADE, 1934, p. 1). Furthermore, there are three stations of the Pillsbury worked up in a modern way by SCHUBERT (1932, p. 378) and three stations of the "Michael Sars" and the "Armauer Hansen" Expedition (HELLAND-HANSEN, 1930; EKMAN and HELLAND-HANSEN, 1931) and finally two stations of the second cruise of the North Atlantic expedition of the "Meteor" in 1938 (published by SCHUBERT, 1944). In all, eighteen stations are available. Table 83 gives a compilation of the main results of the analysis, for the semi-diurnal tide. The measurements were made in various depths. In the table each quantity represents an average value computed from the observations in different depths which are often rather different from each other. This method eliminates, for a large part, possible errors. The principal direction and phase of the current for the individual stations have been entered in Fig. 204 and an attempt made to draw co-tidal lines for tide currents. It is to be seen that the phases are fairly uniform across the width of the entire ocean and supports the old presentation of a tide wave progressing from south to north, whose tidal currents have the form of a rotary current *cum sole* as required by Sverdrup's theory. Figure 204 shows, of course, only approximately the distribution of the tidal currents. It is quite possible that the uniform advance of the co-tidal lines which were interpolated from the few available values, should be replaced by co-tidal lines which are crowded over a short distance. The direction of the tidal current off the American coast is southward, which is opposite to the direction prevailing at the same time off the African coast which is in agreement with a large amphidromy of the semi-diurnal tide in the North Atlantic.

If we omit "Meteor" station 229, which is disturbed by the proximity of the coast, 66 out of 77 current ellipses have a direction of rotation *cum sole*, i.e., 86% of all cases agree with the direction required by the theory. The ratio of the small to the large axis of the current ellipse should be theoretically

$s = [(2\omega \sin \phi) / 2\pi] T = 1.033 \sin \phi$. Table 84 shows that in the whole, this relation is satisfied. From the ratio of the minor to the major axis of the current ellipse V/U and from the difference in time ϵ between the current maximum and that of the occurrence of high water, Proudman and Doodson derived (see p. 565 (equation XI.38)), two equations for the computation of the

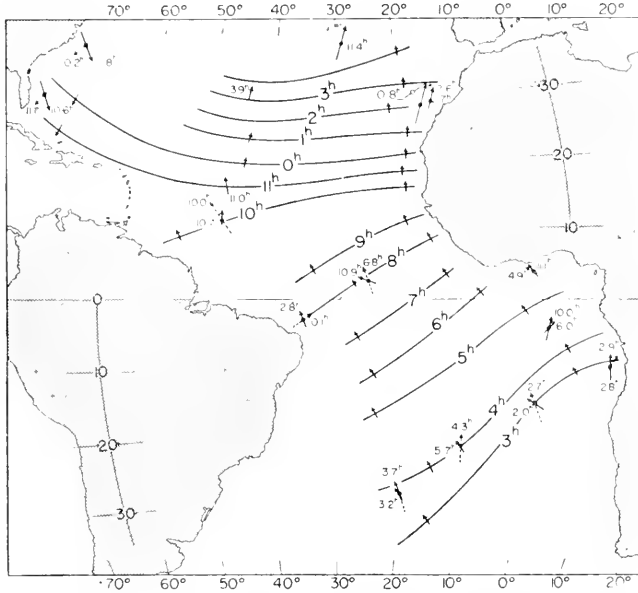


FIG. 204. Direction, phase and intensity of the semi-diurnal tidal current in the Atlantic.
 →, upper layer; ←, deeper layers.

angle ψ enclosed by the co-tidal line and the direction of the current maximum for a certain locality. THORADE (1935, p. 93) has used these equations to compute this angle for the stations in Table 83 by using time of high water as given by Sterneck's map of co-tidal lines (1922) and compared this angle with those given in the map. Table 83 gives in its columns the necessary data and it is to be noted that the observations for different depths have been averaged for the indicated ranges listed in the column denoted by depth. If we exclude station 176, in which the values are too scattered, we find that, for ten out of seventeen stations the difference is less than 30° , for five between 30° and 60° and that only for two it exceeds 60° . This result is not bad considering all the errors inherent in the different values. The two stations with the two greatest discrepancies are close to the coast on the edge of the shelf, and must be regarded as disturbed. If one were to use the new presentation by Dietrich instead of the one by Sterneck, there would be only minor changes because the two presentations are very similar. This result shows that the map of the co-tidal lines of the Atlantic Ocean and the results of the current measurements are in satisfactory agreement and form an oscillatory system closed in itself.

7. Theoretical Considerations on the Semi-diurnal Tides in the Oceans Especially on Those of the Atlantic Oceans

It would be interesting to compare maps of the co-tidal lines of the oceans based on the observations with theoretical maps of the tides. However, it has not been possible hitherto to derive for the oceans tide maps based on an exclusively theoretical mathematical consideration. The complicated configuration of the oceans, the co-oscillation of the water-masses with adjacent seas, the Coriolis force and friction are a few of many factors influencing the tides. We refer to Chapter XI. 2-7 for methods which have been developed

Table 84. Ratio of minor to major axis of tidal current ellipses of semi-diurnal tide as a function of the latitude

Mean latitude ...	36.3°	29.1°	21.5°	14.3°	9.0°	3.4°
Number of stations	2	6	1	4	1	4
Observed ratio	0.570	0.425	0.450	0.315	0.194	0.265
Computed ratio	0.610	0.502	0.378	0.255	0.161	0.062
Difference	+0.040	+0.077	-0.072	-0.060	-0.033	-0.203

in order to obtain at least a first approximation. PROUDMAN and DOODSON (1936, 1938) have given the solution for an ocean of constant depth bounded by two meridians 180° apart, i.e. bounded by a complete meridian (p. 286). The application of these results to the actual oceans can, of course, only be made with reservations. However, it is to be expected that the methods of Proudman and Doodson will be developed in a not too distant future to such an extent that it will be possible to compute the theoretical tide, also for more complicated ocean basins where the boundaries are portions of meridians and circles of latitudes.

In order to obtain footholds regarding the form of the zonal oscillations one may subdivide the ocean in a number of west-east oriented channels bounded at both ends by the continents and apply the improved canal theory of AIRY (p. 290). One then obtains the number of nodal lines and their position which are changed into amphidromies under the influence of the Coriolis Force. Furthermore in order to obtain ideas about the meridional oscillations of the ocean, we may consider them as co-oscillating with the Antarctic belt with which all oceans communicate. These canals being considered by themselves and independently from the neighbouring canals the computations should naturally be used with great caution and be regarded merely as very rough evaluations of possible co-oscillating systems. Prüfer has made such computations for the Indian Ocean, and Dietrich for all three oceans. The forced M_2 tide of the Atlantic Ocean shows a node in its west-east direction between North and South America in the west and Europe and Africa in the

east, except at 30°N. , where the ocean reaches its greatest width. The same applies for the K_1 tide. The free period of the Atlantic Ocean in its meridional axis from about 40°S. lat. up to Iceland is 37.7 h, so that for the M_2 tide $r = 3.04$ and for the K_1 tide $r = 1.58$. Consequently, the co-oscillating tides for these components will have three and two nodes respectively. If we superpose these two oscillating systems in zonal and meridional direction we obtain a picture of the tides which resembles very closely the co-tidal lines derived from the observations.

Conditions are similar in the Indian Ocean. Zonal oceans bounded at 10° and 30°S. give for the M_2 tide two nodes, and for the K_1 tide one node; the co-oscillating tide for which $T_f = 20$ h would have two nodes for the M_2 tide and one node for the K_1 tide. This is mainly what the co-tidal maps show.

In the Pacific Ocean, which widens from the north towards the equator, the number of nodal lines increases. For zonal oscillations we have in 40° and 30°N. two nodes for the semi-diurnal tides, from 20°N. to the equator there are three nodes. Omitting the Tasman Sea and the Coral Sea, there are two nodes in the South Pacific. A meridional co-oscillating tide should have two nodes. The number of amphidromies actually existing corresponds approximately to the points of intersection of these oscillating systems. These considerations are acceptable for the Atlantic and the Indian Ocean, but they seem too risky for an ocean which has the expansion of the Pacific. All that can be said is that the canal theory supports reasonably well the number of amphidromies and nodal lines respectively of the empirically derived oscillating system.

The tides of the Atlantic Ocean have been subjected to a more thorough theoretical treatment. WHEWELL (1833) expressed the opinion when his first map of co-tidal lines was published, that the tide wave of the Atlantic Ocean did not develop in this ocean itself, but penetrated from the south-east. We should observe in the Atlantic Ocean only the effect of a wave which had developed already in the Pacific Ocean or in the Antarctic belt. Later, WARBURG (1922, p. 12) has pointed out that a tidal wave, as required by the theory, can only develop in a belt girding the whole earth and that the tides in the Atlantic Ocean could originate only in this belt.

This conception concerning the origin of the tides in the Atlantic was already contradicted by AIRY (1842), who emphasized that the Atlantic Ocean is sufficiently vast to develop its own tides. Whewell noted later that the Atlantic tides were to be considered as standing oscillations with a nodal line extending from Brazil to Guinea. FERREL (1874, p. 239) has even expressed the opinion that a barrier between South Africa and South America would not alter the tidal wave of the Atlantic Ocean. HARRIS (1904, part IV B, p. 366) explained the co-tidal lines in the Atlantic Ocean by interferences of two oscillations developed in the ocean itself. DARWIN (1910) has taken the position that the wave entering from the south should be of more importance

for the European coasts than the wave developed in the ocean itself. KRÜMMEL (1911, vol. II, p. 250) has discussed all these more qualitative viewpoints, without however attempting to give a more quantitative explanation of the tides in the Atlantic (see THORADE (1931, p. 136)).

STERNECK'S (1922) new presentation of the co-tidal lines has revised the question of explaining the Atlantic tides. DEFANT simplifying considerably the assumptions (1924, pp. 153, 177 and 1926, p. 133) was the first to explain by longitudinal and transverse oscillations the tidal picture as shown by recent maps of co-tidal lines. He assumes that the Atlantic Ocean, including the Arctic Sea, can be represented by a large canal closed at one end, in which the tides result from the superposition of independent tides developed in the ocean itself with tides co-oscillating with those of the large Antarctic belt. These longitudinal oscillations are accompanied by two kinds of transverse oscillations: (1) those caused by the effect of the rotation of the earth on the periodical water displacements resulting from the longitudinal oscillations; and (2) independent transverse oscillations between Europe—Africa and America. The orographical configuration of the ocean was fully taken into account by Defant. All these possible oscillations were calculated numerically by step-wise computation of the different variables. The superposition of all these oscillations gave a tidal picture which in its most essential points, was quite similar to the observed one. There was never any doubt that for tides of the Atlantic Ocean the co-oscillating tide with the periodical water displacements in the Antarctic belt are much more important than the independent tides and that the basic thought of such a hydrodynamical theory is correct.

STERNECK (1926, p. 1) has rejected this simple theory, and he criticizes especially Defant's assumption of transverse oscillations. He published another theory in which he limits his explanations to the centre axis of the ocean. He splits the longitudinal oscillation derived from observations on islands into two oscillations; one with a phase of 1 h and the other one with the phase 4 h. The first one agrees very well, the second one very badly with the values derived from the theory. This is a point which still needs explanation. He disagrees in general with the possibility of splitting the oscillation into longitudinal and transverse oscillations. He tries to make his theory fit the observations made in the N. Atlantic by assuming oscillations in triangle-form which seems rather artificial. However, the introduction of these triangular oscillations means nothing else than splitting the oscillations into separate waves, although he does not use any longer rectangular coordinates, which complicates the question.

DEFANT (1928) has elaborated on his theory of the Atlantic tides in the volume of the "Meteor" Expedition dealing also with the anchor stations. Taking into consideration the more recent theory of the tides in adjacent seas and canals, Defant assumed that a part of the tidal energy penetrating into the Atlantic ocean from the south in the form of a progressive wave, was dissi-

pated partly in the north on the vast shelf of the Arctic Sea and by its ice cover, and has not returned in the form of a reflected wave into the Atlantic Ocean. As mentioned in Ch. XI.3c, p. 345 the form of the co-oscillating tide in such an ocean is no longer a standing wave, but must be represented as a superposition of waves which are displaced with reference to each other.

This explains why in the south Atlantic, the tide wave is almost a pure progressive wave. We would then have in the Atlantic Ocean a similar case as in the North Sea, where the wave coming in from the north loses so much energy in the south by friction that although the reflected wave is sufficient to develop an amphidromy in the Deutsche Bucht superposition in the northern North Sea produces only a progressive wave (see p. 368). The co-oscillating tide in the Atlantic has the phase 1 h in the south (see Chart I), the corresponding orthogonal oscillation the phase 4 h, and these can be computed numerically for the centre axis of the ocean, taking into account the effect of the tide generating forces. The boundary conditions are for the wave with the phase 1 h that at the cross-section zero in the north (Iceland) $\xi_1 = 0$ and η_1 is given an arbitrary value; for the wave with a phase of 4 h, $\eta_4 = 0$

Table 85. *Semi-diurnal tidal constants at islands in the Atlantic*

Place	Latitude	Longitude west	Semi-diurnal tide		Wave amplitude (cm)	
			Amplitude (cm)	Phase lunar hours Greenwich Time	1 h η_1	4 h η_4
Vestmannaeyjar, Heimaey	63.4° N.	20.3	137	6.5 h	-132	+35
Western Azores (average from 8 stations)	38.7° N.	28.5°	60	2.1 ₀ h	+ 50	+33
Bermuda Island	32.3° N.	64.8°	55	11.2 h	+ 32	-44
Two Western Cape Verde Island	17.0° N.	25.2°	63	8.0 ₂ h	- 54	-32
Fernando de Noronha and Rocas	3.8° S.	33.1°	105	6.6 ₂ h	-103	+21
Ascension	7.9° S.	14.4°	45	6.3 ₃ h	- 42	+16
St. Helena	15.9° S.	5.7°	45	3.4 ₈ h	+ 12	+43
Trinidad and Martin Vaz.	20.5° S.	29.1°	42	5.5 h	- 30	+30
Tristan da Cunha	37.0° S.	12.3°	75	0.8 ₂ h	+ 75	- 7

and ξ_4 is given an arbitrary value. The boundary conditions at the other end (co-oscillation with the tides of the Antarctic belt determine the free constants. These constants can also be computed by means of the tidal observations on some islands which are near the centre axis, for instance the Azores and Tristan da Cunha, which has proved to be more practical. In Table 85 are given the amplitude and phase as observed on these islands and also the component values for both waves with the phase 1 and 4 h.

Figures 205 and 206 show that the agreement between theory and observations for amplitude and for the phase is very good. The Atlantic Ocean, therefore, behaves, at least on its centre axis, like a narrow canal.

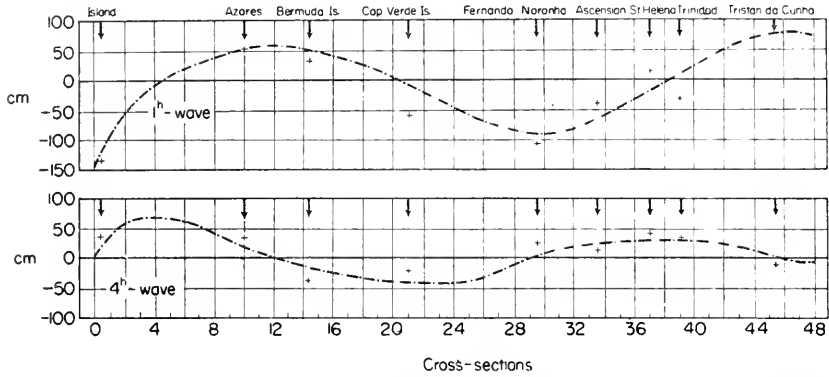


FIG. 205. Distribution of the amplitude for the 1 h and 4 h waves along the centre axis of the Atlantic Ocean. +, tide observations on Atlantic Islands corresponding to Table 85.

The phases of the tidal currents also fit well into this theory (Fig. 207); however, the velocities of these currents are in reality greater than given by the theory. This contradiction, however, is explained, if one considers that the rotation of the earth is not taken into account in the theory. Accord-

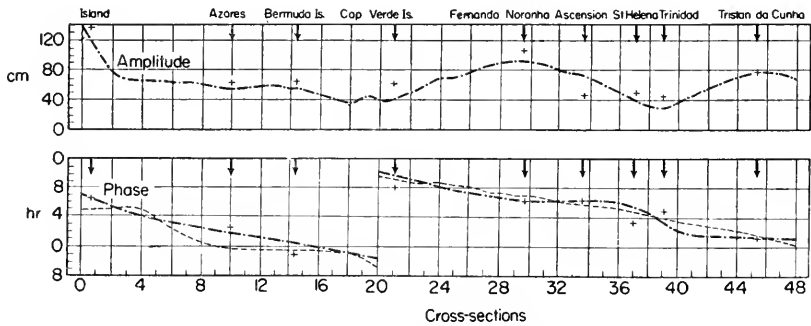


FIG. 206. Theoretically computed semi-diurnal tide along the centre axis of the Atlantic. +, observed values on islands; ----, co-tidal lines according to Sterneck.

ing to Sverdrup, the rotation of the earth increases the velocity of the tidal currents, above those in a long narrow canal by a factor $\frac{1}{1-s^2}$, in which

$$s = \frac{2\omega \sin\phi}{2\pi} T$$

(see equation XI.2). If we multiply by this factor, we have an entirely satisfactory explanation for the observed slow increase of the velocity of the semi-diurnal tidal current to the north. According to this theory, the semi-diurnal

tides in the Atlantic thus become a mixture of independent and co-oscillating tides, in which the latter predominate. We find that the average height of both waves are in a ratio of 2:3.

The diurnal tides of the Atlantic Ocean could also be explained by this theory. The procedure is the same. We can compute theoretically the amplitude and phase for the centre axis. However, for the diurnal tides we have the added difficulty that the current observations have been made in different seasons, and this diurnal tide is very severely subjected to the semi-annual periodical variation. But, fundamentally it seems also possible to explain the picture of the diurnal tides.

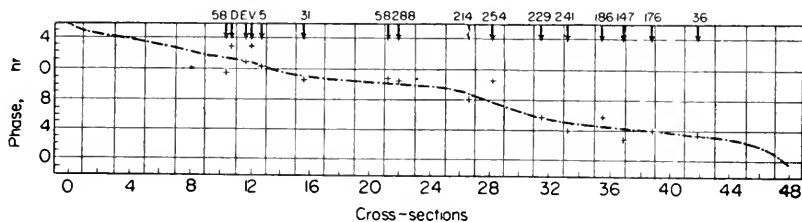


FIG. 207. Phase of the semi-diurnal tidal current for the centre axis of the Atlantic and results of the current measurements (+).

PROUDMAN (1944) has made a new attempt to explain theoretically the tides of the Atlantic. It is mathematically correct that for every area of an ocean the tides and tidal currents are fully defined when one knows, for the chosen boundaries of this area, the tidal ranges or the tidal currents, and if the boundary conditions are fulfilled for the shores. Proudman selects as boundaries of the area of the Atlantic Ocean under consideration the parallel of latitude 45°N. and 35°S. , and considers the tides of this area as a superposition of a number of oscillations which are possible in an ocean in the form of a canal and which fulfils the boundary conditions. He assumes for these oscillations that there is no friction and he neglects any friction along the coasts. Possible oscillations which Proudman considers are:

(1) The independent tide caused by the meridional and zonal tide generating force.

(2) Two waves of the Kelvin type (p. 206), one coming from the north, the other from the south into the area.

(3) Two Poincaré waves, one coming from the north, the other one from the south, taking only the two simplest from the infinite series of these waves (p. 208). We can compute for all these waves the relative tidal ranges and phases, as well as the tidal currents for the entire area under consideration, and taking the morphological configuration fully in account. The superposition of these four waves must agree with the observations made at four coastal localities after deducting the forced tide. This will determine the four free constants necessary to transform the relative values into ab-

solute values for the four waves. The following points were selected: two at the west and east coast at $32^{\circ}5'S.$ and two at $7.5^{\circ}S.$, i.e. south of the gulf of Guinea and of Cape San Roque, where the greatest irregularities in the basin occur. The most important waves seem to be the Kelvin wave travelling northwards and the Poincaré wave travelling southwards. The superposition of all these waves gave, both as to phases and amplitudes, a tidal

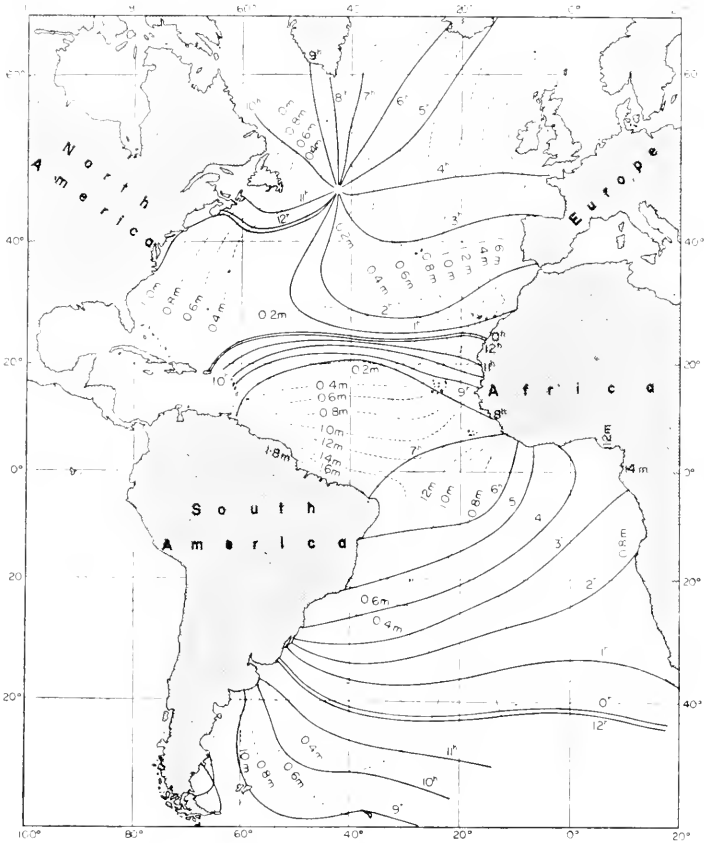


FIG. 207a. Theoretical tides of Atlantic Ocean. Full lines: co-tidal lines referred to moon-transition through meridian of Grw., dashed lines: co-range lines of the semi-diurnal tide M_2 in m (according to Hansen).

picture which from $10^{\circ}N.$ to $35^{\circ}S.$ agrees very well with the values observed at the coasts. If one goes from $10^{\circ}N.$ into the N. Atlantic, the agreement ceases. Perhaps it is possible to make the values agree by increasing the number of waves. This paper of Proudman is an attempt to compute co-tidal lines and co-range lines which satisfy in all respects hydrodynamical principles for an extensive ocean area from coast to coast. However, it is only an attempt to derive the geographical distribution of the tides over the entire expanse

of an ocean from the boundary conditions of the problem. Properly speaking, it is not a theory of the tides of the ocean because this would also have to include the proof as to why each tide wave occurs with its phase and amplitude in the given form.

HANSEN (1949) has used his method, given in Chap. XI, p. 368 to compute the semi-diurnal tides of the Atlantic Ocean. By means of this method isolines of water level are obtained for the North Atlantic. It is shown that there is a fairly good agreement in magnitude between the observations on North Atlantic islands and the corresponding values derived theoretically from coastal observations. Figure 207*a* contains these theoretical tides of the Atlantic, giving isolines of high-water difference referred to the upper transit of the moon through the Greenwich meridian as well as co-tidal lines of the semi-diurnal tide M_2 .

Chapter XV

The Tides in Relation to Geophysical and Cosmic Problems

IN this chapter we will discuss a few problems which are related only indirectly to the tides of the ocean and rather deal with the effect of these tides on the solid earth and its movements. We have treated this matter very summarily, only touching upon the most essential points, because we thought that these questions should be briefly mentioned in a textbook on oceanography. For details we refer to the textbooks on geophysics.

1. The Detection of the Tides of the Solid Earth from Tidal Observations in Shallow Adjacent Seas

In the theory of the tides, as well in the discussion of tidal observations, it is mostly tacitly assumed that the earth is completely rigid and, therefore, not yielding to the tide generating forces. According to observations in geophysics, this assumption is incorrect. In Fig. 208 it is shown how the tides of the oceans are influenced by the tide of the solid earth if the tides obey completely the equilibrium theory (see THORADE, 1933, p. 49). Assume that the ocean bottom BB_0 is rigid and a gauge PP_0 is established at the point P . High water will occur at that point and the water surface will have risen from mean sea level MM_0 to $H'H'_0$, when the tide generating body is in the prolongation PP_0 (in the zenith); the gauge will register a height of water $AN_0 = \bar{\eta}$ above mean sea level at A . At A the surface will be horizontal (maximum) and according to the direction of the tide generating forces (indicated schematically on top of the figure), the surface will slope down on both sides; if this slope is $\bar{\alpha}$, the horizontal component of the tide generating force, which must balance the pressure force, will be $g \tan \bar{\alpha}$ or, $\bar{\alpha}$ being very small, $g\bar{\alpha}$.

This simple picture changes:

(1) When one considers the variation in the height of the tide caused by the tidal protuberance (see p. 284); and

(2) If we assume a certain elasticity in the solid earth which yields to the tide generating forces. The addition of the potential of the protuberance causes a rise of the water level to HH_0 and an increase in the range at the

tide gauge of $AA_0 = \bar{\eta}_0$. The order of magnitude of this increase in the ocean is about one-eighth of the original range.

Let the tide generating forces deform the earth from BB_0 to $B'B'_0$ and let us assume that the surface will rise an amount η_0 from P to P' . The tide gauge in P will register the same rise, so that P_0 becomes P'_0 and the point N on the tide gauge will be at N'_0 , and we have $P_0P'_0 = NN'_0 = \eta_0$.

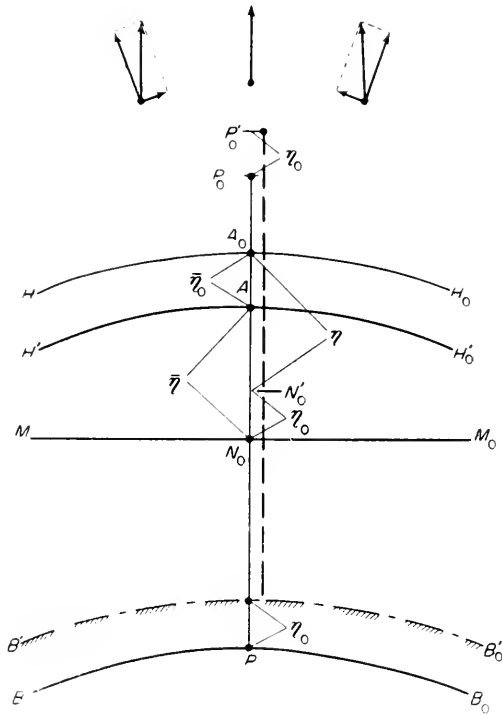


FIG. 208. Tides of the solid earth and oceans.

However, the surface HH_0 does not rise, because its distance from the centre of the earth is governed by the balance between the tide generating force and gravity (equilibrium between tidal forces and pressure forces). The protuberance of the earth could cause to the utmost a slight change, inasmuch as the lower part of the protuberance of the water is now occupied by solid matter instead of water, which changes to some extent the potential of the attraction of the water protuberance. Figure 208 shows that

$$N'_0A_0 = \eta = \bar{\eta} + \bar{\eta}_0 - \eta_0. \tag{XV.1}$$

Likewise, if \bar{a}_0 is the gradient of HH_0 against $H'H'_0$ and a_0 the gradient of $B'B'_0$ against BB_0 , $a = \bar{a} + \bar{a}_0 - a_0$ and the horizontal acceleration will be

$$ga = g(\bar{a} + \bar{a}_0 - a_0). \tag{XVI.2}$$

In investigating the tides of the solid earth, $\bar{\eta}_0$ and η_0 are usually assumed to be proportional to $\bar{\eta}$, as it is for the equilibrium tides, so that if

$$\eta_0 = h\bar{\eta}, \quad \text{and} \quad \bar{\eta}_0 = k\bar{\eta}$$

$$\eta = (1 - h + k)\bar{\eta}.$$

$\gamma = (1 - h + k)$ then represents the ratio between the observed tidal range forced by the tidal generating forces and the tidal range which would be observed if the earth were completely rigid.

It is not possible, in the case of semi-diurnal and diurnal tides to compute the quantity γ for a locality from a comparison between the amplitude of a partial tide derived from the harmonic analysis and the amplitude derived theoretically from the equilibrium theory assuming an absolutely rigid earth, because these waves do not have a tidal development which corresponds approximately to the equilibrium theory. For the long period tides, however (especially the fortnightly and monthly partial tides) there is a probability that they would have their full equilibrium values if the earth were absolutely rigid. It is easy to compute these values; the difficulty is rather in obtaining reliable observations for the semi-monthly and monthly partial tides. The first comparisons of this kind which actually gave a proof of the tides of the earth, were made by THOMSON (LORD KELVIN, 1867) and DARWIN (1883, 1911). Darwin used the harmonic constants of the semi-monthly lunar tide observed on 33 stations and found $\gamma = 0.675$, i.e. the observed tidal range is approximately one-third smaller than the value computed from the equilibrium theory. SCHWEYDAR (1907) has analysed, using the same method, 194 annual observations, and he obtained essentially the same result: for the semi-monthly lunar tides $\gamma = 0.6614$, for the monthly lunar tide $\gamma = 0.6422$. The tides conformed to the theoretical times of high water, so that the assumption of equilibrium tides appears to be justified. Later on it was possible to produce a direct proof of the tides of the solid earth with a horizontal pendulum. See for details GUTENBERG (1929), SCHMEHL and JUNG (1931) and HOPFNER (1936). However, there is a great spread in the derived values for γ , which has probably its origin in secondary phenomena mainly caused by the pressure of the oceanic tides against the continents and by the attraction of the moving water-masses. According to SCHWEYDAR (1929), the most plausible value for $\gamma = 0.841$, whereas PREY (1929) holds that 0.74 is the most probable value. JEFFREYS (1929) gives 0.66 as the most reliable value. It appears therefore that there is not yet sufficient certainty as to the actual value of γ .

PROUDMAN (1928) has proven that the hydrodynamical theory of the tides, at least for narrow waters, like canals, is sufficiently developed to permit the calculation of the tides of the solid earth. The restriction to narrow

waters, whose bottom configuration must be known exactly, means that transverse currents may be neglected. On the other hand, the partial tides with a short period can also be considered, which is of great advantage. Proudman has developed two methods for the computation of γ , which will be explained summarily.

If x is taken in the direction of the longitudinal axis of the narrow sea in the form of a canal, and u represents the average value of the tidal current on a cross-section perpendicular to x , while there is no transverse current, then u will only be a function of x and t . The differential equations of the water motion can be written into the form

$$\left. \begin{aligned} \frac{\partial u}{\partial t} &= -g \frac{\partial}{\partial x} (\eta + \eta_0 - \bar{\eta} - \bar{\eta}_0), \\ 2\omega \sin \phi u &= -g \frac{\partial}{\partial x} (\eta + \eta_0 - \bar{\eta} - \bar{\eta}_0), \end{aligned} \right\} \quad (\text{XV. 3})$$

whereas the equation of continuity takes the form

$$\frac{\partial}{\partial x} (Su) + b \frac{\partial \eta}{\partial t} = 0 \quad (\text{XV. 4})$$

in which S represents the area and b the width of the cross-section at the point x . If u is known the second equation of (XV. 3) helps to reduce the tidal ranges, observed along the coasts to the central axis of the canal.

The first method determines the difference between the tides computed without assuming a tide of the solid earth and the observed tides. If we put, as usual,

$$\begin{aligned} \eta &= H \cos(\sigma t - z) = \eta_1 \cos \sigma t + \eta_2 \sin \sigma t, \\ u &= U \cos(\sigma t - \varepsilon) = u_1 \cos \sigma t + u_2 \sin \sigma t, \end{aligned}$$

we obtain from (XV. 4)

$$\Delta Su_1 = -\sigma H \sin z \cdot b \Delta x \quad \text{and} \quad \Delta Su_2 = +\sigma H \cos z \cdot b \Delta x.$$

If the tidal range along the entire canal is known, one can compute from these relations u_1 and u_2 , i.e. the velocity of the current for each cross-section. With these values we have for all sections the variation of the current velocity during a unit time; because

$$\frac{\partial}{\partial x} (\eta - \bar{\eta}) \quad \text{or} \quad \frac{\partial}{\partial x} (\eta_1 - \bar{\eta}_1) \quad \text{and} \quad \frac{\partial}{\partial x} (\eta_2 - \bar{\eta}_2)$$

are known from the observations, and the theory of the tides' generating forces, in equation (XV. 3) only

$$\frac{\partial}{\partial x} (\eta_0 - \bar{\eta}_0)_1 \quad \text{and} \quad \frac{\partial}{\partial x} (\eta_0 - \bar{\eta}_0)_2$$

are still unknown and can be computed in this way. The method gives,

through numerical integration, the tidal range $\eta_0 - \bar{\eta}_0$ except for one unknown constant; it therefore only gives a relative tide of the solid earth, i.e. the difference between the elevation of the crust η related to the elevation caused by the attraction of the protuberance.

The second method is less dependent upon the accuracy of the observations. If we replace u and $\bar{\eta}$ by $ue^{i\sigma t}$ and $Fe^{i\sigma t}$ and if we take

$$\eta = \gamma\eta_1 + l\eta_2 \quad \text{and} \quad u = \gamma u_1 + lu_2$$

then equations (XV. 3) and (XV. 4) become

$$\left. \begin{aligned} \gamma \left[i\sigma u_1 + g \frac{\partial \eta_1}{\partial x} - F \right] + l \left(i\sigma u_2 + g \frac{\partial \eta_2}{\partial x} \right) = 0, \\ \gamma \left[\frac{\partial Su_1}{\partial x} + i\sigma b\eta_1 \right] + l \left(\frac{\partial Su_2}{\partial x} + i\sigma b\eta_2 \right) = 0. \end{aligned} \right\} \quad \text{(XV. 5)}$$

The two expressions between brackets, put equal to zero, give with the boundary conditions $\eta_1 = 0$ and $Su_1 = 0$ for $x = 0$, a forced oscillation caused by the force $g\bar{\eta}$. The two expressions between parentheses with the boundary condition $\eta_2 = 1$ cm, $Su_2 = 0$ for $x = 0$ give a free oscillation with boundary conditions which are at first arbitrary. A general solution of the equations is then

$$\left. \begin{aligned} \eta &= \{(1-h+k)\eta_1 + l\eta_2\} e^{i\sigma t} \\ u &= \{(1-h+k)u_1 + lu_2\} e^{i\sigma t} \end{aligned} \right\} \quad \text{(XV. 6)}$$

A comparison with the observations on at least one station (section) allows one to compute both the unknown $\gamma = 1-h+k$ and l , while it is also possible to determine differences in phase (4 unknown).

GRACE (1930, p. 273; 1931, p. 301) has applied this method to Lake Baikal and the Red Sea. He used the second method for Lake Baikal. Neglecting the tides of the solid earth, he repeated, first, the computation of Sterneck (see p. 454), and he obtained the same results. The amplitudes at the ends of the lake were 15.7 and 12.3 mm (see Fig. 192). Taking into consideration the tides of the solid earth, and basing himself on the observations made in the Petschannoja Bay, he found $\gamma = 1-h+k = 0.54$ for M_2 and 0.73 for K_1 and at the same time a reduction of the amplitudes to the observed values. The average of the two γ values happens to agree with Jeffreys's value. It can be taken for granted that the tides of the solid earth eliminate the contradiction which existed between the observations, and the results of the theory which, owing to the smallness, narrowness, and great depth of the oscillating water-masses, had to follow the simple equilibrium theory. It is not necessary to attribute these differences to the friction as Sterneck did.

Proudman proposed the Red Sea as especially suitable for the computation of the tides of the solid earth, Grace has made such survey for the M_2 tide for this sea, using both methods. In following the second method there he

eliminated the less reliable harmonic constants of certain localities and there were a still sufficient number of data left to allow the determination of the four unknown quantities.

The result was that, $\gamma = 1 - h + k = -0.42$. This value is entirely at variance with the other values and no explanation can be found for it. However, it is certain that in considering the tides of the solid earth we can represent much better the observations.

The application of the first method shows perhaps the reasons why the second method gives such a different result for γ (see also THORADE, 1933; see p. 411 and Fig. 173). If according to the second method, the assumption that the tides of the solid earth are proportional to the equilibrium tide is correct, then the relative tide of the earth (the excess of the tide of the earth over the rise caused by mutual attraction of water spheroids) should have the same form as the equilibrium tide itself. In reality this is not the case: the curves are very much disturbed, which must probably be attributed to inaccuracies in the observations. If one compares very roughly the difference between the two curves, one gets, according to Grace, a ratio 1:4, from which it follows that

$$h - k = 0.25 \quad \text{or} \quad \gamma = 1 - h + k = 0.75 .$$

The agreement with the value of Prey would be very good. However, this estimation is very inaccurate and all one can tell for sure is that the tides of the Red Sea can hardly be explained with sufficient accuracy without considering the tides of the solid earth, and that the accelerations produced by these latter tides will be approximately of the same order of magnitude as that of the tide generating forces.

2. Deformations of the Solid Earth by Tidal Load

The tides of the solid earth are disturbed and cause the values of γ to vary. The disturbing effect is caused above all by the oceanic tides exercising varying pressures on the shores, which cause deformations of the earth's crust.

These deformations show the same period as the oceanic tides and superimpose themselves on the tides of the solid earth. According to the amplitude of these deformations, the tides of the solid earth may be hardly noticeable. Thus, a coastal gauge will record also oscillations, which besides the general tides can be explained by the attraction exercised by the water-masses which are being periodically moved towards the coast by the tides and by the varying loads exercised by the tides. It can be shown that, when the rocks have the same degree of rigidity as glass, the direct attraction by the water-masses is only one-sixth of the disturbance of the plumb line caused by the loads of the tides. The effects of the variations of the slope are, therefore, by far the more important.

In order to make the effect of the tidal load clearer, DARWIN (1882; 1910,

p. 131) has calculated an ideal, simplified case, which comes as close as possible to conditions existing in nature. The simplifications consist, in the first place, in the fact that the earth is assumed to be level, which assumption can be made without hesitation, inasmuch as the tidal load affects only the upper layers close to the surface; secondly, the ocean is assumed to consist of an indefinite number of wide canals separated from each other by wide strips of land of the same width. It is further assumed that in these seas the water oscillates in the form of simple oscillations (seiches) around a central line, so that when there is high water on one side there is low water on the other side and vice versa. The problem is to find out how the tides change the configuration of the ocean bottom and the strips of land. The result of the computation is

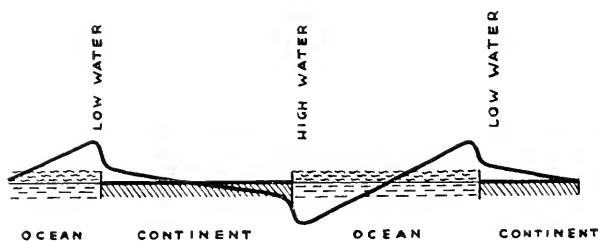


FIG. 209. Deformation of land and ocean bottom by the tidal load (Darwin).

shown in Fig. 209, in which the resulting bottom slope is exaggerated for the sake of clearness. Through the pressure of the water the surface of the land and of the sea, which were level prior to the tidal disturbance, takes the form of the curved line when there is low water to the left of the strip of land and high water to its right. If we interchange N.W. with L.W., the figure is reversed like a mirror-image. One notices that both the solid earth and the ocean bottom oscillate around a central position, which shows that the strip of land appears to be nearly level, the ocean bottom somewhat curved. The sharp bend in the coast line is due to the assumption of a discontinuous form of the solid earth along the shore line; it vanishes if one assumes that the depth of the ocean in front of the coast does not increase suddenly, but gradually. If one assumes that the range of the tide on the coast is 160 cm, the width of the oceans and continents 6280 km each (which corresponds to the average width of the Atlantic Ocean) and that the rigidity of the rocks of the earth is twice that of the most flexible glass and a quarter that of the hardest glass, then the slopes of the land caused by the tidal load at high water are given in Table 86. At low water, the inclinations occur in the opposite direction, so that the variation in inclination during an entire tidal period is double the amount listed in the table. To make the order of magnitude of these inclinations clearer, we will state that two-hundredths of arc second corresponds to an inclination of 1 cm on 103 km; a pendulum at the coast would participate to the fullest extent in this change in inclination of its base.

However, the attraction of the water piled up at the coast at high water causes a further deviation of the pendulum which, with the adopted degree of rigidity of the rocks is computed to be one quarter of the above amount. The total amplitude of the deviation from the plumb line for various distances from the coast is also given in Table 86. In the centre of the continent

Table 86. Deformation of the surface of the earth by tidal load

Distance from shore line (high-water line)	10 m	100 m	1 km	10 km	20 km	100 km
Slope of the solid crust in 1/100 arc second	10	8	6	4	3½	2
Apparent amplitude of the deviation of the plumb line in arc second	0.25	0.20	0.15	0.10	0.084	0.050

(3140 km distant from the coast) the amplitude would be 0.012 arc sec. One can see from these values that the effect of the tidal load at H.W. is sufficiently great to disturb the registration of the tides of the solid earth by the horizontal pendulum. It is very difficult to disentangle these two effects, for the reason that the tidal load is different for each station. Darwin gives a good example of the deformation of the earth through the tidal load, which is illustrated in Fig. 210. The Liverpool observatory at Bridston, where the horizontal

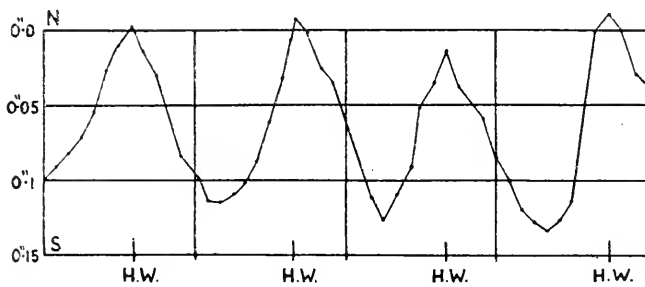


FIG. 210. Deformation of the earth crust by tidal load observed by the Observatory at Bidston.

pendulum was set up, is located 2½ km from the sea, at the estuary of the Mersey (see *Nature Lond.*, 1910, p. 427). The larger mass of the water whose weight causes this deformation should be located north-west of the Observatory. Darwin was right in assuming that the deviation was probably caused by the tides in the open sea rather than by the high waters in the estuary. Figure 211 shows another example by TAKAHASI (1929, p. 85) where, near the shore, the disturbance due to the tidal load of high waters can amount to nearly 50 times the tides of the solid earth.

3. Frictional effects of tidal currents and their relation to cosmic problems

In a number of interesting cosmic problems, the frictional effects of the tidal currents play an important role. At the time the masses of the earth and of the moon were still fluid, this part was a very important one; when the moon was nearer to the earth, the tide produced by the attraction of the earth was very large. Every flood protuberance exercises, however, a frictional effect

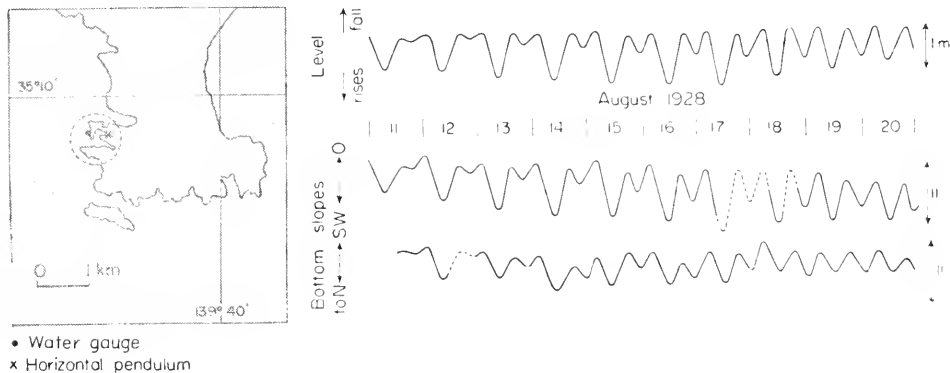


FIG. 211. Action of the oceanic tides in the tilting of the earth crust in the vicinity of the Tokyo coast (Takahasi).

on the rotating body and both protuberances try to reduce the rotation of the celestial body, acting like brake shoes on a spinning wheel. The friction tries constantly to drag the flood protuberances along with the rotation of the moon, so that the line connecting the two fictitious bodies (moon, anti-moon) will precede the protuberances, while the two flood protuberances will retard the rotation. A more accurate picture will be obtained by computing the tides forced by a tide generating force in an equatorial canal when there exists a frictional effect. The case without friction has been discussed in Chapter IX, 3, p. 290. The equation of motion will be modified by introducing at the right a frictional term $-\beta(\partial\xi/\partial t)$ in which the frictional effect has been taken proportional to the velocity of the current. We find (see LAMB, 1932, § 319, p. 565) that to the horizontal tidal disturbing force

$$X = -m \sin 2(nt + \lambda + \varepsilon)$$

correspond a surface elevation.

$$\eta = \frac{H}{2} \frac{1}{\left\{ (1-p^2)^2 + \frac{\beta^2 n^2 a^4}{4c^4} \right\}^{1/2}} \cos 2(nt + \lambda + \varepsilon - \chi), \tag{XV.7}$$

in which $p = nR/c$ and χ is given by

$$\tan^2 \chi = \frac{1}{2} \frac{\beta n a^2}{c^2} \frac{1}{1-p^2}, \tag{XV.8}$$

with

$$0 < \chi < \frac{1}{2}\pi.$$

If $\beta = 0$, we have again equation (IX.12) for the case without friction.

As $nt + \lambda + \varepsilon$ measures the hour-angle of the moon past the meridian of any arbitrary point λ on the canal it appears that high water will follow the moon's transit at an interval t_1 given by $nt_1 = \chi$.

If $p^2 > 1$ we should in the case of very small friction, according to (XV.8), have $\chi = 90^\circ$, i.e. the tides would be inverted. If the frictional influence becomes noticeable the values of χ will be between 90° and 45° , and the time of high water is accelerated by the time equivalent of the angle $90^\circ - \chi$. On the other hand, when $p^2 < 1$ the tides would be direct, and the value of χ lies between 0° and 45° , the time of high water is retarded by the time equivalent of this angle. These two cases are illustrated in Fig. 212. In the direction M , the moon is supposed to be in the plane of the equator. It is

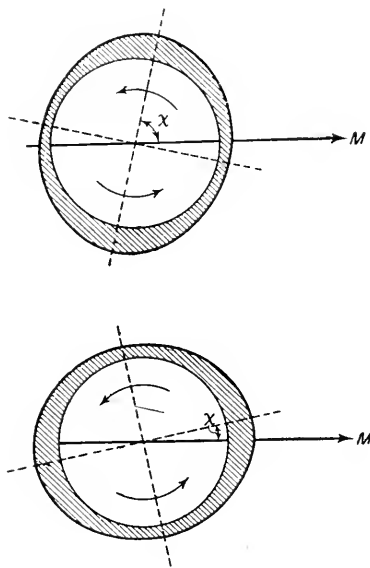


FIG. 212. Tidal friction acting on a tide wave in an equatorial canal (above $p > 1$; below when $p < 1$:). The curved arrows indicate the sens of rotation of the earth; in the direction M is the moon generating the tide.

evident that in each case the attraction of the disturbing system on the elevated water is equivalent to a couple tending to decrease the angular momentum of the rotating system composed of the earth and sea.

The retarding effect of the moon upon the rotation of the earth exists, of course, still today, although it will have been much stronger in ancient times. This retarding effect makes the day grow longer; the amount is still an open question, 1 sec in 100,000 years is regarded as a maximum value (Delaunay).

In the same manner the frictional effect could be used to explain the secular

acceleration of the moon's mean motion, which is about 5 to 12 arc sec in a century. This acceleration would then be a direct consequence of the increase of the time of earth's rotation. A value of 9 arc sec per century, for the secular acceleration of the moon's mean motion will require according to JEFFREYS (1924, p. 216) a dissipation of energy of 1.39×10^{19} erg/sec, which would have to be supplied by the frictional effects of tidal currents. According to Adams and Delaunay, the value of 12 arc sec corresponds to an increase of about 1 sec in the time of rotation of the earth.

The fact that the water height can precede or follow the moon's transit by several hours (establishment) was attributed by AIRY (1842) to the influence of tidal friction. More recent theories have shown that this is a consequence from dynamical principles which will also occur in the absence of any friction. The differences in phase, which can be explained by equation (XV.8) remains very small, even in the case of an equatorial canal of 3510 m (11,250 ft) depth which corresponds to the average depth of the Ocean. From (XV.8), and using the numerical values of page 292,

$$\tan 2\chi = - \frac{1}{1 - 311 h/R} \cdot \frac{1}{n\tau} = -0.191 \frac{2\pi}{n\tau},$$

in which $\tau = 2/\mu$ is the modulus of decay of the free oscillations. It seems rational to suppose that this modulus of decay in the present case would be a considerable multiple of the lunar day $2\pi/n$, in which event the change produced by friction in the time of high water would be comparable with $(2\pi/n\tau) \times 22$ min. Hence we cannot account in this way for phase changes of more than a few minutes. Consequently, the observed differences in phase cannot be explained this way.

As the required dissipation of energy could not possibly be supplied by a tidal friction in the solid body of the earth, the tides of the ocean should supply it. However, as stated above, it appears that the effect of ordinary friction is insufficient to explain either these shifts in phases, or the secular acceleration of the mean sun and moon's motion. It is easy to evaluate the quantities of energy which are available. The components of the tidal current u and v (except the bottom layers) must satisfy the equations of motion (IX.4). As resonance hardly comes into question for the vast expanses of the open oceans, the amplitude of the tide will be of the same order of magnitude as that of the equilibrium tide $\bar{\eta}$. In the open ocean u and v will then have the order of magnitude of 1 cm/sec. The frictional force is $k\rho(u^2 + v^2)$ and is directed against the resultant of the tidal current (see equation (XI.32) and p. 346). The dissipation of energy per unit area is then

$$k\rho(u^2 + v^2)^{3/2}. \quad (\text{XV.9})$$

The factor k has a value between 0.002 and 0.0016. The dissipation of energy per cm^2 will, therefore, be of the order of magnitude 0.004 erg/sec. The surface of all the oceans is nearly 3.62×10^{18} cm^2 , so that the total dissipation of energy in the entire ocean will be of the order of magnitude 10^{16} erg/sec. This is only a small fraction of the dissipation of energy which would be required to explain the secular acceleration of the mean sun and moon.

Therefore the ordinary friction of the tidal currents is not sufficient to account for this secular acceleration.

TAYLOR (1919, p. 1) showed that the loss of energy for the tides of the Irish Sea (see p. 346) is largely of the order of 6×10^{17} erg/sec, which is in itself alone already about 60 times larger than the value found from the open ocean. JEFFREYS (1920, p. 239) assumed therefore that the tidal friction in the adjacent and boundary seas and on the vast coastal shelf could account for the dissipation of energy required by the astronomers. In these shallow seas there is mostly a considerable increase of the tidal ranges, to such an extent that the tidal currents exceed by far 1 cm/sec. As a matter of fact, the area of these seas is small in comparison to those of the ocean, but the dissipation of energy per unit area is proportional to the third power of the velocity. The fact that the small Irish Sea already furnishes one twentieth of the required amount suggests that the friction caused by tides in the adjacent seas is the decisive factor in explaining this secular acceleration.

Jeffreys has applied Taylor's method of evaluation of the dissipation of energy to a large number of adjacent seas and straits in so far as the observations were available in order to obtain an estimate of the total value. His computations refer to spring tides and thus give maximum values listed in Table 87.

Table 87. Average dissipation of frictional energy for the semi-diurnal tide (Unit 10^{18} erg/sec)

European waters		Asiatic waters		North American waters	
Irish Sea	0.6	South China Sea	Small	Hudson Strait	0.2
English Channel	1.1	Yellow Sea	1.1	Hudson Bay	Small
North Sea	0.7	Sea of Okhotsk	0.4	Bay of Fundy	0.4
		Bering Sea	15.0	Northwest Passage	1.6
		Strait of Malacca	1.1		
Total 2.2×10^{19} erg/sec					

The total dissipation of energy for all parts of the oceans considered amounts to 2.2×10^{19} erg/sec. This is more than the amount required by the theory. It should, however, be borne in mind that a reduction to average conditions is necessary.

The superposition of the tidal currents of the lunar tide expressed by $A \cos \sigma t$ and the solar tide expressed by $\nu \cos(1-r)\sigma t$ in the same manner as was done with equation IX.2, (p. 274) gives a total current

$$A[\cos \sigma t + \nu \cos(1-r)\sigma t] = A(1 + \nu^2 + 2\nu \cos r\sigma t)^{1/2} \cos\left(\sigma t - \arctan \frac{\nu \sin r\sigma t}{1 + \nu \cos r\sigma t}\right)$$

The amplitude of the current at spring tide is $A(I + \nu)$. The dissipation of energy is proportional to the third power of the amplitude so that the ratio between the average dissipation of energy and that at spring tide will be average value of $(1 + \nu^2 + 2\nu \cos r \sigma t)^{3/2} : (1 + \nu)^3$ during an entire tidal period. If we neglect ν^6 , the numerator of it will be $\left(1 + \frac{9}{4} \nu^2 + \frac{9}{64} \nu^4\right)$. The mean ratio of the tidal ranges of the lunar and solar tide for coastal localities is approximately $\nu = 1:2.73$ and, if we assume that the mean ratio of the current velocities is about as large, we have for the above ratio 0.51.

This reduction gives for the average dissipation of energy 1.1×10^{19} erg/sec, i.e. 80% of the required amount. It seems that this dissipation of energy is sufficient to explain the observed secular acceleration of the moon. This is the more true, as certainly quite a number of adjacent seas and shelf areas have still been neglected. The Patagonian Shelf, the North American Archipelago, Barents Sea, the vast North Siberian Shelf, the numerous fjords of Norway, Greenland and other coastal regions will certainly be able to make up for the 20% still lacking.

Furthermore we have to consider the frictional losses suffered by the tidal energy on the vast ice covered areas of the Arctic and Antarctic. SVERDRUP's (1926 B) investigations showed how large they can be. Thus there is hardly any doubt that the tidal friction could account for the dissipation of energy required by the astronomers for explaining the secular acceleration of the sun and moon if the eddy viscosity of the tides on the vast shelf areas of the seas is taken into account. However, the frictional effects of the tidal currents in the open oceans are unimportant.

[A rough estimate can be made in the following manner. The total shelf area of all the oceans (depth up till 200 m) is about $27.5 \times 10^6 \text{ km}^2 = 27.5 \times 10^{16} \text{ cm}^2$. The average velocity of the tidal current during a period can be estimated for the shelf as a whole, at about $\frac{1}{2}$ knot, i.e. around 30 cm/sec. Equation (XV. 9) then gives as the dissipation of energy on the shelf 1.53×10^{19} erg/sec, which comes very close to the amount required.]

Chapter XVI

Internal Waves

1. Basic Facts and Theory of the Internal Waves

IN stratified water and in water in which the density varies with depth, waves may occur which are of different type from those appearing on the free surface and which have been discussed in chapters II to V. Because the waves occur inside the water-masses they are called boundary or internal waves. Their principal characteristic is that the largest vertical displacements of the water particles are to be found at the boundary surface between different strata or at some intermediate depth below the free surface. The amplitude of these internal waves is usually considerably larger than that of the ordinary waves at the free surface. The appearance of waves at the boundary surface between two water layers has for a long time escaped the attention of observers, because even when the amplitude of the oscillation at the boundary surface is large, the free surface of the upper layer is only slightly disturbed and remains practically at rest. Only recently, thanks to more numerous and accurate observations, has it become possible to study these internal waves more thoroughly and to prove their importance in oceanography.

(a) *Internal Waves at Boundary Surfaces*

STOKES (1847) was the first to develop the theory of internal waves at the boundary surface in a fluid consisting of two layers of infinite thickness. An excellent treatment of the problem can be found in LAMB (1932, p. 370). If we put the origin of the co-ordinates in the undisturbed boundary surface, we can write for the velocity potentials in the superposed layers the expressions

$$\left. \begin{aligned} \varphi &= C e^{\kappa z} \cos \kappa x e^{i\sigma t}, \\ \varphi' &= C' e^{-\kappa z} \cos \kappa x e^{i\sigma t}. \end{aligned} \right\} \quad (\text{XVI.1})$$

The accents relate to the upper fluid, and the z -axis is taken positive upwards. These expressions satisfy the equations of continuity (II.1) for both layers. The motions represented by them decrease rapidly with increasing distance from the boundary surface and practically vanish at a great distance. The equation of the boundary surface disturbed by the internal wave can be written

$$\eta = a \cos \kappa x e^{i\sigma t}. \quad (\text{XVI.2})$$

Hence, according to equation (II.3), we must have

$$-\kappa C = \kappa C' = i\sigma a. \quad (\text{XVI.3})$$

The equations of motion (II.2) are replaced by the equations

$$\left. \begin{aligned} \frac{p}{\rho} &= \frac{\partial \varphi}{\partial t} - gz, \\ \frac{p'}{\rho'} &= \frac{\partial \varphi'}{\partial t} - gz. \end{aligned} \right\} \quad (\text{XVI.4})$$

The condition for continuity of pressure at the boundary surface ($p = p'$ for $z = 0$) gives

$$\rho(i\sigma C - ga) = \rho'(i\sigma C' - ga). \quad (\text{XVI.5})$$

Substituting the value of C and C' from (XVI.3) we have

$$\left. \begin{aligned} \sigma^2 &= g\kappa \frac{\rho - \rho'}{\rho + \rho'}, \\ \frac{\sigma}{\kappa} &= c, \end{aligned} \right\} \quad (\text{XVI.6})$$

or with

the velocity of propagation of progressive internal waves of the wave length $\lambda = 2\pi/\kappa$ is given by

$$c^2 = \frac{g\lambda}{2\pi} \frac{\rho - \rho'}{\rho + \rho'}. \quad (\text{XVI.7})$$

The presence of the upper fluid has therefore the effect of reducing the velocity of propagation of the internal waves in the ratio $(\rho - \rho')/(\rho + \rho')$. This decrease in the velocity, has a twofold cause; the potential energy of a given deformation of the common surface is decreased in the ratio $1 - \rho'/\rho$, whilst the inertia is increased in the ratio $1 + \rho'/\rho$.

In practice $\rho - \rho'$ is of the order of magnitude 10^{-3} so that the decrease of velocity of the internal waves c against the surface waves is about 45 times, which is quite considerable.

The waves discussed hitherto have the character of surface or "short waves" because their wave length is small compared with the infinite thickness of the two superposed layers.*

Figure 213 shows, according to V. Bjerknes, the stream lines and orbits in the two superposed layers for an internal wave travelling from left to right. It should be noticed that there is a discontinuity of motion at the common surface. The normal velocity $-\partial\varphi/\partial z$ is of course continuous, but the tangential velocity $-\partial\varphi/\partial x$ changes a sign as we cross the surface; in other words, we have a *vortex-sheet*.

* Concerning the application of the equation (XVI.7) to the air-water system see Chapter IV. p. 76.

In nature we deal with cases in which the surface of the upper layer must be considered as a free surface. In this case we can give the velocity potentials of the two superposed layers the form

$$\left. \begin{aligned} \eta &= C \cosh(z+h) \cos \kappa x e^{i\sigma t}, \\ \eta' &= (A \cosh \kappa z + B \sinh \kappa z) \cos \kappa x e^{i\sigma t}, \end{aligned} \right\} \quad (\text{XVI.8})$$

in which h and h' are the thickness of the lower and upper layers respectively. Where we deal with internal waves occurring at the boundary surface between two homogeneous layers of different density, the velocity components

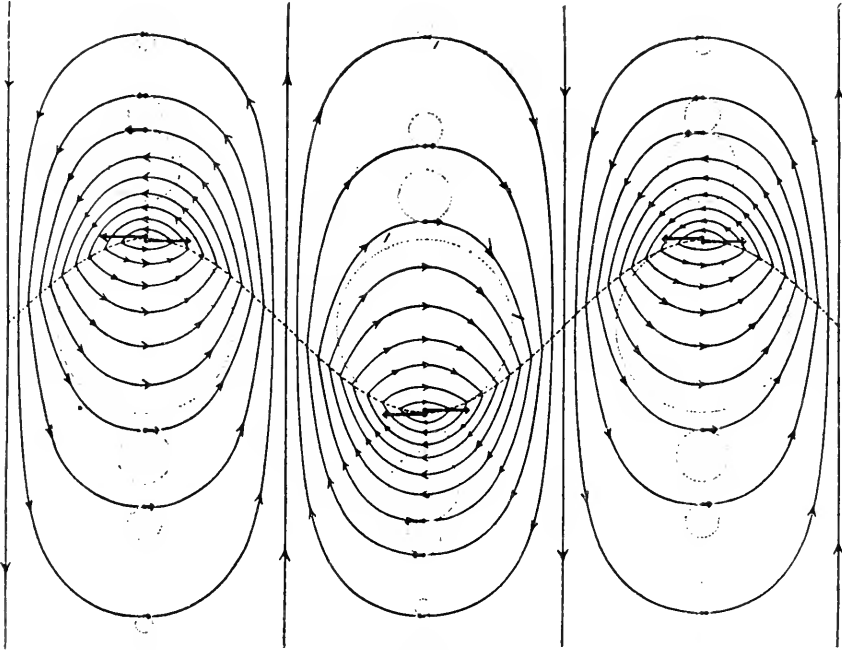


FIG. 213. Streamlines and orbits in a progressive internal wave travelling from left to right at the boundary of two fluids.

must satisfy the kinematic and dynamic boundary conditions both at the free surface and at the internal boundary surface, and also the equation of continuity for both layers. This leads to a quadratic equation for the velocity of propagation c of waves with a wave length $\lambda = 2\pi/\kappa$.

$$c^4(\rho \coth \kappa h \coth \kappa h' + \rho') - c^2 \rho (\coth \kappa h' + \coth \kappa h) \frac{g}{\kappa} + (\rho - \rho') \frac{g^2}{\kappa^2} = 0. \quad (\text{XVI.9})$$

It is shown by this equation that for each wave length two different types of wave may exist. If the difference in density at the discontinuity surface is small, the two following equations are the approximate roots:

$$\left. \begin{aligned} c_1^2 &= \frac{g}{\kappa} \tanh \kappa(h+h'), \\ c_2^2 &= \frac{g}{\kappa} \frac{\varrho - \varrho'}{\varrho \coth \kappa h + \varrho' \coth \kappa h'} \end{aligned} \right\} \quad (\text{XVI.10})$$

The first type of wave is identical with the ordinary surface waves which travel with a velocity c_1 , on a layer of water of the thickness $(h+h')$. With this type of wave the vertical component of the displacements of the water particles decreases gradually with increasing depth from the surface. The surface has the largest amplitude, the boundary surface a smaller one and the phase of the wave motion at the surface is the same as at the boundary surface. This "external" wave, therefore, is in no way different from the ordinary wave at the surface of homogeneous water-masses.

The second type of wave progressing with a velocity of c_2 has its largest amplitude at the boundary surface and it decreases rapidly upwards and downwards. Consequently, this is an *internal wave*. In the upper layer close to the free surface there is a certain depth where the vertical motions vanish. Consequently, the internal boundary surface and the free surface oscillate with opposite phases, but the amplitude at the free surface is so small that for all practical purposes it can be disregarded. The ratio between the amplitude at the free surface and that at the boundary surface is given by

$$\frac{1}{\cosh \kappa h' - (g/c^2 \kappa^2) \sin \kappa h'}. \quad (\text{XVI.11})$$

In practice, the depth of the lower layer is large compared to the wave length. Then we can put $\tanh \kappa h = 1$ and the roots of (XVI.9), and (XVI.10) become

$$c_1^2 = \frac{g}{\kappa},$$

and

$$c_2^2 = \frac{\varrho - \varrho'}{\varrho \coth \kappa h' + \varrho' \kappa} \frac{g}{\kappa}, \quad (\text{XVI.12})$$

the ratio between the amplitudes at the free surface and at the boundary surface becomes

$$- \frac{\varrho - \varrho'}{\varrho} e^{-\kappa h'}. \quad (\text{XVI.13})$$

When ϱ differs slightly from ϱ' this is always a small quantity.

If, on the contrary, the thickness of the upper layer is small compared to the wave length, one can replace $\coth \kappa h'$ by $1/\kappa h'$ and one gets in first approximation:

$$c_1^2 = \frac{g}{\kappa} \quad \text{and} \quad c_2^2 = \frac{\varrho - \varrho'}{\varrho} g h', \quad (\text{XVI.14})$$

and the ratio becomes

$$-\frac{\rho - \rho'}{\rho'}. \quad (\text{XVI.15})$$

GREENHILL (1887) has treated the case of several superposed strata of different densities. Particularly important is perhaps the result that, for instance, if there are three layers, the discontinuity surfaces can oscillate with opposite phases, so that wave crests (-troughs) at one boundary surface correspond to the wave troughs (-crests) at the other boundary surface. For further theoretical problems see also SOLBERG's paper (1928) in which are also treated the conditions in case of wedge-shaped layers.

Internal waves can also be generated in a wave tank in which two layers of different densities, each with a different colour, are superposed. SANDSTRÖM (1908, p. 6) has made such tests in stratified water. In his paper are also indicated the precautions to be taken in order to obtain sharp discontinuity surfaces (see also DEFANT, 1923, p. 83).

(b) *Internal Waves Having the Character of Surface or "Short" Waves*

The equations (XVI.10) to (XVI.15) apply to "short" waves, whose wavelength is small compared to the water depth. As the potential energy necessary for the development of these internal waves at boundary surfaces is very small, any slight pressure disturbances or tangential stresses at the surface of a stratified water-mass will suffice to develop respectively to maintain internal waves at an internal boundary surface. Consequently, these short internal waves must be a frequent phenomenon, not easily recognized because it is not a simple matter to detect them.

The phenomenon of "dead water" is related to these short internal waves. Where rivers flow into the fjords or where ice melts (drift-ice in polar areas) there is frequently a relatively thin layer of fresh or nearly fresh water spreading over the lower layer of higher salinity (heavier water). When the weather is calm and the tides recede so that the layers in the superposed water-masses are maintained, it happens that slow moving vessels are "stuck" in the water and make very little headway. It has been found that frequently an increase in the force of the wind, or the passing-by of another ship at full speed, can make the "dead water" vanish.

This phenomenon was especially observed by Fridjof Nansen during his polar cruise. His vessel "Fram", with its heavy construction and its weak engine and little speed, proved to be very sensitive to the "dead water". The phenomenon has been observed also in the Baltic and in the Kattegat; there is, however, no doubt that it always occurs where a thin layer of light water is superposed on heavier water and when the vessels have a relatively slow speed. Interesting cases have been described by MEYER (1904, p. 20). A slight increase in the speed of the vessels already seems to be sufficient to overcome the effect of the "dead water" on the vessels.

According to the theoretical and experimental studies by EKMAN (in F. NANSEN, *North Polar Exped.* 1893–1896, vol. 5; 1904, p. 562) this “dead water” is due to the fact that a slow moving vessel may create internal waves at the lower boundary of a thin freshwater layer, the thickness of which is not much less nor greater than the draft of the vessel. The motion of the ship creates in the layered system two kinds of waves, external and internal waves. Their velocities of propagation are given by the equations (XVI.12). The external waves are very short, and the wave resistance for the ship will be a normal one. With a given speed of the ship, however, there is also the possibility of generation of internal waves. With the second equation of (XVI.12) it is easy to prove that the quantity $\kappa = 2\pi/\lambda$ is only real if

$$c^2 < \frac{\rho - \rho'}{\rho} gh' . \quad (\text{XVI.16})$$

This means that there is “dead water” when the speed of the ship remains below this critical value. If the speed exceeds this value, then only the external waves are generated, and the wave resistance is practically the same as if there were only one single water-mass. This is confirmed by the observation. Table 88 gives the critical values of c , at which there can be “dead water”, for different thicknesses of the top layer, whose density is determined by its salinity (at 0°C). The lower layer is assumed to have a normal salinity content of 35‰ (see V. BJERKNES, 1933, p. 390).

Table 88. *Critical velocities (m/sec) for the generation of “dead water” waves*

(Lower layer: temp. 0°C., salinity 35‰)

Thickness of upper layer (m)		0.1	0.5	1.0	2.0	5.0	10.0
Salinity of upper layer	30 ‰	0.06	0.14	0.20	0.28	0.44	0.62
	20 ‰	0.11	0.24	0.34	0.48	0.76	1.08
	10 ‰	0.14	0.31	0.44	0.63	0.99	1.40
	0 ‰	0.17	0.37	0.53	0.75	1.18	1.67

It is obvious that the maximum velocity c of a vessel which will generate “dead water” is very small. For smaller vessels (sailing and rowing boats) the order of magnitude is of a few decimeters per sec (thickness of top layer up to 1 m); for larger vessels (thickness of the top layer 10 m) the order of magnitude is 1 m per sec and more (= 1.9 knots). The amplitudes of these internal waves can be very large, and it is these waves which increase considerably the wave resistance.

The tests made by Ekman in a wave tank have confirmed in every way the theoretical explanation of the "dead water". Figure 214 by Ekman shows how at *a* and *b* "dead water" waves are created by the towed vessel; at *c*, with increased speed, the ship has freed itself from the "dead water". There is only a slight denting in the discontinuity surface below the ship, but no internal wave system.

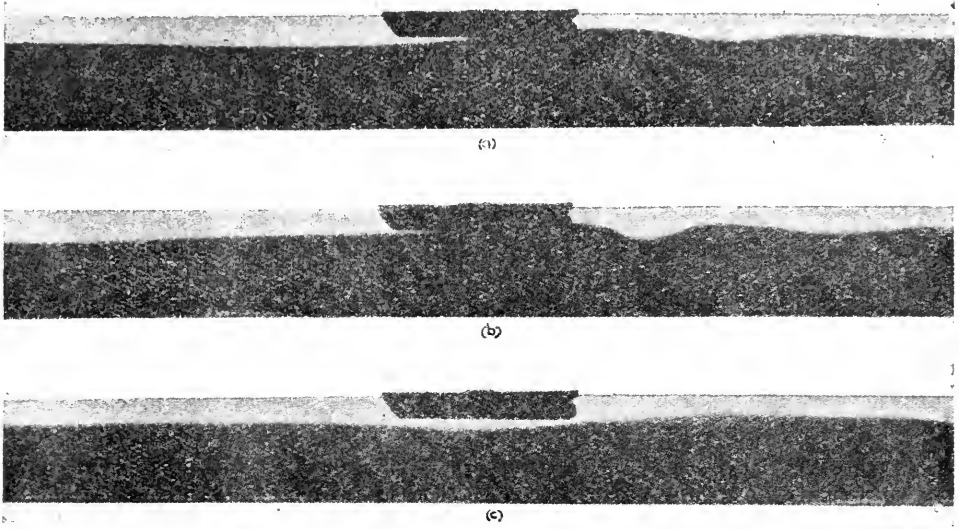


FIG. 214. Ekman's experiments on "dead water" waves. *a* and *b*, "dead water" waves created by a vessel; *c*, the ship is free from "dead water" waves.

When a ship is anchored and a series of observations is taken within short intervals one observes variations in temperature and salinity of short duration; especially if the discontinuity in the vertical distribution of the density is well developed. These variations may be caused by internal waves, but mostly the interval in which the series is made is not sufficient to prove the wavelike nature of the disturbances. One needs continuous registrations of temperature and salinity and such measurements have been made only recently and sporadically. However, there is no doubt that the boundary surfaces are constantly in a wave motion and a state of complete rest is exceptional. We will refer to this later on (p. 531).

(c) *Internal Waves Having the Character of Long Waves*

If the wave length of the internal waves is long in comparison with the total depth ($h+h'$) of the two layers, one can write $1/\lambda h$ and $1/\lambda h'$ instead of the cotangents in (XVI.9) and one gets with sufficient accuracy:

$$c^4 - c^2(h' + h)g + \left(1 - \frac{\rho'}{\rho}\right)g^2hh' = 0.$$

Its two roots are

$$\begin{aligned} c_1 &= \sqrt{g(h+h')}, \\ c_2 &= \sqrt{\frac{\varrho - \varrho'}{\varrho} g \frac{hh'}{h+h'}}. \end{aligned} \quad (\text{XVI.17})$$

For the first of these waves the velocity of progress c_1 is identical with that of ordinary long waves at the surface of a water-mass having the total depth of the two layers. This is the external wave, which will not be discussed here. The value of c_2 is the velocity of progress of the internal wave. If the thickness of the bottom layer h is large compared to h' , this equation is reduced to the second equation of (XVI.14). The amplitude of the internal wave has its maximum at the boundary surface and decreases upwards and downwards. At the free surface it is, according to (XVI.16),

$$\eta_0 = -Z \frac{\varrho - \varrho'}{\varrho}, \quad (\text{XVI.18})$$

if Z is the amplitude at the boundary surface. The negative sign indicates that at the surface the phase is opposite to the phase at the boundary surface. If one assumes $\varrho - \varrho' = 10^{-3}$, which is already a large value corresponding to $\sigma_t = 24.5$ and $\sigma'_t = 23.5$, then if $Z = 10$ m, η_0 becomes of the order of magnitude of 1 cm. It is so small that it can be neglected. At the bottom there is no vertical displacement of the water particles, so that here the internal wave must also vanish. We can assume as it is allowed in a first approximation – that the amplitude of the internal wave increases linearly from the free surface to the boundary surface and decreases linearly from the boundary surface to the bottom. The variation per unit length in the upper layer is then Z/h' , in the bottom layer $-Z/h$. We can compute the amplitude of the horizontal velocities of the water particles from the vertical amplitudes with the equation

$$u = c_2 \frac{\partial \eta}{\partial z} \quad (\text{XVI.19})$$

and one obtains for the two layers

$$U' = c_2 \frac{Z}{h'} \quad \text{and} \quad U = -c_2 \frac{Z}{h} \quad (\text{XVI.20})$$

The amplitudes of the horizontal velocities are constant within each layer; however, they change their sign at the boundary surface; consequently, the velocities have opposite directions on the two sides of the boundary surface. As we have already stated above (p. 518), with internal waves there is always a vortex-sheet at the boundary surface. As, for reasons of continuity, $U'h'$ must equal Uh , these amplitudes of the velocity are inversely proportional to the thickness of the two layers and one obtains

$$U' = Z \sqrt{\left[\frac{\rho - \rho'}{\rho} \frac{gh}{h'(h+h')} \right]} \quad (\text{XVI.21})$$

and

$$U = -Z \sqrt{\left[\frac{\rho - \rho'}{\rho} \frac{gh'}{h(h+h')} \right]}.$$

The order of magnitude of these velocities can be found by calculating a numerical example: If $\rho = 1.025$, $\rho - \rho' = 10^{-3}$, $g = 981 \text{ cm sec}^{-2}$, $h' = 50 \text{ m}$, $h = 200 \text{ m}$ and $Z = 15 \text{ m}$. Then $U' = 18.6 \text{ cm/sec}$ and $U = 4.7 \text{ cm/sec}$. This shows that, already with internal waves of a moderate amplitude, the horizontal particle velocities are relatively large, which can be observed without

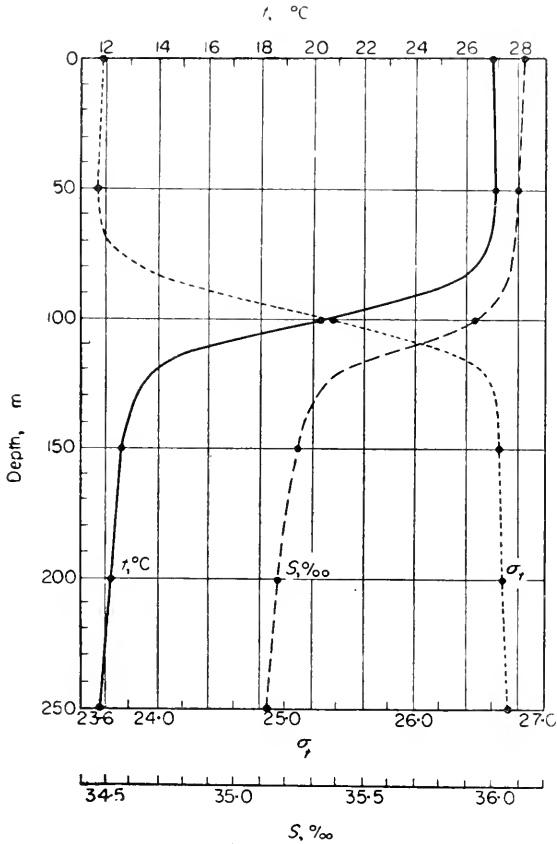


FIG. 215. Vertical distribution of temperature, salinity and density σ_t at the "Meteor" Anchor Station 254.

any difficulties by current measurements. The corresponding velocity of progress of the internal wave is here 63 cm/sec, that of the ordinary long wave at the free surface 4953 cm/sec. Following is an example of these in-

ternal waves of long wave length. On anchor station 254 of the "Meteor" expedition (31 January to 2 February 1927, $\phi = 2^{\circ}26.7'S.$, $\lambda = 34^{\circ}57.4'W.$, average depth $h = 3910$ m) 23 series were lowered down to a depth of 200 m with an interval of approximately 2 h (see DEFANT, 1932, p. 164). These observations give the average vertical distribution of temperature, salinity and the density σ_t , as shown in Fig. 215. It shows that in an average depth of 100 m there was a pronounced discontinuity in the vertical density distribution, which almost had the nature of a discontinuity surface. The nearly

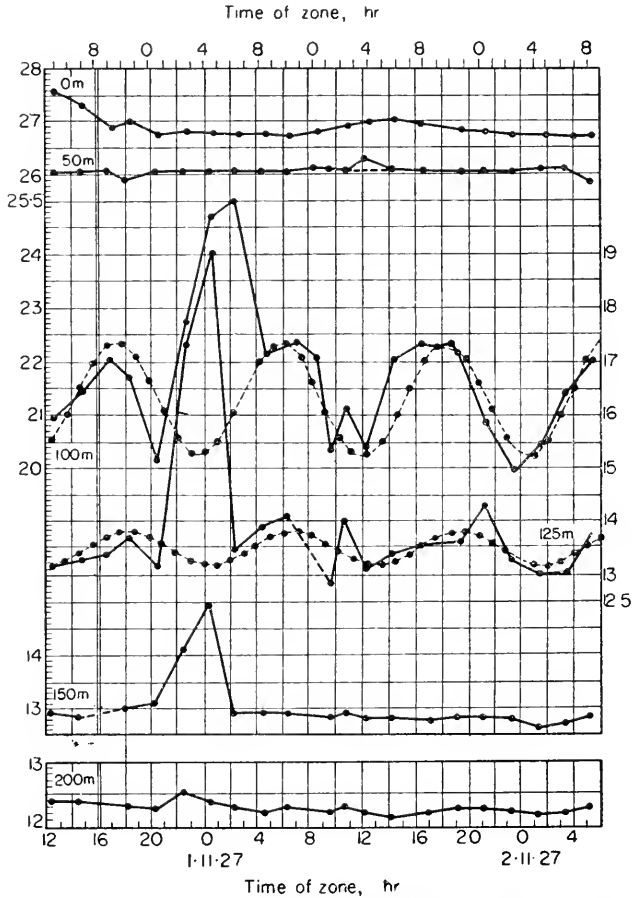


FIG. 216. Temperature variations in different depths at "Meteor" Anchor Station 254.

homogenous top layer had a density of $\sigma'_t = 23.6$ and a thickness of approximately 100 m, the lower layer had a density σ_t of about 26.7 and its depth was very large in proportion to the thickness of the upper layer. The velocity of progress of long internal waves, in this case, according to the equation XVI.14, is $c_2 = 172$ cm/sec.

Figure 216 shows the variation of the temperature in several depths, as observed in the serial observations. Neglecting a disturbance which occurred at midnight, 31 January–1 February one finds that in the vicinity of the discontinuity layer there is a wave with a period of 12.3 h (semi-diurnal lunar period), with a maximum amplitude in 100 m. In 125 m the wave is still noticeable, but in the top layer and downward from 150 m, it is hardly detectable. The variations in salinity are quite similar. The analysis of all the observations reveals that at the boundary surface there was an internal tide wave, with an amplitude of 3.6 m and a phase of 4.3 lunar h (referred to the transit of the moon through the meridian at Greenwich). Current measurements at 0, 25, and 50 m were taken simultaneously with the hydrographic casts. The average velocity for the entire layer was 6.1 cm/sec with a phase of 10.4 lunar h for currents flowing to the north. The difference in phase between the vertical and horizontal motion is therefore 6.1 h, exactly a half period.

The amplitude of the velocity of the current has to be very small in the lower layer because of its great depth; equation (XVI.20) gives for $Z = 3.6$ m and $h' = 100$ m, $U' = 6.15$ cm/sec in complete agreement with the observed value. The influence of the internal tide wave on temperature and salinity is limited to the immediate vicinity of the discontinuity layer of the density.

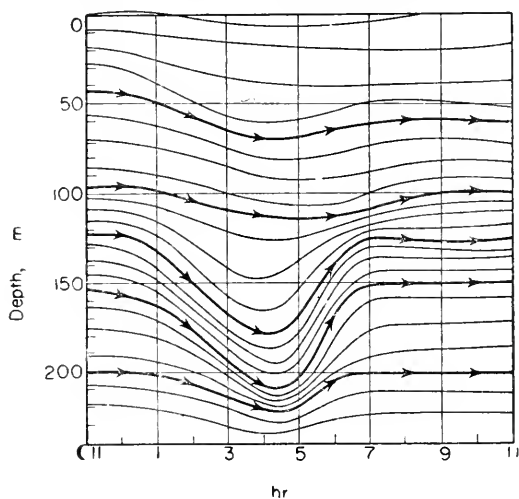


FIG. 217. Streamlines of the lower layers at midnight from 31 January to 1 February at Anchor Station 254.

Vertical displacements of water-masses above and below the discontinuity layer must remain ineffective on the distribution of temperature and salinity because of the nearly homogenous compositions of the layers. For this reason no changes were observed in these properties at 50 and 150 m when the internal wave passed.

The disturbance between 31 January and 1 February, with great changes in temperature and salinity, is of particular interest. The depth from which these water masses originate, can be easily ascertained by means of the vertical distribution of the temperature and salinity at the station — after elimination of the regular semi-diurnal wave. Figure 217 shows the streamlines of this disturbance which was caused by a powerful downward push of nearly 60 m of the upper water masses. Its maximum is located in the region of the discontinuity layer and the disturbance decreases in intensity upward and downward. This disturbance has also the characteristics of an internal wave. Its shape reminds one of the disturbance which SANDSTRÖM (1908, p. 9) created by his experiments in stratified water, when a gust of wind blew upon the water surface and which is illustrated in Fig. 218. It cannot be doubted that at

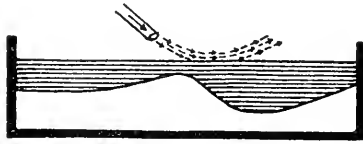


FIG. 218. Sandström's experiment creating an internal wave in stratified water by a gust of wind on the surface.

anchor station 254 a similar process was observed by chance. Some external disturbance can create such an "internal" wave. It travels along the boundary surface with the velocity of internal waves. But observations at one station alone are not sufficient to determine the direction of the wave. The period was about 6.4 h. The length was therefore roughly 40 km, if $c_2 = 172$ cm/sec, which makes it quite plausible that a gust of wind was the cause.

(d) *Internal Waves When the Density is a Continuous Function of the Depth*

(a) *Cellular waves and stability waves.* Until now we have dealt with internal waves at a discontinuity surface of density within a vast water mass. These internal waves have their greatest amplitude at the boundary surface. If there are several discontinuity layers in the vertical distribution of the density, several internal waves can occur simultaneously. Therefore there exists a greater variety of oscillations in such a water mass than in a homogeneous one. It is to be expected, that with an increasing number of discontinuity surfaces, the number of possible internal waves increases accordingly. This leads to the case of a continuous variation of the density with depth and then we can expect an unlimited number of possible internal waves. A water-mass with such continuous variation of the density with depth behaves entirely different from homogenous liquids.

Only the most elementary forms of such wave motions in a stable stratified medium have been studied, as far as "short" waves are concerned. They are the so-called *cellular waves*, where the entire oscillating space is subdivided into "cells" of definite dimensions. In each cell the oscillation occurs

as if between fixed walls and the period is the same for all cells. This is the most elementary case of standing cellular oscillations.

The theory of such cellular waves was developed by LOVE (1891, p. 307, see also HAURWITZ, 1931; BRUNSIDE, 1889, p. 392; LAMB, 1932, p. 379; or PRANDTL, 1942, p. 331). We can find the equation for the frequency only after introducing an assumption for the vertical stratification. The simplest assumption is a water-mass of infinite thickness, in which at rest the density decreases with z (when z is counted positive upwards starting from the bottom) according to an e power, so that

$$\rho_0 = \rho_B e^{-\beta z} = \rho_B e^{-z/H}, \tag{XVI.22}$$

where H is the height, where the density has decreased to the e th part of the density at the bottom.

Let us discuss a two-dimensional case where the horizontal and the vertical displacement of the water particles are represented by ξ and η respectively. Both are functions of x, z , and of the time t . They must satisfy the equations of motion as well as the equation of continuity. The condition of invariability of density has to be added:

$$\frac{d\rho}{dt} = \frac{\partial \rho}{\partial t} + u \frac{\partial \rho}{\partial x} + w \frac{\partial \rho}{\partial z} = 0, \tag{XVI.23}$$

where u and w signify the horizontal and vertical velocities of the particles. The density ρ and the pressure p contain the components at rest ρ_0 and p_0 the components of the disturbance ρ_1 and p_1 . The latter are like u and w quantities of second order, so that products and squares can be neglected. (XVI.23) then becomes

$$\frac{\partial \rho_1}{\partial t} = -\frac{\partial \rho_0}{\partial z} w \quad \text{or} \quad \rho_1 = -\eta \frac{\partial \rho_0}{\partial z}. \tag{XVI.24}$$

This equation signifies that a particle now at the time t at a location x, z was originally at the level $z - \eta$. With this density structure (XVI.22) becomes

$$\rho_1 = \frac{\rho_0}{H} \eta.$$

The linearized equations of the problem are in this case

$$\left. \begin{aligned} \rho_0 \frac{\partial^2 \xi}{\partial t^2} + \frac{\partial p_1}{\partial x} &= 0, \\ \rho_0 \frac{\partial^2 \eta}{\partial t^2} + \frac{\partial p_1}{\partial z} + g(\rho + \rho_1) &= 0, \\ \frac{\partial \xi}{\partial x} + \frac{\partial \eta}{\partial z} &= 0. \end{aligned} \right\} \tag{XVI.25}$$

Then, with the given density distribution, a possible wave solution of cellular type will have the following form:

$$\left. \begin{aligned} \xi &= A e^{z/2H} \cos \kappa x \left[\frac{1}{2H\kappa} \cos \varepsilon z - \frac{\varepsilon}{\kappa} \sin \varepsilon z \right] \cos \sigma t, \\ \eta &= A e^{z/2H} \sin \kappa x \cos \varepsilon z \cos \sigma t. \end{aligned} \right\} \tag{XVI.26}$$

It represents an internal standing cellular wave, where the horizontal wave length is $\lambda_x = 2\pi/\kappa$, the vertical one $\lambda_z = 2\pi/\varepsilon$. Figure 219 shows schematically such an internal oscillation. One recognizes the division of the entire space into "cells" of equal shape. The period of oscillation $T = 2\pi/\sigma$ becomes

$$\begin{aligned}
 T &= 2\pi \sqrt{\left\{ \frac{H}{g} \left[1 + \frac{\varepsilon^2 + 1/4 H^2}{\kappa^2} \right] \right\}} = 2\pi \sqrt{\left\{ \frac{\rho_0}{g\Gamma} \left[1 + \left(\frac{\lambda_x}{\lambda_z} \right)^2 + \frac{\Gamma^2 \lambda_x^2}{16\pi^2 \rho_0^2} \right] \right\}} \\
 &= 2\pi \sqrt{\left\{ \frac{1}{gE} \left[1 + \left(\frac{\lambda_x}{\lambda_z} \right)^2 + \frac{(E\lambda_x)^2}{16\pi^2} \right] \right\}} \quad (\text{XVI.27})
 \end{aligned}$$

If the vertical density gradient is denoted Γ where $\Gamma = -d\rho_0/dz = \rho_0/H$, and if we remember that $\Gamma/\rho_0 = E$ is the stability of the stratification (see vol. I)

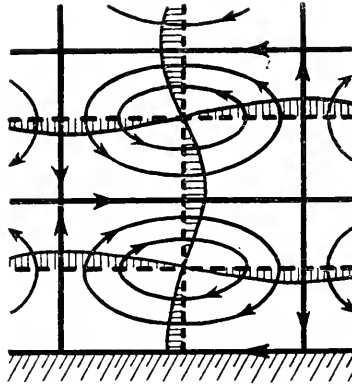


FIG. 219. Presentation of a cellular standing internal wave when the density increases continuously.

we can derive the two other equations in (XVI.27). It will be seen that the period of the cellular oscillations is dependent upon the stability of the stratification and upon the horizontal and vertical dimensions of the cells of oscillation.

Of particular interest is the case where $\varepsilon = 0$, which is identical to $\lambda_z = \infty$. This means that in all z the phase of the oscillation is the same. Then equation (XVI.27) gives a nearly constant period of oscillation for horizontal wave lengths λ_x , which are small compared to $4\pi H$

$$T = 2\pi \sqrt{\frac{\rho_0}{g\Gamma}} \quad (\text{XVI.28})$$

thus independent of λ_x . For regular surface waves on a homogeneous water layer $T = \sqrt{2\pi\lambda_x/g}$ and is thus dependent of the wave length (see II.11). Therefore, there is a considerable difference in the behaviour of internal waves.

If we superpose on a wave (XVI.26), another one of the same type but

with a shift of the phase in x of a quarter of the wave length and a quarter of the period in t . we get internal horizontal progressive waves. Their velocity is

$$c = \frac{\sigma}{\alpha} = \pm \sqrt{\left[\frac{g}{(\alpha^2 + \varepsilon^2)H + \frac{1}{4H}} \right]} = \pm \sqrt{\left[\frac{gI\lambda_x^2}{4\tau^2\varrho_0} \frac{1}{1 + \left(\frac{\lambda_x}{\lambda_z}\right)^2 + \frac{I^2\lambda_x^2}{16\tau^2\varrho_0^2}} \right]} \quad (\text{XVI.29})$$

The velocity of such internal waves therefore depends upon the wave length as well as upon the vertical density distribution. It can be seen that with the same phase of oscillation for all values of z ($\lambda = \infty$) this velocity of internal waves is proportional to the wave length, and not to the root of the wave length as for ordinary surface waves.

Their physical nature becomes understandable only if it is considered that in unstable stratified water masses according to more recent ideas the convection mostly does not take place between individual layers in form of irregular up- and downwards movements of water bodies of arbitrary size, but rather stationary circulations of quite definite form ("cells" of definite extent and shape) occur, in the outer portions of which the medium sinks and rises in their central parts. (Bénard-cells, see Vol. I/1, Chap. 5, Fig. 92.)

Also in case of stable stratified water masses oscillatory processes develop during forced displacements in vertical direction of water bodies (i.e. during dynamic convection), which are of cellular nature. The movement initiated by a single impulse after surpassing the equilibrium position by a certain rate will reverse its direction and the disturbed mass distribution tends

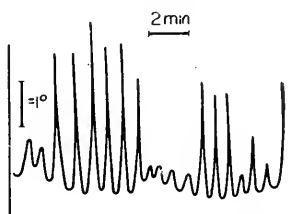


FIG. 220. Stability oscillations (cellular waves) in the Baltic with a period of 45 sec. Taken from temperature registrations in a depth of 7.5 m on 31 July 1944. $\phi = 54^{\circ}34.5'N$. $\lambda = 12^{\circ}18.8'E$.

towards its previously occupied equilibrium position. In this way a cellular oscillation of definite form develops, which will depend upon the stability of stratification. Such cellular gravitational waves are thus denoted as *stability oscillations*.

Ever since the first continuous recorded temperature observations in stratified water masses in lakes and in the ocean, short temperature oscillations

were observed beside wave-like variations with a long period (see KALLE, 1942, p. 383; 1953, p. 145). At first they were believed to be caused by the turbulence of the currents. But there exist frequently cases where the oscillations are entirely of a regular wave-like nature. These are doubtless stability oscillations. Figures 220 and 221 present two cases of such regular oscillations.

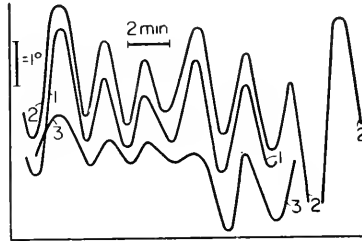


FIG. 221. Stability oscillations in Arkona basin (Baltic) with a period of 2.3 min. Simultaneous temperature registrations at three different places around the ship, 30 July 1944.

lations on two different stations in the Baltic. NEUMANN (1946, p. 282) on the basis of the Baltic observations, tested thoroughly the theoretical results concerning the cellular waves in stratified media with reference to the shape and period of the waves as a function of the stability of the stratification. Figure 222 shows a fairly good agreement between the observed and the theoretically computed periods. The form of the cell is generally rectangular and its horizontal dimension amounts to about $2\frac{1}{2}$ the vertical one. More research will uncover further details about these interesting phenomena, which are certainly connected with turbulence.

(β) *Progressive internal waves of longer periods.* An exhaustive theory of internal progressive waves in water masses, in which the density is a continuous function of depth, was developed by FJELSTAD (1935). He also gave a practical method to compute all possible internal waves for any given distribution of density.

The mathematical basis of the theory is the same as for the cellular waves. Particularly, the same equations (XVI.24), (XVI.25) are valid. In the case of a progressive harmonical wave with a period $T = 2\pi/\sigma$ and with a velocity $c = \sigma/\kappa \xi$ and η can be assumed to be proportional to $e^{i(\sigma t - kx)}$ and finally the differential equation for the vertical displacement will be

$$\frac{d}{dz} \left(\rho_0 \frac{d\eta}{dz} \right) - \frac{\kappa^2}{\sigma^2} \left(g \frac{1}{\rho_0} \frac{d\rho_0}{dz} + \sigma^2 \rho_0 \right) \eta = 0. \quad (\text{XVI.30})$$

The following boundary conditions have to be added:

$$\left. \begin{array}{l} \text{For the bottom } z = 0, \quad \eta = 0, \\ \text{For the free surface } Z = h, \quad \frac{d\eta}{dz} - \frac{\sigma^2}{\kappa^2} g \eta = 0. \end{array} \right\} \quad (\text{XVI.31})$$

A closer investigation of this differential equation shows an infinite number of solutions, corresponding to an infinite number of internal waves of the same period, but with different velocities and different vertical distribution of η . These waves are designated as waves of first, second etc., order, where the wave of zero order is the regular tide wave at the surface. In the wave of first order the vertical displacement in the entire water mass from the surface to the bottom has the same direction with a maximum amplitude

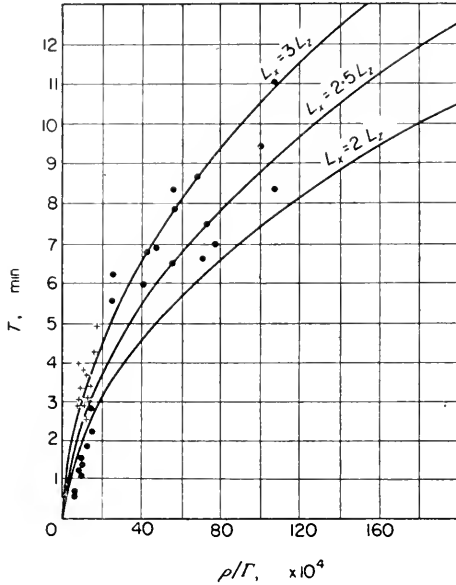


FIG. 222. Relationship between the period T of cellular waves and the stability of the stratification ($E = \Gamma/\rho$) for different ratios between the horizontal (λ_x) and vertical (λ_z) dimensions of the cells; +, observations in the Fehmarnbelt 1937; *, observations in the Baltic 1944 (Neumann).

in one depth. The wave of second order is characterized by vertical displacement in opposite direction within the upper and the lower layer; there are two maxima of amplitudes. The waves of third order have three maxima in the vertical, and the wave of fourth order four maxima, etc. The horizontal velocity is always zero in the depth where the amplitude of the vertical displacement reaches a maximum. Accordingly, the horizontal velocity is zero at one depth for the wave of first order; and within the wave of second order the horizontal velocity is zero at two levels and so on.

In this theory the rotation of the earth and friction have so far been neglected. If one wants to consider the rotation of the earth we have to add to the first equation of (XVI.25) a similar one for the direction of the coordinate y , perpendicular to the direction of progress of the wave. In both equations Coriolis acceleration of $-2\omega\zeta$ and $+2\omega\xi$ respectively has to be added. In this case $\omega = \Omega \sin\phi$ and ζ is the horizontal displacement cross

to the direction of progress of the wave. The other equations remain unchanged. The solutions become more complicated, because there exists now also a variation in the amplitude of the wave cross to the direction of progress. Three different types of waves are to be considered:

(a) In a narrow channel Kelvin waves are possible (see p. 206):

$$\left. \begin{aligned} \eta &= \eta(z)e^{-(2\omega\kappa/\sigma)y} \cos(\sigma t - \kappa x), \\ u &= \frac{\sigma}{\kappa} \frac{d\eta}{dz} e^{-(2\omega\kappa/\sigma)y} \cos(\sigma t - \kappa x), \text{ and } v = 0, \end{aligned} \right\} \quad \text{(XVI. 32)}$$

with the phase velocity $c = \sigma/\kappa$. This solution is the same as the one in the case without rotation of the earth, but the factor $e^{-(2\omega\kappa/\sigma)y}$ is being added to the amplitude in each expression. This factor has here a greater significance than in the case of the regular tide waves, as the values of κ become larger for internal waves. With $\sigma/\kappa = 200$ and $2\omega = 1.3 \times 10^{-4}$ the amplitude perpendicular to the direction of progress of the wave decreases at a distance of 15.3 km to j/e part of its value. Internal waves of this type can gain importance in comparatively narrow channels only.

(b) If the lateral boundaries are neglected one obtains:

$$\left. \begin{aligned} \eta &= \eta(z) \cos(\sigma t - \kappa x), \\ u &= \frac{\sigma}{\kappa} \frac{d\eta}{dz} \cos(\sigma t - \kappa x), \\ v &= -\frac{2\omega}{\kappa} \frac{d\eta}{dz} \sin(\sigma t - \kappa x), \end{aligned} \right\} \quad \text{(XVI.33)}$$

where

$$c = \frac{c_0}{1 - 4\omega^2/\sigma^2},$$

when c_0 represents the velocity in the case of a non-rotating earth.

(c) In a wide channel a wave of the following form is possible: if we assume

$$\varepsilon^2 = \frac{\kappa^2 + \frac{m^2\pi^2}{b^2}}{\sigma^2 - 4\omega^2}.$$

Then

$$\left. \begin{aligned} \eta &= \left[\sin \frac{m\pi}{b} y - \frac{\sigma m\pi}{2\omega\kappa b} \cos \frac{m\pi}{b} y \right] \eta(z) \cos(\sigma t - \kappa x), \\ u &= \left[\frac{\sigma}{\kappa} \sin \frac{m\pi}{b} y - \frac{1}{\varepsilon^2} \frac{m\pi}{2\omega b} \cos \frac{m\pi}{b} y \right] \frac{d\eta}{dz} \cos(\sigma t - \kappa x), \\ v &= -\frac{4\omega^2\kappa^2 + \sigma^2 \frac{m^2\pi^2}{b^2}}{2\omega\kappa \left(\kappa^2 + \frac{m^2\pi^2}{b^2} \right)} \sin \frac{m\pi}{b} y \frac{d\eta}{dz} \sin(\sigma t - \kappa x), \end{aligned} \right\} \quad \text{(XVI. 34)}$$

where the wave velocity is

$$c = \frac{1}{\varepsilon} \sqrt{\frac{\sigma}{\sigma^2 - 4\omega^2 - \frac{m^2\pi^2}{\varepsilon^2 b^2}}}.$$

A necessary condition for the existence of this wave is

$$(\sigma^2 - 4\omega^2)\varepsilon^2 - \frac{m^2\pi^2}{b^2} > 0,$$

that is at least $\sigma^2 > 4\omega^2$. The wave velocity without rotation is in this case $c_0 = 1/\varepsilon$, therefore we can write

$$\frac{m\pi}{b} < \frac{\sigma}{c_0} \sqrt{1 - \frac{4\omega^2}{\sigma^2}}. \quad (\text{XVI.35})$$

For $c = 200$, as before, $m = 1$ and $2\omega = 1.3 \times 10^{-4}$ (60° latitude), it follows $b > 102$ km. Consequently internal waves of such a form may probably occur also in the open ocean. They correspond to the Poincaré-waves at the ocean surface mentioned above (p. 208).

The vertical distribution of η , which characterizes the internal wave, will result from integration of the differential equation (XVI.30). $\eta(z)$ can be ascertained by a comparatively simple numerical integration, when the vertical density distribution is given, as shown by Fjeldstad. With sufficient accuracy we can write

$$\phi = -\frac{1}{\varrho_0} \frac{d\varrho_0}{dz} = 10^{-3} \frac{d\sigma_t}{dz},$$

and as σ^2/g (magnitude in the case of tide waves 10^{-11}) is always very small compared with ϕ , the equation (XVI.30) will be simplified to

$$\frac{d^2\eta}{dz^2} - \frac{\kappa^2}{\sigma^2} g\phi\eta = 0. \quad (\text{XVI.36})$$

Furthermore, the boundary condition for the free surface can be replaced by the more simple one $\eta = 0$. Thereby the wave of zero order is being lost, whose velocity is $c_0 = \sigma/\kappa = \sqrt{gh}$ and which is the regular tide wave. But we want to disregard this "external" wave. The boundary conditions are therefore $w = \eta = 0$ for $z = 0$ and $z = h$. STÖRMER'S (1907) method of integration can be applied in simplified form to this differential equation. It gives the vertical distribution of η with a relatively small amount of computational work, if approximate values of the parameter κ^2/σ^2 are known as Fjeldstad has shown. For more details reference is made to the original publication. As an example we can take station 115 of the "Michael Sars" where the depth to the bottom is 580 m (HELLAND-HANSEN, 1930).

Figure 223 shows its density distribution σ_t as well as Fjeldstad's computed vertical displacements η and horizontal velocities u for the internal waves

of first to fourth order. The computation gives the amplitudes of the vertical displacements and horizontal velocities as relative values, which are plotted on an arbitrary scale. The observations give us absolute values. Furthermore, the theory gives the velocities of progress of these waves of different

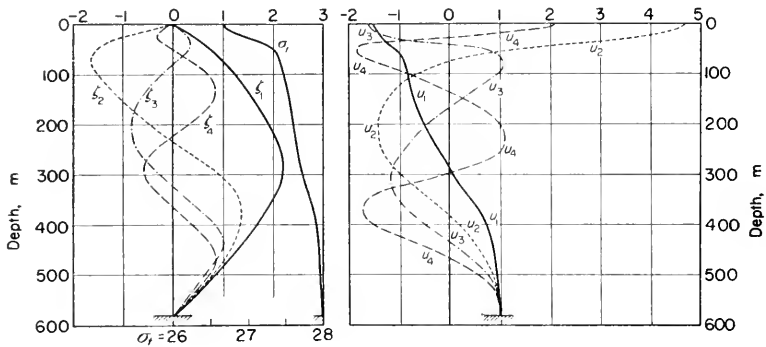


FIG. 223. Left: vertical distribution of the density σ_t and vertical distribution of the vertical displacements η of the internal waves of the 1st until 4th order at the "Michael Sars" Station 115. Right: vertical distribution of the amplitudes of the horizontal velocities corresponding to the internal waves of the 1-4th order. η and u are in arbitrary units (Fjeldstad). (The reader may note that in the picture to the left ζ stands for η .)

orders provided that the depth remains constant and that the distribution of density remains constant in the direction of progress. For this station the velocities are (in cm/sec):

$$c_1 = 70, \quad c_2 = 39, \quad c_3 = 26 \quad \text{and} \quad c_4 = 19.5.$$

The theory does not give the periods or the phase of the waves. Both must be obtained from observations. In this case, the wave lengths of the internal waves, corresponding to waves of 24 lunar hours (diurnal tide wave), will be

$$\lambda_1 = 62.5, \quad \lambda_2 = 34.8, \quad \lambda_3 = 23.2 \quad \text{and} \quad \lambda_4 = 17.4 \text{ km.}$$

The internal tide waves are thus considerably shorter than the tide waves at the surface. The velocity of progress of the internal tide waves will possibly be greater in the open ocean than in the case just discussed, because the velocity of progress of internal waves increases where the difference in density between the upper and lower layers decreases, and also increases with increasing depth to the bottom. The velocity of progress of the wave of first order will seldom exceed 300 cm/sec. For diurnal or semi-diurnal tide waves the corresponding wave lengths will then be about 270 and 135 km respectively; for waves of a higher order they will be correspondingly shorter. If several of such waves occur simultaneously, there is quite a confusion in the time variations of the vertical displacements of the water masses and their corresponding currents.

GROEN (1948) has presented an extension of Fjeldstad's theory, in which he also considers the *short* waves. For a special density increase with depth (two essentially homogeneous layers separated by a transition layer) the computations are carried out until their end analitically. The width of the transition layer which can be chosen arbitrarily, enters the computation as a free parameter. It is rather remarkable that there exist for a given density distribution a lower limit for the period of internal waves. This minimum period seems to be the period of "eigen" or free oscillations of the disturbed stable density distribution about its equilibrium position. This eigen-period is rather small and is for a density increase of $\Delta\rho = 10^{-4}$ per metre of an order of magnitude of some minutes. This should be those stability oscillations already mentioned and discussed above (see p. 531).

2. Observations of Internal Waves in the Oceans; Testing of the Theory

(a) Internal Tide Waves in the Open Ocean

The magnitude of the vertical displacement of the water-masses can be computed from variations of a conservative property of water as temperature, salinity, oxygen content, etc. This can be done without too much effort, if the horizontal gradient of this property is very small. If this property is S , then the condition, that S remains unchanged, will be:

$$\frac{dS}{dt} = 0 \quad \text{or} \quad \frac{\partial S}{\partial t} + u \frac{\partial S}{\partial x} + w \frac{\partial S}{\partial z} = 0.$$

If $S = S_0(z) + S_1(x, z, t)$, and if $\partial S/\partial x$ is small and $w = d\eta/dt$, then

$$S_1 = -\eta \frac{dS_0}{dz} \quad \text{or} \quad \eta = -\frac{S_1}{dS_0/dz}. \quad (\text{XVI.37})$$

The vertical displacement η can be obtained best where the vertical gradient of the property can be determined readily and exactly. This is the usual method whereby the vertical amplitudes of internal waves have been computed from observations of temperature and salinity repeated at short time intervals from an anchored ship.

Not all the variations in oceanographic properties, which are being observed in the various depths, can be attributed to internal waves, even if these changes occur more or less periodically. At the boundaries of neighbouring water-masses oceanographic properties change rapidly within a short distance (fronts). Advances of one water-mass against the other cause oscillations of these properties. The boundary layers between such water bodies are rarely in equilibrium with the existing currents. The disturbances manifest themselves in unperiodical or periodical oscillations of the isolines of the various properties. They then simulate internal waves, and have little to do with true internal waves. In stratified water-masses there occur also periodical oscillations in the slope of the isosteres. They resemble internal

waves only superficially. Let us assume for simplicity only two superposed water bodies. If the water-masses are in stationary equilibrium then the system and currents must satisfy the Margules relation (see vol. I). For instance, the lower water-mass is at rest $u = 0$, h = the height of the boundary surface at the distance L from its intersection with the horizontal, α and α' the specific volume of the lower and upper water-mass, and $f = 2\omega \sin \phi$, then, according to Margules' relation,

$$h = \frac{fL}{g} \frac{\alpha}{\alpha' - \alpha} u'.$$

If the current changes, h changes also, if the steady state is to be maintained and

$$dh = \frac{fL}{g} \frac{\alpha}{\alpha' - \alpha} du'.$$

When

$$f = 10^{-4}, \quad \frac{\alpha}{\alpha' - \alpha} = 10^3 \quad \text{and} \quad du' = 20 \text{ cm/sec},$$

$dh = 2 \times 10^{-3}L$ or at a distance of $L = 10$ km, $dh = 20$ m. The boundary surface will be 20 m higher or lower than before. For a point in the vicinity of the boundary surface, this variation will cause considerable changes in the oceanographic properties. The periodic variations of the tidal currents for example will cause periodic changes in the slope of the isosteric surfaces (normal to the current direction). But such variations are not internal waves in the strict sense of the word, even if they occur periodically.

The first hydrographic observations repeated at short intervals over a long period made by HELLAND-HANSEN and NANSEN (1909) proved the existence of true internal waves. The main waves have often besides meteorological influences also tidal periods. They appear especially where there is a well-developed discontinuity layer of density (see DEFANT, 1938, p. 9). Otto Petterson pioneered in these observations by studying the waters in the Great Belt between the Baltic and the Kattegat; while working from an anchored ship he found such waves with semi-diurnal period. The problem of internal waves at discontinuity surfaces of the density in the free ocean was first investigated on the "Michael Sars" Expedition in the Atlantic Ocean. Later it was studied on the anchor stations of the "Meteor" Expedition 1925-27 in the tropical and sub tropical regions of the Atlantic Ocean, on the anchor stations of the "Snellius" Expedition 1929-30 in the Indonesian waters, and on the anchor stations of the later cruises of the "Meteor" 1937-8. In addition to the temperature and salinity observations in short intervals, also current measurements were taken in various depths. Thus there exist already from many points in the free ocean homogeneous observations on internal waves. The analysis of this material has demonstrated that internal waves exist everywhere and are not limited to discontinuity surfaces. They appear also when the density

increases continuously in the upper layers. It was to be expected that there existed a close connection between vertical displacement of the water-masses and corresponding variations of the velocity, perhaps also in the direction of the current. In most cases it could be verified by current observations. The combined analysis of current and serial observations provides the foundations for the testing of the theory of the internal waves.

First of all reference is made to the observations which FJELSTAD (1938, p. 49) carried out in Herdlefjord, Norway, to prove his theory. The waves can be expected to be of the simple Kelvin type, because of the narrowness of the fjord. The simultaneous hourly observations of temperature, salinity and currents lasted 88 h. The amplitudes and phases of the vertical displacement as well as amplitudes, phase and direction of the current were computed by harmonical analysis (see Table 89). There u represents the velocity of the current in the direction of progress of the wave, v the component normal to it, and τ the direction of the major axis of the current ellipse relative to the east direction. The smallness of v proves that the internal wave corresponded actually approximately to the Kelvin type. The first four internal waves were computed from the mean vertical density distribution to test the theory. Their velocities of propagation are 62.7, 33.4, 23.4 and 17.4 cm/sec. The amplitudes and phases of these four waves can be computed

Table 89. Internal waves in Herdlefjord (Norway), summer 1934

Station 1: 88 h observations (according to J. E. Fjeldstad)

Depth (m)	Vertical displacement				Depth (m)	Current				
	Observed		Computed			In the direc- tion of the wave u (cm/sec)	Normal to the direction of the wave v (cm/sec)	Phase τ in $^{\circ}$	Computed	
	η (cm) Ampli- tude	Phase ε in $^{\circ}$	η (cm) Ampli- tude	Phase ε in $^{\circ}$					u cm/sec	τ in $^{\circ}$
0	63	22 $^{\circ}$	64.3	22.7 $^{\circ}$	5	8.5	0.2	244 $^{\circ}$	12.5	231 $^{\circ}$
10	170	50	167.4	47.8	10	10.5	0.1	239	9.4	233
15	233	49	229.0	50.0	15	5.9	0.5	246	6.7	230
20	273	49	273.8	48.9	35	3.4	0.8	249	2.6	226
30	364	51	362.6	46.8	50	1.0	0.1	213	1.1	227
100	577	27	517.5	46.8	100	1.3	0.9	113	1.4	46

by the method of the least squares, if it is assumed that the observed displacements are mainly caused by these four waves. The assumption is well taken as the table shows. Moreover, the theory provides also the possibility of computing the corresponding currents. But the regular tidal current which belongs to the zero order wave was not included in these theoretical values. The comparison with the observed currents shows an excellent agreement, which

was hardly to be expected. Consequently, the current here must be caused essentially by the internal waves.

Fjelstad published also the observations on another station, no. 3, about 12.3 km distant from station no. 1. The vertical displacements show quite similar values for both stations. The velocity of propagation of the waves on station 1 is known; consequently, the expected waves for station 3 can be computed. A comparison of computed and observed waves is only possible if the observations are simultaneous, which was not the case. Therefore, only relative values can be compared, i.e. the variation of the amplitudes with depth and the phase angles. Table 90 presents such a comparison, which shows nearly complete agreement of the computed and the observed amplitudes. The current measurements on station 3 are not as complete as would be desired; moreover, the current velocities are only small. Nevertheless, observations and theory agree quite well.

The first more exhaustive analysis of periodic variations of oceanographic properties on two stations fairly close to each other in the open ocean was carried out by HELLAND-HANSEN (1930). He worked up the observations of the "Michael Sars" station 115 and the simultaneous observations of the Scotch research vessel "Goldseeker" in the Faero-Shetland Channel. The

Table 90. *Internal waves in Herdlefjord (Norway),
summer 1934*

Station 3: 33 h observations

Depth (m)	Computed from values of Station 1			Observed at Station 3	
	Vertical displacement η (cm)	Phase ε in $^{\circ}$	η Reduced to station 3 (cm)	Vertical displacement η in cm	Phase ε in $^{\circ}$
5	169	194	76	78	175
10	248	204	110	106	200
15	248	202	110	111	179
20	217	200	96	94	198
30	154	206	68	69	(241)
50	124	252	55	—	(215)

ships were stationed at a distance of about 106 km from each other. Table 91 contains the results of the harmonical analysis for the waves of a period of 12 and 24 lunar hours respectively. Essentially the observed variations can be reproduced by superposing the two internal waves of tidal character. The variation in the vertical displacement with depth is quite different on the two stations. The phases also differ strongly so that it may be assumed that the observed variations are caused by progressive waves. From the velocities of the internal waves of the first to the fourth order, which were theoretically

Table 91. Internal waves in the Faero-Shetland Channel. 13-14 August 1910. "Michael Sars" station 115 ($61^{\circ}0'N.$, $2^{\circ}41'W.$, 530 m depth), Scottish station Sc (Goldseeker) ($61^{\circ}32'N.$, $4^{\circ}19'W.$, 725 m depth)

(According to Helland-Hansen)

Depth (m)	Vertical Displacement							
	Semi-diurnal				Diurnal			
	Michael Sars 115		Goldseeker Sc		Michael Sars 115		Goldseeker Sc	
	η (m)	Phase lunar h	η (m)	Phase lunar h	η (m)	Phase lunar h	η (m)	Phase lunar h
100	15	6.3	42	0.7	18	17.0	39	12.3
200	12	8.4	58	11.2	16	15.9	11	14.7
300	24	9.3	22	21.6	9	17.7	8	17.7
400	7	9.5	11	9.2	10	9.0	9	4.4
500	3	6.6	24	11.2	5	11.3	6	5.2
600	—	—	24	7.3	—	—	25	1.2

computed for station 115 (see p. 536 and Fig. 223), it is obvious that the distance of 106 km is so large, that the various waves arrive at the second station with entirely different phases and, consequently, their final composition is here of quite a different form. There exists, however, another possibility, which Helland-Hansen stresses particularly; namely that, with the pronounced transverse

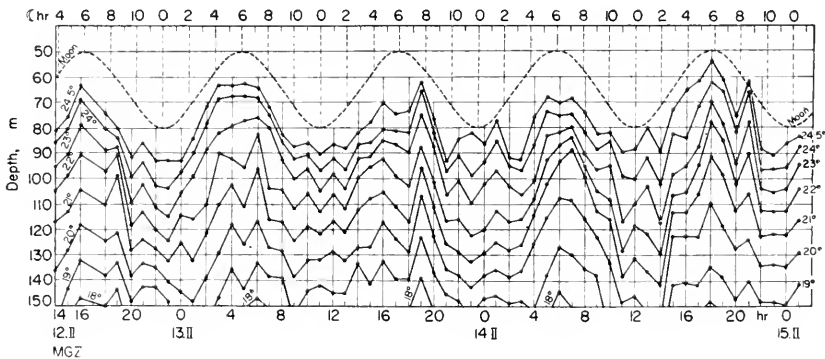


FIG. 224. Depths of the isotherms 18° - 24.5° from 12 February to 15 February 1938 at "Meteor" Anchor Station 385. From 60 series with 1 h interval.

slope of the isosteres (isothermes and isohalines) in the Faero-Shetland trough periodical variations in the currents of the Atlantic Ocean may cause periodical oscillations of the entire system in the transverse direction, which simulate internal waves (see p. 537). In regions with strong horizontal gradients of the oceanographic properties one is never quite certain if one has to deal

with true internal waves or only with displacements of the system, forced by external causes.

SEIWELL (1937) analysed the extensive observations of the "Atlantis" cruises in a region with very small horizontal gradients, north-north-west of Bermuda. He showed that the frequently large oscillations of the oceanographic properties can be presented essentially by waves of 24, 12, and 8 h period, where generally the 8 h wave had the smallest amplitude. Consequently, we are dealing here certainly with true internal waves.

Serial observations repeated in short intervals and extending over several days were made on the anchor stations of the "Meteor" in the Atlantic Ocean and of the "Snellius" Expedition in the Indonesian waters. They formed the basis for exhaustive investigations about internal waves by DEFANT (1932) and LEK (1938). Simultaneous current observation at the various depths were made at these stations. Therefore, the observations are quite complete.

The internal waves on the anchor station 385 of the "Meteor" can be

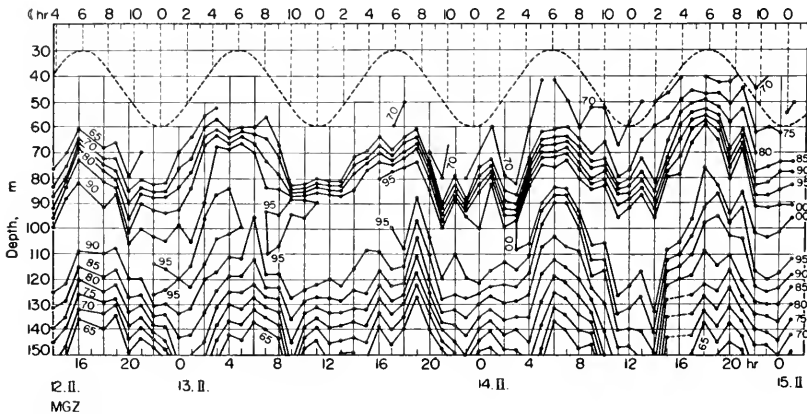


FIG. 225. Depths of the iso-halines 36.65–37.00‰, corresponding to Fig. 224.

taken as a more detailed example (German North Atlantic Expedition, 12–14 February 1938, 16°48.3'N., 46°17.1'W., depth 2900 m). SCHUBERT (1944) reports that altogether sixty repeated series were made to a depth of 150 m in hourly intervals. The current measurements with Böhnecke's current meter were extended to a depth of 800 m. The station was situated over great depths on the mid-Atlantic ridge, at a distance of more than 700 nautical miles from the mainland. The thermo-haline distribution showed the usual subtropical thermocline below an isodense mixed layer of about 60 m depth; the salinity maximum is in 100 m depth. The greatest vertical density gradient is found at 100 m; from 90 to 300 m the density increases rapidly from 24.7 to 27.1. This discontinuity layer was the seat of particularly well-developed internal waves of a period of 12 lunar hours. Figures 224 and 225 show the variations in depth of the isothermes from 18° to 24.5°C

and of the iso-halines from 35.65 to 37.00‰. Lunar period has also been entered; the correlation between the two is clearly recognizable.*

Table 92 shows the mean vertical oscillation (difference between the extreme positions) for individual isothermes and iso-halines. The amplitude of the vertical displacement is greatest at about 100 m, i.e. where the density gradient reaches its maximum. Upwards and downwards the amplitude is dampened. The lowest position occurs at the time of the upper culmination of the moon in Greenwich. The correct harmonical analysis of the semi-diurnal lunar tide of the 24° isotherm gives as its amplitude 12.1 m and the phase 0.24 h lunar time in Greenwich. A glance at Figs. 224 and 225 shows that only the semi-diurnal waves have here any significance.

The results of the analysis of the current measurements are given in Table 93. The conditions are fairly simple in the case of the semi-diurnal tide. The

Table 92. Anchor Station "Meteor" 385 (16°48.3'N., 46°17.1'W., depth 2900 m). Mean vertical variation of isothermes and iso,halines (Five semi-diurnal lunar periods)

Isotherm (°)	Average depth (m)	Mean variation (m)	Iso-haline (‰)	Average depth (m)	Mean variation (m)
24.5	76.5	29	36.75	70	23
24	83	32	36.8	74	24
23	93.5	35	36.85	77	25
22	102	36	36.9	81	26
21	112	34	36.9	115	33
20	128	32	36.85	122	32
			36.80	131	30
			36.75	137	30

phase of the upper layer which extends to the depth of the maximum vertical displacement (maximum density gradient in about 90 m) is 6.6 h, the phase of the lower layer up to 500 m is about 10.6 h. The difference between the phases is here 4 h, which should be 6 h in the case when only a semi-diurnal internal tide wave and no other internal waves, and no normal current at the surface tide were present. The mean velocity of the upper layer is 8.4 cm, of the lower layer 9 cm/sec. The decrease of the amplitude for the semi-diurnal tidal current to the small value of 4.4 cm/sec in a depth of 100 m, is quite characteristic. This depth is in the immediate

* It is of interest that the salinity is not constant in the core of the subtropical under-current with high salinity. During the time the station lasted it increased from 36.9‰ in the beginning to over 37‰ at the end. A definite salinity content is therefore not strictly representative for a definite depth or for an individual water particle during the full duration of the observations and consequently, advection processes must have been of certain importance during this time.

Table 93. Currents at Anchor Station "Meteor" 385 (16°48'3"N., 46°17'1W., depth 2900 m)

Depth (m)	Semi-diurnal tide wave					Diurnal tide wave				
	Principal direction	Amplitude (cm/sec)	Phase lunar h	Ratio of minor to major axis	Sense of rotation	Principal direction	Amplitude (cm/sec)	Phase lunar h	Ratio of minor to major axis	Sense of rotation
5	N. 16° W.	6.4	7.0	0.640	<i>Cum sole</i>	N. 52° E.	7.5	9.7	0.444	<i>Cum sole</i>
10	N. 25° W.	9.4	6.2	0.425	<i>Cum sole</i>	N. 57° E.	6.4	10.0	0.718	<i>Cum sole</i>
30	N. 9° E.	8.9	6.8	0.258	<i>Cum sole</i>	N. 27° E.	4.6	2.7	0.587	<i>Cum sole</i>
50	N. 17° W.	11.6	6.6	0.146	<i>Cum sole</i>	N. 17° E.	4.6	11.5	0.696	<i>Cum sole</i>
100	N. 53° W.	4.4	10.2	0.113	<i>Cum sole</i>	N. 70° E.	2.5	9.5	0.480	<i>Cum sole</i>
300	N. 50° W.	12.3	10.6	0.073	<i>Cum sole</i> <i>Contra</i>	N. 54° E.	4.2	5.0	0.548	<i>Contra</i> <i>solem</i>
500	N. 7° W.	6.3	10.8	0.111	<i>solem</i>	N. 20° E.	3.4	9.0	0.411	<i>Cum sole</i>
800	N.	6.5	0.5	0.477	<i>Cum sole</i>	N. 44° E.	4.9	19.8	0.408	<i>Cum sole</i>

Table 94. Anchor Station "Snellius" 253a (23-24 June 1930, 1°47'5'S., 126°59'4'EL., depth 1740 m). Currents and vertical displacements of the diurnal and semi-diurnal internal tide waves (According to Lek)

Depth (m)	Current		Vertical displacement			Difference between phases of current and vertical displacement (h)
	Amplitude (cm/sec)	Phase lunar h	Depth (m)	Amplitude (m)	Phase lunar h	
			Diurnal tide			
0-50	21.7	9.1	50	10.9	20.0	-10.9
100	13.7	17.1	100	16.3	20.7	-3.6
150	14.0	16.4	150	6.2	5.0	-12.6
200	14.9	15.8	250	16.7	1.7	-9.9
350-500	8.4	21.1	450	16.5	1.2	-4.1
			Semi-diurnal tide			
0	13.6	2.6	—	—	—	—
50	26.1	2.8	50	7.6	5.8	-3.1
100	35.1	4.0	100	7.0	7.4	-3.4
150	39.7	4.0	150	9.2	9.8	-5.8
200	44.2	4.0	250	19.4	11.5	-7.5
350-500	23.5	5.0	450	5.5	10.2	-5.2

proximity of the maximum vertical displacement, where theoretically the velocity ought to become zero. A normal tide current with a phase of approximately 71.0 h superposed on the semi-diurnal internal tide wave could

explain the phase distribution of Table 93. The average phase for the whole layer from surface to 800 m is 10·9 h.

In the case of the diurnal wave the distribution is more irregular in the phase as well as in the amplitude. Here, too, however, the smallest amplitude will be found at the depth of 100 m. The elliptic shape of the current diagrams proves the influences of the Coriolis force in the formation of all internal waves in the open ocean. But the current diagrams are very flat, especially in the case of the semi-diurnal tide. With few exceptions they rotate *cum sole*, as the theory requires.

LEK (1938, p. 69), in his discussion of the observations of the "Snellius" Expedition, investigates station 253a particularly thoroughly. The observations for this station (1°47·5'S., 126°59·4'E., 23 and 24 June 1930) are very complete. Table 94 presents the data which were deduced from the observations. A discussion of the table is hardly necessary. Figure 226 shows

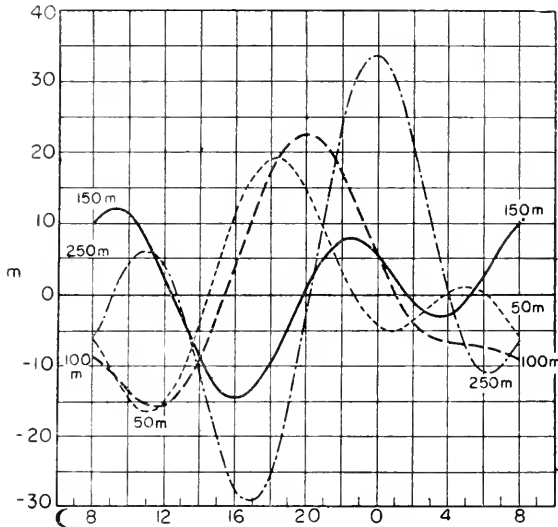


FIG. 226. Diurnal + semi-diurnal vertical displacements in various depths at "Snellius" Anchor Station 253a (Lek).

a graphical presentation of the vertical displacements at the various depths, as a result of the superposition of the semi-diurnal and diurnal components. The resulting complicated picture of the displacements and their importance will be easily recognized. The maximum of 63 m occurred at a depth of 250 m. Lek and Fjelstad applied Fjelstad's theory to this case. The velocities of progress for the first four waves follow; below the velocities are the wave lengths if the period is 24 h:

$$\begin{array}{cccc}
 c_1 = 234, & c_2 = 116, & c_3 = 77, & c_4 = 58 \quad (\text{cm/sec}) \\
 \lambda_1 = 210, & \lambda_2 = 104, & \lambda_3 = 69, & \lambda_4 = 52 \quad (\text{km})
 \end{array}$$

Their superposition shall give for the various depths of observations the observed values of amplitude and phase of the vertical displacement. This enables us to determine the amplitude and the phase of each of the four waves. It has to be emphasized that this is only possible if the number of internal waves under consideration is smaller than the number of depths of observation. Figure 227 (left) shows the vertical distribution of η for the four waves, as well as the related phases. On the right the figure shows the combination of these four waves and a comparison with the observations. A similar, good agreement will be obtained in the case of waves with a diurnal period. But this agreement signifies only that the observations can be reproduced sufficiently exactly by superposing a small number of internal waves. But that will be always possible if one takes as many internal waves as possible in successive order. A better proof of the theory is a comparison between the theoretically computed and observed currents. Table 95 presents such a comparison for the diurnal tide wave. The semi-diurnal wave could not

Table 95. *Currents of diurnal tidal period at "Snellius" Station 253a*
(According to observations and computations based on vertical displacements)

Depth (m)	Amplitude (cm/sec)		Phase	
	Observed	Computed	Observed (°)	Computed (°)
0	21.8	31.4	144.9	126.8
50	21.6	15.1	120.3	139.0
100	13.7	15.6	247.8	247.5
150	14.0	19.5	237.7	247.6
200	14.9	13.0	228.8	225.6
350	9.0	0.5	260.9	202.5
500	7.8	6.1	2.9	352.7

be used to test the theory in this respect. For there are indications that the semi-diurnal wave is not a simple progressive one, therefore will not entirely comply with the assumptions. The table shows quite a good agreement, if it is kept in mind that the observations include also the normal tide current. The greatest difference will be found in a depth of 350 m, where according to the theory, the diurnal wave should disappear almost completely. It is probable that in this depth the observations represent the undistorted normal tide current. It is remarkable, that such complicated periodical variations of the thermohaline structure can be reproduced by a relatively small number of internal waves. But for carrying out such an analysis it is necessary to repeat the serial observations in short intervals and to make simultaneous and continuous current measurements over quite a long period. Of course, other periods than the well-known tidal periods may be present and can confuse the oscillation considerably. During the current measurements, which were made by EKMAN and HELLAND-HANSEN (1931), on the Armauer Hansen

during 1930 in the Atlantic Ocean, quite a number of periods were found other than the tidal periods (see EKMAN, 1942). Their existence seems to be established, but cannot be explained. But they show the difficulties in the interpretation of the phenomenon. They prove, furthermore, that a breakdown of the variations into single component waves is only possible when the observations are very complete.

It is of particular importance that the normal tidal current be eliminated. This current ought to have the same direction and the same velocity in all depths, according to the theory. This elimination is important for the investigation of internal waves as well as for the determination of the tidal currents which are correlated to the surface tides. The customary method is, to compute a mean current for the entire layer from the surface to the bottom (see DEFANT, 1932, p. 164). This, of course, is only possible if the current distribution for the entire depth of the ocean is known. But in general this applies only for the upper layers. However, the formation of mean values for the upper layer of the ocean ought to yield somewhat correct values,

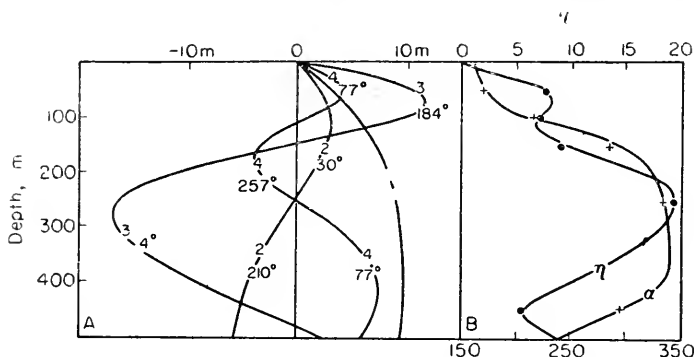


FIG. 227. Left: vertical distribution of the amplitudes of the vertical displacements η of the 1-4th order. The corresponding phases have been entered on the curves. Right: combination of the four waves and comparison with the observations (\bullet for amplitudes η , $+$ for phases) (Lek and Fjeldstad).

because just here the internal waves are particularly well developed on account of the greater density gradient. SVERDRUP (1942, p. 595) showed the theoretical foundation for this method. According to (XVI.19)

$$u_n = c_n \frac{\partial \eta_n}{\partial z},$$

where u_n presents the horizontal current velocity, c_n the velocity of progress and η_n the vertical displacement of the wave of n th order. As the values of η of every internal wave disappear at the surface and the bottom of the sea, it has to be

$$\int_0^h u_n dz = 0. \quad (\text{XVI.38})$$

For waves at the boundary surface between two media this relation will be

reduced to $U'h - Uh = 0$ (see p. 524). The averaging thus eliminates all currents associated with internal waves and leaves only the tidal current, which belongs to the "external" wave.

(b) *Recording Internal Waves and Interpretation of Sneh Records*

It has always been difficult to make extensive observations of internal waves by repeated oceanographic series. O. Pettersson tried in 1909 to record internal waves in not too deep waters by a suitable apparatus. He used for his experiments at the oceanographic station of Bornö (Gullmarfjord) a large submarine float. By carefully balancing of the float it was brought in equilibrium with the discontinuity layer (layer of the maximum density gradient) and participated in its vertical movement (Fig. 228, left). These vertical displacements of the float, which correspond to the vertical displacements of the internal waves, move along a guiding wire, which hangs from a submarine anchored buoy (see Fig. 228, right). A pressure gauge is attached to the float and

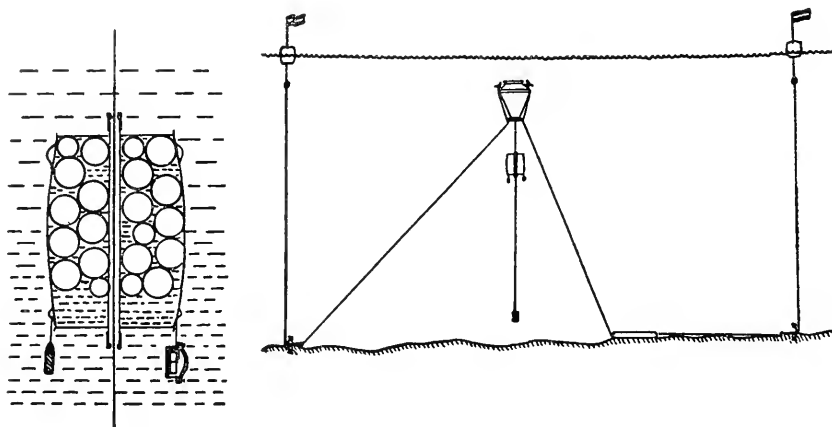


FIG. 228. Left: float of the recording boundary gauge (Kullenberg and Pettersson). Right: way of anchoring it to the bottom (Pettersson).

registers vertical displacements. The technical difficulties of the installation of the apparatus are considerable. KULLENBERG was successful in making a "recording boundary gauge" that could be used in the open ocean (see H. PETTERSSON, 1938, p. 77). In 1932 extensive recordings of internal waves were carried out simultaneously at several places in the central "Kattegat" in the vicinity of the "Fladenbank" shoal ($57^{\circ}10'N.$, $11^{\circ}45'E.$) in order to obtain a series of observations as long as possible. Only such observations make it possible to ascertain if the waves are of the progressive or standing type and also their direction, velocity and origin. KULLENBERG (1935), and PETTERSSON and KULLENBERG (1933) subjected the observations which extended over 15 days to the harmonic analysis and discussed the results thoroughly. Table 96 gives the data for two stations. For the M_2 tide, the amplitude of the first station, which was located closer to the shoal, is con-

Table 96. Records of Internal Tide Waves
Kattegat 6-21 November 1932 (According to Kullenberg)

	M_2		M_4		S_2		S_4	
	Amplitude (cm)	Phase (°)	Amplitude (cm)	Phase (°)	Amplitude (cm)	Phase (°)	Amplitude (cm)	Phase (°)
Station $57^{\circ}14.0'N.$ $11^{\circ}43.4'E.$	66	68	10	315	32	79	7	104
Station $57^{\circ}16.6'N.$ $11^{\circ}40.6'E.$	58	67	6	356	23	45	—	—

siderably greater than at the second one, but the phases are identical. For the tide S_2 the amplitudes are smaller, the phase difference is over 2 h. This is not very significant, considering the difficulty in determining S_2 . These and other results mean that the internal wave was probably of the progressive Kelvin type, travelling in a direction normal to the line connecting the two stations (direction of this line from 60° to 240°). From the data of other stations the wave velocity was found to be 89 cm/sec. This agrees with the value of 93 cm/sec, which was computed from the density distribution and the thickness of the layers (equation XVI.17).

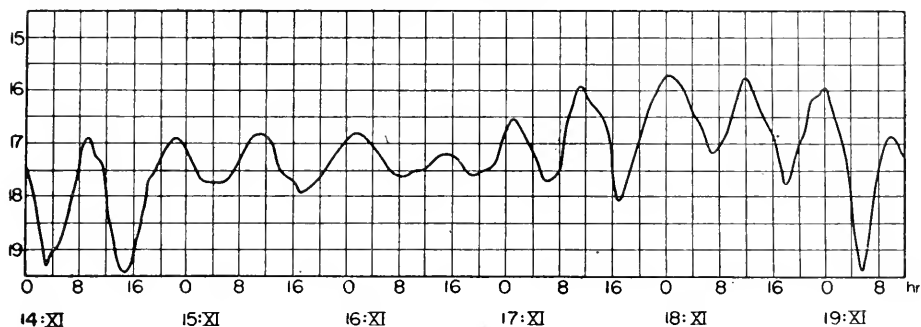


FIG. 229. Records of the recording boundary gauge from Station VII in the Kattegat, 14-19 November 1932 (Kullenberg).

The recordings show in a remarkable way variations of the amplitude with the character of beats (see Fig. 229 as an example). Kullenberg proved with a Schuster periodogram that in addition to the ordinary tidal periods there is a wave with a period of 14.5 h which corresponds to the period of the inertia oscillation of 12 pendulum hours. This follows from the fact that the period of beat is slightly over 3 days, which agrees with the period resulting from the superposition of a wave of 12.3 and one of 14.5 h.* But

* In the case of equal amplitude for both waves

$$a \cos \frac{2\pi}{12.3} t + a \cos \frac{2\pi}{14.5} t = 2a \cos \frac{2\pi}{162.1} t \cdot \cos \frac{2\pi}{13.1} t.$$

The period of beat is consequently $81.06 \text{ h} = 3 \text{ days}, 9 \text{ h}$.

such an internal wave with such an inertia period corresponds to the natural period of free oscillation of the Kattegat if the effect of the rotation of the earth is taken into consideration (see later). For internal waves in the Baltic Sea see also LISITZIN (1953).

By hourly bathythermograph records off the coast of California (40 nm offshore) over 6 days of anchor station on the thermocline in depths of 100–350 ft, well-developed internal waves were measured and analysed (REID, 1956). Waves of semi-diurnal period with amplitudes greater than 30 ft were found at the nearshore station (40 miles offshore in 1080 fm), but little evidence of these waves or any other periodic phenomena was found at the stations farther offshore though there was considerable vertical fluctuation of isotherms. It is suggested that the waves found originate near the coast in the action of the surface tides and that, since the length of such waves, if free, is short, they either dissipate before proceeding far offshore or, more likely, are so distorted by the varying density structure and water velocity that they are no longer recognized.

(c) *Free Internal Oscillations of Large Regions; Internal Inertia Waves*

When a certain thermo-haline distribution of an oceanic region is balanced by existing currents, and when this system is disturbed by some external causes it will try to return to its former state of equilibrium. This always takes place in the way of periodical oscillations around its state of equilibrium. These oscillations will have the period of the free oscillation of the system. The amplitude will depend upon the magnitude of the original disturbance and will gradually decrease because of the influence of friction. The essential data for such a case can be determined from a simple model, like a two-layer ocean. The boundary surface between the upper layer (density ρ' , thickness h') and the lower layer (density ρ , thickness h) will be in equilibrium with the existent currents, according to the Margules condition for boundary layers. Following DEFANT'S (1940) theory, the frequency of the free oscillation of the boundary surface ($\sigma_n = 2\pi/T_n =$ frequency of the free internal waves) can be expressed in first approximation by the quite accurate relation

$$\sigma_n = \sqrt{\left[(2\omega \sin\phi)^2 + \frac{n^2 \pi^2 g}{l^2} \frac{\rho - \rho'}{\rho/h + \rho'/h'} \right]}, \quad (\text{XVI. 39})$$

where l is the length of the area of the oscillation, and where the Coriolis force is taken into consideration. If the earth would not rotate ($\omega = 0$), the frequency would be reduced to the equation for standing internal waves in a basin of length l at the boundary surface between two liquids of different density (see Chapter XVI/1c, p. 523). Then the period of the free oscillation is

$$T_r = \frac{2l}{n} \sqrt{\left[\frac{1}{g(\rho - \rho')} \left(\frac{\rho}{h} + \frac{\rho'}{h'} \right) \right]}. \quad (\text{XVI. 40})$$

Let us assume that for a non-rotating earth the period T_r is great, which is in general the case, considering that the dimensions of the oscillating

system are great. Then the term $(2\omega \sin\phi)^2$ in the equation (XVI.39) becomes large compared with the second term and the period of the free oscillation of the system on the rotating earth becomes

$$T_i = \frac{2\pi}{2\omega \sin\phi} = \frac{12 \text{ h}}{\sin\phi} = \frac{1}{2} \text{ pendulum day}. \quad (\text{XVI.41})$$

On a rotating earth the period of a free oscillation of a stationary boundary surface and their related periodical currents approaches the periods of the inertia oscillation provided the dimensions of the oscillating system are great (see vol. 1). But in general the period T of the free oscillation of the system is

$$T = \frac{T_e}{\sqrt{1 + \left(\frac{T_i}{T_r}\right)^2}}. \quad (\text{XVI.42})$$

The larger T_r is compared to T_i , the more T approaches the period of the inertia oscillations T_i . Two numerical examples shall illustrate these conditions:

(1) The values in the Baltic (Kattegat) (latitude 57°): $\rho - \rho' = 2 \times 10^{-3}$, $h' = 25 \text{ m}$ and $h = 35 \text{ m}$ give as result for the longest oscillation $T_r = 3.75l$ (l in metres). Assuming $T_i : T_r = 0.1$, one obtains $l = 136 \text{ km}$. In a basin of these dimensions the difference between the periods of the free oscillations and the inertia oscillations would be less than 1%. A disturbance developing motion in the inertia circle would probably start oscillations of the boundary surface.

(2) As a numerical example for the open ocean (latitude 45°): $\rho - \rho' = 1 \times 10^{-3}$, $\rho = 1.0273$, $h = 1000 \text{ m}$, $\rho' = 1.0263$, $h' = 100 \text{ m}$ and $l = 150 \text{ km}$, and we obtain for $T = 16.64 \text{ h}$, and for the inertia period $T_i = 16.97 \text{ h}$. The period of the free oscillations in the case of a non-rotating earth would be $T_r = 89.5 \text{ h}$.

In the case of deeper basins or basins in lower latitudes the dimensions of the basins must be quite large if the period of the free oscillation is to approach the period of the inertia oscillations. It must be expected that we will find frequently the inertia period in the variations of the oceanographic properties and currents in the open ocean, because this inertia period is so close to the period of the free oscillation of the system. The foregoing deduction deals only with a two-layer system, but Defant's general result is undoubtedly valid for water-masses where the density increase is continuous.

A typical example is offered by the oceanographic conditions prevailing at the anchor station of the "Altair" on the northern edge of the main axis of the Gulf Stream north of the Azores ($44^\circ 33' \text{N.}$, $38^\circ 58' \text{W.}$, from 16 to 20 June 1938, depth 1110–2390 m), which lasted for 90 h. The current measurements up to 800 m depth showed that the entire water-mass was influenced by the

tide-generating forces in essentially the same way, with the exception of small deviations in the upper layers. The direction of the major axis of the semi-diurnal current ellipse was N. 40° E. the maximum velocity 8.3 cm/sec and the phase 0.5 lunar hours (Gr.). The ratio of the minor to the major axis was 0.43, its direction was *cum sole*. But besides this uniform tide wave there appeared also a 17-hourly wave, which was very much in evidence in the curves of the tidal current through beats. The analysis of the curves gave the values shown in Table 97. These fluctuations leave no doubt that it represents

Table 97. Anchor Station "Altair" (16-20 June 1938, 44°33' N., 38°58' W.).
Analysis of the current observations for a 17 h Wave

Depth (m)	North component		East component		Ratio of amplitudes N:E	Phase h N+4.25h	Difference with east
	Amplitude (cm/sec)	Phase* (h)	Amplitude (cm/sec)	Phase * (h)			
5-15	8.7	14.45	8.2	1.85	1.06	1.70	+0.15
30-100	10.0	7.33	10.0	12.27	1.00	11.58	+0.69
300-500	5.0	9.0	5.0	14.85	1.00	13.25	+1.60
800	8.0	2.0	8.0	8.0	1.00	6.25	+1.75

* Refers to 0 h G. M. T. of 17 June 1938.

an inertia oscillation: according to theory its period $12/\sin\phi = 17.1$ h, the amplitudes of both components are equal, the current is turning to the right and the east component follows the north component by $\frac{1}{4}$ period. Strikingly, there exists a differentiation with depth. The upper layer from the surface to 15 m had a completely inverted course compared with the layer from 30 to 100 m. There seems to exist again a displacement of half a period (8.5 h) between the middle layer and the depth of 800 m. Since the upper layer down to a depth of 100 m shows a well-developed discontinuity in the density (maximal values at a depth of 25 m), it may be assumed, that the 17-hourly wave has the character of internal waves. This was also demonstrated by working up the repeated serial observations over 90 h. Temperature and salinity values in this layer showed a uniform vertical displacement of the water-masses with a phase of 10.5 h and a mean amplitude of 3.0 m. Similar conditions prevailed in a depth between 350 and 450 m, where a discontinuity layer was less pronounced.

From the structure of the entire ocean region near the "Altair" peak it can be concluded, that the length of the oscillating system was about 150 km. Furthermore, $h' = 25$ m, $h =$ approximately 1500 m, $e' = 1.0263$ and $e = 1.0278$; thus $e - e' = 1.5 \times 10^{-3}$. According to equation (XVI.39) the period of the free oscillation of the entire system will be 16.98 h. Compared with the inertia period of 17.1 h, the difference is very slight. The equilibrium of the entire ocean region near the "Altair" peak was probably upset by

atmospheric disturbances (passage of a storm region). After the disturbance subsided the system gradually approached a new equilibrium by its free oscillations.

The internal waves which were observed in the Kattegat with a period of 14.5 h are surely oscillations with the free period of the entire basin. According to computations one needs a width of 136 m to obtain a period of the free oscillation which differs only by 1% from the period of the inertia oscillation which is 14.5 h. The width of the Kattegat is of this order of magnitude. Concerning inertia oscillations in the Baltic, see p. 554.

3. Internal Waves in Lakes and in Basins

The reflection of progressive internal waves at the boundary surfaces of enclosed water-masses, changes these waves into *standing internal waves*. In a basin with an irregular shape, where the density increase is continuous, one can expect an unlimited number of free standing oscillations, because an infinite number of internal waves of different orders may be present and in a horizontal direction the number of nodes may lie between one and infinity. Every internal wave of any order can cause by reflection a standing internal wave. This circumstance makes it likely that there will be always a free-standing internal wave which reacts somehow to an external intermittent disturbance of arbitrary period. Because of the small amount of energy which is necessary to create such internal waves they will occur quite frequently in nature.

In basins of constant depth and of rectangular cross-section (lake), the periods of oscillation of free-standing waves in the presence of two layers are expressed by (see also SCHMIDT, 1908, p. 91)

$$T = \frac{2l}{n} \sqrt{\left(\frac{\rho}{g(\rho - \rho')} \frac{h+h'}{hh'} \right)}, \quad (\text{XVI.43})$$

where h and ρ are the thickness and density of the lower heavier water-mass, h' and ρ' the corresponding values of the upper lighter layer, l is the length of the basin, and $n = 1, 2, 3, \dots$. If the basin is not closed in on all sides, but open on one side (bay), then $2l$ in (XVI.43) has to be replaced by $4l$.

During a large part of the year many lakes and bays have well-developed discontinuity layers of density (thermocline) and internal standing oscillations ought to be a frequent phenomenon. WEDDERBURN (1905, 1907, 1909) proved the existence of such standing internal waves in Scottish lakes and EXNER (1908) did the same for Lake Wolfgang in Austria. They found a very satisfactory agreement between the observed and the theoretically computed values of the periods. According to the corresponding conditions in the case of the surface seiches, it is evident that the shape of the basin exercises a great influence upon the period of oscillation. Since the period of the longer standing internal oscillations in somewhat more extended water-masses is fairly

large, the influence of Coriolis force can be expected to increase. Consequently, equation (XVI.43) should be used with caution.

A particularly beautiful example of temperature seiches in Lake Madü in Pommern, were analysed by HELBFASS and WEDDERBURN (1911) from 25 July to 14 August, 1909. The discontinuity layer of the density was located at a depth of 15 m, and the internal oscillations in this layer were very distinct at that time. Figure 230 shows the course of the isotherms in the layer between 10 and 20 m depth. Solid curves represent the isotherms for a station at the northern end, the dashed curves for a station at the southern end of the lake. The complete inverted course of the two groups of curves shows clearly, that one is dealing with an internal seiche with one node and with

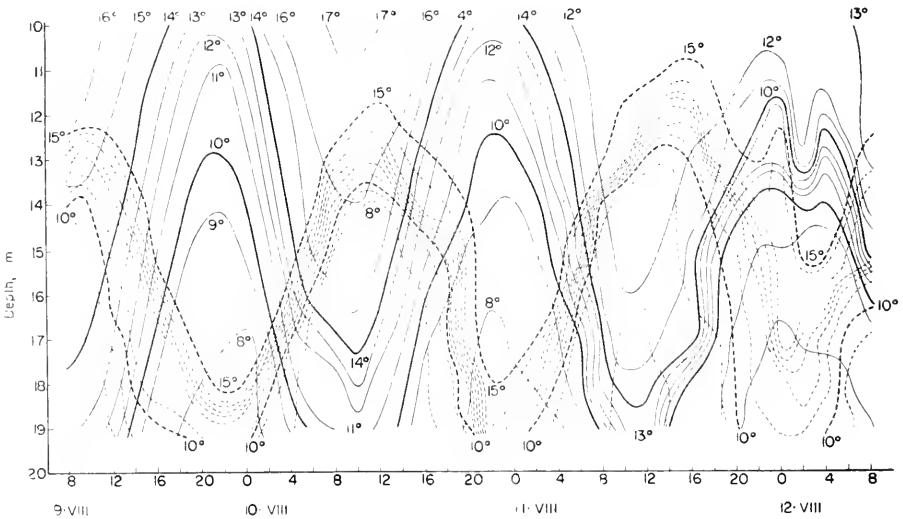


FIG. 230. Internal temperature seiches in Lake Madü (Pommern) from 9th August at 8 h to 11th August, 20 h, 1909; —, isotherms at northern end of the lake; ----, isotherms at southern end of the lake.

an amplitude of roughly 6 m. The period was found to be practically exactly 25 h. The entire discontinuity layer participates in the vertical movement of the water-masses. The dimensions of the oscillating system, substituting for Lake Madü a rectangular trough, are $l = 13.75$ km, $h' = 23$ m, $t' = 17^\circ$, $h = 15$ m, $t = 8^\circ$, in which h' and t' and h and t represent thickness and temperature of the upper and lower layer respectively. Thus one obtains for the period of the internal seiche with 1 node $T = 91,000$ sec = roughly 25 h; in complete agreement with the observed value.

It can be assumed that standing internal oscillations occur also in larger or smaller adjacent seas. But because of the great expansion of the water-masses, the period of the standing internal waves will become very long. Conditions will develop similar to those explained on page 550. The effect

of the Coriolis force has to be considered and the period of the free internal oscillation will approach the period of the inertia oscillation when the size of the oscillating basin increases. Such conditions certainly occur in the Baltic, where variations in the currents showed a period of the inertia oscillation when the water masses are stratified (see GUSTAFSON and KULLENBERG, 1936; KULLENBERG and HELA, 1936). These oscillations in the currents are associated with internal waves of the entire stratified water-mass, and are subjected to the period of the inertia oscillation. Because the oscillations with the inertia period are in general caused by wind disturbances, they persist for some time with a striking constancy and are dampened only slowly. Approaching the coast the amplitude decreases and there they die off.

O. PETTERSSON (1909) found very long periods of internal waves from once-time-daily observations of the stratification of the water-masses of the Gulmarfjord at Bornö. The main period of the internal vertical oscillations was roughly 14 days, with amplitudes up to 25 m. Pettersson believed that these oscillations were caused by the effect of the tide generating forces of the moon (declination tide). But WEDDERBURN (1909, p. 602) could prove, by use of equation (XVI.43) for bays, that in this case one is dealing in all probability with standing internal oscillations of the entire Skagerrak basin. If the entrance of the bay is assumed to be the line connecting Hanstholm (Denmark) and Mandal (Norway) the width of the opening will be 50 km. With $l = 200$ km, $\rho - \rho' = 4 \cdot 10^{-3}$, $h = 100$ or 200 m, $h' = 20$ m and with a correction for the width of the mouth (see equation (VI.75), Table 22) one obtains for the period $T = 13.9$ and 14.2 days respectively. This period derived by theory is in good agreement with the observed one. But it is questionable, if the effect of Coriolis force may be neglected in the case of such long periods.

When the density varies continuously with depth and when the shape of the bay is irregular, an infinite number of internal waves becomes probable. But the waves of high order or of many nodes cannot be expected to last very long because great velocity gradients generate friction which dissipates their energy very fast. An exhaustive investigation on internal waves of the Gulf of California, including this aspect was carried out by SVERDRUP (1939, 1940, p. 170) and MUNK (1941). The hydrographic survey of the Gulf of California from 13 February to 19 March 1939 showed a wave-like pattern in the dynamic topography of the sea surface and of the isobaric surfaces (referred to the 1500 decibar surface). The phenomenon can be explained only by the existence of standing internal waves of a period of roughly 7 days. This wave is of the first order in a vertical direction, and the vertical displacement vanishes at the bottom and at the surface. It is of the fourth order in a horizontal direction with three nodal lines in the Gulf. A nodal line at the entrance of the Gulf indicates that we have to do with a free oscillation. Figure 231 shows the distribution of the water-masses and the position of the various isobaric surfaces within the Gulf, as resulting from the oceanographic

survey. The internal standing wave originates near the entrance of the Gulf as a superposition of two progressive waves of 1000 km wave length and a velocity of progress of 175 cm/sec. The velocity decreases considerably towards the interior of the Gulf. It is interesting to note that this standing wave reflects itself clearly in the sediments of the Gulf. The coarser sediments are deposited along the three nodal lines, where the velocities are great (up to 20 cm/sec), while the finer sediments are collected at the anti-nodes of the oscillations. This difference in the size of the grains of the sediments in a horizontal direction suggests that the standing wave within the Gulf might be a phenomenon which occurs frequently (REVELLE, 1939, p. 1929).

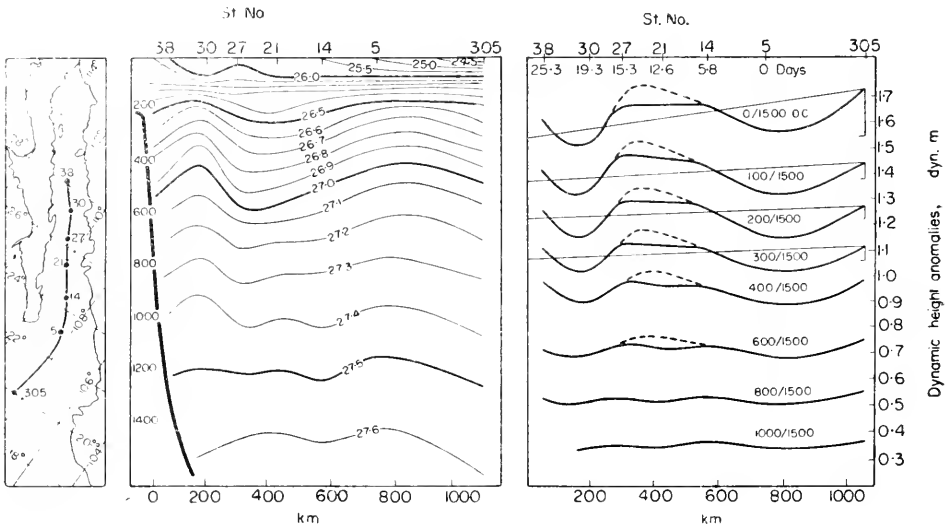


FIG. 231. Vertical distribution of the density σ_t and profiles of the isobaric surfaces (referred to the 1500 deci-bar surface) along a longitudinal section of the Gulf of California (Sverdrup).

MUNK, in a theoretical investigation, examined the problem of the formation of standing oscillations in a bay of variable depth and expanded Fjelstad's theory in this respect. He shows that in this case the expression $f(z) \cdot F(x) \cos \sigma t$ for the horizontal and vertical velocity (z vertical, x horizontal) have to be replaced by those of the form $W(x, z) \cos \sigma t$ whereby the problem becomes considerably more complicated. Developing $W(x, z)$ into a Fourier series

$$W(x, z) = \sum_{i=1}^n C_i W_i(z) \sin k_1 x$$

where

$$k = i\pi/2l$$

and l the length of the bay, the theory requires that all $W(z)$ satisfy analogous differential equations, as in the case of Fjelstad's theory. Furthermore, the

boundary conditions have to be satisfied, so that $W = 0$ for $z = 0$ as well as for $x = 0$. This leads to a determinant D , which has to be a minimum for the period $T = (2\pi/\sigma)$ of the free oscillation of the system.

The orographic configuration, of the Gulf of California can be compared with a canal. Its depth of 1800 m remains roughly constant to about 700 km from the mouth, then it decreases quickly to zero, towards the inner end (near the islands of San Estobal and San Lorenzo). For the outer part, where the depth remains fairly constant, Fjølstad's theory gives a velocity of progress of the wave of first order of 167 cm/sec, and for the depth of the greatest vertical displacement 675 m; which is in good agreement with the observations of 175 cm/sec and 500–600 m depth. For that part of the Gulf of California where the depth decreases to zero the computation of the above-mentioned determinant shows that for waves of the first order, a minimum occurs for a period of 7 days; for waves of the second order for a period of 14.8 days, which corresponds to the observations. It is likely that the more important period of 7 days rather than the period of 14.8 days is caused by the tide generating force of the lunar tide of 13.6 days, since $2 \times 7 = 14$ is closer to 13.6 than the period of the standing wave of the second order. Therefore the 7-day oscillation will dominate, which is in agreement with the observed arrangements of the sediments in the Gulf.

4. Causes of Internal Waves, Particularly of Those with a Tidal Character

In order to investigate closer the causes of the formation of internal waves, it has to be kept in mind that even small amounts of energy are sufficient, to cause oscillations of boundary surfaces between liquids of different density, or vertical displacements in a water-mass where the density increases continuously with depth. Even small pressure disturbances at the surface are already sufficient to cause large vertical displacements within a stratified medium. In the case of the disturbance on the "Meteor" Anchor Station 254 we encountered (p. 527) a condition where in all probability a powerful internal wave was caused by a small gust of wind, started by comparatively small forces; such disturbances of the internal equilibrium of a stratified water-mass, may, under favourable conditions like resonance, increase to an enormous amplitude. Thus it can be expected, that in the case of disturbances of the internal equilibrium in a stratified sea, the return to a new state of equilibrium will be accompanied by internal waves, which are gradually dampened because of the frictional influences.

Since the internal waves observed in the ocean have frequently a decidedly tidal character the question arises, whether internal tide waves in the ocean might be caused by the horizontal and vertical tide generating forces of the sun and the moon. This would explain the tidal character right away. O. PETTERSSON (1909, 1930, 1933, 1934, 1935) thought that especially the vertical component of the tide generating force was the cause of the internal tide

waves. But DEFANT (1932, p. 295; 1934, p. 310) proved theoretically, that tide waves at inner boundary surfaces cannot be caused by such forces. The necessary conditions are never fulfilled under the given circumstances within the ocean, and it has to be stated that the occurrence of inner tide waves can hardly be caused by forces of such kind.

The importance of meteorological influences on the formation of internal waves was discussed by Wedderburn in his work on Scottish lakes. M. PETTERSSON (1920, p. 32) used similarly the daily variations in the vertical distribution of the water-masses at the oceanographic station Bornö (Gullmarfjord), to find possible relations with simultaneous meteorological conditions. The comparison of the variations in the depth of the isohalines with the corresponding force of the winds in the direction of the fjord (NE.-SW.) shows immediately that the curves for most of the cases run parallel (see Fig. 232). A more exhaustive investigation of the correlation between the

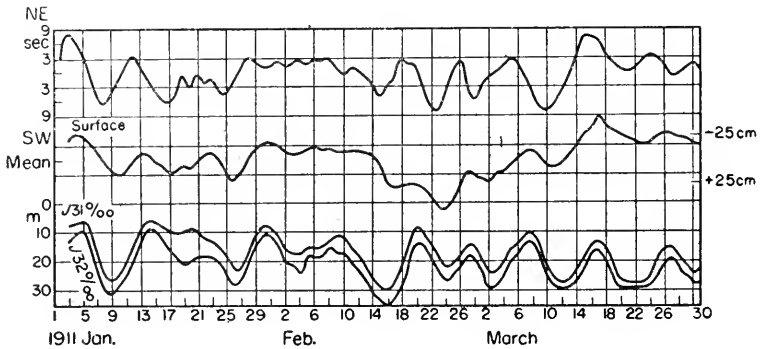


FIG. 232. Relationship between the variations in depths of the isohalines 31 and 32‰ and the surface and the force of the wind in the direction of the Gullmarfjord. Bornö, 1 January–30 March 1911 (H. Pettersson).

vertical displacements and the wind-force confirmed numerically this meteorological influence. Where the wind blows from the ocean towards the fjord the surface water piles up at the inner end of the fjord. This is accompanied by a lowering of the boundary surface between upper and lower layer of the water (mostly with a delay of 1–2 days). Conditions are reversed with the wind blowing towards the sea. Not all oscillations can be traced back to these simple occurrences. But the influence of the wind remains the principal influence for the formation of internal waves, at least in the case of more or less enclosed water-masses.

While investigating the seiches of the Gullmarfjord ZEILON (1912) found the main period of the uninodal wave to be 110 min (see Chapter VI.3a, p. 182). Internal waves of the same period occurred at the discontinuity surface in the fjord. Zeilon, thinks that the currents in the Kattegat near the entrance of the fjord are the outer cause for the generation of these secondary

internal waves. The bottom configuration at this point shows a submarine barrier. Therefore, only the upper water-masses of the fjord are connected with the free ocean. This submarine sill or barrier, which rises nearly to the level of the discontinuity surface, is an obstacle for the development of the horizontal currents of the seiches and these currents cause a disturbance at the boundary surface, which now travels as an internal wave with the period of the seiche along the discontinuity surface into the fjord. ZEILON (1934) could support this explanation by very convincing experiments in the wave tank. He also demonstrated that in an oscillating stratified water-mass a disturbance in the bottom configuration could generate internal waves which then travel along the discontinuity surface of density. Zeilon found in other experiments that internal waves can be formed when a tidal current is advancing toward a wide shelf. If the discontinuity surface is in about the same depth as the outer limit of the shelf, an internal wave is formed on the edge of the shelf and it travels toward the coast in shallow water and also toward the open ocean in deeper water. The two illustrations in Fig. 233 demonstrate

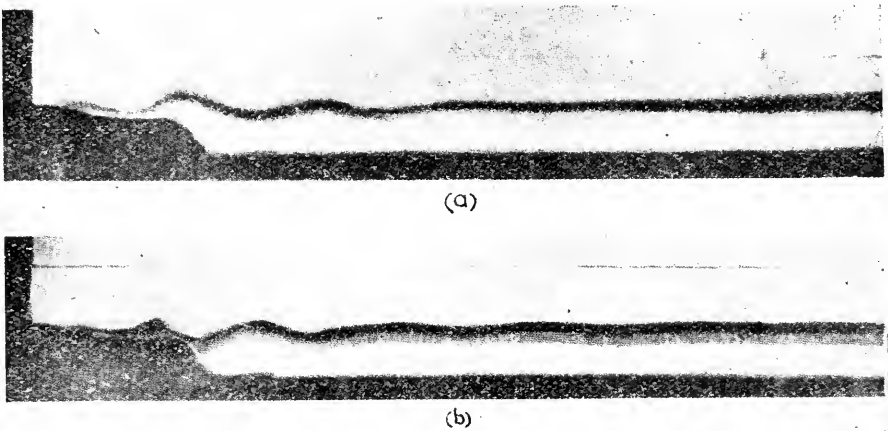


FIG. 233. Tidal current producing internal waves at the edge of the shelf. At *b* the internal wave breaks at the shelf (Zeilon).

Zeilon's experiments. The greatest amplitudes will be found near the shelf in shallow water. Submarine breakers occur during the propagation on the shelf, which can be clearly recognized in the illustration "b".

Further causes for generation of internal waves are the more or less sudden appearance of a strong surface current, which can be caused by a gust of wind (similar to Sandström's experiments, see p. 528), or by the occurrence of a bottom current. The place where the outside disturbance acts upon the water-mass is in both cases the source of the internal waves, which proceed along the boundary surface in the direction of the disturbing current.

These experiments show that in shallow ocean regions (shelf regions) internal periodical displacements might be generated with the same period as the disturbance that caused them. They can occur because of topographical irregularities at the bottom of the ocean or on the edge of the shelf, if the boundary layer is at the right depth. The most frequent disturbance will probably be the periodically returning tidal currents, which ought to cause the generation of internal tide waves in shallow waters. But the influence of such internal tide waves ought to be limited as they are dampened very rapidly, so that their amplitudes decrease quickly when the waves spread out in all directions, as was emphasized by EKMAN (1931).

In the open ocean, topographical bottom influences can hardly be expected to be the cause for the generation of internal waves. External influences from the atmosphere are rather the cause; but these will not have a tidal period. The cause for the internal tide waves, which occur frequently over great depths in the free ocean, far from the continents, cannot yet be stated with certainty. One might think of inhomogeneities in the vertical structure of the main currents, on which the regular tidal current is superposed, which is of the same kind in all depths. But the superposition with the main current causes periodically varying water transport in the superimposed water layers, which ought to be related to the vertical displacements with tidal periods of the boundary layers. The vertical heterogeneity of the main currents is in general dependent upon the vertical distribution of the thermo-haline properties and the discontinuity layers of density are also in most cases discontinuity layers of the field of motion. This heterogeneity in connection with the periodical tidal currents, might well be one of the causes of the so frequently observed internal waves of tidal period.

So far, the effect of the earth's rotation on the internal waves was not considered. Because of the earth's rotation the periods of long internal waves are much shorter and their velocities much larger than without taking into account the Coriolis force; therefore, it is to be expected that the resonance conditions for oscillations at internal surfaces of discontinuity are much more favourable than was supposed previously. This was confirmed by investigations by DEFANT (1950) and HAURWITZ (1950). The main features may be illustrated by the following model. Let the upper water-mass move with the constant velocity U_1 , the lower with the constant velocity U_2 , both parallel to the undisturbed discontinuity layer. A tide generating force,

$$X = f e^{i(\sigma t - \kappa x)},$$

acting in a horizontal direction on the whole system, will produce tide waves at the surface and on the discontinuity layer.

The equations of motion and the continuity equation for both water waves give for the water surface and for the discontinuity layer one wave solution with waves of the frequency σ and the wave numbers κ . The velocity of pro-

pagation $c = \sigma/\kappa$ is determined by the force. In the equations for the amplitudes of the surface and of the boundary layer, the expression

$$c(c-U_1)[(c-U_2)^2\omega_1\omega_2 + (c-U_1)^2\rho_1/\rho_2] - [(c-U_2)^2\omega_1 + (c-U_1)^2\omega_2\rho_1/\rho_2 + c(c-U_1)\omega_1/\rho_1] \cdot g/\kappa + \Delta\varrho g^2/\kappa^2 = D_1 \quad (\text{XVI.43a})$$

always appears as denominator, wherein $\omega_1 = \coth \kappa h_1$ and $\omega_2 = \coth \kappa h_2$. But this expression, when set equal to zero, is the equation which determines the velocity of the *free* waves of the system. For $U_1 = U_2 = 0$ this equation becomes the equation of the velocity of free waves with the wave number κ :

$$c^4(\omega_1\omega_2 + \rho_1/\rho_2) - c^2(\omega_1 + \omega_2)g/\kappa + \Delta\varrho g^2/\kappa^2 = D_2 = 0. \quad (\text{XVI.43b})$$

The two solutions of this equation for long waves are

$$c_1 = \sqrt{g(h_1 + h_2)} \quad \text{and} \quad c_2 = \sqrt{\left[\frac{\Delta\varrho}{g} h_1 h_2 / (h_1 + h_2)\right]}. \quad (\text{XVI.43c})$$

The velocity c_1 is valid for waves at the surface, which are associated with displacements of the boundary layer of smaller amplitudes than those at the surface. c_2 is the velocity of free internal waves. In the case of forced waves the case of resonance corresponds to $D_2 = 0$. Theoretically in this case the amplitude of forced waves will be infinitely large. Note that the internal waves will be infinitely large if the condition $c = c_2$ is exactly fulfilled. But this never occurs, since the magnitude of c for tidal waves in the oceans is about 200 m/sec and that of c_2 only 2 m/sec.

Taking into account the Coriolis force, one obtains in the place of the former (XVI.43b) denominator the expression:

$$\varepsilon^4 - (h_1 + h_2)g\varepsilon^2 + \Delta\varrho g^2 h_1/h_2 = D_3 \quad (\text{XVI.43d})$$

where: $\sigma^2 - f^2/\kappa^2 = \varepsilon^2$.

It has the same form as the relation (XVI.43b), transformed for tidal waves, for the velocity of forced waves c , the influence of the earth's rotation is entered through the quantity ε . Whereas c has the magnitude of 200 m/sec and the quantity D_3 is a large number, under certain conditions ε can be small or nearly equal to the velocity of free internal waves. With these values, however, D_3 will be zero. If T_i is the period of internal waves (equal to 12 pendulum hours), then

$$\varepsilon^2 = c^2[1 - (T/T_i)^2]. \quad (\text{XVI.43e})$$

For the diurnal tide wave, $T = 24$ h and ε will be zero at 30° latitude, but for the semi-diurnal lunar wave, $T = 12.43$ h and ε will be zero at about 74° latitude. For small ε equations (XVI.43d) has, in the first approximation, the form:

$$D_4 = \Delta\varrho g^2 h_1 h_2 - g(h_1 + h_2)\varepsilon^2.$$

D_4 will be zero for

$$\varepsilon^2 = (\Delta\varrho/\varrho)h_1 h_2 / (h_1 + h_2). \quad (\text{XVI.43f})$$

When $\varepsilon = c_2 =$ the velocity of free internal waves, then resonance exists for forced internal waves. In other words, the amplitude of internal tide waves will be very large. This is not the case for the normal tides at the surface, for which

$$D = \varepsilon^2[\varepsilon^2 - g(h_1 + h_2)].$$

D_5 remains a large number when $\varepsilon = c_2$.

Therefore, the rotation of the earth provides a factor which is able to increase the amplitudes of internal waves, and internal waves will thus be a larger wave motion than the tide at the surface (see also the paper by B. HAURWITZ, *The occurrence of internal tides in the ocean* (1954)).

From (XVI.43f) is obtained as resonance wave length of internal waves

$$\lambda_R = 2\pi \sqrt{\left(\frac{1}{(\sigma^2 - f^2)} \frac{\rho_1 h_1 h_2 g}{\rho_2 (h_1 + h_2)} \right)}$$

and, if the frequency of the semi-diurnal or diurnal tides is taken for σ , λ_R as a function of latitude. With wave lengths of this magnitude, internal tidal waves with great amplitudes can always be expected (see KRAUSS, 1957).

5. The Stability of Internal Tide Waves Internal Breakers

The vertical displacements with a tidal period of the discontinuity layer of density occur in most cases in symmetrical form, according to the observations. Examples are the anchor stations "Meteor" 254 (see Fig. 216) and "Meteor" 385 (see Figs. 224 and 225). These tide waves do not show any decay. Their wave profiles are symmetrical, but there are cases where this does not occur, like internal tide waves on the continental shelf or in shallow straits. A typical example are the internal tide waves in the Straits of Gibraltar at springtide. At neap tide, when the discontinuity layer is well-developed between the Atlantic upper current flowing eastward and the Mediterranean under-current flowing westward, these internal waves proceed entirely in a normal fashion and the wave profile is symmetrical. The Danish research vessel "Dana" carried out repeated hydrographic casts on Station 1138 (8–10 October, 1921, 35°59'N., 5°30'W.). Working up this station, JACOBSEN and THOMSON (1934) showed for this period a regular internal tide wave with a range of 43 m and of a phase of 0.7 lunar hours after high water in Gibraltar. The connection between this internal wave and the surface tide within the Strait can be easily explained in this case. The increase of the velocity of the current (main current plus tidal current) in the upper layer, which occurs simultaneously with a decrease in the velocity of the lower current, causes a sinking of the discontinuity layer. A decrease in the velocity of the upper current, together with an increase in the velocity of the lower current, on the other hand, causes a lifting of the discontinuity layer. At neap tide and under normal weather conditions, this internal tide wave occurs

regularly in agreement with theoretical principles and without considerable disturbance. This does not seem to be the case at springtide when the tidal currents are stronger. The repeated serial observations of the "Dana" from 14 to 15 July 1928, which were carefully analysed by Jacobsen and Thomson, show that the internal wave, which was linked with the surface tide, had decayed completely. In the layer between 70 and 150 m the wave is almost turning over. Several values show an instability in the stratification. The wave profile is very asymmetrical and the internal wave assumes the form of an internal bore. It probably traverses the entire strait in the region of the strong tidal currents at springtide. Then it vanishes in the adjoining sea where the depth is so much greater and where the discontinuity in the density is entirely missing, whereas it was well developed in the strait. Figure 234

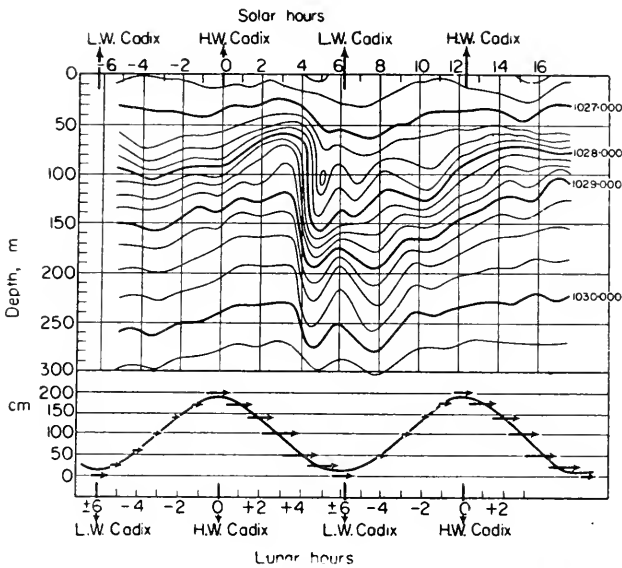


FIG. 234. "Dana" Anchor Station in the Strait of Gibraltar $\phi = 35^{\circ} 57.5' N$, $\lambda = 5^{\circ} 21' W$. 14–15 July 1928. Isopycnals (kg/m^3). Below is given the tide curve for Cadix. The arrows indicate the direction and velocity of the total current (which is the sum of the basis and tidal current) in the upper layers in the centre of the Strait at springtide.

presents the course of the isopycnals (kg/m^3) for the entire duration of the observations up to a depth of 300 m and the unstable internal tide wave within the strait. Also entered in Fig. 234 are the tide curves of Cadix and the curves for the total surface current (main current plus tidal current) for the middle of the Straits.

A number of additional cases of obvious instability of internal tide waves were shown by DEFANT (1948, p. 52) in the observations of the "Meteor" anchor stations on the West African Shelf between the Canary and the Cape Verde Islands. A particularly interesting case was the anchor Station 366

(13–16 April 1937, $10^{\circ}16'N.$, $16^{\circ}38'W.$; 60 repeated casts in 1 hourly intervals). In Fig. 235 the principal isotherms have been averaged from five periods of the semi-diurnal to one period. This figure demonstrates clearly the asymmetrical profile of the internal tide wave in the vertical displacement of the isotherms. The extreme values are shifting with increasing depth, the internal wave is retarded more and more, especially the maximum in the deeper layers lags several hours after the maximum in smaller depths.

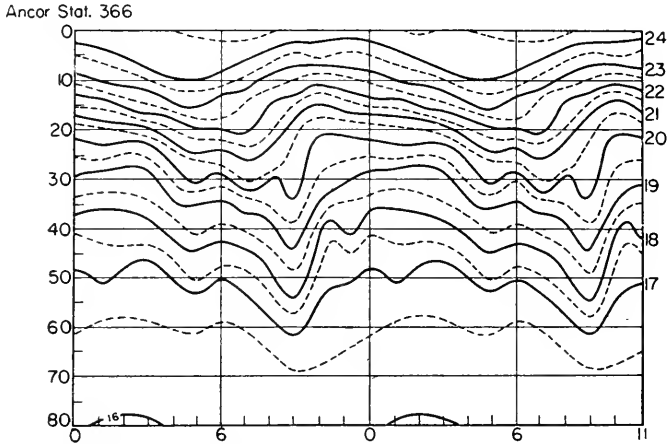


FIG. 235. Isotherms at "Meteor" Anchor Station 366. Average from five periods.

All these facts indicate that the wave profile of internal waves can decay under certain conditions, which can lead finally to internal breakers (surf). One should not think that these internal breakers should have the same energy and have the same speed as the surf of the regular surface waves. This internal surf takes place very slowly, because of the small velocity of the internal waves. Such internal breakers can be produced in a wave tank in a two-layer system. There the phenomenon can be followed closely because of the slowness of the occurrence. A photograph of experiments of such kind will be found in DEFANT (1913, p. 83; 1929, p. 51). Similar phenomena will occur with internal waves in nature.

The question arises as to what causes an internal tide wave to such a turbulent process of degeneration and finally to break down internally. When the amplitude of internal waves becomes great and cannot be considered as small compared to the depth of the water, then the wave changes its profile during its travel. The slope at the front of the wave becomes steeper, and flattens out at the rear of the wave; the wave profile becomes asymmetrical. The increase of this asymmetry leads to the breakers and the surf. Under similar conditions, internal waves will behave the same way as surface waves where the amplitudes were great at shallow depth. Both circumstances are doubtless contributing factors in forcing an asymmetry of the wave profile.

But there are also cases, where these conditions are not sufficient for the explanation of the internal breakers. The circumstances under which internal waves occur, permit the development of dynamic instability. The discussion of the following simple case will be sufficient. Two layers of great thickness are superposed. Let u' be the velocity of the upper, lighter water-mass, u the velocity of the lower, heavier one. The theory shows (see LAMB, 1932, p. 373; V. BJERKNES, 1933, p. 381; HOILAND, 1943), that in this case the velocity of internal waves at the discontinuity surface is given by the expression

$$c = \frac{\rho u + \rho' u'}{\rho + \rho'} \pm \sqrt{\left[\frac{g}{\kappa} \frac{\rho - \rho'}{\rho + \rho'} - \rho \rho' \left(\frac{u' - u}{\rho + \rho'} \right)^2 \right]}. \tag{XVI.44}$$

The first term on the right-hand side represents the convective velocity and may be called the mean velocity of the two currents. Relatively to this the velocity of waves of the length $\lambda = (2\pi/\kappa)$ is represented by the term on the right-hand side under the square root. The first term under the root represents the velocity of progress of the internal waves in the system at rest (p. 518 (XVI.7)), i.e. the velocity of progress of pure gravity waves. The second term under the root with the negative sign is the velocity of pure inertia waves. The term for the gravity waves is always positive, if $\rho > \rho'$, which is of course always the case. Pure gravity waves are always stable. The inertia term, on the other hand, is always negative. Thus it has always an unstable effect and therefore weakens the static stability of the gravity waves. This weakening may become so effective as to produce dynamic instability. This happens if

$$(u' - u)^2 > \frac{g}{\kappa} \frac{\rho^2 - \rho'^2}{\rho \rho'}, \tag{XVI.45}$$

i.e. if for a given wave length and discontinuity of density, the difference in velocities on the discontinuity surfaces become great enough.

In the cases under consideration the thickness of the two superposed water layers are small. This causes a further decrease of the term at the right side of the inequality (XVI.45). Let h and h' be the thickness of the two layers. Then we obtain as inequalities

$$(u' - u)^2 > \frac{g}{\kappa} (\rho - \rho') \left[\frac{1}{\rho \coth \kappa h} + \frac{1}{\rho' \coth \kappa h'} \right]. \tag{XVI.46}$$

If we simplify the case by assuming $h = h'$, and if we consider, that κh is small, we can write with sufficient accuracy

$$\frac{1}{\coth \kappa h} = \tanh \kappa h = \kappa h.$$

Then the inequality becomes

$$u' - u > \sqrt{\left(gh \frac{\rho^2 - \rho'^2}{\rho \rho'} \right)}. \tag{XVI.47}$$

Table 98 was computed with this inequality. For the various values of the discontinuity in density $\varrho - \varrho'$ and for the thickness of the layer h the table presents the difference of velocity, which has to be exceeded, to cause dynamic instability of the internal tide waves.

Table 98. *Dynamic unstable internal waves will be generated when the difference in velocity $u' - u$ in cm/sec between layers exceeds*

$\varrho - \varrho'$	10^{-4}	$5 \cdot 10^{-4}$	10^{-3}
$h = 150$ m	52	117	166
100 m	47	96	135
50 m	30	68	96
25 m	20	48	68

It can be seen from these values that even a relatively small difference of velocity in the currents is sufficient, to cause instability of internal tide waves. The basic currents in sea straits flow always in opposite directions in the two superposed water-masses (compensating currents between ocean and

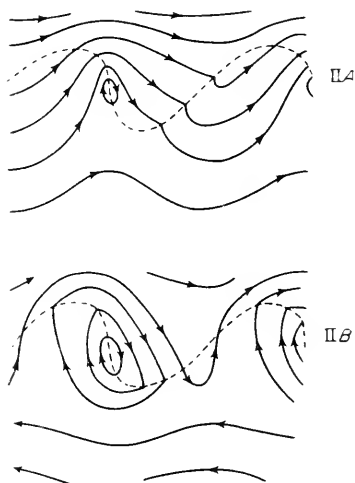


FIG. 236. Wave form and stream lines for dynamic unstable internal waves. II A, upper and lower current having same direction; II B, upper and lower current having opposite directions. Compare with Fig. 213 (V. Bjerknes).

a mediterranean sea). The internal waves at the boundary surface in straits will have therefore a particularly strong tendency towards the degeneration of the wave profile and the formation of internal breakers. This is the case in the Strait of Gibraltar and particularly in the Strait of Messina.

V. Bjerknes computed for other purposes the wave form and the stream lines for such unstable internal waves. Figure 236 presents two of such cases.

In the upper wave the direction of the basic currents is the same in both water-masses; in the lower wave the direction of the basic currents is opposite. In both cases the velocity of the upper water-mass is the greater one, as it is always the case in nature. It will be immediately recognized that the asymmetry of the wave profile reminds one of the slopes of internal tide waves. When the asymmetry of the wave increases it will cause finally powerful internal processes of turbulence. In the case of dynamic instability, the boundary surface curls up into vortices of the same direction, which insert themselves between the two layers which have different motions. Figure 237 shows,

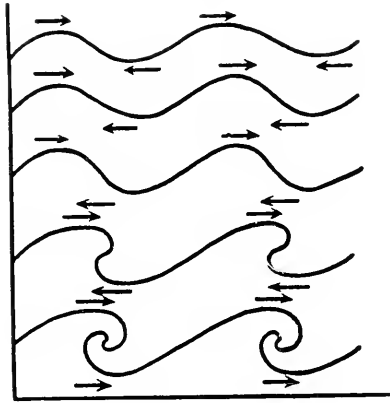


FIG. 237. Transformation of a dynamic unstable internal wave (Rosenhead).

according to ROSENHEAD (1932, p. 170), the transformation of an unstable wave. The final result will be the formation of a mixing layer, caused by the continued vortex motion. There will be then a more or less continuous transition of the density and of the velocities from the lower to the upper layer. The discontinuity of temperature and of salinity decreases rapidly on continental shelves by approaching the shore and then mostly disappears inside a stripe off the coast completely. This is due to the circumstance that the decreasing depth of the ocean causes the internal tide waves to become so unstable that the discontinuity layer disappears. This process is the basic prerequisite for the process of upwelling of cold water along the coasts.

6. Stationary Internal Wave-like Displacements

The oceanographic survey of various regions of shallow depth (on the continental shelf or straits) as well as in the open ocean of not too large a depth, showed frequently vertical cross-sections with striking wave-like distributions of the isotherms and isohalines and of course of the isopycnals. They were apparently of a stationary character. MERZ (1935), for instance, found in the western part of a temperature cross-section through the South Atlantic Ocean in 35°S., large vertical variations of the isotherms, which

extended over several hundred metres. Similar variations but not as large were found in some cross-sections of the "Meteor" Expedition. The occurrence of such stationary wave-like variations of oceanographic properties in straits was demonstrated by several longitudinal sections through these straits. It was pointed out earlier and it can be proven that they are caused by topographical features of the bottom.

Let us assume two superposed water-masses of different density ρ' , h' and ρ , h (density and thickness of the upper and lower layer respectively), where both water-masses have the same velocity c . It can easily be shown theoretically that a disturbance of the bottom causes stationary wave-like displacements, both at the surface of the upper water-mass (the free surface) and at the boundary surface between the two water-masses. Under certain circumstances the displacement of the boundary surface may become very great, many times greater than those of the free surface. If one assumes a simple wave-like profile with the wave length $\lambda = 2\pi/\kappa$ it becomes evident that the stream lines in both water-masses follow the same contour as the bottom configuration and the boundary surface also takes part in these stationary displacements. In the denominator of the equation for the amplitude of these wavy stream lines appears a value N of the form:

$$N = c^4 \left(\coth \kappa h \coth \kappa h' + \frac{\rho'}{\rho} \right) - c^2 (\tanh \kappa h + \coth \kappa h') \frac{g}{\kappa} + \left(1 - \frac{\rho'}{\rho} \right) \frac{g^2}{\kappa^2}. \quad (\text{XVI.48})$$

This expression $N = 0$ is identical with equation (XVI.9) and gives the velocity c of free waves of the wave length $\lambda = 2\pi/\kappa$ at the surface or at the boundary surface in a system at rest (p. 519). Equation (XVI.48) means that the stationary displacements, caused by the bottom configuration can become very large, if the velocity of the currents of the two water-masses equals the wave velocity of the free waves at the surface or of the waves at the boundary surface. Small irregularities in the bottom configuration are thus, under certain conditions, accompanied by great, wave-like, stationary displacements at the boundary surface. In the case that the length of the bottom irregularity becomes great, equation (XVI.48), $N = 0$ gives the two velocities for which this occurs. These velocities are identical with equations (XVI.17). The first value c_1 gives always very great values and cannot be accepted as the velocity of a basic current. The second current velocity c_2 on the other hand has relatively small values. Here the stationary displacements are greatest at the boundary surface, while the free surface remains practically undisturbed. Thus for $\rho - \rho' = 1 \times 10^{-3}$ and if $h' = 50$ m and $h = 100$ m. c_2 becomes 58 cm/sec. This is a reasonable value for basic currents.

The current velocities of the two superposed water-masses are generally different (in the upper water-mass c' , in the lower one c). In that case particularly large stationary wave-like displacements of the boundary surface will occur if the condition

$$c^2 h' + c'^2 h = \left(1 - \frac{\rho'}{\rho}\right) g h h' \tag{XVI.49}$$

is satisfied.

It thus appears as if the frequently observed bulges in the sharp discontinuity layer between the compensating superposed currents, flowing in opposite directions in straits (for instance Bosphorus, Dardanelles, Strait of Gibraltar and others), can be explained in this way as a result of the bottom configuration (see DEFANT, 1929, p. 51).

In the case of currents in a water-mass where the density increase is continuous, stationary wave-like displacements of the isopycnals are also possible. The stream lines will follow then the isopycnals. If a system of progressive internal cellular waves (as discussed on p. 528) with a velocity of progress c (equation (XVI.29)) is superposed by a current with a velocity $U = -c$, the waves become stationary. This is the case of a stratified water-mass flowing with wavy stream lines. For a certain ratio $\varepsilon/\varkappa = \lambda_x/\lambda_z$ the wave length λ of the stationary waves can be computed, if U is known. Since the velocities in the ocean are small, one obtains with sufficient accuracy

$$\lambda_x = \frac{2\pi}{\varkappa} = 2\pi U \sqrt{\left[\frac{H}{g} \left(1 + \frac{\varepsilon^2}{\varkappa^2}\right)\right]} = 2\pi U \sqrt{\left[\frac{\rho}{gI'} \left(1 + \frac{\varepsilon^2}{\varkappa^2}\right)\right]}. \tag{XVI.50}$$

With $\varepsilon/\varkappa = 10^2$ and $\rho/I' = 10^6$ one obtains for $U = 2$ m/sec, a horizontal wave length of 40 km, where the height of the stationary waves will be 400 m (compare Fig. 238). These are conditions which may occur in nature. These

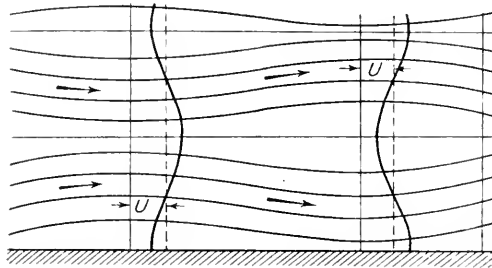


FIG. 238. Stationary waves in a stratified water mass.

waves are of course free waves, which may appear because of a single impulse and then they vanish because of frictional influences. The case is different when external conditions (pressure disturbances on the surface, irregularities of the bottom configuration) cause internal waves of cellular type. The phenomenon of the so-called lee-waves belongs to this type. They occur behind a long outstretched bottom irregularity over which a horizontal current is flowing in a transverse direction. LORD KELVIN (LAMB, 1932, § 246, p. 409) developed the theory of these stationary lee-waves for an incompressible and homogeneous heavy fluid. The examination of the lee-wave disturbances in a

compressible stratified medium was carried out mainly to explain stationary air waves, which occur in the lee of mountains. When lee waves are present in the air they become visible when water vapour is condensed in the form of one or several banks of clouds which have the shape of waves and which are parallel to the chain of mountains (Moazagotl clouds). Such stationary wave-like displacements of the isopycnals may also occur in the ocean, when a current crosses a submarine ridge. Because of the stratification, which takes place in the ocean, these wave-like displacements may take a somehow different shape than similar displacements of pure discontinuity surfaces. An exact computation of such cases should not be too difficult after the more complicated sample cases were discussed. Figure 239 presents, according to

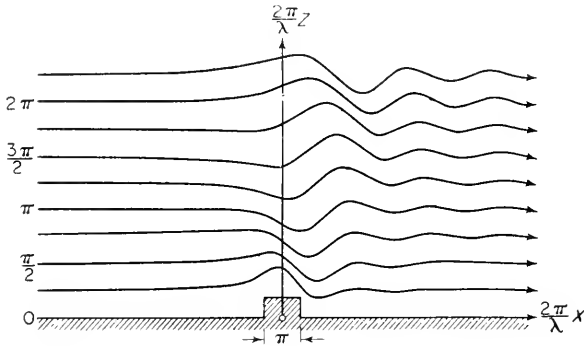


FIG. 239. Stationary internal wave in a stratified medium (streamlines) in the back of rectangular shaped obstacle (Lyra).

LYRA (1940/43) the stream lines of the current, crossing a long extended ridge (see also PRAEDT, 1940, p. 331). The piling up of the current immediately before the obstacle is clearly discernible; above it the stationary lee-waves extend to great heights. These can still be recognized at a great horizontal distance from the obstacle. There is every reason to assume that the wave-like stationary form of the oceanographic properties, which is frequently observed in the ocean, can also be explained in this way.

BIBLIOGRAPHY

- ABERCROMBY, R. (1888). Observations of height, length and velocity of ocean waves. *Phil. Mag.* (5), **25**, 263.
- AIRY, G. B. (1842). Tides and waves. *Encycl. Metrop. London*.
- AIRY, G. B. (1875). On a controverted point in Laplace's theory of tides. *Phil. Mag.* (4), **50**, 227.
- AITKEN, J. (1883). On the effect of oil on a stormy sea. *Proc. Roy. Soc. Edinb.* **12**, 56.
- ALMAGIA, R. (1905). *Reg. Accad. Lincei, Roma* **102**.
- d'ARRIGO, A. (1940). Recenti ricerche sperimentali sul moto ondoso. *Ann. Lavori Publ.* no. 6. Roma. *Atlas der Gezeiten und Gezeitenströme für das Gebiet der Nordsee und der britischen Gewässer*. Publ. by Deutsche Seewarte, new ed. see also Tide Tables.
- d'AURIA, L. (1890, 1891). *Franklin Inst.* (3), **130**, 373; (3), **13**, 49.
- BAGNOLD, R. A. (1939). Interim report on wave-pressure research. *J. Civil Engrs., Lond.*
- BARKOW, E. (1911). Über eine Methode zur Messung der Hochseegezeiten. *Z. Ges. Erdkunde*, Berl. p. 659.
- BARTELS, J. (1926). Barometrische Messungen der Hochseegezeiten. *Ann. Hydr. Mar. Met.* **54**, 211, 227.
- BARTELS, J. (1928). Gezeitenschwingungen der Atmosphäre. *Handb. Experimentalphysik*, **25** (Geophysik, part 1), 163.
- BARTELS, J. (1936). Gezeitenkräfte. *Handb. Geophysik.* **1**, no. 4, 309.
- BARTELS, J. (1956). *Geophysics II* **48**, 734; *Encyclopaedia of Physics*, **2**, 133.
- BATES, H. (1863). *The Naturalist on the Amazons* **2**, 133. London. See also SCHICHEL, 1893.
- BAZIN, M. (1865). Recherches exper. sur la propagation des ondes. *Mem. Sav. Acad. Sci. Imp. Fr.* **19**, 495.
- BERGHAUS, H. (1845, 1892). *Phys. Handatlas*, 1st and 3rd ed. Gotha.
- BERGSTEN, F. (1926). The seiches of Lake Vättern. *Geogr. Ann., Stockh.* **8**, nos. 1, 2.
- BERNOULLI, D. (1741). Traité sur le flux et reflux de la mer. Rec. de pieces qui sont remporte le prix., *Acad. Roy. Paris* **4**, 53.
- BIDLINGMAIER, F. (1908). Ebbe und Flut. *Samml. Meereskunde*, no. 5.
- BJERKNES, V. (1921). On the dynamics of the circular vortex, etc. *Geofys. Publ.* **2**, no. 4.
- BJERKNES and others. (1933). *Physikalische Hydrodynamik*, 797 pp. Berlin: J. Springer.
- BLATON, J. (1937). Versuch einer Anwendung des Fermat'schen Prinzips auf geophysikalische Wellenprobleme. *Biul. Tow. Geof. w Warszawie* **14**, 1.
- BLONDEL, A. (1912). Sur la théorie des marées dans un canal. Appl. à la mer Rouge. *Ann. Fac. Toulouse* **3**, 1912.
- BÖRGEN, C. (1884). Die harmonische Analyse der Gezeitenbeobachtungen. *Ann. Hydr. Mar. Met.* **12**, no. 6, 305.
- BÖRGEN, C. (1890). Über den Zusammenhang zwischen Windgeschwindigkeit und den Dimensionen der Meereswellen, nebst einer Erklärung für das Auftreten von Wellen von langer Periode an freigelegenen Küsten. *Ann. Hydr. Mar. Met.* **18**.
- BÖRGEN, C. (1892). Über die Berechnung eines einzelnen Hoch- und Niedrigwassers nach Zeit und Höhe. *Ann. Hydr. Mar. Met.* **20**. See also Darlegung der Berechnungsweise für die Angaben der Gezeitentafeln, *Ann. Hydr. Mar. Met.* **35**, 1907.
- BÖRGEN, C. (1894a). Über eine neue Methode, die harmonischen Konstanten abzuleiten. *Ann. Hydr. Mar. Met.* **22**.
- BÖRGEN, C. (1894b). Die Gezeitenerscheinungen im Irischen Kanal. *Ann. Hydr. Mar. Met.* **26**, 395, 1894.

- BÖRGEN, C. (1898). Über die Gezeitenerscheinungen im Englischen Kanal und dem südwestlichen Teil der Nordsee. *Ann. Hydr. Mar. Met.* **26**, 414.
- BOUSSINESQ, J. (1871). Théorie de l'intumescence liquide appelée onde solitaire ou de translation, se propageant dans un canal rectangulaire. *C. R. Acad. Sci., Paris* **72**, 755.
- BOUSSINESQ, J. (1877). Essai sur la théorie des eaux courantes. *Mem. Pres. Div. Sav. Acad. Sci. Inst.* (Sec. math., phys.), **23**, 380.
- BOWDEN, K. F. (1948). Some observations of waves and other fluctuations in a tidal current. *Proc. Roy. Soc., A*, **192**, 403–25.
- BOWDEN, K. F. (1950). The effect of eddy viscosity on ocean waves. *Phil. Mag. Ser. 7*, **41**, 907–17.
- BOWDEN, K. F. (1956). The flow of water through the Straits of Dover related to wind and differences in sea level. *Phil. Trans., A*, no. 935, **248**, 517–51.
- BOWDEN, K. F. and PROUDMAN J. (1949). Observations on the turbulent fluctuations of a tidal current. *Proc. Roy. Soc., A*, **199**, 311–27.
- BOWDEN, K. F. and FAIRBAIRN L. A. (1952*a*). Further observations on the turbulent fluctuations of a tidal current. *Phil. Trans. A*, no. 883, **244**, 335–56.
- BOWDEN, K. F. and FAIRBAIRN, L. A. (1952*b*). A determination of the frictional forces in a tidal current. *Proc. Roy. Soc., A*, **214**, 371–92.
- BROWN, P. R. (1953). *Marine Observer* **23**, 94.
- BRUNS, E. (1936). Oberflächenwellen in der Ostsee. V. Hydrolog. *Konf. Balt. Staaten, Finland, Bericht II A*.
- BRUNSIDE. (1889). On the small wave motions of a heterogeneous fluid under gravity. *Proc. Lond. Math. Soc.* **20**, 392.
- BURGERS, J. (1927). Sur quelques recherches de Helmholtz et de Wien relatives à la forme des ondes se propageant à la surface de séparation de deux liquides. *Rend. Acad. Linnei*, **5**, 333.
- BURLING, R. W. (1955). *Proc. Conf. on Coastal Engineering. U.S. Coun. on Wave Research*. The Eng. Foundation, **1**.
- CALOI, P. (1938). Sesse dell'Alto Adriatico con part. riguardo al golfo di Trieste. *Mem. Com. talassogr. Ital.* no. 24. Venezia.
- CAUCHY, A. (1815). Théorie de la propagation des ondes à la surface d'un fluide pesant d'une profondeur infinie. *Mem. Acad. Roy. Sci. Inst.* (Sec. Math. Phys.), **1**.
- CHAMPION, H. and CORKAN, R. (1936). The bore in the Trent. *Proc. Roy. Soc., A*, **154**, 158.
- CHANDON, E. (1930). Sur les marées de la mer Rouge et du Golfe de Suez. Thèse pres. a la fac. d. scien. d. Paris, Gauthier-Villars et Cie.
- CHAPMAN, S. (1919). *Quart. J. Met. Soc.* **45**, 128.
- CHOLNOKY, E. V. (1897). Limnologie des Plattensees. *Res. wiss. Erf. Plattensees*, **1**, no. 3. Wien.
- CHRYSTAL, G. (1904). Some results in the math. theory of seiches. *Proc. Roy. Soc. Edinb.* **25**, 325.
- CHRYSTAL, G. (1905*a*). Some further results in the math. theory of seiches. *Proc. Roy. Soc. Edinb.* **25**, 637.
- CHRYSTAL, G. (1905*b*). On the hydrodyn. theory of seiches. *Trans. Roy. Soc. Edinb.* **41**, 599.
- CHRYSTAL, G. (1908). An investigation of the seiches of Loch Earn, Part. IV. Effect of meteorological conditions upon the denivellements of lakes. *Trans. Roy. Soc. Edinb.* **46**, no. 20.
- CHRYSTAL, G. (1909). An investigation of the seiches of Loch Earn. Part V. Mathematical Appendix on the effect of pressure disturbances upon the seiches in a symmetric parabolic lake. *Trans. Roy. Soc. Edinb.* **46**, 455.
- CIALDI, A. (1886). *Sul moto ondoso del mare e sul le correnti di esso, specialmente sul quelle litorali*. 2nd ed., Rome.
- COCHRANE, J. D. and ARTHUR, R. S. (1948). Reflection of Tsunami. *J. Mar. Res.* **7**, 239–51.
- COMOY, M. (1881). *Études pratique sur les marées fluviales et le mascaret*. Paris.
- CORKAN, R. H. (1948). *Storm Surges in the North Sea*, Vols. 1 and 2. H. O. Misc. 15072, Washington, D. C.
- CORKAN, R. H. (1950). The levels in the North Sea associated with the storm disturbance of 8 January 1949. *Phil. Trans., A*. no. 853, **242**, 483–525.

- CORKAN, R. H. and DOODSON, A. T. (1952). Free tidal oscillations in a rotating square sea. *Proc. Roy. Soc. A.*, **215**, 147–162.
- CORNISH, V. (1900). *Nature, Lond.* **14**, 44.
- CORNISH, V. (1910). *Waves of the Sea and other Water Waves*. London.
- CORNISH, V. (1934). *Ocean Waves and Kindred Geophysical Phenomena*, p. 164, Cambridge Univ. Press.
- LA COUR, D. (1917). Abnorme Vandstandsforhold i de Danske Farvande. *Publ. Danske met. Inst.* **4**. Copenhagen.
- COURTIER, A. (1938). *Marces. Serv. Hydr. Marine, Paris*. See also DIETRICH, G. (1944a).
- CREDNER, R. (1888). Über den "Seebar" der west. Ostsee vom 16. und 17. Mai 1888. *Pomm. Geogr. Ges., Greifswald*.
- CRONE, C. (1906). Flux et reflux des mers qui envoient le Danemark. *Rapp. trav. serv. mareogr. Inst. meteor. Danemark*. Copenhagen.
- DALHUISEN, H. (1907). *Publ. de Circonst.* no. 36. Copenhagen.
- DARBYSHIRE, J. (1952). The generation of waves by wind. *Proc. Roy. Soc., A.*, **215**, 299.
- DARLINGTON, C. R. (1954). The distributions of wave heights and periods in ocean waves. *Quart. J. Roy. Met. Soc.* **80**, 619–26.
- DARWIN, G. H. (1882). Appendix to the second report on lunar disturbance of gravity. *Brit. Ass. Rep. Southampton*, 1882.
- DARWIN, G. H. (1883). Report on the harmonic Analysis of tidal observations. *Brit. Ass. for adv. Sci. Rep.* See also *Scient. Pap.* 1, Cambridge, 1907.
- DARWIN, G. H. (1886a). *Proc. Roy. Soc.* **41**, 337.
- DARWIN, G. H. and TURNER, H. (1886b). On the correction of the equilibrium theory of tides for the continents. *Proc. Roy. Soc. Pap.* 1, p. 328.
- DARWIN, G. H. (1902). *Nature, Lond.* **66**, 445.
- DARWIN, G. H. (1910). *The Tides and Kindred Phenomena in the Solar System*. Cambridge.
- DARWIN, W. (1947). *Encycl. Brit.* 9th ed., **23**, p. 359.
- DAVISON, C. (1897). Note on an error in the method of determining the mean depth of the ocean from velocity of seismic waves. *Phil. Mag.* (5), **43**, 33.
- DAWSON, B. W. (1894–1902). Survey of tides and currents in Canadian waters. *Rep. Stream Meas. Can.*
- DAWSON, B. W. (1899). The bore of Moneton. Survey of Tides and Currents in Canadian Waters, p. 22. Ottawa.
- DAWSON, B. W. (1902). *Nature, Lond.* **66**, 85.
- DAWSON, B. W. (1905). The currents at the entrance of the Bay of Fundy. *Rep. of Tidal and Current Survey*. Ottawa.
- DAWSON, B. W. (1907a). *J. Soc. Canada*, p. 216.
- DAWSON, B. W. (1907b). The current in the Belle-Isle Strait. *Rec. Tidal and Current Survey*. Ottawa.
- DAWSON, B. W. (1913a). *The Currents in the Gulf of St. Lawrence*. Dep. Naval Service, Ottawa, 1913.
- DAWSON, B. W. (1913b). *The Currents in the Entrance of the St. Lawrence*. Dep. Naval Service, Ottawa.
- DAWSON, B. W. (1920). The tides and tidal streams, with illustrative examples from Canadian waters. *Rep. Tidal and Current Survey*. Ottawa.
- DAWSON, B. H. (1924). Estuary Tides. Amer. Geoph. Union, Meet. Apr. 1923. *Bull. Nat. Res. Coun., Wash.*, no. 41, p. 141.
- DEACON, G. E. R. (1946). Ocean waves and swell. *Oceanogr. Pap. "Challenger" Soc.* no. 1, p. 13.
- DEACON, G. E. R. (1949). in Haurwitz B. and coll. (1949).
- DEFANT, A. (1911). Über die Periodendauer der Eigenschwingungen des Adriatischen Meeres. *Ann. Hydr. Mar. Met.* **39**.
- DEFANT, A. (1914). Zur Theorie der Gezeiten des Adriatischen Meeres. *Ann. Hydr. Mar. Met.* **42**, 270.
- DEFANT, A. (1916). Theoretische Ueberlegungen über Seespiegelschwankungen in Seen und Meeresbuchten. *Ann. Hydr. Mar. Met.* **44**, 29.

- DEFANT A. (1917). Die Lösung des Euripus-Problems. *Ann. Hydr. Mar. Met.* **45**.
- DEFANT, A. (1918). Neue Methode zur Ermittlung der Eigenschwingungen (Seiches) von abgeschlossenen Wassermassen (Seen, Buchten usw.). *Ann. Hydr. Mar. Met.* **46**, 78.
- DEFANT, A. (1919a). Untersuchungen über die Gezeitenerscheinungen in Mittel- und Randmeeren, Buchten und Kanälen, Part I: Die Methoden der Untersuchung. *Denkschr. Wiener Akad. Wiss.* p. 105. See also Defant (1925a).
- DEFANT, A. (1919b). Untersuchungen a. s. o. Part II—III—IV, *Denkschr. Wiener Akad. Wiss.* **96**, 110.
- DEFANT, A. (1919c). Die hydrodynamische Theorie der Gezeiten und Gezeitenströmungen im Englischen Kanal und dem südwestlichen Teil der Nordsee. Untersuchungen a. s. o. Part V. *Denkschr. Wiener Akad. Wiss.* **96**. See also THORADE (1921).
- DEFANT, A. (1920). Untersuchungen a. s. o. Part VI: Die Gezeiten und Gezeiten Strömungen im Irischen Kanal. *S. B. Wiener Akad. Wiss. (Math.-Natur. Kl.)* **129**, 253.
- DEFANT, A., KLEINSCHMIDT, E. and BARTELS J., (1922). Bemerkungen zu Spitalers Abhandlung "Eine neue Theorie der taglichen Luftdruckschwankungen a. s. o. *Ann. Hydr. Mar. Met.* **50**, 22, 322.
- DEFANT, A. (1923a). Grundlagen einer Theorie der Nordseegezeiten. *Ann. Hydr. Mar. Met.* **51**, 57.
- DEFANT, A. (1923b). Die Gezeiten der Nordsee, Beobachtungen und Theorie. *Ann. Hydr. Mar. Met.* **51**, 177.
- DEFANT, A. (1923c). Theoretische Ueberlegungen und experimentelle Untersuchungen zum Aufbau hoher Zyklonen und Antizyklonen. *S. W. Wiener Akad. Wiss. (Math.-Phys. Kl.)* **132**, 83.
- DEFANT, A. (1924). Die Gezeiten des Atlantischen Ozeans und des Arktischen Meeres. *Ann. Hydr. Mar. Met.* **52**, 153, 177.
- DEFANT, A. (1925a). Gezeitenprobleme des Meeres in Landnähe. *Probl. kosm. Physik* **6**, 80.
- DEFANT, A. (1925b). Bemerkungen zu Sternecks Arbeiten. *Ann. Hydr. Mar. Met.* **53**, 231.
- DEFANT, A. (1926a). Gezeiten und Gezeitenströmungen in Roten Meer. *Ann. Hydr. Mar. Met.* **54**, 185.
- DEFANT, A. (1926b). Zur Theorie der halbtägigen Gezeiten des Atlantischen Ozeans. *Ann. Hydr. Mar. Met.* **54**, 133.
- DEFANT, A. (1928). Mitschwingungsgezeit und Gezeitenreibung. *Ann. Hydr. Mar. Met.* **56**, 274.
- DEFANT, A. (1929). *Dynamische Ozeanographie. Einführung in die Geophys.* **9**, Berlin, J. Springer.
- DEFANT, A. (1932a). Beiträge zur theoretischen Limnologie. *Beitr. Phys. frei. Atmos.* **19**, 143.
- DEFANT, A. (1932b). Die Gezeiten und inneren Gezeitenwellen des Atlantischen Ozeans. *Wiss. Ergebn. Atl. Exp. "Meteor" 1925-27*, **7**.
- DEFANT, A. (1933). Zur Erklärung der Seiches des Schwarzen Meeres. *Ann. Hydr. Mar. Met.* **61**, 56.
- DEFANT, A. (1934a). *Gedanken über interne Wellen. J. Johnstone Mem. Vol.*, Liverpool, p. 310.
- DEFANT, A. and SCHUBERT, O. V., (1934b). Strommessungen und ozeanographische Serienbeobachtungen der 4-Länder-Unternehmung im Kattegat, Aug. 1931. *Veröff. Inst. Meeresk., Univ. Berl., N. F. A.*, no. 25.
- DEFANT A. (1938). Oscillations internes dans les oceans. *C. R. Congr. Int. Geogr. Amst.* **12**, Sect. II B, p. 9.
- DEFANT, A. (1940a). Scylla und Charybdis und die Gezeitenströmungen in der Strasse von Messina. *Ann. Hydr. Mar. Met.* **68**, 145. See also *Geofis. pura appl.* **2**, Messina, 1940.
- DEFANT, A. (1940b). Die ozeanogr. Verhältnisse während der Ankerstation des "Altair" am Nordrand des Hauptstromstriches des Golfstroms nördlich der Azoren. *Wiss. Ergeb. Golfstr.-Untern.* 1938. See also *Ann. Hydr. Mar. Met.* **68**, Nov.-Beiheft, 1940.
- DEFANT, A. (1942). Die Gezeiten der festen Erde, des Meeres und der Atmosphäre. *Vortr. Preuss. Akad. Wiss.*, no. 10.
- DEFANT, A. (1948). Über interne Gezeitenwellen und ihre Stabilitätsbedingungen. *Arch. Met. Geophys.* **1**, Wien.
- DEFANT, A. (1950). On the origin of internal tide waves in the open sea. *J. Mar. Res.* **9**, 111-19.
- DEFANT, F. (1953). Theorie der Seiches des Michigansees und ihre Abwandlung durch Wirkung der Corioliskraft. *Arch. Met., Wien*, **A**, **6**, No. 2.

- DIETRICH, G. (1943). Über ozeanische Gezeitenerscheinungen in geograph. Betrachtungsweise. *Ann. Hydr. Mar. Met.* **71**, 123.
- DIETRICH, G. (1944*a*). Die Gezeiten des Weltmeeres als geograph. Erscheinung. *Z. d. ges. Erdkunde*, p. 69. Berlin. See also COURTIER, A. (1938).
- DIETRICH, G. (1944*b*). Die Schwingungssysteme der halb- und eintägigen Tiden in den Ozeanen. *Veröff. Inst. Meeresk.*, Univ. Berlin, N. F. A., 10, 41.
- DOODSON, A. D., CAREY, R. M. and BALDWIN, R. (1920). Theoretical determination of the longitudinal seiches of Lake Geneva. *Trans. Roy. Soc. Edinb.* **52**/3, no. 25, p. 629.
- DOODSON, A. T. (1922). The harmonic development of the tide-generating potential. *Proc. Roy. Soc.*, A, **100**, 305.
- DOODSON, A. T. (1924). Perturbations on harmonic constants. *Proc. Roy. Soc.*, A, **106**, 513.
- DOODSON, A. T. (1928*a*). The analysis of tidal observations. *Phil. Trans.*, A, **227**, 223.
- DOODSON, A. T. (1928*b*). Application of num. methods of interpretation to tidal dynamics. *Mon. Not. R. Astr. Soc. (Geophys. Suppl.)* **1**, 541.
- DOODSON, A. T. (1929). *Geophys. Mem.* **47**.
- DOODSON, A. T. and CORKAN, R. (1932). The principal constituent of the tides in the English and Irish Channels. *Phil. Trans.*, A, **234**.
- DOODSON, A. T. and PROUDMAN, J. (1936, 1938). Tides in the oceans bounded by meridians, Parts I-III. *Phil. Trans.*, A, **235**, 273; **237**, 311.
- DOODSON, A. T. (1938). Instructions for analysing tidal observations. *The Admiralty Tide Tables*, 3. London.
- DOODSON, A. T. (1947). Storm surges. *Intern. Hydrogr. Rev.* **24**.
- DOODSON, A. T. (1956). Tides and storm surges in a long uniform gulf. *Proc. Roy. Soc.*, A, **237**, 325-43.
- DOODSON, A. T., ROSSITER, J. R. and CORKAN, R. H. (1954). Tidal charts based on coastal data: Irish Sea. *Proc. Roy. Soc. Edinb.*, A, **64**, Pt. I, 90-111.
- DOODSON, A. T. See also PROUDMAN and DOODSON.
- DOOS, B. (1907). Über ostbaltische Seebären. *Gerl. Beitr. Geophys.* **8**, 368.
- ECKHARDT, A. (1931). Erfahrung über Wellenwirkung beim Bau des Hafens von Helgoland. *Jb. hafenbautechn. Ges. Hamburg*.
- EINSTEIN, A. (1916). Elementare Theorie der Wasserwellen und des Fluges. *Naturwissenschaften*, p. 509.
- EKMAN, W. (1904). Über Totwasser. *Ann. Hydr. Mar. Met.* **32**, 562.
- EKMAN, W. (1906). On Dead Water. *The Norw. North Polar Exp. 1893-1896*, ed. by Fr. Nansen, 5. Christiania.
- EKMAN, W. and HELLAND-HANSEN, B. (1931). Measurements of ocean currents. *K. fysiogr. Sällsk. Lund Forh.* **1**, no. 1.
- EKMAN, W. (1942). Turbulenzstudier i Atlanten. *Medd. fran Lunds Geogr. Inst.* no. 176.
- EMDEN, R. (1905). Der Energiegehalt der Seiches. *Jr. Sankt Gallischen naturw. Ges.*
- ENDRÖS, A. (1903). Seeschwankungen (Seiches) beobachtet am Chiemsee. Diss. München.
- ENDRÖS, A. (1908). Vergleichende Zusammenstellung der Hauptseichesperioden der bis jetzt untersuchten Seen u. s. w. *Peterm. Mittl.* **54**.
- ENDRÖS, A. (1914*a*). Die Gezeiten, Seiches und Strömungen des Meeres bei Aristoteles. *S. B. bayer. Akad. Wiss. (math.-phys. Kl.)*, p. 99.
- ENDRÖS, A. (1914*b*). Zum Problem des Euripus. *S. B. bayer. Akad. Wiss. München*.
- ENDRÖS, A. (1927). Vergleichende Zusammenstellung der Hauptseichesperioden der bis jetzt untersuchten Seen mit Anwendung auf verwandte Probleme. *Peterm. Mittl.*
- ENDRÖS, A. (1930). Gezeitenbeobachtungen in Binnenseen. *Ann. Hydr. Mar. Met.* **58**, 305.
- ENDRÖS, A. (1932). Die Seiches des Schwarzen Meeres und Asowschen Meeres und die dortigen Hubhöhen der Gezeiten. *Ann. Hydr. Mar. Met.* **60**, 442.
- ENDRÖS, A. (1934). Beobachtungen über die Dämpfung der Seiches in Seen. *Gerl. Beitr. Geophys.* **41**, no. 2, 130.

- ERTEL, H. (1933). Eine neue Methode zur Berechnung der Eigenschwingungen von Wassermassen in Seen unregelmässiger Gestalt. *S. B. preuss. Akad. Wiss.* **24**. Berlin, 1933.
- EXNER, F. (1908). Über eigentümliche Temperaturschwankungen von eintätiger Periode im Wolfgangsee. *S. B. Wien. Akad. Wiss. (Math.-Nat. Kl.)*, **117**, 9.
- FAIRBAIRN, L. A. (1954). The semi-diurnal tides along the equator in the Indian Ocean. *Phil. Trans. A*, **247**, no. 927, 191–212.
- FERREL, W. (1874). Tidal researches. *U. S. Coast and Geod. Surv. Rep.* pp. 154, 239, 245. Washington.
- FJELDSTAD, J. (1923). Litt. om tidvandet i Nordishavet. *Naturen* **47**, 161. Bergen and Copenhagen.
- FJELDSTAD, J. (1929). Contributions to the dynamics of free progressive tidal waves. *Sci. Res. Norweg. North Polar Exped. "Maud" 1918–1925.* **4**, no. 3. Bergen.
- FJELDSTAD, J. (1935). Interne Wellen. *Geofys. Publ.* **10**, no. 8 (Norske Vid. Akad., Oslo).
- FJELDSTAD, J. (1938). Interne Wellen. *C. R. Congr. Intern. Geogr. Amst.* **12**, sect. II b, p. 49.
- FJELDSTAD, J. (1941). Tidal waves of finite amplitude. *Astrophys. Norveg.* **3**, no. 10, Oslo.
- FORCHHEIMER, P. (1903). *S. B. Wien. Akad. Wiss. (Math.-Naturwiss. Kl.)*, **112 a**.
- FORCHHEIMER, P. (1924). *Hydraulik*, 2nd ed. Leipzig and Berlin: A. G. Teubner.
- FOREL, F. (1879). *Comp. Rend.* **39**, 859.
- FOREL, F. (1895). *Le Leman.* **2**, 39. Lausanne.
- FRANCIS, I. R. D. (1954). *Weather* **9**, 163.
- FRANZIUS, L. and SONNE (1879). *Der Wasserbau*. Plate 48, Leipzig. See also *Peterm. Mittl.* (1880), p. 299.
- FRANZIUS and others (1901). *Handbuch der Ingenieurwissenschaften*, 3, *Der Wasserbau*, 3rd ed. pp. 22, 229. Leipzig.
- GAILLARD, D. (1904). Wave action in relation to engineering structures. *Prof. Pap. Corps Eng., U.S. Army, Wash.*, no. 31.
- GASSENMAYER, O. (1896). Wellenmessungen im Atlantischen Ozean. *Mittl. Gebiet Seewesens*, **24**, 190. Pola.
- S.M.S. "GAZELLE". (1888/90). *Die Forschungsreise, Reichsmarineamt* **2**, 128. Berlin.
- GEISSLER, H. (1939). Auslegung von Hochseepegeln. *Ann. Hydr. Mar. Met.* **67** (Beiheft Jan.), p. 18.
- GEISSLER, H. (1941). Die deutschen Hochseepegel. *Arch. dtsh. Seewarte, Hamburg* **61**, no. 1.
- GEPPERT, H. (1929). Die permanenten Wellen in ringförmigen Kanälen. *Math. Ann.* **101**, 424.
- GERSTNER, F. (1802). Theorie der Wellen u. s. w., *Abh. Kgl. Böhm. Ges. Wiss., Prag*.
- GLEINITZ, E. (1878). *Nova acta Leop. Car. Acad. Naturf.* **40**, no. 9. Halle.
- GOLDSBROUGH, G. R. (1913). The dynamical theory of the tides in a polar basin. *Proc. Lond. Math. Soc.* **14**, 31.
- GOLDSBROUGH, G. R. (1914). The dynamical theory of the tides in a zonal basin. *Proc. Lond. Math. Soc.* **14**, 207.
- GOLDSBROUGH, G. R. (1927). The tides in oceans on a rotating globe. *Proc. Roy. Soc., A*, **117**, 692.
- GOLDSBROUGH, G. R. (1931). The tidal oscillations in rectangular basins. *Proc. Roy. Soc., A*, **132**, 689.
- GOLDSBROUGH, G. R. (1933). The tides in oceans on a rotating globe. Part IV. *Proc. Roy. Soc., A*, **140**, 241.
- GOLDSBROUGH, G. R. (1954). Wind effects on the motion of the sea in a infinite channel and in a rectangular gulf. *Proc. Roy. Soc., A*, **222**, 477–89.
- GOLDSTEIN, S. (1929). Free and forced oscillations in a rotating elliptic basin of uniform depth. *Mon. Not. R. Astr. Soc. Geophys. Suppl.* **2**, no. 4, p. 213.
- GRABLOVITZ, G. (1891). La isorachia della marea nel Mediterraneo. *Rend. R. Acad. Linnei*, **7**, p. 132, 1891.
- GRABLOVITZ, G. (1909). Le attuali conoscenze sul fenomeno della marea nel Mediterraneo. *Mem. geogr. (Suppl. alla Riv. geogr. Ital.)*, no. 9. Florenz.
- GRACE, S. (1929). Internal friction in certain tidal currents. *Proc. Roy. Soc. A*, **24**, 150.
- GRACE, S. (1930). The semi-diurnal tidal motion of the Red Sea. *Mon. Not. R. Astr. Soc. Geophys. Suppl.* (March), p. 274.

- GRACE, S. (1931a). The influence of the friction on the tidal motion of the Gulf of Suez. *Mon. Not. R. Astr. Soc. Geophys. Suppl.* (Jan).
- GRACE, S. (1931b). Tidal oscillations in rotating rectangular basins of uniform depth. *Mon. Not. R. Astr. Soc. Geophys. Suppl.* p. 385.
- GRACE, S. (1931c). The semi-diurnal lunar tidal motion of the Lake Baikal and the derivation of the earth-tides from the water-tides. *Mon. Not. R. Astr. Soc. Geophys. Suppl.* 2. no. 7, 301.
- GRACE, S. (1932). The principal diurnal constituent of tidal motion in the Gulf of Mexico. *Mon. Not. R. Astr. Soc. Geophys. Suppl.* p. 70.
- GRACE, S. (1933). The principal semi-diurnal constituent, etc. *Mon. Not. R. Astr. Soc. Geophys. Suppl.*
- GRACE, S. (1936). Friction in the tidal currents of the Bristol Channel. *Mon. Not. R. Astr. Soc. Geophys. Suppl.*
- GRACE, S. (1937). Tidal friction in the tidal currents of the English Channel. *Mon. Not. R. Astr. Soc. Geophys. Suppl.* (May).
- GREEN, L. (1837). On the motion of waves in a variable canal of small depth and width. *Trans. Phil. Soc. Lond.* 6.
- GREENHILL, (1887). Wavemotion in Hydrodynamics. *Amer. J. Math.* 9.
- GROEN, P. (1948). Contribution to the theory of internal waves. *K. Nederl. Met. Inst. Medel. Verhand. Serie B.* 2, no. 11.
- GROEN, P. (1954). On the behaviour of gravity waves in a turbulent medium, with application to the decay and apparent period increase of swell. *K. Nederl. Met. Inst. Medel. Verhand.* 63, 1–23.
- GROEN, P. and DORRESTEIN R. (1950). Ocean swell: its decay and period increase. *Nature, Lond.* 165, 445–47.
- GROSSMAN, J. (1892). *Die Bekämpfung der Sturzseen durch Oel und ihre Bedeutung für die Schifffahrt.* Wien.
- GUSTAFSON, J. and OTTERSTEDT, G. (1933). Sven. Strömmätningar i Kattegat 1930. *Sven. Hydr.-Biol. Kom. Skr. Hydr.* X, 1933.
- GUSTAFSON, J. and KULLENBERG, B. (1936). Untersuchungen von Trägheitsströmungen in der Ostsee. *Sven. Hydr.-Biol. Kom. Skr. Ny Ser. XIII.* Lund.
- GWYHER, R. F. (1900). The classes of progressive long waves. *Phil. Mag.* (5), 50, 213, 349.
- HAGEN, G. (1878). *Handbuch der Wasserbaukunst. Part III. Allgemeine Erscheinungen im Meere.* 2nd ed. 1, 87. Berlin.
- HALBFASS, W. (1911). Gibt es im Madü-See Temperatureisches? *Int. Rev. Ges. Hydrobiol. Hydrogr.* 3 (Suppl.).
- HALBFASS, W. (1923). Grundzüge einer vergleichenden Seekunde, pp. 354. Berlin.
- HANN, J. v. (1939). *Lehrbuch der Meteorologie*, 5th ed., Leipzig. See also L. W. POLLAK.
- HANSEN, W. (1938). Amplitudenverhältnis und Phasenunterschied der harmonischen Konstanten in der Nordsee. *Ann. Hydr. Mar. Met.* 66, 429.
- HANSEN, W. (1940). Ein Verfahren zur Berechnung der eintägigen Tiden. *Ann. Hydr. Mar. Met.* 68, 41.
- HANSEN, W. (1942). Alternierende Gezeitenströme a. s. o. *Ann. Hydr. Mar. Met.* 70, 65.
- HANSEN, W. (1943). Ermittlung der Gezeiten in beliebig geformten Meeresgebieten unter Benützung der Randwerte. *Ann. Hydr. Mar. Met.* 71, 135.
- HANSEN, W. (1948). Die Ermittlung der Gezeiten beliebig gestalteter Meeresgebiete mit Hilfe des Randwertverfahrens. *Dtsch. Hydr. Z.*, 1, 157–63.
- HANSEN, W. (1949). Die halbtägigen Gezeiten im Nordatlantischen Ozean. *Dtsch. Hydr. Z.* 2, 44–51.
- HANSEN, W. (1956). Theorie zur Berechnung des Wasserstandes und der Strömungen in Randmeeren nebst Anwendungen. *Tellus.* 8 no. 3, 287–300.
- HARMONIC ANALYSIS (1928). Handweiser zur harmonischen Analyse. *Prager Geophys. Studien* 2.
- HARMONIC CONSTANTS (1930, 1933, 1936, 1940), *Spec. Publ. Hydrogr. Bureau Intern. Monaco*, Spec. Publ. no. 26. Monaco.
- HARRIS, R. A. (1894–1907). Manual of tides. Parts I–V. Appendices. *U.S. Coast and Geod. Surv. Rep.*, Wash.

- HARRIS, R. A. (1911). Arctic tides. *U. S. Coast and Geod. Surv. Rep.*, Wash.
- HARVEY, H. W. (1955). *The Chemistry and Fertility of Sea Waters*, pp. 1–224. Cambridge University Press.
- HAURWITZ, B. (1931). Zur Theorie der Wellenbewegung in Luft und Wasser. *Veröff. Geophys. Inst. Lpz.* **5**, no. 1, Ser. 2.
- HAURWITZ, B. (1950). Internal waves of tidal character. *Trans. Amer. Geophys. Union* **31**, no. 1, 47–52.
- HAURWITZ, B. (1954). The occurrence of internal tides in the ocean. *Arch. Met. Geophys. Biokl.* **7**, 406–24.
- HAURWITZ, B. and others (1949). Ocean surface waves. *Ann. N. Y. Acad. Sci.* **51**, 347–72.
- HAYFORD, J. (1922). Effects of winds and of barometric pressure on the Great Lakes *Publ. Carnegie Inst. Wash.*
- HELLAND-HANSEN, B. and NANSEN, F. (1909). The Norwegian Sea. *Norv. Fish and Mar. Invest. Rep.* **2**, no. 1 and 2.
- HELLAND-HANSEN, B. (1930). Physical oceanography and meteorology. *Rep. Sci. Res. "Michael Sars" North Atl. Deep-Sea Exp.* 1910. **1**. Bergen.
- HELLAND-HANSEN, B. and EKMAN, W. (1931). Measurements of ocean currents (Experiments in the North Atlantic). *K. fysiogr. Sällsk. Lund Förh.* **1**, no. 1 (May).
- HELMHOLTZ, H. v. (1889). Zur Theorie von Wind und Wellen. *S. B. K. Akad. Wiss. Berl.*, p. 761.
- HELMHOLTZ, H. v. (1890). Die Energie der Wogen und des Windes. *S. B. K. Akad. Wiss., Berl.*, p. 853.
- HENRY, A. (1902). Wind Velocity and Fluctuations of Water Level on Lake Erie. Washington.
- HESSEN, K. (1920*a*). Über eine neue Methode, die harmonischen Konstanten der langperiodischen Tiden der Mondzeiten abzuleiten. *Ann. Hydr. Mar. Met.* **48**, 441.
- HESSEN, K. (1920*b*). Über die Börgen'sche Methode der harmonischen Analyse der Meereszeiten, deren Vereinfachung und Erweiterung. *Ann. Hydr. Mar. Met.* **48**, 1.
- HIDAKA, K. (1932*a*). Theory of uninodal longitudinal seiches in Lake Yamanaka. *Geophys. Mag.* **5**. Tokyo.
- HIDAKA, K. (1932*b*). Seiches of viscous water. *Geophys. Mag.* **5**, no. 1. Tokyo.
- HIDAKA, K. (1935). Seiches due to a submarine bank (bank seiches). A theory of shelf seiches. *Mem. Imp. Mar. Obs. Kobe* **6**, no. 1.
- HIDAKA, K. (1931*a*). Problems of water oscillations in various types of basins and canals. Part I. The oscillations of water in spindle-shaped and elliptic basins as well as the associated problems. *Mem. Imp. Mar. Obs. Kobe* **4**, no. 2.
- HIDAKA, K. (1931*b*). Problems of water oscillations in various types of basins and canals. Part II. The free oscillations of water in a canal of spindle-shaped plane. *Mem. Imp. Mar. Obs. Kobe* **4**, no. 4.
- HIDAKA, K. (1932*a*). Problems of water oscillations in various types of basins and canals. Part III, IV and VI. Tidal oscillations in a rectangular basin of variable depth. *Mem. Imp. Mar. Obs. Kobe* **5**, no. 1; or *Geophys. Mag.* **5**, no. 3.
- HIDAKA, K. (1932*b*). Problems of water oscillations in various types of basins and canals. Part V. Tidal oscillations in a circular basin with an elevation or depression at its centre. *Mem. Imp. Mar. Obs. Kobe* **5**, no. 2.
- HIDAKA, K. (1934). Problems of water oscillations in various types of basins and canals. Part VII. Oscillations of water in a fan-shaped basin. *Geophys. Mag.* **8**, no. 2.
- HIDAKA, K. (1935*a*). Problems of water oscillations in various types of basins and canals. Part VIII. The oscillations of water in canals of asymmetric plane. *Mem. Imp. Mar. Obs. Kobe* **5**, no. 4.
- HIDAKA, K. (1935*b*). Problems of water oscillations in various types of basins and canals. Part IX. Seiches in a channel. *Mem. Imp. Mar. Obs. Kobe* **5**, no. 4.
- HIDAKA, K. (1936). Problems of water oscillations in various types of basins and canals. Part X. Seiches in an infinite canal with undulatory bed. *Geophys. Mag.* **10**, no. 1.
- HIDAKA, K. (1936). Application of Ritz Variation method to the determination of seiches in a lake. *Mem. Imp. Mar. Obs. Kobe* **6**, no. 2.

- HILLEBRAND, C. (1913). Die dynamische Theorie der Gezeiten auf einem MacLaurin'schen Ellipsoid. *Denkr. Akad. Wiss. Wien, (Math.-Naturwiss. Kl.)* **89**.
- HOCHSTETTER, F. V. (1868, 1869, 1870). *S. B. Akad. Wiss. Wien.* **58**, 837; **59**, 112, **60**, 818.
- HOFF, B. E. (1907). Elementare Theorie der Sonnentiden. *Ann. Hydr. Mar. Met.* **35**, 122.
- HOILAND, E. (1943). On the wave motions in sliding layers with internal static stability. *Arch. Math. Naturw.* **47**, no. 3. Oslo.
- HONDA, ISITANI, TERADA and IOSHIDA, (1908). Secondary undulations of oceanic tides. *J. Coll. Sci. Imp. Univ. Tokyo*, **24**, 1.
- HOPFNER, F. (1936). Die Gezeiten der Erd feste. In B. Gutenberg, *Handbuch der Geophysik* **1**, Pt. 5. Berlin.
- HORN, W. (1943). Gezeitenerscheinungen, *Lehrbuch der Navigation*, Pt. 1, p. 411, Bremen.
- HOUGH, S. (1897, 1898). On the application of harmonic analysis to the dynamical theory of the tides. *Phil. Trans.*, A, **189**, 201; **191**, 139.
- IMAMURA, A. and KAWASE, Z. (1933). The Sanriku Tsunami of 1933. *Jap. J. Astr. Geophys.* **9**, no. 1, 17.
- ISHIMOTO, M. (1933). Preliminary notes on the Tsunami of 2 March, 1933. *Jap. J. Astr. Geophys.* **9**, no. 1, 1.
- JACOBSEN, J. (1913). Strommessungen in der Tiefe der dänischen Gewässer, 1909-1911. *Medd. Kom. Havundersøgelser (Ser. Hydr.)*, **2**. Copenhagen.
- JACOBSEN, J. and THOMSON H. (1934). Periodical variations in temperature and salinity in the Straits of Gibraltar. *J. Johnson. Mem. Vol.* Liverpool.
- JAMES, R. W. (1954). An example of a wave forecast based on energy spectrum methods. *Trans. Amer. Geophys. Un.* **35**, 153-60.
- JEFFREYS, H. (1920). Tidal friction in shallow seas. *Phil. Trans. A.* **221**, 239.
- JEFFREYS, H. (1924). On water waves near the shore. *Phil. Mag.* (6), **48**, 44.
- JEFFREYS, H. (1925, 1926). On the formation of water waves by wind. *Proc. Roy. Soc. A*, **107**, and **110**.
- JEFFREYS, H. (1929). *The Earth*, 2nd ed. pp. 278. Cambridge Univ. Press.
- JEFFREYS, H. (1934). Additional notes in V. Cornish, *Ocean Waves and Kindred Geophysical Phenomena*, p. 139, 1934. Cambridge Univ. Press.
- JERIMOW, A. and KRAWETZ T. (1926). Vorläufige Mitteilung über die Gezeiten des Baikalsees. *Der Baikal, Verh. Magn. Met. Obs. Irkutsk*, **1**, 54.
- KALLE, K. (1942). Über die innere thermische Unruhe des Meeres. *Ann. Hydr. Mar. Met.* **70**, 383.
- KALLE, K. (1953). Zur Frage der inneren thermischen Unruhe des Meeres. *Dtsch. Hydr. Z.* **6**, 145-70.
- KAPLAN, K. (1950). Inst. Eng. Res., Univ. Calif., Berkeley, Calif., *Tech. Rep. H. E.* 116-316.
- KELLAND, P. (1839). On the theory of waves. *Trans. Roy. Soc. Edinb.* **14**, 497.
- KEMPF, G. (1936). Windstärken und Seegänge auf den verschiedenen Meeren. *Lilienthal Ges. Luftfahrtforsch. Jahrb.* Berlin.
- KESSLITZ, W. v. (1910). Das Gezeitenphänomen in Hafen von Pola. *Mittl. Geb. Seewesens, Pola*.
- KESSLITZ, W. v. (1913). Die Gezeiten des Adriatischen Meeres. *Mittl. Geb. Seewesens, Pola* **41**.
- KESSLITZ, W. v. (1919). Die Gezeitenerscheinungen in der Adria: Die Beobachtungsergebnisse der Flutstationen. *Denkschr. Akad. Wiss. Wien*, **96**. (Discussion by A. DEFANT, *Ann. Hydr. Mar. Met.* **48**, 163, 1920).
- KEYSER, H. (1946). Results of the Intern. observations of swell in the North Atlantic Ocean, Nov. 1914/15. *K. Nederl. Met. Inst.* no. 126, De Bilt.
- KEYSER, H. (1946). Results of the intern. observations of swell in the North Atlantic Ocean, Nov. 14-19, 1938. A. Ships observations. *K. Nederl. Met. Inst.* no. 126.
- KLEBBA, A. (1945). A summary of shore recording wavemeters. *Prelim. Rep. Woods Hole Oceanogr. Inst.*
- KÖPPEN, W. (1893). Verhalten der Oele und Seifen auf Wasserflächen. *Ann. Hydr. Mar. Met.* **21**, 134.
- KOHLRAUSCH, F. (1935). *Lehrbuch der praktischen Physik*, 17th ed. Leipzig and Berlin, 1935.

- KOHLSCHÜTTER, E. (1909). *Wellen- und Küstenaufnahmen. Forschungsreise S.M.S. "Planet"*, 1906/07, 3, chap. 6, p. 135. Berlin.
- KORTEWEG and VRIES, (1895). On the change of form of long waves advancing in a rectangular canal, and on a new type of long stationary waves. *Phil. Mag.* (5), 39.
- KOTCHINE, N. (1927). Détermination rigoureuse des ondes permanentes d'ampleur finie à la surface de séparation de deux liquides de profondeur finie. *Math. Ann.* 98, 582.
- KRAUSS, W. (1957). Interne Wellen grosser Amplitude. *Dtsch. Hydrogr. Z.* 10, no. 5, 191–201.
- KREY, H. (1926). Die Flutwelle in Flussmündungen und Meeresbuchten. *Mittl. d. Versuchsanstalt. Wasserbau. Schiffsbau.* Berlin.
- KRÜMMEL, O. (1888). Zum Problem des Euripus. *Peterm. Mittl.* p. 331.
- KRÜMMEL, O. (1911). *Handbuch der Ozeanographie* 2, pp. 766 (2nd ed.). Stuttgart: J. Engelhorn.
- KULLENBERG, B. (1935). Interne Wellen im Kattegat. *Svenska Hydr. Biol. Komm. Skrifter, Ny Ser. Hydrografi* XII.
- KULLENBERG, B. and HELA, J. (1936). Om Träghetssvängningar i Ostersjön. *Svenska Hydr. Biol. Komm. Skrifter, Ny. Ser. XVI.* Lund.
- KULLENBERG, B. See also Pettersson and Kullenberg.
- KURTSCHATOFF, J. W. (1925). Die Seiches des Schwarzen Meeres und des Asow'schen Meeres. *Nachr. Zbl. Hydromet., Leningrad* 4.
- LAGRANGE, J. L. (1781). Mémoire sur la théorie du mouvement des fluides. *Nouv. Mém. Ac. Roy. Berlin, Oeuvres*, 4.
- LAMB, H. and SWAIN, L. (1915). A tidal problem. *Phil. Mag.* (6), 29, 737.
- LAMB, H. (1932). *Hydrodynamics*, Cambridge University Press. 6th ed. pp. 883.
- LAPLACE, P. S. (1775, 1776). Recherches sur quelques points de système du monde, *Mem. Acad. Roy. Sci.* (See also *Mechanique céleste* 4, no. 1, 1799.)
- LARISCH-MOENNICH, F. (1925). Sturmsee und Brandung. *Monogr. Erkunde*, no. 33 (Velhagen u. Klasing).
- LEK, L. (1938a). Interne Wellen in den Niederländisch-Ostindischen Gewässern. *C. R. Congr. Int. Geogr., Amst.* 12, sect. II B, p. 69.
- LEK, L. (1938b). Die Ergebnisse der Strom- und Serienmessungen. *Snellius Exped. in the Eastern Part of the Netherlands East-Indies, 1929–30*, 2, pt. 3.
- LENTZ, H. (1873). *Von der Ebbe und Flut des Meeres.* Hamburg.
- LETTAU, H. (1932a). Über die Periode freier Schwingungen von unvollständig abgeschlossenen Wassermassen (Mündungskorrektion bei Seiches). *Gerl. Beitr. Geophys.* 37, 41.
- LETTAU, H. (1932b). Freie Schwingungen (Seiches) des Kurischen Haffs. *Schrift. Phys.-ökon. Ges. Königsberg.* 67.
- LETTAU, H. (1932c). Seiches des Frischen Haffs. *Ann. Hydr. Mar. Met.* 60, 229.
- LETTAU, H. (1934). Ausgewählte Probleme bei stehenden Wellen in Seen. *Ann. Hydr. Mar. Met.*, 62, 13.
- LEVI-CIVITA, T. (1922). Über die Transportgeschwindigkeit einer stationären Wellenbewegung. *Vorträge aus dem Gebiet der Hydro und Aerodynamik*, p. 85. Innsbruck, Berlin, 1922 and 1924.
- LEVI-CIVITA, T. (1925). Determination rigoureuse des ondes permanentes d'ampleur finie. *Math. Ann.* 93, 264.
- LEVY, M. (1898). *Leçons sur la théorie des marées.* 1, Paris.
- LISITZIN, E. (1943). Die Gezeiten des baltischen Meerbusens. *Fennia* 67 no. 4, Helsinki.
- LISITZIN, E. (1944). Die Gezeiten des Finnischen Meerbusens. *Fennia* 68 no. 2, Helsinki.
- LISITZIN, E. (1953). On internal waves in the northern Baltic. *Havsforknings Inst. Skrift* no. 161, 1–9 Helsinki.
- LONGUET-HIGGINS, M. S. (1952). On the statistical distribution of the heights of sea waves. *J. Mar. Res.* 11, 245–46.
- LOVE, A. (1891). Wave motion in a heterogeneous liquid. *Proc. Math. Soc. Lond.* 22, 307.
- LUBBOCK, J. (1839). An elementary treatise on the tides. *Phil. Trans.* (See also other publications in *Phil. Trans.* 1830–1850).

- LYRA, G. (1943). Theorie der stationären Leewellenströmung in der freien Atmosphäre. *Z. angew. Math.* **23**, no. 1. (See also *Beitr. Z. Phys. fr. Atmos.*, **26**, 1940).
- MACCOWAN, (1891). On the solitary waves. *Phil. Mag.* (5). **32**, 45.
- MACCOWAN, (1892). On the theory of long waves and its application to the tidal phenomena of rivers and estuaries. *Phil. Mag.* (5), **33**, 250.
- DE MARCHI, L. (1908). La marea nel Mediterraneo. *Atti R. Acad. Lincei.* (Cl., at. nat. Ser.), 5, no. 1, 12.
- MATTHIESEN, L. (1889). *Ann. Phys. Chem.* **38**, 118.
- MATUZAWA, T., KANBARA, K., and MINAKAMI T. (1933). Horizontal movement of water in the lunami of March 3, 1933. *Jap. J. Astr. Geophys.* **11**, no. 1.
- MAURER, H. (1924). Zur Entstehung der Seebären. *Ann. Hydr. Mar. Met.* **52**, 63.
- MAZELLE, E. (1907). Die Phys. Erforschung des Adriatischen Meeres. *Oest. Rundschau*, **12**.
- MAZZARELLI, G. (1938). I vortici, i tagli e altri fenomeni delle correnti dello stretto di Messina. *Atti real. Ac. Peloritana* **40**. Messina.
- MEISNER, O. (1924). Zur Frage nach der Entstehung der Seebären. *Ann. Hydr. Mar. Met.* **52**, 14. See also *Ann. Hydr. Mar. Met.* **52**, 63, 76.
- MEISNER, O. (1922). Seiches der Ostsee. *Phys. Z.*
- MEISNER, O. (1925). Seiches der Ostsee. *Ann. Hydr. Mar. Met.* **53**.
- MERZ, A. (1914). Unsere Kenntnis von den Gezeiten des Mittelmeeres. *Z. Ges. Erdkunde, Berl.*, no. 2.
- MERZ, A. (1921). Gezeitenforschungen in der Nordsee. *Ann. Hydr. Mar. Met.* **49**, 393.
- MERZ, A. (1923). *Die Gezeiten der Nordsee. Nordseehandbuch. südl. Teil*, p. 30. Berlin.
- MERZ, A. (1935). Die Deutsche Atl. Expedition auf dem Vermessungs- und Forschungsschiff "Meteor". *S. B. preuss. Akad. Wiss. (Phys.-Math. Kl.)* **31**.
- MEYER, H. (1904). Totwasser. *Ann. Hydr. Mar. Met.* **32**, 20.
- MICHELL, J. H. (1893). The highest waves in water. *Phil. Mag.* (5). **36**, 430.
- MICHEL-MOROT, J. (1908). Universal tide-predicting machine Roberts. *Rev. Gén. Industr., Paris*, p. 394.
- MITCHIM, C. F. (1940). Oscillatory waves in deep water. *The Milt. Eng Publ. Soc. Amer. Mil. Engrs.* **32**, no. 182. Washington.
- MIYAHARA, S. and NIIMI, M. (1939). *On the Treatment of a Short Series of Tidal Observations.* Hydr. Depart. Tokyo.
- MÖLLER, L. (1933). Das Tidegebiet der Deutschen Bucht. Die Vertikalkomponente der Gezeiten. *Veröff. Inst. Meereskunde, Berl.*, N. F. Reihe A, Heft 23, 1933.
- MÖLLER, L. (1937). Hydr. Untersuchungen im Frischen Haff. *Z. Ges. Erdkunde, Berl.*, p. 262.
- MÖLLER, M. (1896). *Z. Arch. Ing. Wiss.* **2**, 479.
- MONTGOMERY, R. B. See ROSSBY and MONTGOMERY.
- MOORE, W. U. (1888). *J. China Branch Asiatic Soc. Shanghai* **23**, 183.
- MOORE, W. U. (1888, 1893). *Further Report of the Bore of the T sien-Tang-Kiang, H.M.S. "Rambler"*. Adm. Publ. London.
- MOTZFELD, H. (1937). Die turbulente Strömung an welligen Wänden. *Z. angew. Math. Mech.* **17**, 193.
- VON DER MÜHL, K. (1886). Über die Bewegung tropfbarer Flüssigkeiten in Gefäßen. *Math. Ann.* **27**, 575.
- MUNK, W. H. (1941). Internal waves in the Gulf of California. *J. Mar. Res.* **4**, no. 1.
- MUNK, W. H. (1944). Measurement of waves from pressure fluctuations at the ocean bottom. *Scripps Inst. Wave Project Rep.* no. 5.
- MUNK, W. H. and TRAYLOR, M. A. (1947). Refraction of ocean waves: a process linking underwater topography to beach erosion. *J. Geol.* **16**, no. 1.
- MUNK, W. H. (1947a). Tracking storms by forerunners of swell. *J. Met.* **4**, no. 2.
- MUNK, W. H. (1947b). Increase in the period of waves travelling over larger distances, with special applications to tsunamis, swell and seismic waves. *Trans. Amer. Geophys. Un.* **28**, no. 2.

- MUNK, W. H. (1952). *Forecasting Ocean Waves. Compendium of Meteorology*, Amer. Met. Soc. 1952, pp. 1082-89.
- MUNK, W. H. See also Sverdrup and Munk.
- MURAMOTO, A. (1932). On the main stream in the Taguru Kaikyo. *Hydr. Bull.* **11**, 227.
- NANSEN, F. See HELLAND-HANSEN and F. NANSEN.
- NEUMANN, G. (1941). Eigenschwingungen der Ostsee. *Archiv Dtsch. Seewarte* **61**, no. 4.
- NEUMANN, G. (1942). Periodische Strömungen im finnischen Meerbusen im Zusammenhang mit den Eigenschwingungen der Ostsee. *Gerl. Beitr. Geophys.* **59**, 1.
- NEUMANN, G. (1943). Über die Periode freier Schwingungen in zwei durch einen engen Kanal miteinander verbundener Seen. *Ann. Hydr. Mar. Met.* **71**, 409.
- NEUMANN, G. (1944a). Die Impedanz mechanischer Schwingungs-Systeme und ihre Anwendung auf die Theorie der Seiches. *Ann. Hydr. Mar. Met.* **72**, 65.
- NEUMANN, G. (1944b). Eine Methode zur Berechnung der Eigenperiode zusammengesetzter (gekoppelter) Seebeckensysteme. *Ann. Hydr. Mar. Met.* **72**, 193.
- NEUMANN, G. (1946). Stehende, zellulare Wellen im Meer. *Naturwissenschaften*, Heft. 9, p. 282.
- NEUMANN, G. (1949). Stabilitätsschwingungen und die innere thermische Unruhe im Meer und in der Atmosphäre. *Dtsch. Hydrogr. Z.* **2**, Nos. 1-3, 52.
- NEUMANN, G. (1949). Die Entstehung der Wasserwellen durch Wind. *Dtsch. Hydrogr. Z.* **2**, no. 5, 187-99.
- NEUMANN, G. (1952). Über die komplexe Natur des Seeganges, 1. Teil. *Dtsch. Hydrogr. Z.* **5**, 95-110. 2. Teil. *Dtsch. Hydrogr. Z.* **5**, 252-77.
- NEUMANN, G. (1953a). On ocean wave spectra and a new method of forecasting wind generated sea. Beach Erosion Board, Washington D. C. Techn. Mem. no. 43.
- NEUMANN, G. (1953b). On the energy distribution in ocean wave spectra at different wind velocities. *Trans. Amer. Geophys.* See HAURWITZ. (1949).
- NEUMANN, G. (1954). Zur Charakteristik des Seeganges. *Arch. Met. Geophys. Biokl., A*, **7**, 352-377.
- NISIDA, K. (1927). Results of the current measurements in the adjacent seas Tyosen, 1923-1926. *Rep. Oceanogr. Invest. Fish. Exp. Sta. Husan* **2**.
- NISIDA, K. (1928). Results of the current observations made in the vicinity of Husan. *Umito Sora (Sea and Sky)* **8**.
- NISIDA, K. (1930). Results of the tidal current observations in the eastern channel of the Tushima Kaikyo. *Umito Sora (Sea and Sky)* **10**.
- NOMITSU, T. (1935). A theory of Tsunamis and Seiches produced by wind and barometric gradient. *Mem. Coll. Sci. Imp. Univ. Kyoto, A*, **18**, no. 4.
- NOMITSU, T. and HABU, K. (1935). Proper oscillations of the sea on continental shelf. *Mem. Coll. Sci. Imp. Univ. Kyoto, A*, **18**, no. 5.
- NOMITSU, T. and NAKAMIJA. (1937). Proper oscillations of lake-shelves. *Mem. Coll. Sci. Imp. Univ. Kyoto* **20**, no. 1.
- O'BRIEN, M. P. and others (1942). A summary of the theory of oscillatory waves. *Tech. Rep. U.S. Beach Erosion Board*, no. 2. 1942.
- ODDONE, E. (1908). Il problema delle odulazioni secondarie di mare. *Boll. Soc. Sism. Ital.* **12**.
- ODDONE E. (1910). Per lo studio delle cause del fenomeno delle sesse. *Rend. Reg. Acad. Lincei (Cl. fis.-mat.)* **19**.
- OGURA, S. (1923). The tides in the Gulf of Tartary. *Miscell. Rep. Hydr.* **10**, 89.
- OGURA, S. (1926). On the tides in the seas of Eastern Asia. *Proc. 3rd Pan. Pacif. Sci. Congr., Tokyo*.
- OGURA, S. (1932). On the tides in the Taguru Kaikyo. *Hydr. Bull.* **11**, 1.
- OGURA, S. (1933a). On the tidal currents and tides in the northern part of the Hwang Hai (Yellow Sea). *Hydr. Bull.* **12**, 47, 89, 137.
- OGURA, S. (1933b). On the tides in the Liautung Gulf. *Hydr. Bull.* **11**, 269.
- OGURA, S. (1933c). The tides in the seas adjacent to Japan. *Hydr. Bull. Dep. Imp. Jap. Navy* **7**.
- OGURA, S. (1934a). Analysis of the results of tidal current observations made at two stations in the northern part of Tung Hai. *Hydr. Bull.* **13**, 431, 471.

- OGURA, S. (1934*b*). Further notes on the tides and tidal currents in the Liautung Gulf. *Hydr. Bull.* **13**, 91, 133, 179.
- OGURA, S. (1936). On the tides and tidal currents in Pwok Hai. *Hydr. Bull.* **15**, 147, 181.
- OKADA, T., FUJIWHARA S. and MAEDA S. (1913). On thunderstorms as a cause of seiches. *Math.-Phys. Soc. Tokyo* **7**, no. 12, 210.
- PABST, W. (1933). *Z. f. Mechanik*.
- PÂRIS, A. (1867). *Compt. Rend.* **64**, 731.
- PÂRIS, A. (1871). Des mouvements des vagues. *Rev. Mar. Colon.* **31**, 111.
- PARTIOT, H. (1861). Memoires sur le mascaret. *Ann. Ponts Chaussees* (4), p. 17.
- PAULSEN, A. (1906). *Rapp. Trav. Serv. Hydr. Mareogr.* p. 13. Copenhagen.
- PETTERSSON, H. (1920). Internal movement in coastal waters and meteorological phenomena. *Geogr. Ann.* p. 32. Stockholm.
- PETTERSSON, H. and KULLENBERG B. (1933). Boundary waves in the Kattegat. *Medd. Oceanogr. Inst. Goetborg*, no. 4.
- PETTERSSON, H. (1938). Internal waves in Canadian waters. *C. R. Congr. Int. Geogr., Amst.*, **12**, sect. 2*b*, p. 77.
- PETTERSSON, O. (1909). Gezeitenähnliche Bewegungen des Tiefenwassers. *Publ. Circonst. Cons. Expl. Mer.* no. 47. Copenhagen.
- PETTERSSON, O. (1930). The tidal force, a study in Geophysics. *Geogr. Ann., Stockholm*.
- PETTERSSON, O. (1933*a*). Interne Gezeitenwellen. *Rapp. Cons. Expl. Mer.* **82**, Copenhagen.
- PETTERSSON, O. (1933*b*, 1934, 1935). Tidvattnets Problem, I-IV, *Arkiv. Math., Astr. Fys., Stock.*, **A**, **23**, no. 23; **24**, nos. 16, 17; **25**, no. 1.
- PETTERSSON, O. (1934). La Marée interne. *J. Johnstone Mem. Vol.* Liverpool, p. 294.
- PETTERSSON, O. (1935). The internal parallax tide in the transitional area. *Rapp. Cons. Expl. Mer* **94**. Copenhagen.
- PIERSON, W. I. (1952). An unified mathematical theory for the analysis, propagation and refraction of storm generated ocean waves. I and II. *Coll. Engr. Dep. Univ. New York*.
- PIERSON, W. I. (1953). An interpretation of the observable properties of sea waves in terms of the power spectrum of the Gaussian record. *34th Annual Meeting of the A.G.U. Washington D.C.* May 4-6, 1953.
- PIERSON, W. I., NEUMANN, G. and JAMES, R. W. (1953). Practical methods for observing and forecasting ocean waves by means of wave spectra and statistics. *Tech. Rep. Res. Div., Coll. Engr. New York Univ.* no. 1.
- PLATANIA, G. (1907). Nuove ricerche sulle librazioni del mare. *Ann. reg. Inst. Naut.* **1**. Catania. See also *Atti del V Congr. Geogr. Ital.*, Napoli, 1904.
- PLATANIA, G. (1910). *Bol. Soc. Sismol. Ital.* 1908-1909, **13**, fasc. 7,8. Rome.
- POINCARÉ, H. (1910). *Leçons de mécanique céleste*. Vol. 3, *Theorie des marées*, p. 409, Paris: Gauthier-Villars, 1910.
- POISSON, S. (1816). Memoire sur la théorie des ondes. *Mem. Acad. Roy. Sci. Inst. Fr.* 1818.
- POLLAK, L. (1926). *Rechentafeln zur harmonischen Analyse*, Leipzig. See also *Harmonic Analysis*.
- PRANDTL, L. (1942). *Führer durch die Strömungslehre*. 3rd ed. pp. 382. Braunschweig: Vieweg und Sohn, 1942.
- PREY, A. (1929). Über die Elastizitätskonstanten der Erde. *Gerl. Beitr. Geophys.* **23**.
- PROUDMAN, J. (1913). On some cases of tidal motion on rotating sheets of water. *Proc. Roy. Soc. Math.*, (2), **35**, 75.
- PROUDMAN, J. (1941*a*). Diffraction of tidal waves on flat rotating sheets of water. *Proc. Lond. Math. Soc.* (2), **14**, 89.
- PROUDMAN, J. (1941*b*). Free and forced longitudinal tidal motion in a lake. *Proc. Lond. Math. Soc.* (2), **14**.
- PROUDMAN, J. (1916, 1931). On the dynamical equations of the tides, Part I-III, and Part IV. *Proc. Lond. Math. Soc.* **18**, 1; **34**, 294.

- PROUDMAN, J. (1920). Harmonic analysis of tidal observations in the British Empire. *Brit. Ass. Adv. Sci.* 1920, p. 328.
- PROUDMAN, J. and DOODSON, A. T. (1923). The tides of the Irish Sea. "*Merseyside*" *Handbook of Liverpool*. (Sept. 1923).
- PROUDMAN, J. and DOODSON, A. T. (1924*a*). Time relations in meteor effects on the sea. *Proc. Lond. Math. Soc.* (2), **24**, no. 2, 140.
- PROUDMAN, J. and DOODSON, A. T. (1924*b*). The principal constituent of the tides of the North sea. *Phil. Trans. A*, **224**, 185.
- PROUDMAN, J. (1925*a*). Tides in a channel. *Phil. Mag.* (6) **49**, 465.
- PROUDMAN, J. (1925*b*). On tidal features of local coastal origin and on sea-seiches. *Mon. Not. R. Astr. Soc. Geophys. Suppl.* **1**, no. 6, 247.
- PROUDMAN, J. (1927). *Newton's Work on the Theory of Tides*, p. 78, Mem. Vol. issued by Math. Soc. Lond.
- PROUDMAN, J. (1928*a*). On the tides in a flat semi-circular sea of uniform depth. *Mon. Not. R. Astr. Soc. Geophys. Suppl.* **2**, 32.
- PROUDMAN, J. (1928*b*). Deformation of earth-tides by means of water-tides in narrow seas. Bull. no. 11, *Sect. oceanogr. cons. de recherches*, Venedig.
- PROUDMAN, J. (1929). The effects on the sea of changes in atmospheric pressure. *Mon. Not. R. Astr. Soc. Geophys. Suppl.* **2**, no. 4, 196.
- PROUDMAN, J. (1939). On the currents in the North Channel of the Irish Sea. *Mon. Not. R. Astr. Soc. Geophys. Suppl.* (Jan.).
- PROUDMAN, J. (1942*a*). On the distribution of tides over a channel. *Proc. Lond. Math. Soc.* (2), **49**, 211.
- PROUDMAN, J. (1942*b*). On Laplace's differential equations for the tides. *Proc. Roy. Soc., A*, **179**, no. 978, p. 261.
- PROUDMAN, J. (1944). The tides of the Atlantic Ocean. *Mon. Not. R. Astr. Soc. Geophys. Suppl. Suppl.* **104** no. 5
- PROUDMAN, J. (1946). On the distribution of tides over a channel. *Math. Soc. Lond. Proc.* (2), **49**, 211.
- PROUDMAN, J. (1955*a*). The propagation of tide and surge in an estuary. *Proc. Roy. Soc., A*, **231**, 8-24.
- PROUDMAN, J. (1955*b*). The effect of friction on a progressive wave of tide and surge in an estuary. *Proc. Roy. Soc., A*, **233**, 407-8.
- PROUDMAN, J. (See also A. T. DOODSON).
- PUTZ, R. R. (1952). Statistical distribution for ocean waves. *Trans. Amer. Geophys. Union.* **33**, 685-92.
- PRÜFER, G. (1936). Die Gezeiten des Indischen Ozeans. *Veroff. Inst. Meereskunde, Berl., N. A. F.*, no. 37.
- RALTRAY, M. and BURT, W. V. (1956). A comparison of methods for forecasting wave generation. *Deep-sea Res.* **3**, 140-4.
- RANKINE, W. (1864). On the exact form of waves near the surface of deep water. *Phil. Trans.* **108**, 127.
- RAUSCHELBACH, H. (1921, 1924). Die deutsche Gezeitenrechenmaschine. *Z. Instr. Kunde*, 285, and *Ann. Hydr. Mar. Met.* **49**, 93.
- RAUSCHELBACH, H. (1924). Harmonische Analyse der Gezeiten des Meeres. *Arch. Dtsch. Seewarte.* **62**, no. 1. Hamburg.
- RAUSCHELBACH, H. (1932*a*). Grundlagen für einen neuen Hochseepegel. *Ann. Hydr. Mar. Met.* **60**, 129.
- RAUSCHELBACH, H. (1932*b*). Zur Geschichte der Hochseepegel. *Ann. Hydr. Mar. Met.* **60**, 73.
- RAUSCHELBACH, H. (1934). Die Hochseepegelbeobachtungen im südlichen Kattegat im August 1931. *Ann. Hydr. Mar. Met.* **62**, 177-233.
- RAYLEIGH LORD (1876). On waves. *Phil. Mag.* **1**, 257.

- RAYLEIGH LORD (1894). *Theory of Sound*, pp. 480 and 504. London and New York, Macmillan and Co.
- RAYLEIGH LORD (1903). *Phil. Mag.* (6), **5**. See also *Sci. Pap.* **5**, 93, 1903.
- RAYLEIGH LORD (1909). *Proc. Roy. Soc., A*, **82**. See also *Sci. Pap.* **5**, 89, 497.
- RAYLEIGH LORD (1914). On the theory of long waves and bores. *Proc. Roy. Soc. A*, **40**, paper 6. See also LAMB (1932).
- REDFIELD, A. C. (1950). The analysis of the tidal phenomena in narrow embayments. *Pap. Phys. Oceanogr. Met. Woods Hole Oceanogr. Inst.* **9**, no. 4.
- REDFIELD, A. C. (1953). Interference phenomena in the tides of the Woods Hole region. *J. Mar. Res.* **121**, 121-40.
- REQUIST, H. (1926). Ein Seebär in Finnland. *Geogr. Annaler*, p. 230. Stockholm.
- REVELLE, R. (1939). Sediments of the Gulf of California. *Geol. Soc. Amer. Bull.* **50**, p. 1929.
- REYNOLDS, O. (1880). On the effect of oil-destroying waves on the surface of water. *Brit. Ass. Rep.* 1880.
- RIED, J. L. (1956). Observations of internal tides in October 1950. *Trans. Amer. Geophys. Union*, **37** **3**, 278-86.
- ROBERT, S. A. (1946). Refraction of water waves by islands and shoals with circular bottom-contours. *Trans. Amer. Geophys. Un.*, **27**, 168.
- ROBERTS, E. (1870). *Proc. Roy. Soc.*, **29**.
- ROLL, H. U. (1948). Das Windfeld über den Meereswellen. *Naturwissenschaften*, **35**, 230-34.
- ROLL, H. U. (1951). Neue Messungen zur Entstehung von Wasserwellen durch Wind. *Ann. Meteor.* **4**, 269-86.
- ROLL, H. U. (1952). Über die Grössenunterschiede der Meereswellen bei Warm- und Kaltluft. *Dtsch. Hydr. Z.* **5**, 111-13.
- ROLL, H. U. (1953, 1954). Höhe, Länge und Steilheit der Meereswellen im Nordatlantik (Statistik der Wellenbeobachtung der Ozean-Wetterschiffe). *Dtsch. Wetterdienst, Seewetteramt Hamburg Einzelveröff.* Nos. 1, 6. Hamburg.
- ROLL, H. U. (1957). Oberflächen-Wellen des Meeres. *Encycl. Physics* **48**, 671-733.
- ROSENHEAD, L. (1932). The formation of vortices from a surface of discontinuity. *Proc. Roy. Soc. A*, **134**.
- ROSSBY, C. G. and MONTGOMERY, R. B. (1935). The layer of frictional influence in wind and ocean currents. *Pap. Phys. Oceanogr. Met.* **3**, no. 3, 101.
- ROSSBY, C. G. (1936). On the frictional forces between air and water and on the occurrence of a laminar boundary layer next to the surface of the sea. *Pap. Phys. Oceanogr. Met.* **4**, no. 3.
- ROSSBY, C. G. (1945). On propagation of frequencies and energy in certain types of oceanic and atmospheric waves. *J. Met.* **2**, 187.
- ROSSITER, J. R. (1954). The North Sea storm surge of 31 January and 1 February 1953. *Phil. Trans. A*, **246**, no. 915, 371-400.
- ROTTOCK, E. (1888). Die Beruhigung der Wellen durch Oel. Berlin.
- DE ROUVILLE, A., BESSON, P. and PETRY P. (1938). État des études intern. sur les efforts des aux lames. *Ann. Ponts et Chaussées*. Paris.
- RUDOLPH, E. (1887, 1895, 1898). Über submarine Erdbeben und Eruptionen. *Gerl. Beitr. Geophys.* **1**, **2**, and **3**, 133, 537 and 273.
- DE SAINT VÉNANT (1870). Démonstration élémentaire de la formule de propagation d'une onde ou d'une intumescence dans un canal prismatique. *Comp. Rend.* **71**, Paris.
- SANDSTRÖM, J. (1908). Dynamische Versuche mit Meerwasser. *Ann. Hydr. Mar. Met.* **36**, 6.
- SCHAFFERNICHT, W. (1937). Horizontalpendelbeobachtungen über Lotschwankungen in Marburg a. L. *Ann. Phys.* **29**, 349.
- SCHICHEL, (1893). Der Amazonenstrom. Diss. Strassburg. See also BATES H. W. 1863.
- SCHMEHL and JUNG (1931). Figur, Schwere und Massenverteilung der Erde, in Wien-Harms, *Handbuch der Experimentalphysik*, p. 315, Leipzig.

- SCHMIDT, W. (1908). Stehende Schwingungen in der Grenzschicht zweier Flüssigkeiten, *S. B. Akad. Wiss. Wien.* (Abt. IIa), **117**, p. 91.
- SCHMIDT, W. (1934a). Turbulence near the ground. *Coun. R. Aeronaut. Soc.*, Lect. no. 583.
- SCHMIDT, W. (1934b). Untersuchungen über den Feinbau des Windes. *Dtsch. Forschung*, no. 14 (*Ans Arb. Notgemeinschaft. Wiss.*), p. 54.
- SCHOOLEY, A. H. (1955). Curvature-distributions of wind-created water waves. *Trans. Amer. Geophys. Un.* **36**, 273.
- SCHOTT, G. (1893). *Wiss. Erg. einer Forschungsreise zur See. Peterm. Mittl. Erg.* **109**, 73. Gotha.
- SCHUBERT, O. v. (1932). Die Strommessungen Pillsburys in moderner Bearbeitung. *Ann. Hydr. Mar. Met.* **60**, 378.
- SCHUBERT, O. v. (1944). Ergebnisse der Strommessungen und der ozeanogr. Serienmessungen auf den beiden Stationen der 2. Teilfahrt. *Wiss. Erg. Dtsch. Nordatl. Exp. 1937-38*, and *Ann. Hydr. Mar. Met.* **72**, (Beiheft Jan.).
- SCHUMACHER, A., and THORADE H. (1923). Die Gezeiten der Sylter Gewässer. *Arch. Dtsch. Seewarte, Hamburg*, **41**, no. 2, 48.
- SCHUMACHER, A. (1924). Darstellung des Gezeitevorganges in der Nordsee durch Isohypsenkarten der Meeresoberfläche. *Ann. Hydr. Mar. Met.* **52**.
- SCHUMACHER, A. (1936). (Untersuchungen des Seegangs mit Hilfe der Stereophotogrammetrie. *Jb. Lilienthal-Ges. Luftfahrtforschung, Berl.*
- SCHUMACHER, A. (1939). Stereophotogr. Wellenaufnahmen. *Wiss. Erg. dtsch. Atl. Exp. "Meteor" 1925-27*, **7**, no. 2. Berlin.
- SCHWEYDAR, W. (1907a). Ein Beitrag zur Bestimmung des Starrheitskoeffizienten der Erde. *Gerl. Beitr. Geophys.* **9**.
- SCHWEYDAR, W. (1907b). Bemerkungen zur Abhandlung von Prof. Hoff. *Ann. Hydr. Mar. Met.* **35**, 179, 375.
- SCHWEYDAR, W. (1931). Lotschwankung und Deformation der Erde durch Flutkräfte. *Veröff. Int. Erdmess.* no. 38, Berlin, 1921. See also *Veröff. geod. Inst. Potsdam*, 1912 and 1919.
- SCOTT RUSSELL, J. (1838). Rep. Comm. Waves. *Brit. Ass. Rep. no. 7, Meet. Liverpool, 1837*, p. 417. London.
- SCOTT RUSSELL, J. (1845). Report on waves. *Brit. Ass. Rep. 14, Meet. London, 1844*. London.
- SEIWELL, H. (1937). Short-period vertical oscillations in the western basin on the North Atlantic. *Pap. Phys. Oceanogr. Met. Woods Hole Oceanogr. Inst.* **5**, no. 2.
- SEIWELL, H. R. (1948). Results of research on surface waves of the western North Atlantic. *Pap. Phys. Oceanogr. Met. Mass. J. Tech.* **10**, no. 4, 1-56.
- SEIWELL, H. R. (1949). The principles of time series analyses applied to ocean wave data. *Proc. Nat. Acad. Sci. Washington.* **35**, no. 9, 518-28.
- SEIWELL, H. R. and WADSWORTH, G. P. (1949). A new development in ocean wave research. *Science*, **109**, 271-74.
- SERVAIS, F. (1957). Exploration hydrobiologique du Lac Tanganika. *Res. Sci.* **2**, no. 3, Bruxelles.
- SHOULEJKIN, W. (1926). Hydrodynamics of the tides in a small sea communicating with the ocean (White Sea). *Gerl. Beitr. Geophys.* **15**, 321.
- SHUREMAN, P. (1924). A manual of harmonic analysis and prediction of tides. *U.S. Coast and Geod. Surv.*, no. 98.
- SOLBERG, H. (1936). Über die freien Schwingungen einer homogenen Flüssigkeitsschicht auf der rotierenden Erde, Part I. *Astrophys. Norveg.*, **1**, no. 7. Oslo.
- SPITALER, R. (1921). Eine neue Theorie der täglichen Luftdruckschwankungen, sowie der Ebbe und Flut überhaupt. *Ann. Hydr. Mar. Mat.* **49**, 220.
- SPRINGTUBE, H. (1934). Die Gezeitenerscheinungen im St. Lorenz-Golf. *Arch. Dtsch. Seewarte, Hamburg*, **53**.
- STAHLBERGER, E. (1874). *Die Ebbe und Flut in der Reede von Fiume*. Budapest.
- STANTON, T. (1932). The growth of waves on water due to the action of the wind. *Proc. Roy. Soc., A*, **137**.

- STENJI, S. (1932). Zur Theorie der Wasserschwingungen in einem begrenzten Meeresbecken mit bes. Berücksichtigung des Einflusses des Luftdrucks. *Soc. Sci. Fen. Comm. Phys.-math.* **6**, no. 16. Helsinki.
- STENJI, S. (1936). Über das Hochwasser im Finnischen Meerbusen am 23 Sept. 1924. *V. Hydr. Konf. balt. Staaten, Finnland*, Bericht 15, D.
- STERNECK, R. v. (1912*a*). Das Gezeitenphänomen in westlichen Mittelmeer. *S. B. Akad. Wiss. Wien*, **121**, 1245.
- STERNECK, R. v. (1912*b*). Über die Gezeiten des Schwarzen Meeres. *Akad. Anz. Akad. Wiss. Wien* (17 Oct.).
- STERNECK, R. v. (1914*a*). Über die Gezeiten des Aegäischen Meeres. *Akad. Anz. Akad. Wiss. Wien*, (10 Dec.).
- STERNECK, R. v. (1914*b*). Über den Einfluss der Erdrotation auf die halbtägigen Gezeiten der Adria. *S. B. Akad. Wiss. Wien*, **123**, ser. 3, 3. Discussion by A. DEFANT, *Ann. Hydr. Mar. Met.* **42**, 556, 1917.
- STERNECK, R. v. (1914*c*). Über "Seiches" an den Küsten der Adria. *S. B. Akad. Wiss. Wien*, 123. (Abt. IIa).
- STERNECK, R. v. (1915*a*). Zur hydrodynamischen Theorie der Adriagezeiten. *S. B. Akad. Wiss. Wien*. (Math.-Naturwiss. Kl.), **124**, 147.
- STERNECK, R. v. (1915*b*). Zur Theorie der Gezeiten des Mittelmeeres. *S. B. Akad. Wiss. Wien*. (Abt. IIa), **122**. Discussion by A. DEFANT, *Ann. Hydr. Mar. Met.* p. 561.
- STERNECK, R. v. (1915*c*). Hydrodynamische Theorie der halbtägigen Gezeiten des Mittelmeeres. *S. B. Akad. Wiss. Wien*, (Abt. IIa), **124**, 905. Discussion by A. DEFANT, *Ann. Hydr. Mar. Met.* **44**, 465.
- STERNECK, R. v. (1916). Zur Theorie der Euripus-Strömungen. *S. B. Akad. Wiss. Wien*. (Abt. IIa), **125**.
- STERNECK, R. v. (1919*a*). Die Gezeitenerscheinungen der Adria, II. Teil. Die theor. Erklärung der Beobachtungstatsachen. *Denkschr. Akad. Wiss. Wien*, **96**.
- STERNECK, R. v. (1919*b*). Ergänzende Rechnung zur Theorie der Adriagezeiten. *Akad. Anz. d. Akad. d. Wiss. Wien*, no. 19.
- STERNECK, R. v. (1920-1). Die Gezeiten der Oceane. 1. und 2. Mitteilung. *S. B. Akad. Wiss. Wien*. (Math.-Naturwiss. Kl.), **129**, 131; 130, 363.
- STERNECK, R. v. (1922*a*). Neue Weltkarten der Flutstundenlinien. *Ann. Hydr. Mar. Met.* **50**, 145.
- STERNECK, R. v. (1922*b*). Schematische Theorie der Gezeiten des Schwarzen Meeres. *S. B. Akad. Wiss. Wien*. (Math.-Naturw. Kl.), **131**, 81.
- STERNECK, R. v. (1922*c*). Harmonische Analyse und Theorie der Mittelmeergezeiten. *S. B. Akad. Wiss. Wien*. (Math.-Naturwiss. Kl.), **131**.
- STERNECK, R. v. (1923*a*). Zur Praxis der harmonischen Analyse der Gezeitenbeobachtungen. *Ann. Hydr. Mar. Met.* **51**.
- STERNECK, R. v. (1923*b*). Die Eintagstiden im Mittelmeer. *Ann. Hydr. Mar. Met.* **51**, 215.
- STERNECK, R. v. (1925). Zu den halbtägigen Gezeiten der Nordsee. *Ann. Hydr. Mar. Met.* **53**, 147.
- STERNECK, R. v. (1926*a*). Die Zerlegungs- und Kanaltheorie der Gezeiten. *Z. Geophys.* **2**, 319.
- STERNECK, R. v. (1926*b*). Harmonische Analyse und Theorie der Gezeiten des Schwarzen Meeres. *Ann. Hydr. Mar. Met.* **54**, 289.
- STERNECK, R. v. (1926*c*). Zur Theorie der halbtägigen Gezeiten des Atlantischen Ozeans. *Ann. Hydr. Mar. Met.* **54**.
- STERNECK, R. v. (1927). Selbstständige Gezeiten und Mitschwingen im Roten Meere. *Ann. Hydr. Mar. Met.* **55**, 129.
- STERNECK, R. v. (1928*a*). Die Gezeiten im nördlichen Eismeer. *Ann. Hydr. Mar. Met.* **56**, 21, 1928.
- STERNECK, R. v. (1928*b*). Die Gezeiten des Baikalsees. *Ann. Hydr. Mar. Met.* **56**, 221, See also *Verh. Magn. Met. Obs. Irkutsk*, **2**, no. 3.
- STEVENSSON, T. (1850). Observations on the force of waves. *Brit. Ass. Rep. Lond.* (App. 1851). See also *New Edinb. Phil. J.* **53**, 358, 1852.

- STEVENSSON, T. (1864). *Design and Construction of Harbours*, pp. 64. Edin. Adam and Ch. Black.
- STÖRMER, C. (1907). Sur les trajectoires des corpuscules électrisés dans l'espace. *Arch. Sci. Phys. Nat. Geneve*.
- STOK, P. VAN DER (1897). *Wind, Weather, Currents, Tides and Tidal Streams of the East Indian Archipelago*. Batavia. See also *Med. Verh. Kgl. nederl. Met. Inst.* no. 102. Utrecht, 1910.
- STOK, P. VAN DER (1905). Études des phénomènes sur les côtes Néerlandaises, nos. I-III. Utrecht.
- STOK, P. VAN DER (1911). Elementare Theorie der Gezeiten u. s. w. *Ann. Hydr. Mar. Met.* **39**, 227, 303, 354.
- STOKES, G. (1847). On the theory of oscillatory waves. *Cambridge Trans.* VIII (Papers I, p. 212).
- STOKES, G. (1880). Supplement to a paper on the theory of oscillatory waves. *Math. and Phys. Papers*, I, Cambridge.
- STRUJK, D. (1926). Détermination rigoureuse des ondes irrotationnelles périodiques dans un canal à profondeur finie. *Math. Ann.* **95**, 595.
- SVERDRUP, H. U. (1926*a*). Dynamics of tides on the North Siberian Shelf. *Geofys. Publ.* **4**, no. 5. Oslo.
- SVERDRUP, H. U. (1926*b*). The tides on the North Siberian Shelf, their bearing on the existence of land in the arctic sea and their dynamics. *J. Wash. Acad. Sci.* **16** (Dec.).
- SVERDRUP, H. U. (1939). The Gulf of California. *Proc. Sixth Pac. Sci. Congr. Berkeley*, 1939.
- SVERDRUP, H. U. (1940). The Gulf of California. *Ass. Océanogr. Phys. Procès-Verb.* no. 3, p. 170.
- SVERDRUP, H. U. and MUNK, W. H. (1944). Breakers and Surf. Principles in forecasting. *Hydrogr. Off. U. S. Navy*, no. 234.
- SVERDRUP, H. U., JOHNSON and FLEMING. (1946*a*). *The Oceans*. New York.
- SVERDRUP, H. U. and MUNK, W. H. (1946*b*). Empirical and theoretical relations between wind, sea and swell. *Trans. Amer. Geophys. Un.* **27**, no. 6.
- SVERDRUP, H. U. and MUNK, W. H., (1946*c*). Theoretical and empirical relations in forecasting breakers and surf. *Trans. Amer. Geophys. Un.* **27**, no. 6.
- SVERDRUP, H. U. (1947*a*). Period increase of ocean swell. *Trans. Amer. Geophys. Un.* **28**, no. 3.
- SVERDRUP, H. U. (1947). Period increase of ocean swell. *Trans. Amer. Geophys. Un.* **28**, no. 3, 407-17.
- SVERDRUP, H. U. and MUNK, W. H. (1947*b*). Wind, sea and swell: theory of relations for forecasting. *Tech. Rep. U. S. Hydrogr. Office*, no. 1, Publ. 601.
- SYMONS, G. (1888). The eruption of Krakatoa and subsequent phenomena. *Rep. Krakatoa Comm. Roy. Soc. Lond.*
- TAKAHASI, R. (1929). Tilting motion of the earth crust caused by tidal loading. *Bull. Earthquake Res. Inst.* **6**, 85.
- TAYLOR, G. (1919). Tidal friction in the Irish Sea. *Phil. Trans. A*, **220**, 32.
- TAYLOR, G. (1920). Tidal oscillations in gulfs and rectangular basins. *Proc. Lond. Math. Soc.*, (2), **20**, nos. 2 and 3,
- TAYLOR, G. (1921). Tides in the Bristol Channel. *Proc. Camb. Phil. Soc.* **20**, 3, 320.
- TENANI, M. (1929). Considerazioni teorico-sperimentali sul regime delle maree del mare Adriatico. *Rend. R. Acad. Lincei*, **10**, Ser. 6. Rome.
- TENANI, M. (1930). Sur les marées de la Méditerranée orientale. *Comp. Rend.* 21 July.
- TENANI, M. (1931). Contributo alla conoscenza delle maree dell'oceano artico. *Rend. Acad. Lincei*, **13**, 879, Rome.
- THOMSON, H. See J. P. JACOBSEN and H. THOMSON.
- THOMSON, W. and TAIT (1867, 1883). *Treatise on Natural Philosophy*. Cambridge and Oxford.
- THOMSON, W. (1871). Hydrokinetic solutions and observations. *Phil. Mag.* (4), **41**, 1871.
- THOMSON, W. (1875*a*). On an alleged error in Laplace's theory of the tides. *Phil. Mag.* (4), **50**, 227.
- THOMSON, W. (1875*b*). Note on the oscillations of the first species in Laplace's theory of the tides. *Phil. Mag.* (4), **50**, 279.
- THOMSON, W. (1879). On gravitational oscillations of rotating water. *Proc. Roy. Soc. Edinb.* **10**, 92 (Pap. 4, p. 141).
- THOMSON, W. (1881). *The Engineer*, 1879. Inst. Civ. Eng. **65**.

- THOMSON, W. (1891). *Popular Lectures and Addresses*, 3, 1, 201. Lond.
- THORADE, H. (1918). Die Sturmflut vom 15. u. 16. Jan. 1916 in den dänischen Gewässern. *Ann. Hydr. Mar. Met.* **46**, 234.
- THORADE, H. (1921). Die Gezeiten als stehende Wellen. (Nach A. Defants neueren Arbeiten). *Ann. Hydr. Mar. Met.* **49**, 100.
- THORADE, H. (1924*a*). Flutstundenlinien und Flutwelle. *Ann. Hydr. Mar. Met.* **52**, 27.
- THORADE, H. (1924*b*). Bemerkungen zu Defant's letzten Gezeitenarbeiten. *Ann. Hydr. Mar. Met.* **52**, 63.
- THORADE, H. (1926*a*). Flutwellen über unebenem Grund. *Ann. Hydr. Mar. Met.* **54**, 217.
- THORADE, H. (1926*b*). Fortschreitende Wellen bei veränderlicher Wassertiefe. *Mittl. Math. Ges. Hanburg*, 6, no. 5, 203.
- THORADE, H. (1928*a*). Newton's Anschauungen über Ebbe und Flut. *Ann. Hydr. Mar. Met.* **56**, 366.
- THORADE, H. (1928*b*). Gezeitenuntersuchungen in der Deutschen Bucht der Nordsee. *Arch. dtsh. Seewarte Hamburg*, **46**.
- THORADE, H. (1929). Beiträge zur Theorie der Gezeitenströme. *Gerl. Beitr. Geophys.* **21**, 290.
- THORADE, H. (1930). Ebbe und Flut in der Nordsee. Ein geschichtlicher Rückblick. *Peterm. Mittl.* no. 209, p. 195. Gotha.
- THORADE, H. (1931). Probleme der Wasserwellen. *Probl. Kosm. Physik*, **13**, **14**, 219. Hamburg.
- THORADE, H. (1933). Erdgezeiten und Meeresgezeiten. *Ann. Hydr. Mar. Met.* **61**, 49.
- THORADE, H. (1934). Die Gezeiten des Atlantischen Ozeans. *Ann. Hydr. Mar. Met.* **62**, 1.
- THORADE, H. (1935). Bemerkungen über die Halbtagsgezeiten des Atlantischen Ozeans. *Ann. Hydr. Mar. Met.* **63**, 93.
- THORADE, H. See SCHUMACHER and THORADE, 1923.
- Tides and tidal streams*, (1909). 1st ed. London, H.M. Stationery Office.
- Deutsche Gezeitentafeln* (1939). Anleitung zur Berechnung der Gezeiten nach dem harmonischen Verfahren. Berlin.
- The Admiralty Tide Tables*, Pt. II. London, 1938.
- Description of the U. S. Coast and Geodetic tide-predicting machine* (1918). No. 2, Spec. Publ., no. 32. Washington.
- TOMASCHEK, R. and SCHAFFERNICHT W. (1932). Untersuchungen über die zeitlichen Aenderungen der Schwerkraft, I. *Ann. Phys.* **15**, 787. See also R. TOMASCHEK (1933), Die Messungen der zeitl. Aenderungen der Schwerkraft. *Erg. exakt. Naturwiss.* **12**, Berlin: J. Springer.
- VERCELLI, F. (1925*a*). Campagna idrogr. scient. nel Mare Rosso. Parte I. Correnti e maree. *Istit. Idrogr. R. Mar. Ital. Genova*.
- VERCELLI, F. (1925*b*). *Crociere per lo studio dei fenomeni nello stretto di Messina* (R. N. Marsigli 1922–23). Vol. **1**: *Il regime delle correnti e delle maree nello stretto di Messina*. Com. Intern. del Mediterraneo, Venezia.
- VERCELLI, F. (1941). Le Marree e le sesse nel porto di Zara. *Ric. Scient.* **12**, no. 1. p. 32.
- DE VRIES, See Korteweg and de Vries.
- WARBURG, H. D. (1922). *Tides and Tidal Streams*, p. 12. Cambridge.
- WATTERS, I. K. A. (1953). *N. Z. J. Sci. Tech. B*, **34**, 408.
- Shore Wave recorder drawings* (1946). College of Engineering, Navy Dep. Bureau of Ships, *Contr. Rep.* no. 216. (Univ. of Calif.).
- WEDDERBURN, E. (1905, 1907). *Proc. Roy. Soc. Edinb.* **28**, **29**.
- WEDDERBURN, E. (1909). Temperature observations in Loch Garry. Observations on deep water oscillations. *Proc. Roy. Soc. Edinb.* **29**, 98, 602.
- WEGEMANN, G. (1908). Über sekundäre Gezeitenwellen. *Ann. Hydr. Mar. Met.* **36**, 532.
- WEGEMANN, G. (1913). Die Gezeiten des Mittelmeeres. *Ann. Hydr. Mar. Met.* **41**, 555.
- WEINBLUM, G. and BLOCK, W. (1938). *Naturwissenschaften*, **26**, 193.
- WEINBLUM, G. and BLOCK, W. (1935). *Stereophotogr. Wellenaufnahmen. Schiffsbautechn. Ges.* **36**. *Hauptvers.* Berlin.

- WERENSKJOLD, W. (1916). An analysis of current-measurements in the open sea. *Det 16de Skand. Naturforsmöte*, pp. 306-83.
- WESTPHAL, A. (1899). *Verh. d. 7. Geogr. Kongr., Berl.* **2**, 53.
- WHARTON and EVANS (1888). On the seismic sea-waves caused by the eruption of Krakatoa, Aug. 26 and 27, 1883. *Rep. Krakatoa Comm. Roy. Soc. Lond.*
- WHEELER, W. (1903). *The Sea Coast* **2**, 37. London.
- WHEWELL, W. (1833). Essay towards a first approximation to a map of cotidal lines. *Phil. Trans.* **1**, 147.
- WHEWELL, W. (1836). On the results of an extensive system of tide observations. *Phil. Trans.* p. 289.
- WHEWELL, W. (1848). On the tides of the Pacific and on the diurnal inequality. *Phil. Trans.* p. 1.
- WIEN, W. (1894). Über den Einfluss des Windes auf die Gestalt der Meereswellen. *S. B. Preuss. Akad. Wiss.* **2**, 509.
- WIEN, W. (1900). *Lehrbuch der Hydrodynamik*, pp. 319. Leipzig: S. Hirzel.
- WILKES, Ch. (1845). *Narrative of the U. S. Exploring Expedition, 1838-1842*, **1**, 135. London.
- WITTING, R. (1911). Tidvattnen i Ostersjön och Finska Viken. *Fennia*, **29**, Helsingfors.
- WUST, W. (1949). *Z. angew. Math. Mech.* **29**, 239.
- ZEILON, N. (1912). On tidal boundary waves. K. Svenska. Vetens. Akad. Handl. Stockholm.
- ZEILON, N. (1913). On the seiches of the Gullmar Fiord. Svensk. Hydr.-Biol. Komm. Skrifter, **5**.
- ZEILON, N. (1934). Experiments on boundary tides. Medd. Goteborgs Högskolas, Oceanogr. Inst, no. 8.
- ZIMMERMANN, E. (1920). Aufsuchung von Mittelwerten für die Formen ausgewachsener Meereswellen auf Grund alter und neuer Beobachtungen. *Schiffbau*, **21**, 663. Berlin.

Author Index

- ABERCROMBY, R., 42, 43, 571
AIRY, G. B., 17, 122, 123, 148, 281, 290, 364, 365,
469, 496, 497, 514, 571
AITKEN, J., 140, 571
ALMAGIA, R., 571
D'ARRIGO, A., 135, 571
ARTHUR, R. S., 134, 244, 572
D'AURIA, L., 135, 571
- BAGNOLD, R. A., 136, 137, 571
BALDWIN, R., 167, 575
BARTELS, J., 251, 266, 452, 571, 574
BATES, H., 457, 571
BAZIN, M., 116, 124, 472, 571
BÉNARD, 531
DE BENAZE, 43
BERGHAUS, H., 475, 571
BERGSTEN, P., 183, 184, 220, 571
BERNOULLI, D., 25, 74, 272, 571
BESSON, P., 135, 585
BIDLINGMAIER, F., 275, 571
BJERKNES, V., 124, 296, 297, 518, 522, 565, 566,
571
BLATON, J., 128, 571
BLONDEL, A., 408, 571
BLOCK, W., 46, 589
BOERGEN, C., 95, 266, 304, 366, 380, 381, 387,
571
BOUSSINESQ, J., 116, 572
BOWDEN, K. F., 349, 381, 572
BREITSCHNEIDER, 93, 106
BROWN, P. R., 45, 572
BRUNS, E., 572
BRUNSIDE, 23, 529, 572
BURGERS, J., 76, 572
BURLING, R. W., 45, 572
BURT, W. V., 98, 584
- CALOI, P., 189, 224, 572
CAREY, R. M., 167, 575
CAUCHY, A., 68, 69, 74, 572
CHAMPION, H., 469, 471, 572
CHANDON, E., 408, 572
CHAPMAN, S., 252, 572
CHOLNOKY, E. V., 454, 572
CHRYSAL, G., 161, 163, 167, 169, 172, 182, 183,
184, 220, 222, 340, 415, 572
CIALDI, A., 125, 572
COCHRANE, J. D., 244, 572
COMOY, M., 457, 459, 461, 462, 470, 572
CORKAN, R. H., 217, 230, 381, 385, 388, 469,
471, 572, 575
CORNISH, V., 43, 44, 45, 75, 95, 96, 102, 469, 573
LA COUR, D., 229, 573
COURTIER, A., 306, 572
COX., 239
CREDNER, R., 237, 573
CRONE, C., 374, 573
- DALHUISEN, H., 380, 573
DARBYSHIRE, J., 97, 98, 99, 106, 573
DARLINGTON, C. R., 51, 573
DARWIN, G. H., 266, 278, 281, 299, 304, 305,
314, 389, 476, 497, 506, 509, 511, 573
DAVISON, C., 239, 573
DAWSON, B. W., 309, 439, 444, 445, 457, 469,
471, 573
DEACON, G. E. R., 38, 106, 573
DEFANT, A., 157, 164, 165, 176, 179, 183, 185,
189, 197, 198, 199, 200, 201, 213, 216, 254, 336,
337, 340, 342, 344, 345, 347, 360, 361, 366, 368,
369, 372, 381, 387, 388, 390, 395, 401, 408, 410,
412, 413, 414, 427, 436, 445, 447, 448, 477, 494,
498, 521, 526, 538, 542, 547, 550, 551, 558, 560,
563, 564, 569, 573, 574, 587
DEFANT, FR., 173, 183, 185, 202, 573
DELAUNAY, 513
DIETRICH, G., 295, 306, 418, 419, 420, 478, 479,
480, 483, 487, 488, 491, 494, 495, 496, 575
DOODSON, A. T., 157, 158, 167, 168, 217, 222,
225, 226, 230, 231, 232, 266, 267, 286, 287, 289,
290, 299, 304, 309, 310, 311, 360, 361, 367, 368,
381, 385, 388, 495, 496, 573, 575, 584
DOOS, B., 237, 575
DORRESTEIN, R., 106, 577
DOUGLAS, 60
DUBNOW, 194
DU BOYS, 151, 154, 160
- ECKART, 87
ECKHARDT, A., 113, 114, 575
EINSTEIN, A., 75, 575
EKMAN, W., 323, 327, 328, 494, 522, 523, 546,
547, 560, 575, 578
EMDE, 68, 110
EMDEN, R., 220, 575
ENDROES, A., 176, 182, 185, 186, 187, 189, 200,
201, 202, 406, 436, 453, 454, 575
ERTEL, H., 172, 173, 183, 576
EULER, 272
EVANS, 239, 590
EXNER, F., 553, 576
- FAIRBAIRN, L. A., 349, 487, 572, 576
FERREL, W., 281, 436, 476, 497, 575
FJELDSTAD, J., 122, 144, 326, 329, 331, 333, 334,
350, 446, 466, 532, 535, 536, 537, 539, 540, 545,
547, 556, 576
FORCHHEIMER, P., 124, 128, 178, 576
FOREL, F., 43, 151, 155, 160, 182, 188, 189, 220,
576
FRANCIS, I. R. D., 45, 576
FRANZIUS, L., 135, 457, 460, 462, 464, 465, 576
FROUDE, 37, 38
FUJIWHARA, S., 220, 583
- GAILLARD, G., 43, 72, 116, 124, 127, 135, 136,
576

- GASSENMAYER, O., 42, 43, 102
 GEDGE, 410
 GEISSLER, H., 251, 576
 GEPPERT, H., 23, 576
 GERSTNER, F., 23, 24, 26, 28, 576
 GLEINITZ, E., 238, 576
 GOLDSBROUGH, G. R., 230, 231, 286, 287, 576
 GOLDSTEIN, S., 201, 216, 576
 GRABLOVITZ, G., 389, 576
 GRACE, S., 336, 347, 406, 407, 411, 436, 438, 456, 508, 576, 577
 GREEN, J., 239
 GREEN, L., 120, 150, 153, 154, 466, 577
 GREENHILL, 521, 577
 GROEN, P., 106, 537, 577
 GROSSMANN, J., 139, 577
 GUSTAFSON, J., 374, 555, 577
 GUTENBERG, B., 506
 GWYTHYR, R. F., 117, 577

 HABU, K., 234
 HALBFASS, W., 182, 554, 577
 HANN, J. V., 275, 303, 577
 HANSEN, W., 232, 233, 362, 372, 467, 468, 469, 503, 577
 HARRIS, R. A., 305, 366, 377, 390, 407, 427, 433, 436, 439, 441, 446, 447, 453, 476, 491, 497, 577, 578
 HAURWITZ, B., 529, 560, 562, 578
 HAYFORD, J., 202, 454, 578
 HELA, 555, 580
 HELLAND-HANSEN, B., 494, 535, 538, 540, 541, 546, 575, 578
 HELMHOLTZ, H. v., 75, 578
 HENRY, A., 202, 453, 578
 HERSCHEL, 445
 HESSEN, K., 304, 305, 578
 HIDAKA, K., 157, 163, 169, 171, 183, 185, 197, 198, 234, 235, 578
 HILLEBRAND, C., 284, 579
 HOCHSTETTER, F. v., 238, 579
 HOFMEIER, 457
 HOILAND, E., 565, 579
 HONDA, 164, 176, 187, 579
 HOPFNER, F., 506, 579
 HORN, W., 249, 579
 HOUGH, S., 282, 284, 286, 579

 IMAMURA, A., 579
 IOSHIDA, 164, 187, 579
 ISHIMOTO, M., 579
 ISITANI, 164, 187, 579

 JACOBSEN, J., 374, 562, 563, 579
 JAMES, R. W., 54, 63, 98, 107, 579, 583
 JÄHNKE, 68, 110
 JEFFREYS, H., 29, 75, 83, 84, 86, 87, 122, 473, 506, 514, 515, 579
 JERIMOY, A., 454, 579
 JUNG, K., 506, 585

 KALLE, K., 532, 579
 KAPLAN, K., 78, 579
 KELLAND, P., 145, 579
 KELVIN, LORD (*see* THOMSON, W.)
 KEMPF, G., 61, 579
 KESSLITZ, W. v., 199, 317, 399, 579
 KEYSER, H., 62, 103, 579
 KLEBBA, A., 38, 579

 KOPFEN, W., 139, 579
 KOHLRAUSCH, F., 9, 579
 KOHLSCHÜTTER, E., 46, 49, 50, 111, 580
 KORTEWEG, 109, 125, 580
 KRAUSS, W., 562, 580
 KRAWETZ, T., 454, 579
 KREY, H., 467, 580
 KRUFMEL, O., 48, 67, 96, 101, 112, 125, 127, 136, 188, 189, 237, 366, 414, 417, 434, 440, 441, 443, 470, 475, 476, 498, 580
 KULLENBERG, B., 548, 549, 555, 580, 577, 583
 KURTSCHATOFF, J. W., 200, 580

 LAGRANGE, J. L., 18, 144, 145, 146, 580
 LAMB, H., 13, 17, 21, 24, 25, 66, 68, 69, 76, 109, 119, 122, 164, 201, 281, 285, 290, 293, 326, 340, 473, 512, 517, 529, 565, 569, 580
 LAPLACE, P. S., 279, 282, 283, 284, 290, 580
 LARICH-MOENNICH, F., 33, 42, 43, 100, 580
 LEK, L., 542, 544, 545, 547, 580
 LENTZ, H., 580
 LETTAU, H., 158, 192, 580
 LEVI-CIVITÀ, T., 23, 26, 109, 580
 LEVY, M., 465, 580
 LISITZIN, E., 377, 550, 580
 LONGUET-HIGGINS, M. S., 58, 59, 580
 LOVE, A., 529, 580
 LUBBOCK, S., 311, 580
 LYRA, G., 570, 581

 MACCOWAN, 117, 145, 147, 581
 MACDONALD, 239
 MACH, 258
 MACLAURIN, 272 (*see* BERNOULLI, D., 571)
 MAEDA, S., 220, 583
 MARCHI, DE L., 389, 581
 MARINI, 395
 MASON, 129
 MATHIESEN, L., 78, 581
 MATUZAWA, T., 243, 581
 MAURER, H., 237, 581
 MAZELLE, E., 188, 581
 MAZZARELLI, G., 395, 398, 581
 MEISSNER, O., 194, 237, 581
 MERIAN, 154, 159, 166, 174, 189
 MEISNER, O., 194, 237, 581
 MERZ, A., 368, 370, 371, 389, 567, 581
 MEYER, H., 521, 581
 MICHELL, J. H., 24, 117, 581,
 MICHEL-MOROT, J., 319, 581
 MITCHIM, C. F., 31, 581
 MIYAHARA, S., 305, 581
 MOELLER, L., 192, 372, 581
 MÖLLER, M., 465, 581
 MONTGOMERY, R. B., 96, 581, 585
 MOORE, W. U., 470, 581
 MOTZFELD, H., 81, 82, 84, 87, 88, 581
 VON DER MÜHL, K., 154, 581
 MÜLLER, 258
 MUNK, H. W., 15, 22, 37, 40, 72, 73, 74, 85, 86, 88, 89, 92, 93, 97, 107, 121, 125, 126, 128, 130, 132, 133, 134, 240, 555, 556, 581, 582, 588
 MURAMOTO, A., 430, 582

 NAKAMIYA, 234, 582
 NANSEN, F., 521, 522, 538, 578, 582
 NEUMANN, G., 51, 52, 54, 55, 58, 63, 87, 92, 97, 99, 107, 176, 179, 192, 194, 195, 203, 204, 218, 219, 532, 533, 582, 583

- NEWTON, 272, 279
 NIIMI, M., 305, 581
 NISIDA, K., 429, 582
 NOMITSU, T., 234, 235, 236, 582

 O'BRIEN, M. P., 129, 582
 ODDONE, E., 188, 220, 582
 OGIURA, S., 424, 425, 426, 427, 429, 430, 431, 433, 488, 582, 583
 OKADA, T., 220, 583
 OITIRSTEDT, G., 374, 577

 PABST, W., 37, 583
 PARIS, A., 37, 42, 43, 102, 583
 PARTIOT, H., 469, 583
 PAULSEN, A., 188, 583
 PETRY, P., 135, 585
 PETTERSSON, H., 548, 558, 583
 PETTERSSON, O., 548, 555, 557, 583
 PIERSON, W. I., 54, 58, 63, 65, 107, 583
 PLATANIA, G., 188, 583
 POINCARÉ, H., 208, 278, 467, 501, 502, 535, 583
 POISSON, S., 68, 69, 74, 583
 POLLAC, L., 303, 583
 PRAEDT, 570
 PRANDTL, L., 19, 529, 583
 PREY, A., 506, 509, 583
 PROUDMAN, J., 148, 157, 158, 167, 168, 174, 183, 206, 208, 210, 222, 225, 226, 227, 231, 237, 254, 287, 290, 298, 309, 349, 354, 359, 360, 361, 367, 368, 385, 388, 410, 411, 495, 496, 501, 502, 506, 508, 572, 575, 583, 584
 PRÜFER, G., 295, 487, 584
 PUTZ, R. R., 51, 584

 RALTRAY, M., 98, 584
 RAUSCHELBACH, H., 251, 266, 299, 319, 584
 RAYLEIGH, LORD, 19, 23, 30, 116, 121, 150, 164, 174, 175, 177, 216, 473, 584, 585
 REDFIELD, A. C., 350, 354, 585
 RENQUIST, H., 237, 585
 REVELLE, R., 556, 585
 REYNOLDS, O., 140, 585
 RIBAUD, 395
 RIED, J. L., 550, 585
 ROBERTS, E., 309, 318, 585
 ROLL, H. U., 45, 51, 65, 82, 87, 88, 585
 ROSENHEAD, L., 76, 567, 585
 ROSSBY, C. G., 15, 85, 86, 96, 585
 ROSSITER, J. R., 230, 388, 575, 585
 ROTTOCK, E., 139, 585
 ROUVILLE, DE, 135, 585
 RUDE, 250
 RUDOLPH, E., 237, 585

 SANDSTRÖM, J., 528, 559, 585
 SCHAFFERNICHT, W., 269, 270, 585, 589
 SCHICHEL, 457, 585
 SCHILLING, 135
 SCHMEHL, 506, 585
 SCHMIDT, W., 80, 553, 586
 SCHOOLEY, A. H., 87, 586
 SCHOTT, G., 42, 43, 470, 586
 SCHUBERT, O. v., 336, 494, 542, 586
 SCHUMACHER, A., 46, 48, 60, 366, 474, 586
 SCHWEYDAR, W., 269, 506, 586
 SCOTT RUSSEL, J., 10, 31, 66, 116, 117, 124, 466, 586
 SHWELL, H. R., 51, 57, 542, 586

 SERVAIS, F., 183, 185, 229, 586
 SHEPARD, 239
 SHOULEJKIN, W., 445, 586
 SHUREMAN, P., 305, 319, 478, 586
 SOLBERG, H., 297, 521, 586
 SPITALER, R., 258, 586
 SPRINGSTUBE, H., 441, 442, 443, 586
 STAHLBERGER, E., 188, 586
 STANTON, T., 81, 84, 586
 STENJI, S., 161, 194, 222, 587
 STERNECK, R. v., 165, 176, 188, 189, 200, 367, 368, 388, 389, 390, 393, 401, 402, 403, 404, 405, 406, 407, 410, 412, 431, 436, 447, 453, 454, 456, 476, 477, 478, 483, 484, 491, 495, 498, 508, 587
 STEVENSSON, T., 95, 124, 127, 134, 587, 588
 STÖRMER, C., 535, 588
 STOK, VAN DER, P., 306, 380, 417, 588
 STOKES, G., 16, 17, 22, 23, 24, 517, 588
 STRUIK, D., 109, 588
 SVERDRUP, H. U., 11, 22, 37, 71, 72, 73, 74, 85, 86, 88, 89, 92, 93, 97, 106, 107, 121, 125, 126, 132, 250, 321, 326, 329, 330, 333, 350, 448, 449, 451, 500, 516, 547, 555, 556, 588
 SWAIN, L., 293, 580
 SYMONS, G., 239, 588

 TAIT, 278, 588
 TAKAHASHI, R., 511, 512, 588
 TAYLOR, G., 210, 212, 213, 214, 215, 217, 346, 347, 358, 368, 387, 515, 588
 TENANI, M., 399, 448, 588
 TERADA, 164, 187, 579
 THOMSON, H., 562, 563, 588
 THOMSON, W. (LORD KELVIN), 76, 206, 208, 210, 211, 212, 214, 216, 266, 278, 281, 299, 318, 322, 341, 342, 366, 368, 501, 502, 506, 534, 539, 549, 569, 588, 589
 THORADE, H., 24, 26, 29, 35, 43, 69, 110, 147, 151, 229, 254, 323, 326, 329, 331, 334, 335, 361, 364, 366, 383, 474, 494, 495, 498, 504, 586, 589
 TOMASCHEK, R., 269, 270, 589
 TRAYLOR, M. A., 121, 128, 130, 133, 134, 581
 TURNER, H., 278, 573

 VÉNANT DE SAINT, 144, 585
 VERCELLI, F., 183, 199, 395, 398, 408, 589
 DA VINCI, L. 10, 31
 DE VRIES, 109, 125

 WADSWORTH, G. P., 57
 WARBURG, H. D., 497, 589
 WATTERS, I. K. A., 51, 589
 WEBER-BROTHERS, 112
 WEDDERBURN, E., 183, 553, 554, 555, 558, 589
 WEGEMANN, G., 390, 436, 589
 WEINBLUM, G., 46, 48, 87, 589
 WERENSKIÖLD, W., 331, 590
 WESTPHAL, A., 188, 590
 WHARTON, 239, 590
 WHEELER, W., 125, 590
 WHIEWELL, W., 364, 365, 446, 475, 497, 590
 WIEN, W., 75, 590
 WILKES, CH., 36, 590
 WITTING, R., 374, 375, 376, 590
 WÜST, W., 86, 87, 590

 YOUNG, 364

 ZEILON, N., 176, 182, 558, 559, 590
 ZIMMERMANN, E., 41, 42, 44, 96, 590

Subject Index

- Aegean Sea, tides 403
Adjacent seas, tides 364
Adriatic Sea, tides 399
Amphidromy 290
Analysis,
 harmonic of tidal observations 299
 harmonic of tidal potential 263
 periodogram 56
 spectral 52
- Baltic Sea, tides 372
Bearing Sea, tides 433
Black Sea, tides 404
Bore 469
 internal 562
Break, of waves 120
 of internal waves 562
- California Gulf, tides 434
Canal theory, of tides (Airy) 290
Cellular waves 528
Co-oscillation, tidal 337
Co-range lines 354
 disturbance of by islands 358
 of the World Oceans 479
Co-tidal charts 475
 charting and observing 477
Co-tidal lines 354
 disturbance of by islands 358
 in vicinity of a cape and in a bay 357, 360
 of the World Oceans 479
Cosmic problems, and tides 504
Current,
 due to internal waves 546
 measurements, results 332
 tidal measurements in relation to cosmic problems 512
- Dead water 523
Decrement, logarithmic 9
Deformation, of solid earth by tidal load 509
Dislocation waves 237
Displacement, of stationary internal waves 567
Diurnal tide (K_1), in Atlantic 491
 Dynamical theory of tides 279
 remarks concerning 296
- Eastern China Sea, tides 423
East Indian Archipelago, tides 417
Energy,
 equation of waves 71, 90
 of full-risen sea 54
 kinetic 22
 potential 22
 spectrum 52
 Wave 20
English Channel, tides 377
Equilibrium theory, of tides 272
 corrected 293
 further development 277
Establishment 246
Estuaries, tides 457
Euripus problem 190
Explosion waves 237
- Fetch 98
Forces, tidal,
 experimental proof 268
 as function of zenith-distance 258
 radial and horizontal components 261
 tide generating 254
 tide-generating of moon 257
 tide-generating of sun 257
Friction, influence on waves 78
 effect of on oscillations in basins 155
 of tidal currents in relation to cosmic problems 512
Fundy-Bay, tides 443
- Gauges 250
Geophysical problems,
 and tides 504
Group velocity 12
- Harmonic-components, of tides 267
 analysis of tidal potential 263
 analysis of tidal observations 299
Haough-theory, of tides 284
- Impedance 179
 theory 179

- Inequality, semi-monthly 246
 declinal 248
 diurnal 248
 monthly 247
- Inertia, internal waves 550
- Inland Seas, tides of
 Baikal Lake 454
 Lake Balaton 453
 Lake Geneva 454
 Michigan Lake 453
 Lake Superior 453
- Instability, of internal waves 565
- Internal waves, theory 517, 537
 bore 562
 inertia waves 550
 of long wave character 523
 progressive internal waves of long period 532
 of surface or short wave character 521
 tides, stability 562
 tides in ocean 524
 waves, causes 557
 wave instability 565
 wave records 548
 wave-like displacements 567
 waves, observation 537
- Irish Sea, tides 384
- Japan Sea and Okhotsk Sea, tides 426
- Kattegat, tides 372
- K_1 -tide (diurnal tide), in Atlantic 491
- Lake surface, action of wind and atmospheric pressure 221
- Laplace-theory, of tides 279
- Lines,
 co-range 354
 co-tidal 354
- Machines, predicting of tides 311
- Mediterranean, tides 364, 388
- Mexican Gulf, tides 435
- Motion orbital 5, 19, 21, 50, 124, 519
 of internal waves 519
 sea 60
 trochoidal 28
- M_2 -tide (Semi-diurnal tide)
 in Atlantic 481
 in Indian Ocean 483
 in Pacific 488
- Neap time 247
- North Polar Basin, tides 446
- North Sea tides 365
- Observations, tidal 250
 concerning internal waves in open ocean 537
- Opening correction 174
- Orbital motions 5, 19, 21, 50, 124, 519
 motions of internal waves 519
- Oscillations, of connected systems 175
 free, in a rotating basin 210
 generation and growth of 219
 in lakes, bays and adjacent seas 182, 187, 194
 in the "Haffe" 192
- Oscillations, of shelf 234
- Persian Gulf, tides 413
- Potential, tidal 259
- Predicting machines 311, 317
 harmonic methods 315
 of tides, methods of reference stations 315
- Pressure, normal 83
 atmospheric action on lake surface 221
- Propagation, of waves 66, 68
- Range, tidal 247
- Records of internal waves 548
- Red Sea, tides 407
- Refraction, of waves 127
- Resonance 9
- Revolution 255
- River, tides 458
 tides, theoretical considerations 464
- Sea, motion 60
 scale of sea motion 60
 state of sea and wind 64
 wind-generated 97
- Seiches, in the Black Sea 200
 in adjacent seas 194
 in Adriatic Sea 188, 199
 in Aegean Sea 109
 in bays 187
 Chrystal's method 161
 causes of 219
 in a closed basin, influence of Earth rotation 217
 in lakes 182
 Japanese method 164
 in Mediterranean Sea 189
 method of A. Defant 165
 method of Ertel 172
 in the Sea of Asow 201
 theory of 161
- Semi diurnal, tide (M_2) in Atlantic 481
 in Indian Ocean 483
 in Pacific 488
 theory 496
- Solid earth, and tides in ocean 504
- Spectrum co-cumulative power 54
- Spring time 247

- Stability, waves 528
 of internal tide waves 562
- St. Lawrence Gulf, tides 439
- Strait, tides in of Messina 395
- Stress, tangential 83
- Surf 109
 breaking against cliffs 134
 of flat and steep coasts 123
 multiple 127
- Surface, tension 77
- Surges, storm 229, 245
- Swell 61
 observation of 99
 photographs of 131
 theory of 99
- Tension surface 77
- Tidal-currents 245, 320, 494
 constants 307
 currents in Atlantic 494
 currents, influence of earth rotation 320
 currents, relation between and co-tidal and
 co-range lines 354
 influence of friction 326
 load on solid earth 509
 observations 250
 phenomena in narrow embayments 350
 tables 311
 variation of constants 308
- Tidal, friction 514
- Tides
 in the Adriatic 399
 of the Mediterranean 388
 in adjacent seas 337
 in adjacent seas, effect of earth rotation 341
 in adjacent seas, influence of friction 342
 in the Aegean Sea 403
 of Bering Sea 433
 of Black Sea 404
 of California Gulf 435
 Canal-theory (Airy) 290
 computation from tidal current measurement
 359
 co-oscillating 337
 of East Indian Archipelago 417
 of Eastern China Sea 423
 of English Channel and SW-North Sea 377
 independent 377
 of Irish Sea 384
 of Fundy-Bay 443
 in Kattegat and Baltic Sea 372
 in Mediterranean and adjacent seas 364
 in the North Sea 364
 Form-“zahl” characteristics 305
 predicting machines 311
 in an ocean bounded by a complete meridian
 287
 of Persian Gulf 413
 of Red Sea 404
 of Sea of Japan and Okhotsk 426
- Tides (*Contd.*)
 of the St. Lawrence Gulf 439
 in the Strait of Messina 395
 tables 311
 prediction 311
 equilibrium theory 272
 dynamical theory 279
 in estuaries 457
 interaction between lunar and solar 274
 in Inland Seas 452
 harmonic components of 267
 Hough-theory 284
 internal in ocean 524
 Luni-tidal interval 246
 partial 267
 in a polar basin 286
 of North Polar Basin 446
 Laplace-theory 279
 in rivers 458
 Review of phenomena 245
 relation to geophysical and cosmic problems
 504
 range 247
 semi-monthly inequality 246
 of solid earth 504
 stability of internal 562
 of the World Oceans 475
- Trochoid 28
- Tsunami 234, 239
- Velocity,
 group 12
 Langrange 18
 of propagation or progress 11
- Waves,
 apparent characteristics 57
 break 120
 classification 2
 co-cumulative power spectrum 54
 choical 110
 comparison between theory and observation
 49
 cellular 528
 calming effect of oil on 139
 deep and shallow 10
 dislocation and explosion 237
 energy equation of 71
 energy spectrum 52
 energy 20
 form of 120
 free and forced 8
 frictional influence 78
 generation 66
 growth 66, 87, 93
 group velocity 12
 General remarks 1
 Gerstner's rotational 26
 influence of surface tension 77
 internal 517

Waves (*Contd.*)

- internal inertia waves 550
- internal in lakes and basins 553
- internal, causes 557
- internal 76
- Kelvin 206
- Logarithmic decrement 9
- long (in channels) 142
- laboratory experiments 31
- Mitchell 24
- orbital motion 5, 19, 21
- observation and measurement 31, 33, 93, 99
- progressive 2, 532
- progressive internal of long periods 532
- propagation 66, 68
- Poincaré 208
- resonance 9
- recorder 39
- refraction 127
- reflection of Kelvin 210
- stability 74, 76
- standing 6, 142
- shallow water 109
- surf 109
- standing (in closed basins) 154
- standing (in partially open basins) 173
- surface 10, 20

Waves (*Contd.*)

- short-crested 29
- significant 37, 87
- stability 528
- stereophotogrametric measurement 46
- Taylor 210
- theory of internal waves 517
- tidal 202
- tidal waves, influence of earth rotation 202
- theory of short and long 16
- theory of generation and growth 74
- trochoidal motion 28
- velocity of propagation 11, 66
- wind-generated 50
- White Sea and Gorlo
- tides 445
- Wind
- action on lake surface 221
- duration of action 98
- fields above waves 80
- normal pressure forces of 83
- state of sea and wind 64
- tangential stress of 83
- World Ocean
- co-range lines 479
- co-tidal lines 479
- tides 475

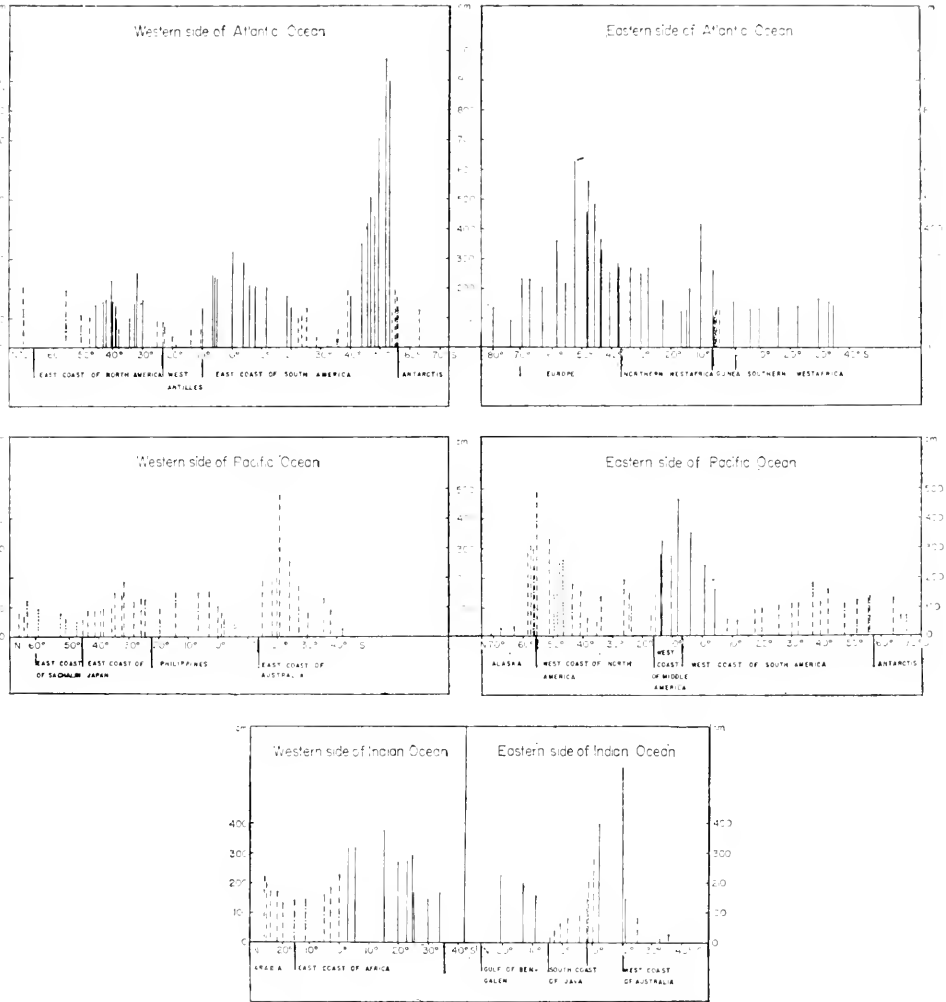


CHART III. Average range at springtide of semi-diurnal tides $2(M_2 + S_2)$ in centimetres. The character of tide $F = \frac{(K_1 + O_1)}{(M_2 + S_2)}$ is designated by —————: $0 < F < 0.25$ semi-diurnal tides; — — — —: $0.25 < F < 1.5$ mixed, mainly semi-diurnal tides; — — — — —: $1.5 < F < 3.0$ mixed, mainly diurnal tides; — — — — — —: $3.0 < F < \infty$ diurnal tides.

(See: Vol. II, Pt. II, p. 480.)

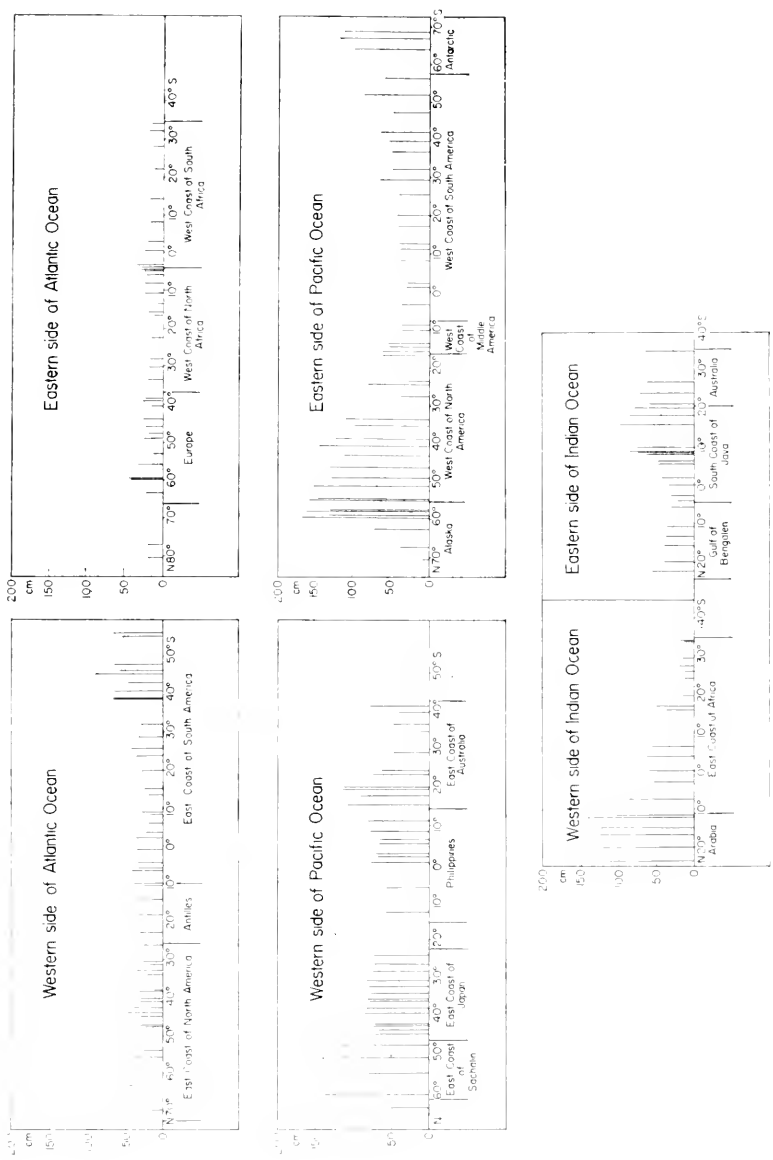


CHART IV. Average range of spring tide $2(K_1 + O_1)$ in centimetres.
 (See: Vol. II, Pt. II, p. 480.)

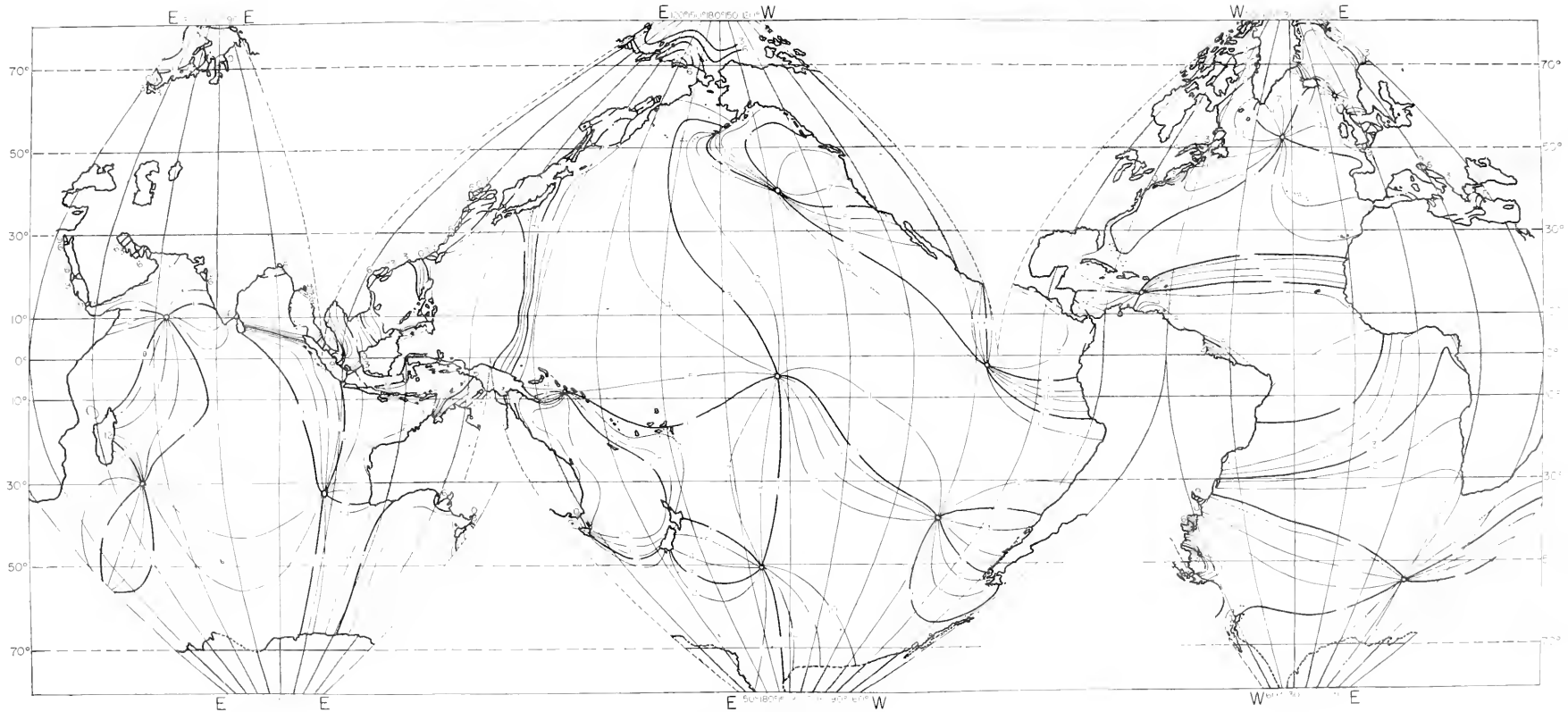


CHART I Semi-diurnal tides in the Oceans.

Co-tidal lines of the semi-diurnal tide M_2 referred to the upper culmination of the moon in Greenwich (DU RUIJ 1944).

(See Vol. II, Pt. II, p. 479)

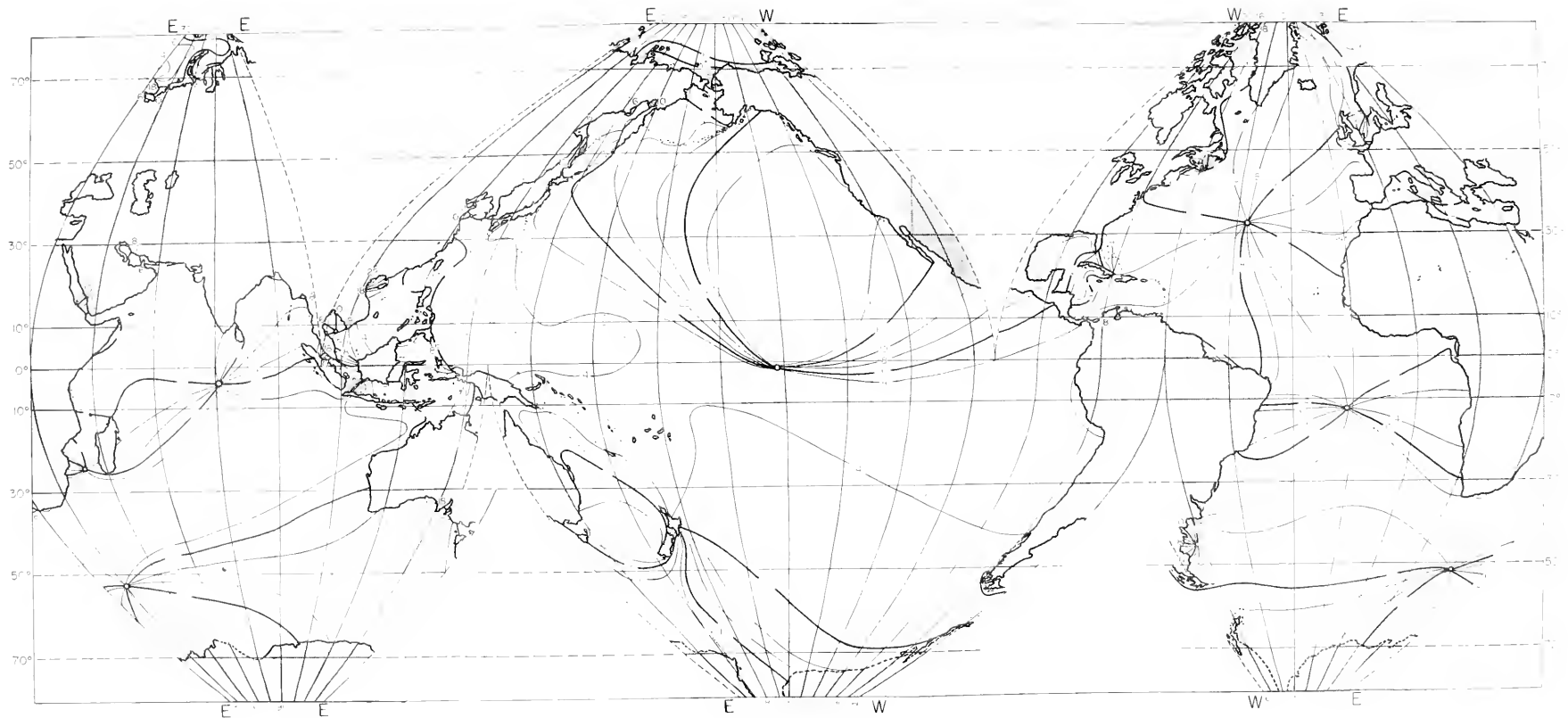


CHART II Diurnal tides in the oceans.

Co-tidal lines of the K_1 tide referred to Greenwich (DITTRICH 1944).

(See Vol. II, Pt. II, p. 479.)

